Investigation into pathological neuronal-myeloid cell interactions and rescue of hyper-reactive immune responses in Huntington's disease

Lucianne Dobson

University College London

A thesis submitted in partial fulfilment of the requirements for the degree of Doctor of Philosophy from University College London

2017

Declaration

I, Lucianne Dobson, confirm that the work presented in this Thesis is my own. Where information has been derived from other sources or contributions of others are involved, I confirm that this has been clearly indicated in this Thesis.

Acknowledgements

I would firstly like to thank my principal supervisor and mentor, Prof. Sarah Tabrizi, for giving me the wonderful opportunity to develop as a scientist under her excellent guidance. Her incredible enthusiasm, wealth of knowledge and determination to improve the lives of people with Huntington's disease is inspiring and motivating, and I feel privileged to have been her student. I express enormous gratitude to my subsidiary supervisor, Dr. Jennifer Pocock, for her mentoring, expertise, encouragement, friendship and unwavering support in both professional and personal matters through times good and bad. I don't think I would have come this far without her.

Thanks to members of the Tabrizi research group past and present for sharing their ideas, experience, resources and valuable time in contribution towards my research. I would like to extend special thanks to Dr. Ralph André, Dr. Rhia Ghosh, Dr. Rob Goold, Dr. Jamie Miller, Dr. Jennifer Parker and Dr. Alison Wood-Kaczmar for their friendship, humour, motivation, shared enthusiasm for science and our much-loved lunch dates. Ralph was also my lab mentor, advisor and friend, and I would like to thank him for all those hours mulling over the technical details of my research and his support during the most difficult moments.

I would also like to show my appreciation to my colleagues at the MRC Prion Unit and UCL Department of Neurodegenerative Disease for creating such a vibrant and motivating environment in which to do my research. The lab technicians and other PhD students have become good friends and we have shared every stressful and exciting moment of our research together. I am especially grateful to Kevin Williams for his constant unconditional support in all matters from freezer failure emergencies to personal crises, and of course for our lunch dates at Fryer's Delight. Any challenging moment can be turned around in his company - he is the life and soul of the research department. I also thank Laura Jane Pulford for being part of my life and sharing with me her vibrant enthusiasm and positive nature - and introducing me to HelloFresh and Nespresso! She was a beautiful person, inside and out, and though she will be missed I take with me the wonderful memories we created together and her amazing approach to living life to the fullest. Additional thanks also go to my personal mentor, Nicholas Little, who helped me through the toughest moments.

I wish to express sincere appreciation to the Huntington's disease patients and their families and carers who donated blood samples, and staff at the Huntington's disease clinic, without whom this research project would not have been possible. Also to BBSRC, GSK and Teva Pharmaceutical Industries, whose funding supported my

research, and our collaborators Dr. Liat Hayardeny and Prof. Pippa Loupe at Teva for their advice and guidance on pre-clinical drug testing and scientific paper writing.

Finally, I would like to thank my friends and family for their love, care, support, encouragement and guidance. Dr. Elspeth Brzezińska, Katarína Feketeová, Sarah Roberts, Pavol Šedík and Dr. Phillip Smethurst are the truest of friends, and I thank them for their kindness and patience, for giving me the strength to keep going, for understanding my past, for believing in my future and for loving me just the way I am. Thanks to my darling Matej Šedík for lighting up my life and bringing me so much happiness. Thanks to my partner, best friend and soul mate Lenart Seničar for his love, care and support, especially during the writing-up period when at times life has been trying. Thanks to my parents, Jacqueline Ray and Steven Dobson, for loving me, nurturing me, encouraging me and supporting me with their non-judgemental guidance; to my sister, Hollie Dobson, for her friendship and excellent sense of humour; to my step-parents, Andy Ray and Greta Dobson, for supporting my parents and me; to my auntie, Carol Birkett, for the laughs and cheering me on; and to my grandparents, Stella Birkett and John Deryk Birkett, for encouraging me to make the most of myself. To these people, I dedicate this Thesis, for none of this would have been possible without them.

Abstract

The innate immune system is known to play a significant role in the pathogenesis of Huntington's disease (HD). However, whether the myeloid cell activation and inflammation associated with neurodegeneration and disease progression in HD is protective or damaging remains to be clearly defined. Here, neuronal-myeloid cell interactions were examined in novel co-culture models of HD, with the aim of investigating the contribution of myeloid cells to neurotoxicity or neuroprotection in the pathogenesis of HD. HD and non-HD human NSC-derived neuronal cell lines expressing human huntingtin (*HTT*; full-length or exon 1) were developed and characterised. These cell lines can be differentiated into mature neuronal cultures, and HD neuronal cultures expressing mutant *HTT* exon 1 exhibit several characteristics of pathologically affected neurons in the HD patient brain. Additionally, a novel technique was discovered for the induced differentiation of primary blood monocyte cultures, from healthy volunteers or HD patients, into microglia-like cells (BMD-microglia). BMD-microglia are similar to human brain-resident microglia *in vivo* by both morphological and antigenic criteria. In co-culture, BMD-microglia rescued HD neurons from mutant HTT-induced neurotoxicity and reduced neuronal death. This was associated with elevated levels of brain-derived neurotrophic factor (BDNF) release and M2 polarisation shift. During chronic stimulation, HD patient BMD-microglia became more M2-polarised than healthy volunteer BMD-microglia and released BDNF at three-fold higher levels. In contrast, BMD-macrophages, differentiated from primary monocyte cultures from healthy volunteers or HD patients, were neurotoxic in co-culture with HD or non-HD neurons, and this was associated with increased release of the proinflammatory cytokines interleukin (IL)-1β, IL-6 and tumour necrosis factor (TNF)α. Inherent dysfunctional upregulation of cytokine release was also demonstrated in HD patient monocytes. Overall, the findings presented in this Thesis highlight myeloid cell phenotypes as an important modulator of neurotoxicity in HD, and harnessing the innate immune system in order to promote neuroprotective myeloid cell phenotypes whilst inhibiting neurotoxic phenotypes is an attractive therapeutic target. Laquinimod, a novel immunomodulatory drug which has been shown to have beneficial effects in multiple sclerosis patients, was shown here to dampen hyper-reactive cytokine production in HD patient monocytes. Modulation of peripheral immune responses has previously been demonstrated to impact on central pathology and disease progression in HD, and therefore laquinimod may be a promising candidate for dampening the harmful effects of a dysfunctional innate immune system in HD.

Table of contents

Index of figures

Index of tables

Abbreviations list

17β-HSD14	17β-hydroxysteroid dehydrogenase type 14
24hPT	24 hours pre-treatment
24hPT+24hCT	24 hours pre-treatment with 24 hours continued treatment
2hPT	2 hours pre-treatment
3-HK	3-hydroxykynurenine
6-FAM	6-Carboxyfluorescein
A2UCOE	A2 ubiquitous chromatin opening element
AAO	Age at onset
AAV	Adeno-associated virus
ABI	Applied Biosystems Incorporation
ABS	Absorbance
ACDP	Advisory Committee on Dangerous Pathogens
AD	Alzheimer's disease
ADP	Adenosine diphosphate
AhR	Aryl hydrocarbon receptor
ALS	Amyotrophic lateral sclerosis
ampr	Ampicillin resistance gene
ANOVA	Analysis of variance
AP	Alkaline phosphatase
AP-1	Activator protein-1
ASO	Antisense oligonucleotide
ATP	Adenosine triphosphate
Aβ	Amyloid-beta
BAC	Bacterial artificial chromosome
BBB	Blood-brain barrier
BCA	Bicinchoninic acid
BDNF	Brain-derived neurotrophic factor
BF	Brightfield
bFGF	Basic fibroblast growth factor
BL	Borderline (significance)
BMD	Blood monocyte-derived
bp	Base pair
BSA	Bovine serum albumin
C(#)	Clone (*number*)
CAG	Cytosine-adenine-guanine
cAMP	Cyclic adenosine monophosphate
CB_2	Cannabinoid receptor 2
CCG	Cytosine-cytosine-guanine
CCL	Chemokine (C-C motif) ligand

CD	Cluster of differentiation
cDNA	Complementary deoxyribonucleic acid
CDS	Cytosolic deoxyribonucleic acid sensor
C/EBP	CCAAT/enhancer-binding protein
c-Fos	Cellular Fos
CHDI	Cure Huntington's Disease Initiative
c-Jun	Cellular Jun
CLR	C-type lectin receptor
CNS	Central nervous system
COX-2	Cyclooxygenase-2
cPPT	Central poly-proline tract
CREB	cAMP response element binding
CSF	Cerebrospinal fluid
CSF1	Colony-stimulating factor 1
CSF1R	Colony-stimulating factor 1 receptor
DAMP	Damage-associated molecular pattern
DAP12	DNAX activation protein 12
DAPI	4',6-diamidino-2-phenylindole
db-cAMP	Dibutyryl cyclic adenosine monophosphate
dbSNP	Database of Single Nucleotide Polymorphism
DCL	Diagnostic confidence level
DD	Days differentiation
ddH_2O	Deionised distilled water
DHEA	Dehydroepiandrosterone
DIC	Differential interference contrast
DIV	Days *in vitro*
DMEM	Dulbecco's Modified Eagle Medium
DMEM:F-12	Dulbecco's Modified Eagle Medium: Nutrient Mixture F-12
DMSO	Dimethyl sulfoxide
DNA	Deoxyribonucleic acid
DPBS	Dulbecco's Phosphate-Buffered Saline
dsRNA	Double-stranded ribonucleic acid
DTI	Defined Trypsin Inhibitor
EAE	Experimental autoimmune encephalomyelitis
EDTA	Ethylenediaminetetraacetic acid
EGF	Epidermal growth factor
eGFP	Enhanced green fluorescent protein
EGTA	Ethylene glycol-bis(β-aminoethyl ether)-N,N,N',N'-tetraacetic acid
ERK	Extracellular signal-regulated kinase
ERβ	Oestrogen receptor-β
FACS	Fluorescence-activated cell sorting
FBS	Foetal bovine serum

FITC	Fluorescein isothiocyanate
FL	Full-length
g	Gram
GABA	Gamma-amino butyric acid
GAD	Glutamic acid decarboxylase
GAG	Group antigens
GAPDH	Glyceraldehyde 3-phosphate dehydrogenase
G-CSF	Granulocyte-colony stimulating factor
GDNF	Glial-derived neurotrophic factor
GM-CSF	Granulocyte macrophage colony-stimulating factor
GWAS	Genome-wide association study
h	Hour
HBSS	Hank's Balanced Salt Solution
HCS	High Content Screening
HD	Huntington's disease
HDAC	Histone deacetylase
HEK293T	Human Embryonic Kidney (cell line 293 with T antigen)
Hi-Di	Highly deionised
HLA	Human leukocyte antigen
HMGB1	High-mobility group box 1 protein
HPA	Hypothalamic–pituitary–adrenal
HRP	Horseradish peroxidase
HTT	Huntingtin gene (human)
HTT	Huntingtin protein (human)
Htt	Huntingtin gene (mouse)
Htt	Huntingtin protein (mouse)
HV	Healthy volunteers
hyg	Hygromycin
hygr	Hygromycin resistance gene
Iba1	Ionized calcium-binding adapter molecule 1
ICC	Immunocytochemistry
IFC	Imaging flow cytometry
IFN	Interferon
IFNGR	Interferon-gamma receptor
Ig	Immunoglobulin
IGF	Insulin-like growth factor
I.I.	Integrated intensity
IKK	IκB kinase
IL	Interleukin
IL-1R	Interleukin 1 receptor
IL-1RA	Interleukin 1 receptor antagonist
iNOS	Inducible nitric oxide synthase

INT	2-(4-iodophenyl)-3-(4-nitrophenyl)-5-phenyl-2*H*-tetrazolium
IoN	Institute of Neurology
iPSC	Induced pluripotent stem cell
IR	Infrared
IRAK	Interleukin-1 receptor-associated kinase
IRES	Internal ribosome entry site
IRF	Interferon regulatory factor
IVF	*In vitro* fertilisation
IκB	Inhibitor of kappa-light-chain-enhancer of activated B cells
Jak	Janus kinase
JNK	c-Jun N-terminal kinases
Kb	Kilobases
KCL	King's College London
KDa	Kilodaltons
KMO	Kynurenine 3-monooxygenase
KYNA	Kynurenic acid
LB	Luria-Bertani
LBP	Lipopolysaccharide-binding protein
LDH	Lactate dehydrogenase
LOD	Limit of detection
LPS	Lipopolysaccharide
LTR	Long terminal repeats
MACS	Magnetic-activated cell sorting
Mal	Myeloid differentiation primary response gene 88 adaptor-like
manHD	Manifest Huntington's disease patients
MAPK	Mitogen-activated protein kinase
MC-CM	Monocyte-conditioned medium
MCI	Mild cognitive impairment
MCP-1	Monocyte chemoattractant protein-1
MCS	Multiple cloning site
MD-2	Myeloid differentiation protein 2
MG-CM	Microglia-conditioned medium
MHC	Major histocompatibility complex
mHTT	Mutant huntingtin gene (human)
mHTT	Mutant huntingtin protein (human)
mHtt	Mutant huntingtin gene (mouse)
mHtt	Mutant huntingtin protein (mouse)
min	Minute
MKK	MAPK kinase
MMP	Matrix metalloproteinase
MOI	Multiplicity of infection
MRC	Medical Research Council

MRI	Magnetic resonance imaging
mRNA	Messenger ribonucleic acid
MS	Multiple sclerosis
MSCV	Murine stem cell virus
MSD	MesoScale Discovery
MSN	Medium spiny neuron
MyD88	Myeloid differentiation primary response gene 88
Mφ-CM	Macrophage-conditioned medium
N2a	Neuro-2a (neuroblastoma cell line)
NAD^+	Nicotinamide adenine dinucleotide (oxidised)
NADH	Nicotinamide adenine dinucleotide (reduced)
NAP1	NFκB-activating kinase-associated protein 1
NCA	Not commercially available
NCBI	National Center for Biotechnology Information
NCCD	Nomenclature Committee on Cell Death
N-CM	Neuron-conditioned medium
NCOR2	Nuclear receptor co-repressor 2
NEMO	NFκB essential modulator
NFκB	Nuclear factor kappa-light-chain-enhancer of activated B cells
NGF	Nerve growth factor
NHNN	National Hospital for Neurology and Neurosurgery
NK	Natural killer
NLR	NOD-like receptor
NLRP3	NOD-, LRR- and pyrin domain-containing 3
NM	Neuronal medium
nm	Nanometres
NMDA	*N*-methyl-D-aspartate
NO	Nitric oxide
NOD	Nucleotide-binding oligomerization domain
Nrf2	Nuclear factor E2-related factor 2
NS	Not significant
NSAID	Non-steroidal anti-inflammatory drug
NSC	Neural stem cell
NT	Neurotrophin
P	Phosphorylated/phosphate group
p75NTR	p75 neurotrophin receptor
PAGE	Polyacrylamide gel electrophoresis
PAMP	Pathogen-associated molecular pattern
PBMC	Peripheral blood mononuclear cell
PBR	Peripheral benzodiazepine receptor
PBS	Phosphate-buffered saline
PBST	Phosphate-buffered saline Tween-20

PCR	Polymerase chain reaction
PD	Parkinson's disease
PDE	Phosphodiesterase
PDL	Poly-D-lysine
p.d.u.	Procedure defined unit
PE	R-phycoerythrin
PEI	Polyethylenimine
PET	Positron emission tomography
PFA	Paraformaldehyde
PGE2	Prostaglandin E2
PGK	Phosphoglycerate kinase
PI	Propidium iodide
PI3K	Phosphatidylinositol-4,5-bisphosphate 3-kinase
PLA	Proximity Ligation Assay
PMSF	Phenylmethylsulfonyl fluoride
polyQ	Poly-glutamine
PPAR	Peroxisome proliferator-activated receptor
preHD	Pre-manifest Huntington's disease gene carrier
PRR	Pattern recognition receptor
puro	Puromycin
puror	Puromycin resistance gene
PVDF	Polyvinylidene fluoride
QA	Quinolinic acid
RAGE	Receptor for advanced glycation end-products
RCA	Rolling-circle amplification
Rhes	Ras homologue enriched in striatum
RIG-I	Retinoic acid-inducible gene 1
RIP1	Receptor-interacting serine/threonine-protein kinase 1
RIPA	Radioimmunoprecipitation assay
RLR	RIG-I-like receptor
RLU	Relative light units
RM	Repeated measures
RMS	Root mean square
RNA	Ribonucleic acid
RNAi	Ribonucleic acid inhibitor
RNS	Reactive nitrogen species
ROS	Reactive oxygen species
rpm	Revolutions per minute
RPMI	Roswell Park Memorial Institute
RT	Room temperature
s	Seconds
SARM	Sterile-alpha and Armadillo motif-containing protein

SD	Standard deviation
SDS	Sodium dodecyl sulphate
SEM	Standard error of the mean
SIN	Self-inactivating
SINTBAD	Similar to NAP1 TBK1 adaptor
siRNA	Small interfering ribonucleic acid
SNP	Single nucleotide polymorphism
SNS	Sympathetic nervous system
SOC	Super Optimal broth with Catabolite repression
SOD	Superoxide dismutase
ssRNA	Single-stranded ribonucleic acid
STAT	Signal transducer and activator of transcription
T3	Tri-iodo-thyronine
T4	L-Thyroxine
TAB	TAK1-binding protein
TAK1	TGFβ-activated kinase 1
Tb	Terbium
TBE	Tris/Borate/EDTA
TBK1	TANK-binding kinase 1
TBST	Tris-buffered saline Tween-20
TDP-43	Transactive response DNA binding protein 43
TGFβ	Transforming growth factor beta
TH	Tyrosine hydroxylase
Th1	T helper type 1
Th2	T helper type 2
TIR	Toll/interleukin-1 receptor
TIRAP	TIR domain-containing adaptor protein
TLR	Toll-like receptor
TMB	3,3’,5,5’-Tetramethylbenzidine
TNF	Tumour necrosis factor
TNFR	Tumour necrosis factor receptor
TRAF	TNF receptor-associated factor
TRAM	TRIF-related adaptor molecule
TREM2	Triggering receptor expressed on myeloid cells 2
TR-FRET	Time-resolved fluorescence resonance energy transfer
TRIF	TIR domain-containing adaptor inducing IFNβ
Trk	Tyrosine receptor kinase
Ub	Ubiquitin
Ubc13	Ubiquitin-conjugating enzyme E2 13
UCL	University College London
Uev1a	Ubiquitin-conjugating enzyme E2 variant 1A
UHDRS	Unified Huntington’s Disease Rating Scale

UK	United Kingdom
UV	Ultraviolet
V	Volts
VM	Ventral mesencephalon
VSV-G	Vesicular stomatitis glycoprotein G
WGA	Wheat germ agglutinin
WPRE	Woodchuck post-transcriptional regulatory element
WT	Wild-type
YAC	Yeast artificial chromosome
Ym	Chitinase-like proteins
Δ5-ADIOL	5-androstene-3β,17β-diol

1 Introduction

1.1 Huntington's disease

Huntington's disease (HD) is a genetic neurodegenerative disorder characterised by pathology in the brain and peripheral tissues, along with progressive motor, cognitive and neuropsychiatric symptoms. HD is a highly debilitating and fatal condition which displays a pattern of progressive decline over approximately twenty years from when symptoms become manifest, which is usually in middle-age (Walker 2007). The condition was first described in detail by George Huntington in 1872 as a hereditary chorea with a psychiatric component and age-onset (Huntington 1872). Approximately 12 per 100,000 persons suffer from HD in the United Kingdom (UK) (Evans *et al.* 2013) and there is currently no cure, nor are there any treatments which can delay onset or slow progression of the disease.

1.1.1 Clinical features of HD

Symptoms of HD display delayed onset despite presence of the disease-causing gene, mutant huntingtin (*mHTT*), and protein (mHTT) throughout the entire lifetime. Symptoms usually become manifest at 35-44 years of age, but can begin at any time from infancy to senescence (Walker 2007).

Motor abnormalities include involuntary movement disturbances (chorea), such as hyperkinetic, irregular and uncontrollable movements. With disease progression, motor symptoms become more severe with abnormal posturing and writhing motions, until rigidity-akinesia ensues in the final stages (Wild and Tabrizi 2007). Cognitive dysfunction in HD includes deficits in attention, executive functioning and working memory, and ultimately dementia (Montoya *et al.* 2006). The most commonly reported neuropsychiatric symptoms in HD patients are depressed mood, anxiety, irritability, and apathy (van Duijn *et al.* 2007).

HD gene carriers can present with one or all of the symptom domains comprising the HD triad (motor, cognitive and neuropsychiatric), and in any order (Victorson *et al.* 2014). Being such a clinically heterogeneous disease, it can be difficult to clearly discern symptom onset. While many patients display evidence of cognitive and psychiatric problems before any manifestation of motor symptoms, a definitive

diagnosis of HD is usually only made when motor abnormalities are noted on examination (Wild and Tabrizi 2007).

Approximately 7 % of HD patients become manifest at under twenty years of age and are diagnosed with Juvenile HD. Disease progression is generally faster in Juvenile HD, and symptoms differ from the adult onset disease in that akinetic-rigidity, rather than chorea, is the dominant motor abnormality and many individuals additionally suffer with seizure disorder (Nance and Myers 2001).

Life expectancy of HD patients is around twenty years from symptom onset, and the most common primary causes of death are aspiration pneumonia and cardiovascular diseases (Heemskerk and Roos 2012; Sørensen and Fenger 1992). Suicide rates are also much higher in HD patients than in the general population (Schoenfeld *et al.* 1984; Sørensen and Fenger 1992).

1.1.2 HD genetics and other contributing factors

HD is an autosomal dominantly inherited condition caused by a cytosine-adenine-guanine (CAG) trinucleotide repeat expansion in exon 1 of the *HTT* gene, which is located on the short arm of chromosome 4 at 4p16.3 (The Huntington's Disease Collaborative Research Group 1993). The CAG codons are translated into a poly-glutamine (polyQ) stretch of amino acids in the HTT protein, which is ubiquitously expressed (van der Burg *et al.* 2009; Ellrichmann *et al.* 2013).

The CAG repeat region in *HTT* can vary in length between individuals and is very closely related to HD manifestation and phenotype (Harper 1999; Walker 2007). In HD patients, CAG repeat length accounts for approximately 60 % of the variation in age at onset (AAO) and rate of disease progression; individuals with longer repeats become manifest at a younger age and progress faster (Andrew *et al.* 1993; Snell *et al.* 1993; Harper 1999; Walker 2007). Less than 27 CAG repeats is normal and individuals do not develop HD. *HTT* with 27-35 repeats is considered an intermediate genotype as individuals are generally unaffected but there is a potential risk of expansion and inheritance of the mutant gene by offspring (Ha *et al.* 2012). Trinucleotide CAG repeats in the intermediate range or longer become increasingly unstable with length during replication, especially in spermatogenesis, leading to dynamic mutations and an increased likelihood of expansions over generations (Snell *et al.* 1993; Walker 2007). Repeats of 36-40 give a mutant gene which has reduced penetrance and symptoms may not appear until late in adult life, if at all (Rubinsztein *et al.* 1996; Walker 2007). With CAG repeats of more than 40 a fully penetrant mutant gene is produced and carriers will be affected by HD (Walker 2007). If the *mHTT* gene has 60 or more repeats, the individual will manifest with Juvenile HD (Nance and Myers 2001).

The majority of HD patients are heterozygous gene carriers, and the chance of HD inheritance by offspring is 50 %. Some individuals, however, are homozygous for the mutant gene, increasing heritability to 100 %. Interestingly, AAO remains within the same range as heterozygotes carrying similar repeat lengths to the homozygote allele with the longest CAG repeat (Squitieri *et al.* 2003). Rate of progression in homozygous HD gene carriers is, however, more rapid, suggesting that there may be different mechanisms underlying AAO and disease progression (Squitieri *et al.* 2003).

CAG-repeat length accounts for some, but not all, of the variation in AAO and progression rate in HD, and other contributors such as genetic modifiers and environmental factors are attributable for the remaining variation in HD pathogenesis (Wexler *et al.* 2004; Gusella *et al.* 2014; Sun *et al.* 2016). Recently, analysis of a genome-wide association study (GWAS) revealed variants in genes associated with deoxyribonucleic acid (DNA) handling and repair mechanisms to be significant modifiers of HD AAO (Genetic Modifiers of Huntington's Disease (GeM-HD) Consortium 2015). This could be linked to CAG-repeat somatic expansion, particularly in brain regions that are targets for neurodegeneration, which has been found to occur at a higher rate in individuals with earlier AAO (Swami *et al*. 2009). Environmental factors which may influence AAO include poverty, diet, exposure to pollutants and poor sanitation (Wexler *et al.* 2004).

Since identification of the HD gene, individuals who are at risk can choose to undergo genetic testing, preceded by genetic counselling, to confirm whether or not they have inherited the defective gene. The most common reasons for genetic testing are family planning and making career choices (Walker 2007). For example, HD gene carriers may opt for *in vitro* fertilisation (IVF) along with preimplantation genetic diagnostics to select for unaffected embryos (Stern 2014). Genetic testing in HD also offers a unique opportunity for researchers to study the processes of neurodegenerative disease in the pre-manifest stages, potentially opening up avenues of therapeutic intervention before the onset of symptoms.

1.1.3 HD neuropathology

Neuropathology in HD is hallmarked by neuronal dysfunction and atrophy of the dorsal striatum, resulting in extreme shrinkage of the caudate nucleus and putamen and expansion of the frontal horns of the lateral ventricles (Vonsattel *et al.* 1985) (Figure 1.1). Gamma-amino butyric acid (GABA)ergic medium spiny neurons (MSNs) are particularly vulnerable, leading to loss of inhibitory input to the indirect pathway of basal ganglia-thalamocortical circuitry involved with movement initiation, and consequently manifestation of hyperkinesis and chorea (Purves *et al.* 2001). Other brain areas

particularly affected in HD include the substantia nigra, cortical layers 3, 5, and 6, the CA1 region of the hippocampus, the angular gyrus in the parietal lobe, Purkinje cells of the cerebellum, lateral tuberal nuclei of the hypothalamus, and the centromedial-parafascicular complex of the thalamus (Walker 2007). There is also profound white matter loss in manifest patients, with basal ganglia-cortical connectivity being particularly affected (Novak *et al.* 2015), in addition to progressive astrogliosis and accumulation of reactive microglia in affected brain regions (Vonsattel *et al.* 1985; Sapp *et al.* 2001). Structural and functional brain changes throughout the disease course correlate with symptom manifestation and severity, with the specific regions affected relating to associated motor, cognitive and neuropsychiatric symptoms (Kuwert *et al.* 1989; Mayberg *et al.* 1992; Montoya *et al.* 2006; Novak *et al.* 2015).

Figure 1.1: Large-scale progressive neuropathology in the HD brain

Volumetric magnetic resonance imaging (MRI) scans in a healthy volunteer (HV), a pre-manifest HD gene carrier (preHD) and a manifest HD patient (manHD) in the early stages of clinical symptomatic disease, reveal progressive regional and whole-brain atrophy in HD (Tabrizi et al. 2009). Striking changes, which can be observed in the images above, include expansion of the lateral ventricles, atrophy of the caudate and putamen, and thinning of the cortex. (Re-printed with minor amendments from Lancet Neurology, Volume 8, Issue 9, 'Biological and clinical manifestations of Huntington's disease in the longitudinal TRACK-HD study: cross-sectional analysis of baseline data', Page 795, Figure 1, Tabrizi et al., ©2009, with permission granted by Elsevier Health Science Journals via Copyright Clearance Center, License ID: 3931970923439).

Neuropathology at the cellular level is characterised by presence of nuclear and cytoplasmic inclusion bodies containing ubiquitinated mHTT aggregates (Davies *et al.* 1997; DiFiglia *et al.* 1997). The full-length HTT protein is proteolytically cleaved into several smaller N-terminal fragments all containing the polyQ region, and in HD the smallest fragments, including an exon 1 only HTT protein, accumulate into a detergent-insoluble complex (Landles *et al.* 2010). It is thought that the polyQ expansion in mHTT alters the physiochemical properties of the final protein structure, especially in the shorter fragments, such that the final proteins do not fold normally and are instead

drawn together by their highly polar polyQ tracts to form hydrogen-bonded accumulating aggregates (Arrasate and Finkbeiner 2012). Other cellular neuropathology includes dysfunction of synapses, cytoskeletal integrity and axonal transport (Walker 2007).

1.1.4 Normal HTT function

HTT is a very large protein, approximately 350 kilodaltons (KDa) in its full-length form (Cattaneo *et al.* 2005), which is expressed in all human and mammalian cells (Walker 2007; Ellrichmann *et al.* 2013). The *HTT* gene sequence is also highly conserved phylogenetically (Cattaneo *et al.* 2001) suggesting a fundamental role of HTT in cellular function.

HTT is transcribed widely during embryogenesis (Buraczynska *et al.* 1995) and homozygous *Htt* knock-out is embryonic lethal in mouse models (Duyao *et al.* 1995; Nasir *et al.* 1995; Zeitlin *et al.* 1995), indicating an essential role of HTT in development. HTT interacts with numerous other proteins involved with a variety of biological functions including transcriptional regulation, endocytosis, intracellular trafficking and vesicle transport, cell viability and apoptosis, cell signalling, and morphogenesis (Cattaneo *et al.* 2001; Harjes and Wanker 2003), suggesting that HTT is also involved with these processes.

Highest concentrations of HTT are found in the brain and testes (Walker 2007), and several identified roles of the protein relate specifically to neuronal function. HTT regulates fast axonal trafficking, vesicle transport and synaptic transmission, and protects neurons from excitotoxicity (Cattaneo *et al.* 2001; Cattaneo *et al.* 2005). HTT is also required for normal excitatory synapse development in the cortex and striatum (McKinstry *et al.* 2014), and is involved in the production and transport of brain-derived neurotrophic factor (BDNF), a neurotrophin which protects neurons and regulates neurogenesis (Cattaneo *et al.* 2005). HTT is therefore crucial for normal brain function.

1.1.5 Mutant huntingtin and cellular pathogenesis

It is unlikely that HD pathogenesis is caused by a loss of normal HTT function, but rather a toxic gain of function by the mutant protein. It is known that expression of mHTT causes neuronal dysfunction and degeneration, and there is accumulating evidence that fragments of mHTT exon 1 are the toxic species. HD pathology could, however, be caused by soluble misfolded mHTT, mHTT-containing inclusion bodies, or any species that exist inbetween (compact β-sheet structures, protofibrils, fibrils, aggregation foci or visible aggregates) (Bates 2003; Rubinsztein and Carmichael 2003). Full-length HTT and/or smaller N-terminal fragments could be involved, and even *mHTT* messenger ribonucleic acid (mRNA)-mediated mechanisms of

neurotoxicity have been implicated (Nalavade *et al.* 2013). Any of these species could be toxic, redundant or even protective.

Accumulation of aggregates, especially nuclear inclusions, may cause mechanistic interference with normal cell signalling, and have been shown to correlate with toxicity in several animal and cell models (Rubinsztein and Carmichael 2003). Aggregation inhibition by specific antibodies directed at HTT has been shown to prevent death in an HD cell culture model, and antibodies which stimulated aggregation increased apoptotic cell death (Khoshnan *et al.* 2002). Aggregates may also sequester HTT-interaction proteins and normal HTT into inclusions via retained binding sites and polar polyQ interactions, resulting in a dominant negative effect by interfering with normal HTT function (Walker 2007). However, it has also been argued that the development of inclusions is a protective mechanism implemented by cells to compartmentalise toxic mHTT species to reduce their overall concentration and toxicity. Cells which form inclusion bodies have been shown to survive longer than those that don't (Arrasate *et al.* 2004), and a compound which enhances aggregate formation may even lessen some aspects of cellular pathology (Bodner *et al.* 2006). In transgenic HD mouse models the most toxic species seems to be mHTT exon 1, as these fragment models display the most aggressive disease phenotype, much more so than full-length mHTT or larger N-terminal fragments (Heng *et al.* 2008).

Whatever the toxic species, mHTT expression has been shown to cause cellular pathogenesis via several mechanisms. These include excitotoxicity, mitochondrial dysfunction, metabolic impairment, increased production of free radicals, oxidative stress, impairment of autophagy and proteasomal degradation systems, transcriptional dysregulation, caspase activation, calcium homeostasis dysregulation, apoptosis, and inflammatory processes (Rubinsztein and Carmichael 2003; Ross and Tabrizi 2011; Soulet and Cicchetti 2011; Ellrichmann *et al.* 2013).

The reasons for specific vulnerability of striatal and cortical neurons to mHTT in HD pathogenesis are not known. One theory is that the connectivity properties of striatal MSNs with the neocortex leave these cells more susceptible to hyper-excitation and excitotoxicity is aggravated. Therefore, by non-cell-autonomous neuronal circuit-mediated effects, these cells have a heightened vulnerability to the cell-autonomous toxicity of mHTT (Saxena and Caroni 2011). Another explanation for selective vulnerability in HD could be that mHTT interacts with Ras homologue enriched in striatum (Rhes), a protein localised selectively to the striatum which has been shown to greatly enhance toxicity by eliciting mHTT sumoylation, disaggregation and cell death (Subramaniam *et al.* 2009).

1.1.6 Peripheral pathology in HD

Despite the primary pathology in HD occurring in the brain, numerous reports have now described abnormalities in peripheral tissues of HD patients. These include weight loss, skeletal muscle wasting, cardiac failure, testicular atrophy, osteoporosis, diabetes, and dysfunction of blood-derived cells (van der Burg *et al.* 2009) (Figure 1.2). It seems that dysfunction in peripheral tissues can be partly accounted for as secondary effects of central nervous system (CNS) pathology, or due to general sickness. However, there is a growing body of evidence which indicates peripheral pathologies are directly caused by cell-autonomous effects of mHTT expression.

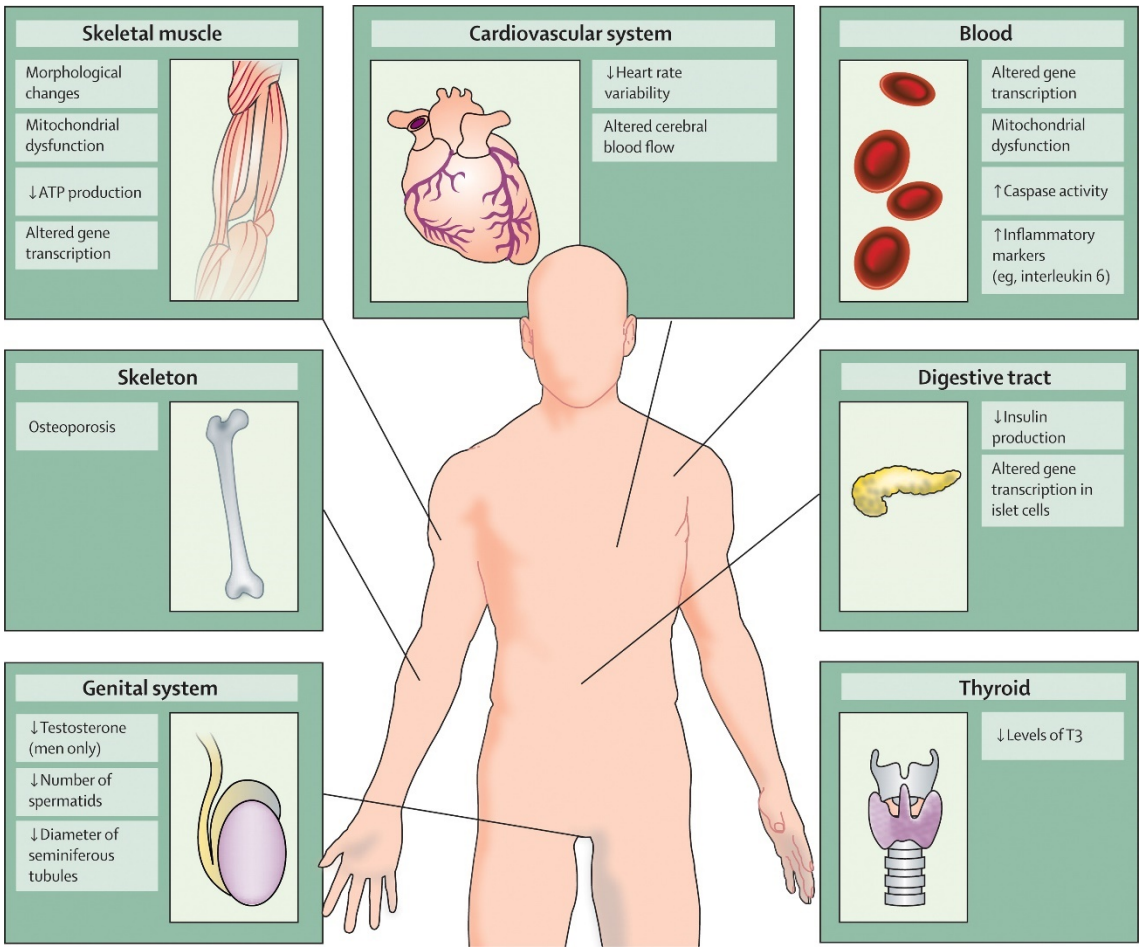

Figure 1.2: Peripheral pathology in HD patients

In addition to neurological symptoms, HD patients also suffer with non-neurological symptoms as a result of dysfunction in peripheral tissues caused by the ubiquitous expression of mHTT. (Re-printed from Lancet Neurology, Volume 8, Issue 8, 'Beyond the brain: widespread pathology in Huntington's disease', Page 768, Figure 2, van der Burg et al., ©2009, with permission granted by Elsevier Health Science Journals via Copyright Clearance Center, License ID: 3931941045883).

Intracellular mHTT aggregates are present in peripheral organs of transgenic HD mouse models (Sathasivam *et al.* 1999; Orth *et al.* 2003) and peripheral cells isolated from HD patients are dysfunctional when in isolation (van der Burg *et al.* 2009), indicating cell intrinsic effects of mHTT which are not secondary to pathological brain function. For example, monocytes isolated from HD patients are hyper-reactive in response to a pathogenic stimulus (Björkqvist *et al.* 2008). Weight loss and skeletal muscle atrophy may result from increased metabolic rate and altered muscle energy metabolism in HD patient cells, and osteoporosis has been linked to disrupted endocrine signalling, such as increased cortisol concentrations (van der Burg *et al.* 2009).

Blood-derived cells are dysfunctional in HD patients (van der Burg *et al.* 2009) and evidence is increasing for an active role of the immune system in HD (Ellrichmann *et al.* 2013). Blood plasma levels of proinflammatory cytokines are elevated in HD patients on average sixteen years before onset of clinical symptoms and peripheral blood mononuclear cells (PBMCs) have altered inflammatory signalling (Björkqvist *et al.* 2008). This could occur in reaction to cellular pathology such as aggregate formation, oxidative damage or necrotic cell death, however there is also evidence to suggest a direct role of intrinsic mHTT expression in disrupted PBMC inflammatory signalling (Träger *et al.* 2014a). It is possible that both cell-autonomous and non-cell-autonomous mechanisms of hyperactive inflammatory processes are at play, leading to a cycle of chronic inflammation. An elevated inflammatory state may additionally contribute to further neuropathology and peripheral pathology in HD, including neuroinflammation, weight loss and muscle wasting (van der Burg *et al.* 2009).

It is important to study peripheral pathologies in HD because some contribute significantly to mortality, and treating non-neurological symptoms could reduce morbidity and improve quality of life. Peripheral tissues may also offer valuable insight for molecular and cellular pathogenic disease mechanisms that are shared with the CNS. Peripheral cells, such as PBMCs, are easier and less invasive to sample from HD patients, and are less expensive to study than CNS-derived cells. As they can be isolated from living HD patients, they can be used to monitor pathogenesis over the disease course, and could serve as a window into central pathogenic events. There is also potential for peripheral biomarkers which track disease progression (Strand *et al.* 2005; Dalrymple *et al.* 2007; Björkqvist *et al.* 2008; Weiss *et al.* 2012).

1.2 The innate immune system

The innate immune system is an evolutionarily conserved, non-specific branch of the immune system which provides a broad first line of defence against invading microbial

pathogens, endogenous cellular and tissue damage, and other potential threats. The innate immune system comprises physical and chemical barriers against infectious agents as well as innate leukocytes which destroy and clear pathogens and other dangerous molecules via a variety of different mechanisms. When a local threat or cellular damage is detected by tissue-resident leukocytes, a process of acute inflammation is initiated. The cells become activated and release inflammatory mediators such as histamine, bradykinin, leukotrienes and prostaglandins, which induce vasodilation, increase vascular permeability, and have chemotactic effects on other circulating leukocytes (Yoshikai 2001). Phagocytes, such as neutrophils and macrophages, migrate towards the chemoattractant stimuli and are recruited into the inflammatory response, where they can additionally engulf and phagocytose smaller pathogens, damaged cells and dangerous molecules. Activated phagocytes release cytokines and chemokines which recruit other leukocytes and mediate the inflammatory response. Another important function of innate immune cell activation is the subsequent initiation of a pathogen-specific adaptive immune response, via antigen presentation, for long-lasting immunological memory through B and T lymphocytes (Hoebe *et al.* 2004; Iwasaki and Medzhitov 2015).

1.2.1 Myeloid cells

Myeloid cells of the innate immune system include basophils, dendritic cells, eosinophils, monocytes, macrophages (and microglia), mast cells, natural killer (NK) cells and neutrophils.

Neutrophils are circulating granular polymorphonuclear leukocytes which are generally the first cells to be recruited to an inflammatory site, and can kill microorganisms by production of toxic antimicrobial molecules, or by phagocytosis (Kolaczkowska and Kubes 2013). Basophils and eosinophils are also polymorphonuclear granulocytes, and they play important roles in parasite infections by activating the release of chemical mediators such as histamine, which also implicates these cells as initiators of chronic allergy responses (Karasuyama *et al.* 2009; Rosenberg *et al.* 2013). Mast cells share similar characteristics with basophils, but unlike their circulating counterparts they are tissue-resident (Karasuyama *et al.* 2009). Mast cells contain secretory granules harbouring pre-formed immunomodulatory and vasoactive compounds, and when appropriately activated they undergo degranulation whereby these compounds are rapidly released into the extracellular surroundings (Wernersson and Pejler 2014). NK cells are mononuclear leukocytes that produce immunomodulatory cytokines as well as cytotoxic molecules which can directly destroy infected, damaged or cancer cells via cytolytic processes (Vivier *et al.* 2008). Monocytes are peripheral blood circulating mononuclear cells which migrate into tissues where they produce inflammatory

mediators and terminally differentiate into macrophage or dendritic cell populations (Shi and Pamer 2011). Tissue-resident macrophages have important roles in the maintenance of homeostasis by sensing and responding to local infection or tissue injury. They produce inflammatory mediators and present antigens to T cells for initiation of a secondary adaptive immune response. They also employ specialised phagocytic mechanisms to engulf and degrade pathogens, lipoproteins, debris and dead cells (Lavin *et al.* 2015). Microglia are a specialised population of CNS-resident macrophages which are the primary responding cells for pathogen infection and injury in the CNS. They release inflammatory mediators and engage in phagocytosis in response to a threat, but also function in maintenance of normal tissue homeostasis and play important roles in the development and remodelling of the CNS (Saijo and Glass 2011). Both monocytes and macrophages (and their sub-populations) also play roles in tissue repair following infection and injury, and are essential for wound healing processes. Dendritic cells are the major antigen-presenting cells and their main function is to process and present pathogenic antigens to T cells and promote their activation (Gabrilovich *et al.* 2012).

1.2.1.1 Monocytes and macrophages

Monocytes originate from self-renewing multipotent haematopoietic stem cells in the bone marrow which differentiate over sequential steps to produce mature, specialised myeloid cells (Gabrilovich *et al.* 2012). Circulating human monocytes can be classified into three subsets based on their expression of cluster of differentiation (CD) cell surface markers and phenotypes: classical monocytes ($CD14^{hi}CD16^{-}$), intermediate monocytes ($CD14^{hi}CD16^{+}$), and non-classical monocytes ($CD14^{low}CD16^{+}$) (Ziegler-Heitbrock *et al.* 2010). Classical monocytes are inflammatory and phagocytic, produce inflammatory cytokines such as interleukin (IL)-6 and tumour necrosis factor (TNF)α, generate reactive oxygen species (ROS), and migrate into tissues where they differentiate into inflammatory M1 classified macrophages which are involved in mediation of an inflammatory response, phagocytosis, proteolysis, antigen presentation and T cell activation (Yang *et al.* 2014). Non-classical monocytes are anti-inflammatory and patrolling, produce anti-inflammatory cytokines such as IL-10, and migrate into tissues where they differentiate into anti-inflammatory M2 classified macrophages which are involved in wound healing, tissue fibrosis and angiogenesis (Yang *et al.* 2014). During steady state, circulating pools of monocytes in the blood are predominantly of the classical or non-classical definition, and their expression and phenotypic profiles can change between these two major subtypes, via the intermediate monocyte group, to maintain a steady composition of monocyte subsets (Ziegler-Heitbrock *et al.* 2010; Yang *et al.* 2014).

While tissue-resident macrophages can be produced by differentiation of infiltrating monocytes (Figure 1.3), it has recently been discovered that the majority of macrophage populations originate from erythromyeloid precursors which migrate from yolk sac into specific tissues during early embryogenesis, and terminally differentiate into specialised macrophage sub-populations with tissue-specific phenotypes (Lavin *et al.* 2015). Tissue-specific functional specialisation is thought to occur in response to cytokines and metabolites that are released by the stroma and drive the expression of unique transcription factors (Lavin *et al.* 2015). Under normal homeostatic conditions most tissue macrophage populations are maintained by self-renewing embryonic precursors independently of monocytes, but following local innate immune responses macrophage numbers can be replenished by differentiation of infiltrating monocytes (Lavin *et al.* 2015).

Macrophage activation has been historically classified as classical or alternative, ‘M1’ or ‘M2’ respectively. Classical activation can be triggered by inflammatory cytokines such as interferon gamma (IFNγ), which is produced by T helper type 1 (Th1) cells, and alternative activation can be triggered by IL-4 or IL-13, which are produced by T helper type 2 (Th2) cells, hence the respective M1 versus M2 macrophage activation nomenclature (Martinez and Gordon 2014). M1 macrophages have increased proinflammatory cytokine, inducible nitric oxide synthase (iNOS) and ROS production; increased expression of major histocompatibility complex (MHC) class II molecules and CD68; increased antigen presentation; and increased microbicidal activity (Gordon and Taylor 2005). M2 macrophages have increased endocytic activity; increased expression of mannose receptor, dectin-1 and arginase; increased cell growth; increased tissue repair; and increased parasite killing (Gordon and Taylor 2005). An additional ‘M0’ activation state may also be considered, whereby macrophages are deactivated by anti-inflammatory IL-10 or transforming growth factor beta (TGFβ) leading to increased production of IL-10, TGFβ and prostaglandin E2 (PGE2); and reduced expression of MHC class II molecules (Gordon and Taylor 2005).

While the M1 versus M2 classification of macrophages may still be used to describe the extreme phenotypes of macrophage function, it is now more generally accepted that these cells are highly plastic and exist in a dynamic continuum between M1 and M2 activation states (Martinez and Gordon 2014). Based on a growing body of evidence, it is now considered that macrophage markers and function reflect their tissue microenvironment and these cells are highly sensitive to local deviations from homeostasis, adapting their phenotypes accordingly (Gabrilovich *et al.* 2012; Yang *et al.* 2014).

1.2.1.2 Microglia

Microglia are CNS-resident macrophages which are derived by primitive haematopoiesis in the foetal yolk sac and seed CNS tissue during early embryogenesis (Ginhoux *et al.* 2010; Saijo and Glass 2011; Goldmann *et al.* 2016). Yolk sac-derived embryonic myeloid precursors are exposed to factors in CNS tissue which drive the expression of specific genes for differentiation into functionally specialised microglia (Saijo and Glass 2011; Lavin *et al.* 2015) (Figure 1.3). Recent studies have shown that the molecular signatures of microglia define them as a distinct cell population compared to other cells of myeloid lineage (Michell-Robinson *et al.* 2015). Unlike other tissue macrophages, none of the microglia sub-populations originate from haematopoietic stem cells in the bone marrow, and under normal physiological conditions circulating monocytes do not contribute to the myeloid cell pool in the CNS (Ginhoux *et al.* 2010; Saijo and Glass 2011). Rather, maintenance and local expansion of microglia is solely dependent on self-renewing CNS-resident microglial progenitors (Ajami *et al.* 2007). Under neuroinflammatory conditions, however, circulating monocytes may be recruited to a CNS lesion site where they differentiate into macrophages or dendritic cells (Mildner *et al.* 2007; Greter *et al.* 2015).

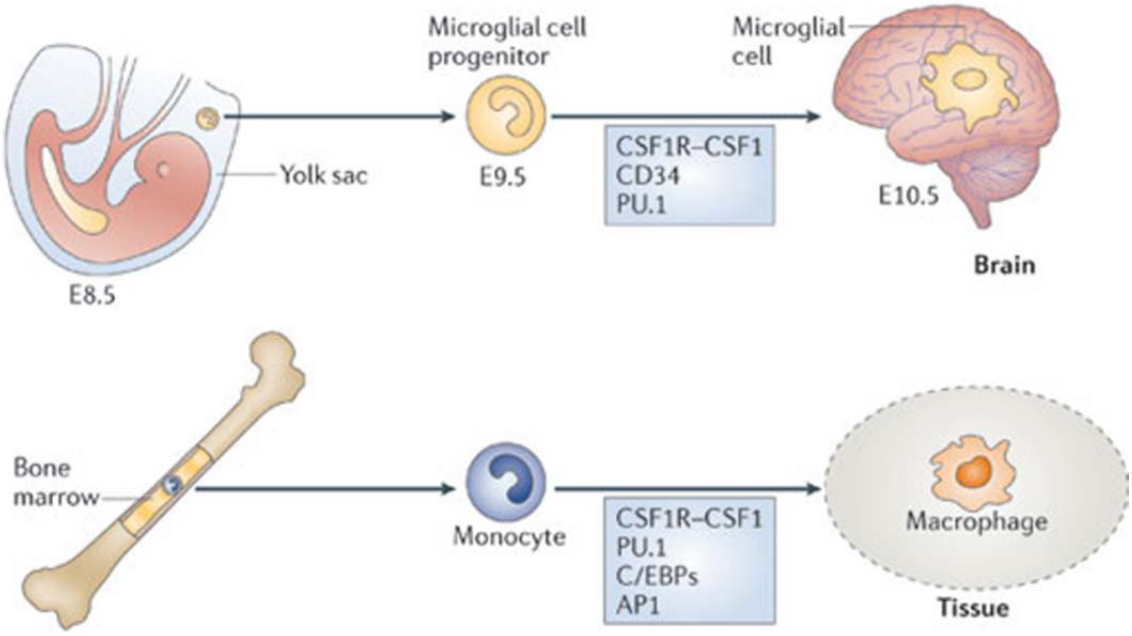

Figure 1.3: Microglia and BMD-macrophage differentiation

Microglia (top) are derived from primitive haematopoiesis and migrate from the foetal yolk sac to the brain during the early days of embryonic (E[days]) development. Microglia differentiation and proliferation is initiated by colony-stimulating factor 1 (CSF1) and its receptor (CSF1R), CD34 and transcription factor PU.1. Blood monocyte-derived (BMD)-macrophages (bottom) originate from haematopoietic stem cells in the bone marrow, enter the circulation as monocytes, and take up residence in peripheral tissues as macrophages. BMD-macrophage

differentiation and proliferation is initiated by CSF1-CSF1R and transcription factors PU.1, CCAAT/enhancer-binding proteins (C/EBPs) and activator protein 1 (AP1). (Re-printed with minor amendments from Nature Reviews Immunology, Volume 11, Issue 11, 'Microglial cell origin and phenotypes in health and disease', Page 776, Figure 1, Saijo and Glass, ©2011, with permission granted by Nature Publishing Group (Permissions) via Copyright Clearance Center, License ID: 3932010960492).

Microglia remove damaged neurons and infections as well as playing important roles in brain development, tissue maintenance and repair. Neuron-microglia cross-talk occurs throughout CNS development via soluble factors, physical regulation of the number of neural progenitor cells, and direct interaction with developing synapses (Michell-Robinson *et al.* 2015). Microglia also modulate neurite outgrowth and myelin formation in the developing and adult brain. Under normal homeostatic conditions, microglia exhibit a different morphology than peripheral macrophages, with ramified branches which extend from the cell body and dynamically survey the local environment and communicate with neurons and other glial cells. In response to infection or traumatic stimuli, microglia rapidly adopt an amoeboid morphology and become migratory and phagocytic, releasing proinflammatory mediators such as cytokines, chemokines, ROS and nitric oxide (NO) (Saijo and Glass 2011) (Figure 1.4). Microglia hyperactivity or chronic activation, however, is associated with neurotoxicity and myelin loss and can contribute to the progression of neurodegenerative and neoplastic diseases (Saijo and Glass 2011).

Like peripheral macrophages, it is considered that microglia can exist in a dynamic continuum between M1 and M2 polarised states (Figure 1.4), and microenvironmental conditions can selectively modify unique microglia phenotypes and functions (Michell-Robinson *et al.* 2015). Microglia morphology is also highly variable depending on the developmental and functional state as well as anatomical location. The structural and functional signatures of primary microglia can be modulated by the local microenvironment, and peripheral blood monocyte-derived (BMD)-macrophages and microglia show morphological and functional similarities when cultivated under identical conditions (Gordon *et al.* 1988; Schmid *et al.* 2009; Butovsky *et al.* 2014). Under neuroinflammatory conditions *in vivo*, there is a large phenotypic overlap between microglia and recruited BMD-macrophages, introducing technical difficulty for the definition of microglia-specific functions in inflammation. Microglia and certain BMD-cells have even been deemed phenotypically indistinguishable (Enose *et al.* 2005; Greter *et al.* 2015). It is possible that BMD-macrophages recruited to a site of neuroinflammation adopt a functional and morphological state similar to resident microglia due to an equal response to the same environmental stimuli (O'Koren *et al.*

2016). Therefore, whilst recent studies have presented unique molecular signatures as a means of reliably distinguishing between populations of resident microglia and infiltrating myeloid cells (Greter *et al.* 2015; Michell-Robinson *et al.* 2015), these cell types are highly dynamic and become almost phenotypically indistinguishable when exposed to the same microenvironment.

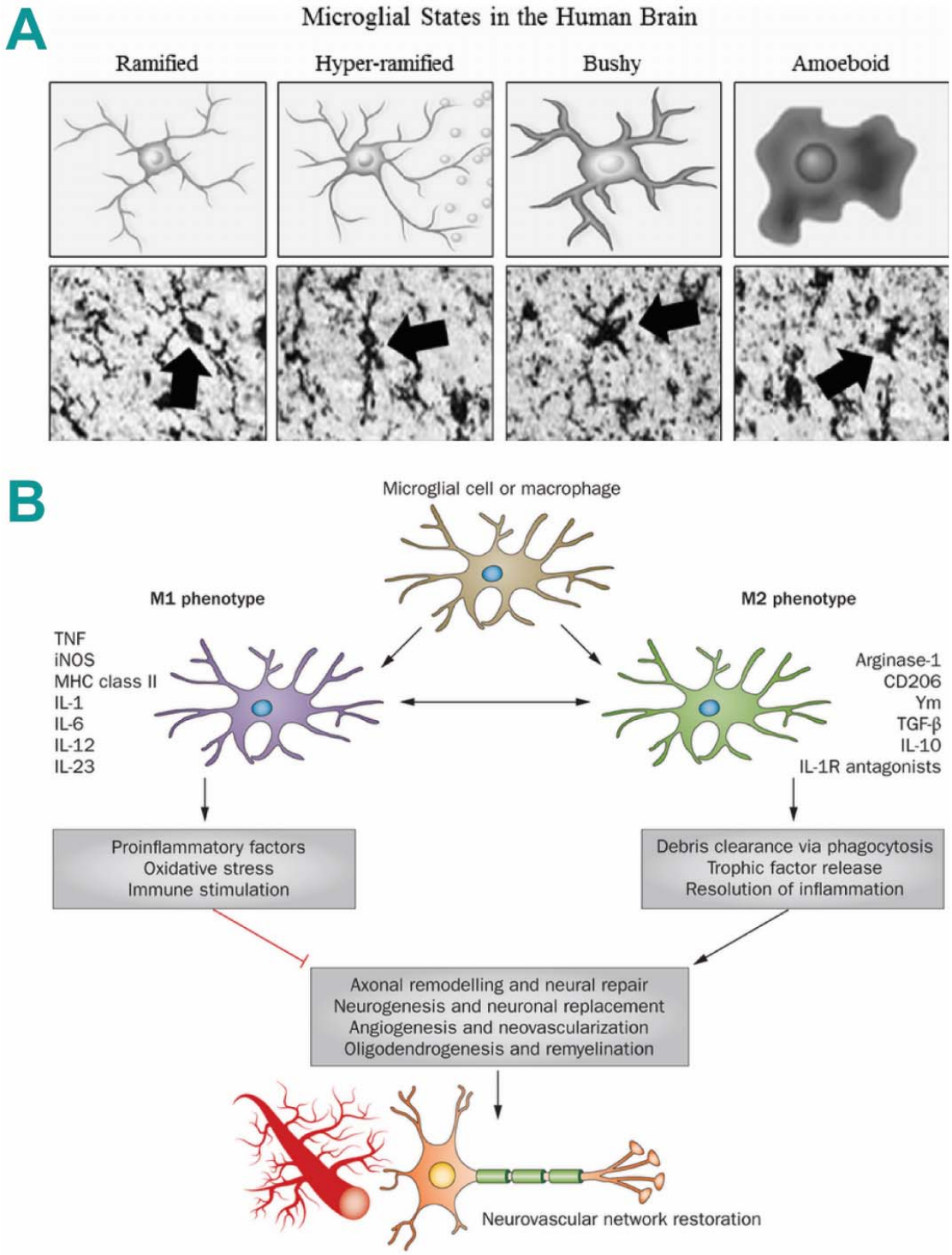

Figure 1.4: Microglial morphology and activation phenotypes

A) *Schematic representations (top panel) and photomicrographs (Iba1 microglial-marker immunohistochemistry, bottom panel) of human brain microglia, depicted at various*

morphological stages of activation. Ramified/resting microglia have long, ramified processes with small cell bodies; hyper-ramified microglia are mildly activated and display longer processes with increased branching in addition to proinflammatory cytokine production; bushy microglia are intermediate in their activation state and are characterised by swollen, truncated processes and enlarged cell bodies; amoeboid/phagocytic microglia display rounded, macrophage-like morphology with no/few processes and are associated with maximal proinflammatory activation, ROS production, and microglial apoptosis (Crews and Vetreno 2016). (Re-printed from Psychopharmacology, Volume 233, Issue 9, 'Mechanisms of neuroimmune gene induction in alcoholism', Page 1544, Figure 1, Crews and Vetreno, ©2016, with permission granted by Springer-Verlag Berlin/Heidelberg via Copyright Clearance Center, License ID: 3932500986976). ***B)*** *Microglial/macrophage activation is a dynamic process existing between M1 (classical activation) and M2 (alternative activation) poles. M1 populations release proinflammatory mediators and free radicals which promote neuroinflammation and removal of pathogens but impair brain repair and regeneration. M2 populations promote brain repair and regeneration by increasing phagocytosis, releasing trophic factors and resolving neuroinflammation (Hu et al. 2015). (Re-printed from Nature Reviews Neurology, Volume 11, Issue 1, 'Microglial and macrophage polarization—new prospects for brain repair', Page 57, Figure 1, Hu et al., ©2015, with permission granted by Nature Publishing Group (Permissions) via Copyright Clearance Center, License ID: 3932500035088). Abbreviations not yet stated: CD206, also known as mannose receptor; IL-1R, interleukin 1 receptor; Ym, chitinase-like proteins.*

1.2.2 Myeloid cell signalling

1.2.2.1 Pattern recognition receptors (PRRs)

Monocyte-, macrophage- and microglia-mediated inflammatory responses can be activated through stimulation of a diverse and extensive array of pattern recognition receptors (PRRs) expressed by these myeloid cells. PRRs recognise pathogen-associated molecular patterns (PAMPs) and damage-associated molecular patterns (DAMPs). PAMPs are structures conserved amongst microbial species such as flagellin (flagellated bacteria), zymosan (certain fungi), double-stranded RNA (dsRNA) (viruses) and lipopolysaccharide (LPS) (Gram-negative bacterial cell wall component) (Akira *et al.* 2006). DAMPs are endogenous danger signals including components from damaged, necrotic or dying cells such as intracellular proteins, protein fragments from the extracellular matrix and pathologically aggregated proteins (for example, heat-shock proteins, fibrinogen and mHTT) (Akira *et al.* 2006). PRRs are germ-line encoded, evolutionarily conserved molecules, and include Toll-like receptors (TLRs), for example TLR4 which recognises LPS, nucleotide-binding oligomerization domain (NOD)-like receptors (NLRs), Retinoic acid-inducible gene 1 (RIG-I)-like receptors (RLRs), cytosolic DNA sensors (CDS) and C-type lectin receptors (CLRs) (Takeuchi and Akira

2010; Mahla *et al.* 2013). Activation of different PRRs leads to initiation of different signalling cascades resulting in upregulated transcription of genes involved in inflammatory responses, such as proinflammatory cytokines, type I IFNs, chemokines and antimicrobial proteins, proteins involved in the modulation of PRR signalling, and many uncharacterised proteins (Takeuchi and Akira 2010).

1.2.2.2 Toll-like receptors (TLRs)

TLRs are characterised by N-terminal leucine-rich repeats and a transmembrane region followed by a cytoplasmic Toll/IL-1 receptor homology (TIR) domain (Medzhitov *et al.* 1997; Rock *et al.* 1998). Ten different types of TLR (TLR1-10) have been identified in humans and twelve in mice, all recognising a variety of different PAMPs and DAMPs (Takeuchi and Akira 2010). When stimulated, each TLR activates shared but distinct signalling pathways via different adaptor molecules which are recruited to the TIR domain (Akira *et al.* 2006). Stimulation of TLR signalling leads to the activation of transcription factors such as nuclear factor kappa-light-chain-enhancer of activated B cells (NFκB) and interferon regulatory factors (IRFs), and the induction of various cellular immune responses such as production of proinflammatory cytokines, chemokines and IFNs (Mahla *et al.* 2013).

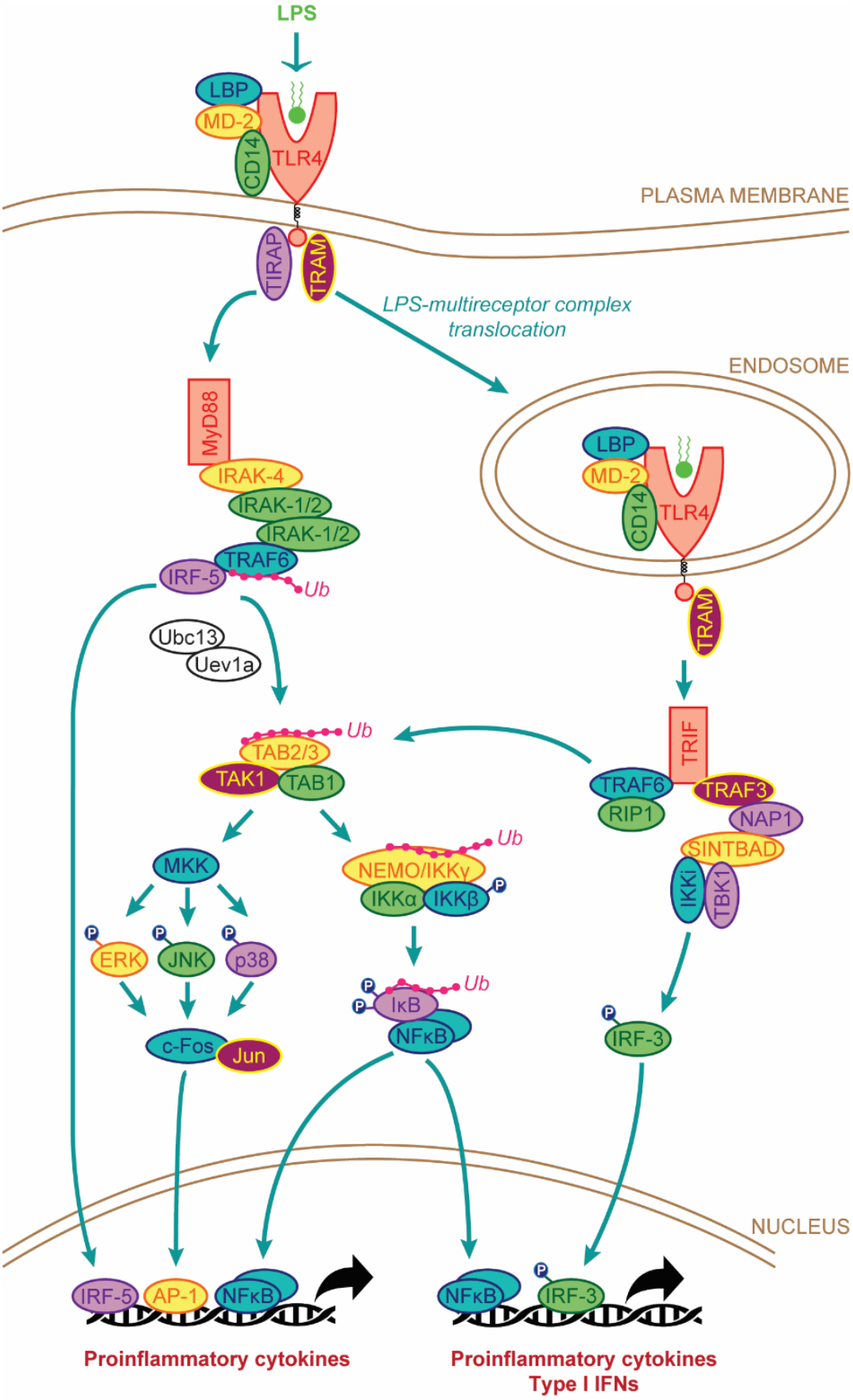

Figure 1.5: TLR4 signalling cascades triggered by LPS stimulation

When TLR4 recognises LPS, an LPS-multireceptor assembles at the plasma membrane with the recruitment of CD14, MD-2 and LBP. Depending on the associated adaptor proteins

involved, a signalling cascade is initiated via the MyD88-dependent pathway (TIRAP/Mal and MyD88) or MyD88-independent pathway (TRAM and TRIF). MyD88 recruitment to the TIR-domain induces formation of a complex of IRAKs, the E3 ubiquitin ligase TRAF6, and IRF-5. TRAF6 catalyses the ubiquitination of itself and NEMO/IKKγ with Ubc13 and Uev1a, and via interaction with the complex formed by TAK1, TAB1 and TAB 2/3 regulates phosphorylation and subsequent activation of the IKK complex. Phosphorylated IκB undergoes ubiquitination and is targeted for degradation by the proteasome, allowing freed NFκB to translocate to the nucleus and induce transcription of proinflammatory cytokine genes. TAK1 is released into the cytoplasm directing additional activation of MAPK (ERK, JNK and p38) cascades, ultimately leading to the activation of AP-1 which is critical for the induction of cytokine genes. MKK phosphorylates MAPKs which in turn initiates the heterodimerisation of c-Fos and c-Jun and the formation of AP-1 complex. TRAM recruitment to the TIR-domain triggers translocation of the LPS-multireceptor into endosomes, which is controlled by CD14. From endosomes, TLR4 is able to interact with the modulator protein TRIF which activates NFκB and IRF-3, inducing their nuclear translocation and induction of proinflammatory and type I IFN gene transcription, respectively. TRIF regulates formation of a complex of TRAF6 and RIP1 which leads to NFκB activation, and TRAF3 which is responsible for phosphorylation of IRF-3 by TBK1/IKKi, inducing its translocation. NAP1 and SINTBAD are required for the activation of TBK1/IKKi. (Akira et al. 2006; Takeuchi and Akira 2010; Brubaker et al. 2015). Abbreviations not yet stated: c-Fos, cellular Fos; c-Jun, cellular Jun; ERK, extracellular signal-regulated kinase; IKK, IκB kinase; IRAK, interleukin-1 receptor-associated kinase; IκB, inhibitor of kappa-light-chain-enhancer of activated B cells; JNK, c-Jun N-terminal kinases; MAPK, mitogen-activated protein kinase; MKK, mitogen-activated protein kinase kinase; NAP1, NFκB-activating kinase-associated protein 1; NEMO, NFκB essential modulator (also known as IKKγ subunit); P, phosphorylated (phosphate group); RIP1, receptor-interacting serine/threonine-protein kinase 1; SINTBAD, similar to NAP1 TBK1 adaptor; TAB, TGFβ-activated kinase 1-binding protein; TAK1, TGFβ-activated kinase 1; TBK1, TANK-binding kinase 1; TRAF, TNF receptor-associated factor; Ub, ubiquitin; Ubc13, ubiquitin-conjugating enzyme E2 13; Uev1a, ubiquitin-conjugating enzyme E2 variant 1A.

There are five TLR TIR domain-containing adaptor molecules: Myeloid differentiation primary response gene 88 (MyD88), TIR domain-containing adaptor inducing IFNβ (TRIF), TIR domain-containing adaptor protein (TIRAP)/MyD88 adaptor-like (Mal), TRIF-related adaptor molecule (TRAM), and Sterile-alpha and Armadillo motif-containing protein (SARM) (Takeuchi and Akira 2010). TLR signalling can be divided into two distinct pathways depending on the usage of MyD88 or TRIF adaptor molecules. MyD88 is essential for the induction of inflammatory cytokines triggered by all TLRs except TLR3, and TRIF is implicated in the TLR3- and TLR4-mediated MyD88-independent pathway (Takeda and Akira 2004; Takeuchi and Akira 2010). TLR4 is expressed on the plasma membrane and on endosomes. It is the principle

LPS receptor but also recognises other PAMPs such as viral proteins and polysaccharide, and DAMPs such as low-density lipoprotein, β-defensins, heat shock proteins and pathologically aggregated proteins (Walter *et al.* 2007; Brubaker *et al.* 2015). The TLR4 response to LPS requires a multireceptor complex consisting of LPS-binding protein (LBP), CD14, and myeloid differentiation protein 2 (MD-2), which act sequentially to extract LPS from bacteria and promote TLR4 signalling (Brubaker *et al.* 2015). TLR4 activation triggers both the MyD88-dependent and TRIF-dependent signalling pathways, although unlike TLR3, TLR4 requires another adaptor, TRAM, for activating TRIF (Takeuchi and Akira 2010). Ultimately, the MyD88-dependent signalling cascade results in activation of NFκB, activator protein 1 (AP-1) and IRF-5 transcription factors and subsequent production of proinflammatory cytokines, and the TRIF-dependent signalling cascade results in activation of NFκB and IRF-3 which induce production of proinflammatory cytokines and type I IFNs (Akira *et al.* 2006; Takeuchi and Akira 2010). Figure 1.5 shows details of the signalling pathways activated when TLR4 is stimulated with LPS.

1.2.2.3 Cytokines

Monocytes, macrophages and microglia produce both Th1- and Th2-type cytokines, depending on their phenotype. Th1- and Th2-type cytokines are so-called because they are also produced by Th1 and Th2 cells, respectively. Th1-type cytokines, such as IFNγ, IL-1β, IL-6, IL-8, IL-12 and TNFα, promote classical inflammation and tend to produce proinflammatory responses like activation of phagocytosis and cytotoxic T cells. Th2-type cytokines, such as IL-4, IL-5, IL-10 and IL-13, are produced in alternative activation states and are involved in T cell-dependent activation of B cells and promotion of immunoglobulin (Ig) E and eosinophilic responses. Excessive Th1-type proinflammatory responses can lead to chronic inflammation-related tissue damage, and Th2-type cytokines can counteract some Th1-mediated actions to achieve an optimal, balanced immune reaction (Berger 2000). See Table 1.1 for details of specific IFN, interleukin and TNF cytokines.

Table 1.1: Cytokines

Interferons (IFNs)	
• Glycoprotein cytokines which activate immune cells via signal transducer and activator of transcription (STAT) signalling complexes (Brocker *et al.* 2010) • Predominantly known for their ability to mediate cellular responses to viral infection (Brocker *et al.* 2010) • Five classes of type I IFNs found in humans: IFNα, IFNβ, IFNε, IFNκ and IFNω (Pestka *et al.* 2004) • One class of type II IFN: IFNγ (Pestka *et al.* 2004)	
Type I IFNs:	• Activate intracellular antimicrobial programmes • Modulate cell fate, differentiation and migration • Regulate the development of almost every effector cell of the innate and adaptive immune responses (Hertzog and Williams 2013; Ivashkiv and Donlin 2014)
Type II IFN (IFNγ):	• Principle Th1-type cytokine • Activates macrophages • Upregulates pathogen recognition, antigen processing and presentation • Directly inhibits viral replication • Inhibits cellular proliferation and modulates apoptosis • Activates microbicidal effector functions • Mediates leukocyte trafficking • General roles in immunomodulation (Schroder *et al.* 2003) • Ligand for the interferon-gamma receptor (IFNGR) - IFNGR activates Janus kinase (Jak)1 and Jak2, leading to the phosphorylation and activation of STAT1. This forms a transcription factor (STAT1α) which translocates to the nucleus and drives the expression of IFNγ-regulated genes (Pestka *et al.* 2004) • STAT3 and STAT5 are also sometimes activated by IFNγ, as well as phosphatidylinositol-4,5-bisphosphate 3-kinase (PI3K), Akt (protein kinase B), NFκB and mitogen-activated protein kinases (MAPKs) (Pestka *et al.* 2004)
Interleukins (ILs)	
• Cytokines which modulate growth, differentiation and activation during an immune response	

• First observed as a number of secreted molecules produced by leukocytes (The information about interleukins in this table was acquired from a review written by Brocker and colleagues (Brocker *et al.* 2010)).	
IL-1β:	• Th1-type cytokine • Rapidly induces transcription of hundreds of downstream targets, including other cytokines/chemokines, NOS and matrix metalloproteinases (MMPs) • Induces production of adhesion molecules to enable transmigration of leukocytes into inflamed tissues • Involved in the induction of fever
IL-2:	• Does not specifically promote a Th1- or Th2-type immune response • Along with the Th2-type cytokine IL-4, influences proliferation, differentiation and survival of innate and adaptive immune cells, including T cells, B cells, NK cells, natural killer T cells and dendritic cells
IL-4:	• Th2-type cytokine • Along with IL-5 and granulocyte macrophage colony-stimulating factor (GM-CSF), facilitates granulocyte maturation • Regulation of Ig class switching in B cells, for example, induction of IgE secretion • Mast cell recruitment • Multiple effects on the function and differentiation of monocytes and macrophages
IL-5:	• Th2-type cytokine • Along with IL-4 and GM-CSF, facilitates granulocyte maturation • Stimulates B cell growth and immunoglobulin secretion • Stimulates eosinophil production, activation and localisation
IL-6:	• Th1-type cytokine • Plays key roles in the acute phase immune response • Mediates systemic inflammation and fever • Induces differentiation and maturation of B cells into Ig-secreting plasma B cells • Initiates T cell activation, growth and differentiation
IL-8:	• Th1-type cytokine • Attracts neutrophils to the vascular endothelium during inflammation, behaving more like a chemokine than a cytokine

IL-10:	• Th2-type cytokine • Key anti-inflammatory cytokine - an extremely important anti-inflammatory and immunosuppressive cytokine in humans • Inhibits Th1-type cytokine expression • Potent suppressor of monocyte and macrophage functions • Regulates and terminates inflammatory responses • Enhances B cell survival, proliferation and antibody production
IL-12p70:	• Th1-type cytokine • The active heterodimer of IL-12 • Promotes differentiation of naïve T cells into Th1 cells • Stimulates production of IFNγ and TNFα • Inhibits IL-4-induced proliferation of Th2 cells • Mediates cytotoxic activity of NK cells and cytotoxic T cells
IL-13:	• Th2-type cytokine • Closely related to IL-4 and shares similar effects • Regulation of Ig class switching in B cells, for example, induction of IgE secretion • Mast cell recruitment • Multiple effects on the function and differentiation of monocytes and macrophages
Tumour necrosis factors (TNFs)	
• Cytotoxic cytokines which can induce cell death by apoptosis or regulated necrosis • Important molecules in the immune response to tumours	
TNFα:	• Th1-type cytokine • Plays key roles in the acute phase immune response • Mediates systemic inflammation • Triggers multiple cell signalling pathways leading to apoptosis, proliferation, differentiation, chemoattraction and cytokine production (Aggarwal 2003)

1.2.2.4 Neurotrophins

Neurotrophins are a family of polypeptide growth factors that are essential for the development, function and maintenance of the nervous system. They promote neuronal growth and survival, have significant direct effects on synaptic transmission and plasticity, and any neurotrophin gene knock-out is embryonic lethal indicating their

essential roles in development (Chao 2003). The neurotrophin family includes nerve growth factor (NGF), BDNF, neurotrophin (NT)-3 and NT-4. They can bind to the low-affinity p75 neurotrophin receptor (p75NTR), or the high-affinity tyrosine receptor kinase (Trk) receptors (TrkA, TrkB and TrkC). P75NTR is a member of the TNF receptor superfamily, and it is involved in the induction of pro-apoptotic programmes, the control of axonal regeneration, and mediates the migration of Schwann cells (Chao 2003; Vega *et al.* 2003). P75NTR also acts as a regulator of Trk receptor activation by modulating the binding affinity and specificity of the receptors for their different neurotrophin ligands (Segal 2003). TrkA is the preferred receptor for NGF; TrkB for BDNF and NT-4; and TrkC for NT-3 (Vega *et al.* 2003). Neurotrophins and their receptors are widely expressed in the peripheral and CNS, as well as by cells of the immune system, and may be involved in mediating interactions between neurons and immune cells (Kleij and Bienenstock 2007).

Monocytes, macrophages and microglia produce NGF and BDNF, and express their high affinity receptors (TrkA and TrkB, respectively) (Vega *et al.* 2003; Kleij and Bienenstock 2007). Both neurotrophins influence the expression profile and production of inflammatory mediators such as IFNγ, IL-1β, IL-4, IL-5, TGFβ and TNFα (Vega *et al.* 2003; Kleij and Bienenstock 2007); promote activation (Kleij and Bienenstock 2007; Mizoguchi *et al.* 2014); promote proliferation and differentiation (Kleij and Bienenstock 2007; Gomes *et al.* 2013); induce chemotaxis and migration (De Simone *et al.* 2007; Zhang *et al.* 2014); and can have pro- or anti-inflammatory effects depending on the situation and concentration of the neurotrophin (Kleij and Bienenstock 2007). Microglia constitutively secrete low levels of BDNF during homeostasis, but during CNS inflammation or following injury, BDNF production is chronically upregulated and NGF production is induced (Nakajima *et al.* 2001; Kleij and Bienenstock 2007; Venkatesan *et al.* 2010; Gomes *et al.* 2013). The TrkA and TrkB receptors can behave as autoreceptors, regulating myeloid cell neurotrophin synthesis and release as well as responding to neurotrophins in the environment (Kleij and Bienenstock 2007; Zhang *et al.* 2014). Positive feedback loops of autocrine BDNF signalling may contribute to prolonged microglial activation and chronic neuroinflammation in CNS diseases (Zhang *et al.* 2014), however the neurotrophin has also been shown to have neuroprotective effects in several CNS injury and disease models (Linker *et al.* 2010; Lee *et al.* 2012). NGF can contribute to inflammatory hypersensitivity, but also suppresses inflammation by switching the immune response to an anti-inflammatory, suppressive mechanism (Kleij and Bienenstock 2007).

1.2.2.5 Complement

The complement system is involved in rapid, non-specific sensing and responding to tissue alterations and pathogen antigens. It is an integral part of the innate immune response, but also acts as a bridge between the innate and adaptive immune systems. The complement system comprises approximately twenty-five proteins and peptides which are present in the plasma and on cell surfaces as inactive precursors, which can be activated at the site of inflammation. Via a coordinated sequential enzyme cascade, complement mediates responses to inflammatory triggers by enhancing recognition, opsonisation and lysis of foreign or damaged cells (Nesargikar *et al.* 2012). The system 'complements' both innate and adaptive immune cell functions by attracting phagocytic cells, triggering cytokine expression, initiating cell lysis by the membrane attack complex, and can be activated by and work with IgG and IgM antibodies produced by B cells (Nesargikar *et al.* 2012).

1.3 Neural-immune interactions

The CNS and immune system are intimately linked, and neural-immune interactions are bi-directional. The complex communication between these systems occurs at multiple levels, from whole system to cellular interactions and sub-cellular and molecular mechanisms. Neuroendocrine and neuronal pathways control humoral and cellular immune responses via the hypothalamic–pituitary–adrenal (HPA) axis and direct sympathetic innervation of the lymphoid organs, respectively; and the immune system influences the CNS via immune mediators and cytokines (Eskandari and Sternberg 2002; Wrona 2006). At cellular and molecular levels, neurons and immune cells interact via hormones, neurotransmitters, neuropeptides, cytokines and growth factors, and their receptors (Wrona 2006).

1.3.1 Healthy neural-immune interactions

1.3.1.1 Communication between the CNS and immune system

CNS control of the immune system is primarily mediated via the HPA axis and sympathetic nervous system (SNS). HPA axis activity results in the production of glucocorticoids which regulate a wide variety of immune cell functions, including production of cytokines and other inflammatory mediators, maturation and differentiation, chemoattraction and migration, and expression of adhesion molecules, as well as causing a Th1- to Th2-type shift in immune responses (Eskandari and Sternberg 2002). Immune organs, including the thymus, spleen and lymph nodes, are innervated by the SNS, and immune cells express adrenergic receptors which allow them to respond to the catecholamine neurotransmitters released by sympathetic nerves. Like glucocorticoids, systemic adrenaline and noradrenaline promote a Th2-

type immune response over a Th1-type response by inhibiting production of proinflammatory cytokines such as IFNγ, IL-12 and TNFα, and stimulating the production of anti-inflammatory cytokines like IL-10 and TGFβ (Eskandari and Sternberg 2002). In certain local responses, however, catecholamines may also promote a proinflammatory immune reaction by inducing IL-1β, IL-8 and TNFα production (Eskandari and Sternberg 2002).

Peripheral immune cells can also regulate activity in the CNS, and this is primarily mediated by cytokines. Peripherally-derived cytokines can affect the CNS via several mechanisms: they can cross the blood-brain barrier (BBB) at 'leaky' sites, for example, at the organum vasculosum lamina terminalis or median eminence; they can cross the BBB by carrier-mediated transport mechanisms; they can trigger the production of CNS-derived mediators in the brain parenchyma via a relay involving endothelial cells and circumventricular organs at the internal milieu-brain interface; or they can signal the CNS by stimulating peripheral afferent neurons such as those of the vagus nerve (Eskandari and Sternberg 2002; Wrona 2006). In general, the peripheral immune system signals the CNS to influence feedback regulation of systemic immune responses, as well as to induce or suppress the physiological (for example; fever) and behavioural (for example; anorexia, immobility, social withdrawal, depressed mood, disturbed sleep) symptoms of sickness (Eskandari and Sternberg 2002; Poon *et al.* 2015).

Cytokines produced by peripheral monocytes and macrophages and CNS-resident microglia can have direct effects on neurons in the CNS by activating their neuronal receptors. The proinflammatory cytokines IL-1β, IL-6 and TNFα have been shown to have neuromodulatory properties by impacting synaptic transmission and neuronal excitability: the activation of their neuronal receptors rapidly alters neuronal excitability via post-translational modifications of either voltage-gated or receptor-coupled ion channels, and by promoting presynaptic changes in neurotransmission (Vezzani and Viviani 2015). IL-2 and the Th1-type cytokines granulocyte-colony stimulating factor (G-CSF), IFNγ, IL-1α, IL-1β, IL-6, IL-12 and TNFα regulate numerous pathways in neurons, including cytokine–receptor interactions, MAPKs, TLRs, apoptosis, peroxisome proliferator-activated receptor (PPAR) signalling, cell adhesion molecules, antigen processing and Jak-STAT signalling (Benjamins 2013). These cytokines also upregulate production of certain neurotransmitters and their receptors, elements of the ubiquitin-proteasome pathway, iNOS, superoxide dismutase (SOD)2 and genes involved in the Wnt and Notch signalling pathways (Benjamins 2013). The Th2-type cytokines IL-4, IL-5, IL-10 and TGF-β regulate genes related to neuroactive ligand-receptors, calcium and long-term potentiation, upregulate arginase 1 expression

leading to decreased NO generation and enhanced neurite outgrowth, and downregulate the gene for nuclear receptor co-repressor 2 (NCOR2) which could potentially lead to inhibition of histone demethylases and promotion of neuronal differentiation (Benjamins 2013).

1.3.1.2 Neuronal-microglial cell interactions

Neurons and microglia engage in dynamic communication essential for CNS development and maintenance, as well as to produce appropriate immune responses in the event of injury or infection. Neurons secrete factors such as chemokines, classic neurotransmitters and purines which modulate or maintain microglial activation states, properties and behaviours. Microglia produce cytokines, neurotrophic factors and other mediators, as well as making direct physical contact with neuronal elements, playing important roles in neurodevelopment, neuronal cell fate, the function and maintenance of neuronal synapses and circuitry, and the surveillance and resolution of neuronal injury or infection.

CD200 and the chemokine fractalkine (CX3CL1) are expressed on the surface of neurons in the CNS, and are unique ligands for their receptors CD200R and CX3CR1, respectively, which are expressed by microglia in the CNS parenchyma. When CD200 activates CD200R, microglia are maintained in a quiescent and unactivated state. When CX3CL1 activates CX3CR1 in models of inflammation, microglia are maintained in a non-neurotoxic, quiescent state and basal microglial process dynamism, motility and surveillance activities are promoted (Eyo and Wu 2013). It has also been suggested that neurons suppress the activation of microglia through cell-to-cell contact via interaction between the neuronal cell-surface proteins CD47 and CD22 and their respective microglial cell receptors CD172 and CD45 (Saijo and Glass 2011). Microglial activity is also affected by local neurotransmission, whereby motility is decreased by GABAergic inhibitory neurotransmission and increased by glutamatergic excitatory neurotransmission (Eyo and Wu 2013). GABA and glutamate have also been shown to have direct effects on microglial activation state and phenotype via interaction with their microglia-expressed neurotransmitter receptors (Mead *et al.* 2012). When injured, neurons release purines including adenosine triphosphate (ATP) and its degradation products; adenosine diphosphate (ADP) and adenosine. Purines diffuse into the extracellular space where they can activate P1 (A3) and P2 (P2Y12) microglial purinergic receptors, leading to ATP-induced microglial chemotaxis, migration and branch extension towards the injury site. Following microglial activation, adenosine can also activate A2a receptors that mediate microglial branch retraction (Eyo and Wu 2013).

During homeostasis, microglia secrete neurotrophic factors, such as BDNF, insulin-like growth factor (IGF)1, NGF and TGFβ, which support neuronal survival, function and tissue repair and maintain CNS homeostasis (Saijo and Glass 2011). Microglial processes also make transient direct physical contact with synaptic neuronal dendritic spines, suggesting neuro-modulatory roles for microglia during normal physiology (Eyo and Wu 2013). Microglia regulate the development and maintenance of neuronal synapses and circuitry through various signalling pathways including fractalkine, complement receptor, and the DNAX activation protein 12 (DAP12)/triggering receptor expressed on myeloid cells 2 (TREM2) signalling complex (Eyo and Wu 2013). DAP12/TREM2 is also involved in the maintenance of microglia in a quiescent, unactivated state (Saijo and Glass 2011). Microglia also play key roles in synaptic pruning during development, and their phagocytic functions support neurogenesis (Saijo and Glass 2011). In response to local injury or infection, microglia are activated to a proinflammatory, phagocytic, M1-type state which although in principle is neuroprotective, can be neurotoxic, especially if the inflammation becomes chronic. There are therefore several mechanisms which actively regulate the transition of microglia from the activated state to a quiescent, neuroprotective phenotype, and some of these are through direct communication with neurons. IL-10, TGFβ, steroid hormones, fatty acid metabolites and various nuclear receptor ligands have been shown to contribute to the restoration of the resting microglial cell phenotype and the resolution of microglial cell-mediated inflammation (Saijo and Glass 2011). For example, IL-10 induces the expression of 17β-hydroxysteroid dehydrogenase type 14 (17β-HSD14), which mediates the conversion of dehydroepiandrosterone (DHEA) to 5-androstene-3β,17β-diol (Δ5-ADIOL), an anti-inflammatory ligand of oestrogen receptor-β (ERβ). 17β-HSD14 can also be suppressed by TLR4 signalling, allowing acute inflammatory activation to occur during a threat and resolution of the inflammatory response when the threat is no longer present; an integrated response mediated by the ERβ nuclear receptor (Saijo and Glass 2011).

1.3.2 Neural-immune interactions in neurodegenerative diseases

In principle, inflammation is a protective, natural response to tissue damage or infection. However, chronic activation of the immune system or incomplete resolution of the immune response can trigger tissue pathology. Neuroinflammation, along with upregulation of peripheral immune responses, is a hallmark of several neurodegenerative diseases, including HD, Alzheimer's disease (AD), Parkinson's disease (PD) and amyotrophic lateral sclerosis (ALS). The extent to which inflammation is protective or deleterious in these neurodegenerative diseases, and whether immune activity is not only a consequence of but also a contributor to neuropathology, is

currently not well understood. Dissecting the complex mechanisms underlying neural-immune interaction have recently become a key focus of research in neurodegenerative diseases as there is potential for immunomodulation as a beneficial therapeutic target.

Neurodegenerative diseases share common features, including the aggregation, accumulation and deposition of certain misfolded proteins; progressive dysfunction and loss of specific CNS neuronal populations leading to related cognitive, psychiatric or motor dysfunction; age-dependent symptom onset and progressive disability until directly or indirectly fatal; chronic innate immune activation; and neuroinflammation. It may therefore be considered that neurodegenerative diseases share common mechanisms of pathology, including those underlying the bidirectional communication between neurons and immune cells and their roles in disease progression. Discoveries in the context of AD, PD and ALS can shed light on similar mechanisms which may be at play in HD; and as a dominantly inherited genetic condition, HD may serve as a model for studying neural-immune interactions over the entire disease-course, including a unique opportunity to investigate the pre-symptomatic phase of a neurodegenerative disease in patients. In this section, the role of neural-immune interactions in neurodegenerative diseases is discussed, with a particular focus on AD, PD and ALS. Immune system dysfunction and neural-immune interactions in HD are discussed in more detail in section 1.4.

1.3.2.1 Characteristics of neurodegenerative diseases

AD is both the most common neurodegenerative disease and the most common dementing illness, and is characterised by the parenchymal deposition of amyloid-beta (Aβ) peptides into Aβ plaques, the formation of neurofibrillary tangles composed largely of hyperphosphorylated microtubule-associated tau protein, and the progressive atrophy of hippocampus and neocortex leading to progressive memory decline and cognitive dysfunction (Amor *et al.* 2014; Heneka *et al.* 2014; Doty *et al.* 2015). PD is the second-most common neurodegenerative disorder. It is characterised by abnormal accumulation of α-synuclein aggregates in neurons, nerve fibres or glial cells, and the formation of Lewy bodies composed of intracellular proteinaceous inclusions containing α-synuclein and ubiquitin. PD is hallmarked by neurodegeneration of extrapyramidal motor neurons, in particular the loss of dopaminergic neurons of the basal ganglia from the substantia nigra pars compacta to the striatum (caudate and putamen). This results in movement disturbances such as resting tremor, bradykinesia, rigidity and gait dysfunction (Amor *et al.* 2014; Doty *et al.* 2015). ALS is characterised by ubiquitin-positive cytoplasmic inclusions containing transactive response DNA binding protein 43 (TDP-43) in pathologic neurons, and selective degeneration and loss of upper and

lower motor neurons in the motor cortex, brainstem and spinal cord. This leads to corticospinal tract signs such as hyper-reflexia and fasciculations, and the wasting and atrophy of targeted muscles, ultimately resulting in complete paralysis (Heneka *et al.* 2014; Doty *et al.* 2015).

1.3.2.2 Microglial activation and chronic neuroinflammation in neurodegenerative diseases

While neuronal dysfunction and death are the main phenomena leading to cognitive, psychiatric and physical disability in neurodegenerative diseases, there is a growing body of evidence for a key role of innate immune activation and neuroinflammation in pathogenesis. In HD, AD, PD and ALS, neuroinflammation is routinely documented in pathologically affected areas of the CNS, and involves microgliosis (activation, proliferation and migration of microglia at/to a site of injury or infection); astrogliosis (altered molecular expression, cellular hypertrophy and proliferation of astrocytes, potentially leading to glial scar formation); elevated production of proinflammatory cytokines, chemokines and complement; increased expression of PRRs including TLRs; and in some cases activation and infiltration of peripherally-derived immune cells like T cells, NK cells and BMD-macrophages (Amor *et al.* 2014; Heneka *et al.* 2014; Doty *et al.* 2015). Neuroinflammation and immune activation develop early in the course of the disease, often prior to symptom onset and large-scale neuronal loss, and neuronal injury occurs in an inflammatory environment (Doty *et al.* 2015). Complex interplay occurs between different immune cells and degenerating neurons, and polymorphisms of several common immunomodulators involved in this cross-talk have been associated with increased risk of neurodegeneration or altered rate of disease progression in recent GWASs (Durrenberger *et al.* 2014; Heneka *et al.* 2014; Doty *et al.* 2015).

In neurodegenerative diseases, neuroinflammation can be triggered via stimulation of PRRs on different brain cell types (including microglia, astrocytes, neurons and endothelial cells) by disease-associated DAMPs such as misfolded proteins, aggregated peptides or mislocalised nucleic acids (including mHTT, Aβ and α-synuclein aggregates) (Saijo and Glass 2011; Heneka *et al.* 2014; Doty *et al.* 2015). Other DAMPs occurring as a result of neuronal injury or death can also trigger neuroinflammation, such as heat-shock proteins, high-mobility group box 1 protein (HMGB1), histones and ATP (Saijo and Glass 2011; Amor *et al.* 2014). A continued presence of high levels of DAMPs in the diseased brain leads to chronic microglial activation and production of proinflammatory factors which can have autocrine effects to reinforce and maintain the inflammatory phenotype (Doty *et al.* 2015). Such factors may also stimulate responses from astrocytes, which feedback to microglia driving

recruitment and neuroinflammatory modulation, as well as having both neurotrophic or neurotoxic effects on neurons (Saijo and Glass 2011; Doty *et al.* 2015). Neurotoxic effects of mediators released by microglia and astrocytes in the neuroinflammatory milieu leads to further neuronal injury and death and the subsequent release of more DAMPs which activate microglia. Additionally, due to the damage and loss of neuronal populations in neurodegenerative diseases, there is a reduction in the neuroimmunoregulatory molecules normally expressed by these cells to provide inhibitory input to maintain or restore microglial quiescence and regulatory functions, indirectly driving a pro-activation state in local microglia (Amor *et al.* 2014). As a consequence, a chronic cycle of neuroinflammation is initiated (Figure 1.6).

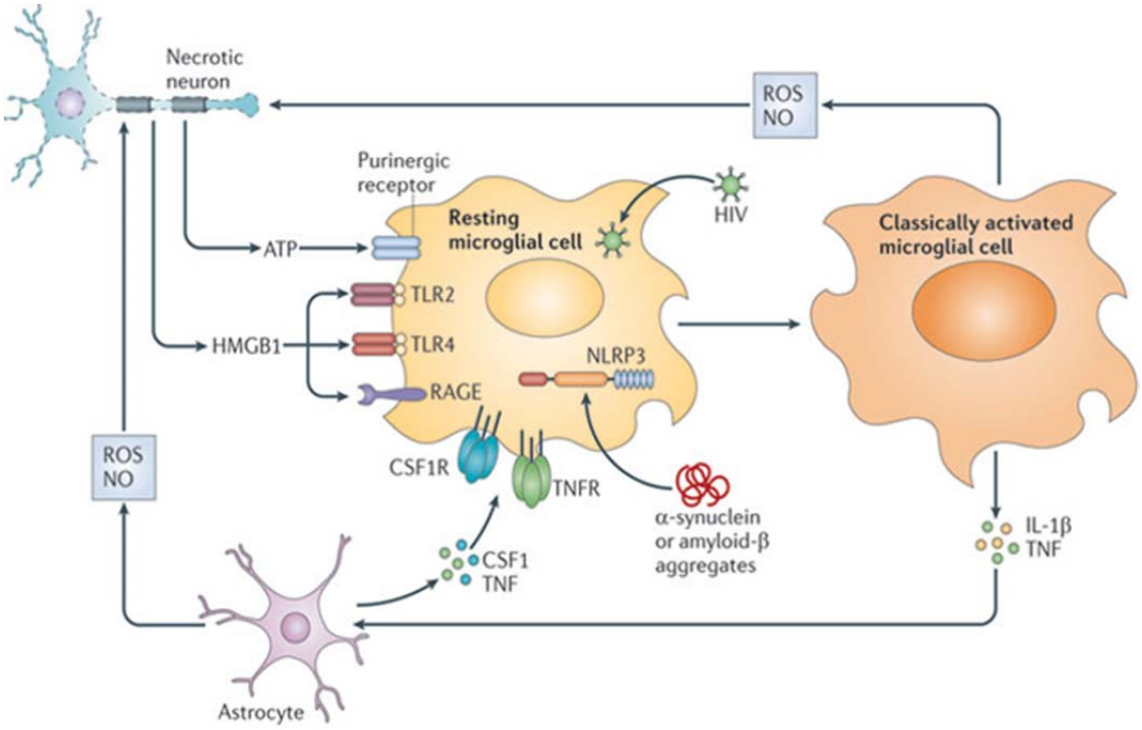

Figure 1.6: Generation of a feed-forward cycle of chronic neuroinflammation in neurodegenerative diseases

Degenerating neurons release DAMPs which are detected by PRRs and purinergic receptors on microglia, leading to their activation. Disease-associated protein aggregates may also be recognised as DAMPs. The fibril form of Aβ has also been reported to stimulate the activity of the NLRP3 inflammasome in microglia, which promotes the maturation of IL-1β. Classically activated microglia release proinflammatory mediators such as cytokines, ROS and NO which maintain the proinflammatory state by activating other microglial cells and astrocytes, which amplify neuroinflammatory signals by releasing their own inflammatory mediators. This causes further neuronal damage, resulting in the release of more DAMPs (Saijo and Glass 2011). (Re-printed from Nature Reviews Immunology, Volume 11, Issue 11, 'Microglial cell origin and phenotypes in health and disease', Page 782, Figure 4, Saijo and Glass, ©2011, with permission granted by Nature Publishing Group (Permissions) via Copyright Clearance Center,

License ID: 3932560951122). Abbreviations not yet stated: NLRP3, NOD-, LRR- and pyrin domain-containing 3; RAGE, Receptor for advanced glycation end-products.

Neuroinflammation can be directly neurotoxic because inflammatory mediators such as cytokines, free radicals and proteolytic enzymes cause neuronal damage (Amor *et al.* 2014; Doty *et al.* 2015). Alternatively, neuroinflammation can result in indirect neurotoxicity due to the shift in microglial phenotypes away from quiescent microglia performing homeostatic and beneficial functions, such as the production of neurotrophic factors and supporting normal neuronal function (Heneka *et al.* 2014). For example, the sustained release of proinflammatory mediators has been shown to suppress axonal transport, adult neurogenesis and synaptic plasticity, and this is thought to be a combined effect of the directly suppressive effects of cytokines and NO along with the phenotypic change in microglia away from the ramified form which has been associated with synapse remodelling via direct neuronal contact through microglial processes (Heneka *et al.* 2014). Additionally, when microglia become excessively and chronically activated, they cease to engage in beneficial communication with neurons, and microglial cytokine production can become dysregulated. This promotes harmful actions of the defence mechanisms leading to neurotoxicity, and disturbance of normal neural cell functions due to the sensitivity of neurons to cytokine signalling (Hanisch 2002). Prolonged activation of microglia has also been shown to reduce their phagocytic functions, restricting their abilities to degrade and clear misfolded and aggregated proteins (Heneka *et al.* 2014).

Neurons which are injured in neurodegenerative diseases may be more vulnerable to progressive damage caused by both direct and indirect mechanisms of inflammation-related neurotoxicity. In support of a toxic role for inflammation in neurodegenerative diseases, epidemiologic studies have shown long-term use of non-steroidal anti-inflammatory drugs (NSAIDs) reduce the risk of developing AD or PD by approximately fifty percent (Lucin and Wyss-Coray 2009; Heneka et al. 2014), and anti-inflammatory agents have been reported to reduce microglial activation in association with reduced neuronal loss in experimental animal models of PD (Doty *et al.* 2015). Also, by visualising ongoing proinflammatory microglial activity using positron emission tomography (PET), high levels of neuroinflammation predicts development of clinical AD in patients experiencing mild cognitive impairment (MCI), and the extent of microglial cell activation positively correlates with the severity of clinical symptoms in ALS (Heneka *et al.* 2014). A recent study demonstrated that classical NFκB activation leading to proinflammatory cytokine production occurs in microglia in the spinal cord of ALS patients, and constitutive activation of this pathway alone was enough to induce

the pathological hallmarks of ALS in wild-type mice. Conversely, the selective inhibition of microglial NFκB signalling rescued motor neurons from microglial-mediated death by dampening proinflammatory microglia activation, and the consequence of this was to extend survival and delay disease progression by almost fifty percent in a mouse model of ALS (Frakes *et al.* 2014). This study highlights the significance of microglia-mediated neurotoxicity in this neurodegenerative disease.

Alternatively, there are many cases in which innate immune activation and neuroinflammation have been shown to be protective in neurodegenerative diseases, especially in early phases of the neurodegeneration process. For example, phagocytic microglia can clear Aβ aggregates and promote efflux of amyloid from the brain to the blood stream (Doty *et al.* 2015). This has been shown to reverse amyloid burden and prevent amyloid deposition in animal models of AD (Cagnin *et al.* 2006). Also, microglia populations existing on the continuum between the classically activated and quiescent poles have important functions in healing and supporting neuronal survival. It is possible that in the early stages of neurodegenerative diseases activated microglia perform neuroprotective functions, and in later stages become neurotoxic in their role on account of dysregulated neural-immune communication and damage to microglial populations themselves as a result of prolonged stimulation over years of the disease course. In support of this, *ex vivo* microglia from an ALS mouse model in early-stage disease were shown to be alternatively activated (M2 phenotype) and neuroprotective, whereas microglia from late-stage animals were more classically activated (M1 phenotype) and neurotoxic to motor neurons in co-culture (Doty *et al.* 2015). Moreover, an increased ratio of M1 to M2 markers has been observed in the mid-brain of aged mice and blocking microglial polarisation to the M2 phenotype in substantia nigra dramatically exacerbated the death of dopaminergic neurons in a mouse model of PD (Tang *et al.* 2014). This suggests that ageing is a factor in switching microglial phenotypes away from protective M2-type microglia to neurotoxic M1-type microglia in PD. In addition, microglia may be driven to a more toxic phenotype in later stages of the neurodegenerative process as a result of chronic activation. For example, prolonged stimulation of microglia has been demonstrated to induce aberrant and uncontrolled production of proinflammatory mediators and cause restricted abilities to phagocytose and clear protein aggregates (Cagnin *et al.* 2006; Heneka *et al.* 2014).

1.3.2.3 Cytokines and neurotrophins in the pathogenesis of neurodegenerative diseases

Cytokines are essential mediators for neural-immune communication in the pathogenesis of neurodegenerative diseases, and their functions have been shown to have both beneficial and deleterious effects.

Elevated levels of the proinflammatory cytokines IL-1β, IL-6, IL-8, IL-12 and TNFα have been detected in cerebrospinal fluid (CSF), in areas surrounding Aβ plaque formation and neuronal damage, and in plaque-associated microglia in AD patients (Heneka *et al.* 2014; Doty *et al.* 2015). IL-1β signalling initiates activation of NFκB which drives proinflammatory gene expression and production of NO and ROS which can promote bystander neuronal death. Over-expression of IL-1β in AD brain has been directly linked to plaque progression and tangle formation (Doty *et al.* 2015). IL-6 drives gliosis in response to Aβ and promotes tau hyperphosphorylation, as well as having roles in immune resolution and behaving as a neurotrophic factor. Inhibiting IL-12 or TNFα in AD mouse models leads to decreased levels of Aβ and reduced pre-plaque pathology along with fewer learning and memory deficits (Czirr and Wyss-Coray 2012; Heneka *et al.* 2014; Doty *et al.* 2015).

In PD, elevated levels of IFNγ, IL-1β, IL-2, IL-4, IL-6, TGFα, TGFβ and TNFα, along with an upregulation of NFκB activation, have been reported in patient CSF and in the substantia nigra and striatum (Nagatsu *et al.* 2000a; Reale *et al.* 2009a; Doty *et al.* 2015). TGFβ1 and TGFβ2 may serve to protect against neuronal cell damage in the brain parenchyma (Reale *et al.* 2009a). Blocking TNFα in mouse models of PD prevents microglial activation and attenuates the progressive degeneration of dopaminergic neurons (Nagatsu *et al.* 2000a; Czirr and Wyss-Coray 2012; Reale 2015), however TNFα has been shown to have neuroprotective as well as toxic effects. Chronic low expression of TNFα levels reduced the nigrostriatal neurodegeneration in a mouse model of PD, while chronic expression of high levels of TNFα induced a slow and progressive neurodegeneration accompanied by gliosis and an infiltration of peripheral monocytes and macrophages (Chertoff *et al.* 2011). This suggests that the level and time of expression of a particular cytokine can determine whether it causes CNS damage or protection.

Cytokines detected in ALS spinal cord and CSF are similar to AD and PD, and include IL-1β, TNFα, and IL-6. The excessive production and release of IL-1β is a common feature of neurodegenerative disease, and as a result of the proinflammatory cascades it induces, IL-1β is considered to be a major driver of chronic neuroinflammation in AD, PD and ALS (Heneka *et al.* 2014; Doty *et al.* 2015).

Neurodegenerative diseases are also associated with dysregulation and altered distribution of neurotrophins and their receptors. Neurotrophins are produced by neurons, astrocytes, microglia and peripheral myeloid cells, and they can directly impact neuronal function and survival. In neurodegenerative diseases, levels of NGF and BDNF and their primary high affinity receptors TrkA and TrkB, respectively, have

been reported to be increased, decreased or displaying no change in patient brain, CSF and serum. There are several potential reasons for these conflicting results, including variations in neurotrophin levels over the disease course, large patient-to-patient variability, medication or supplements used by patients which affect neurotrophin levels and lead to confounding results, or even differences in methodology. Whilst disease-related changes in the levels of NGF and BDNF still remain to be clearly defined, the general consensus is that lower levels of NGF or BDNF in disease-associated brain areas, CSF or serum correlate with worse outcome and higher levels correlate with better outcome in measures such as neuronal fate, brain atrophy rate, disease progression, and symptoms or behaviours in patients and animal models of various neurodegenerative diseases (Howells *et al.* 2000; Nagatsu *et al.* 2000b; Lorigados Pedre *et al.* 2002; Schindowski *et al.* 2008; Salehi and Mashayekhi 2009; Weinstein *et al.* 2014; Budni *et al.* 2015; Forlenza *et al.* 2015; Passaro *et al.* 2015; Wang *et al.* 2016).

1.3.2.4 The role of peripheral immune cells in the pathogenesis of neurodegenerative diseases

While it is clear that a strong link has been defined between neuroinflammation and neurodegeneration, peripherally-derived innate immune cells may also play a significant role in disease progression, either directly by infiltration to sites of neurodegeneration in the CNS, or indirectly via the release of inflammatory mediators. CNS infiltration of T cells has been shown to modulate microglial phenotypes and neuroinflammation, and affects disease progression in PD and ALS (Park *et al.* 2016). In AD, circulating monocytes have been demonstrated to play a role in the elimination of Aβ, whereby they are attracted to and crawl onto the luminal wall of Aβ-positive veins and carry Aβ back into the peripheral blood stream (Michaud *et al.* 2013). Increases in the concentrations of inflammatory mediators in the periphery, which can occur as a result of obesity, reduced physical activity or a history of systemic infection, are known risk factors for AD (Heneka *et al.* 2014). Also, AD patients who experience an acute systemic infection display accelerated cognitive decline which has been correlated with peripheral levels of IL-1β and TNFα (Holmes *et al.* 2003; Holmes *et al.* 2009), and there is a strong correlation between peripheral proinflammatory cytokine levels and rate of disease progression in PD (Reale 2015). IL-2, IL-1β, IL-6 and TNFα have all been reported to be elevated in the periphery in AD and PD. IFNγ, IL-4, IL-8 and IL-10 are also increased in PD, and TGFβ is increased in AD (Brodacki *et al.* 2008; Reale *et al.* 2009a). This indicates that neurodegenerative diseases are not only hallmarked by neuroinflammation, but are associated with a more widespread

inflammatory state, and PBMCs are a likely source of enhanced and dysregulated cytokine production in the periphery (Reale *et al.* 2009b).

While sustained microglial activation is most likely triggered by disease-associated and neuronal injury-related DAMPs in neurodegenerative diseases, it is possible that peripheral proinflammatory events may also contribute directly to the chronic cycle of neuroinflammation ongoing in the CNS by amplifying microglial responses and exacerbating neurodegeneration. For example, pre-symptomatic ALS animal models show an accelerated course of disease development in response to chronic peripheral LPS exposure (Heneka *et al.* 2014). In PD high plasma concentrations of IL-6 result in an increased risk of developing the disease (Chen *et al.* 2008), and people with high levels of circulating IL-1β or TNFα produced by PBMCs are more likely to develop AD (Tan *et al.* 2007). Also, CNS entry of peripherally-derived proinflammatory factors such as TNFα has been shown to directly activate microglia and induce their production of more inflammatory factors (including TNFα, monocyte chemoattractant protein-1 (MCP-1), IL-1β and NFκB p65) leading to progressive neurodegeneration of dopaminergic neurons in the substantia nigra of adult wild-type mice (Qin *et al.* 2007). This suggests that peripheral proinflammatory cytokines do not only contribute to chronic neuroinflammation leading to neurodegeneration, but may also trigger it.

While there is substantial evidence that peripheral inflammatory events can impact on the development and progression of neurodegenerative diseases, there is also scope for the injured CNS affecting the peripheral immune system. Delivery of an inflammatory stimulus, such as Aβ, IL-1β or an endotoxin, by intracerebroventricular injection, induces production of cytokines such as IL-6, which are secreted from the brain and directly contribute to the pool of systemic cytokines, or stimulate cytokine production by peripheral immune cells via the HPA axis (De Simoni *et al.* 1990; Romero *et al.* 1996; Song *et al.* 2001; Reale *et al.* 2009a). It may therefore be considered that the peripheral immune alterations observed in neurodegenerative diseases occur as a consequence of brain immune activation as well as contributing to it. Hence, when attempting to dissect the complex neural-immune interactions in the self-propagating cycle of chronic inflammation and neuronal injury in neurodegenerative diseases, it is important to include the roles of peripheral immune cells.

1.3.2.5 Intervention by immunomodulation in neurodegenerative diseases

Studying the immune components of neurodegenerative diseases has yielded common themes, and by unifying these concepts there is increased potential for the development of immune-based therapeutics for treatment of HD, AD, PD and ALS.

Chronic neuroinflammation and associated neurotoxicity is a characteristic of all of these diseases, and it could be argued that directly inhibiting proinflammatory processes with an anti-inflammatory agent would be neuroprotective. There is a large body of evidence in support of this theory, including epidemiological studies which have shown long-term use of NSAIDs to reduce the risk of developing AD or PD (Lucin and Wyss-Coray 2009; Heneka et al. 2014). However, increasing expression of the key ant-inflammatory cytokine, IL-10, in AD mouse models was recently shown to suppress microglial Aβ phagocytosis, increase Aβ plaque accumulation and exacerbate memory impairment (Chakrabarty *et al.* 2015). Conversely, suppression of IL-10 has been shown to be beneficial, promoting Aβ clearance and mitigating synaptic and cognitive deficits in AD mice (Guillot-Sestier *et al.* 2015). The IL-10 signalling pathway is abnormally elevated in AD patient brains, and it is thought that suppressing IL-10 may rebalance innate immunity and mitigate AD pathology (Guillot-Sestier *et al.* 2015). Expression of proinflammatory molecules has also been demonstrated to improve disease-relevant outcomes in several animal models of neurodegenerative disease (Doty *et al.* 2015). From these studies, it can be considered that due to the complexity of neural-immune interactions, and the dual roles of inflammation in both neuroprotection and neurotoxicity, a general dampening of all immune responses is unlikely to yield a beneficial treatment for neurodegenerative diseases. Rather, a targeted immunomodulatory approach should aim to dampen neurotoxic aspects of immune cell activation and neuroinflammation whilst promoting beneficial immune cell behaviours. To achieve this, a better understanding of the communication between neurons and immune cells during homeostasis and in neurodegenerative diseases is required.

1.4 Innate immune system dysfunction in the pathogenesis of HD

As in other neurodegenerative diseases, the innate immune system is now recognised to play a significant role in the pathogenesis of HD. Neuroinflammation, involving microglial activation, astrogliosis and elevated levels of proinflammatory factors, is an early and active component of the disease course, and is accompanied by parallel inflammatory events in the periphery mediated by monocytes and macrophages. Chronic inflammation and aberrant myeloid cell behaviour accelerate alongside progressive neurodegeneration and peripheral pathology. This is likely due, in part, to cell-autonomous dysfunction caused by the expression of mHTT in immune cells. As is the case in other neurodegenerative disease like AD, PD and ALS, it is also probable that cell-to-cell interaction mechanisms involving neurons, immune cells and astrocytes play a role in generating a ‘feed-forward’ cycle of myeloid cell activation and chronic

inflammation; triggered by DAMPs produced by damaged and degenerating neurons and sustained by the accumulating presence of proinflammatory and neurotoxic factors which affect all interacting cells.

Evidence suggests that peripheral innate immune cell dysfunction and systemic inflammation in HD may serve as a window into central pathological events, or could even directly modulate neuroinflammation and impact on neurodegenerative processes in the brain. Whether the myeloid cell activation and inflammation associated with neurodegeneration in HD is protective or damaging remains to be clearly defined, and the extent to which innate immune system dysfunction in HD is a reactive process or has an active influence on disease progression has not yet been fully elucidated. Recent evidence, however, indicates that targeting immune disruption, centrally or peripherally, may modify disease onset and/or progression. Therefore, it is important that we develop further understanding of the influence of inflammation on HD pathogenesis, as innate immune cells hold potential as a meaningful therapeutic target to slow disease progression or forestall the onset of disease.

1.4.1 Microglial activation and chronic neuroinflammation in HD

HD is characterised by cellular and molecular features of neuroinflammation, including microgliosis, astrogliosis, elevated levels of proinflammatory cytokines and chemokines, strong activation of the complement system, and production of ROS and reactive nitrogen species (RNS); and microglia are the main effector cells.

Post-mortem study of HD brain tissue and PET analyses in living HD patients (using a ligand for the peripheral benzodiazepine receptor (PBR), PK11195, expressed selectively by activated microglia in the CNS), have shown an early and progressive accumulation of activated microglia in affected regions of the HD brain, such as the cortex and striatum, and this correlated with loss of neuronal function, brain atrophy, and disease severity (Sapp *et al.* 2001; Pavese *et al.* 2006; Politis *et al.* 2011). Microglial activation has also been detected in pre-symptomatic HD gene carriers up to fifteen years before predicted AAO, and this correlated with striatal neuronal dysfunction and rate of disease progression (Tai *et al.* 2007a; Tai *et al.* 2007b; Politis *et al.* 2011). Interestingly, a higher level of microglia activation correlated with a lower level of dopamine D2 receptor binding sites and this was associated with a higher probability of developing HD in five years (Tai *et al.* 2007b). Additionally, activated microglia can be observed in degenerating white matter, which is a key early pathological event in HD (Tabrizi *et al.* 2013). Taken together, these findings indicate that microglial activation is an early event in HD pathogenesis and shares a spatial and progressive temporal relationship with neuropathology, suggesting an active role of

microglial activation in neurodegeneration, including subclinical disease progression. Indeed, activated microglia have been shown to proliferate in the vicinity of degenerating neurites in HD brain slice cultures and mHTT-expressing neuronal cell models of HD (Kraft *et al.* 2012), indicating a direct association between microgliosis and neuronal damage in an isolated *in vitro* setting.

Microglial activation is accompanied by a distinct profile of inflammatory mediators in HD patient CSF and post-mortem HD brain tissue (Silvestroni *et al.* 2009). IL-1β and TNFα were found to be increased only in the striatum, while IL-6, IL-8 and MMP-9 were also upregulated in cortex and cerebellum (Silvestroni *et al.* 2009). The mRNA levels of IL-6, IL-8, IL-10, MCP-1 and TNFα are also increased in the CSF and diseased brains of HD patients (Björkqvist *et al.* 2008; Silvestroni *et al.* 2009) (Figure 1.7). Elevated levels of inflammatory mediators can similarly be observed in the brains of well-established HD transgenic mouse models, such as the R6/2 model which expresses human mHTT exon 1 driven by the human huntingtin promoter (Mangiarini *et al.* 1996), and the BACHD and YAC128 models which express full-length human mHTT from the human genomic locus on a bacterial artificial chromosome (BAC) (Gray *et al.* 2008) or yeast artificial chromosome (YAC) (Hodgson *et al.* 1999; Slow *et al.* 2003; Van Raamsdonk *et al.* 2007), respectively. Like in human HD patient brain, microglial accumulation has been observed in the striatum of HD mouse models (Simmons *et al.* 2007), and this is associated with elevated levels of proinflammatory cytokines such as IL-1β, IL-6 and TNFα (Ona *et al.* 1999; Björkqvist *et al.* 2008; Bouchard *et al.* 2012; Alto *et al.* 2014). Analysis of striatal tissue gene expression in symptomatic R6/2 mice has revealed Th1-type cytokines as potential regulators of disease (Crocker *et al.* 2006), and both IL-6 and TNFα have been demonstrated to influence the disease course in HD (Bouchard *et al.* 2012; Hsiao *et al.* 2014). Administration of an IL-6 neutralising antibody into R6/2 mice diminished weight loss and partially rescued motor deficits (Bouchard *et al.* 2012). Intracranial infusion of a TNFα inhibitor into R6/2 mice decreased the elevated levels of TNFα in the cortex and striatum, decreased gliosis and reduced caspase activation, and this was associated with fewer mHTT aggregates, increased neuronal density and improved motor function (Hsiao *et al.* 2014). These studies indicate a pathological role of the proinflammatory cytokines IL-6 and TNFα in HD, and findings suggest they are key mediators of disease progression. IL-1β is another proinflammatory cytokine which is elevated in the brains of HD patients and in the R6/2 mouse model (Ona *et al.* 1999; Ellrichmann *et al.* 2013). IL-1β is known to augment inflammatory signals in the CNS, including direct stimulation of astrogliosis, and is involved in neuronal cell death (Ona *et al.* 1999).

Other aspects of neuroinflammation, such as astrogliosis and increased complement biosynthesis and activation, can also be observed in affected regions of HD patient brains (Singhrao *et al.* 1999). Astrocytes expressing mHTT are more prone to support neuroinflammation and may amplify proinflammatory signalling initiated by microglia (Crotti and Glass 2015). Complement activators and regulators have been shown to be constitutively expressed at much higher levels in the HD brain compared with normal brain; and in the striatum, neurons, astrocytes and myelin show deposition of complement components on their surface (Singhrao *et al.* 1999). It is thought that complement production is elevated in local microglia and activated on neuronal membranes, contributing to neuronal necrosis and proinflammatory activities (Singhrao *et al.* 1999). The complement peptide receptor mRNAs, C5a receptor and C3a receptor, are strongly expressed in HD caudate (Singhrao *et al.* 1999). These receptors may be involved in the recruitment and stimulation of glial cells and phagocytes bearing specific complement receptors, and have been shown to activate microglia and induce their migration *in vitro* (Nolte *et al.* 1996; Möller *et al.* 1997).

Recently, magnetic resonance imaging (MRI) techniques and post-mortem tissue analyses have been used to assess blood vessel impairments in HD patients, and it was discovered that there were alterations in the cerebral vasculature leading to BBB leakage (Drouin-Ouellet *et al.* 2015). The BBB was also found to be compromised in the R6/2 mouse model (Drouin-Ouellet *et al.* 2015). This suggests that there may be uncontrolled passage of innate immune cells and blood-borne factors between the brain and periphery, however, CNS influx of peripherally-derived immune cells has not been reported in neuropathological studies of HD (Silvestroni *et al.* 2009; Möller 2010). Therefore, neuroinflammation in HD appears to be mediated solely via cellular interactions between microglia, neurons and astrocytes. There may, however, be communication between central and peripheral inflammatory events mediated via molecular messengers, such as cytokines.

1.4.2 Peripheral innate immune system dysfunction in HD

Like in the CNS, peripherally, inflammatory molecules are elevated in plasma up to sixteen years prior to AAO (Björkqvist *et al.* 2008; Dalrymple *et al.* 2007; Wild *et al.* 2011; Chang *et al.* 2015), providing further evidence for a possible active role of the innate immune system during progression to symptomatic disease. Plasma levels of IL-6, IL-8, TNFα and clusterin (a protein associated with the clearance of cellular debris and apoptosis) are elevated in pre-manifest HD, become more abundant with clinical manifestation, and continue to increase in correlation with disease severity (Dalrymple *et al.* 2007; Björkqvist *et al.* 2008; Heneka *et al.* 2014) (Figure 1.7). Plasma levels of other cytokines and chemokines, including chemokine (C-C motif) ligand (CCL)4,

CCL11, CCL26, IFNγ, IL-1β, IL-4 and IL-10 also increase with disease progression (Björkqvist *et al.* 2008; Wild *et al.* 2011; Ellrichmann *et al.* 2013). Similarly, serum levels of inflammatory molecules have been shown to be elevated in several HD mouse models (Björkqvist *et al.* 2008; Nguyen *et al.* 2010; Chang *et al.* 2015). As is the case in the CNS, several members of the complement cascade have also been detected in HD patient plasma samples (Dalrymple *et al.* 2007). These studies indicate a peripheral immune response in HD which occurs in parallel to microglial activation and neuroinflammation in the CNS.

Peripheral myeloid cells are the likely source of elevated systemic levels of inflammatory molecules in HD. Monocytes and macrophages isolated from HD patients are hyper-reactive in response to external proinflammatory stimulation (Björkqvist *et al.* 2008; Träger *et al.* 2014a), exhibit increased levels of phagocytosis (Träger *et al.* 2014b), and are impaired in their ability to migrate towards chemo-attractant stimuli (Kwan *et al.* 2012b). The intrinsic phenotype of T cells, however, is not altered in HD patients (Miller *et al.* 2015). HD monocytes from pre-manifest HD gene carriers, up to sixteen years prior to AAO, produce elevated levels of IL-6 compared to healthy volunteer monocytes when stimulated with IFNγ and LPS *ex vivo,* and this can additionally be observed in both microglia and macrophages isolated from HD mouse models (Björkqvist *et al.* 2008). Increased IL-6, IL-8 and TNFα production has also been observed in stimulated pre-manifest and manifest HD patient monocytes and BMD-macrophages differentiated *in vitro* (Träger *et al.* 2014a) (Figure 1.7). These responses, observed in myeloid cells *ex vivo*, account for elevated levels of proinflammatory cytokines in the brain, CSF and plasma of HD patients over the disease course.

The extent to which central and peripheral inflammation in the pathogenesis of HD are independent and parallel events, or occur in synchronisation as a consequence of interactive communication, is not entirely understood. For example, HD patient peripheral myeloid cells (Björkqvist *et al.* 2008; Weiss *et al.* 2012; Träger *et al.* 2014a), like microglia (Shin *et al.* 2005; Simmons *et al.* 2007), express mHTT, and this results in immune cell dysfunction (Kwan *et al.* 2012b; Träger *et al.* 2014a) which could promote equivalent hyper-reactive proinflammatory molecule secretion in the CNS and plasma (Björkqvist *et al.* 2008). As microglia respond to DAMPs produced by neuronal injury, peripheral myeloid cells may also encounter DAMPs produced by mHTT-induced peripheral tissue pathology or mHTT itself (van der Burg *et al.* 2009), possibly leading to initiation and maintenance of chronic inflammation in the periphery as occurs in the CNS. In these cases, cell-autonomous mHTT-induced immune cell dysfunction and hyper-reactive responses to progressive pathology in the CNS and periphery

would occur in parallel, but independently, and these events would accelerate with disease progression. Alternatively, microglial activation and neuroinflammation could directly impact peripheral immune behaviour (Eskandari and Sternberg 2002; Saleh *et al.* 2009) and/or peripheral inflammatory events could contribute to neuroinflammation and neurodegenerative processes in the CNS (Eskandari and Sternberg 2002; Wrona 2006). It is probable that both independent cell-autonomous mechanisms and synchronised CNS-peripheral immune system interactions play roles in the generation and maintenance of chronic neuroinflammation and systemic inflammation in HD.

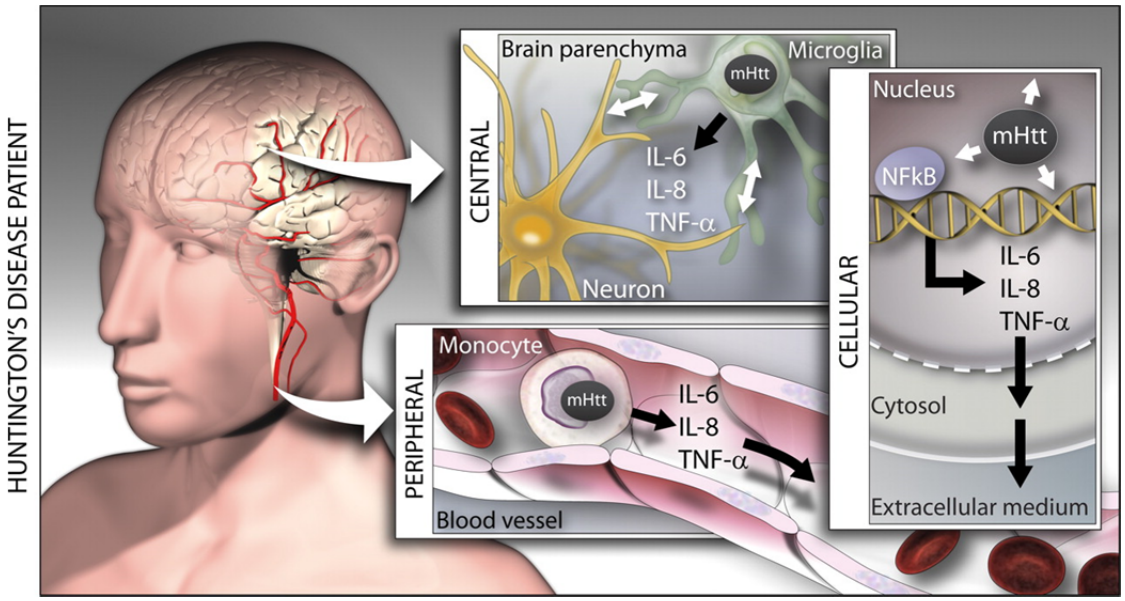

Figure 1.7: Central, peripheral and cellular inflammatory events in the HD patient

Levels of key proinflammatory cytokines, including IL-6, IL-8 and TNFα, are elevated in the CNS and blood plasma of HD patients, up to sixteen years prior to expected AAO. This is strongly linked to disease progression. Degenerating neurons stimulate microglial activation in the brain parenchyma leading to cytokine production. The cell-autonomous expression of mHTT by microglia and peripheral monocytes (and macrophages) also leads to hyper-reactive proinflammatory cytokine production by these cells. This is due, in part, to direct transcriptional dysregulation caused by mHTT expression, as well as interaction of mHTT with elements of the NFκB pathway (and key myeloid-lineage determining factors in microglia) which up-regulates proinflammatory responses. (Björkqvist *et al.* 2008). *(Re-printed from The Journal of Experimental Medicine, Volume 205, Issue 8, 'A novel pathogenic pathway of immune activation detectable before clinical onset in Huntington's disease', Page 1874, Figure 4, Björkqvist et al., 2008).*

Evidence for parallel cell-autonomous effects of mHTT-induced immune cell dysfunction comes from studies examining central and peripheral myeloid cell

behaviour *ex vivo*. The expression of mHTT was shown to compromise cell migration and the motility of cellular processes in microglia and monocytes derived from HD mouse models and HD patients (Kwan *et al.* 2012b). Monocytes isolated from HD patient blood were also shown to release elevated levels of proinflammatory cytokines when stimulated, compared with healthy volunteer monocytes, and this was reversed after delivery of small interfering (si)RNAs which lowered HTT expression (Träger *et al.* 2014a).

There has been very little research into the direct effects of neuroinflammation on the peripheral immune system in HD. However, there is some evidence to suggest that the HPA axis may be altered in HD patients. Levels of cortisol, a major immunosuppressant and the main glucocorticoid produced by the adrenal cortex in humans, were found to be higher in HD patient blood than in healthy volunteers (Saleh *et al.* 2009). However, this was independent of adrenocorticotropic hormone levels which stimulates the adrenal cortex to produce cortisol, indicating alterations in the HPA axis in HD, possibly due to chronic stress (Saleh *et al.* 2009). These findings may indicate dysfunction of a major pathway of communication between the CNS and the peripheral immune system in HD.

Multiple studies have shown peripheral immune dysfunction as a key modifier of neuroinflammation and central pathogenesis in HD. Peripheral administration of LPS at doses unlikely to penetrate the CNS induces changes such as increased microglial activation in the brains of YAC128 mice (Franciosi *et al.* 2012). The dampening of peripheral immune responses has also been shown to confer benefits in the brains of HD mouse models. For example, peripherally-restricted inhibition of kynurenine 3-monooxygenase (KMO), an enzyme highly expressed in peripheral immune cells, ameliorates neurodegeneration in R6/2 mice by raising CNS levels of neuroprotective metabolite kynurenic acid (KYNA) and consequently preventing hyperactive microglial activity (Zwilling *et al.* 2011). Transplantation of wild-type bone marrow into YAC128 and BACHD mice resulted in normalisation of circulating proinflammatory cytokine levels, increased synaptic connections in the cortex, and partial suppression of motor and neuropathological defects (Kwan *et al.* 2012a). Conversely, signalling through cannabinoid receptor 2 (CB_2) dampens immune activation, and genetic deletion of these receptors in BACHD mice accelerated the onset of motor deficits and exacerbated their severity (Bouchard *et al.* 2012). Treatment of R6/2 mice with a CB_2 agonist extended life-span and suppressed motor deficits, synapse loss, and neuroinflammation, while a peripherally restricted CB_2 antagonist blocked these effects (Bouchard *et al.* 2012). Inhibition of systemic IL-6 also partially rescues motor deficits and weight loss in R6/2 mice (Bouchard *et al.* 2012). These studies provide evidence

that peripheral immune cell dysfunction is an important modifier of HD pathogenesis, and plays active roles in central pathology, including microglial activation, neuroinflammation and neurodegeneration, and impacts on disease onset, progression and severity.

1.4.3 Cellular mechanisms of myeloid cell dysfunction in HD

Myeloid cells are known to be dysfunctional in HD, and there is evidence that both cell-autonomous and non-cell-autonomous cellular mechanisms play a role. In HD patients, the mHTT protein is constitutively and ubiquitously expressed, however *mHTT* mRNA expression in immune cells is approximately three-fold higher than in other cell-types (Genomics Institute of Novartis Research Foundation, transcript 202389_s_at) (Soulet and Cicchetti 2011). Mutant HTT levels measured in PBMCs isolated from HD patients were also found to correlate with markers of disease progression such as disease stage, disease burden score and caudate atrophy rates (Weiss *et al.* 2012). It is therefore considered that mHTT expression causes cell-autonomous dysfunction in myeloid cells, contributing to HD pathogenesis. In support of this, it has been revealed in a recent study that HD patient monocytes display innate transcriptional dysregulation associated with proinflammatory pathway activation in their basal, unstimulated state (Miller *et al.* 2016), indicating a cell-autonomous mechanism in myeloid cells for the elevated release of proinflammatory molecules in HD. Miller *et al.* found increased resting expression of numerous proinflammatory cytokines and abnormal basal activation of the NFκB pathway was thought to play a key role in mediating these transcriptional changes (Miller *et al.* 2016). Indeed, others have demonstrated mHTT to directly interact with components of the NFκB pathway leading to upregulation of proinflammatory gene expression in monocytes and macrophages (Träger *et al.* 2014a). Similarly, mHTT has been shown to enhance the transcriptional activities of myeloid lineage-determining factors in microglia, resulting in increased production of proinflammatory cytokines (Crotti *et al.* 2014). Mutant HTT also directly impairs immune cell migration, and it is proposed that this is due to interaction with components of the actin machinery (Kwan *et al.* 2012b).

Non-cell-autonomous mechanisms of myeloid cell dysfunction in HD include chronic inflammation induced and sustained by hyper-reactive responses to mHTT-induced DAMPs produced by other cells, and mHTT itself. It is possible that mHTT expression primes immune cells in their resting state, leading to an exaggerated inflammatory response when a stimulus is encountered. Therefore, myeloid cells are not only in an abnormal diseased environment which promotes inflammatory responses, but are also maladaptive to this environment due to the cell-autonomous expression of mHTT. In support of this, the addition of mHTT-expressing microglia to wild-type neuronal

cultures has been shown to cause neuronal apoptosis, and the extent of this neurotoxicity is considerably increased under conditions of sterile inflammation (Crotti *et al.* 2014).

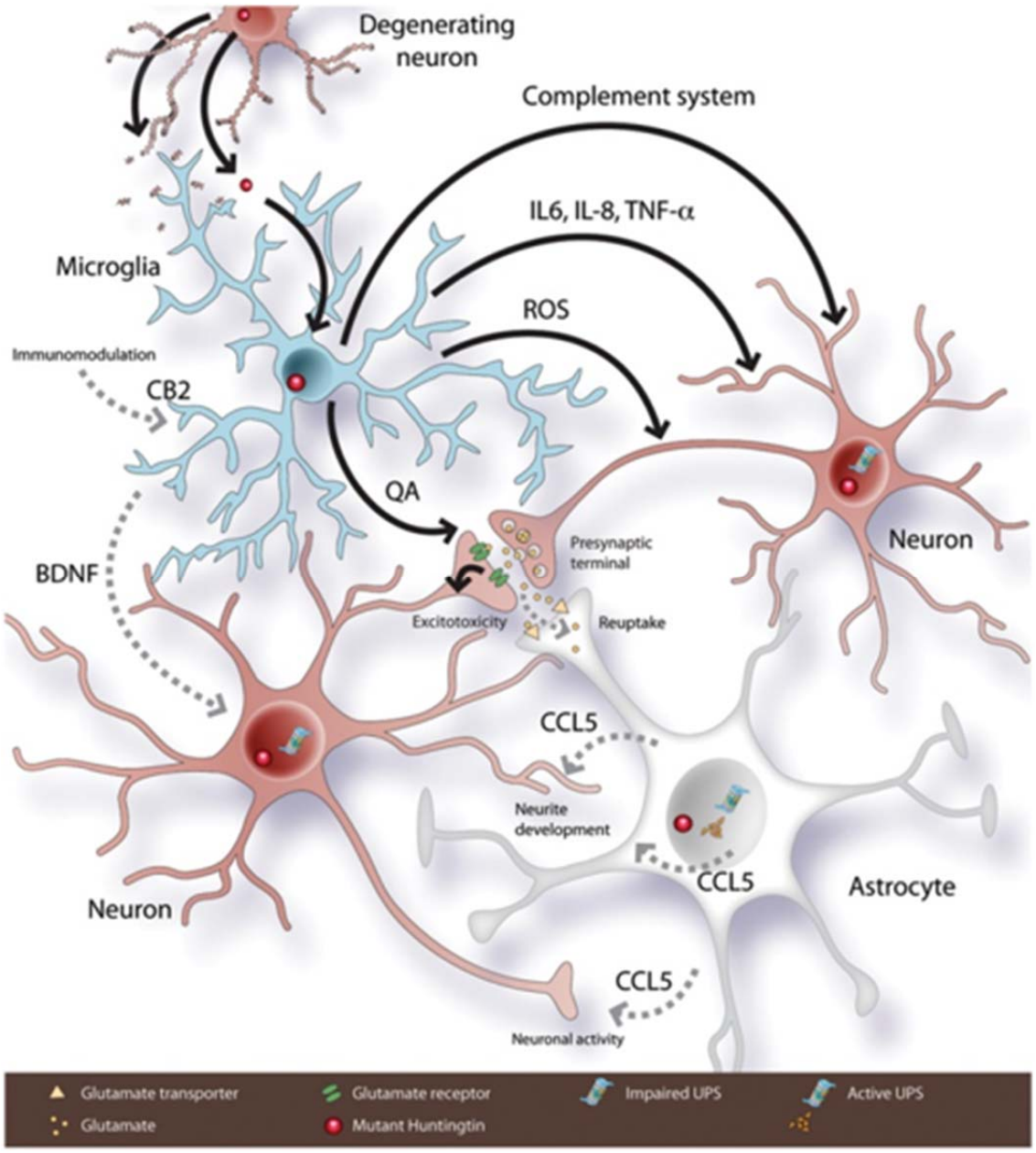

Figure 1.8: Cellular and molecular mechanisms of the immune response in HD

Myeloid cells may contribute to HD pathogenesis by cell-to-cell interaction mechanisms as well as cell-autonomous mechanisms. In the former case, degenerating neurons release DAMPs and mHTT which activate microglia and trigger neuroinflammation. In the latter case, constitutive expression of mHTT by microglia and peripheral myeloid cells primes, or even triggers, a heightened immune response. This includes the release of proinflammatory cytokines and ROS, and activation of the complement system. Induction of the kynurenine pathway also leads to the release of ROS and production of neurotoxic metabolite quinolinic acid (QA), which causes excitotoxicity by over-stimulating neuronal glutamatergic N-methyl-D-aspartate (NMDA) receptors. All of these inflammatory mediators can cause further damage to

neurons (black arrows). Microglial QA release, in combination with astrocytic deficiencies in glutamate reuptake, exacerbate excitotoxicity in neurons. Mutant HTT expression in astrocytes also leads to downregulation of CCL5, attenuating its beneficial effects on neurite development and neuronal activity. Reactive microglia, however, also release neurotrophic factors such as BDNF, which may promote neuroprotection (dashed arrows). Modulation of CB_2 signalling can alter myeloid cell inflammatory phenotypes; signalling through this receptor can downregulate inflammatory responses and promote neuroprotection. Finally, cell-specific, differential proteasome activity may negatively correlate with the toxicity of the soluble form of mHtt. (Soulet and Cicchetti 2011). (Re-printed from Molecular Psychiatry, Volume 16, Issue 9, 'The role of immunity in Huntington's disease', Page 893, Figure 3, Soulet and Cicchetti, ©2011, with permission granted by Nature Publishing Group (Permissions) via Copyright Clearance Center, License ID: 3934220747498)

1.4.3.1 Non-cell-autonomous mechanisms of myeloid cell activation in HD

When cells are damaged or killed by mHTT-induced toxicity, DAMPs are released and detected by myeloid cells as immunogenic molecules, triggering an inflammatory response (Soulet and Cicchetti 2011; Crotti and Glass 2015) (Figure 1.8). It is possible that extracellular soluble or aggregated forms of mHTT could also be detected as DAMPs and induce immune responses, as occurs when Aβ is taken up by macrophages via phagocytic or receptor-mediated endocytic processes (Morten et al. 2007). It has been demonstrated that immortalised cell lines in culture are capable of ingesting synthetic polyQ peptides from the extracellular space, which then translocate to the nucleus and induce cytotoxicity (Yang *et al.* 2002). Internalised fibrillar aggregates have also been shown to interact with soluble cytoplasmic proteins (Ren *et al.* 2009). It is therefore plausible that mHTT fragments could be detected and trigger similar processes in myeloid cells. *Mutant HTT* mRNA may also serve as a trigger for immune cell activation. CAG trinucleotide repeats can form hybrid dsRNAs which are subsequently cleaved by the ribonuclease, Dicer, into single-stranded (ss)RNA CAG repeat septamers, that can activate intracellular TLRs and cause cell death (Richards *et al.* 2013; Heneka *et al.* 2014). This mechanism was shown to drive neurotoxicity in a *Drosophila melanogaster* model of HD (Richards *et al.* 2013; Samaraweera *et al.* 2013).

1.4.3.2 NFκB pathway dysregulation in HD myeloid cells

Hyper-reactivity of the innate immune response in HD is due partly to NFκB pathway dysregulation (Khoshnan *et al.* 2004; Hsiao *et al.* 2013; Träger *et al.* 2014a) (Figure 1.7). In HD myeloid cells, dysregulation is observed upon activation of TLRs using LPS, implicating a possible mechanism of dysfunctional signalling downstream of TLR4, the principal LPS receptor (Poltorak *et al.* 1998; Qureshi *et al.* 1999). Signalling down-

stream of TLR4 is highly complex, including activation of the NFκB signalling pathway, as well as MAPKs and IRFs (Figure 1.5). Aberrant NFκB signalling has been demonstrated in cultured cells expressing mHTT and striatal cells from HD patients and HD mouse models, where mHTT was shown to interact with the IKKγ subunit, leading to elevated NFκB activity and increased NFκB-dependent gene expression (Khoshnan *et al.* 2004; Hsiao *et al.* 2013). This was also observed in peripheral myeloid cells isolated from HD patients, along with a more rapid degradation of IκB following LPS stimulation in HD patient monocytes compared to healthy volunteer monocytes (Träger *et al.* 2014a). Under baseline conditions, IκB binds NFκB transcription factors such as p65 (*RELA*) and RelB, thereby preventing their nuclear translocation. When a stimulus activates TLR4, the MyD88-dependent and/or MyD88-independent signalling cascades are triggered, leading to assembly of the IKK complex which phosphorylates IκB. The subsequent degradation of IκB liberates NFκB transcription factors for nuclear translocation where they initiate gene transcription for production of proinflammatory cytokines and type I IFNs (Akira *et al*. 2006; Takeuchi and Akira 2010; Brubaker *et al*. 2015). In HD patient myeloid cells, mHTT directly interacts with the γ subunit of the IKK complex, resulting in enhanced degradation of IκB, increased and prolonged NFκB translocation, and elevated production of proinflammatory cytokines (including IL-1β, IL-6, IL-8 and TNFα) following stimulation (Khoshnan *et al.* 2004; Björkqvist *et al.* 2008; Träger *et al.* 2014a) (Figure 1.9). Moreover, IKK has been shown to phosphorylate mHTT at amino acid S13, enhancing the clearance of mHTT via the ubiquitin-proteasome and autophagy degradation systems and regulating its neurotoxicity (Thompson *et al.* 2009; Steffan 2010).

In addition, mHTT-induced transcriptional dysregulation affects key inflammatory signalling pathways, including elements of the NFκB pathway, in HD patient myeloid cells (Figure 1.7). Basal, resting RNA expression levels of several genes downstream of TLR4 activation are increased, including Akt, c-Fos, c-Jun, IRAK-1, MyD88 and TRAM (Träger *et al.* 2014a) (Figure 1.5). When HTT expression was knocked-down by delivery of anti-*HTT* siRNAs, the observed transcriptional dysregulation in HD myeloid cells was reversed, and the elevated production of IL-6, IL-8 and TNFα was also decreased (Träger *et al.* 2014a). Immortalised human monocyte and rat microglial cell lines could also be induced to release elevated levels of proinflammatory cytokines in response to stimulation (Träger *et al.* 2014a), and elevated proinflammatory gene transcripts (Crotti *et al.* 2014), respectively, by transduction with *mHTT*. These findings provide further evidence for HD myeloid cells existing in a cell-autonomous, mHTT-induced primed state leading to hyper-reactive responses when a stimulus is encountered.

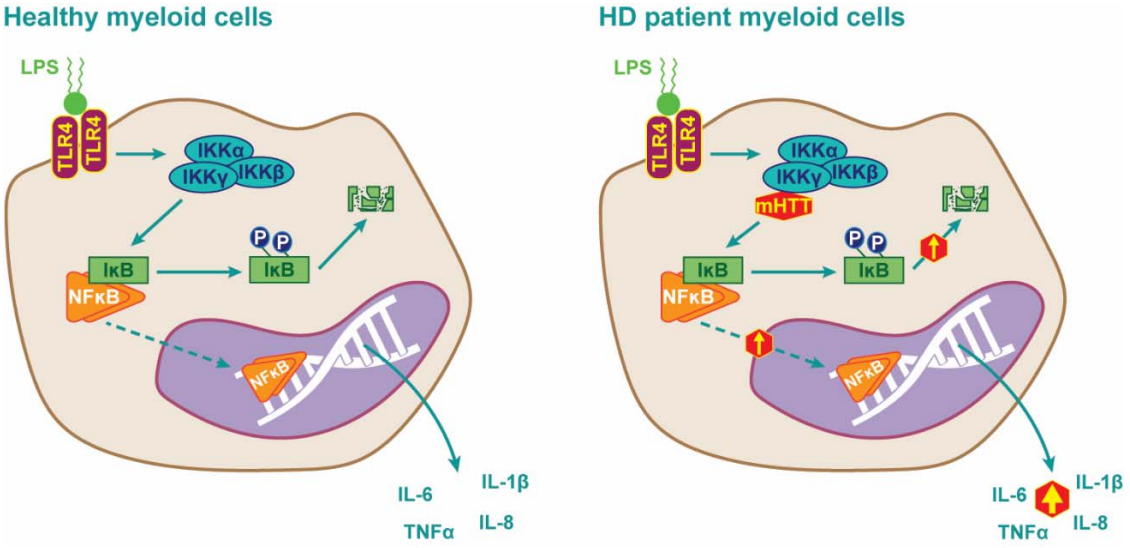

Figure 1.9: NFκB pathway dysfunction in HD patient myeloid cells

Cell-autonomous mHTT expression in HD patient microglia, monocytes and macrophages leads to hyper-reactive proinflammatory cytokine production in response to LPS stimulation. Mutant HTT directly interacts with the γ subunit of the IKK complex (also known as NEMO) leading to increased IκB degradation, and subsequently nuclear translocation of NFκB is enhanced and prolonged. NFκB initiates transcription of genes for proinflammatory cytokines and type I IFNs which are released from the cell at elevated levels.

1.4.3.3 mHTT promotes microglial activation via myeloid lineage-determining factors

While mHTT has been shown to promote autonomous hyper-reactivity in myeloid cells by enhancing the activities of the transcription factor NFκB (Träger *et al.* 2014a), mHTT has also been demonstrated to promote microglial activation in a basal, resting state via myeloid lineage-determining factors (Crotti *et al.* 2014) (Figure 1.7). The expression of *mHTT* in a rat microglial cell line conferred a cell-autonomous increase in proinflammatory gene expression associated with the increased expression and transcriptional activities of myeloid lineage-determining factors PU.1 and CCAAT/enhancer-binding protein (C/EBP) (Crotti *et al.* 2014). Binding sites for PU.1 and C/EBPs were highly enriched in enhancers and promoters associated with genes exhibiting constitutive upregulation in primary microglia isolated from HD mouse models, and enhanced binding of the two transcription factors in combination was observed nearby genes such as *Il6* and *Tnfa*, correlating with their increased expression. Microglia in the striatum and cortex of HD patient brains were also shown to express elevated levels of PU.1 (Crotti *et al.* 2014). This molecular mechanism of mHTT-induced enhanced basal proinflammatory activation was reported to be microglia-specific, as it was not observed in peripheral macrophages isolated from HD mouse models or in HD patient monocytes (Crotti *et al.* 2014).

1.4.3.4 Signalling through CB_2 dampens proinflammatory activation and promotes neuroprotective phenotypes in HD myeloid cells

CB_2 is expressed by microglia and peripheral myeloid cells (Palazuelos *et al.* 2009; Bouchard *et al.* 2012), and its expression is increased in striatal microglia in the brains of HD patients and HD mouse models (Palazuelos *et al.* 2009). It has been demonstrated that signalling through this receptor both suppresses proinflammatory activation of immune cells and confers a neuroprotective phenotype (Figure 1.8). Administration of CB_2 agonists to transgenic and chemical HD animal models reduces neuroinflammation, systemic levels of proinflammatory cytokines, brain oedema, striatal neuronal loss, synapse loss and motor deficits, and extends life-span (Palazuelos *et al.* 2009; Sagredo *et al.* 2009; Bouchard *et al.* 2012). Conversely, genetic ablation of CB_2 or administration of CB_2 antagonists in HD animal models enhances microglial activation, increases disease-related neurotoxicity, accelerates the onset of motor deficits, increases severity of motor symptomatology, and reduces life-span (Palazuelos *et al.* 2009; Sagredo *et al.* 2009; Bouchard *et al.* 2012). A peripherally-restricted CB_2 antagonist was also shown to have these effects (Bouchard *et al.* 2012). These studies demonstrate a link between CB_2 signalling in peripheral and central myeloid cells and the onset and severity of neurodegeneration in HD, and indicate an association between the attenuation of myeloid cell activation and the prevention neurodegeneration.

1.4.3.5 Kynurenine pathway modulation in HD myeloid cells

The kynurenine pathway, for the metabolism of L-tryptophan and formation of nicotinamide adenine dinucleotide (NAD^+) (Moroni 1999), has received interest in the study of HD pathogenesis because it generates several metabolites with neuroactive properties (Amori *et al.* 2009; Schwarcz *et al.* 2010). KYNA has a neuroprotective effect through modulation of mitochondrial function (Beal *et al.* 1990), while 3-hydroxykynurenine (3-HK) and quinolinic acid (QA) are neurotoxic because they induce oxidative stress via generation of ROS (Crotti and Glass 2015), and cause excitotoxicity by over-stimulating neuronal glutamatergic *N*-methyl-D-aspartate (NMDA) receptors (Schwarcz and Pellicciari 2002), respectively. Several studies have investigated the levels of kynurenine pathway metabolites in HD patients and HD mouse models, and generally found increased levels of neurotoxic metabolites and decreased levels of neuroprotective metabolites (Möller 2010; Schwarcz *et al.* 2010). In a yeast suppressor screen, it was discovered that genetic deletion of KMO, the enzyme that converts kynurenine into 3-HK, suppresses mHTT toxicity (Giorgini *et al.* 2005). Inhibition of KMO decreases levels of neurotoxic metabolites and increases KYNA levels (Andre *et al.* 2016). In the CNS, KMO is mainly expressed by microglia, and is

not found in neurons (Guillemin *et al.* 2003; Giorgini *et al.* 2008), implicating a non-cell-autonomous mechanism for microglia involvement in HD pathogenesis. A follow-up study by Giorgini *et al.* (2008) demonstrated that microglia isolated from R6/2 mice synthesise increased levels of neurotoxic metabolites via the kynurenine pathway, and that these increases can be reduced by histone deacetylase (HDAC) inhibitors (Giorgini *et al.* 2008). Interestingly, oral treatment with a peripherally-restricted KMO inhibitor has also been shown to protect against synaptic loss and improve behavioural defects in HD mice, implicating a role of peripheral immune cells, as well as microglia, in the modulation of neurodegeneration via the kynurenine pathway in HD (Zwilling *et al.* 2011) (Figure 1.8).

1.4.3.6 Motility and migration deficits in HD myeloid cells

Mutant HTT expression has been linked to impaired immune cell motility and migration. Microglia isolated from BACHD mice and monocytes and macrophages isolated from HD patient blood are defective in their ability to migrate towards chemoattractant stimuli (Kwan *et al.* 2012b). Microglia also displayed reduced process extension and increased process retraction, and a delayed response to injury in the brains of HD mice *in vivo* (Kwan *et al.* 2012b). These migration and motility deficits were reversed when mHTT expression was inhibited specifically in macrophages by conditional *HTT* deletion (Kwan *et al.* 2012b), demonstrating a cell-autonomous mechanism of immune cell dysfunction caused by expression of mHTT. The authors proposed that mHTT directly interacts with cofilin, a component of the actin machinery, disrupting the dynamic turnover of cofilin/phosphorylated-cofilin which drives membrane alterations required for cell migration (Kwan *et al.* 2012b).

1.4.4 Neurotoxic versus neuroprotective effects of innate immune system dysfunction in HD

In the study of neurodegenerative diseases, the consequences of inflammation for neurodegenerative processes is an important area of research. The same is true for HD, where central and peripheral immune activation and inflammation is recognised to play key roles in the onset, progression and modulation of neuropathology. Exactly what these roles are, and to what extent they are beneficial or harmful, however, still need to be completely elucidated. A fully comprehensive understanding of the complex neural-immune interactions underpinning communication between the nervous and immune systems in HD is likely to reveal targets for appropriate therapeutic intervention with the aim of delaying disease onset and/or slowing disease progression.

There is a huge body of evidence in support of microglial activation and neuroinflammation causing neurotoxicity in HD, and increased inflammation has been

clearly linked to a more severe disease phenotype and symptomatic progression (Heneka *et al.* 2014). In one study, induction of sterile inflammation by stereotactic injection of LPS into the striatum of mice expressing mHTT only in microglia, resulted in enhanced neuronal death compared to non-transgenic control mice (Crotti *et al.* 2014). This response was also observed *in vitro* when the addition of primary murine mHTT-expressing microglia to wild-type murine neuronal-astrocyte cultures increased neuronal apoptosis (Crotti *et al.* 2014). Inflammatory changes in mHTT-expressing host microglia have also been shown to cause specific striatal projection neuron toxicity in non-HD grafts in human patients (Cicchetti *et al.* 2009). These results suggest that mHTT-expressing microglia have the capacity to initiate and/or amplify neuroinflammation, and that this is enough to cause neurotoxicity, even in non-HD neurons.

Excessive proinflammatory cytokine release by microglia and peripheral myeloid cells have been demonstrated to contribute to neurotoxicity, and inhibition of IL-6 or TNFα, centrally or peripherally, has been shown to have beneficial therapeutic effects in HD (Bouchard *et al.* 2012; Hsiao *et al.* 2014). Chronic elevated proinflammatory cytokine release may also have direct impact on peripheral tissues, such as muscle and fat, leading to exacerbated symptoms of muscle wasting and weight loss in HD patients (van der Burg *et al.* 2009).

The presence of mHTT is also a trigger of oxidative stress (Crotti and Glass 2015). Aggregates of mHTT have been shown to cause generation of ROS and RNS in neuronal and non-neuronal cells, including myeloid cells (Wyttenbach *et al.* 2002; Hands *et al.* 2011), and this is possibly due to mHTT-induced defects in mitochondrial metabolism (Crotti and Glass 2015). HTT is an iron-regulated protein (Hilditch-Maguire *et al.* 2000) and mHTT inclusions are iron-dependent centres of oxidative stress (Firdaus *et al.* 2006). This has been proposed as a direct mechanism of neuronal injury, as well as an indirect mechanism via microgliosis; which has been demonstrated to be attenuated, along with neurodegeneration, in rat models of iron deprivation (Shoham and Youdim 2000). Conversely, iron supplementation to iron deprivation rats increased microgliosis and neuronal damage, demonstrating a tight relationship between iron and neurotoxic microgliosis (Shoham and Youdim 2000). Abnormal accumulation of iron has been observed in HD brains (van den Bogaard *et al.* 2013), and while iron is required for normal mitochondrial function, when it is in excess this can lead to uncontrollable generation of ROS (Crotti and Glass 2015). Oxidative stress can cause neurotoxicity in HD by damaging neuronal DNA, lipids and proteins (Barja 2004; Shirendeb *et al.* 2011). However, in addition to the excessive production of free radicals, over-expression of antioxidants, such as the glutathione peroxidases

peroxiredoxin 1 and peroxiredoxin 6, has also been observed in HD (Sorolla *et al.* 2008; Mason *et al.* 2013), and it is suggested that this is an adaptive response to restore the balance of ROS and RNS (Sorolla *et al.* 2008). Glutathione peroxidase activity has even been shown to be neuroprotective in HD mouse models (Mason *et al.* 2013). Ferritin, an iron storage protein with antioxidant properties, has been found to accumulate in mHTT aggregates in striatal microglia from R6/2 mice and in HD patient tissue, and ferritin accumulation increased with disease progression (Simmons *et al.* 2007). It is considered that ferritin accumulation may be a protective response to reduce the free iron pool and consequently reduce oxidative stress (Möller 2010; Crotti and Glass 2015).

While current evidence generally points to a neurotoxic role for immune cell activation and inflammation in HD (Andre *et al.* 2016), it is possible that myeloid cell phenotypes may shift throughout different stages of the disease course. For example, in early stages of disease, immune responses to neuronal damage may be protective and beneficial, but when neurodegeneration becomes extensive the inflammatory events may shift to become chronic, uncontrolled and neurotoxic. Surprisingly, however, a study looking at macrophage M1-M2 polarisation over the clinical disease course in HD, found pre-manifest and early-stage manifest HD patient macrophages to be predominantly of a proinflammatory M1 phenotype, and late-stage manifest HD patient macrophages displayed changes in the expression of surface markers in favour of an anti-inflammatory M2 phenotype (Di Pardo *et al.* 2013). This correlated with increased IL-12 and NFκB expression in pre-manifest HD macrophages and reduced levels of anti-inflammatory TGFβ1 in pre-manifest HD serum, all of which returned to normal levels along with an increase in IL-10-expressing macrophages in progressing symptomatic disease (Di Pardo *et al.* 2013). These findings suggest an active inflammatory state in pre-manifest and early-stage HD, which shifts to a more down-regulated, neuroprotective state in late-stage disease, possibly outlining tissue repairing attempts. The authors suggested a possible M1/M2 polarisation shift dysfunction in HD macrophages, mediated by aberrant NFκB pathway signalling which changes due to altered microenvironment signals over the disease course (Di Pardo *et al.* 2013).

Activated microglia are generally considered to be of a neurotoxic phenotype, however, microglial activation can also occur as a protective response to neuronal dysfunction and changes in the tissue microenvironment, and microglial provision of phagocytic clearance and trophic support could be beneficial during neurodegeneration (Andre *et al.* 2016). This has been demonstrated in HD brain slice cultures and a rodent HD cell culture model, where microglia became activated and proliferated in the vicinity of

degenerating neurites (Kraft *et al.* 2012). Co-culture of wild-type microglia with mHTT-expressing neurons also increased neuronal survival (Kraft *et al.* 2012). Activated microglia can therefore be neuroprotective, however cell-autonomous dysfunction caused by expression of mHTT in HD patient immune cells may reduce these protective functions (Heneka *et al.* 2014).

It has also been argued that microglial activation and neuroinflammation are simply reactive processes; responding to neurodegeneration but not contributing to it in either a beneficial or harmful capacity. For example, BACHD mice showed marked amelioration of disease with reduction of mHTT in cortical and striatal neurons, without affecting its expression in microglia (Wang *et al.* 2014a). The general consensus, however, is that cell-autonomous toxicity as well as cell-to-cell interactions, involving neurons, astrocytes and microglia, are necessary for the generation of striatal pathogenesis in HD (Gu *et al.* 2005; Gu *et al.* 2007; Bradford *et al.* 2009; Bradford *et al.* 2010; Möller 2010; Crotti and Glass 2015).

1.5 Therapeutic intervention in HD

1.5.1 Management of symptoms in HD

There are currently no curative treatments for HD, and no therapies which slow or delay disease progression (Mestre and Ferreira 2012; Pidgeon and Rickards 2013; Frank 2014; Killoran and Biglan 2014; Dayalu and Albin 2015). Pharmacological intervention aims at symptomatic relief (Pidgeon and Rickards 2013; Brett *et al.* 2014; Killoran and Biglan 2014; Dayalu and Albin 2015), and these treatments generally focus on the motor aspects of HD (Pidgeon and Rickards 2013; Frank 2014). For example, tetrabenazine, a dopamine-depleting agent and the only drug officially approved for the treatment of HD, is effective for reducing chorea (Mestre and Ferreira 2012; Pidgeon and Rickards 2013; Frank 2014; Killoran and Biglan 2014). However, the use of this agent carries a risk of potentially serious adverse effects, so some newer neuroleptic agents, such as olanzapine and aripiprazole, are often administered as alternatives due to their adequate efficacy for treating chorea and psychosis with a more favourable adverse effect profile (Frank 2014; Killoran and Biglan 2014). For the management of psychiatric disturbances, selective serotonin reuptake inhibitors and mood stabilizers are often used (Killoran and Biglan 2014). No known effective treatment is available for cognitive dysfunction in HD (Killoran and Biglan 2014).

Overall, the evidence base for the pharmacological management of HD is poor, with only tetrabenazine showing any clinically meaningful effect on chorea and few clinical studies focussing on pharmacotherapy for non-motor symptoms of HD (Pidgeon and

Rickards 2013). There is some evidence for the usefulness of physical therapy, occupational therapy and speech therapy, but such non-drug treatments are still limited in improving quality of life (Walker 2007). This highlights a significant need for high quality clinical trials and clinical research efforts with the aim of finding effective and safe treatments for motor, cognitive and neuropsychiatric symptoms of HD (Mestre and Ferreira 2012; Pidgeon and Rickards 2013).

1.5.2 Current therapeutic strategies under investigation for treatment of HD

In addition to ongoing clinical research into the treatment of symptoms in HD, multiple therapeutic strategies are currently under investigation with the aim of preventing/delaying disease onset and/or slowing disease progression. These potential therapies target a variety of biological aspects of this complex disease.

Pharmacological approaches include administration of BDNF (Giampà *et al.* 2013) or dopamine stabilisers (Huntington Study Group HART Investigators 2013) to preserve remaining neural activity; cannabinoids which have anti-inflammatory, neuroprotective and neuroregenerative properties (Sagredo *et al.* 2012); KMO inhibitors to tip the balance of kynurenine pathway metabolites in the favour of neuroprotective KYNA production and away from neurotoxic 3-HK and QA production (Zwilling *et al.* 2011); phosphodiesterase (PDE) inhibitors targeting transcriptional dysregulation within the cyclic adenosine monophosphate (cAMP) and cAMP response element binding (CREB) signalling cascades in striatal neurons, and restoring synaptic function (DeMarch *et al.* 2008; Giampà *et al.* 2010); HDAC inhibitors which alter gene transcription and aberrant post-translational modifications of mHTT (Gray 2011); non-allele specific RNA inhibitors (RNAi) (Manth *et al.* 2012) and antisense oligonucleotides (ASOs) (Lu and Yang 2012) to knock down expression of *HTT*; and allele-specific silencers which target single nucleotide polymorphisms (SNPs) in the mutant gene (Kay *et al.* 2014).

Surgical approaches, which have already been shown to have some benefit in other neurodegenerative diseases, such as PD, involve the neurotransplantation of neural and mesenchymal stem cells in an attempt to replace neurons that have already succumbed to disease pathology and provide trophic support for remaining cells (Lescaudron *et al.* 2012; Maucksch *et al.* 2013; Kerkis *et al.* 2015). Pre-implantation genetic engineering of stem cells to over-express BDNF may also serve as a useful CNS delivery method for this neurotrophin (Pollock *et al.* 2016). Recent advances in induced pluripotent stem cell (iPSC) technology, in combination with emerging specific RNAi and ASO gene therapies to silence the *mHTT* gene, highlight potential for patient-specific cell replacement therapy which would provide a readily obtainable

source of graft material which can be differentiated into specific neuronal populations, and eliminate problems of immunological rejection (Liu *et al.* 2016).

1.5.3 Potential therapies targeting the immune system in HD

Numerous reports have described dysfunction of the innate immune system in HD, and an active role in neuropathology has been clearly demonstrated in HD mouse models and HD patients. Consequently, novel therapeutic approaches targeting immune cells and inflammation are under investigation for the treatment of HD.

The first attempt to reduce neuronal damage by immunomodulation in HD was the use of minocycline (Ellrichmann *et al.* 2013). Minocycline displays high tolerance and excellent bioavailability to the brain and has been clinically tested for several disorders of the CNS, including ALS and PD, due to its widespread neuroprotective and anti-inflammatory actions (Soulet and Cicchetti 2011). Minocycline is a caspase inhibitor, known to suppress microglial activation and IL-1β, TNFα and iNOS production, and has been demonstrated to significantly delay disease progression and mortality in the R6/2 mouse model (Chen *et al*. 2000). In a small study, the drug was also shown to be safe and well tolerated in HD patients (Thomas *et al.* 2004), however the primary endpoint of a 25 % improvement in TFC score was not met in a subsequent futility study (Huntington Study Group DOMINO Investigators 2010).

Taking a more general anti-inflammatory approach, treatments with two NSAID cyclooxygenase-2 (COX-2) inhibitors, acetylsalicylate and rofecoxib, already in widespread human use for the treatment of inflammation and pain, were analysed. Both drugs were administered to transgenic HD mouse models from weaning, at doses comparable to those tolerated in humans, but had no beneficial effects on weight loss, behavioural changes, or gross cerebral and striatal atrophy (Norflus *et al.* 2004).

More recently, the fumaric acid ester, dimethylfumarate, an immunomodulator approved for the treatment of relapsing-remitting multiple sclerosis (MS) (Tecfidera, Biogen), has been shown to have beneficial effects on neuronal degeneration, motor functions, weight loss and length of survival in R6/2 and YAC128 mouse models (Ellrichmann *et al.* 2011). Dimethylfumarate has pronounced effects on macrophages (Schilling *et al.* 2006) and potentially exerts neuroprotective effects via induction of nuclear factor E2-related factor 2 (Nrf2), a transcription factor which activates detoxification pathways and subsequently protects against oxidative damage and free radicals triggered by inflammation (Ellrichmann *et al.* 2011; Linker *et al.* 2011).

A more specific anti-cytokine approach also holds potential for reducing inflammation and modifying disease progression in HD. Administration of an IL-6 neutralising

antibody to R6/2 mice partially rescued motor deficits and prevented weight loss (Bouchard *et al.* 2012). Inhibition of TNFα, another proinflammatory cytokine which is elevated in HD, has also been demonstrated to have therapeutic effect in HD mouse models. Intracerebroventricular infusion of XPro1595, a dominant negative inhibitor of soluble TNFα, decreased elevated levels of TNFα in the cortex and striatum, improved motor function, reduced caspase activation, diminished the amount of mHTT aggregates, increased neuronal density and decreased gliosis in brains of R6/2 mice (Hsiao *et al.* 2014). Systemic injection of XPro1595 reduced the peripheral inflammatory response and improved motor function in R6/2 mice (Hsiao *et al.* 2014).

Modulation of the kynurenine pathway in peripheral immune cells has also been shown to have potential as a therapeutic target in HD. Oral administration of JM6, a peripherally-restricted small-molecule prodrug inhibitor of KMO, into R6/2 mice, inhibited KMO (which is expressed at high levels in peripheral immune cells such as macrophages (Heyes *et al.* 1992)) in the blood, and increased KYNA levels and reduced extracellular glutamate in the brain (Zwilling *et al.* 2011). This was associated with extended life span, reduced loss of synapses and a decrease in abnormal microglial activation (Zwilling *et al.* 2011). It is thought that KYNA is neuroprotective by reducing glutamate receptor-mediated excitotoxicity and free radical formation (Zwilling *et al.* 2011). The Cure Huntington's Disease Initiative (CHDI) foundation have recently developed a novel peripherally-acting KMO inhibitor, CHDI-340246, that may increase the levels of kynurenine and KYNA in the brains of rodent HD models and in the CSF of non-human primates (Mrzljak 2013).

Signalling through the CB_2 receptor dampens immune activation, and administration of the CB_2 receptor agonist, GW405833, has been demonstrated to ameliorate motor deficits, synapse loss, and CNS inflammation, and prolong survival in the BACHD mouse model (Bouchard *et al.* 2012). Co-administration with a peripherally-restricted CB_2 antagonist reversed these beneficial effects (Bouchard *et al.* 2012), suggesting that GW405833 acts peripherally, and providing further evidence for peripheral immunomodulation as a viable therapeutic target in the treatment of HD.

Thus far, while anti-inflammatory strategies for the treatment of HD have shown potential at pre-clinical stages of research, few have led to meaningful benefits in patients (Soulet and Cicchetti 2011). A possible reason for this is that a general suppression of immune responses inhibits the beneficial roles of the immune system as well as the detrimental roles. Complex communication between neurons and immune cells in the degenerating brain include reparative and neuroprotective interactions, and these processes may need to be maintained or enhanced while damaging interactions

are inhibited. A specific immunomodulatory approach aiming to promote neuroprotective roles of the immune system while inhibiting its deleterious features, rather than a general anti-inflammatory approach, may therefore have more therapeutic value for the treatment of HD.

1.5.4 Novel immunomodulatory drug laquinimod

Laquinimod (Figure 1.10) is a novel orally-active immunomodulatory drug that has been shown to downregulate immune cell activation and inflammation in the CNS (Brück *et al.* 2012; Mishra *et al.* 2014) and periphery (Yang *et al.* 2004; Schulze-Topphoff *et al.* 2012). The drug has already been studied in human immunomodulation and has been shown to affect neuropathological processes. Laquinimod was demonstrated to be safe and well-tolerated in humans, as well as having beneficial effects on inflammation, brain atrophy and disease progression in two Phase III clinical trials for the treatment of MS (Comi *et al.* 2012; Filippi *et al.* 2014; Vollmer *et al.* 2014). Inflammation has been implicated in myelin, axonal and neuronal loss in MS pathology, and the same is true for HD (Ellrichmann *et al.* 2013). It is therefore plausible that laquinimod could slow brain atrophy rate and disease progression in HD through central and peripheral immunomodulatory mechanisms, as it has been shown to do in MS.

Laquinimod

2D structure:

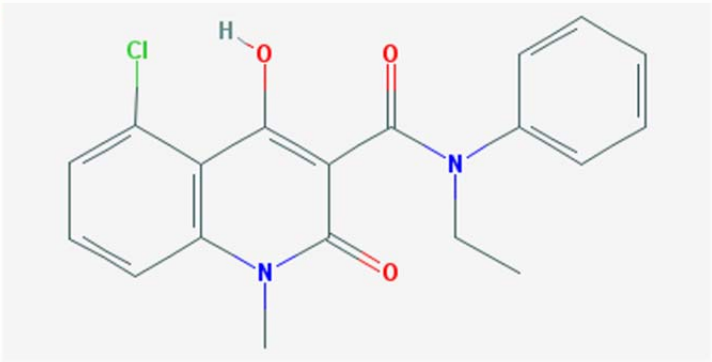

Chemical name: 5-CHLORO-N-ETHYL-4-HYDROXY-1-METHYL-2-OXO-N-PHENYL-1,2-DIHYDROQUINOLINE-3-CARBOXAMIDE
Molecular formula: $C_{19}H_{17}ClN_2O_3$
Molecular weight: 356.806 g/mol

Figure 1.10: Compound summary for laquinimod

Chemical structure, chemical name, molecular formula and molecular weight for novel orally-active immunomodulatory drug laquinimod (National Center for Biotechnology Information; PubChem Compound Database; CID=54677946, https://pubchem.ncbi.nlm.nih.gov/compound/54677946; accessed Apr. 9, 2017).

In cuprizone-treated mice (a model of MS), laquinimod administration reduced the proportion of astrocytes with nuclear NFκB (p65/RelA) immune-reactivity (Brück *et al.*

2012), and in *ex vivo* cultures of adult human microglia, laquinimod treatment decreased cytokine release in response to LPS stimulation (Mishra *et al.* 2014). In mice with induced experimental autoimmune encephalomyelitis (EAE), laquinimod markedly reduced demyelination, axonal damage and inflammation within the brain by suppressing T cell recruitment (Wegner *et al.* 2010). It may also restore BDNF levels (Aharoni *et al.* 2012). In the periphery, laquinimod has been shown to induce an immunomodulatory shift in immune cell phenotypes away from M1/Th1-type responses and towards M2/Th2-type responses. Primary cultures of human PBMCs released lower levels of IL-17, IL-3 and G-CSF following laquinimod treatment (Brück and Wegner 2011). Mononuclear cells isolated from the spleen of a laquinimod-treated MS rat model displayed evidence of a shift from proinflammatory Th1-type to anti-inflammatory and regulatory Th2-type cytokine expression profiles, with a laquinimod-induced change in favour of Th2-type cytokines IL-4, IL-10 and TGFβ and reductions in the Th1-type cytokines TNFα and IL-12 (Yang *et al.* 2004). Laquinimod has also been shown to promote splenic development of M2-polarised monocytes and dendritic cells in mice, leading to reduced cellular production of Th1-type cytokines IL-6, IL-12 and TNFα and a corresponding increase in production of anti-inflammatory Th2-type cytokine IL-10 (Schulze-Topphoff *et al.* 2012). As an immunomodulatory drug, rather than an anti-inflammatory drug, laquinimod may therefore have the potential to promote reparative and neuroprotective inflammatory phenotypes in immune cells whilst suppressing proinflammatory and neurotoxic phenotypes.

The immunomodulatory effects of laquinimod in the periphery and CNS have recently been found to be mediated via induction of the aryl hydrocarbon receptor (AhR) (Berg *et al.* 2016; Kaye *et al.* 2016; Birnberg *et al.* 2017). The AhR pathway modulates the differentiation and function of several cell populations, many of which play an important role in neuroinflammation (Kaye *et al.* 2016). Laquinimod can bind and activate the AhR leading to downstream gene transcription (Berg *et al.* 2016; Kaye *et al.* 2016), and while laquinimod treatment has been shown to have a pronounced effect on clinical symptoms, CNS inflammation, leukocyte infiltration and demyelination in EAE-afflicted wild-type mice, these effects were abolished in AhR-deficient mice (Berg *et al.* 2016; Kaye *et al.* 2016). Interestingly, laquinimod treatment resulted in increased BDNF production associated with neuroprotection in AhR-deficient mice (Berg *et al.* 2016), suggesting that the immunomodulatory effects of laquinimod occur by different mechanisms than the neuroprotective effects in EAE.

In addition to the AhR pathway, laquinimod has also been shown to modulate multiple genes within the NFκB pathway, including the downregulation of proinflammatory monocyte genes (Birnberg *et al.* 2017). In a high-throughput gene expression study

using DNA microarrays, laquinimod-treated human PBMC cultures were revealed to express increased IκB whilst downstream NFκB genes were decreased (Gurevich *et al.* 2010). Imaging flow cytometry (IFC) experiments have also shown laquinimod-induced reduction of p65 translocation in primary murine astrocytes (Brück *et al.* 2012). IκB degradation is increased and NFκB translocation enhanced and prolonged in HD patient myeloid cells in response to stimulation (Träger *et al.* 2014a), and it is plausible that laquinimod could rescue this dysfunctional hyper-reactive phenotype and dampen the consequential elevated production of proinflammatory cytokines by these cells (Björkqvist *et al.* 2008). Laquinimod may also suppress another proinflammatory signalling pathway by reducing phosphorylation and activation of the MAPKs p38 and JNK (Mishra *et al.* 2012).

While laquinimod has been shown to have both peripheral and central affects, when orally-administered the drug is quickly absorbed into the blood stream from where only a small percentage (7-8 %) crosses the BBB and penetrates the CNS. It is therefore likely that laquinimod acts primarily on peripheral immune cells. Intervention of peripheral inflammatory events has previously been shown to modulate central neuropathology and disease progression in HD (Zwilling *et al.* 2011; Bouchard *et al.* 2012; Kwan *et al.* 2012a), therefore laquinimod has potential for slowing disease progression in HD patients by affecting peripheral immune cells. Indeed, laquinimod is currently under investigation for its potential effects in HD and a Phase II clinical trial (LEGATO-HD) aimed at evaluating the efficacy, safety and tolerability of laquinimod as a treatment in patients with HD is in progress (Teva Pharmaceutical Industries 2016).

1.6 Thesis aims

1.6.1 General research goals

The overarching goal was to investigate the physiological and pathophysiological roles of inflammatory processes in HD. Aims were to examine neuroprotective and neurotoxic interactions between myeloid cells and neurons in HD, and to determine whether dysfunctional hyper-reactive and proinflammatory phenotypes in HD myeloid cells may be rescued by novel immunomodulatory drug, laquinimod.

1.6.2 Specific aims

1) Develop and characterise novel human neuronal-myeloid cell co-culture models of HD using three main experimental approaches:
    i. Develop and characterise novel human neural stem cell-derived neuronal cell models expressing human *HTT* exon 1 or full-length human *HTT* with varying CAG repeat lengths in the pathogenic and non-pathogenic range.

ii. Develop and characterise a novel primary human blood monocyte-derived microglia cell model, differentiated *in vitro* from *ex vivo* primary monocyte cultures (taken from healthy volunteers, pre-manifest HD gene carriers and manifest HD patients), using a novel technique.

iii. Develop and characterise control and HD co-culture paradigms with neuronal cell lines, blood monocyte-derived macrophages and blood monocyte-derived microglia.

2) Investigate neuronal-myeloid cell interactions in HD co-culture models

i. Determine the effects of resting or activated (by acute or chronic stimulation) healthy volunteer and HD patient myeloid cells on wild-type and HD neuronal survival.

ii. Analyse M1/Th1- and M2/Th2-type cytokines and neurotrophin production by healthy volunteer and HD patient myeloid cells and assess differential effects on wild-type and HD neurons in co-culture.

3) Investigate the effects of laquinimod on rescuing hyper-reactive immune cell dysfunction in HD patient myeloid cells.

i. Analyse M1/Th1- and M2/Th2-type cytokine production in untreated and laquinimod-treated healthy volunteer and HD patient monocytes.

ii. Investigate modulation of the NFκB pathway as a potential mechanism of action for laquinimod in HD patient myeloid cells.

2 Materials and methods

All materials and reagents were purchased from Sigma unless otherwise stated. Non-sterile ultra-pure deionised distilled water (ddH_2O) was obtained using a Milli-Q ultrapure water purification system (18 MΩ·cm resistivity at 25 °C) [Merck Millipore].

2.1 Cell culture

All cell cultures were maintained in Heracell 150i incubators [Thermo Scientific] at 37 °C; 5 % CO_2. Unless otherwise stated, all culture media and reagents were warmed to 37 °C prior to use, in a digitally-controlled stable temperature water bath [Grant] designated for tissue culture. All cell culture procedures, including those involving work with viruses, were performed in Containment Level II Safety Cabinets in a designated tissue culture facility, and aseptic practices were followed in order to maintain sterile conditions and adhere to safety protocols. All work involving whole blood samples was carried out in a tissue culture facility specifically designated for handling human blood. Non-primary cells were subject to routine mycoplasma screening using LookOut Mycoplasma PCR Detection Kit. All biological material waste, including cells and viruses, was decontaminated in Virkon disinfectant for at least 2 h prior to disposal; other than waste from human primary cell culture which was decontaminated in 2 M sodium hydroxide for a minimum of 2 h, in accordance with safe disposal guidelines.

2.1.1 Cell lines

2.1.1.1 HEK293T, Phoenix-AMPHO and HeLa

Human embryonic kidney cell line 293, containing the SV40 T antigen (HEK293T) and the second-generation Phoenix amphotropic cell line (Phoenix-AMPHO) based on HEK293T, were used for packaging lentiviral and retroviral plasmids, respectively. HEK293T were additionally used to test and titrate lentiviruses expressing *HTT* exon 1. Both cell lines were kind gifts from Prof. Parmjit S. Jat (Medical Research Council (MRC) Prion Unit, Institute of Neurology (IoN), London, UK). The HeLa cell line was derived from human cervical adenocarcinoma cells. The line was a kind gift from Dr Adrian M Isaacs (University College London (UCL) IoN, London, UK) and was used to test and titrate retroviruses expressing full-length *HTT*.

These cell lines were cultured in sterile Nunclon cell culture-treated polystyrene flasks [Nunc] and maintained in DMEM/FBS culture medium (Appendix I-i) in the incubator.

Medium was changed 2-3 times per week, and once the cells reached 70-80 % confluence they were passaged into fresh culture flasks. To passage, medium was removed with a serological pipette [Corning] and cells were washed in Dulbecco's Phosphate-Buffered Saline (DPBS) [Life Technologies]. Enough Trypzean-Ethylenediaminetetraacetic acid (EDTA) [Lonza] was added to the cells to just cover the culture surface and cells were incubated at 37 °C; 5 % CO_2 for 5 min. Fresh culture medium was then added to inhibit further trypsinisation, and then cells were triturated from the culture surface and collected into a 15 mL Falcon tube [BD Falcon] using a serological pipette. Cells were pelleted out of solution by centrifugation at 300 × *g* for 5 minutes (min) at room temperature (RT) and re-suspended in fresh DMEM/FBS culture medium. Cells were counted using a haemocytometer and seeded at a minimum density of 1.4×10^4 cells/cm^2 in fresh culture flasks. Cells were then returned to the incubator.

When HEK293T or Phoenix-AMPHO cells were used for viral packaging, they were thawed from cryopreserved stocks which had undergone less than ten passages, and were expanded for only one passage in culture before use.

2.1.1.2 N2a_R2

Neuro-2a (N2a) is a murine neuroblastoma cell line of which R2 is a sub-clone made by, and a kind gift from, Dr. Peter C. Klöhn (MRC Prion Unit, IoN, London, UK). N2a_R2 cells were received as cryopreserved stocks at their third passage post-sub-cloning. Once thawed, the cell line was used in experiments between one and three subsequent passages in culture. N2a_R2 were cultured in sterile Nunclon cell culture-treated polystyrene flasks and maintained in OptiMEM/FBS culture medium (Appendix I-ii) in the incubator. Medium was changed every 3-4 days and once cells reached 80-90 % confluence, they were passaged into fresh culture flasks. To passage, medium was removed and cells were gently washed in DPBS. Culture medium was added to the flask and cells were triturated from the culture surface using a serological pipette. The cell suspension was then added to fresh culture flasks containing pre-warmed medium, at a split of 1:10-1:7 densities. Cells were then returned to the incubator.

2.1.1.3 ReNcell VM NSC culture

The ReNcell VM neural stem cell (NSC) line was a kind gift from ReNeuron (Guilford, UK). ReNcell VM was derived from 10-week-old human foetal ventral mesencephalon immortalised by retroviral transduction with a *v*-myc oncogene and expanded long-term as undifferentiated NSCs. ReNcell VM can be routinely cultured in their replicating form, and stable karyotype has been confirmed for up to a minimum of 80 passages (ReNeuron). NSCs can be spontaneously differentiated into pan-neuronal cultures, and

some astrocytes, upon removal of the growth factors epidermal growth factor (EGF) and basic fibroblast growth factor (bFGF) from the culture medium (Donato *et al.* 2007). The NSCs were received as cryopreserved stocks at their seventeenth passage, and once thawed they were used in experiments between one and ten passages in culture.

NSCs were plated in sterile laminin-coated Nunclon cell culture-treated polystyrene flasks. To laminin-coat, 10 µg/mL cold mouse laminin-1 PathClear [Trevigen] in cold DMEM: Nutrient Mixture F-12 (DMEM:F-12) [Life Technologies] was added to culture flasks at approx.130 µL/cm^2 and incubated at 37 °C; 5 % CO_2 for at least 2 hours (h). Before seeding NSCs, the laminin solution was removed and laminin-coated surfaces were washed in pre-warmed DMEM:F-12. For experiments, NSCs were seeded in a sterile laminin-coated 4-well, 6-well, 24-well or 96-well Nunclon cell culture-treated MultiDish [Nunc] at 5 × 10^4 cells/cm^2. In some cases, NSCs were seeded onto sterile laminin-coated 13 mm diameter round glass coverslips [VWR International] at a density of 1 × 10^5 cells/coverslip. Coverslips were sterilised by baking in an electric oven at 200 °C for 6 h. To laminin-coat, sterile coverslips were placed in a 4-well or 24-well cell culture dish and 200 µL 20 µg/mL cold mouse laminin-1 PathClear in 20 mM cold Tris-HCl [Sigma], pH 7, was pipetted onto each coverslip. The culture dish was then placed in the incubator for at least 24 h. Before seeding NSCs, the laminin solution was removed and laminin-coated surfaces were washed in pre-warmed DMEM:F-12.

NSCs were maintained in ReN/NSC culture medium (Appendix I-iii) with fresh media changes every 3-4 days, and were passaged on reaching 80-90 % confluence. To passage, medium was removed and cells were washed with Hank's Balanced Salt Solution (HBSS) [Life Technologies]. Enough Trypzean-EDTA was added to the cells to just cover the culture surface and cells were incubated at 37 °C; 5 % CO_2 for 5 min until cells had detached from the flask. Trypsinisation was inhibited by the addition of Defined Trypsin Inhibitor (DTI) solution [Life Technologies] at equal volume to Trypzean-EDTA, and then cells were triturated and collected into a 15 mL Falcon tube using a serological pipette. NSCs were pelleted out of solution by centrifugation at 300 × *g* for 5 min at RT, and re-suspended in fresh ReN/NSC culture medium. Cells were counted using a haemocytometer and then plated as a monolayer in laminin-coated culture flasks at a density of 1.4 × 10^4 cells/cm^2. Cells were then returned to the incubator.

2.1.1.4 Cryopreservation and revival of cell lines

Once cultures reached 80-90 % confluence, cells were collected from the culture flask as described above for the relevant cell line. Viable cells were counted by Trypan Blue exclusion (section 2.6.4) using a haemocytometer. Cultures with greater than 95 % cell

viability were taken forward for cryopreservation. Cells were pelleted out of solution by centrifugation, re-suspended in relevant culture medium supplemented with 8 % dimethyl sulfoxide (DMSO), to a density of 3 × 10^6 viable cells/mL, and aliquoted into 1.6 mL cryovials [Nunc] at 1 mL per vial. Cryovials were then placed into a Mr Frosty Freezing Container [Thermo Scientific] and frozen to −80 °C. The following day, cryovials were placed in a liquid nitrogen tank under vapour-phase nitrogen for long-term storage.

To revive cell lines under cryopreservation, cryovials were taken from liquid nitrogen storage and immediately placed in a 37 °C water bath for rapid thawing. Cells were then quickly added to 10 mL pre-warmed relevant culture medium in a 15 mL Falcon tube and pelleted by centrifugation at 300 × *g* for 5 min at RT. Cells were re-suspended in 15 mL relevant culture medium and plated in 75 cm^2 culture flasks. ReNcell VM NSCs were an exception, as they were added directly to laminin-coated culture flasks containing pre-warmed culture medium, immediately following rapid thaw and without undergoing centrifugation. This was due to the fragility of this cell line and vulnerability to lysis by centrifugation during revival. The following day, all cultures were given a fresh media change and thereafter received media changes every 2-3 days until they were ready to passage.

2.1.2 Primary human cell cultures

All human experiments were performed in accordance with the Declaration of Helsinki and approved by UCL/UCL Hospitals Joint Research Ethics Committee. All blood donors provided informed written consent for research on Huntington's disease.

2.1.2.1 Classification of human samples

Blood samples were collected from healthy volunteers, pre-manifest HD gene carriers and manifest HD patients, who were recruited from the HD clinic at the National Hospital for Neurology and Neurosurgery (NHNN), London, UK. Healthy volunteers were generally spouses, partners and/or carers of HD patients. Pre-manifest HD were genetically diagnosed patients with a diagnostic confidence level (DCL) of less than 4 on the standardised motor exam of the Unified Huntington's Disease Rating Scale (UHDRS). Manifest HD were genetically diagnosed patients with early or moderate stage disease and a DCL of 4 with unequivocal extrapyramidal motor signs consistent with HD. Donors with inflammatory or infectious conditions, and/or taking anti-inflammatory or immunomodulating medication were excluded. Samples were collected from both males and females, and average age and age range of participants were matched as much as possible between groups for each experiment. Each blood sample collected was designated an anonymised five-digit number for blinded analysis.

2.1.2.2 Isolation of primary human monocytes from whole blood

Whole blood samples were collected from donors and decanted into 50 mL heparinised tubes (50 µL prescription grade heparin [CP Pharmaceuticals] in standard 50 mL Falcon tubes). Twenty-five millilitres whole blood was then carefully layered onto 20 mL Histopaque-1077. Histopaque-1077 is a solution of polysucrose and sodium diatrizoate, adjusted to a density of 1.077 g/mL. It is designed to facilitate recovery of viable peripheral blood mononuclear cells (PBMCs) from small volumes of whole blood. Whole blood was separated through the Histopaque-1077 gradient by centrifugation in a swinging bucket rotor at 400 × *g* for 30 min at RT with no brake. Erythrocytes are aggregated by polysucrose and rapidly sediment, and granulocytes become slightly hypertonic, increasing their sedimentation rate, resulting in pelleting of erythrocytes and granulocytes at the bottom of the centrifuge tube. PBMCs remain at the plasma/Histopaque-1077 interface and were isolated by removal with a Pasteur pipette. PBMCs were washed in magnetic-activated cell sorting (MACS) buffer (Appendix II-i) and pelleted out of wash solution by centrifugation at 350 × *g* for 10 min at 4 °C. Cells were re-suspended in 1 mL MACS buffer and 60 µL anti-CD14 MACS MicroBeads [Miltenyi Biotec] were added to the suspension. The MicroBeads are highly specific antibodies directed at the CD14 antigen, a plasma membrane receptor expressed by monocytes, conjugated to 50 nm superparamagnetic particles. The MicroBeads were mixed with PBMCs by quick vortex and the mixture was incubated for 15 min at 4 °C. Cells were then pelleted by centrifugation at 350 × *g* for 5 min at 4 °C, and re-suspended in fresh MACS buffer before being applied to MACS columns [Miltenyi Biotec] mounted on a magnetic separator [Miltenyi Biotec]. MACS columns contain a matrix composed of ferromagnetic spheres, and when placed on a magnetic separator, they amplify the magnetic field by 10,000-fold, inducing a high gradient within the column. PBMCs run slowly through the column, and magnetically labelled $CD14^+$ monocytes are held in suspension within the column, while unlabelled cells drip through and were discarded. Magnetically-isolated CD14+ monocytes were plunged out of the column into a separate collection tube, washed in DPBS by suspension and centrifugation, and re-suspended in RPMI/FBS culture medium (Appendix I-iv).

2.1.2.3 Ex vivo culture of primary human monocytes

A total cell count was made before seeding monocytes into 6-well or 24-well Primaria culture dishes [BD Falcon] at a density of 2.5×10^5 cells/cm^2 and placing them in the incubator. For some experiments, monocytes were seeded onto sterile poly-D-lysine (PDL)-coated coverslips at a density of 1×10^5 cells/coverslip. Coverslips were sterilised using 100 % ethanol and were allowed to air-dry before placing into a 4-well or 24-well cell culture dish. To PDL-coat, 200 µL 0.1 mg/mL PDL in sterile tissue

culture grade distilled water [Life Technologies] was pipetted onto each coverslip and incubated for 5 min at RT. PDL solution was then removed and coverslips were thoroughly washed in sterile distilled water before being allowed to air-dry for at least two hours. If monocytes were differentiated *in vitro* the PDL-coating step was skipped, as following differentiation steps, the cells much better adhere to glass. Pre-testing using fluorescence-activated cell sorting (FACS) analysis has shown the purity of cultures described here to be at least 95 % $CD14^+$ monocytes (Björkqvist *et al.* 2008), and they were used in experiments up to 4 days *in vitro* (DIV).

2.1.2.4 Differentiation of human blood monocyte-derived (BMD) macrophages in vitro

Ex vivo human monocyte cultures were prepared as described above (section 2.1.2.2) with the addition of 20 ng/mL GM-CSF to RPMI/FBS culture medium on seeding. Cells were given a complete medium change with addition of fresh GM-CSF at 3 DIV, and returned to the incubator. These cells have previously been confirmed by factor analysis to be fully differentiated macrophages at 6 DIV, and were used in experiments 6-10 DIV.

2.1.2.5 Differentiation of human BMD-microglia in vitro

Primary human macrophage cultures were prepared as described above (section 2.1.2.4). At 7 DIV, macrophages were given a complete medium change into neuronal medium (NM) (Appendix I-v) and returned to the incubator for a further 4 days. At 11 DIV, cells displayed morphological and phenotypic characteristics of primary human microglia, as is shown later in this Thesis (sections 3.5.4.2 and 3.5.4.3), and were used in experiments at this stage.

2.1.2.6 Stimulation of human myeloid cells

Unless stated otherwise, where primary human myeloid cells (monocytes, BMD-macrophages and BMD-microglia) are described as “stimulated” in this Thesis, cells were given a media change with the addition of 2 µg/mL LPS and 10 ng/mL IFNγ [R&D Systems]. In “acute stimulation” paradigms cells were given a pulse stimulation for 1 h followed by a fresh media change, and in “chronic stimulation” paradigms cells were stimulated continuously for 24 or 48 h. Myeloid cells described as “non-stimulated” were given the same media changes without the addition of LPS and IFNγ. In the investigation into the effects of laquinimod on rescuing hyperactive immune cell dysfunction in HD patient myeloid cells (Chapter 5), myeloid cells were stimulated with 1 µg/mL LPS and 10 ng/mL IFNγ for 24 h. Due to potential batch-to-batch variability in the potency and content of LPS, myeloid cells were stimulated with LPS from the same source and batch (Sigma, L6529, *E. coli* 055:B5) across all experiments.

2.1.3 ReNcell VM neuronal differentiation

2.1.3.1 Spontaneous differentiation of ReNcell VM NSCs into neuronal cultures

ReNcell VM NSCs can be spontaneously differentiated into mature neuronal cultures by removal of EGF and bFGF from the ReN/NSC culture medium (Neuronal medium (NM); Appendix I-v). Mature neuronal cultures also contained some glial cells, including astrocytes. ReNcell VM NSCs were seeded in sterile laminin-coated culture flasks, as described above (section 2.1.1.3), at a higher density of 5×10^5 cell/cm^2. NSCs, which had undergone less than ten passages post-thawing, were maintained in ReN/NSC culture medium until reaching 90-100 % confluence (1-2 days), when they were given a complete media change into NM and returned to the incubator. Differentiating cultures were given fresh media changes every 4-5 days and were used at various stages of differentiation (days differentiation, DD), depending on the experiment.

2.1.3.2 Induced differentiation of ReNcell VM NSCs into neuronal cultures

In some cases, an alternative protocol was used to differentiate ReNcell VM NSCs, with the aim of achieving a higher neuronal yield and fewer glial cells in the mature cultures. The following optimised protocol was adapted from Donato *et al*. (2007). Following standard NSC passage, as described above (section 2.1.1.3), cells which had undergone less than ten passages post-thawing were cultured as neurospheres by seeding in non-laminin-coated culture flasks in standard ReN/NSC culture medium at a density of 3×10^4 cells/cm^2. NSCs were then returned to the incubator and allowed to form neurospheres over 5-7 days. Once neurospheres had formed, they were pelleted out of culture medium by centrifugation at 300 × *g* for 5 min at RT, washed in DPBS, and disaggregated by incubation in Trypzean-EDTA for 15 min at 37 °C. Trypsinisation was then inhibited by 1:1 addition of DTI, and cells were pelleted out of solution by centrifugation at 300 × *g* for 5 min at RT. Cells were re-suspended in ReN/NSC culture medium, seeded in laminin-coated culture flasks at a density of 5×10^4 cells/cm^2 and returned to the incubator. Once cells reached 90-100 % confluence (1-2 days post-seeding), they were given a complete medium change into NM supplemented with dibutyryl-cAMP (db-cAMP) and glial-derived neurotrophic factor (GDNF) (NM/cAMP/GDNF; Appendix I-vi), and returned to the incubator. Differentiating cultures were given fresh media changes in supplemented NM every 4-5 days for the first 2 weeks, and in standard NM (Appendix I-v) thereafter, and used in characterisation experiments from 10-25 DD.

2.1.4 Co-culture

2.1.4.1 Preparation of conditioned media and myeloid cell lysates

Primary human myeloid cells were cultured in 24-well plates and treated in 1 mL relevant culture medium per well, in accordance with the relevant experiment. Whole culture medium was harvested per well; monocyte-conditioned medium (MC-CM), macrophage-conditioned medium (Mφ-CM) or microglia-conditioned medium (MG-CM). Conditioned medium was transferred from culture wells to 0.5 mL microcentrifuge tubes [Eppendorf] using a 1000 µL pipette [Gilson], centrifuged at 400 × *g* for 5 minutes to deposit out any remaining cells, supernatant passed through a 0.22 µL cellulose acetate sterile syringe filter [Triple Red] to remove cell debris and any other potential contaminants, and aliquoted into separate fresh microcentrifuge tubes. Conditioned medium was then snap frozen in a dry ice/ethanol cooling bath and stored at −80 °C.

For some experiments, analysis results for conditioned medium content were normalised to total protein. Therefore, upon removal of conditioned medium from a culture, cell lysates were prepared by adding 100 µL 4 °C radioimmunoprecipitation assay (RIPA) buffer (Appendix II-ii) directly to each well. Culture plates were then incubated at 4 °C for 15 min on a shaking platform set to 400 revolutions per minute (rpm). Cell lysates were homogenised by pipetting, collected into separate 0.5 mL microcentrifuge tubes and stored at −80 °C.

This process was repeated on a routine basis as blood sample donations became available bi-monthly through the HD clinic, and was continued until relevant sample sizes had been processed and stored. Generally, 5-6 samples were processed at a time, with at least one sample per subject group processed together.

2.1.4.2 Co-culture by conditioned media transfer

ReNcell VM NSCs were seeded at 2 × 10^4 cells/well in sterile laminin-coated cell culture-treated Nunc MicroWell 96-well Microplates, and differentiated into mature neuronal cultures as described above (section 2.1.4.1). When neuronal cultures reached 10 or 25 DD, Mφ-CM or MG-CM was thawed slowly on ice and gradually warmed to 37 °C. Culture medium was removed from neuronal cultures and replaced with 100 µL Mφ-CM or MG-CM per well, in triplicate. Control wells were cultured in 100 µL fresh non-conditioned NM, and Mφ-CM transfer co-culture experiments also had additional control wells cultured in 100 µL RPMI/FBS culture medium. Neuronal cultures were then returned to the incubator and maintained in conditioned media treatments for 24 h. All conditioned medium related to the same experiment was used to treat neuronal cultures at the same time.

2.1.4.3 Co-culture by medium shared concurrently

Monocytes were cultured on 13 mm diameter glass coverslips in 24-well cell culture dishes and differentiated into macrophages until 5 DIV. ReNcell VM NSCs were cultured on coverslips in 24-well cell culture dishes and differentiated into 11 DD mature neuronal cultures by spontaneous differentiation. One coverslip of each cell type was then transferred into a 10 cm diameter sterile cell culture-treated petri-dish [Nunc] and both cell types were co-cultured in shared RPMI/FBS culture medium (Appendix I-iv) for a further 3 days.

2.1.4.4 Co-culture by direct physical contact

Monocytes were cultured in 6-well cell culture dishes and differentiated into BMD-microglia. At 11 DIV, culture medium was removed and discarded, and BMD-microglia were lifted from the culture surface by scraping in ice-cold 2 mM EDTA in DPBS. Cells were transferred from culture dishes to 15 mL Falcon tubes using a pipette, pooling together cells from the same donor. A viable cell count was made using Trypan Blue exclusion (section 2.6.3) and a haemocytometer. BMD-microglia were then pelleted out of solution by centrifugation at 400 × *g* for 5 min at 4 °C, washed in pre-warmed DPBS, and re-suspended in pre-warmed NM to a density of 2×10^5 cells/mL. NSCs were cultured on coverslips in 24-well cell culture dishes and differentiated into mature neuronal cultures by induced differentiation to 18 DD. Half of the neuronal culture medium, 500 µL, was removed per well and replaced with 500 µL BMD-microglia cell suspension in NM, equivalent to 1×10^5 BMD-microglia per coverslip. Cells were then returned to the incubator in direct co-culture.

2.2 Molecular biology

Samples suspected to contain viral vectors were handled in a Class II Microbiological Safety Cabinet situated within an Advisory Committee on Dangerous Pathogens (ACDP) Containment Level II laboratory with strict adherence to local rules of safe working practice. Samples, and any waste from bacterial work, were decontaminated with Virkon disinfectant for at least 2 h and autoclaved prior to disposal.

2.2.1 Viral plasmids

2.2.1.1 Human HTT exon 1 lentiviral expression system plasmids

Human *HTT* exon 1 lentiviral plasmids and related control vectors were a kind gift from Prof. Gillian P. Bates (King's College London (KCL), London, UK), and made by Dr. Eva C. Sirinathsingh of the same research group. The entire coding sequence of human *HTT* exon 1 with 29 (normal genotype), 71 (expanded, HD genotype) or 129 (highly expanded, HD genotype) CAG repeats, and the first 21 base pairs (bp) of *HTT*

intron 2, was cloned into a pHR-self-inactivating (SIN) lentivirus vector backbone under the bidirectional A2 ubiquitous chromatin opening element (A2UCOE) promoter. The A2UCOE element is a CpG island which confers resistance to DNA methylation-mediated silencing of lentiviral vectors, for stable, reliable and sustained transgene expression (Zhang *et al.* 2010). Following *HTT* exon 1 is an internal ribosome entry site (IRES) controlling concurrent expression of reporter gene enhanced green fluorescent protein (eGFP). A central poly-purine tract (cPPT) and Woodchuck post-transcriptional regulatory element (WPRE) are incorporated to increase transduction efficiency and transgene expression (Barry *et al.* 2001). The entire sequence is flanked by long terminal repeats (LTRs) to facilitate integration into the host genome, with a deletion in the 3' LTR rendering the virus self-inactivating after integration, in adherence with safety guidelines. An ampicillin resistance gene (*ampr*) is also present within the lentiviral backbone to allow for selection of expressing bacterial colonies during plasmid amplification. See Figure 2.1 for a schematic representation of the A2UCOE *HTT* exon 1 constructs, and Figure 2.2 for detailed plasmid maps of the A2UCOE *HTT* exon 1 constructs (*HTT* exon 1 129 CAG presented as an example) and an A2UCOE eGFP reporter only control vector, without the *HTT* exon 1 transgene, which was also cloned.

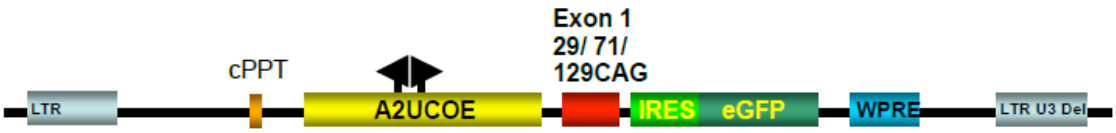

Figure 2.1: Schematic representation of A2UCOE HTT Exon 1 constructs

pHR-SIN backbone including cPPT and WPRE regulatory elements and flanking LTRs. Exon 1 genes with 29, 71 or 129 CAG repeats have been inserted under control of the A2UCOE promoter, and are followed by an IRES initiating concurrent expression of eGFP.

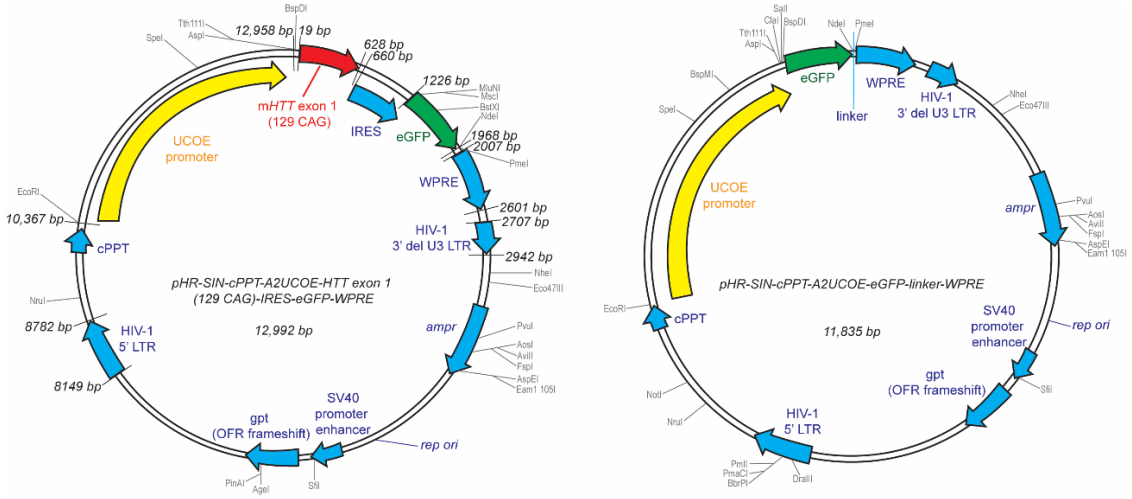

Figure 2.2: Plasmid maps for A2UCOE *HTT* Exon 1 lentiviral vectors

Full plasmid map for pHR-SIN-cPPT-A2UCOE-HTT exon 1-IRES-eGFP-WPRE (left), with mHTT 129 CAG construct presented as an example. Base pair (bp) numbers are indicated in black. An eGFP reporter only control construct was also created; pHR-SIN-cPPT-A2UCOE-eGFP-linker-WPRE (right). Restriction enzyme sites are indicated in grey on both plasmids.

2.2.1.2 Full-length human HTT retroviral expression system plasmids

Full-length human *HTT* retroviral plasmids were a kind gift from Prof. Michael R. Hayden (University of British Columbia, Canada). Full-length human *HTT* complementary DNA (cDNA) with 15 CAG repeats was synthesised from the ~10 Kb transcript variant of *HTT* ribonucleic acid (RNA) by reverse transcription. This produced the control *HTT* gene, which was a 10,030 bp transcript including the entire coding DNA sequence, and a non-coding DNA region followed by a poly A tail. A highly expanded pathological length CAG repeat region was then sub-cloned into *HTT* (15 CAG) to produce a HD *mHTT* gene with 138 CAG repeats (Goldberg *et al.* 1996). *HTT* (15 CAG) and *mHTT* (138 CAG) were cloned into the multiple cloning site (MCS) of Clontech murine stem cell virus (MSCV) vectors, with puromycin (puro) or hygromycin (hyg) antibiotic resistance genes, *puror* and *hygr* respectively, to produce MSCVpuro+full-length *HTT* (15 CAG) and MSCVhyg+full-length *mHTT* (138 CAG) (Figure 2.3). The MSCV expression systems are optimised for the introduction and expression of target genes in pluripotent stem cells, such as the ReNcell VM NSC line. Transgene expression is under the control of a retroviral promoter, Ψ^+, and a phosphoglycerate kinase (PGK) promoter following the transgene induces concurrent expression of the puro or hyg antibiotic resistance gene. *Ampr* is also present in each construct to allow for selection of expressing bacterial colonies during plasmid amplification.

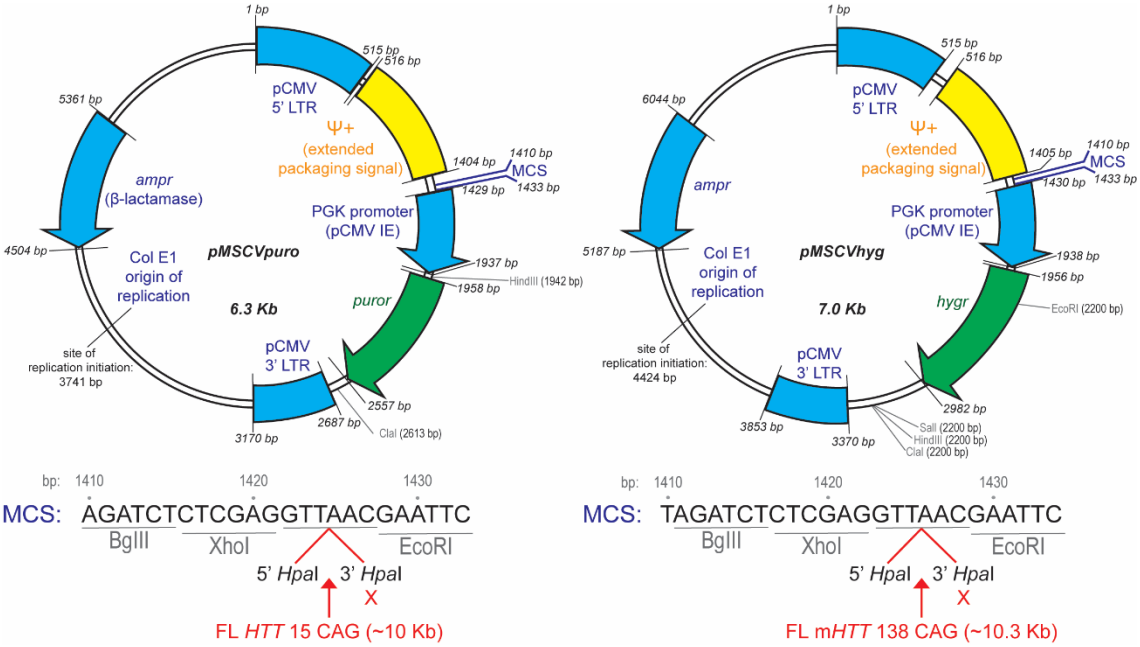

Figure 2.3: Plasmid maps for MSCV full-length *HTT* retroviral vectors

MSCVpuro (left) and MSCVhyg (right) Clontech retroviral plasmid vectors. Full-length (FL) human HTT cDNA was inserted into the MCS at the HpaI site in both constructs, with the resulting ablation of the 3' HpaI site (HTT (15 CAG) into MSCVpuro and mHTT (138 CAG) into pMSCVhyg).

2.2.2 Amplification and purification of plasmid DNA

Plasmid DNA (viral vectors and relevant viral packaging plasmids) was amplified in One Shot TOP10 Chemically Competent *E. Coli* [Invitrogen]. 100 ng plasmid DNA was added to one vial of One Shot cells and mixed gently. The vial was then incubated on ice for 30 min before heat-shocking the cells in a water bath for 30 seconds (s) at 42 °C and returning to ice for a further 2 min. 250 µL pre-warmed Super Optimal broth with Catabolite repression (SOC) medium was aseptically added to the vial to enhance transformation, and cells were shaken horizontally at 37 °C for 1 h at 225 rpm in a shaking incubator. Transformation mix was spread, at 200 µL per plate, on pre-warmed Luria-Bertani (LB) agar plates containing 50 ng/µL ampicillin, at 1:1, 1:10 or 1:100 dilutions in LB Broth. Plates were inverted and incubated overnight at 37 °C. Single bacterial colonies were picked from plates on which the colonies were well spaced, and used to inoculate 2 mL LB Broth culture medium containing 100 µg/mL ampicillin. Transformed bacteria were expanded in increasing volumes of LB Broth (with ampicillin), up to a volume of 1.5 L per culture, over 24 h at 37 °C with horizontal shaking at 225 rpm. During expansion, small samples of the bacterial culture were taken to create glycerol stocks for long-term storage of DNA plasmids (section 2.2.2.1). *E. Coli* were harvested from the culture medium by centrifugation at 6000 × *g* for 15 min at 4 °C, and plasmid DNA was isolated and purified using Qiagen Plasmid Maxi Kit

and the protocol for plasmid DNA purification using Qiagen Plasmid Midi and Maxi Kits [Qiagen], as per the manufacturer's protocol. Briefly, the bacterial pellet was re-suspended in lysis solution, and DNA was precipitated from the lysate. The lysate was cleared from the supernatant containing precipitated DNA by centrifugation and filtration steps, and then DNA was purified by wash steps through a Qiagen-tip 500 column. Purified plasmid DNA was then eluted from the column, and precipitated in isopropanol before pelleting by centrifugation at 6000 × *g* for 1 h at 4 °C. The DNA pellet was washed in 5 mL ethanol and centrifuged at 6000 × *g* for 1 h at 4 °C. The pellet was then air-dried and re-dissolved in ddH2O. Plasmid DNA was assessed for concentration and purity by NanoDrop (section 2.2.7).

2.2.2.1 Creating and using bacterial glycerol stocks

For long-term storage of plasmids, samples of transformed bacterial cultures were taken during the amplification phase. Five hundred microlitres bacterial culture was added to 500 µL 50 % glycerol in a 2 mL cryovial [Nunc] and gently mixed before freezing at −80 °C. For revival of bacteria, glycerol stocks were removed from the freezer, and without thawing, a sterile loop was used to scrape frozen bacteria from the top of the glycerol stock. Bacteria was then streaked onto LB agar plates containing 50 ng/µL ampicillin and colonies were grown overnight in an incubator at 37 °C. Bacterial glycerol stocks were returned to the freezer without thawing.

2.2.3 DNA sequencing

2.2.3.1 DNA sequencing primers and design

DNA sequencing primers were designed using online tool Primer3 (Untergasser *et al.* 2012), and selected based on their relative melting/annealing temperatures, low guanine-cytosine (G-C) bp percentage and minimal likelihood of complementary pair annealing between primers. See Table 2.1 for primers used to sequence ReNcell VM *HTT* exon 1 genomic DNA, *HTT* exon 1 transgenes in A2UCOE lentiviral plasmid vectors and full-length *HTT* transgenes in MSCV retroviral plasmid vectors. Forward and reverse primer sites for sequencing *HTT* exon 1 transgenes were within the A2UCOE plasmid backbone, 5' and 3' to the transgene inserts. The eGFP reporter only control A2UCOE vector was also sequenced using the same primers. Due to the large size of full-length HTT transgenes in MSCV, 17 primer pairs were designed to sequence shorter, overlapping fragments along the entire transgene, and these were matched up for analysis of the whole full-length transgene. These primer pairs were designed based on the Clontech plasmid sequences flanking the transgenes and the published National Center for Biotechnology Information (NCBI); nucleotide; RefSeqGene reference sequence NG_009378.1, for the ~10.3 Kb transcript variant of

full-length *Homo sapiens* HTT cDNA (IT15), chromosome 4. The same reference sequence was used to design forward and reverse primers for sequencing ReNcell VM genomic HTT exon 1.

Table 2.1: DNA sequencing primers

Primer name	Sequence (5' to 3')
ReNcell VM genomic DNA *HTT* exon 1 forward	TGCTTCTCGCTGCACTAATC
ReNcell VM genomic DNA *HTT* exon 1 reverse	CTGAGGACCCCAAGTGTGAC
A2UCOE *HTT* exon 1 forward	CCCGGGTCTAGAATCGATAA
A2UCOE *HTT* exon 1 reverse	TTTTCCACCATATTGCCGTC
MSCV full-length *HTT* 681 forward	ATGGTGCCCCTCGGAGTT
MSCV full-length *HTT* 879 reverse	GCAAAATTGCCAAAAGAAGC
MSCV full-length *HTT* 1054 forward	TGTCGAGGATGAACACTCCA
MSCV full-length *HTT* 1264 reverse	ATTGTGGTCTTGGTGCTGTG
MSCV full-length *HTT* 1533 forward	TCAGCAGCTCTGCCTTAACA
MSCV full-length *HTT* 1736 reverse	TATCCTCCTCATCCCCATCA
MSCV full-length *HTT* 1993 forward	GGAGGCCTTCAGGAACTCTT
MSCV full-length *HTT* 2222 reverse	AAGCAGATAAAAGGCGGACA
MSCV full-length *HTT* 2522 forward	ACATTTTCTTTGGCGGATTG
MSCV full-length *HTT* 2799 reverse	AAAAAGCTCACCAGCCTGAA
MSCV full-length *HTT* 3193 forward	CACATCAACCACCAGAGCAC
MSCV full-length *HTT* 3409 reverse	ATGGGCTGAGAGATCCAATG
MSCV full-length *HTT* 3702 forward	AGGGGAAGGAGAAAGAACCA
MSCV full-length *HTT* 3931 reverse	CGTGCTGTTCTGAAGATCCA
MSCV full-length *HTT* 4295 forward	GAGCAGGAGAACGACACCTC
MSCV full-length *HTT* 4510 reverse	CGCCAGCAAATCTAAAACCT
MSCV full-length *HTT* 4849 forward	CCAAAAAGAGGTGGTGGTGT
MSCV full-length *HTT* 5008 reverse	GGCTAACATTGGGAGGATGA
MSCV full-length *HTT* 5435 forward	GTGGAAATGAGTGAGCAGCA
MSCV full-length *HTT* 5608 reverse	GTTCAAGCTGTCCAGGGTGT
MSCV full-length *HTT* 6011 forward	ATCCAGGCAATTCAGTCTCG
MSCV full-length *HTT* 6220 reverse	ATTTGCAGCCAGAAGCATTT
MSCV full-length *HTT* 6504 forward	AAGGTGCAGAGCTGGTGAAT
MSCV full-length *HTT* 6723 reverse	TGGAAGACATGATGGACAGC
MSCV full-length *HTT* 7061 forward	GCCTGCTCCCTCATCTACTG
MSCV full-length *HTT* 7247 reverse	TTTCTGCCACCATCTCACAG
MSCV full-length *HTT* 7609 forward	GAGCCCACCAGAAGAAGACA
MSCV full-length *HTT* 7821 reverse	TCTTGCTCCACAATCCCTCT

MSCV full-length *HTT* 8292 forward	GCAACCAGTTTGAGCTGATG
MSCV full-length *HTT* 8530 reverse	GTCGCACTCCAGCACATAGA
MSCV full-length *HTT* 8846 forward	CTGGTCAAGCTGAGTGTGGA
MSCV full-length *HTT* 9028 reverse	AGATACCCGCTCCATAGCAA
MSCV full-length *HTT* 9262 forward	GCTGTCCCTCTCCAACTTCA
MSCV full-length *HTT* 9505 reverse	CACCTCAAGCACAGACTGGA

2.2.3.2 DNA sequencing polymerase chain reaction and analysis

DNA sequencing polymerase chain reactions (PCR) were carried out in ThermoFast non-skirted 96-well microplates [Thermo Fisher Scientific]. One reaction (15 µL final volume) was prepared with 1 µL BigDye Terminator v1.1 (Cycle Sequencing Kit) [Applied Biosystems], 5 µL Better Buffer [Microzone Limited], 0.75 µL primer (5 µM), 1 µL template DNA (150 ng/µL) and 7.25 µL ddH_2O. Plates were covered and placed on a Tetrad 2 BioRad thermal cycler with the program outlined in Table 2.2.

Table 2.2: Thermal cycling program for DNA sequencing PCR

Step	Temperature	Duration	Number of cycles
Initial denaturation	96 °C	1 min	1
Denaturation	96 °C	30 s	30
Annealing/extension	60 °C	3 min 15 s	
Reaction stop	15 °C	5 min	1

To purify extension products, 3.75 µL 0.125 M EDTA and 45 µL 100 % ethanol was added to each sequencing reaction and mixed by pipetting. Reactions were then incubated at RT for 15 min before centrifugation of the plate at 3000 × *g* for 30 min at 4 °C to pellet precipitated DNA. Waste products were removed by gently inverting the plate onto tissue and centrifugation for 1 min at 100 × *g*. Sixty microlitres 70 % ethanol was added to each DNA pellet and the plate was centrifuged at 1650 × *g* for 15 min at 4 °C. The plate was then inverted onto tissue and centrifuged again for 1 min at 185 × *g* to remove excess liquid. The plate was then placed, uncovered, on a thermocycler set to 37 °C for 5 min to allow any final traces of ethanol to evaporate. Dried DNA pellets were frozen to −20 °C and handed to Gary Adamson, Genetics and Diagnostics, MRC Prion Unit (IoN, London, UK), for sequencing. Samples were sequenced using the automated Applied Biosystems 3730xl DNA Analyser. Electropherograms for each sample were analysed in the forward and reverse directions using Geneious Pro (Biomatters Ltd.).

Sequencing results for ReNcell VM NSC genomic *HTT* exon 1, A2UCOE *HTT* exon 1 transgenes and MSCV full-length *HTT* transgenes were assessed for homology against the NCBI; nucleotide; RefSeqGene reference sequence NG_009378.1, for the ~10.3 Kb alternatively polyadenylated transcript variant of full-length *Homo sapiens HTT* cDNA (IT15), chromosome 4. DNA sequences were assessed for CAG repeat length, any mutations in exon 1, and any coding mutations in the rest of the full-length transgene. Genomic DNA was additionally assessed for SNPs in exon 1.

2.2.4 HD genotyping by CAG repeat-sizing

ReNcell VM NSCs were grown to approximately 80 % confluence in a 75 cm^2 culture flask, removed from the culture surface and pelleted as per the usual protocol (section 2.1.1.3). Cells were re-suspended in 200 µL 1× phosphate-buffered saline (PBS, prepared from 10× PBS solution diluted in ddH_2O). ReNcell VM Genomic DNA was then extracted using Qiagen DNeasy Blood and Tissue Kit [Qiagen; #69504] according to the manufacturer's Spin-Column Protocol for purification of total DNA from animal blood or cells. DNA was eluted in 200 µL Qiagen Buffer AE (10 mM Tris-Cl; 0.5mM EDTA; pH 9.0) and nucleic acid concentration and purity were determined using NanoDrop (section 2.2.7).

ReNcell VM genomic DNA was then sent to Andrea Haworth (Neurogenetics, NHNN, London, UK) for CAG repeat sizing, using the same method as is used for HD patient diagnostics through the HD clinic. Two primer pairs (HD3F/HDE and HD3F/HD5; see Table 2.3) were used to amplify across the CAG repeat by PCR. The HD3 primer is conjugated to 6-Carboxyfluorescein (6-FAM) fluorophore (HD3F). The HD3F/HD5 primer pair sequences across the polymorphic cytosine-cytosine-guanine (CCG) repeat region adjacent to the CAG repeat tract, and can be used to check for diploidy at the *HTT* gene site and HD gene homozygosity. Results from this PCR can also be used to confirm any positive results. One reaction was prepared with 12.5 µL Amplitaq Gold 360 Master Mix, 2.5 µL GC enhancer, 5 pmol of each primer, 1 µL DNA (50 ng/µL) and ddH_2O to a final volume of 25 µL. Two expansion positive controls, one with an expansion of 40-50 repeats and one with a large expansion of >70, were included in each analysis. A negative control was also included which was homozygous for a normal repeat size with HD3F/HDE, or heterozygous with HD3F/HD5. PCR was then performed according to the thermal cycling program outlined in Table 2.4.

Table 2.3: CAG repeat-sizing PCR primers

PCR primer	Sequence (5' to 3')
HD3F	6-FAM-CCTTCGAGTCCCTCAAGTCCTT
HDE	GGCGGTGGCGGCTGTTGCTGCTGCTGCTGC
HD5	CGGCTGAGGCAGCAGCGGCTGT

Table 2.4: Thermal cycling program for *HTT* CAG repeat-sizing PCR

Step	Temperature	Duration	Number of cycles
Initial denaturation	95 °C	10 min	1
Cycling	95 °C	30 s	30
	58 °C	30 s	
	72 °C	30 s	
Final extension	72 °C	7 min	1
Reaction stop	4 °C	-	1

Ten microlitres PCR product was transferred to a 3.5 % agarose minigel and subjected to agarose gel electrophoresis (section 2.2.6). DNA was visualised by exposure to ultraviolet (UV) light using the Gene Genius gel documentation system. The agarose gel was used to check that the PCR had worked and that there was no contamination of the samples. Capillary electrophoresis of the PCR product was then performed. One microlitre PCR product was added to 12 µL highly deionised (Hi-Di) formamide and 0.3 µL 500 Liz dye-labelled fragment size standard in a 96-well plate. The plate was then heat-sealed with plastic film using an Eppendorf Heat Sealer; before briefly spinning down the samples by centrifugation. Samples were heated at 95 °C for 3 min, immediately cooled on ice for 3 min, briefly spun down again, and then loaded onto an Applied Biosystems Incorporation (ABI) 3730 XL DNA Analyzer for capillary electrophoresis and fragment analysis. Sizing data was analysed using GeneMapper Software, and repeat sizes were calculated as shown in Table 2.5. The size, shape and peak height of PCR products was examined for interpretation of homozygosity and expanded alleles. The agarose gel was compared with capillary electrophoresis data to check for consistency of results.

Table 2.5: CAG repeat size calculation

Primer pair	CAG repeat number
HD3F/HDE	$\frac{allele\ size - 39}{3} \pm 2$
HD3F/HD5	$\frac{allele\ size - 108}{3} \pm 2$

The range of normal alleles is 8-26 repeats, intermediate alleles sizes range from 27-35 repeats, expanded alleles 36-75+ (36 to 39 reduced penetrance; ≥40 fully penetrant). Repeat allele sizes have been empirically ascertained to be accurate within a range of ± 2 repeats.

2.2.5 Restriction enzyme digestion of DNA

For each reaction, 1 µg plasmid DNA and 1 µL of each specific restriction enzyme was diluted in 1 × appropriate restriction enzyme buffer [NEBuffer; New England BioLabs], supplemented with 100 µg/mL bovine serum albumin (BSA) if specified by the manufacturer's protocol for use of the specific restriction enzyme, to a final volume of 10 µL in DNAse/RNAse free molecular biology grade water. Reactions were incubated for 1 h at 37 °C. DNA fragments were visualised by agarose gel electrophoresis (section 2.2.6). Restriction enzyme digests were used to size A2UCOE and MSCV plasmid backbones and their transgene inserts as confirmation of their presence at correct sizes and no contamination between transgenes. See Table 2.6 for details of restriction enzymes used for each digest and the conditions used.

Table 2.6: Restriction enzyme plasmid sites and reaction conditions

Plasmid	Restriction enzyme	Reaction conditions	Digestion sites
A2UCOE+ *HTT* exon 1	*Bam*HI	NEBuffer[3] + BSA	***HTT* exon 1 transgene + A2UCOE plasmid backbone** Double cut in A2UCOE either side of transgene
MSCV+ full-length *HTT*	Double digest: *Eco*RI *Hpa*I	NEBuffer[4]	**Fragmented full-length *HTT* transgene + MSCV plasmid backbone** *Eco*RI: MCS 3' to transgene, bp 4698 and 5175 *HTT* cDNA, within *hygr* *Hpa*I: MCS 5' to transgene
MSCV+ full-length *HTT*	*Xho*I	NEBuffer[4] + BSA	**5' fragment of full-length *HTT* transgene including CAG repeat** MCS 5' to transgene and bp 824 *HTT* cDNA

2.2.6 Agarose gel electrophoresis

Zero point eight to one point two percent agarose gels were prepared by heating 0.8-1.2 grams (g) UltraPure Agarose [Invitrogen] in 100 mL 1 × Tris/Borate/EDTA (TBE) buffer (Appendix II-iii) in a microwave, with occasional swirling, until the agarose was completely dissolved. The solution was allowed to cool to approximately 50 °C before adding ethidium bromide to 0.5 µg/mL final concentration and pouring into a casting tray where it was allowed to solidify. Once set, the agarose gel was removed from the casting tray and placed in an electrophoresis unit [Thermo Scientific]. The gel tray was filled with TBE buffer until the gel was completely covered. BlueJuice Gel Loading Buffer [Invitrogen] was added to each DNA digest, and samples were carefully loaded into wells of the agarose gel. HyperLadder I/IV DNA ladders (Bioline) were loaded alongside the samples. DNA fragments were electrophoresed at 100-120 Volts (V) for 30-60 min, until the dye line had run approximately 80 % of the way through the gel. DNA fragments were visualised under UV light using the BioRad Gel Doc XR system with Quantity One software (version 4.5.1, BioRad). The size of DNA fragments was interpreted using the DNA ladders as a guide.

2.2.7 Determining concentration and purity of DNA

Nucleic acid concentration was determined by measuring absorbance at 260 nm (A260) using a NanoDrop ND-1000 spectrophotometer [NanoDrop Technologies]. Absorbance measurement at 280 nm (A280) was used to determine protein concentration, and absorbance at 230 nm (A230) was used to determine presence of other contaminants within the sample. A260/A280 and A260/A230 ratios were calculated and used as a measure of purity in DNA samples, with an A260/A280 ratio of ~1.8 and an A260/A230 ratio of 2.0-2.2 being considered pure DNA. Deionised distilled H_2O was used to blank the machine before each sample absorbance reading.

2.3 Viral vectors and transduction of NSCs

All procedures involving viruses or virus parts were performed under biosafety level 2 conditions and appropriate risk assessments and safety measures were in place. All materials and waste associated with the use of viruses or virus parts were decontaminated for at least 2 h in 5 % Virkon disinfectant prior to disposal, as per the recommended safety guidelines.

2.3.1 Packaging plasmids into viruses

2.3.1.1 Packaging A2UCOE+HTT exon 1 into lentiviruses in HEK293T

A2UCOE+*HTT* exon 1 with 29, 71 or 129 CAG repeats, and A2UCOE eGFP reporter only plasmids were packaged into lentiviral vectors with a Vesicular Stomatitis Virus glycoprotein G (VSV-G) envelope, encoded from VSV-G-expressing plasmid MD.G2. Group antigens (GAG) and pol (reverse transcriptase, RNase H and integrase functions) proteins were encoded from the packaging plasmid CMVRd8.74. MD.G2 and CMVRd8.74 plasmids were produced by Plasmid Factory, and the patent is held with Michael Antoniou, KCL, London, UK.

HEK293T cells of low passage number were seeded at 12 × 10^6 cells per 175 cm^{-2} culture flask and incubated at 37 °C for 24 h, as described above (section 2.1.1.1). For each flask of cultured cells, viral parts were prepared by adding 50 µg specific viral vector construct, 17.5 µg VSV-G envelope plasmid (MD.G2) and 32.5 µg GAG/pol packaging plasmid (pCMVRd8.47) to 5 mL serum-free Dulbecco's modified Eagle medium (DMEM). Polyethylenimine (PEI) transfection reagent was prepared by adding 1 µL 10 mM pH 7.0 PEI to 5 mL DMEM. Viral parts and PEI solution were sterilised by passing through a 0.22 µm cellulose acetate syringe filter before gently mixing them together and incubating for 20 min at RT. Culture medium was removed from HEK293T cultures, and the cells were washed in serum-free DMEM before transfection was initiated by adding 10 mL viral parts and PEI mixture to each flask. Cells were returned

to the incubator for 4 h. The transfection mixture was then replaced with 15 mL standard DMEM/FBS culture medium (Appendix I-i) and cells were incubated for a further 24 h. Following this, lentiviral supernatants were harvested, passed through a 0.45 µm cellulose acetate syringe filter [Nalgene] into Falcon tubes to remove any cells or cellular debris, and promptly frozen in a −80 °C freezer where they were stored until ready for use.

2.3.1.2 Packaging MSCV+full-length HTT into retroviruses in Phoenix-AMPHO

MSCVpuro+full-length *HTT* (15 CAG) and MSCVhyg+full-length *mHTT* (138 CAG) were packaged into retroviral vectors with a pseudotyped dual 4070A (amphotropic) and VSV-G envelope. The additional VSV-G envelope protein was incorporated to increase the stability of retrovirus particles for the purpose of virus concentration by ultracentrifugation (section 2.3.2). The 4070A envelope and GAG/pol proteins were encoded from constructs carried by the second-generation Phoenix-AMPHO retrovirus producer cell line, and VSV-G was encoded from VSV-G-expressing plasmid MD.G2.

Phoenix-AMPHO cells of low passage number were plated at 2.5×10^6 per 75 cm^{-2} culture flask and grown to approximately 60 % confluence, as described above (section 2.1.1.1). Cells were transfected with MSCVpuro+full-length *HTT* (15 CAG) or MSCVhyg+full-length *mHTT* (138 CAG) using FuGene HD Transfection Reagent [Promega], as was recommended by the manufacturer for use with this cell line. For each flask,16.3 µL transfection reagent and 7.5 µg VSV-G envelope plasmid (MD.G2) was added to 136 µL serum-free DMEM, and incubated at RT for 5 min. Thirteen point six micrograms specific viral vector construct was then added to the mixture and incubated at RT for a further 15 min. The mixture was added drop-wise to Phoenix-AMPHO cells and swirled to mix evenly with the cells, before returning the cultures to the incubator for 24 h. The transfection medium was then removed from the cells and replaced with 10 mL fresh standard DMEM/FBS culture medium (Appendix I-i). After a further 48 h incubation, retroviral supernatants were harvested, passed through a 0.45 µm cellulose acetate syringe filter and promptly frozen in a −80 °C freezer where they were stored until ready for use.

2.3.2 Concentration of viruses

Viral supernatants were concentrated to increase multiplicity of infection (MOI) when transducing cells (section 2.3.4; Stable transduction of NSCs), and to allow for re-suspension of virus pellets in NSC-compatible culture media. A2UCOE+*HTT* exon 1 lentivirus or MSCV+full-length *HTT* retrovirus frozen supernatants were rapidly thawed in a 37 °C water bath. Twenty millilitres supernatant was transferred into an ultracentrifuge tube [Polyallomer Konical 30 mL Beckman Coulter]. Virus supernatant

was underlain with 5 mL filter-sterilised [0.22 µm cellulose acetate filter and vacuum pump; Millipore] 25 % sucrose in PBS, then the remaining supernatant was added and tubes were topped up with serum-free DMEM. The virus suspension was then centrifuged through the sucrose gradient by ultracentrifugation in a Sorvall Ultra Pro 80 centrifuge with a Sorvall Surespin 630 (36 mL) rotor, in a vacuum at 98,000 × *g* for 2 h at 4 °C, with fast acceleration and slow deacceleration. Supernatant was removed and discarded, and each viral pellet was re-suspended in 200 µL DMEM:F-12, aliquoted into cryovials [Nunc] and stored at −80 °C until ready for use.

2.3.3 Virus viability testing and titration

2.3.3.1 Testing and titrating A2UCOE+HTT exon 1 lentiviruses in HEK293T cells

A2UCOE+*HTT* exon 1 with 29, 71 or 129 CAG repeats, and A2UCOE+eGFP reporter only lentiviral supernatants were tested for transduction viability in HEK293T cells, and the concentrated lentiviruses were titred in the same cell line.

To test for presence of viable lentivirus in supernatants, HEK293T cells were seeded in 25 cm^{-2} flasks at 3 × 10^5 cells per flask and incubated for 8 h, as described above (section 2.1.1.1). Lentivirus supernatants were removed from −80 °C freezer storage and rapidly thawed in a 37 °C water bath. Culture medium was then removed from HEK293T cell cultures and replaced with 5 mL 1:1 fresh culture medium: lentiviral supernatant and 8 µg/mL hexadimethrine bromide (polybrene). Polybrene is a cationic polymer which neutralises the charge repulsion between virus particles and sialic acid on the cell surface, increasing the efficiency of retroviral infection. Cell cultures were returned to the incubator for 24 h, given a fresh media change, then incubated for a further 48 h. Transduction efficiency was assessed by monitoring eGFP expression by live-cell fluorescence microscopy with a fluorescein isothiocyanate (FITC) filter (section 2.7.2).

To titrate concentrated lentiviruses, HEK293T cells were seeded in 24-well culture plates at 1 × 10^5 cells per well and incubated overnight, as described above (section 2.1.1.1). Concentrated lentivirus was removed from −80 °C freezer storage and rapidly thawed in a 37 °C water bath. HEK293T cells were treated in duplicate with concentrated lentivirus at 1:100, 1:500, 1:1000, 1:5,000, or 1:10,000 dilution, or no lentivirus (control), in 500 µL standard culture medium with 8 µg/mL polybrene, for 24 h. Cells were then given a fresh medium change and returned to the incubator for a further 48 h. Transduction efficiency was assessed by monitoring eGFP expression by live-cell fluorescence microscopy with a FITC filter, and calculating the average percentage eGFP-positive cell population across two repeats, per concentrated lentivirus dilution. The optimum lentivirus treatment was considered to be the dilution

which resulted in ~50 % average eGFP-positive cell population, as greater than 50 % infection increases the likelihood of multiple transductions per cell, and less than 50 % would yield low transduction efficiency. These optimum conditions were taken forward for the transduction of ReNcell VM NSCs with *HTT* exon 1.

2.3.3.2 Testing and titrating MSCV+full-length HTT retroviruses in HeLa cells

MSCVpuro+full-length *HTT* (15 CAG) and MSCVhyg+full-length *mHTT* (138 CAG) retroviral supernatants were tested for transduction viability in HeLa cells, and the concentrated retroviruses were titred in the same cell line.

To test for presence of viable retrovirus in supernatants, HeLa cells were seeded in 6-well culture plates at 5×10^4 cells per well and incubated overnight, as described above (section 2.1.1.1). Retrovirus supernatants were removed from −80 °C freezer storage and rapidly thawed in a 37 °C water bath. Culture medium was then removed from HeLa cell cultures and replaced with 2 mL 1:1 fresh culture medium: retroviral supernatant and 8 µg/mL polybrene. Cell cultures were returned to the incubator for 24 h, given a fresh media change, then incubated for a further 48 h, reaching sub-confluence. Keeping all cells, transduced cultures were passaged into 75 cm^{-2} culture flasks, as previously described, and incubated overnight. Antibiotic selection of successfully transduced cells was then commenced by the addition of 0.2 µg/mL puromycin (puromycin dihydrochloride from *Streptomyces alboniger*) to the culture medium of cells infected with MSCVpuro+full-length *HTT* (15 CAG) retrovirus and 300 µg/mL Hygromycin B (from *Streptomyces hydroscopicus*) [Invitrogen] to cultures infected with MSCVhyg+full-length *mHTT* (138 CAG). Culture medium changes with the addition of fresh antibiotics were performed every 48 h. The optimum conditions and concentrations of antibiotics used here for antibiotic selection were ascertained by performing puromycin or Hygromycin B antibiotic kill curves in HeLa cells (section 2.3.4.1). Retrovirus viability was assessed by monitoring the number of surviving cells (cell density) after four days puromycin selection or seven days Hygromycin B selection. Infections with retroviral supernatants which resulted in at least 5 % surviving cells after 4 days puromycin selection or 7 days Hygromycin B selection, followed by an exponential growth phase under continued selection, were considered to contain viable retrovirus with reasonable transduction efficiency, and were subsequently taken forward for concentration.

To titrate concentrated retroviruses, HeLa cells were seeded in 24-well culture plates at 5×10^4 cells per well and incubated overnight, as described above (section 2.1.1.1). Concentrated retrovirus was removed from −80 °C freezer storage and rapidly thawed in a 37 °C water bath. HeLa cells were treated in duplicate with concentrated retrovirus

at 1:100, 1:1000 or 1:10,000 dilutions, or no retrovirus (control), in 500 µL standard culture medium with 8 µg/mL polybrene, for 24 h. Cells were then grown to confluence, passaged into 25 cm^{-2} culture flasks, and subjected to antibiotic selection, in the same way as is described above for testing retrovirus viability in supernatants. Transduction efficiency was assessed by monitoring the average number of surviving cells (cell density) after four days puromycin selection or seven days Hygromycin B selection, per retrovirus dilution, over two repeats. The optimum retrovirus treatment was considered to be the dilution which resulted in 15-20 % average surviving cell population after 4 days puromycin selection or 7 days Hygromycin B selection (with the no retrovirus treatment control cultures reaching 100 % cell death alongside), followed by an exponential growth phase under continued selection. These optimum conditions were taken forward for the transduction of ReNcell VM NSCs with full-length *HTT*.

As additional measures of MSCVpuro+full-length *HTT* (15 CAG) and MSCVhyg+full-length *mHTT* (138 CAG) retrovirus viability and transduction success, HeLa cells which had survived antibiotic selection were expanded and presence of the full-length (*m*)*HTT* protein produced from the transgene was assessed by Western blotting and immunocytochemistry (ICC) techniques. Increased expression of *HTT* in transfected HeLa cells compared with non-transfected cells was considered to indicate presence of either transgene. Expression of *mHTT* in HeLa cells transfected with full-length *mHTT* (138 CAG) compared with non-transfected cells or cells transfected with full-length *HTT* (15 CAG) was considered to indicate presence of the full-length *mHTT* (138 CAG) transgene.

2.3.4 Stable transduction of NSCs

2.3.4.1 Antibiotic kill curves

MSCVpuro+full-length *HTT* (15 CAG) and MSCVhyg+full-length *mHTT* (138 CAG) carry *puror* and *hygr* antibiotic resistance genes, respectively, which are co-expressed alongside the *HTT* transgene in transduced cells. Consequently, cells which carry the transgene can be selected for in a mixed culture by treatment with the relevant antibiotic. The optimum antibiotic selection concentration for each cell type was determined using kill curves. HeLa cells or ReNcell VM NSCs were seeded in 6-well culture plates at 5×10^4 cells per well and incubated overnight, as described above (sections 2.1.1.1 and 2.1.1.3). Cells were then given a media change with the addition of a range of antibiotic concentrations, each tested in triplicate. HeLa cells were treated with twelve different puromycin concentrations in the range of 0-15 µg/mL, or ten different Hygromycin B concentrations in the range of 0-500 µg/mL. ReNcell VM NSCs were treated with seventeen different puromycin concentrations in the range of 0-1

µg/mL, or ten different Hygromycin B concentrations in the range of 0-400 µg/mL. Cells were given a media change with the addition of fresh antibiotics every 2 days. Percentage surviving cells was monitored daily, and determined by direct visualisation of cell cultures under a light microscope (section 2.7.1), taking an average interpretation from three treatment repeats. The optimum antibiotic selection concentration was considered to be the minimum concentration required to give 100 % cell death after 3-4 days for puromycin, and 7-8 days for Hygromycin B.

2.3.4.2 Transduction of ReNcell VM NSCs with HTT exon 1 or full-length HTT

ReNcell VM NSCs which had undergone one passage post-thawing were seeded in 24-well culture plates at 5×10^4 cells per well and incubated overnight, as previously described (section 2.1.1.3). Cells were then infected with concentrated A2UCOE+*HTT* exon 1 lentiviruses or MSCV+full-length *HTT* retroviruses at 1:100 dilutions, in 500 µL culture medium with 8 µg/mL polybrene per well, for 24 h. For full-length *HTT* transductions, cells were then given another consecutive 24 h infection with the aim of increasing MOI, because the concentrated retroviruses were of very low titre. All cells were then given a fresh medium change and returned to the incubator. Once cells had been allowed to grow to confluence, they were passaged into larger culture vessels, keeping all cells.

2.3.4.3 Selecting for HTT transgenes in transduced NSCs

Transgene expression was confirmed in A2UCOE+HTT exon 1-infected cells by screening for the eGFP reporter using live-cell fluorescence microscopy with a FITC filter (section 2.7.2). NSC+HTT exon 1 (29, 71 or 129 CAG) and NSC+eGFP reporter only cultures were then expanded, and cells carrying the transgene and co-expressing the eGFP reporter were selected for by FACS (section 2.5.4); performed by Dr. Eva C. Sirinathsingh, Prof. Gillian P. Bates' research group, KCL, London, UK).

NSC cultures which had been infected with MSCVpuro+full-length *HTT* (15 CAG) or MSCVhyg+full-length *mHTT* (138 CAG) retroviruses were treated with 0.125 µg/mL puromycin or 40 µg/mL Hygromycin B, respectively, to select for transduced cells. Culture medium was changed every 2 days with the addition of fresh antibiotics, and cultures were maintained under antibiotic selection for 1 week (puromycin) or 2 weeks (Hygromycin B).

2.3.4.4 Confirmation and maintenance of ReNcell VM+HTT exon 1 and ReNcell VM+full-length HTT NSC lines

ReNcell VM NSC+*HTT* exon 1 and ReNcell VM NSC+full-length *HTT* cell lines were expanded long-term and kept under cryopreservation at a maximum total passage number of twenty-one (section 2.1.1.4), or maintained in routine cell culture in the same

way as wild-type ReNcell VM NSCs (section 2.1.1.3). Transgenic lines were used in experiments as NSCs or differentiated into mature neuronal cultures at less than ten passages post-expansion or post-thawing (less than a total passage number of 31). Production of exon 1 or full-length HTT proteins with appropriate polyQ lengths was confirmed by a combination of Western blotting (sections 2.4.4 and 2.5.1), dot blotting (section 2.4.5), ICC (section 2.5.2), MSD assay (section 2.5.6.2) and TR-FRET assay (section 2.5.7). Stable expression of the transgenes was checked every 3-4 passages by monitoring continued eGFP reporter expression in *HTT* exon 1 lines, and antibiotic resistance in full-length *HTT* lines.

2.4 Protein biochemistry

2.4.1 Preparation of cell lysates

2.4.1.1 Standard preparation of cell lysates for Western blotting or dot blotting

Cells were harvested from the culture surface and pelleted out of culture medium using the same methods as were applied in routine cell culture (section 2.1.1). Differentiated ReNcell VM neuronal cultures were treated the same way as NSC cultures. Cells were washed in PBS and re-suspended in ice-cold Lysis Buffer (Appendix II-iv) by pipetting until achieving a homogenous solution. Suspended lysates were then incubated on ice, with agitation, for 15-20 min. Small samples of lysate were taken and protein concentration was quantified by Bradford protein assay [Bio-Rad] (section 2.4.2.1) or bicinchoninic acid (BCA) assay (section 2.4.2.2). For Western blot lysates, to precipitate proteins, reduce aggregation, and remove lipids, 100 µL lysate was added to 900 µL ice-cold methanol in a 1.5 mL Eppendorf tube, and incubated at −20 °C for at least 30 min. Samples were then centrifuged at 18,000 × *g* for 10 min at 4 °C, methanol was poured off, and the pellet was left to air dry. Dry pellets were re-suspended to 1 mg/mL protein in 1× Sample buffer (Appendix II-v) and incubated on a shaking heater at 95 °C, 800 rpm for 10 min, until pellets had completely dissolved.

2.4.1.2 Preparation of myeloid cell lysates

Culture medium was removed and myeloid cells were lysed directly in the culture vessel with the addition of ice-cold RIPA buffer (Appendix II-ii). For BMD-macrophages and BMD-microglia, culture plates were then incubated at 4 °C for 15 min on a shaking platform set to 400 rpm to remove the cells from the culture surface. Cell lysates were homogenised by pipetting, collected into 0.5 mL Eppendorf tubes and stored at −80 °C until ready for use. When ready to prepare samples, cell pellets were thawed on ice and a quantification of total protein was made by BCA assay (section 2.4.2.2). Lysates

were mixed with 1× Sample buffer (Appendix II-v) to a final protein concentration of 1 mg/mL, and incubated at 95 °C for 10 min.

2.4.2 Quantification of total protein

2.4.2.1 Bradford Assay (Bio-Rad)

The Bio-Rad protein assay is a colorimetric assay based on the Bradford dye-binding method (Bradford 1976), and works on the principle that Coomassie brilliant blue G-250 dye binds to amino acid residues and the resultant colour change, which can be measured by reading its absorbance, is linear in relation to the amount of protein within a solution. The assay was used to quantify total protein concentration of cell lysates prepared in buffers which did not contain high concentrations of detergents, which are known to interfere with this assay, as per the manufacturer's instructions and Standard Procedure for Microtiter Plates protocol. Firstly, dye reagent was prepared by diluting one-part Dye Reagent Concentrate with four parts ddH_2O, and syringe filtering the solution to remove particulates. Five dilutions of BSA were prepared as protein standards (0, 50, 100, 300 and 500 µg/mL), and samples were prepared as pure, 1:2, 1:10 and 1:20 dilutions in PBS. Ten microlitres of each protein standard and sample dilution was pipetted into separate wells of a clear, flat-bottomed 96-well assay plate [Greiner], in duplicate. Then 200 µL diluted dye reagent was added to each well, and thoroughly mixed by pipetting. Samples were incubated for 5 min at RT before measuring the absorbance at 595 nanometres (nm) on a TECAN X-Fluor4 v4.51 plate reader [Sunrise]. The BSA protein standards were used to create a linear standard curve from which unknown protein concentrations were determined, using Microsoft Excel.

2.4.2.2 Bicinchoninic acid (BCA) assay

The BCA protein assay [Pierce, Thermo Fisher Scientific] is a colorimetric assay which works on the principle that peptide bonds in protein reduce Cu^{2+} ions from copper(II) sulfate to Cu^{+} ions, in a temperature-dependent reaction. The number of Cu^{2+} ions reduced is directly proportional to the amount of protein in a solution, and is measured by reading the absorbance of a purple-coloured complex which forms when BCA molecules chelate with Cu^{+} ions. The assay was used to quantify total protein in highly concentrated samples (BCA Assay has a broader dynamic range than Bradford Assay) prepared in buffers which contained high concentrations of detergents (known to interfere with the Bradford Assay), as per the manufacturer's instructions. Firstly, BSA protein standards were prepared at the following concentrations: 0, 25, 125, 2500, 500, 750, 1000, 1500 and 2000 µg/mL in appropriate buffer. Cell lysates were diluted 1:5 in PBS. Twenty-five microlitres of each protein standard and sample dilution was pipetted

into separate wells of a clear, flat-bottomed 96-well assay plate, in duplicate. Then 200 µL prepared BCA Working Reagent was added to each well, and the plate was mixed thoroughly on a plate shaker for 30 s. The plate was then incubated in the dark for 30 min at 37 °C. After allowing the plate to cool to RT, absorbance was measured at 562 nm on a TECAN X-Fluor4 v4.51 plate reader. The BSA protein standards were used to create a linear standard curve from which unknown protein concentrations were determined, using Microsoft Excel.

2.4.3 Sodium dodecyl sulphate (SDS) polyacrylamide gel electrophoresis (PAGE)

Pre-cast Novex 8, 10, 12 or 4-20% Tris-Glycine 1.5 mm gels with 10 or 15 wells [Invitrogen] were assembled in an Invitrogen Novex Mini-Cell Gel tank and the chambers were filled with 1× Tris/Glycine/SDS Running buffer (Appendix II-vi). Cell lysates prepared in Sample Buffer (section 2.4.1) were loaded into separate gel wells at 20 µL (20 µg protein, as determined by Bradford Assay or BCA assay (sections 2.4.2.1 and 2.4.2.2, respectively)) per lane, against 9 µL BioRad Precision Plus Protein Kaleidoscope, BioRad Precision Plus All Blue, HiMark Pre-Stained high molecular weight protein standard [Invitrogen] or Novex SeeBlue Plus2 Prestained standard [Life Technologies] molecular weight markers. Gels were run at 90 V constant voltage for approx. 10 min until samples had stacked at the stacking gel: resolving gel interface, then the voltage was increased to 150 V for approx. 1 h until samples had reached the end of the gel (or 3-4 h for full-length HTT protein to reach the middle of the gel).

2.4.4 Electroblotting of proteins

Following SDS-PAGE, proteins were transferred from the polyacrylamide gel to nitrocellulose membrane [Thermo Fisher Scientific] or Immobilon polyvinylidene fluoride (PVDF) membrane [Millipore]. The gel, membrane, Whatmann filter papers and sponges, which had been pre-soaked thoroughly in Electroblotting buffer [National Diagnostics] (Appendix II-vii) for at least 15 min, were assembled in a Novex blot module [Invitrogen] in an XCell Surelock Mini-Cell tank, according to the manufacturer's instructions. The central chamber of the transfer tank was filled with Electroblotting buffer and the outer chambers with water to act as a coolant, and proteins were transferred from the gel to the membrane at 15 V overnight. For transfer of very large proteins, such as full-length HTT, the electroblotting process was conducted for 24 h at 15 V followed by a further 1 h at 35 V. As full-length HTT is also prone to aggregation, 0.1 % SDS was included in the Electroblotting buffer in these cases. Following transfer, the membrane was removed from the transfer apparatus and buffer was washed off by three 10 min washes in PBS on a gentle shake.

2.4.5 Dot-blotting

Dot blotting apparatus was assembled with pre-soaked filters and a nitrocellulose membrane. Cell lysates prepared in Lysis Buffer (section 2.4.1.1) were dotted, in triplicate, onto the membrane at 20 µg per dot (as determined by BCA assay (section 2.4.2.2)). All blank wells were blocked or filled with Lysis Buffer (Appendix II-iv) to ensure good draining. The vacuum was then applied to draw proteins into the membrane.

2.5 Immunostaining and detection techniques

2.5.1 Western blot or dot blot protein detection

Following electroblotting of proteins separated by SDS-PAGE from polyacrylamide gel to a membrane (section 2.4.4; for Western blotting) or transfer of proteins from dotted cell lysates to a membrane by vacuum (section 2.4.5; for dot blotting), proteins were detected by different techniques depending on the optimal conditions for the specific protein or antibodies used for detection.

2.5.1.1 Western blot or dot blot protein detection by infrared (IR) fluorescence

The nitrocellulose membrane was incubated in Odyssey Blocking Buffer [LI-COR] for 1 h at RT on a gentle shake. The membrane was then incubated in primary antibodies at the appropriate dilution (see Table 2.7 for details of primary antibodies used for immunoblotting) in Odyssey Blocking Buffer at RT for 2 h, or at 4 °C overnight, on a shaking platform. In some cases, two different primary antibodies were added at the same time, assuming the primary antibodies were raised in different species and the relevant secondary antibodies were conjugated to IR dyes of different wavelengths and there was no potential for cross-reactivity. Excess, unbound primary antibodies were then washed off the membrane by six 10 min washes in 0.1 % PBS Tween-20 (PBST), with gentle shaking throughout. The membrane was then incubated in IRDye secondary antibodies (see Table 2.8 for details of secondary antibodies used for immunoblotting) at 1:10,000 dilution in Odyssey blocking buffer, for 1 h at RT with gentle shaking, in the dark. Excess, unbound secondary antibodies were washed off the membrane with three 10 min washes in 0.1 % PBST, followed by three 10 min washes in PBS only, with gentle shaking in the dark throughout. IRDye secondary antibodies were visualised directly on the membrane by scanning using a LI-COR Odyssey Scanner. Protein levels were quantified by calculating relative fluorescence of background-subtracted integrated intensities (I.I.) on the digital images using Odyssey Software v2.1. Sample I.I.s were normalised to I.I.s generated from loading control probes.

2.5.1.2 Western blot protein detection by chemiluminescence

Western blotting for the assessment of IκB degradation kinetics in stimulated myeloid cells was performed by Dr. Ulrike Träger (Prof. Sarah J. Tabrizi's research group, UCL IoN, London, UK). Proteins were transferred to PVDF membrane, as described above (section 2.4.4). The washed membrane was incubated in 5 % non-fat dried milk in Tris-buffered saline, pH 7.0, containing 0.1 % Tween-20 (TBST), for 2 h at RT on a gentle shake. The membrane was then incubated with anti-IκB primary antibodies (see Table 2.7 for details of primary antibodies used for immunoblotting) in 5 % non-fat dried milk in PBST, at 4 °C overnight, on a shaking platform. Excess, unbound primary antibodies were then washed off the membrane by six 10 min washes in TBST, with gentle shaking throughout. The membrane was then incubated with alkaline phosphatase (AP)-conjugated secondary antibodies (see Table 2.8 for details of secondary antibodies used for immunoblotting) in 5 % non-fat dried milk in PBST, for 1 h at RT with gentle shaking. Excess, unbound secondary antibodies were washed off the membrane with six 10 min washes in TBST, with gentle shaking throughout. To develop the AP signal, the membrane was washed twice in Tropix assay buffer [Applied Biosystems] (Appendix II-viii), and then incubated with Tropix CDP-Star chemiluminescent AP-substrate [Applied Biosystems] for 5 min at RT. The signal was visualised by exposure to BioMax MR-1 film [Kodak], followed by development and fixation using a Xograph Imaging Machine [Xograph Imaging Systems]. The membrane was stripped by 10 min incubation in 1:10 diluted ReBlot Plus Strong solution [Millipore] on a gentle shake, and reprobed with anti-glyceraldehyde 3-phosphate dehydrogenase (GAPDH) primary antibodies (see Table 2.7 for details) and AP-conjugated secondary antibodies (see Table 2.8 for details) as a loading control. Developed blots were scanned using an HP Scanjet N6350 scanner and quantified by densitometry analysis of digital images at three different exposures using TotalLab TL100 image analysis software [Sigma Aldrich].

2.5.1.3 Details of antibodies used for immunoblotting

Table 2.7: Primary antibodies for immunoblotting

Antibody/ antigen	Host	Dilution	Cat No.	Supplier
4C9/ aa65-84 HTT	Mouse (IgG1)	1:1000 (1.38 mg/mL stock)	NCA	Kind gift from Dr. Andreas Weiss (Novartis, Switzerland)
CD68	Mouse (IgG2b)	1:200	MAB20401	R & D Systems
CSF1R	Rabbit	1:1000	LS-C167079	LifeSpan Biosciences

CX3CR1	Rabbit	1:500	NBP1-76872	Novus Biologicals
ERK1/2	Rabbit	1:2000	M5670	Sigma
GAPDH	Rabbit	1:3000	G9545	Sigma
GFP	Rabbit	1:1000	A11122	Invitrogen
Iba1 (isoforms 1 and 3)	Goat	1:500	NB100-1028	Novus Biologicals
IκB	Rabbit	1:500	sc-371	Santa Cruz Biotechnology
mAB2166/ aa181-810 HTT	Mouse (IgG1)	1:1000	MAB2166	Millipore
MW1/ HTT polyQ	Mouse (IgG2b)	1:2000 (2.3 mg/mL stock)	NCA	Kind gift from Dr. Andreas Weiss (Novartis, Switzerland)
P2Y12	Rabbit	1:400	ab183066	Abcam
PU.1	Mouse (IgG1)	1:500	ab88082	Abcam
S830/ mHTT polyQ	Sheep	1:2000	NCA	Kind gift from Prof. Gillian P. Bates (KCL, London, UK)
β-actin	Rabbit	1:10,000	SAB5500001	Sigma
β-actin	Mouse (IgG1)	1:10,000	A5441	Sigma

NCA, not commercially available

Table 2.8: Secondary antibodies for immunoblotting

Antibody	Dilution	Cat No.	Supplier
AP-conjugated anti-Rabbit IgG	1:10,000	A3687	Sigma
IRDye 680LT Donkey anti-Mouse IgG	1:10,000	925-68022	LI-COR
IRDye 680LT Donkey anti-Rabbit IgG	1:10,000	925-68023	LI-COR
IRDye 680LT Goat anti-Rabbit IgG	1:10,000	925-68021	LI-COR
IRDye 800CW Donkey anti-Goat IgG	1:10,000	925-32214	LI-COR
IRDye 800CW Donkey anti-Mouse IgG	1:10,000	925-32212	LI-COR
IRDye 800CW Goat anti-Mouse IgG	1:10,000	925-32210	LI-COR
IRDye 800CW Goat anti-Rabbit IgG	1:10,000	925-32211	LI-COR

2.5.2 Immunocytochemistry (ICC)

2.5.2.1 Preparation of coverslips for ICC

Cells were seeded into 24-well culture plates at 1 × 10^5 cells per well on 13 mm diameter glass coverslips. For NSC cultures (and differentiated neuronal cultures), coverslips were sterilised by baking in an electric oven at 200 °C for 6 h, and laminin-coated by incubating in 200 µL 20 µg/mL cold mouse laminin-1 PathClear in 20 mM cold Tris-HCl, pH 7, per coverslip, at 37 °C for 24 h. Before seeding NSCs, the laminin solution was removed and laminin-coated surfaces were washed in pre-warmed DMEM:F-12. For HeLa, N2a_R2 or primary MC cultures, coverslips were sterilised by soaking in 100 % ethanol for at least 10 min before allowing to air-dry in a tissue culture safety cabinet. Coverslips were then PDL-coated by incubating in 200 µL 0.1 mg/mL PDL in sterile tissue culture grade distilled water, per coverslip, for 5 min at RT. Before seeding cells, PDL solution was removed and coverslips were thoroughly washed in sterile distilled water and allowed to air-dry for at least two hours. For BMD-macrophage and BMD-microglia cultures, coverslips were sterilised in 100 % ethanol and allowed to air-dry before seeding. No cell attachment aids were required for these cells because they already adhere well to glass.

2.5.2.2 Standard ICC

When ready to perform ICC, cells were washed three times in PBS and fixed in 4 % paraformaldehyde (PFA) [Polysciences] in PBS for 15 min at RT. PFA was removed with five washes in PBS, then cells were permeabilised in 100 % ice-cold methanol for 15 min at −20 °C. Methanol was removed with five washes in PBS. Cells were then incubated with 10 % BSA in PBS at 37 °C for 30 min, followed by a 1 h incubation with primary antibodies at the appropriate dilution (see Table 2.9 for details of primary antibodies used for ICC) in 1 % BSA in PBS at 37 °C. In some cases, two or more different primary antibodies were added at the same time, assuming the primary antibodies were raised in different species or were of different isotypes, and the relevant secondary antibodies were conjugated to different fluorophores and there was no potential for cross-reactivity. Excess, unbound primary antibodies were removed with five washes in PBS, then cells were incubated with 1:1000 dilution Alexa Fluor-conjugated secondary antibodies (see Table 2.10 for details of secondary antibodies used for ICC) in 1 % BSA at 37 °C for 45 min. Excess, unbound secondary antibodies were removed with five washes in PBS. Coverslips were then mounted, cells down, on Superfrost glass microscope slides [Thermo Scientific] in Antifade Fluorescence Mounting Medium [Dako] containing 1 µg/mL 4',6-diamidino-2-phenylindole (DAPI). Immunofluorescent staining was visualised by confocal microscopy (section 2.7.3).

2.5.2.3 ICC with differentiated neuronal cultures

Neuronal cultures were washed three times in PBS and fixed in 4 % PFA in PBS for 15 min at RT. PFA was removed with five washes in PBS, then cells were permeabilised in 0.2 % Triton X-100 in PBS for 10 min at RT. Triton X-100 was removed with five washes in PBS. Cells were then incubated with 10 % goat serum (or donkey serum if primary antibodies were raised in sheep or goat e.g. S830); 1 % BSA in PBS for 1 h at RT, followed by an overnight incubation with primary antibodies at the appropriate dilution (see Table 2.9 for details of primary antibodies used for ICC) in 1 % BSA at 4 °C. Excess, unbound primary antibodies were removed with five washes in 0.05 % PBST, then cells were incubated with 1:1000 dilution Alexa Fluor-conjugated secondary antibodies (see Table 2.10 for details of secondary antibodies used for ICC) in 1 % BSA at RT for 1 h. Excess, unbound secondary antibodies were removed with five washes in 0.05 % PBST. Coverslips were then mounted on Superfrost glass microscope slides in Antifade Fluorescence Mounting Medium [Dako] containing 1 µg/mL DAPI or 1 µg/mL Hoechst 33342. Immunofluorescent staining was visualised by confocal microscopy (section 2.7.3).

2.5.2.4 Details of antibodies used for ICC

Table 2.9: Primary antibodies for ICC

Antibody/ antigen	Host	Dilution	Cat No.	Supplier
2B7/ aa1-17 HTT	Mouse (IgG1)	1:500 (4.854 mg/mL stock)	NCA	Kind gift from Dr. Andreas Weiss (Novartis, Switzerland)
CD11b	Mouse (IgG1)	1:50	MCA551	Serotec
CD14	Mouse (IgG1)	1:50	MA5-14773	Thermo Scientific
GAD67	Mouse (IgG2a)	1:100	MAB5406	Millipore
GFAP (conjugated to cy3)	Mouse (IgG1)	1:200	C9205	Sigma
GFP	Rabbit	1:1000	A11122	Invitrogen
Iba1 (isoforms 1 and 3)	Goat	1:20	NB100-1028	Novus Biologicals

mAB2166/ aa181-810 HTT	Mouse (IgG1)	1:250	MAB2166	Millipore
Mannose receptor (CD206)	Rabbit	1:250	ab125028	Abcam
MW1/ HTT polyQ	Mouse (IgG2b)	1:1000 (2.3 mg/mL stock)	NCA	Kind gift from Dr. Andreas Weiss (Novartis, Switzerland)
S830/ mHTT polyQ (aggregates)	Sheep	1:500	NCA	Kind gift from Prof. Gillian P. Bates (KCL, London, UK)
TREM2	Goat	1:20	LS-C150090	LifeSpan Biosciences
Tyrosine hydroxylase	Mouse (IgG1)	1:250	MAB318	Millipore
βIII-tubulin	Mouse (IgG2a)	1:500	ab78078	Abcam

NCA, not commercially available

Table 2.10: Secondary antibodies for ICC

Antibody	Dilution	Cat No.	Supplier
Alexa Fluor 488 Donkey anti-Goat IgG (H+L)	1:1000	A-11055	Invitrogen
Alexa Fluor 488 Goat anti-Mouse IgG (H+L)	1:1000	A-11001	Invitrogen
Alexa Fluor 488 Goat anti-Mouse IgG2a	1:1000	A-21131	Invitrogen
Alexa Fluor 488 Goat anti-Mouse IgG2b	1:1000	A-21141	Invitrogen
Alexa Fluor 488 Goat anti-Rabbit IgG (H+L)	1:1000	A-11034	Invitrogen
Alexa Fluor 546 Donkey anti-Goat IgG (H+L)	1:1000	A-11056	Invitrogen
Alexa Fluor 568 Goat anti-Mouse IgG1	1:1000	A-21124	Invitrogen
Alexa Fluor 647 Donkey anti-Rabbit IgG (H+L)	1:1000	A-31573	Invitrogen

2.5.3 Proximity ligation assay (PLA)

Proximity ligation assay (PLA) allows for the detection, visualisation and quantification of proteins which directly interact, or are in close proximity, within cell samples prepared for microscopy. PLA was used to determine the level of interaction between HTT and IKKγ in primary BMD-macrophages in various treatment paradigms, as per the manufacturer's instructions [Duolink In Situ PLA, Olink Bioscience].

Monocytes were seeded on coverslips in 24-well culture plates at 1 × 10^6 cells per well and differentiated into BMD-macrophages as per the usual protocol (section 2.1.2.4).

Following treatments relevant to the specific experiment, cells were fixed in 4 % PFA and stained with 1 µg/mL fluorescent wheat germ agglutinin (WGA) [Life Technologies] for 5 min at 37 °C to label membranes. Excess WGA was removed with ten washes in PBS. Cells were then permeabilised in 100 % ice-cold methanol for 15 min at −20 °C, and then blocked with 10 % BSA in PBS for 30 min at 37 °C. Cells were probed with primary antibodies in 1 % BSA in PBS for 1 h at 37 °C (see Table 2.11 for details of primary antibodies and Table 2.12 for antibody pairs used for PLA). Excess, unbound primary antibodies were washed off with three 5 min washes in PBS with gentle agitation.

To perform PLA, cells were then incubated with anti-mouse and anti-rabbit secondary antibodies conjugated with oligonucleotides (PLA probe MINUS and PLA probe PLUS). To do this, firstly the PLA probe was prepared by incubating 8 µL PLA PLUS with 8 µL PLA MINUS in 24 µL 1 % BSA in PBS, for 20 min at RT. Each coverslip was removed from the culture plate and sandwiched in parafilm with 40 µL pre-prepared PLA probe, and incubated for 1 h at 37 °C in a humidified chamber. Coverslips were then returned to culture plates and given two 5 min washes in Duolink In Situ Wash Buffer A (Appendix II-ix) with gentle agitation, before transferring back to parafilm. Two oligonucleotides were then hybridised to the two PLA probes by incubation in 1 × Duolink In Situ Ligation Solution (consisting of the two oligonucleotides and Ligase) for 30 min at 37 °C in a humidified chamber. If the oligonucleotides were in close proximity, they would join to form a closed circle. Coverslips were then returned to culture plates and given two 5 min washes in Duolink In Situ Wash Buffer A with gentle agitation, before transferring back to parafilm. The DNA template was then amplified in a rolling-circle amplification (RCA) reaction. Coverslips were incubated in 1 × Duolink In Situ Red Amplification Solution (consisting of nucleotides and fluorescently labelled oligonucleotides) with Polymerase for 100 min at 37 °C in a humidified chamber. One of the oligonucleotides hybridised to one of the PLA probes acts as a primer for a RCA reaction using the ligated circle as a template, and the fluorescently labelled oligonucleotides hybridise to the RCA product. Coverslips were then returned to culture plates and given two 10 min washes in 1 % Duolink In Situ Wash Buffer B (Appendix II-x) followed by one 2 min wash with 0.01 % Duolink In Situ Wash Buffer B, with gentle agitation, in the dark. Finally, coverslips were mounted on glass microscope slides in 7 µL Duolink In Situ Mounting Medium with DAPI, and confocal fluorescence microscopy was used to detect and visualise fluorescently labelled oligonucleotides (section 2.7.3).

Positive interactions, indicating two proteins which directly interact or are in close proximity, appear as distinct fluorescent red spots. Positive interactions were quantified as average number of spots per cell, from at least seven random fields of view per

experiment condition per subject. Cell perimeters were determined based on WGA staining and spot count quantification parameters were gated against positive and negative controls (see Table 2.12). Confocal images were processed, analysed and quantified using Volocity high performance 3D imaging software v6.1.1 [PerkinElmer], according to the protocol outlined in section 2.7.3.1.

Table 2.11: Primary antibodies for PLA

Antibody/ antigen	Host	Dilution	Cat No.	Supplier
4C9/ aa65-84 HTT	Mouse (IgG1)	1:300 (1.38 mg/mL stock)	NCA	Kind gift from Dr. Andreas Weiss, Novartis, Switzerland
IKKγ	Rabbit	1:100	sc-8330	Santa Cruz Biotechnology
IKKβ	Mouse	1:50	sc-271782	Santa Cruz Biotechnology

Table 2.12: Antibody pairs used in PLA

Type of pair	Primary antibodies	PLA probes
Assay pair	4C9 (HTT) -and- IKKγ	PLA probe MINUS anti-mouse -and- PLA probe PLUS anti-rabbit
Positive control	IKKβ -and- IKKγ	PLA probe MINUS anti-mouse -and- PLA probe PLUS anti-rabbit
Negative control	4C9 only	PLA probe MINUS anti-mouse -and- PLA probe PLUS anti-rabbit
Negative control	IKKγ only	PLA probe MINUS anti-mouse -and- PLA probe PLUS anti-rabbit

IKKγ and IKKβ primary antibody pair was used as a positive control as these proteins are known to directly interact under the conditions tested.

2.5.4 Fluorescence-activated cell sorting (FACS)

FACS is a type of flow cytometry which can be used to physically separate cells into groups based on their light scattering and fluorescent properties. To select for ReNcell VM NSCs expressing *HTT* exon 1 transgenes following transduction (section 2.3.4.2), cells were sorted by detection of the co-expressed eGFP reporter. FACS was performed entirely by Dr. Eva C. Sirinathsingh (Prof. Gillian P. Bates' research group, KCL, London, UK).

2.5.5 Imaging flow cytometry (IFC)

IFC is an analytical technique which combines flow cytometry with fluorescent confocal microscopy, allowing for high-throughput fluorescent and morphological analysis of cellular events. IFC was used to detect, visualise and quantify NFκB nuclear translocation in various treatment paradigms, in monocytes.

Monocytes were seeded into 6-well culture plates at 2 × 10^6 cells per well, as per the usual protocol (section 2.1.2.3). Following treatment relevant to the specific experiment, culture medium was removed and cells were harvested by scraping from the culture surface in ice-cold PBS and transferring into a clear V-bottom 96-well assay plate [Greiner]. Cells were fixed with intracellular fixation buffer [IC Fixation Buffer, eBioscience] for 15 min at 4 °C with gentle shaking. Fixation buffer was removed with three 5 min washes in PBS, and then cells were permeabilised in 1 × Permeabilization Buffer [eBioscience] for 10 min at 4 °C with gentle shaking. Cells were given one 5 min wash in PBS then incubated with NFκB p65 XP Rabbit antibodies [Cell Signaling Technology; Cat No. 8242] diluted 1:200 in 1 × Permeabilization Buffer for 60 min at 4 °C with gentle shaking. Excess, unbound primary antibody was washed off with two 5 min washes in PBS, and then cells were incubated with donkey anti-rabbit IgG (H+L) R-phycoerythrin (PE)-conjugated secondary antibodies [eBioscience; Cat No. 12-4739] diluted 1:100 in FACS buffer (Appendix II-xi) for 60 min at RT, with gentle shaking in the dark. Excess, unbound secondary antibody was washed off with two 5 min washes in FACS buffer. Cells were then re-suspended in FACS buffer and stained with 1 µg/mL DAPI immediately prior to analysis.

Prepared samples were run on the ImageStream MkII [Amnis by EMD Millipore] IFC machine using INSPIRE for the ISX MkII software [EMD Millipore]. PE was excited by the 488 nm laser and DAPI by the 405 nm laser, and both were detected in different channels at 40× magnification. Full brightfield (BF) illumination images were also taken. A minimum of 10,000 images were acquired per experiment condition, per subject, and analysed using IDEAS software [Amnis]. Images were firstly gated for ‘single cells’ which were ‘in focus’ and ‘double-stained’. These gated cells provided a total cell number from which the percentage ‘translocated’ cells were calculated i.e. the percentage of cells which showed nuclear localisation of NFκB rather than cytoplasmic localisation. See Table 2.13 for details of gating parameters.

Table 2.13: Gating parameters for IFC analysis

Name of gate	X axis plot	Y axis plot	Meaning	Gate position
#1 Single cells	BF area	BF aspect ratio	Circularity	Images with 50-300 area and 0.5-1.0 aspect ratio
#2 In focus	BF RMS gradient	Normalised frequency	Contrast	50+ RMS gradient
#3 Double-stained	DAPI intensity	PE intensity	Nucleus and NFκB co-staining	Cell population in upper right quadrant
#4 Translocated	BF object mask defining cell boundary ↓ Eroded by 2 pixels to exclude cell membrane ↓ DAPI/PE similarity feature	Normalised frequency	Degree to which DAPI and NFκB staining overlap	2.5+ similarity feature within the defined mask

Similarity feature is a log transformed Pearson's correlation coefficient used to measure the degree to which two images are linearly correlated, relating in this case to a comparison of DAPI and PE intensity. RMS, root mean square.

2.5.6 Solid-phase immunoassays

2.5.6.1 Enzyme-linked immunosorbent assay (ELISA)

MG-CM and BMD-microglia lysates were prepared, harvested and stored as previously described (section 2.1.5.1). When ready to perform the ELISA, MG-CM was removed from −80 °C storage and thawed slowly to RT. ELISAs were performed using the Human BDNF or Human beta-NGF ELISA Kits for serum, plasma, cell culture supernatant and urine [Sigma Aldrich] according to the manufacturer's instructions and the protocol for Sandwich Assay Procedure. Samples and BDNF or beta-NGF protein standards were added, in duplicate, at 100 µL per well into a supplied 96-well assay plate pre-coated with capture antibodies, and incubated for 2.5 h at RT with gentle shaking. Solution was removed and plates were washed four times with 1× Wash

Buffer, patting out any remaining liquid by inverting the plate and blotting on clean paper towels. Biotinylated Human BDNF or Human beta-NGF Detection Antibody Solution was then added at 100 µL per well and the plate was incubated for 1 h at RT with gentle shaking. The solution was discarded and wash steps were repeated as above. Horseradish peroxidase (HRP)-Streptavidin solution was then added at 100 µL per well and the plate was incubated for 45 min at RT with gentle shaking. The solution was discarded and wash steps were repeated as above before adding 3,3',5,5'-Tetramethylbenzidine (TMB) One-Step Substrate Reagent at 100 µL per well. The plate was incubated for 30 min at RT with gentle shaking. Stop Solution was then added at 50 µL per well, and the absorbance was read immediately at 450 nm on a TECAN X-Fluor4 v4.51 plate reader. The BDNF or beta-NGF protein standards were used to create a standard curve from which unknown neurotrophin concentrations in MG-CM were determined, using GraphPad Prism v5.00 for Windows [GraphPad Software; La Jolla California, USA] and Microsoft Excel.

BMD-microglia lysates were removed from −80 °C storage and thawed slowly to RT before performing BCA assay to determine protein concentrations of each lysate (section 2.4.2.2). MG-CM neurotrophin concentrations were normalised to total protein from the relevant cell lysates.

2.5.6.2 MesoScale Discovery (MSD) assay

MC-CM, Mφ-CM or MG-CM and monocyte, BMD-macrophage or BMD-microglia lysates, respectively, were prepared, harvested and stored as previously described (section 2.1.5.1). When ready to perform MSD, conditioned media was removed from −80 °C storage and thawed slowly to RT. Cytokine levels in MC-CM were measured using Human Th1/Th2 10-Plex Tissue Culture Kit [MSD] analysing ten different cytokines simultaneously (IFNγ, IL-1β, IL-2, IL-4, IL-5, IL-8, IL-10, IL-12p70, IL-13 and TNFα), or Human IL-6 Singleplex Kit [MSD], according to the manufacturer's instructions. Cytokine levels in Mφ-CM were measured using V-PLEX Human Proinflammatory Panel I (4-Plex) [MSD] analysing four different cytokines simultaneously (IFNγ, IL-1β, IL-6 and TNFα), according to the manufacturer's instructions. Cytokine levels in MG-CM were measured using V-PLEX Human Proinflammatory Panel I (10-Plex) [MSD] analysing ten different cytokines simultaneously (IFNγ, IL-1β, IL-2, IL-4, IL-6, IL-8, IL-10, IL-12p70, IL-13 and TNFα), according to the manufacturer's instructions.

For the Human Th1/Th2 10-Plex Tissue Culture Kit, an initial blocking step was required. One percent MSD Blocker B (containing blocking and stabilising agents) in PBS was added to a provided 96-well assay plate, at 150 µL per well. The plate was

sealed with an adhesive plate cover and incubated for 1 h at RT with shaking at 1000 rpm. Solution was discarded and plates were washed three times with 0.05 % PBST, patting out any remaining liquid by inverting the plate and blotting on clean paper towels. This blocking step was not required for other MSD assays. Pre-prepared standards and samples (diluted as appropriate in provided Diluent 2 (containing proteins, blockers and preservatives), as determined by calibration optimisation in pre-testing) were added at 50 µL, in duplicate, to a provided 96-well assay plate pre-coated with capture antibodies immobilised on a working electrode surface. Analyte capture antibodies are organised in a single spot for singleplex plates, or in a patterned array of spots for multiplex plates. The plate was sealed with an adhesive plate cover and incubated for 2 h at RT with shaking at 1000 rpm. Solution was removed and wash steps were performed as above. Pre-prepared Detection Antibody Solution containing cytokine-specific Detection Antibodies conjugated with electrochemiluminescent labels (MSD SULFO-TAG), was then added at 25 µL per well and the plate was covered and incubated for 2 h at RT with shaking at 1000 rpm. Wash steps were repeated as above, and then 2 × Read Buffer T (with surfactant) was added at 150 µL per well, catalysing the electrochemiluminescent reaction. The plate was then loaded onto a Sector Imager 6000 (Model 1200) MSD instrument, operated using MSD Discovery Workbench software. A voltage was applied to the plate electrodes causing the captured labels to emit light, for which the intensity was measured to provide a quantitative measure of analytes in the sample. Sample concentrations were calculated by the software, using the calibrator standards of known analyte concentrations.

Cell lysates were removed from −80 °C storage and thawed slowly to RT before performing BCA assay to determine protein concentrations of each lysate (section 2.4.2.2). Analyte concentrations were normalised to total protein from the relevant cell lysates.

2.5.6.3 HTT quantitation using MSD

Total HTT and expanded HTT levels were quantified in ReNcell VM+*HTT* exon 1 NSC and 10 DD neuronal cultures using the MSD platform and a proprietary, optimised protocol. Cell pellets were sent to Evotec-CHDI HTT Quantitation Service, Hamburg, Germany. Total human HTT was detected using 2B7/4C9 antibody pair (service HTT assay reference #39) and polyQ expanded (mutant) HTT was detected using 2B7/MW1 antibody pair (service HTT assay reference #6). Both assays were quantified by standard recombinant HTT reference protein (Human HTT NF573Q23 spiked into 0.01 mg/mL of a wild-type mouse whole brain lysate (C57BL/6)). Cell pellets were lysed in 120-300 µL MSD lysis buffer (depending on pellet size) and protein concentration was determined by BCA assay (section 2.4.2.2). All lysates were run in parallel on the same

MSD plate and tested in technical triplicates at a final concentration of 0.01 mg/mL. Standard proteins were applied at a final concentration range between 0.001 and 1 fmol/µL. Final buffer concentrations can be found in Appendix II-xii. Samples were analysed in a total of two assay runs.

2.5.7 Time-resolved fluorescence resonance energy transfer (TR-FRET)

Time-resolved fluorescence resonance energy transfer (TR-FRET) was used to quantify levels of total HTT and expanded HTT in ReNcell VM+full-length *HTT* NSC lines. Dry cell pellets were sent to Dr. Andreas Weiss (IRBM-Promidis, Italy) who performed TR-FRET as described in 'Microtiter plate quantification of mutant and wild-type huntingtin normalized to cell count' (Weiss *et al.* 2011). Two antibody pairs, 2B7/4C9 and 2B7/MW1, were used to simultaneously detect wild-type HTT and mHTT, respectively. 2B7 was labelled with the donor fluorophore terbium (Tb) cryptate Lumi4, which when excited transfers energy over non-overlapping emission spectra to excite two acceptor fluorophores, D2 (labelling MW1) and Alexa488 (labelling 4C9), simultaneously. After excitation of the Tb donor at 320 nm and a time delay of 100 µs, emission signals of Alexa488 and D2 were detected at 520 and 665 nm, respectively. The 2B7/4C9 antibody pair displays preferential detection of wild-type HTT because the epitopes are separated by the polyQ stretch, and polyQ elongation in mHTT increases the distance between the two labelled antibodies resulting in a reduced TR-FRET signal. The 2B7/MW1 antibody pair displays preferential detection of mHTT due to the specificity of MW1 for elongated polyQ stretches. The HTT signals were normalised to PicoGreen signal, a highly sensitive fluorescent double-stranded specific DNA dye, whose signal intensity correlates with the amount of double-stranded DNA, and therefore the number of cells in a sample. PicoGreen was excited at 485 nm and detected at 535 nm.

2.6 Cytotoxicity assays

2.6.1 Lactate dehydrogenase (LDH) cytotoxicity assay

CytoTox 96 Non-Radioactive Cytotoxicity Assay [Promega] is a colorimetric assay which was used to quantitatively measure lactate dehydrogenase (LDH) in cell culture supernatants as a broad indicator of total cell death by apoptosis and/or necrosis. LDH is a stable cytosolic enzyme which is released upon cell lysis. The assay was performed, according to the manufacturer's instructions, to measure cytotoxicity in neuronal or myeloid cell cultures following media titration, in neuronal cultures treated with Mφ-CM or MG-CM in co-culture experiments, and in primary monocytes treated with a range of laquinimod concentrations.

Culture supernatants were added, at least in duplicate, to a 96-well clear flat-bottomed assay plate at 50 µL per well. A control culture well, or all cultures, were then lysed in 0.9 % v/v Triton X-100 for 45 min on a shaking platform at 400 rpm, releasing all LDH from the cells into the culture supernatant (Total LDH). Total LDH supernatants were added to the assay plate. In order to measure background LDH, media only and/or Mφ-CM or MG-CM from the same aliquot which had been used to treat the neurons were also included in the assay. Prepared Substrate Mix reconstituted in Assay Buffer was added at 50 µL per well, and the plate was incubated for 30 min at RT in the dark. In a coupled enzymatic reaction, LDH converts oxidised NAD+ and lactate to reduced nicotinamide adenine dinucleotide (NADH) and pyruvate. In turn, NADH and the tetrazolium salt 2-(4-iodophenyl)-3-(4-nitrophenyl)-5-phenyl-2H-tetrazolium (INT) are converted into a red formazan product (and NAD+) by NADH dehydrogenase. The amount of colour formed is proportional to the number of lysed cells. Stop Solution (1 M acetic acid) was then added at 50 µL per well and absorbance of the red formazan product was measured at 490 nm on a TECAN X-Fluor4 v4.51 plate reader. Data was analysed using Microsoft Excel, and percentage cell death for each condition was calculated using the following formula:

$$Percentage\ cell\ death\ = \frac{Supernatant\ LDH\ -\ background}{Total\ LDH\ -\ background}\ \times\ 100$$

2.6.2 ATP cell viability assay

CellTiter-Glo Luminescent Cell Viability Assay [Promega] was used to measure the number of viable cells in a culture by quantifying their levels of ATP, indicative of metabolic activity. The assay was performed, according to the manufacturer's instructions, to measure cell viability in neuronal or myeloid cell cultures following media titration in pre-testing for co-culture. It is important to note that due to mHTT-induced mitochondrial dysfunction, ATP levels may be affected in mHTT-expressing cells, and consequently results from this assay should be interpreted with caution. In all cases, an alternative measure of cytotoxicity/viability was used in conjunction with this assay.

Cells were cultured in 96-well plates and treated as per the relevant experiment. When ready to perform the assay, culture medium was removed and replaced with 100 µL fresh RT culture medium. In order to measure background luminescence, media was also added to wells without any cells. Pre-prepared Cell-Titer Glo Reagent was added at 100 µL per well, and the mixture was pipetted up and down to detach cells from the culture surface. The culture plate was incubated for 2 min at RT with vigorous shaking to induce cell lysis, then cells were transferred into a 96-well white, flat-bottomed, chimney-well assay plate [Greiner] and incubated at RT without shaking for a further 10

min to stabilise the luminescent signal. A thermostable luciferase (Ultra-Glo Recombinant Luciferase) generates a stable “glow-type” luminescence when, along with magnesium ions, it catalyses the reaction of Beetle Luciferin, ATP and oxygen to Oxyluciferin, adenosine monophosphate (AMP), pyrophosphate and carbon dioxide. The luminescent signal is proportional to the amount of ATP present, which is proportional to the number of viable cells (Crouch *et al.* 1993). Luminescence was recorded using a TECAN Infinite plate reader and TECAN iControl software, and data was analysed using Microsoft Excel. Average background luminescence was subtracted from all sample readings.

2.6.3 Propidium iodide (PI) viable cell exclusion

PI is a red fluorescent stain which intercalates in DNA. As it is also membrane impermeant, PI stains only the nuclei of dead or compromised cells, and is generally excluded from viable cells. PI staining was used to quantify the number of non-viable cells in neuronal cultures following media titration in pre-testing for co-culture, and following treatment with Mφ-CM or MG-CM in co-culture. PI viable cell exclusion measures cellular demise at a snap shot in time and can be used simulatenously with a nuclear stain, such as Hoechst, to distinguish apoptotic cells from healthy or necrotic cells by assessment of nuclear shape and condensation.

Neurons were cultured on coverslips and treated as per the relevant experiment. To measure cytotoxicity, PI was added directly to the culture medium at 1.25 µg/mL final concentration and cells were returned to the incubator for 20 min. Hoechst 33342 was then added directly to the culture medium at 0.8 µg/mL final concentration and cells were returned to the incubator for a further 10 min. Coverslips were then carefully removed from culture wells and floated face-down on 3 µL 37 °C DPBS on a glass microscope slide. Cells were imaged immediately using a Zeiss LSM 710 confocal microscope (section 2.7.3), and images were quantified using the methods described in section 2.7.3.1.

2.6.4 Trypan Blue viable cell exclusion

Trypan Blue is a dye which is impermeant to the intact cell membranes of viable cells. It can, however, traverse the compromised membranes of non-viable cells, staining them blue. Trypan Blue exclusion was used to count viable cells in routine cell culture and before cryopreservation of cell lines. A 0.4 % solution of Trypan Blue [Thermo Fisher Scientific] in DPBS was added 1:10 to a small volume of cells in suspension. Ten microlitres cell suspension was pipetted onto a haemocytometer, and cells were visualised using a light microscope to count total number of viable cells per millilitre of cell suspension.

2.7 Microscopy

All images were visualised, analysed and quantified blinded to experiment condition and subject group to eliminate experimenter bias.

2.7.1 Phase-contrast microscopy

A Zeiss Axiovert 25 inverted microscope, equipped with 10×, 20× and 40× objectives, was used to view and monitor cells during routine cell culture. A NIKON Eclipse TS100 inverted microscope equipped with 10×, 20× and 40× objectives and linked to photo viewing software was used to acquire phase-contrast images.

2.7.2 Live-cell epifluorescence microscopy

A NIKON Eclipse TS100 inverted microscope equipped with a FITC filter (465-495 nm) was used to detect native eGFP reporter expression in cells transduced with *HTT* exon 1 by infection with A2UCOE lentiviruses. Images were acquired using linked photo viewing software.

2.7.3 Confocal fluorescence microscopy

A Zeiss LSM 710 confocal microscope was used to acquire confocal images of cells with immunofluorescent staining. DAPI and Hoechst 33342 were excited by the 405 nm laser. Alexa Fluor 488 and WGA were excited by the 488 nm laser. PI was excited by the 514 nm laser. Alexa Fluor 568 and the red fluorescent spots produced by PLA were excited by the 561 nm laser. Zeiss Immersol Immersion Oil 518F was dabbed onto each coverslip before viewing cells via Plan-Apochromat 40×/1.4 or 63×/1.4 oil differential interference contrast (DIC) M27 objectives. All images were taken with constant gain and pinhole settings at a resolution of 1024 × 1024 pixels. Operation of the microscope and processing of acquired images was performed using ZEN Imaging Software (Black edition) [Zeiss].

Confocal microscopy images of mHTT aggregates in ReNcell VM+*HTT* exon 1 neuronal cultures were acquired using the Opera LX High Content Screening (HCS) system [PerkinElmer; Waltham, Massachusetts, USA]. The system was operated by Dr. Christin Luft (Dr. Robin Ketteler's research group, Laboratory for Molecular Cell Biology (LMCB)-MRC, UCL, London, UK).

2.7.3.1 Confocal image quantification methods

All confocal images acquired for quantification of any form were taken from at least five random fields of view per coverslip from at least duplicate coverslips.

To perform cell counts on acquired confocal images, ImageJ image analysis software (Schneider et al. 2012) was used to perform automated cell counts using the built-in

ImageJ Quantitation Tasks outlined in Figure 2.4. This method was used for quantification of: percentage eGFP reporter positive cells in NSCs transduced with *HTT* exon 1; percentage full-length *mHTT* expressing cells (by ICC with 2B7/MW1 co-stain (section 2.5.2) in NSCs transduced with full-length *HTT* (138 CAG); and percentage non-viable cells (by PI viable cell exclusion (section 2.6.3)) in wild-type neuronal cultures for co-culture media titration, or following treatment with Mφ-CM or MG-CM in co-culture. Total cell counts were acquired using the software and then the number of eGFP positive, 2B7/MW1 co-stained, and PI positive cells, respectively, were counted manually. Percentage positive cells was calculated from at least ten random fields of view, taken at a maximum magnification of 40×, from at least duplicate cultures.

To identify expression of the transgene in a subclone of ReNcell VM+full-length *mHTT* (138 CAG) NSCs, levels of HTT and mHTT were detected by ICC with 2B7 and MW1 respectively. Intensity of staining was quantified using Volocity v6.1.1 and the built-in Volocity Quantitation Tasks outlined in Figure 2.5, and compared to wild-type NSCs. Volocity software was also used to quantify the average number of red fluorescent spots per cell in BMD-macrophages following PLA (section 2.5.3), using the built-in Volocity Quantitation Tasks outlined in Figure 2.6.

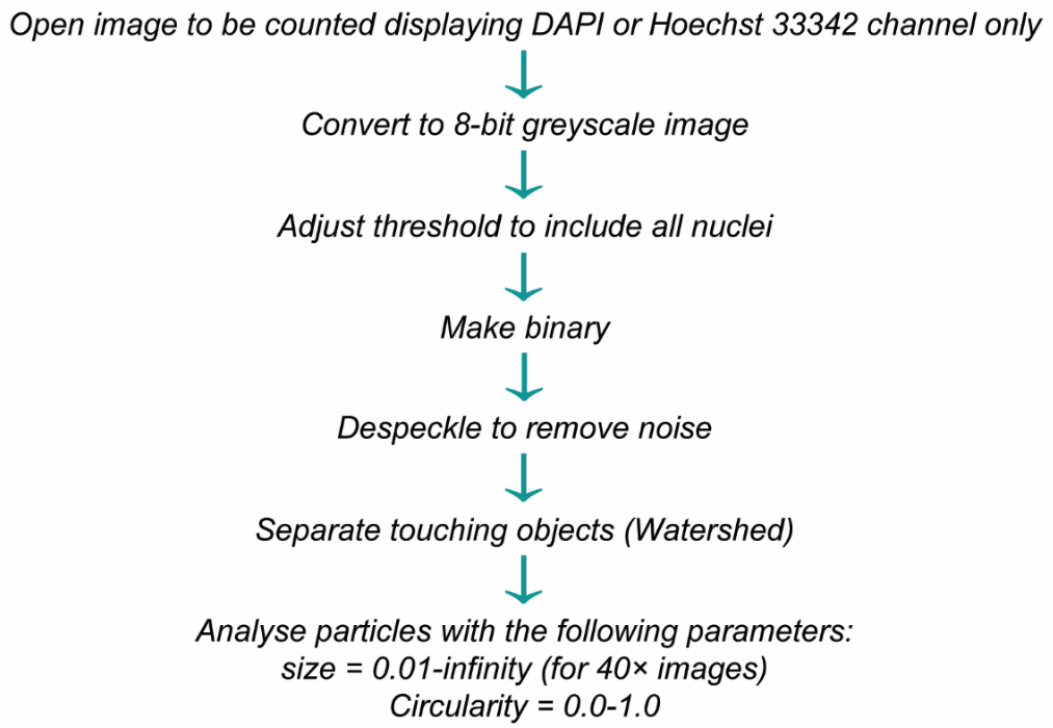

Figure 2.4: ImageJ Quantitation Tasks for automated cell counting

Each image was quantified independently. Cell counts for each image were recorded in Microsoft Excel and used in further calculations.

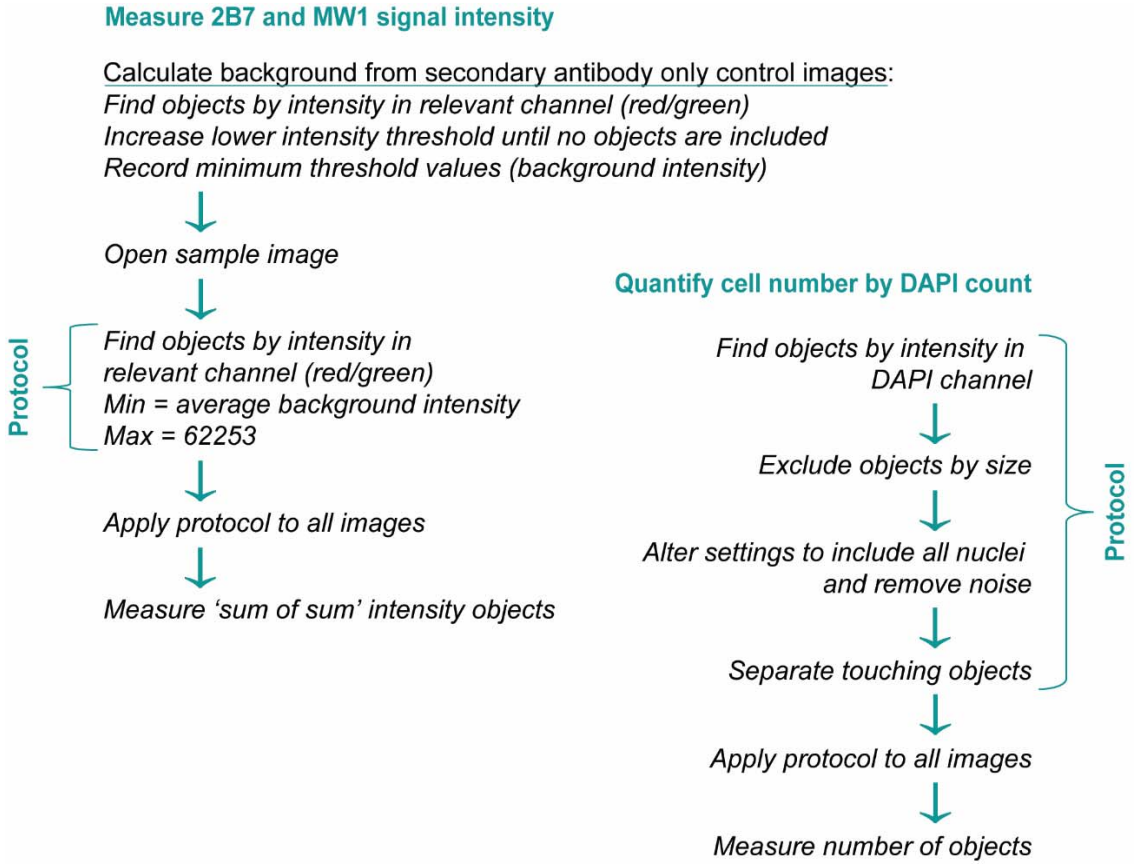

Figure 2.5: Volocity signal intensity Quantitation Tasks

HTT and mHTT levels quantified in cells by measuring intensity of 2B7 (red) and MW1 (green) staining, respectively, in confocal images following ICC. Total intensity and cell number (DAPI count) were measured. Data was extracted from Volocity and imported into Microsoft Excel for analysis. Total intensity per image was divided by total cell number per image to give average intensity per cell.

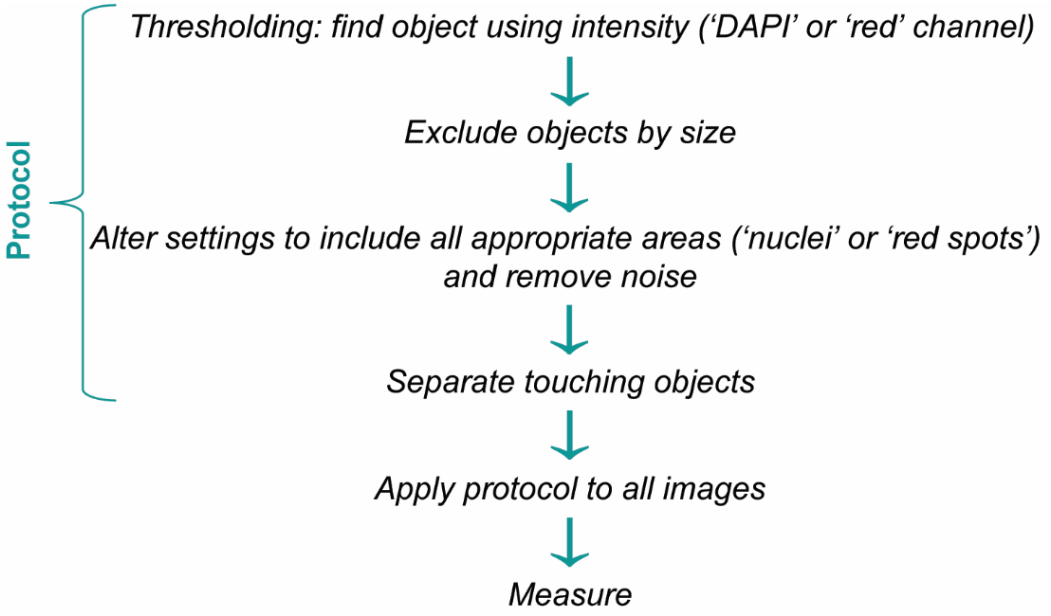

Figure 2.6: Volocity Quantitation Tasks for PLA image analysis

Parameters (protocol) were set using positive control images before applying to all sample images and negative controls. Data was extracted from Volocity and imported into Microsoft Excel for analysis. Total number of red spots was divided by total DAPI count to give average number of spots per cell for each image.

2.8 Small molecule drug testing (laquinimod)

Pre-clinical drug testing of laquinimod in primary HD patient myeloid cells (monocytes and BMD-macrophages from healthy volunteers, pre-manifest HD gene carriers and manifest HD patients), was performed in collaboration with Teva Pharmaceutical Industries Ltd. Laquinimod, a quinolone-3-carboxamide, was received as a white powder, and was reconstituted in sterile tissue culture grade water. The lowest therapeutic dose tested in humans (for the treatment of MS) is 0.6 mg, which equates to a plasma level of 1 μM active drug (98 % albumin-bound; 1.8-2.0 % free active drug). Laquinimod has an 80 h half-life in humans and a 3.5 h half-life in mice.

2.8.1 Testing drug cytotoxicity *in vitro*

Monocyte cultures were treated with a range of laquinimod concentrations (0, 0.001, 0.01, 0.1, 0.5, 1, 5, 10, 50 or 100 μM), in duplicate, for 24 or 48 h. Cell death levels post-treatment were assessed by LDH cytotoxicity assay, as described in section 2.6.1., and compared to cell death levels in untreated monocyte cultures.

2.8.2 Measuring cytokine release in laquinimod-treated myeloid cells

Monocyte cultures were treated with 1 or 5 μM laquinimod for 2 or 24 h, or were untreated. Cells were then given a media change, and for cultures in the "stimulated" condition, 1 μg/mL LPS and 10 ng/mL IFNγ was included. Cultures were returned to

the incubator for 24 h. Three drug treatment durations and two drug concentrations were tested: 2 h pre-treatment (2hPT) or 24 h pre-treatment (24hPT) with 1 or 5 μM laquinimod, and 24 h 5 μM pre-treatment with 24 h continued 5 μM laquinimod treatment during stimulation (24 h pre-treatment with 24 h continued treatment, 24hPT+24hCT). MC-CM and cell lysates were collected, processed and stored as described in section 2.1.5.1, and cytokine levels were measured using MSD Human Th1/Th2 10-Plex Tissue Culture Kit or Human IL-6 Singleplex Kit, as described in section 2.5.6.2. Results for IFNγ levels were not considered in the analysis due to presence of this cytokine in monocyte culture medium as a priming agent for stimulated conditions.

2.8.3 Investigating NFκB pathway modulation as laquinimod mechanism of action

The effects of laquinimod on dysfunctional NFκB signalling in HD myeloid cells was assessed by monitoring IκB degradation kinetics, p65 nuclear translocation, and interactions between mHTT and IKKγ in laquinimod-treated cells.

IκB degradation kinetics in response to LPS stimulation were assessed by Western blotting techniques. Monocytes received 24hPT with 5 μM laquinimod, or were untreated, then were stimulated with 1 μg/mL LPS over a time-course of 0-60 min. Cell lysates were prepared as described in section 2.4.1.2 and Western blots were performed as described in sections 2.4.3, 2.4.4 and 2.5.1.2.

NFκB p65 nuclear translocation in response to LPS stimulation was assessed by IFC. Monocytes received 24hPT with 5 μM laquinimod, or were untreated, then were stimulated with 1 μg/mL LPS for 45 min. IFC was then performed as described in section 2.5.5.

Interactions between mHTT and IKKγ were assessed by PLA. BMD-macrophages were treated with 5 μM laquinimod for 24 h, or were untreated. Cells were then fixed and PLA was performed as described in section 2.5.3.

2.9 Statistical analyses and data presentation

Experiment results which were analysed statistically included at least three biological repeats i.e. parallel measurements of biologically distinct samples (e.g. the same experiment performed on different days using the same cell line at different passage numbers; or measuring responses in primary cells from several different subjects receiving the same treatments at the same time). Experiments were performed with at least two internal replicates per condition i.e. repeated measurements of the same condition (e.g. duplicate cell treatment wells) and/or sample (e.g. triplicate assay read-

outs). Mean average results from experiment internal replicates were calculated using Microsoft Excel.

Unless otherwise stated, statistical analysis of data was performed using GraphPad Prism v5.00 for Windows, and data were presented graphically using the same software. Data are presented as mean ± standard error of the mean (SEM), or in some cases as mean ± standard deviation (SD). Statistical *p*-values are graphically presented as follows: *$p<0.05$, **$p<0.01$, ***$p<0.001$, ****$p<0.0001$.

2.9.1 Student's *t*-test

To compare the mean differences between two groups (e.g. laquinimod-treated versus untreated), based on a single response variable (e.g. percentage p65 nuclear translocation), a two-tailed, Student's *t*-test was used. If the two groups could be matched (e.g. comparing the effects of two different treatments in the same subjects), the *t*-test was paired.

2.9.2 Analysis of variance (ANOVA)

To compare the mean differences between three or more groups (e.g. healthy volunteer, pre-manifest HD and manifest HD subject groups), based on a continuous response variable (e.g. percentage neuronal culture death), an analysis of variance (ANOVA) was used. When groups of a single factor were compared based on a single response variable (e.g. comparing subject groups by percentage cell death), a one-way ANOVA was used. When groups of two or more factors were compared based on a single response variable (e.g. comparing percentage cell death in different subject groups over various time-points), a two-way ANOVA was used.

If the groups could be matched (e.g. comparing IκB degradation kinetics over time in laquinimod-treated or untreated cells from the same subjects), and no data was missing for each condition, repeated measures (RM) were used in the ANOVA. If subject matching was found to be significant ($p<0.05$) by the ANOVA, this indicated that RM had successfully separated between-subject variability from within-subject variability, therefore controlling for factors that cause variability between subjects and resulting in a powerful statistic test. If subject matching was found to be non-significant ($p>0.05$), this indicated that the matching was not effective, and consequently repeated measures is a much less powerful statistical test due to having fewer degrees of freedom. In cases of ineffective subject matching, an ordinary ANOVA (without RM) was used.

To compare each group mean with every other group mean, one-way ANOVAs were performed with Tukey post-hoc tests. If each group mean was compared to one control

mean, a Dunnett post-hoc test was performed. If two-way ANOVAs were performed, appropriate sets of means were compared by Bonferroni post-hoc multiple comparison tests.

2.9.3 Linear mixed regression model

Statistical analysis of cytokine levels in MC-CM from laquinimod-treated (and untreated) monocytes was performed by an independent statistician, Ruth Farmer (London School of Hygiene & Tropical Medicine, Department of Medical Statistics, London, UK). Her description of the statistical model she used to analyse the data set, taken from the publication of this collaborative work in Journal of Neurochemistry ('Laquinimod dampens hyperactive cytokine production in Huntington's disease patient myeloid cells' (Dobson *et al.* 2016) (Appendix III-i)), is as follows:

"The data set was split into two - stimulated and non-stimulated conditions - to perform statistical analysis. Not every subject had a measurement for every condition due to some samples failing quality control, leading to unbalanced data. Data were log transformed prior to analysis to improve normality assumptions. A linear mixed model was fitted to each of the subsets separately, assuming exchangeable correlation, with robust standard errors to allow for misspecification of the covariance structure. Comparisons of interest were calculated using linear contrasts. This approach allows for data from a subject to be used even if some of the conditions are missing, under a missing at random assumption. For the HD combined comparisons, a weighted combination of pre-manifest HD and manifest HD was used, based on the total number of patients in those subgroups. All analyses were additionally adjusted for age. Multiple comparison adjustments were not made due to the small sample size and lack of independency in cytokine activity, and this was taken into consideration when reviewing the findings from these analyses. All results of cytokine levels and statistical analysis of this data are graphically presented and reported on the logarithmic scale. It is important to note that natural differences in cytokine release from primary human monocytes leads to highly variable data, and the sample size limits the precision for which estimates of between condition and between group differences can be made. Therefore, in cases where there is absence of statistical evidence it is not possible to determine whether this is due to no effect or that the random variation in measurements masks any effect that may be present."

2.9.4 Power calculations

In some cases, power calculations were performed to determine appropriate sample sizes using DSS Researcher's Tool Kit Sample Size Calculator [online source at www.dssresearch.com, DSS Research, DC, USA]. Data from preliminary experiments

with a sample size of at least *n*=3 were used to provide test values, and sample averages and SDs for each sample. The confidence level (α-error level) i.e. the probability of incorrectly rejecting the null hypothesis that there is no difference in the average values, was set to 5 % (an alpha of 5 % to a 95 % confidence interval). Statistical power (β-error level) i.e. the probability of incorrectly failing to reject the null hypothesis, was set to 50 %. Sample sizes required to give the power to observe differences between sample groups were then automatically calculated.

3 Development and characterisation of human neuronal-myeloid cell co-culture models of HD

3.1 Background

To assess neuronal-myeloid cell interactions in the pathogenesis of HD, there is a requirement for the development of novel HD cell models and co-culture models. Current HD cell culture models include primary cells isolated from HD animal models or HD patients, immortalised human cell lines over-expressing N-terminal fragments of mHTT or the full-length gene and iPSC lines derived from HD patients. While all of these models have provided invaluable insight into pathological cellular mechanisms of HD, they are also limited in their usefulness for investigating pathogenic neuronal-myeloid cell interactions in HD due to model-specific drawbacks. Primary neurons and microglia are either not of human origin or lack availability on a large scale, immortalised human neuronal and myeloid cell lines generally fail to represent their primary human cell counterparts, and the derivation of specific neuronal subtypes or microglia from iPSCs is not yet fully established. With the aim of assessing cellular interactions between neurons and myeloid cells in HD, there is a requirement for the development of novel neuronal and microglial HD cell models.

Transgenic mice are the most commonly used animal models in HD research, and can be classified as fragment, full-length or knock-in models depending on how they were generated. Fragment models, such as R6/2 (Mangiarini *et al.* 1996), express N-terminal fragments of human *mHTT* on a wild-type diploid murine *Htt* background; full-length models, such as BACHD (Gray *et al.* 2008) or YAC128 (Hodgson *et al.* 1999; Slow *et al.* 2003; Van Raamsdonk *et al.* 2007), express full-length human *mHTT* on a wild-type diploid murine *Htt* background; and knock-in models, such as Hdh (Q150/Q150) (Shelbourne *et al.* 1999), express the endogenous murine *Htt* gene with CAG repeats added, or ‘knocked-in’, to create an expanded murine *Htt* gene. Various different primary cell types have been isolated from these HD mouse models and cultured *ex vivo*, and studying them has led to the discovery of several cellular and molecular mechanisms underlying key pathological processes caused by mHTT expression. Of particular importance, is the availability of primary neurons throughout

the disease course, which recapitulate many features of neurons *in vivo* (Ross and Tabrizi 2011), and cannot be isolated from humans until post-mortem.

HD mouse models have been shown to mimic some of the pathological features and symptoms of HD, such as widespread aggregate deposition throughout the brain, neurodegeneration and late-onset behavioural phenotypes including motor abnormalities (Heng *et al.* 2008). However, a major issue confounding the study of cells from these models is that HD is an illness which only occurs in humans, and no individual animal model fully recapitulates the complex pathological phenotypes and progressive motor, cognitive and psychiatric impairments observed in HD, including the massive striatal neuronal degeneration seen in humans (Ross and Tabrizi 2011). Consequently, while animal models have been invaluable in improving our understanding of the human condition and provide means to screen potential therapeutic compounds in an *in vivo* setting, it is essential that HD is additionally studied on a human background alongside the use of animal models.

With the aim of studying cellular neural-immune interactions in HD pathogenesis and discovering immunomodulatory agents to alter the course of disease, another significant issue is that immune systems are species specific. Key differences have been reported between human and murine primary microglia (Smith and Dragunow 2014; Watkins and Hutchinson 2014) and many of the therapeutic immunomodulatory reagents recently developed are human specific (Shultz *et al.* 2012). HD mice and the primary cell cultures derived from them are therefore flawed for investigation of the immune system and neural-immune interactions in HD.

Immortalised human cell lines have also been used to model HD *in vitro*. Human HD cell lines have been developed using transient transfection, stable transduction and inducible expression strategies with N-terminal fragments of *mHTT* or the full-length gene. Most commonly, cell models of HD utilise the exon 1 fragment of *mHTT*. Exon 1 contains the expanded CAG repeat region leading to HD and has been shown to exist, independently of the full-length protein, *in vivo* in the neuronal nuclei of the Hdh (Q150/Q150) knock-in mouse model (Landles *et al.* 2010), in HD post-mortem brain (DiFiglia *et al.* 1997) and in HD patient peripheral immune cells (Weiss *et al.* 2012), following aberrant splicing of *mHTT* mRNA (Sathasivam *et al.* 2013) and/or proteolytic cleavage and fragmentation of the full-length protein (Landles *et al.* 2010; Weiss *et al.* 2012). There is a large body of evidence which suggests the exon 1 protein fragment is the primary pathogenic species in HD, and is sufficient to cause neuronal dysfunction and death (Mangiarini *et al.* 1996; Ross and Tabrizi 2011). Indeed, the R6/2 model, expressing human mHTT exon 1, has the most severe and fast-progressing disease

phenotype of any HD mouse model (Heng *et al.* 2008) along with a distinct proinflammatory immune profile representative of the human condition (Björkqvist *et al.* 2008). Cell lines expressing only exon 1 of mHTT therefore represent highly relevant cell models of HD, and due to its small size (exon 1 coding sequence; 269 bp (21 CAG)), exon 1 can easily be packaged into virus particles and efficiently inserted into the genomic DNA of a cell line for stable, long-term expression over multiple passages.

The full-length *HTT* gene is very large, spanning 180 Kb and consisting of 67 exons. *HTT* exon transcripts are expressed as two alternatively polyadenylated forms; a larger transcript of approximately 13.7 Kb which is expressed predominantly in brain, and a smaller transcript of approximately 10.3 Kb which is more widely expressed. Consequently, introduction of the full-length mutant transgene into the genomic DNA of a cell line is complex; viral delivery can be very inefficient and ultimately translation into the final 350 KDa protein is often unsuccessful. For this reason, very few HD cell lines exist with stable expression of full-length mHTT. While exon 1 models have led to novel insights into the pathophysiology of HD, it may also be important to study the HD mutation in the context of the whole HTT gene and protein. Native mHTT has been shown to exist in its full-length form in HD patient post-mortem brain, in the brains of BACHD mice, and in the brains and primary neurons from a Q140/Q140 knock-in mouse model of HD (Sapp *et al.* 2012). *In vitro* the expanded polyglutamine region within the monomeric full-length mHTT protein has been associated with increased cellular toxicity (Sapp *et al.* 2012), and in a HD *Drosophila* model and BACHD mice, neuropathology and behavioural phenotypes occur with expression of human full-length mHTT in the absence of detectable N-terminal fragments (Gray *et al.* 2008; Romero *et al.* 2008). This is evidence to indicate a role of full-length mHTT in the pathogenesis of HD and thus there is a requirement for the development of better full-length cellular models.

Immortalised human HD cell lines have proved valuable for biochemical investigations (Ross and Tabrizi 2011), and being human cells they more closely recapitulate human-specific biological processes (Shultz *et al.* 2012) than primary murine cells. However, immortalised cell lines have often been transformed with oncogenes, viruses and other inducible modifications which may alter their phenotype and affect the outcome of experiments. Additionally, for one of the main cell types of interest, microglia, none of the available immortalised human cell lines (for example CHME3, HMC3 and HMO6 (Janabi *et al.* 1995; Nagai *et al.* 2001)) fully recapitulate the phenotypes of these cells *in vivo*, or even of their primary human microglia counterparts.

In order to combat the limitations of animal cells or immortalised cell lines, primary human cells can also be isolated from healthy volunteers or HD patients, cultured *ex vivo* and manipulated in an *in vitro* setting. Primary human HD cells can be obtained from blood samples, buccal smears or biopsies of skin, fat or muscle in the living patient. Experiments using such samples have proven very useful for studying general cellular pathophysiology caused by native mHTT expression, and for drug screening strategies, over the disease course in an *ex vivo* HD patient setting. More specifically, protocols have been highly optimised for the isolation and differentiation of specific peripheral immune cell subtypes from whole blood samples, including the isolation of monocytes and *in vitro* differentiation into BMD-macrophages (Björkqvist *et al.* 2008; Träger *et al.* 2014a), allowing for the study of immune cell dysfunction in primary HD patient cells directly. Primary human neuronal and microglial cultures, however, are much more difficult to obtain. Isolation protocols are highly invasive, involving surgical brain biopsies, which are seldom performed for therapeutic or diagnostic purposes in HD patients, or cultures taken immediately post-mortem. Such samples are therefore not ideal for large-scale experiments due to their lack of availability, and generally only provide a window into end-stage disease on post-mortem. The development and screening of therapeutics in cells, with the aim of slowing or preventing HD progression, requires the use of models which can recapitulate pre-manifest and early stages of manifest disease, as this is the optimal window for intervention before large-scale neuronal loss.

While the culture of primary HD microglia is not feasible on a large-scale due to difficulties in obtaining samples and lack of availability, it has also been reported that despite having different developmental origins (Ginhoux *et al.* 2010; Saijo and Glass 2011; Goldmann *et al.* 2016) and unique molecular signatures (Greter *et al.* 2015; Michell-Robinson *et al.* 2015), microglia and BMD-macrophages are highly dynamic and become almost phenotypically indistinguishable when exposed to the same microenvironment (Enose *et al.* 2005; Greter *et al.* 2015). Under neuroinflammatory conditions there is a large phenotypic overlap between microglia and recruited BMD-macrophages, and it is thought this may be because BMD-macrophages adopt a functional and morphological state similar to resident microglia in an equal response to the same environmental stimuli (O'Koren *et al.* 2016). Indeed, when cultured *ex vivo* under identical conditions, primary microglia and BMD-macrophages display structural and functional similarities (Gordon *et al.* 1988; Schmid *et al.* 2009; Butovsky *et al.* 2014). Therefore, in the interest of developing a microglial cell model which better represents the phenotypes of human microglia than current immortalised cell lines, it may be feasible to differentiate *ex vivo* HD patient monocytes into microglia-like cells

by exposing differentiating cultures to stimuli representative of the CNS environment. Ohgidani and colleagues recently reported direct induction of ramified microglia-like cells from human monocytes by treatment with GM-CSF and IL-34 (Ohgidani *et al.* 2014).

Recently established iPSCs derived from HD patients (Park *et al.* 2008) offer many of the positive aspects of both primary human cell culture and immortalised cell lines, and may be especially useful for the culture of HD patient neurons *in vitro*. Fibroblasts can be isolated from HD patients and re-programmed as pluripotent stem cells via the introduction of genes for specific transcription factors (Takahashi and Yamanaka 2006; Park *et al.* 2008). Following this, pluripotent stem cells can be differentiated *in vitro* into cell types of interest, including specific neuronal subtypes, some of which have been shown to exhibit some disease-relevant phenotypes (Lu and Palacino 2013). However, they have limitations including genetic heterogeneity and phenotypic variability between cell lines, a lack of isogenic genetic controls, absence of mHTT aggregates, lack of a robust neurodegenerative phenotype, and long differentiation protocols of greater than ninety days. Also, protocols for differentiation of iPSCs into authentic MSNs (the main neuronal subtype of interest for the study of HD) or microglia, are not yet fully established.

A human NSC-derived neuronal model, ReNcell VM, addresses many of the deficiencies outlined above for iPSC-derived neuronal models. ReNcell VM was derived from human foetal ventral mesencephalon and immortalised by retroviral transduction with a *v*-myc oncogene (Donato *et al.* 2007). NSCs were expanded long-term and can be differentiated into mature neuronal cultures which have been well reported as a valid model of human neurons in culture (Hoffrogge *et al.* 2006; Donato *et al.* 2007; Wood-Kaczmar *et al.* 2008; Gandhi *et al.* 2009; Morgan *et al.* 2009; Choi *et al.* 2014). ReNcell VM has also been demonstrated to successfully model neurodegenerative diseases *in vitro*, including AD (Choi *et al.* 2014) and PD (Wood-Kaczmar *et al.* 2008; Gandhi *et al.* 2009), following disease-relevant genetic manipulation of the cell line. ReNcell VM therefore shows potential for modelling human HD neurons by stable transduction with human *mHTT* exon 1 or the full-length *mHTT* gene. Wild-type and HD lines may be derived from NSCs from a renewable source with an isogenic background, which maintain genotype over at least 80 passages and can be robustly and consistently differentiated into cultures with high neuronal yields and minimal phenotypic variability over a period of only 5-14 days (Hoffrogge *et al.* 2006; Donato *et al.* 2007; Wood-Kaczmar *et al.* 2008; Gandhi *et al.* 2009; Morgan *et al.* 2009; Choi *et al.* 2014).

Overall, it is clear that there is requirement for new neuronal and microglial cell models of HD which more accurately represent the human disease while being easily obtainable and useable on a large scale. Here, ReNcell VM neuronal lines with stable expression of human *mHTT* exon 1 or full-length *mHTT* were generated and a novel differentiation protocol for induction of microglia-like cells from *ex vivo* HD patient monocyte cultures was discovered. These cell models have the potential to meet necessary requirements while avoiding many of the deficiencies of the aforementioned HD cell models. Once established, these novel neuronal and microglial models of HD were placed in various co-culture paradigms, along with BMD-macrophages which can be differentiated *in vitro* from *ex vivo* primary monocyte cultures using a previously established protocol (Träger *et al.* 2014a), in order to investigate neuronal-myeloid cell interactions in the pathogenesis of HD. Various novel neuronal-myeloid cell HD co-culture models were developed and characterised here and their usefulness for investigation of HD pathophysiology was assessed.

3.2 Aims

1) Characterise wild-type ReNcell VM NSCs and differentiated neuronal cultures.
2) Generate novel human ReNcell VM NSC-derived neuronal cell lines with stable expression of human *HTT* exon 1 with CAG repeats in the pathogenic and non-pathogenic range.
3) Generate novel human ReNcell VM NSC-derived neuronal cell lines with stable expression of full-length human *HTT* with CAG repeats in the pathogenic and non-pathogenic range.
4) Develop a novel differentiation protocol for induction of microglia-like cells from *ex vivo* monocyte cultures isolated from healthy volunteers and HD patients, and characterise BMD-microglia as a model of human microglia in culture.
5) Develop HD and control co-culture models using *HTT* exon 1 and full-length *HTT* cell lines in combination with BMD-macrophages and BMD-microglia.

3.3 Methods

A summary of methods used in this Chapter is outlined below. Full details of experimental protocols can be found in Chapter 2: Materials and Methods.

ReNcell VM NSCs were cultured as described in section 2.1.1.3 and differentiated into mature neuronal cultures by spontaneous differentiation (section 2.1.4.1) or induced differentiation (section 2.1.4.2). Wild-type ReNcell VM NSCs and neuronal cultures were characterised using phase-contrast microscopy (section 2.7.1) and ICC (section

2.5.2) with confocal fluorescence microscopy (section 2.7.3), and genotyped using CAG repeat-sizing (section 2.2.4) and sequencing of native *HTT* exon 1 (section 2.2.3).

ReNcell VM+*HTT* exon 1 and ReNcell VM+full-length *HTT* neuronal cell lines were generated by transduction with retroviruses carrying A2UCOE (section 2.2.1.1) or MSCV (section 2.2.1.2) viral vectors, respectively, containing human *HTT* transgenic inserts. A2UCOE+*HTT* exon 1 and MSCV+full-length *HTT* plasmid DNA was amplified and purified as described in section 2.2.2, and presence of the correct plasmids and *HTT* transgenes was confirmed by restriction enzyme digests (sections 2.2.5 and 2.2.6) and sequencing (section 2.2.3). Concentration and purity of plasmid DNA was determined by NanoDrop (section 2.2.7). A2UCOE+*HTT* exon 1 and MSCV+full-length *HTT* plasmids were packaged into retroviruses using HEK293T and Phoenix-AMPHO (section 2.1.1.1) packaging cell lines, respectively, as described in section 2.3.1. Retroviruses were subsequently concentrated by ultracentrifugation (section 2.3.2). A2UCOE+*HTT* exon 1 lentivirus and MSCV+full-length *HTT* retrovirus viability and transduction efficiency was tested in HEK293T and HeLa cells (section 2.1.1.1), respectively, as described in section 2.3.3. Expression of eGFP reporter was monitored by live-cell fluorescence imaging with a FITC filter (section 2.7.2) in HEK293T cells transduced with A2UCOE+*HTT* exon 1 lentiviruses, and HeLa cells transduced with MSCV+full-length *HTT* retroviruses were subjected to antibiotic selection (using antibiotic concentrations determined by kill curves, which were performed in HeLa cells and ReNcell VM NSCs as described in section 2.3.4.1). Expression of HTT or mHTT trans-protein was monitored in selected HeLa cells using Western blotting (sections 2.4.1.1, 2.4.2.1, 2.4.3, 2.4.4 and 2.5.1) and ICC techniques with confocal fluorescence microscopy. Viruses were used to infect ReNcell VM NSCs (section 2.3.4.2). Successfully transduced NSCs, ReNcell VM+*HTT* exon 1 or ReNcell VM+full-length *HTT*, were selected for by expression of eGFP reporter or antibiotic resistance, respectively, (as described in section 2.3.4.3), using FACS (section 2.5.4) or antibiotic treatment (sections 2.3.4.1 and 2.3.4.3), respectively.

ReNcell VM transgenic cell lines were confirmed and maintained as described in section 2.3.4.4. ReNcell VM+*HTT* exon 1 NSCs and differentiated neuronal cultures were characterised by phase-contrast microscopy to assess cell morphology; Western blotting to detect exon 1 trans-protein expression; MSD assay (section 2.5.6.2) to quantify levels of HTT trans-protein expression; ICC with confocal fluorescence microscopy to determine cellular composition of the cultures and confirm eGFP reporter and HTT trans-protein expression; ICC with Opera LX HCS system (section 2.7.3) to detect mHTT aggregates; and LDH cytotoxicity assay (section 2.6.1) to assess mHTT-induced neurotoxicity. ReNcell VM+full-length *HTT* NSCs and

differentiated neuronal cultures were characterised by ICC with confocal fluorescence microscopy to detect HTT over-expression and mature neurons. Clonal cell lines were generated by expansion from single-cell seeding, and clonal lines were characterised by dot-blot (sections 2.4.1.1, 2.4.2.2, 2.4.5 and 2.5.1) and TR-FRET assay (section 2.5.7) to assess HTT and/or mHTT expression levels; Western blot to confirm HTT over-expression was full-length; ICC with confocal fluorescence microscopy to confirm HTT over-expression and content of mature neuronal cultures in the selected final clone; and LDH cytotoxicity assay to assess mHTT-induced neurotoxicity.

Primary human samples were classified as described in section 2.1.2.1. Primary human monocytes were isolated from whole blood (section 2.1.2.2) and cultured *ex vivo* (section 2.1.2.3) or were differentiated into BMD-macrophages (section 2.1.2.4) or BMD-microglia (section 2.1.2.5). Mutant HTT expression in HD patient myeloid cell cultures was detected by ICC with confocal fluorescence microscopy. BMD-microglia cultures were characterised by phase-contrast microscopy to assess morphological phenotypes; and expression of specific microglial cell markers was confirmed by Western blotting and ICC with confocal fluorescence microscopy. N2a_R2 cells (section 2.1.1.2) were used as a negative control for detection of microglia cell markers by ICC. In some cases, myeloid cell cultures were stimulated, as described in section 2.1.3.2.

Neuronal-BMD-macrophage and neuronal-BMD-microglia co-culture models were developed as described in sections 2.1.5.1 and 2.1.5.2 (co-culture by conditioned medium transfer), 2.1.5.3 (co-culture by medium shared concurrently) and 2.1.5.4 (co-culture by direct physical contact). Media titrations were also performed and various stimulation paradigms were trialled. Co-culture models were analysed by phase-contrast microscopy, ATP cell viability assay (section 2.6.2), PI viable cell exclusion (section 2.6.3), Bio-Rad Protein Assay (section 2.4.2.1) and LDH cytotoxicity assay.

Statistical analyses were performed as described in section 2.9.

3.4 Contributions

- Dr. Jennifer Parker (Prof. Sarah J. Tabrizi's research group, UCL IoN, London, UK) optimised the protocol for induced differentiation of ReNcell VM NSCs into neuronal cultures to promote development of specific neuronal subtypes. Dr. Parker also provided the original ICC confocal microscopy images for characterisation of neuronal subtypes within ReNcell VM differentiated neuronal cultures, which are presented in Figure 3.2; panels C, F and G.

- Andrea Hawarth (Neurogenetics, NHNN, London, UK) genotyped ReNcell VM NSC *HTT* alleles by CAG repeat-sizing.
- Dr. Ralph André (Prof. Sarah J. Tabrizi's research group, UCL IoN, London, UK) sequenced ReNcell VM NSC genomic *HTT* exon 1 and provided the original ICC confocal images of ReNcell VM+full-length *HTT* differentiated neuronal cultures (Figure 3.16; B).
- Gary Adamson (Genetics and Diagnostics, MRC Prion Unit, IoN, London, UK) operated the automated DNA sequencing machine for analysis of *HTT* exon 1 and full-length *HTT* transgenes in A2UCOE and MSCV plasmid vectors, respectively.
- Dr. Eva C. Sirinathsingh (Prof. Gillian P. Bates' research group, KCL, London, UK) selected for eGFP-expressing ReNcell VM NSCs by FACS.
- Total HTT and expanded HTT levels were quantified in ReNcell VM+*HTT* exon 1 NSC and neuronal cultures by MSD assay, performed by Evotec-CHDI HTT Quantitation Service, Hamburg, Germany.
- Dr. Rhia Ghosh (Prof. Sarah J. Tabrizi's research group, UCL IoN, London, UK) provided the original ICC images showing mHTT aggregation in ReNcell VM+*HTT* exon 1 neuronal cultures (Figure 3.10). The Opera LX HCS system which was used to acquire the images was operated by Dr. Christin Luft (Dr. Robin Ketteler's research group, LMCB-MRC, UCL, London, UK).
- Dr. Alison Wood-Kaczmar (Prof. Sarah J. Tabrizi's research group, UCL IoN, London, UK) carried out the single-cell cloning of ReNcell VM+full-length *HTT* cell lines and provided the original ICC images showing HTT over-expression in ReNcell VM+full-length *HTT* (138 CAG) clone 8 (Figure 3.18).
- Dr. Rob Goold (Prof. Sarah J. Tabrizi's research group, UCL IoN, London, UK) performed dot blots and Western blots for HTT quantification in ReNcell VM+full-length *HTT* clonal lines, and provided the original images of these which are presented in Figure 3.17; A-C.
- Dr. Andreas Weiss (IRBM-Promidis, Italy) analysed HTT and mHTT expression levels in ReNcell VM+full-length *mHTT* (138 CAG) clonal NSC lines by TR-FRET assay.

3.5 Results

3.5.1 Characterisation of ReNcell VM NSCs and differentiated neuronal cultures

ReNcell VM NSCs were differentiated by either spontaneous differentiation or induced differentiation techniques and cell morphology was assessed throughout the differentiation process by phase-contrast microscopy. NSCs in culture displayed a

classic paving-stone like morphology. Following initiation of spontaneous differentiation, cells proliferated for a further 2-3 days, and by 5-7 DD cell bodies had shrunk and begun to develop processes. Over the following two weeks, processes grew longer and thinner, arborizing and connecting in a web-like network. Cultures thinned out as undifferentiated cells died off and were washed away by media changes. ReNcell VM morphology throughout the differentiation process can be seen in Figure 3.1. Differentiated neuronal cultures have been maintained for up to 7 weeks with no obvious changes in morphology from 21 DD onwards.

Successful spontaneous differentiation of NSCs into mature neuronal cultures was determined by ICC with confocal fluorescence microscopy. Antibodies directed at βIII-tubulin identified a high yield of mature neurons in cultures post-10 DD, and GFAP stained a sub-population of NSC-derived astrocytes, all of which also expressed native HTT as detected by anti-HTT 2B7 antibody (Figure 3.2; A-E). Differentiation by induction promoted the development of neuronal subtypes expressing tyrosine hydroxylase (TH) and glutamic acid decarboxylase (GAD)67, indicative of dopaminergic and GABAergic neurons, respectively (Figure 3.2; F and G).

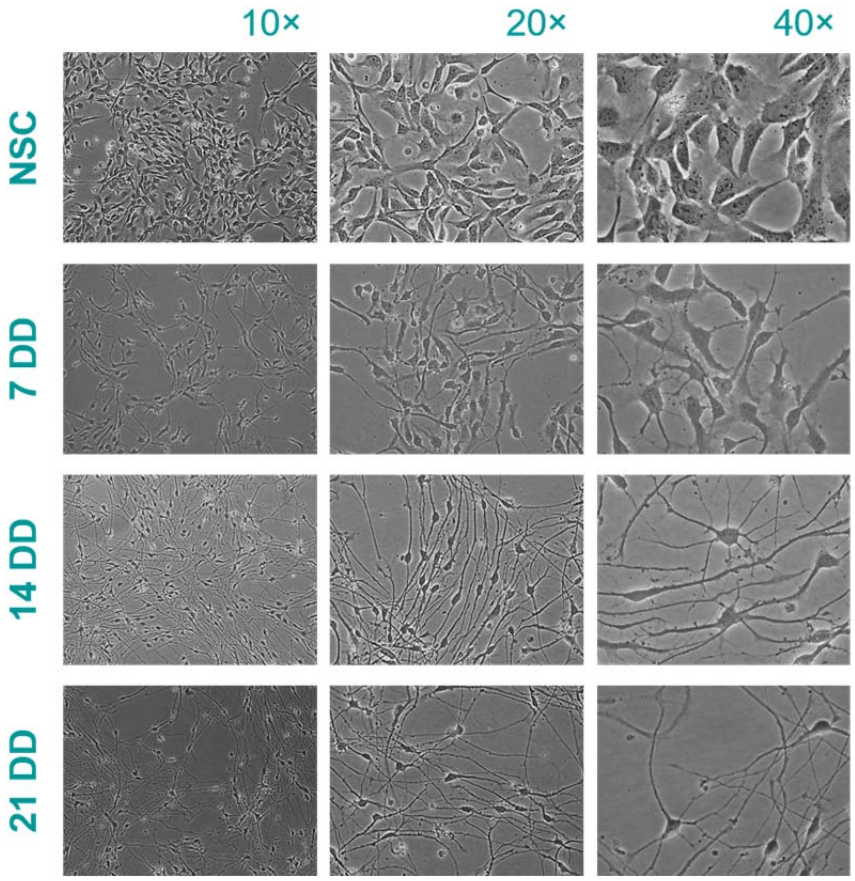

Figure 3.1: Morphological analysis of ReNcell VM differentiation

ReNcell VM NSCs were differentiated by spontaneous differentiation. Phase-contrast images were taken of the cultures at 0 (NSC), 7, 14 and 21 DD using 10×, 20× and 40× objectives.

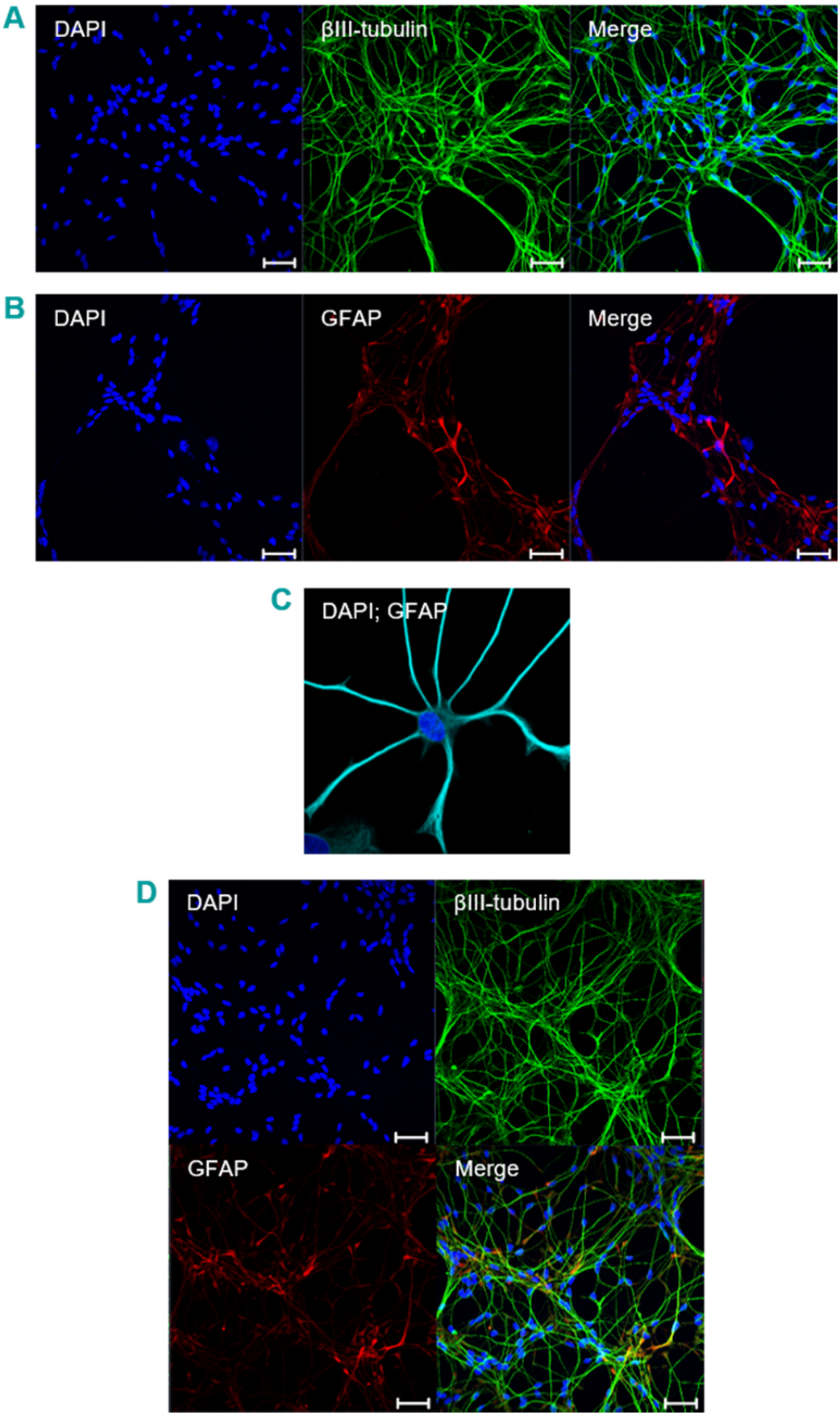
A
DAPI
βIII-tubulin
Merge
B
DAPI
GFAP
Merge
C
DAPI; GFAP
D
DAPI
βIII-tubulin
GFAP
Merge

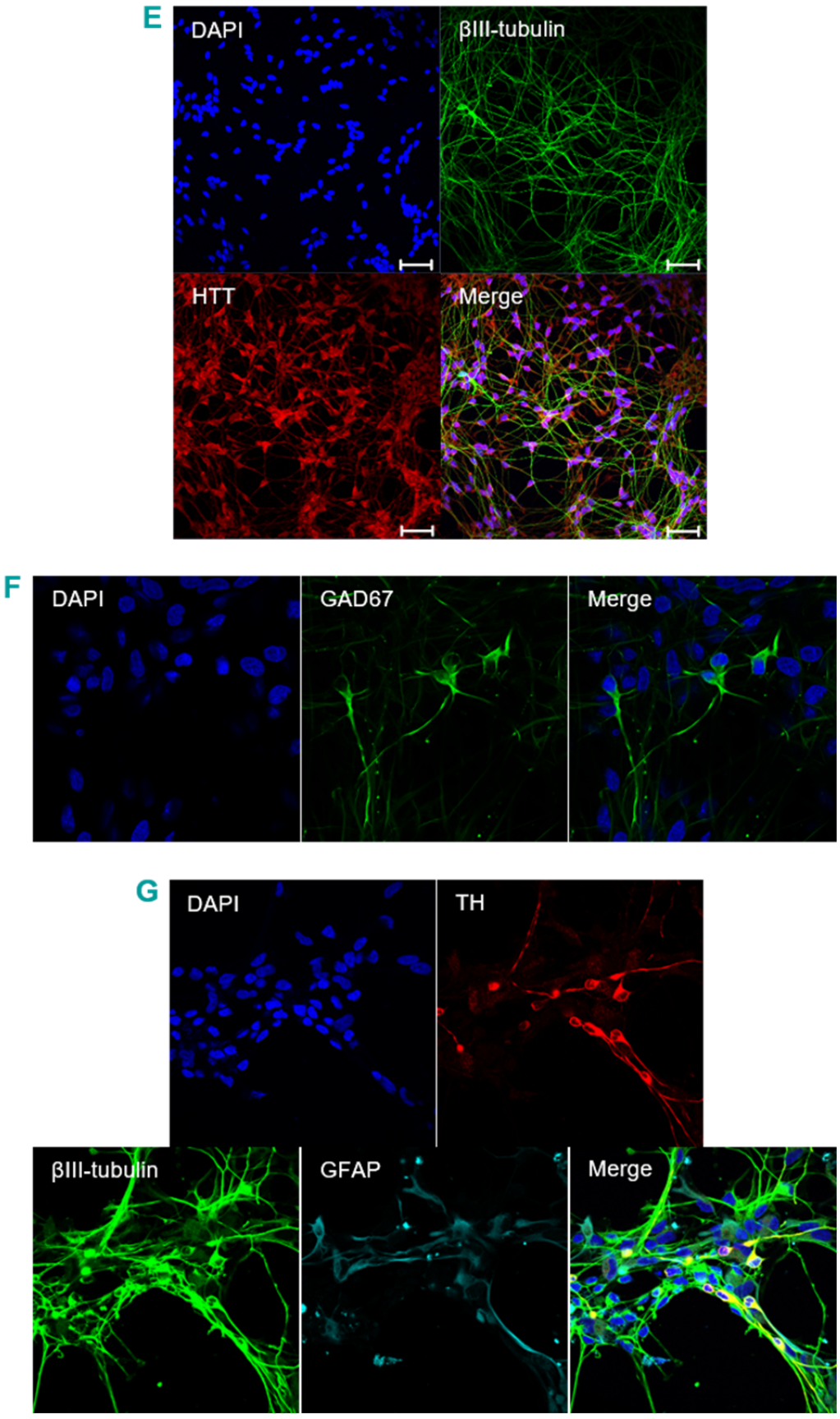

Figure 3.2: Characterisation of ReNcell VM neuronal culture composition

Confocal fluorescence microscopy images of 10 DD ReNcell VM neuronal cultures following ICC for neuronal and astrocytic expression markers. Spontaneous differentiation resulted in a

*high yield of cells with βIII-tubulin expression indicative of a pan-neuronal phenotype (**A**) and a smaller GFAP+ astrocytic sub-population (**B-D**), all of which express native HTT, as determined by staining with 2B7 anti-HTT antibody (**E**). Induced differentiation resulted in development of very small populations of GAD67+ GABAergic (**F**) and TH+ dopaminergic (**G**) neuronal subtypes. Scale bars, where indicated = 50 µm; Image C = 63×; Panels F and G = 40×.*

To ensure ReNcell VM had native *HTT* CAG repeats within the normal range, genomic DNA was extracted from the cells and genotyped by CAG repeat-sizing. ReNcell VM genomic *HTT* exon 1 was also sequenced. CAG repeat-sizing confirmed that ReNcell VM was diploid for *HTT* with CAG repeat sizes of 16 and 20 (± 2), in the non-pathogenic range, and sequencing results revealed no genetic mutations within exon 1. This NSC-derived neuronal model was therefore taken forward for the development of *HTT* exon 1 and full-length *HTT* HD transgenic cell lines.

3.5.2 Generation of human HD neuronal cell lines with stable expression of human mHTT exon 1

A2UCOE lentiviral vectors containing human *HTT* exon 1 with 29, 71 or 129 CAG repeats, and an eGFP alone control vector, were a kind gift from Prof. Gillian P. Bates (KCL, London, UK), and made by Dr. Eva C. Sirinathsingh of the same laboratory research group. Full details of the expression systems, including plasmid maps, can be found in section 2.2.1.1.

A2UCOE+*HTT* exon1 (29, 71 or 129 CAG) and A2UCOE+eGFP alone plasmid vector DNA was amplified and purified, then restriction digests were performed to confirm correctness of the plasmids and check for DNA contamination. Firstly, plasmid DNA was digested with *Bam*HI and resulting DNA fragments were separated by agarose gel electrophoresis and sized against HyperLadder I DNA ladder which was run in parallel. *Bam*HI recognises two sites within A2UCOE; one site 2225 bp 5' to the *HTT* exon 1 transgene, and one site 21 bp 3' to the transgene. Therefore, Bam*HI* was expected to cut out the whole transgenic insert (entire coding sequence of *HTT* exon 1 + first 21 bp of *HTT* intron 2), which had a predicted size of 616 bp (129 CAG), along with 2250 bp flanking plasmid DNA. Figure 3.3 shows that digestion of each vector with *Bam*HI produced DNA fragments at sizes appropriate to represent *HTT* exon 1 transgenes + flanking plasmid; in the region of 2500-3000 bp with increasing size in correlation with expanding CAG repeat length.

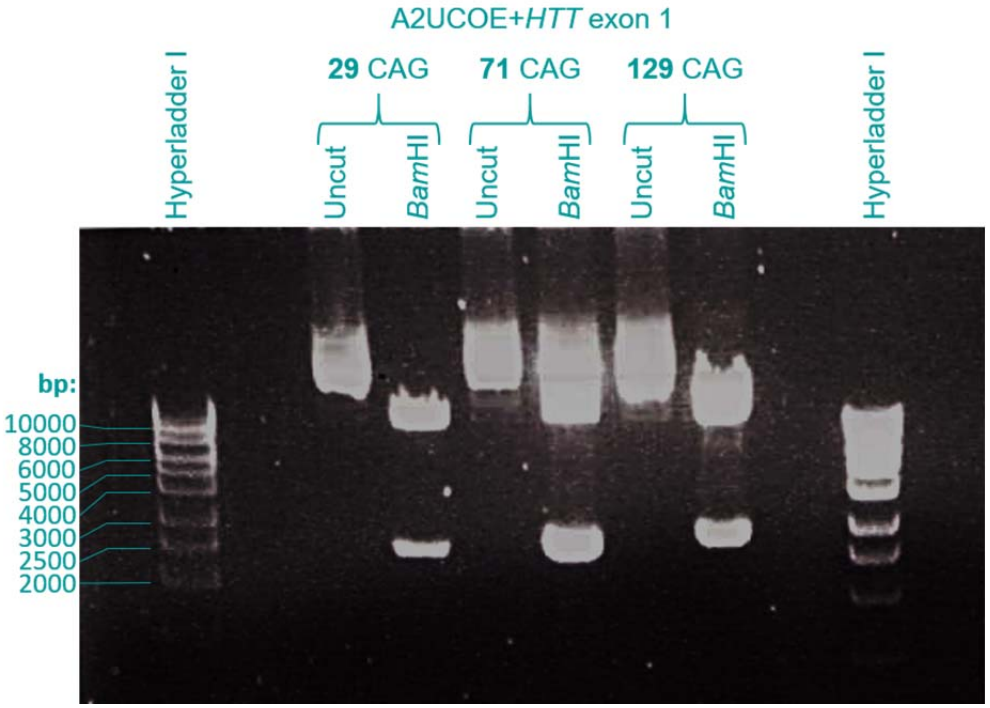

Figure 3.3: Restriction digest of A2UCOE+*HTT* exon 1 plasmid vectors

*A2UCOE+HTT exon 1 (29, 71 or 129 CAG) plasmid vectors were digested with restriction enzyme Bam*HI *and resulting DNA fragments were separated by agarose gel electrophoresis alongside DNA ladder HyperLadder I. Each digested (Bam*HI*) plasmid sample was run alongside an undigested (uncut) control sample. DNA was visualised by exposure of intercalated ethidium bromide to UV light and an image of the gel is presented above. Smaller fragments in digested samples (transgene + flanking plasmid) appear between 2500 and 3000 bp, and increase in size in correlation with expanding CAG repeat length; expected sizes were 2566 (29 CAG), 2692 (71 CAG) and 2866 (129 CAG). Expected size of remaining plasmid was 10126 bp, and a band of this approximate size can be seen in all digested samples.*

HTT exon 1 transgenes were then sequenced in order to confirm their presence within the lentiviral vectors, and to check their CAG repeat lengths and any mutations. Analysis confirmed that each of the vectors contained a human *HTT* exon 1 transgene, other than the eGFP alone control construct which did not contain any *HTT* exon 1 sequence, as expected. All *HTT* sequences were in frame, with no mutations, and shared 100 % homology with the published NCBI; nucleotide; RefSeqGene reference sequence NG_009378.1 for *Homo sapiens* HTT cDNA (IT15), chromosome 4. However, there were some variations from the predicted sequences in the CAG repeat regions: A2UCOE+*HTT* exon 1 (29 CAG) actually had 30 CAG repeats and A2UCOE+*HTT* exon 1 (129 CAG) had 122 CAG repeats. A2UCOE+*HTT* exon 1 (71 CAG) had 71 CAG repeats as expected. For reasons of clarity, the plasmids (and lentiviruses and cell lines created using them) will still be referred to as A2UCOE+*HTT* exon 1 (29, 71 or 129 CAG) throughout this Thesis. In addition, all three *HTT* exon 1

transgene CAG repeat regions had a CAA interruption in place of the ninth penultimate CAG codon. While individuals with 29 or 30 CAG repeats in *HTT* are unaffected by HD, this is considered to be an intermediate genotype because the CAG repeat is unstable and there is potential risk of expansion into the disease range (Ha *et al.* 2012), especially in cells with high replication rates (Snell *et al.* 1993; Walker 2007). It is possible that presence of the CAA interruption may reduce the propensity for expansion within the CAG tract. The BAC in BACHD mice, for example, was engineered to include a mixed CAG/CAA repeat in human *mHTT* exon 1, and unlike R6/2 mice which have a purely CAG repeat tract, the repeat length remains stable in the germline over many generations (Yang and Gray 2011). As both CAA and CAG encode glutamine, an uninterrupted polyQ stretch should still be translated in the final HTT exon 1 protein. Figure 3.4 shows an annotated electropherogram from *HTT* exon 1 transgene sequencing.

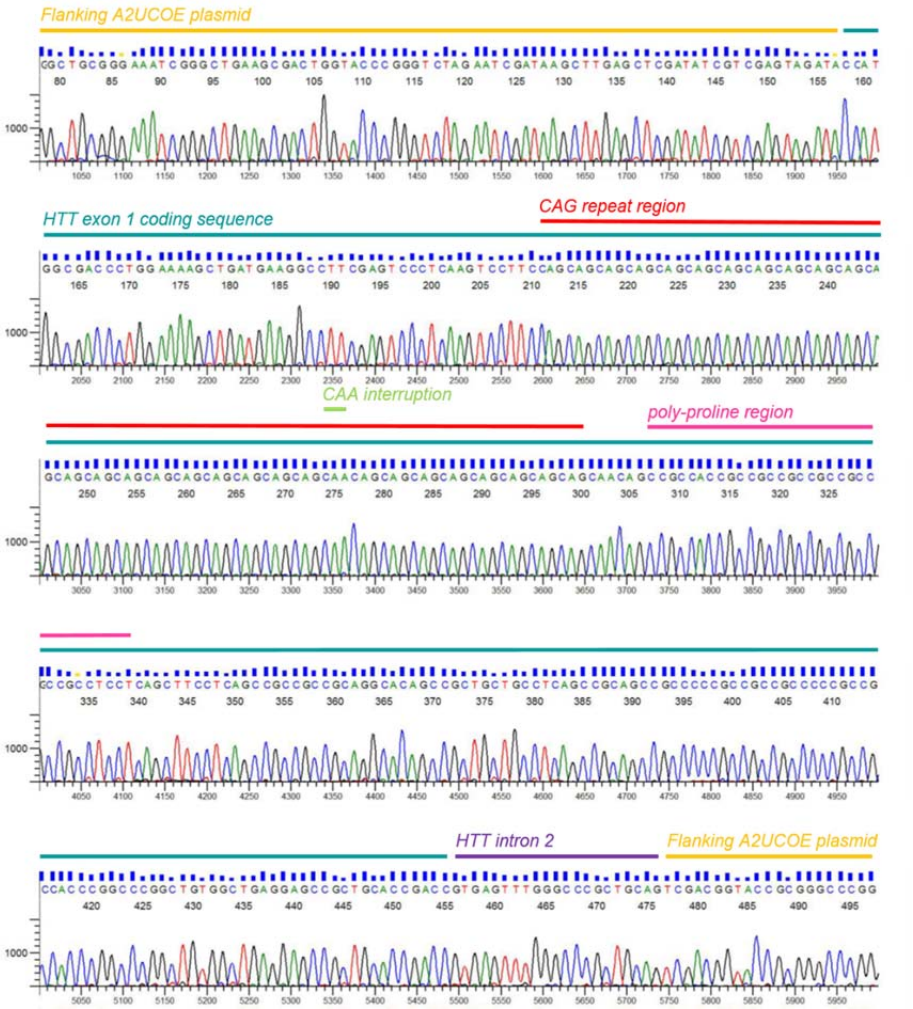

Figure 3.4: Annotated electropherogram from automatic DNA sequencing of A2UCOE+*HTT* exon 1 (29 CAG)

HTT exon 1 transgenes were sequenced in A2UCOE lentiviral plasmid vectors, with flanking primers (Table 2.1), using an automated DNA analyser. Electropherograms for each sample

were analysed in the forward and reverse directions using Geneious Pro. An example electropherogram (HTT exon 1 (29 CAG)) is shown above, with regions of interest labelled.

The concentration and purity of A2UCOE+*HTT* exon1 (29, 71 or 129 CAG) and A2UCOE+eGFP reporter only plasmid DNA was determined by NanoDrop, and results are reported in Table 3.1. A260/A280 ratios were approximately 1.9 for all plasmids, indicating no protein or RNA contamination within the samples (protein and RNA contaminants are expected to produce ratios of less than 1.8 or more than 2.0, respectively). A260/A230 ratios were above 2.0 for all plasmids, indicating no other contaminants within the DNA samples. All plasmid DNA was therefore considered to be sufficiently pure and of high quality for use in transfection procedures.

Table 3.1: A2UCOE+*HTT* exon 1 plasmid DNA concentration and purity

Plasmid	DNA concentration/ ng/µL	A260/A280	A260/A230
A2UCOE+*HTT* exon 1 (29 CAG)	2637.6	1.89	2.22
A2UCOE+*HTT* exon 1 (71 CAG)	1866.4	1.91	2.25
A2UCOE+*HTT* exon 1 (129 CAG)	2482.9	1.89	2.13
A2UCOE+eGFP reporter only	1602.6	1.91	2.26

A2UCOE+*HTT* exon 1 (29, 71 or 129 CAG) and A2UCOE+eGFP reporter only plasmid vectors were packaged into VSV-G coated lentiviruses by PEI-mediated transfection into the HEK293T packaging cell line along with VSV-G-expressing envelope plasmid MD.G2 and GAG/pol-expressing packaging plasmid CMVRd8.74. Lentiviral supernatants were collected and tested for viability and transduction efficiency by infection of fresh HEK293T cell cultures and monitoring of eGFP reporter expression. Figure 3.5 shows eGFP reporter expression in HEK293T cells 3 days post-infection with A2UCOE+*HTT* exon 1 lentiviral supernatants.

Positive eGFP reporter expression was detected in all HEK293T cultures following infection with each lentiviral supernatant, and no eGFP signal was detected in the polybrene only negative control treatment condition. This confirmed the viability of all A2UCOE+*HTT* exon 1 lentiviral supernatants. Viral titre appeared to be very low on account of a MOI of ~1 % in HEK293T cells. Lentiviral supernatants were therefore subsequently concentrated by ultracentrifugation through a sucrose gradient with the aim of increasing titre. Concentrated lentiviruses were tested and titrated in fresh HEK293T cell cultures in the same way as described above for lentiviral supernatants

(and in more detail in section 2.3.3.1), and 1:100 was determined to be the optimum dilution for all concentrated lentiviruses, resulting in a MOI of ~50 % in HEK293T cells.

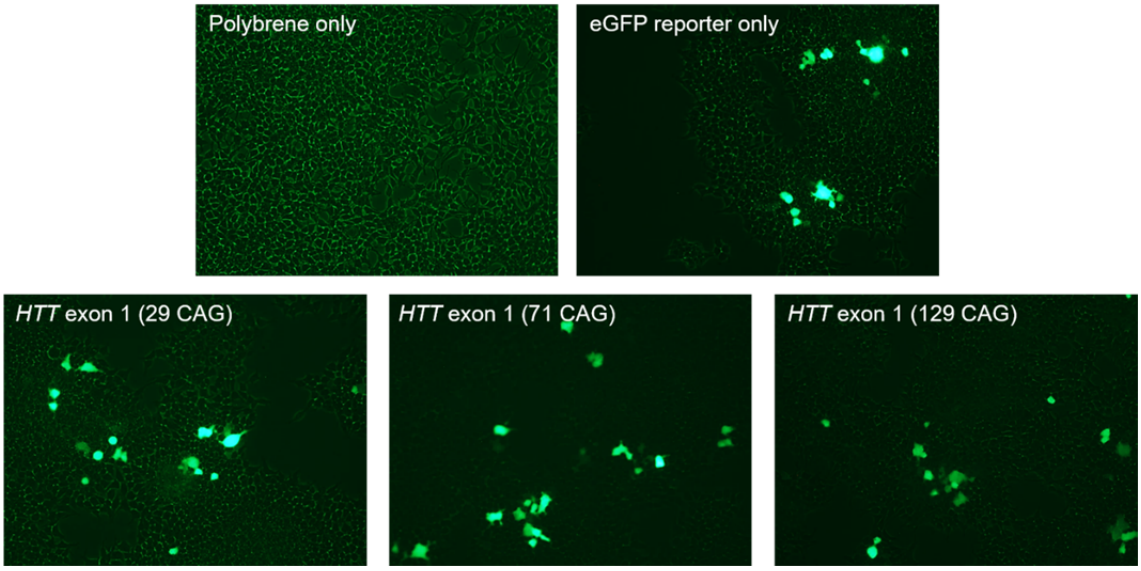

Figure 3.5: eGFP reporter expression in HEK293T cell cultures infected with A2UCOE+*HTT* exon 1 lentiviral supernatants

HEK293T cells were infected with A2UCOE+HTT exon 1 (29, 71 or 129 CAG) or A2UCOE+eGFP reporter only lentiviral supernatants for 24 h. Cells were then given a fresh culture medium change and returned to the incubator for a further 48 h. Successful transduction with HTT exon 1 transgenes was determined by detection of eGFP reporter expression using live-cell fluorescence microscopy with a FITC filter. Three random fields of view per condition were imaged, and one example image for each condition is presented above. As polybrene was used to aid infection, a polybrene only treatment condition (without lentiviral supernatant) was added as a negative control for eGFP detection.

Concentrated A2UCOE+*HTT* exon 1 (29, 71 or 129 CAG) and A2UCOE+eGFP reporter only lentiviruses were then used to infect ReNcell VM NSCs, at 1:100 dilution, as described in detail in section 2.3.4.2. Successful transduction was initially confirmed by detection of eGFP reporter expression, using live-cell fluorescence microscopy with a FITC filter, 3 days post-infection. NSC cultures were then expanded, and expression of the transgenes was confirmed by ICC techniques using antibodies directed at eGFP and mHTT, as shown in Figure 3.6. Five random fields of view were taken for each infected NSC culture using confocal fluorescence microscopy, and the average number of eGFP-expressing cells in each culture was calculated using these images and the quantification methods outlined in section 2.7.3.1, in order to determine transduction efficiency. The results of this analysis can be found in Table 3.2.

ReNcell VM NSC+*HTT* exon 1 cultures were then selected for eGFP-expressing cells by FACS. Cells of similar eGFP expression levels across the different NSC lines were expanded for characterisation and use in experiments.

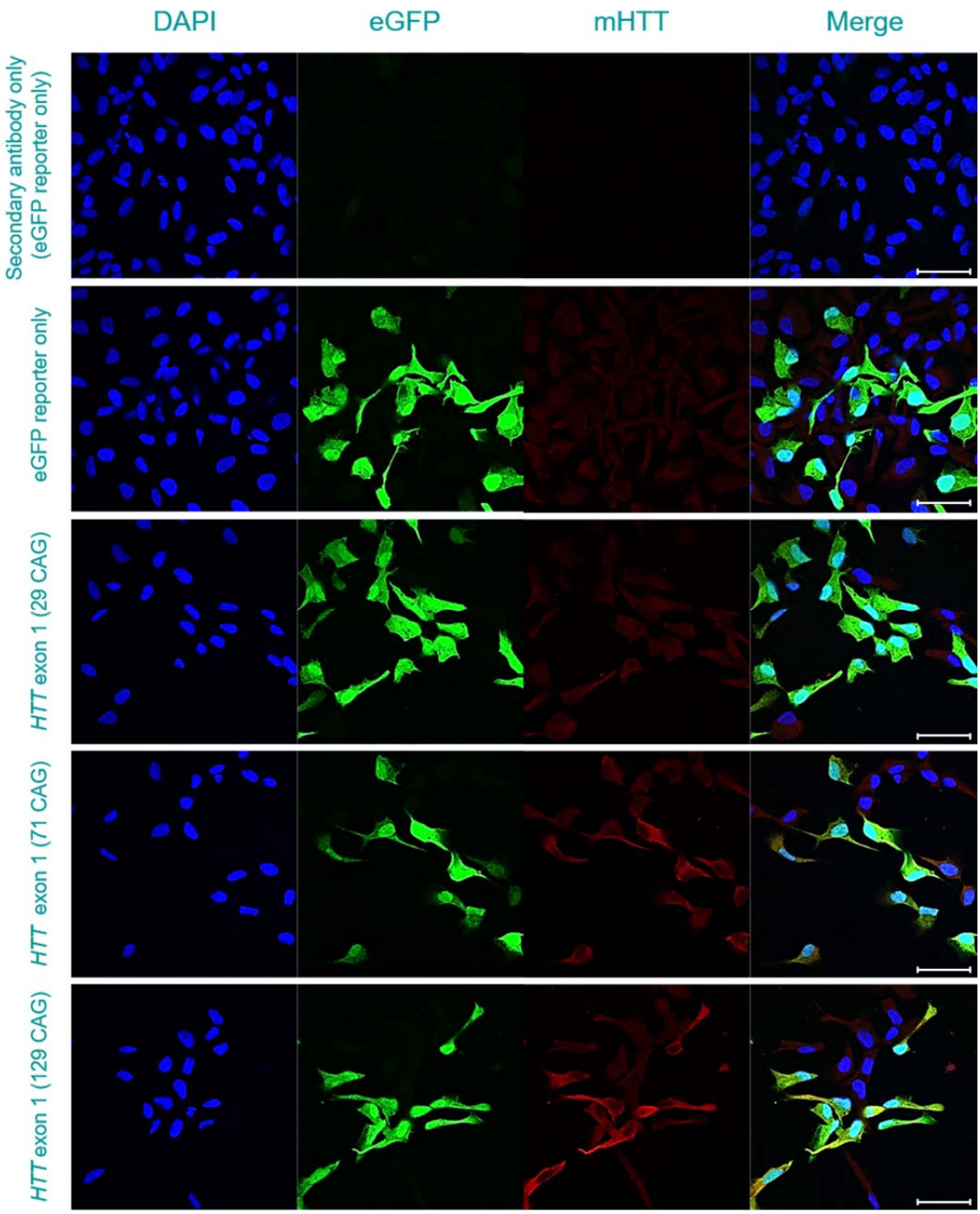

Figure 3.6: Confirmation of *HTT* transgene and eGFP reporter expression in transduced ReNcell VM NSCs

ReNcell VM NSCs were infected with A2UCOE+HTT exon 1 (29, 71 or 129 CAG), or A2UCOE+eGFP reporter only lentiviruses, and expanded. ICC with antibodies directed at eGFP revealed expression of the eGFP reporter (green) in all cultures. MW1 antibody binds to the polyQ region of HTT *and displays preferential binding to elongated polyQ stretches, resulting in*

increased binding in correlation with expanding polyQ length and a preference for mHTT *over normal* HTT. *ICC with MW1 resulted in a signal (mHTT; red) which can be seen to increase with expanding HTT CAG repeat length in the images above, indicating successful expression of HTT exon 1 transgenes in NSCs. Images were taken with a confocal fluorescence microscope and are examples from 5 random fields of view taken per infected NSC culture. Secondary antibodies only were directed at eGFP reporter only-expressing NSCs as a negative control and to determine background fluorescence detection levels (top panel). Scale bars = 50 μm.*

Table 3.2: Transduction efficiency of A2UCOE+*HTT* exon 1 lentiviruses in ReNcell VM NSCs

A2UCOE+eGFP only lentivirus-infected ReNcell VM NSCs			
Field	**Total cell count**	**No. eGFP-expressing NSCs**	**% transduced NSCs**
1	34	5	14.71
2	53	19	35.85
3	56	16	28.57
4	24	3	12.50
5	51	26	50.98
		Mean average transduction efficiency:	**28.52**
A2UCOE+*HTT* exon 1 (29 CAG) lentivirus-infected ReNcell VM NSCs			
Field	**Total cell count**	**No. eGFP-expressing NSCs**	**% transduced NSCs**
1	20	15	75.00
2	25	22	88.00
3	22	18	81.82
4	21	16	76.19
5	26	14	53.85
		Mean average transduction efficiency:	**74.97**
A2UCOE+*HTT* exon 1 (71 CAG) lentivirus-infected ReNcell VM NSCs			
Field	**Total cell count**	**No. eGFP-expressing NSCs**	**% transduced NSCs**
1	20	15	75.00
2	29	27	93.10
3	18	9	50.00
4	20	13	65.00
5	18	12	66.67
		Mean average transduction efficiency:	**69.95**

A2UCOE+*HTT* exon 1 (129 CAG) lentivirus-infected ReNcell VM NSCs			
Field	**Total cell count**	**No. eGFP-expressing NSCs**	**% transduced NSCs**
1	36	16	44.44
2	33	14	42.42
3	21	12	57.14
4	26	8	30.77
5	18	11	61.11
		Mean average transduction efficiency:	**47.18**

3.5.2.1 Characterisation of ReNcell VM+HTT exon 1 neuronal cell lines

All ReNcell VM NSC+*HTT* exon 1 NSC cultures grew well in culture and expanded at comparative rates to wild-type, non-transduced NSCs. NSC cultures were all of similar morphology, although *HTT* exon 1 (71 CAG) NSCs appeared spindlier. This could be an indication of a mHTT-induced morphological phenotype in these cells. Upon differentiation, using the induced differentiation protocol, all NSC cultures adopted neuronal-like morphology with changes occurring in line with wild-type NSC differentiation and over a similar time-course. By 25 DD, some minor differences could be observed between the neuronal cultures: *HTT* exon 1 (71 CAG) and *HTT* exon 1 (129 CAG) neuronal cultures had thinned out more than *HTT* exon 1 (29 CAG), eGFP reporter only and wild-type neuronal cultures, leaving larger and more numerous gaps between surviving cells. This could be due to a toxic phenotype of the expanded CAG repeats in these mHTT-expressing neurons. Interestingly, *HTT* exon 1 (29 CAG) neuronal cultures appeared to be denser than eGFP reporter only and wild-type neuronal cultures, and cells bunched into patches. This could indicate a higher survival rate of differentiated cells or a prolonged turnover of NSCs prior to differentiation. Images of ReNcell VM NSC+*HTT* exon 1 NSC cultures and 25 DD neuronal cultures can be seen in Figure 3.7.

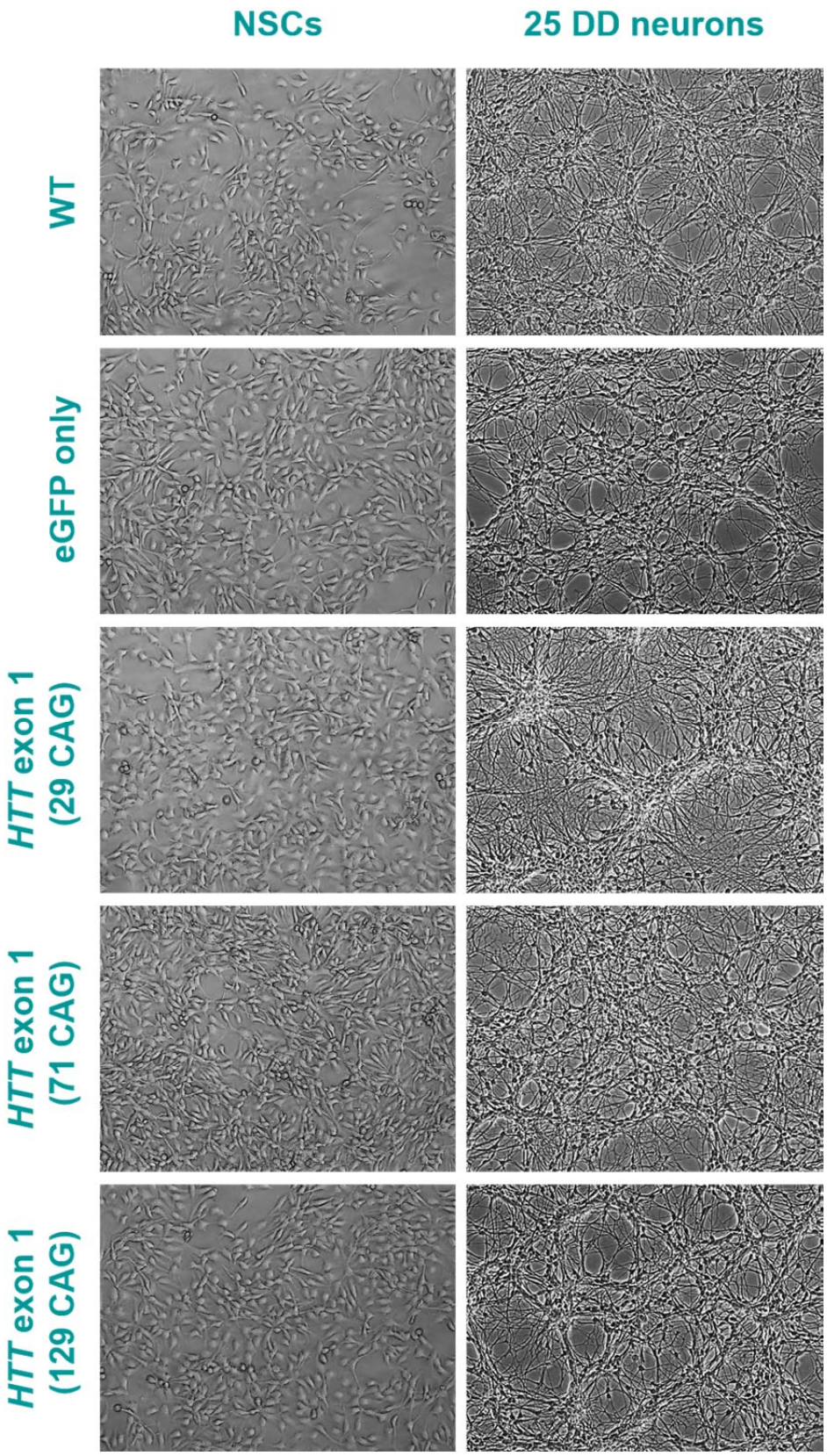

Figure 3.7: Morphology of ReNcell VM+*HTT* exon 1 NSC lines and differentiated neuronal cultures

Phase-contrast images of ReNcell VM+HTT exon 1 NSCs and 25 DD neuronal cultures (induced differentiation). Wild-type (WT; non-transduced) ReNcell VM cultures presented for comparison (top panel). All images taken with 10× objective.

Expression of HTT exon 1 trans-protein with 29Q, 71Q or 129Q was confirmed by Western blotting in ReNcell VM+*HTT* exon 1 (29, 71 or 129 CAG), ReNcell VM+eGFP reporter only and wild-type ReNcell VM NSCs and 25 DD (induced differentiation) neuronal cultures. Proteins which co-stained with 4C9 and S830 were detected in ReNcell VM+*HTT* exon 1 (29 CAG), ReNcell VM+*HTT* exon 1 (71 CAG) and ReNcell VM+*HTT* exon 1 (129 CAG) NSC and DD25 neuronal cultures (Figure 3.8). The sizes of these proteins were consistent with those expected for HTT exon 1 with approximately 29, 71 or 129 polyQ, respectively, with larger glutamine repeats becoming more retarded in the gel during SDS-PAGE (Landles *et al.* 2010). 4C9 alone detected several bands in all samples which could be associated with fragments of native HTT (Weiss *et al.* 2012). S830 is directed at mHTT polyQ and has preference for expanded polyQ regions, however it will still bind to polyQ stretches within the normal range. Over-expression of HTT exon 1 within the normal polyQ range (29Q) was detected in ReNcell VM+*HTT* exon 1 (29 CAG) NSCs and DD25 neuronal cultures by increased S830 signal, in co-stain with 4C9, compared with wild-type and ReNcell VM+eGFP reporter only cultures. It was therefore confirmed that ReNcell VM NSCs which had been transduced with *HTT* exon 1 (29, 71 or 129 CAG) were successfully expressing HTT exon 1 trans-protein of the correct size, and that this was also the case following differentiation into mature neuronal cultures.

Interestingly, N-terminal fragments smaller than exon 1 were detected in ReNcell VM+*HTT* exon 1 (129 CAG) NSC and DD25 neuronal cultures, which may be a result of post-translational proteolytic cleavage of the highly-expanded exon 1 fragment. Also, protein co-staining for 4C9 and S830 was detected in the region transferred directly from the polyacrylamide gel wells in both of the mHTT-expressing DD25 neuronal cultures (ReNcell VM+*HTT* exon 1 (71 CAG) and ReNcell VM+*HTT* exon 1 (129 CAG)). This may indicate presence of mHTT aggregates in the mature HD neuronal cultures, which were more resistant to denaturation processes during preparation of the cell lysates and were therefore too large to enter the gel during electrophoresis (Figure 3.8).

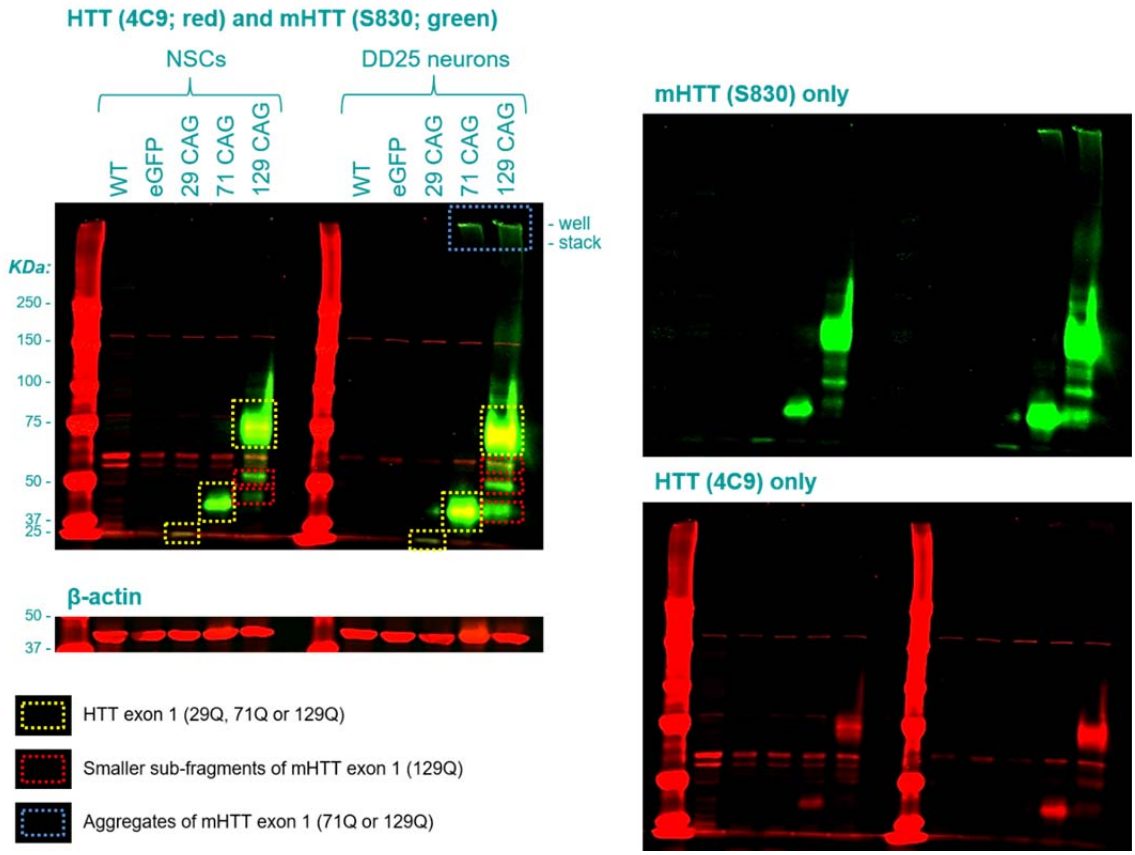

Figure 3.8: Confirmation of HTT exon 1 protein expression in ReNcell VM+*HTT* exon 1 neuronal cell lines

Wild-type (WT) ReNcell VM, ReNcell VM+HTT exon 1 (29, 71 or 129 CAG) and ReNcell VM+eGFP reporter only (eGFP) NSC and DD25 (induced differentiation) neuronal cultures were harvested and cell lysates prepared. Proteins were separated according to their electrophoretic mobility by SDS-PAGE and transferred into a membrane by electroblotting. The membrane was then probed with 4C9 and S830 primary antibodies, directed against HTT *and* mHTT*, respectively, and IRDye-conjugated secondary antibodies. IR signals were visualised directly on the membrane using a LI-COR Odyssey Scanner (*HTT*, red;* mHTT*, green). Presented here is a representative example of two repeat Western blots. The blot is pictured as an annotated image with merged 4C9/S830 signals (top left panel), and as 4C9 only and S830 only images (right). The Western blot was also probed for β-actin (red; 42 KDa) as a loading control (bottom left panel). Detected proteins were sized against BioRad Precision Plus All Blue protein standard. Dotted yellow boxes highlight* HTT *exon 1 proteins expressed from the transgenes. Dotted red boxes highlight shorter N-terminal fragments of* mHTT *which may occur due to proteolytic cleavage of* mHTT *exon 1 produced by mHTT transgenes. The dotted blue box highlights possible aggregates of* mHTT *which have remained in the gel wells during SDS-PAGE.*

Total HTT and expanded HTT in the NSCs and 25 DD neuronal cultures was then quantified using the MSD platform and a proprietary, optimised protocol. Total HTT was measured using 2B7/4C9 antibody pair and expanded HTT was measured using

2B7/MW1 antibody pair, in wild-type ReNcell VM, ReNcell VM+*HTT* exon 1 (29, 71 or 129 CAG) and ReNcell VM+eGFP reporter only NSC and 10 DD neuronal cultures (induced differentiation). Results of the MSD analysis are presented in Figure 3.9.

Total HTT levels were found to be higher in all cells expressing *HTT* exon 1 transgenes (ReNcell VM+*HTT* exon 1 (29, 71 or 129 CAG) NSCs and neurons) compared with cells which did not (wild-type ReNcell VM and ReNcell VM+eGFP reporter only NSCs and neurons). This occurs due to induction by the A2UCOE promoter as well as expression of the transgenes on a diploid native *HTT* background, and provided further confirmation of successful trans-protein production in the cell lines. Expanded HTT was also only detected in cells expressing the *mHTT* exon 1 transgenes (ReNcell VM+*HTT* exon 1 (71 or 129 CAG) NSCs and neurons). Total HTT was of similar levels in ReNcell VM+*HTT* exon 1 (71 CAG) and ReNcell VM+*HTT* exon 1 (129 CAG) NSCs; 51.67 and 58.33 fmol/mg, respectively. However, total HTT levels were approximately three-fold higher, 169.33 fmol/mg, in ReNcell VM+*HTT* exon 1 (29 CAG) NSCs, which may indicate higher expression of the *HTT* exon 1 (29 CAG) transgene. Ideally, all ReNcell VM+*HTT* exon 1 lines would express the transgene to equal levels, however as it was the control line with CAG repeats in the normal range which had higher total HTT levels, this was considered to be acceptable. Expanded HTT levels were higher in neuronal cultures than NSCs, suggesting a potential build-up of mHTT exon 1 protein in the post-mitotic cells. This could be an indication of mHTT aggregation in these neurons. Expanded HTT levels were also higher in ReNcell VM+*HTT* exon 1 (129 CAG) than ReNcell VM+*HTT* exon 1 (71 CAG), potentially indicating that mHTT with more expanded polyQ has a higher propensity for build-up and/or aggregation. However, as the MW1 antibody (used for detection of expanded HTT in this assay) has more affinity for expanded polyQ, the detection of higher MW1 signal in ReNcell VM+*HTT* exon 1 (129 CAG) may just be due to more antibodies binding to each individual exon 1 protein.

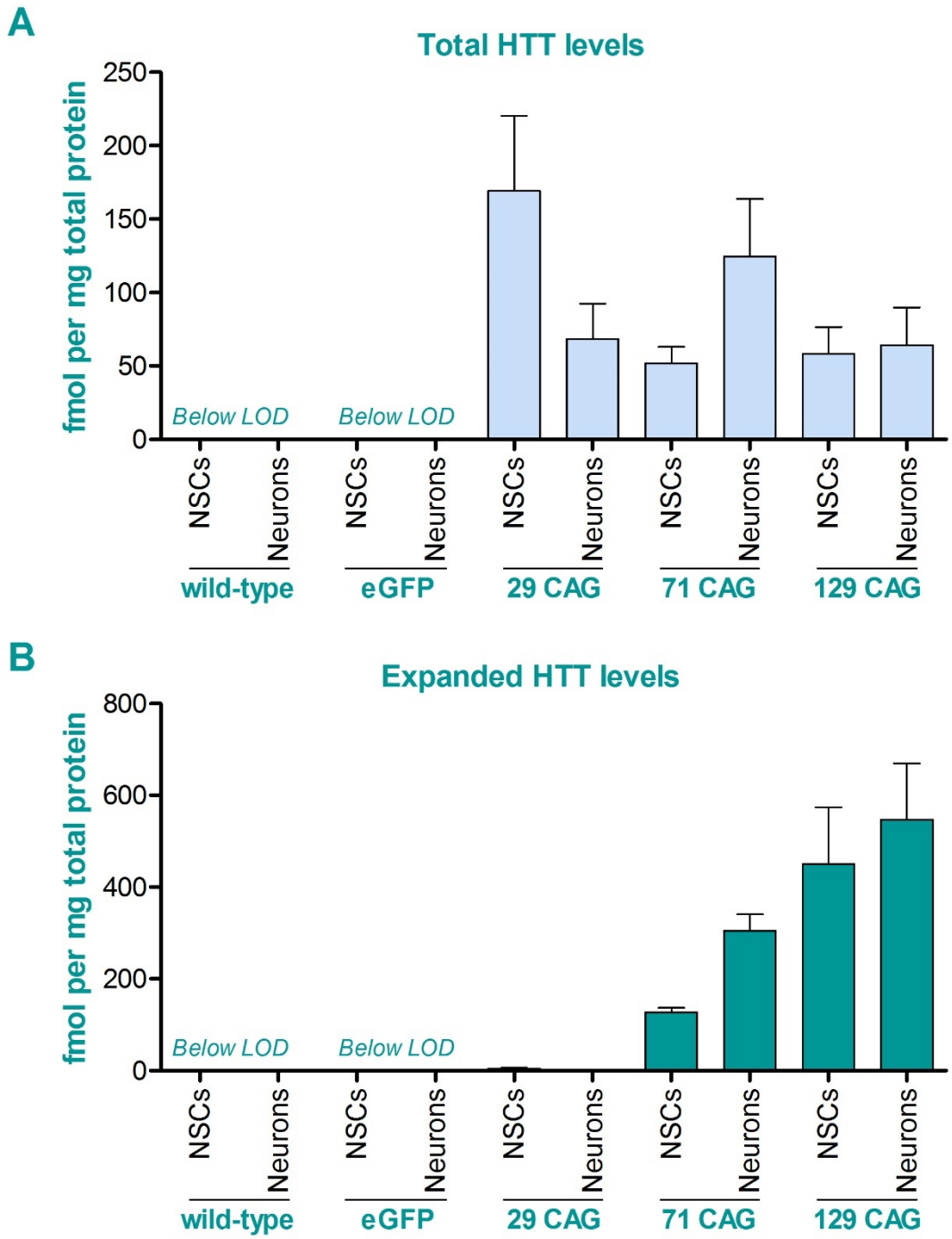

Figure 3.9: Levels of total and expanded HTT in ReNcell VM+*HTT* exon 1 NSCs and neuronal cultures

*Total HTT and expanded HTT levels were measured by MSD assay in wild-type ReNcell VM, ReNcell VM+HTT exon 1 (29, 71 or 129 CAG) and ReNcell VM+eGFP reporter only (eGFP) NSC and DD10 (induced differentiation) neuronal cultures. Total HTT levels (**A**) were measured using 2B7/4C9 antibody pair and expanded HTT levels (**B**) were measured using 2B7/MW1 antibody pair. All measurements were normalised to total protein concentration per culture. It is important to note that the assay for measurement of total HTT was performed independently from the assay for measurement of expanded HTT, and due to differential kinetics of the two*

assays, comparisons should not be made across the two data sets. Bars = mean average of three independent assay measurments from the same culture; error bars = SD; Below LOD, below limit of detection.

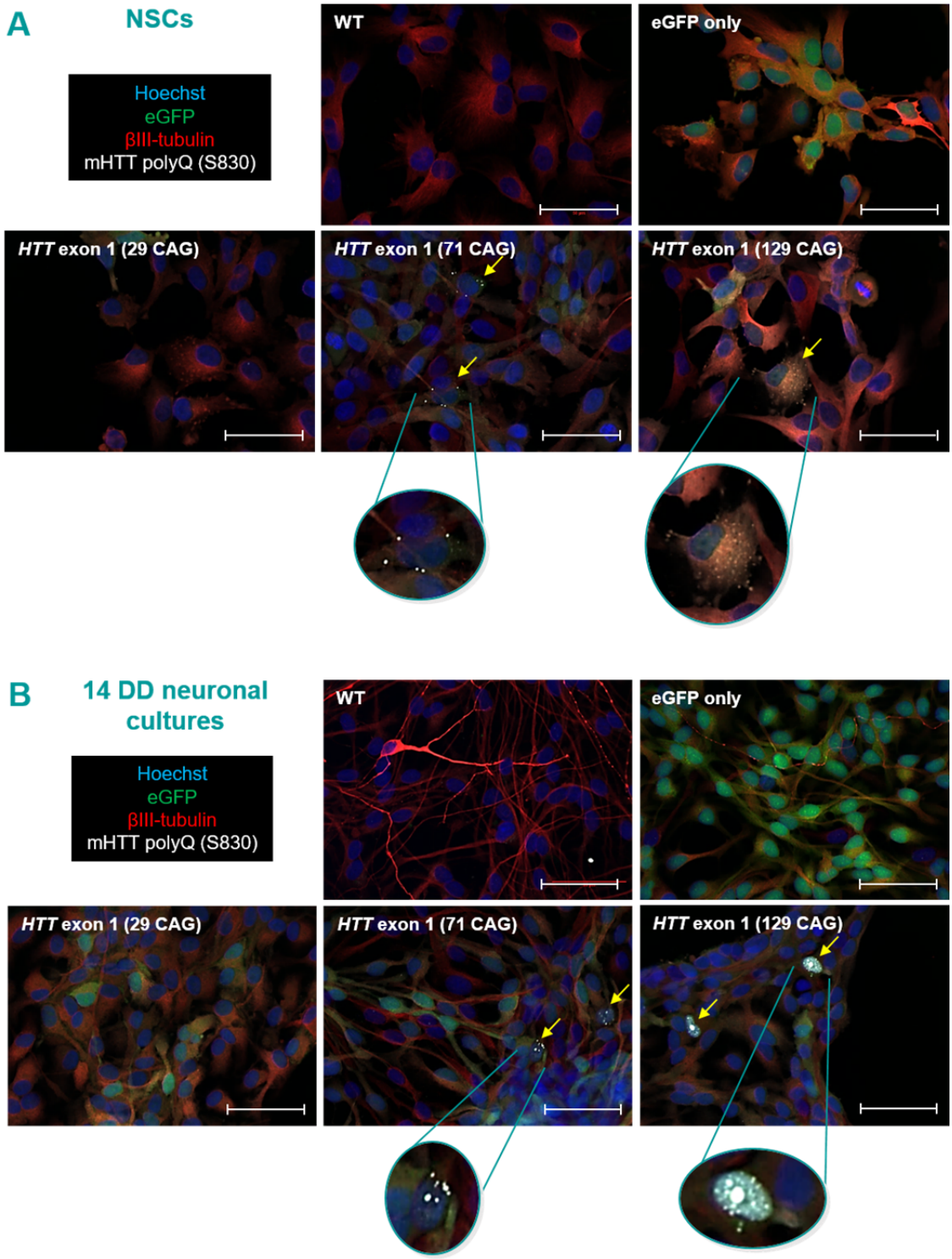

Figure 3.10: Detection of mHTT aggregates in ReNcell VM+*mHTT* exon 1 (71 or 129 CAG) NSCs and differentiated neuronal cultures

*Wild-type (WT) ReNcell VM, ReNcell VM+HTT exon 1 (29, 71 or 129 CAG) and ReNcell VM+eGFP only NSCs (**A**) and 14 DD neuronal cultures (**B**; induced differentiation) were probed*

with antibodies directed at mHTT polyQ (S830; white), eGFP (green) and βIII-tubulin (red) using ICC techniques. Nuclei were stained with Hoechst 33342 (blue). Cultures were then imaged using the Opera LX HCS system. Cells containing aggregates of mHTT exon 1 are indicated with yellow arrows, and some examples are magnified below the images for closer inspection. Scale bars = 50 µm.

MSD assay analysis of expanded HTT levels had shown potential build-up of mHTT in neurons expressing *HTT* exon 1 with 71 or 129 CAG (Figure 3.9), and Western blot results had provided some evidence for the presence of mHTT aggregates in these neurons (Figure 3.8). ICC techniques utilising S830 anti-mHTT polyQ antibodies were therefore applied to NSC and 14 DD neuronal cultures (induced differentiation) with the aim of detecting mHTT aggregates. Cultures were then imaged using the Opera LX HCS system, and some examples are presented in Figure 3.10.

A punctate S830 signal was detected in some cells in ReNcell VM+*HTT* exon 1 (71 CAG) and ReNcell VM+*HTT* exon 1 (129 CAG) NSC and neuronal cultures, confirming the presence of mHTT aggregates. This was not detected in wild-type ReNcell VM, ReNcell VM+eGFP reporter only or ReNcell VM+*HTT* exon 1 (29 CAG) cultures. In NSCs, the aggregates were cytoplasmic or perinuclear and appeared small and diffuse. In 14 DD neuronal cultures, the aggregates were much larger and had formed intranuclear inclusions. Intranuclear inclusions were found in cells which stained positively for βIII-tubulin, confirming them as neurons. Additionally, all cells in transduced ReNcell VM NSC and neuronal cultures stained positively for eGFP, showing that 100 % cells were expressing the transgenes.

In order to determine whether there was any mHTT-induced toxicity in ReNcell VM+*HTT* exon 1 (71 CAG) and ReNcell VM+*HTT* exon 1 (129 CAG) neurons, LDH cytotoxicity assays were performed on neuronal cultures. ReNcell VM+eGFP reporter only and ReNcell VM+*HTT* exon 1 (29, 71 or 129 CAG) NSCs were differentiated until 10 DD by spontaneous differentiation. Cells were given a fresh culture medium change and returned to the incubator for a further 24 h. LDH cytotoxicity assays were then performed and results are displayed in Figure 3.11.

Neuronal culture type was a significant source of variation in neuronal culture death (p=0.010). Expression of *mHTT* exon 1 (71 CAG) resulted in significantly more neuronal death than expression of *HTT* exon 1 (29 CAG), p<0.05, suggesting that mHTT exon 1 71Q is more toxic than HTT exon 1 29Q and an indication of mHTT-induced neurotoxicity in this HD neuronal cell model. Interestingly, expression of *mHTT* exon 1 with a more expanded CAG tract (129 CAG) resulted in similar levels of death as *HTT* exon 1 (29 CAG), and significantly less death than *HTT* exon 1 (71 CAG),

p<0.01. This suggests that mHTT exon 1 71Q is more neurotoxic than mHTT exon 1 129Q in this model.

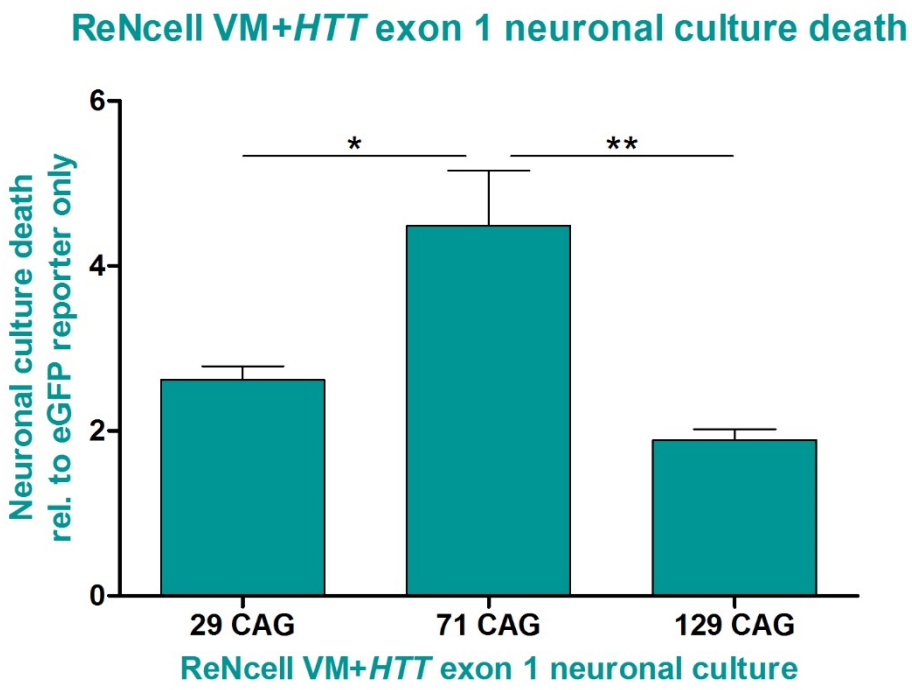

Figure 3.11: mHTT exon 1-induced cytotoxicity in ReNcell VM neuronal cultures

*LDH cytotoxicity assays were performed on ReNcell VM+HTT exon 1 (29 CAG), ReNcell VM+mHTT exon 1 (71 CAG), ReNcell VM+mHTT exon 1 (129 CAG) and ReNcell VM+eGFP reporter only neuronal cultures (11 DD, spontaneous differentiation) after 24 h incubation in standard NM culture medium. Results are presented as mean average neuronal culture death (calculated as described in section 2.6.1) relative to untreated eGFP reporter only neuronal culture death (baseline death levels), from three independent cultures per cell line, each with three internal experimental replicates, ± SEM. Data were statistically analysed using one-way ANOVA with Tukey post-hoc analyses; *p<0.05, **p<0.01.*

3.5.3 Generation of human HD neuronal cell lines with stable expression of human full-length mHTT

MSCVpuro+full-length *HTT* (15 CAG) and MSCVhyg+full-length *mHTT* (138 CAG) retroviral vectors were a kind gift from Prof. Michael R. Hayden (University of British Columbia, Canada). Full details of the expression systems, including plasmid maps, can be found in section 2.2.1.2.

MSCVpuro+full-length *HTT* (15 CAG) and MSCVhyg+full-length *mHTT* (138 CAG) plasmid DNA was amplified and purified, then restriction digests were performed to confirm correctness of the plasmids and check for DNA contamination. Firstly, plasmid

DNA was digested with *Xho*I and resulting DNA fragments were separated by agarose gel electrophoresis and sized against HyperLadder I and HyperLadder IV DNA ladders which were run in parallel. *Xho*I recognises two sites within each plasmid; one site in MSCV MCS located 12 bp 5' to the *HTT* transgene, and one naturally occurring sequence within *HTT* cDNA located 387 bp 3' to the CAG repeat tract. Therefore, *Xho*I was expected to cut out an N-terminal *HTT* fragment containing the CAG repeat + 12 bp flanking plasmid DNA, which had predicted sizes of 494 bp for MSCVpuro+full-length *HTT* (15 CAG) and 863 bp for MSCVhyg+full-length *mHTT* (138 CAG).

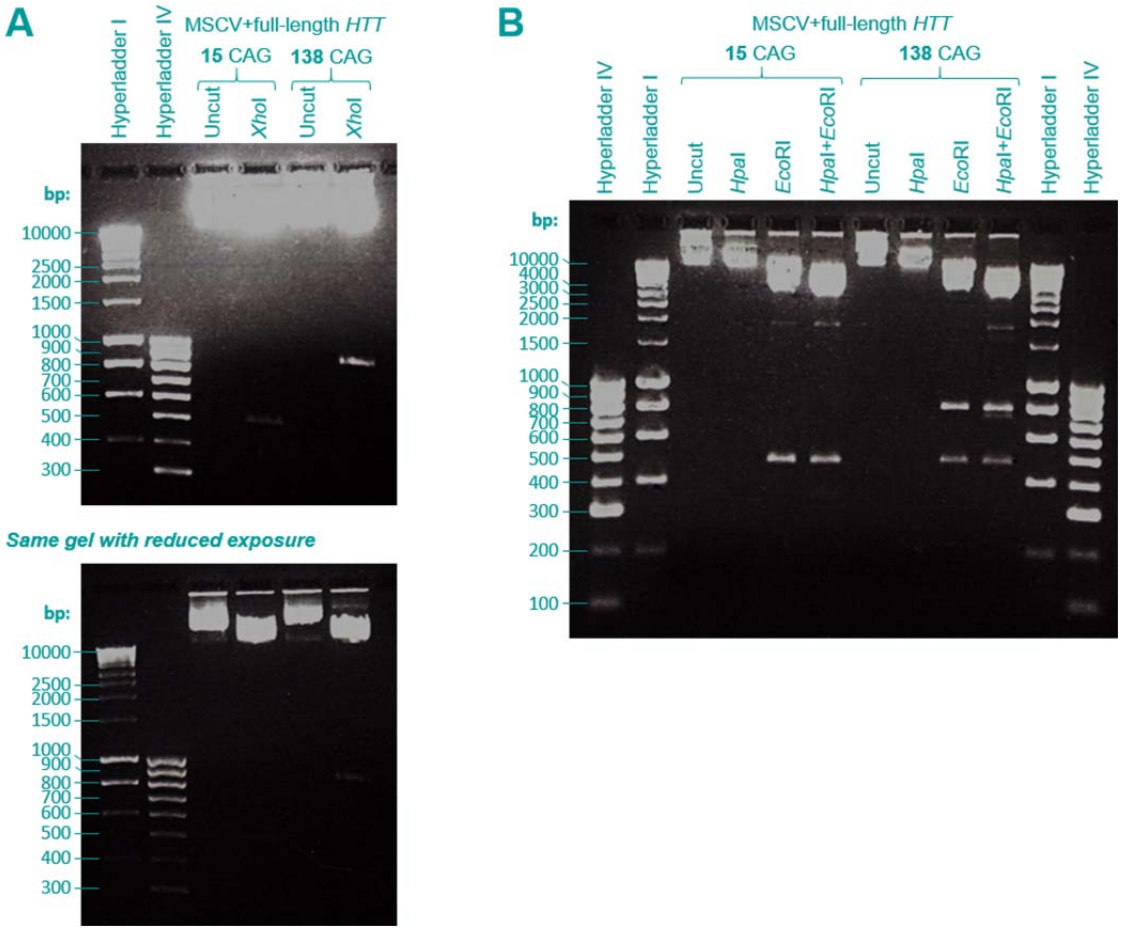

Figure 3.12: Restriction digest of MSCV+full-length *HTT* plasmid vectors

*MSCVpuro+full-length HTT (15 CAG) and MSCVhyg+full-length mHTT (138 CAG) plasmid vectors were digested with restriction enzyme Xho*I (***A***) *or Eco*RI *and Hpa*I (***B***) and *resulting DNA fragments were separated by agarose gel electrophoresis alongside DNA ladders HyperLadder I and HyperLadder IV. Each digested (Xho*I, *Hpa*I, *Eco*RI or *Hpa*I+*Eco*RI*) plasmid sample was run alongside an undigested (uncut) control sample. DNA was visualised by exposing intercalated ethidium bromide to UV light and images of the gels are presented above. Xho*I *digestion DNA gel results (****A****) are presented at two different exposures to more clearly demonstrate DNA bands representing N-terminal HTT fragments containing the CAG repeat (top) and remaining plasmid (bottom). Clear bands can be seen at ~500 bp in MSCVpuro+full-length HTT (15 CAG) and ~850 bp in MSCVhyg+full-length mHTT (138 CAG) samples following*

*digestion with Xho*I (***A***), *confirming CAG repeat tracts of the correct approximate size. Digestion with Eco*RI *and Hpa*I *also produced DNA bands at the estimated sizes (**B**), confirming correctness of both plasmids.*

Figure 3.12; A shows that digestion of each vector with *Xho*I produced DNA fragments at sizes appropriate to represent N-terminal *HTT* fragments with 15 or 138 CAG repeats, as predicted. The plasmid vectors were then digested with *Eco*RI and *Hpa*I. *Eco*RI recognises two sites within the *HTT* cDNA sequence (bp 4698 and bp 5175) and a site in MSCV MCS located directly 3' to the *HTT* transgene. In MSCVhyg+full-length *mHTT* (138 CAG), *Eco*RI also recognises a site within *hygr.* Therefore, digestion of MSCVpuro+full-length *HTT* (15 CAG) with *Eco*RI alone was predicted to produce three DNA fragments of 477 bp (*HTT* cDNA bp 4535-5012 (15 CAG)), 4405 bp (*HTT* cDNA bp 5012 (15 CAG)-MCS) and ~11 Kb (the remainder of the plasmid). Digestion of MSCVhyg+full-length *mHTT* (138 CAG) was expected to produce four DNA fragments of 477 bp, 4405 bp, ~11 Kb, and an additional fragment of unknown size due to the restriction site within *hygr* (full Clontech plasmid sequence is proprietary). *Hpa*I recognises only one site in each vector, which is located in MSCV MCS directly 5' to the *HTT* transgene. Digestion with *Hpa*I alone was consequently expected to linearize each plasmid, producing single DNA fragments of 15.7 Kb for MSCVpuro+full-length *HTT* (15 CAG) (6.3 Kb MSCVpuro + 9.4 Kb full-length *HTT* cDNA with 15 CAG) or 16.8 Kb for MSCVhyg+full-length *mHTT* (138 CAG) (7.0 Kb MSCVhyg + 9.8 Kb full-length *mHTT* cDNA with 138 CAG). Following digestion of each plasmid with *Eco*RI and *Hpa*I, alone or in combination, resulting DNA fragments were separated by agarose gel electrophoresis and sized against HyperLadder I and HyperLadder IV DNA ladders which were run in parallel. DNA bands of the predicted sizes were detected in each digested sample, as shown in Figure 3.12; B, which confirmed that each of the plasmids was correct and contained full-length *HTT* transgenes with CAG repeats in the correct range. No additional bands were detected, other than a faint band at ~2000 bp in *Eco*RI digestions which was attributed to star activity of this enzyme, confirming no contamination of plasmid DNA.

Full-length *HTT* transgenes were then sequenced in order to confirm their presence within the retroviral vectors, and to check their CAG repeat lengths and any mutations. Analysis confirmed that each of the vectors contained a full-length human *HTT* cDNA transgene with 15 CAG repeats for MSCVpuro+full-length *HTT* (15 CAG) and 136 CAG repeats for MSCVhyg+full-length *mHTT* (138 CAG). For reasons of clarity, the latter plasmid (and retroviruses and cell lines created using it) will still be referred to as MSCV+full-length *mHTT* (138 CAG) throughout this Thesis. The expanded *HTT*

transcript also contained 13 CAA interruptions in the CAG repeat tract. The transgenic inserts included the full coding DNA transcript followed by 600 bp non-coding DNA and a polyadenylated tail. Sequences were in frame, had no mutations in exon 1, and shared exact homology with the published NCBI; nucleotide; RefSeqGene reference sequence NG_009378.1 for *Homo sapiens* HTT cDNA (IT15) 10.3 Kb transcript, chromosome 4, other than the exceptions outlined in Table 3.3. Variations from the reference sequence were mostly synonymous substitutions or located in the non-coding sequence, so would not lead to changes in the final HTT protein. There were, however, three nonsynonymous nucleotide substitutions leading to amino acid coding changes: two of which were identified in both transgenes (codons for arginine instead of lysine and histidine instead of tyrosine), and one which was identified only in the full-length *mHTT* (138 CAG) transgene (codon for asparagine instead of threonine). Threonine → asparagine (bp 5165) and tyrosine → histidine (bp 6933) are known natural variants (SNPs) in HTT, which correspond to variants rs363125 and rs362331, respectively, in the Database of Single Nucleotide Polymorphism (dbSNP) (https://www-ncbi-nlm-nih-gov.libproxy.ucl.ac.uk/SNP/). Lysine → arginine (bp 3721) is not recorded as a known natural variant in HTT (UniProtKB – P42856; http://www.uniprot.org/uniprot/P42858), however polymorphisms in the *HTT* gene have not yet been fully established. Lysine and arginine are similar amino acids (both have electrically charged, basic side chains and are of similar size), therefore this variation should make little difference to the tertiary structure of the final HTT protein. Also, as the same variation occurs in both the *HTT* (15 CAG) and *mHTT* (138 CAG) transgenes, it was not considered to be problematic.

Table 3.3: Description of sequencing results for full-length *HTT* cDNA transgenes

HTT transgene	
Full-length human *HTT* cDNA (15 CAG)	**Full-length human *mHTT* cDNA (138 CAG)**
Size	
Full transgene = 10030 bp Coding sequence = 9417 bp	Full transgene = 10358 bp Coding sequence = 9780 bp
CAG repeat size	
15	136 (including 13 CAA interruptions)
Variations from reference sequence	
	bp 281: GAA → GAG *Synonymous substitution (glutamic acid)*

bp 1196: ACC → ACT *Synonymous substitution (threonine)*	
bp 3721: AAA → AGA *Nonsynonymous substitution (lysine → arginine)*	
	bp 5165: ACT → AAT *Nonsynonymous substitution (threonine → asparagine)*
bp 6933: TAC → CAC *Nonsynonymous substitution (tyrosine → histidine)*	
bp 7184: CTA → CTC *Synonymous substitution (leucine)*	
bp 9811: C → G *Non-coding sequence*	
bp 9923: C → A *Non-coding sequence*	
bp 9958: C → T *Non-coding sequence*	

Reference sequence = NCBI; nucleotide; RefSeqGene; NG_009378.1 for Homo sapiens HTT cDNA (IT15) 10.3 Kb transcript, chromosome 4. bp numbers refer to locations in the cDNA reference sequence. A, adenine; C, cytosine; G, guanine; T, tyrosine.

The concentration and purity of MSCVpuro+full-length *HTT* (15 CAG) and MSCVhyg+full-length *mHTT* (138 CAG) plasmid DNA was determined by NanoDrop, and results are reported in Table 3.4. A260/A280 ratios were 1.9 for both plasmids, indicating no protein or RNA contamination within the samples, and A260/A230 ratios were above 2.0, indicating no other contaminants within the DNA samples. Plasmid DNA was therefore considered to be sufficiently pure and of high quality for use in transfection procedures.

Table 3.4: MSCV+full-length *HTT* plasmid DNA concentration and purity

Plasmid	DNA concentration/ ng/µL	A260/A280	A260/A230
MSCVpuro+full-length *HTT* (15 CAG)	2814.2	1.90	2.21
MSCVhyg+full-length *mHTT* (138 CAG)	2507.9	1.90	2.22

MSCVpuro+full-length *HTT* (15 CAG) and MSCVhyg+full-length *mHTT* (138 CAG) plasmids have wild-type genomes of 6.3 and 7.0 Kb, respectively, and *HTT* transgene inserts of 10.0 Kb and 10.3 Kb, respectively. For a retroviral expression system, which usually have insert size capacities in the range of 2.5-5.0 Kb, these plasmids are very large, and therefore viral titre was expected to be very low. MSCV retroviral expression systems are, however, optimised for introducing and expressing target genes in pluripotent cell lines, including human stem cells such as ReNcell VM NSCs, and viral expression systems with larger insert size capacities, such as adenovirus gene delivery systems, do not facilitate transgene integration into the genome of the target cell. Adeno-associated virus (AAV) expression systems have a much larger typical titre, but again, do not generally facilitate genome integration. The MSCV retroviral expression system was therefore selected for introducing and expressing the full-length *HTT* transgenes in ReNcell VM NSCs. As viral titre was predicted to be very low, it was expected that retroviral supernatants would require concentration. For this reason, pseudotyped viruses were created with VSV-G foreign viral envelope protein, to increase stability of the viral particles and maintain their structural integrity during ultracentrifugation. MSCVpuro+full-length *HTT* (15 CAG) and MSCVhyg+full-length *mHTT* (138 CAG) plasmid vectors were packaged into dual 4070A (amphotropic)/VSV-G coated retroviruses by transfection into the Phoenix-AMPHO retrovirus producer cell line, along with VSV-G-expressing envelope plasmid MD.G2, using FuGene HD Transfection Reagent. The 4070A envelope and GAG/pol packaging proteins were encoded from constructs carried by Phoenix-AMPHO.

Retroviral supernatants were collected and tested for viability by infection of HeLa cell cultures and monitoring survival rates under antibiotic selection. Firstly, puromycin and hygromycin antibiotic kill curves were performed in HeLa cells, as described in detail in section 2.3.4.1. Cells were treated with a range of puromycin (0-15 µg/mL) or Hygromycin B (0-500 µg/mL) concentrations and approximate percentage cell survival was interpreted daily by visualisation of HeLa cultures using phase-contrast microscopy. The optimum antibiotic selection concentration was considered to be the minimum concentration required to give 100 % HeLa cell death after 3-4 days for puromycin, which was 0.2 µg/mL, and 7-8 days for Hygromycin B, which was 300 µg/mL (Figure 3.13). Four days post-infection with MSCVpuro+full-length *HTT* (15 CAG) or MSCVhyg+full-length *mHTT* (138 CAG) retrovirus supernatants, 0.2 µg/mL puromycin or 300 µg/mL Hygromycin B, respectively, was added to the HeLa cell culture medium, and medium changes with the addition of fresh antibiotics were performed every two days. Retrovirus viability was assessed by monitoring cell survival under antibiotic selection. Infections with retroviral supernatants which resulted in at

least 5 % surviving cells after four days puromycin selection or seven days Hygromycin B selection, followed by an exponential growth phase under continued selection, were considered to contain viable retrovirus, and were subsequently taken forward for concentration by ultracentrifugation.

Concentrated MSCVpuro+full-length *HTT* (15 CAG) and MSCVhyg+full-length *mHTT* (138 CAG) retroviruses were tested for viability and transduction efficiency in HeLa cells, as described in detail in section 2.3.3.2. HeLa cells were infected with concentrated retrovirus at 1:100, 1:1000 and 1:10,000 dilutions, or received no infection, and were subjected to antibiotic selection. After four days puromycin selection or 7 days Hygromycin B selection, non-infected cells were completely dead, cells which received no antibiotic treatment had reached 100 % confluence, and infected cultures had ~15-20 % surviving cell populations. The exception was HeLa cells infected with MSCVpuro+full-length *HTT* (15 CAG) concentrated retrovirus at 1:10,000 dilution, which did not survive under antibiotic selection, indicating low viability or poor transduction efficiency. All other infections were deemed to contain viable retroviruses with reasonable transduction efficiency.

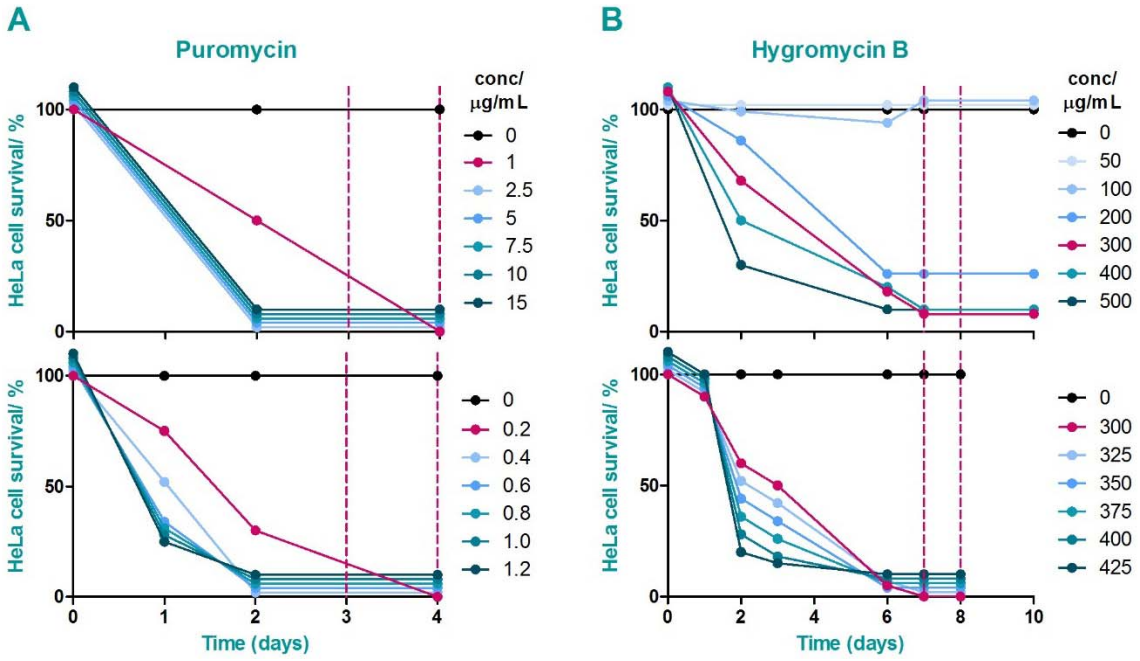

Figure 3.13: Antibiotic kill curves in HeLa cell cultures

*HeLa cells were treated, in triplicate, with puromycin (**A**) or Hygromycin B (**B**) at a range of concentrations. Average percentage surviving cells compared to untreated cells was monitored daily, and determined by visualisation of cell cultures using a light microscope. Cells were given a media change with the addition of fresh antibiotics every 2 days. The optimum antibiotic selection concentration was considered to be the minimum concentration required to give 100 % cell death after 3-4 days for puromycin, and 7-8 days for Hygromycin B (purple dashed lines indicate optimum day range; purple line graphs indicate optimum antibiotic concentrations). Kill*

curves were performed firstly with a broad concentration range (top graphs) and again with a narrower concentration range (bottom graphs).

While MSCV retroviral expression systems are optimised for the delivery and expression of target genes in pluripotent cell lines, there was still a possibility that transgene silencing may occur in transduced NSCs due to the highly dynamic epigenetic regulation taking place in these cells. Therefore, in order to ensure that the retroviruses were functional, successful expression of the transgenes was firstly tested in the transduced HeLa cells. Cultures which had survived antibiotic selection were grown to confluence and expanded, and expression of full-length HTT trans-protein was detected by Western blotting and ICC techniques with confocal fluorescence microscopy.

Full-length HTT protein runs at ~350 KDa by SDS-PAGE, and anti-HTT antibody mAB2166 detected proteins of this size in Western blots of transduced HeLa cell lysates. Cells transduced with full-length *HTT* had stronger expression of this protein than non-transduced (wild-type) cells (Figure 3.14; A, mAB2166), indicating expression of the trans-proteins. When Western blots were probed with anti-mHTT polyQ antibody MW1, protein bands were detected in HeLa cell cultures transduced with full-length *mHTT* (138 CAG), but not in wild-type cultures or cultures transduced with full-length *HTT* (15 CAG) (Figure 3.14; A, MW1), indicating presence of mHTT with expanded polyQ in these cells. MW1 labelled very faint bands at ~350 KDa (full-length mHTT), and stronger bands ranging between 150 and 250 KDa, indicating possible fragmentation of the full-length protein. Cultures which had received the most concentrated infections (1:100 concentrated retrovirus) were taken forward for testing by ICC, as described in sections 2.3.3.2 and 2.5.2. Fixed cells were probed with 2B7 (anti-HTT) and MW1 (anti-mHTT polyQ) antibodies, which detected over-expression of HTT in both transduced cultures compared with wild-type HeLa cells, and mHTT expression in cultures transduced with full-length *mHTT* (138 CAG) (Figure 3.14; B). This provided further evidence for expression of the HTT trans-proteins and confirmed that the retroviruses were viable.

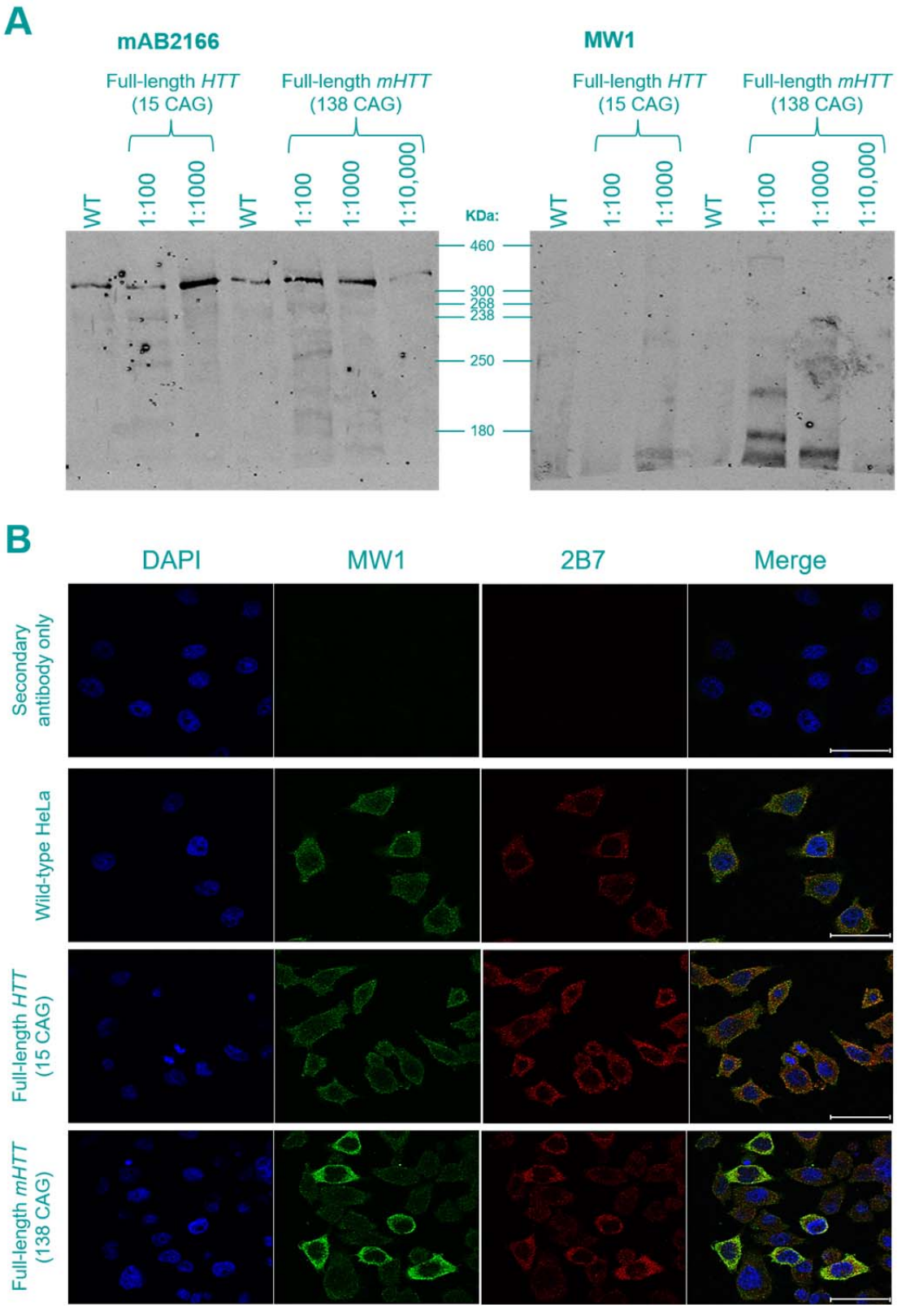

Figure 3.14: Full-length HTT trans-protein expression in HeLa cell cultures infected with MSCV+full-length *HTT* concentrated retroviruses

A) *Western blots of lysates from wild-type (WT) HeLa cell cultures, and HeLa cell cultures infected with concentrated MSCVpuro+full-length HTT (15 CAG) or MSCVhyg+full-length mHTT (138 CAG) retroviruses at 1:100, 1:1000 or 1:10,000 dilutions. Membranes were probed with*

*mAB2166 (anti-HTT) (**left**) and MW1 (anti-mHTT polyQ) (**right**) primary antibodies which were detected by IRDye-conjugated secondary antibodies and visualised using a LI-COR Odyssey Scanner. Protein weight was determined by two high molecular weight protein standards which were run alongside. **B)** ICC showed increased expression of HTT in transduced HeLa cells compared with wild-type HeLa cells (2B7; red), and mHTT expression in cells transduced with full-length mHTT (138 CAG) (MW1; green). DAPI (blue) was used to stain nuclei. Cell cultures were imaged using confocal fluorescence microscopy. Example images presented from six random fields of view per culture. Scale bar = 50 µm.*

As expected, viral titre was very low, and therefore the highest concentration of retrovirus was used for subsequent infections of ReNcell VM NSCs, as described in detail in section 2.3.4.2. Additionally, a double infection method was used to improve transduction efficiency. ReNcell VM NSCs were infected with concentrated MSCVpuro+full-length *HTT* (15 CAG) or MSCVhyg+full-length *mHTT* (138 CAG) retroviruses at 1:100 dilution for 24 h, followed by another consecutive 24 h infection to increase MOI. Cells were then expanded over one passage before undergoing antibiotic selection. NSC cultures transduced with full-length *HTT* (15 CAG) were selected with 0.125 µg/mL puromycin and NSC cultures transduced with full-length *mHTT* (138 CAG) were selected with 40 µg/mL Hygromycin B. These optimum antibiotic concentrations had been determined previously by performing kill curves in ReNcell VM NSCs (Figure 3.15). Cultures were maintained under antibiotic selection for 1 week (puromycin) or 2 weeks (Hygromycin B), at which point small colonies of surviving cells had begun to expand. Cultures were then grown to confluence and expanded over two passages.

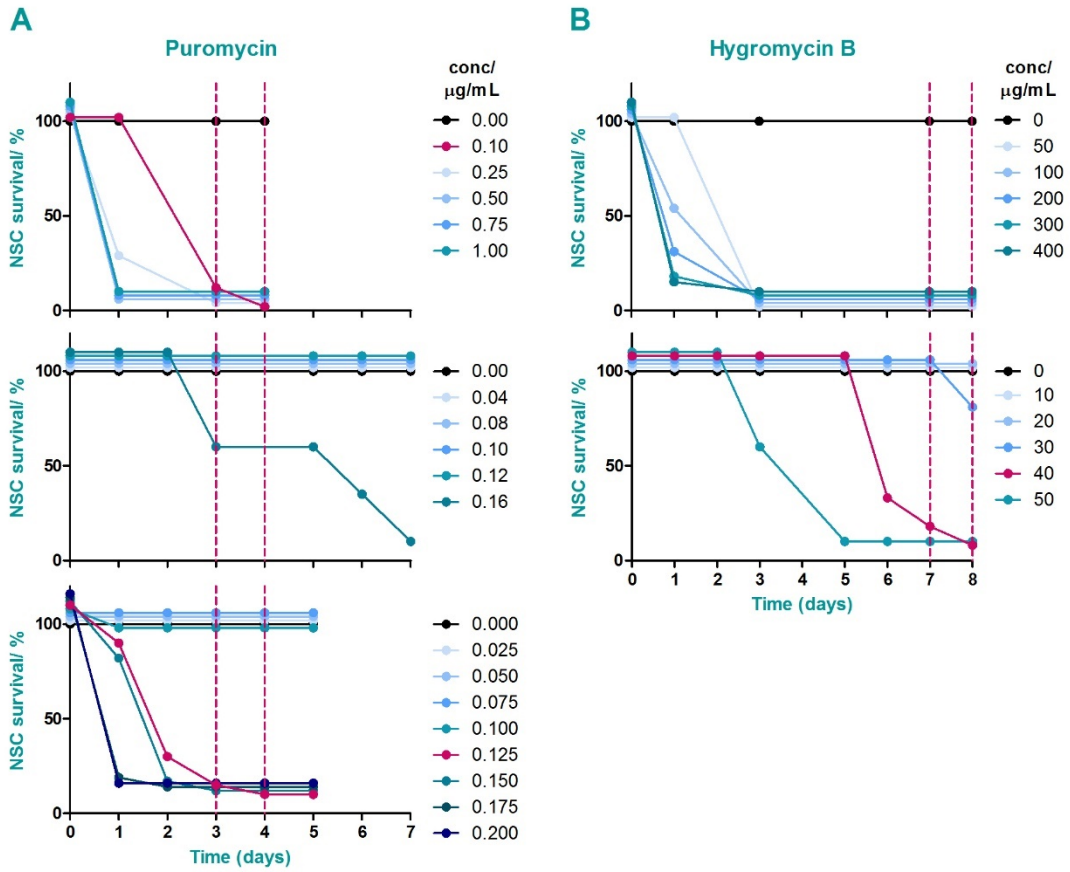

Figure 3.15: Antibiotic kill curves in ReNcell VM NSC cultures

*ReNcell VM NSCs were treated, in triplicate, with puromycin (**A**) or Hygromycin B (**B**) at a range of concentrations. Average percentage surviving cells compared to untreated cells was monitored daily, and determined by visualisation of cell cultures using a light microscope. Cells were given a media change with the addition of fresh antibiotics every 2 days. The optimum antibiotic selection concentration was considered to be the minimum concentration required to give 100 % cell death after 3-4 days for puromycin, and 7-8 days for Hygromycin B (purple dashed lines indicate optimum day range; purple line graphs indicate optimum antibiotic concentrations). Kill curves were performed firstly with a broad concentration range (top graphs) and again with narrower concentration ranges (bottom graphs).*

3.5.3.1 Characterisation of ReNcell VM+full-length HTT neuronal cell lines

Stable expression of the trans-proteins in ReNcell VM+full-length *HTT* (15 CAG) and ReNcell VM+full-length *mHTT* (138 CAG) NSCs was determined by ICC (as described for HeLa+full-length *HTT* cell lines above, and in detail in section 2.5.2) (Figure 3.16; A). Like wild-type ReNcell VM, these transduced NSCs could be differentiated into mature neuronal cultures by spontaneous differentiation (Figure 3.16; B).

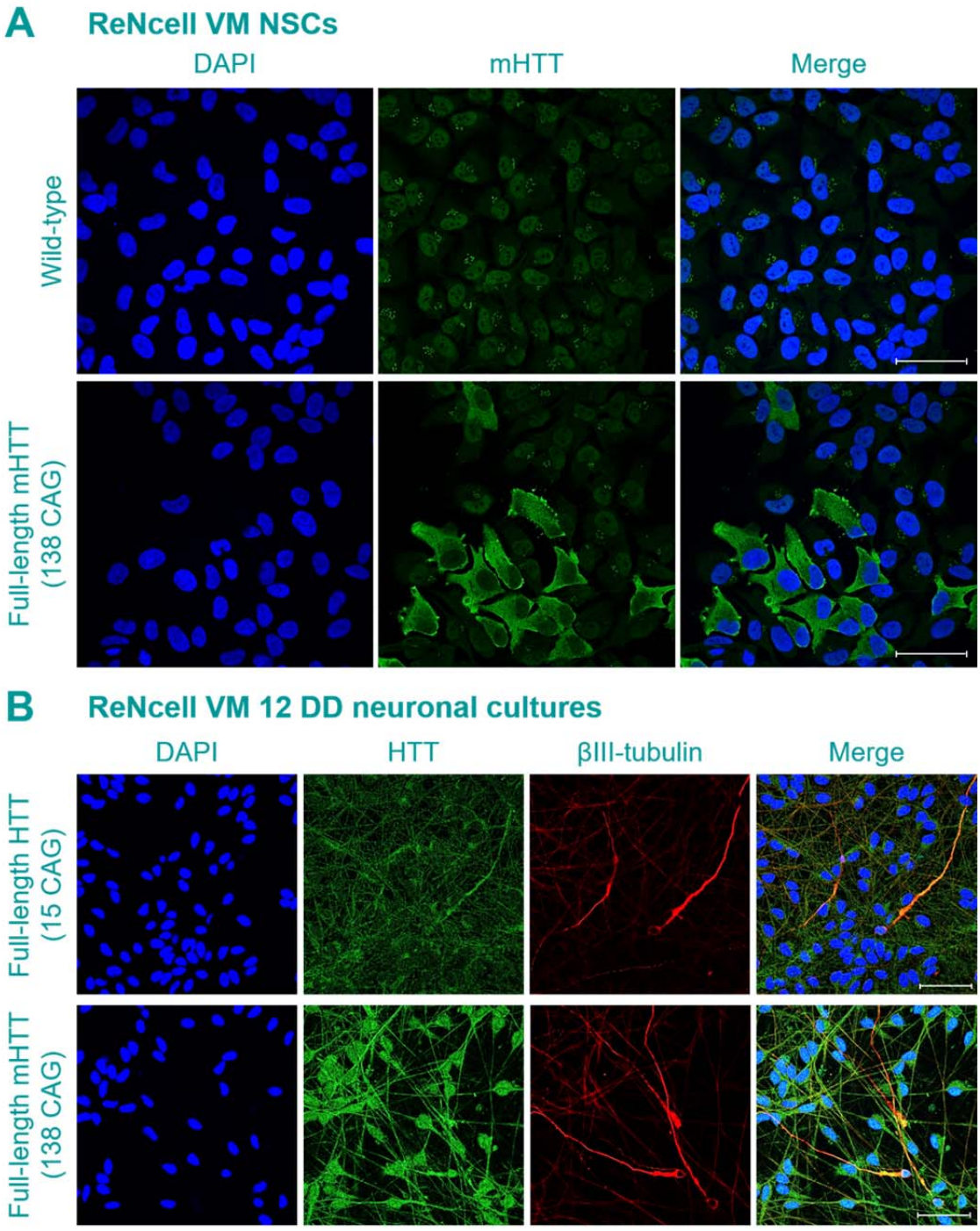

Figure 3.16: Characterisation of selected ReNcell VM+full-length *HTT* cell lines

*Confocal fluorescence microscopy images of wild-type ReNcell VM and ReNcell VM+full-length mHTT (138 CAG) NSC cultures (**A**) show expression of* mHTT *trans-protein in the transgenic cell line following ICC with antibodies directed at* mHTT *polyQ (MW1; green). ReNcell VM+full-length HTT (15 CAG) and ReNcell VM+full-length mHTT (138 CAG) can be differentiated into mature neuronal cultures (spontaneous differentiation) (**B**) which express HTT (mAB2166; green) and βIII-tubulin (red). All images are representative examples from at least five random fields of view from two cultures. Nuclei stained with DAPI (blue). Scale bars = 50 μm.*

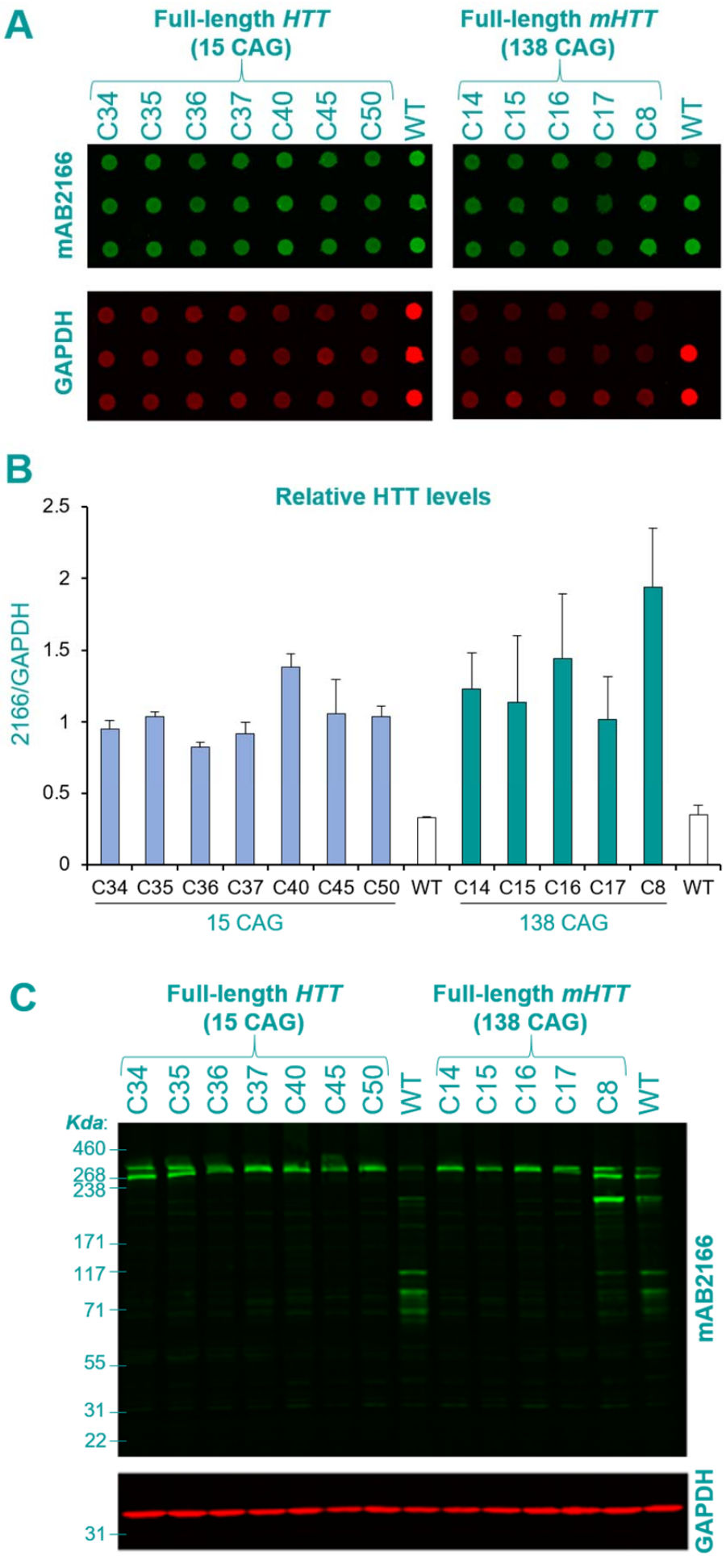
A
Full-length HTT
(15 CAG)
Full-length mHTT
(138 CAG)
C34 C35 C36 C37 C40 C45 C50 WT
C14 C15 C16 C17 C8 WT
mAB2166
GAPDH
B
Relative HTT levels
2166/GAPDH
2.5
2
1.5
1
0.5
0
C34 C35 C36 C37 C40 C45 C50 WT C14 C15 C16 C17 C8 WT
15 CAG
138 CAG
C
Full-length HTT
(15 CAG)
Full-length mHTT
(138 CAG)
C34 C35 C36 C37 C40 C45 C50 WT C14 C15 C16 C17 C8 WT
Kda:
460
268
238
171
117
71
55
31
22
mAB2166
31
GAPDH

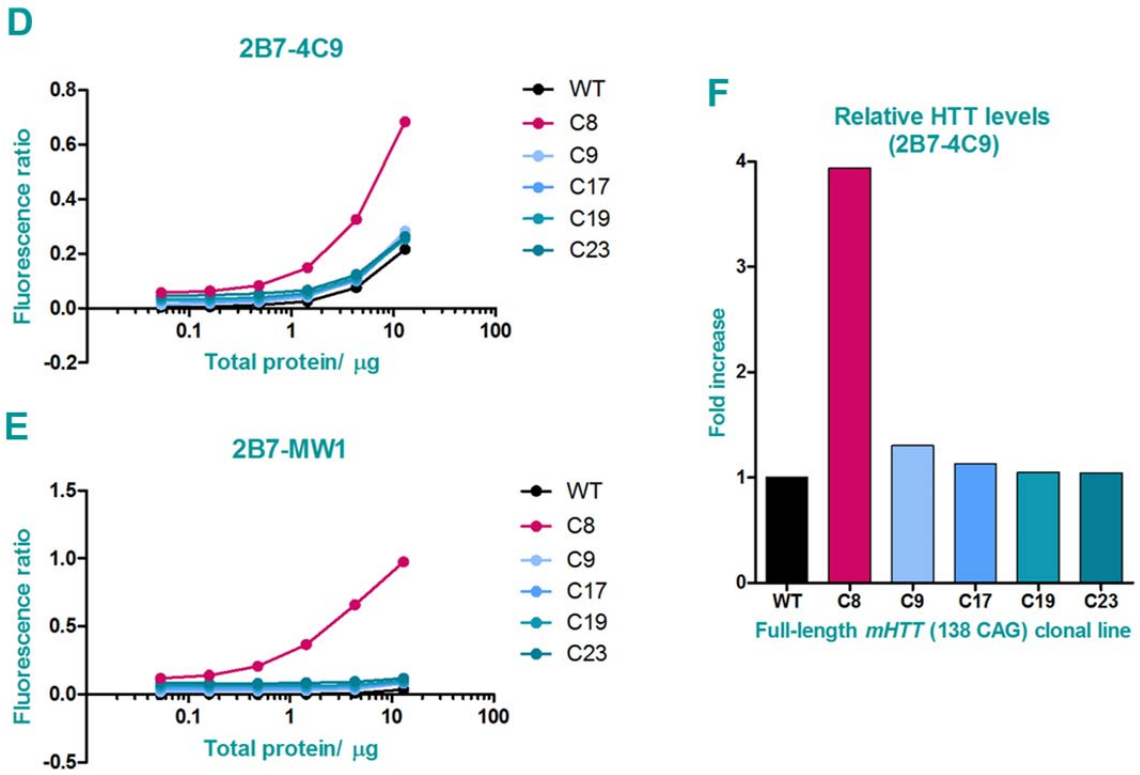

Figure 3.17: HTT quantification in ReNcell VM+full-length *HTT* clonal lines

*Wild-type ReNcell VM NSC and ReNcell VM+full-length HTT (15 CAG) and ReNcell VM+full-length mHTT (138 CAG) NSC clone lysates were dot blotted (**A**) or Western blotted (**C**) and probed for HTT (mAB2166) and GAPDH (loading control). IRDye-labelled secondary antibodies bound to HTT (green) and GAPDH (red) were visualised by LI-COR Odyssey scanner. Relative HTT levels were calculated by normalising HTT levels to GAPDH levels (**B**), as detected by dot blot. HTT levels in ReNcell VM+full-length mHTT (138 CAG) NSC clones relative to wild-type NSCs were confirmed by TR-FRET assay (**F**) utilising results from 2B7-4C9 antibody pair analysis (**D**). 2B7-MW1 antibody pair analysis (**E**) confirmed expression of mHTT in ReNcell VM+full-length mHTT (138 CAG) C8 NSCs. All panels presented in this figure are examples taken from several different clone screening batches.*

It was observed that there was large cell-to-cell variability in HTT expression levels within each culture (Figure 3.16; A), indicating variable transgene expression, and consequently there was a requirement for generation of clonal transgenic cell lines. ReNcell VM+full-length *HTT* (15 CAG) or ReNcell VM+full-length *mHTT* (138 CAG) NSCs were seeded into a 96-well culture plate at 1 cell per well and cultures which grew to confluence were expanded as individual clonal cell lines. From single-cell seeding, approximately 40 clonal cell lines of each original ReNcell VM+full-length *HTT* line survived and were expanded. Of these clones, approximately 20 of each line were screened for presence and expression level of the trans-proteins by dot blotting, Western blotting and TR-FRET assay. Wild-type ReNcell VM NSC and ReNcell VM clone lysate samples were dot blotted, in triplicate, and probed with antibodies directed

at HTT (mAB2166) and GAPDH (Figure 3.17; A). Clone HTT levels, relative to wild-type NSCs, were determined by normalising HTT levels to GAPDH levels in each sample (Figure 3.17; B), and clones with HTT levels at least two-fold higher than wild-type NSCs were confirmed as expressing the trans-protein. Cell lysates were then run on Western blots and again probed for HTT (mAB2166) to check the sizes of the HTT fragments against a protein ladder (Figure 3.17; C). TR-FRET assay was performed on selected ReNcell VM+*mHTT* (138 CAG) NSC clones which had been shown to over-express HTT by dot blotting and Western blotting techniques. 2B7-4C9 antibody pair was used to quantify HTT levels in each of the clones, and in wild-type ReNcell VM NSCs, (Figure 3.17; D) and 2B7-MW1 antibody pair was used to simultaneously quantify mHTT levels (expanded polyQ) (Figure 3.17; E). HTT levels in each clone were then calculated relative to wild-type ReNcell VM NSC HTT levels, using results from the 2B7-4C9 TR-FRET assay (Figure 3.17; F).

ReNcell VM+*mHTT* (138 CAG) Clone 8 (C8) was determined, by dot blot and TR-FRET assay, to have approximately four-fold HTT over-expression compared to wild-type ReNcell VM NSCs. Over-expression of HTT protein within the full-length size range was also detected by Western blot, along with smaller over-expressing fragments, and C8 was the only full-length *mHTT* (138 CAG) clone for which mHTT with expanded polyQ was detected by TR-FRET (2B7-MW1 antibody pair). HTT over-expression in C8 was also observed by ICC, as can be seen in Figure 3.18. ReNcell VM+*mHTT* (138 CAG) C8 was therefore confirmed to be expressing the full-length *mHTT* trans-protein.

Due to the large volume of work required to generate, expand and screen each clonal line, this process was carried out in batches and ReNcell VM+*mHTT* (138 CAG) clones were completed first. At the time of writing this Thesis, no final ReNcell VM+*HTT* (15 CAG) clones had been fully verified.

To assess mHTT-induced neurotoxicity in the full-length line, wild-type and ReNcell VM+full-length *mHTT* (138 CAG) C8 ReNcell VM were differentiated (spontaneous differentiation) to 10 DD. Neuronal cultures were then given a fresh medium change and returned to the incubator for 24 h before performing LDH cytotoxicity assays. Percentage cell death over this 24 h window was not found to be affected by expression of full-length *mHTT* (Figure 3.19).

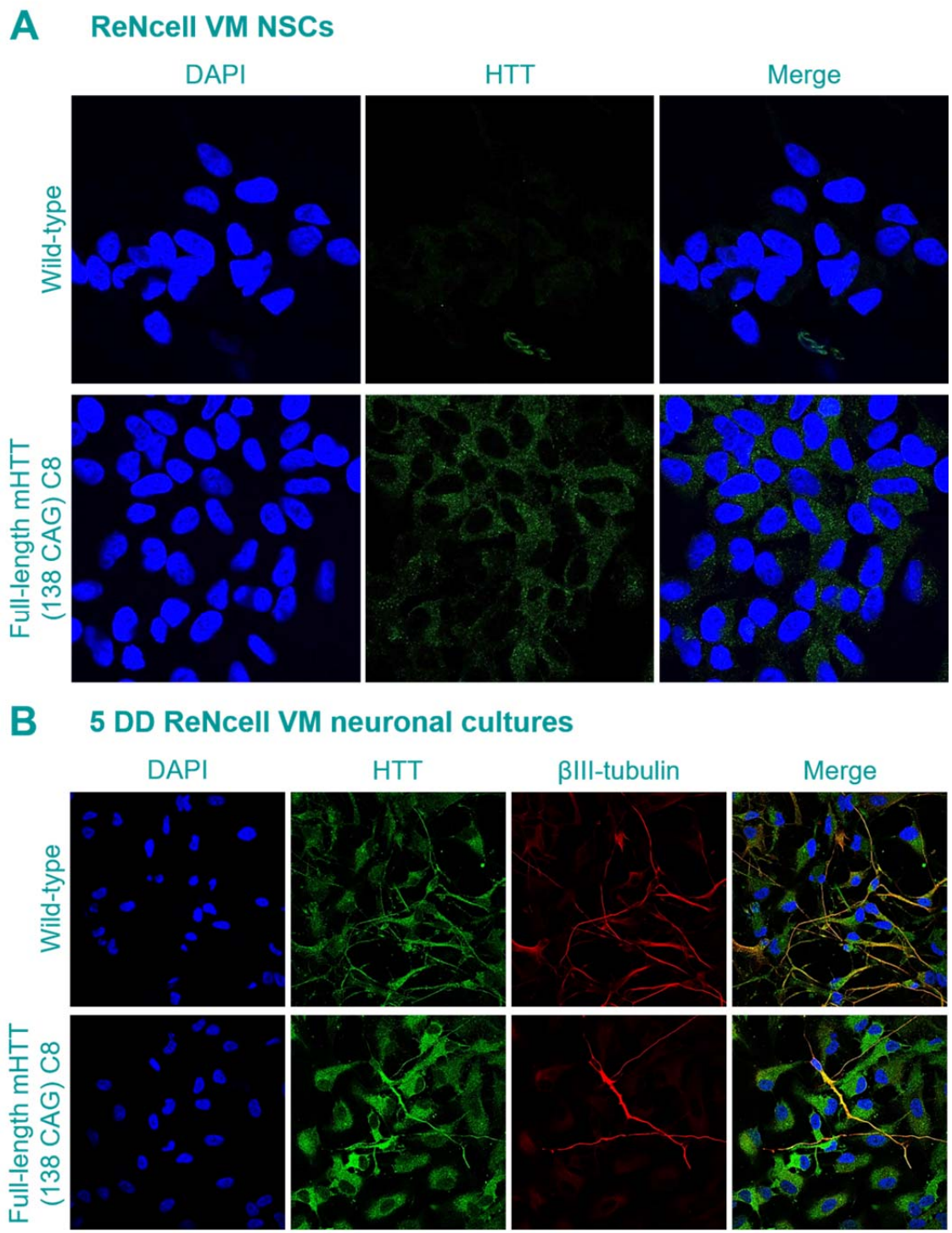

Figure 3.18: HTT over-expression in ReNcell VM+full-length *mHTT* (138 CAG) C8

*Confocal fluorescence microscopy images following ICC of wild-type ReNcell VM and ReNcell VM+full-length mHTT (138 CAG) C8 NSC cultures (**A**) and 5 DD neuronal cultures (spontaneous differentiation) (**B**) with antibodies directed at HTT (mAB2166; green) show over-expression of HTT in C8 of the transgenic line. Mature neurons stained positively for βIII-tubulin (red) indicating successful differentiation. Interestingly, mHTT-expressing cultures appeared to differentiate more slowly than wild-type cultures, as can be seen by the higher number of NSCs and lower number of mature neurons at 5 DD. Nuclei were stained with DAPI (blue).*

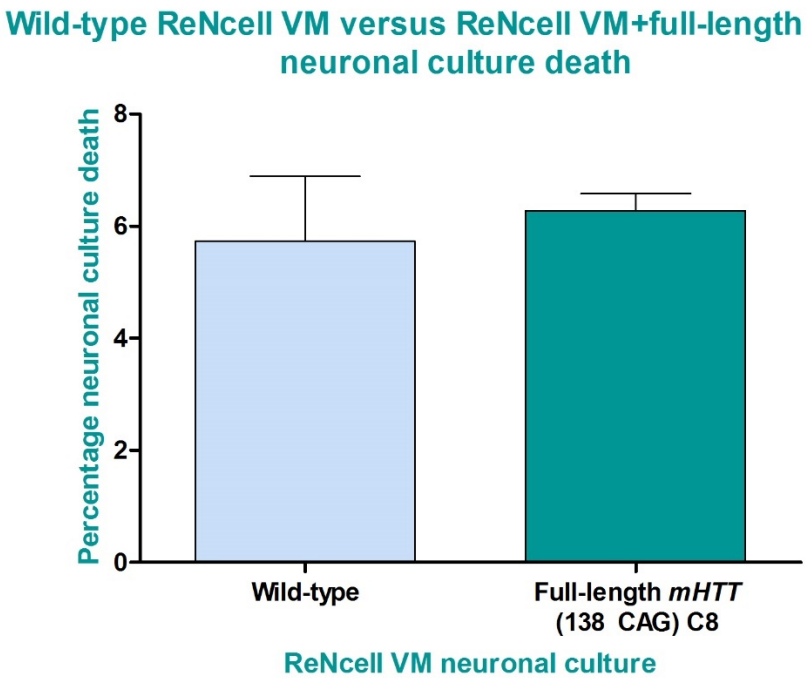

Figure 3.19: Full-length mHTT-induced neurotoxicity in ReNcell VM neuronal cultures

Ten DD (spontaneous differentiation) wild-type ReNcell VM and ReNcell VM+full-length mHTT (138 CAG) C8 neuronal cultures were cultured in fresh medium for 24 h before performing LDH cytotoxicity assays, in triplicate cultures, to assess neurotoxicity. Results presented as mean average percentage cell death (calculated as described in section 2.6.1) of two independent biological repeats ± SEM. Data were statistically analysed using two-tailed, paired t-test and the difference in the means was found to be not significant (p=0.639).

3.5.4 Differentiation of primary human monocytes into macrophages and microglia-like cells in culture

3.5.4.1 HD patient myeloid cells express mHTT

Primary human monocytes were isolated from whole blood samples collected from healthy volunteers and manifest HD patients and cultured *ex vivo*. Monocytes were then differentiated into BMD-macrophages using a previously published and well-establish protocol (Akagawa *et al.* 2006; Kwan *et al.* 2012b; Träger *et al.* 2014a), which is described in section 2.1.2.4. Differentiation was induced by GM-CSF, which promotes the development of macrophages with a proinflammatory M1-type phenotype. HD patient BMD-macrophages were shown to express mHTT by ICC and confocal fluorescence microscopy (Figure 3.20).

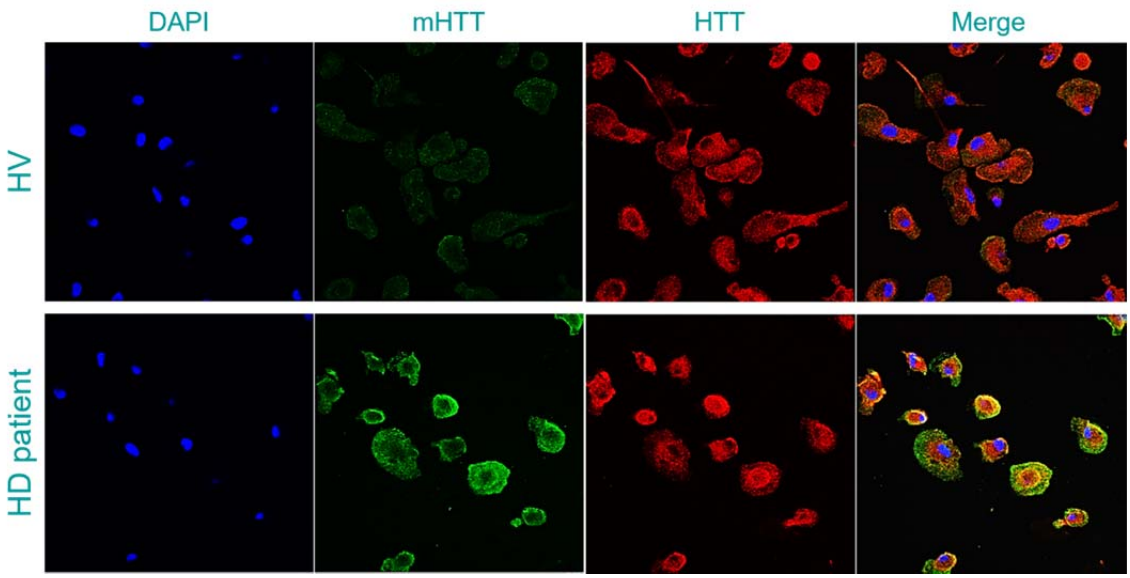

Figure 3.20: mHTT expression in HD patient BMD-macrophages

Confocal fluorescence microscope images of BMD-macrophages differentiated from monocytes isolated from a healthy volunteer (HV; top panel) or HD patient (bottom panel) following ICC with antibodies directed at HTT (2B7; red) and mHTT polyQ (MW1; green). Nuclei were stained with DAPI (blue). MW1 has preference for expanded HTT polyQ and can be seen above to produce higher signal in HD patient BMD-macrophages than healthy volunteer BMD-macrophages, indicating expression of mHTT in these cells. Images presented here are representative examples from three healthy volunteer cultures and five manifest HD patient cultures, with at least five fields of view per culture. Images taken at 40× objective.

3.5.4.2 In vitro differentiation of primary human monocytes into microglia-like cells

Most co-culture set-ups require both cell types to be cultured in the same medium, and therefore a compatible culture medium must be used. For the development of neuronal-myeloid cell co-culture models of HD, media titrations were performed, as described in detail below (section 3.5.5), in both ReNcell VM neuronal cultures and BMD-macrophage cultures using standard neuronal culture medium (NM) and standard BMD-macrophage medium (RPMI/FBS). Surprisingly, while observing BMD-macrophages during culture in increasing titrations of NM, these cells became microglia-like in their morphology and behaviour. BMD-macrophages initially exhibited a classic round, ‘fried egg’ morphology and were transformed into ramified cells with dendritic-like, arborizing processes which appeared to actively and physically survey the local micro-environment. This transformation occurred over a period of four days and was more pronounced with higher NM titrations. On account of this interesting morphological transformation, these cells were investigated further as a potential model of human microglia in culture.

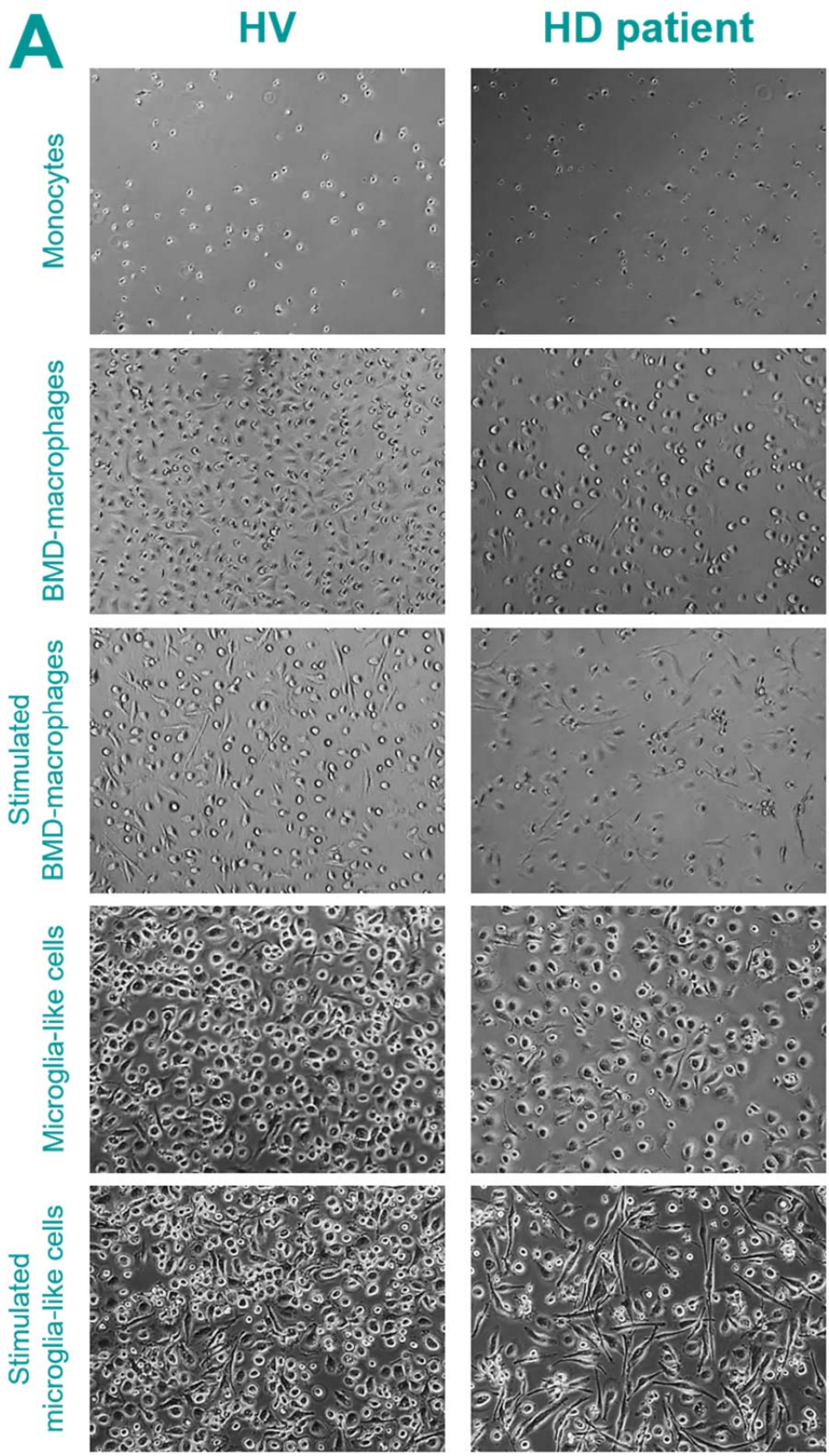
A
HV
HD patient
Monocytes
BMD-macrophages
Stimulated BMD-macrophages
Microglia-like cells
Stimulated microglia-like cells

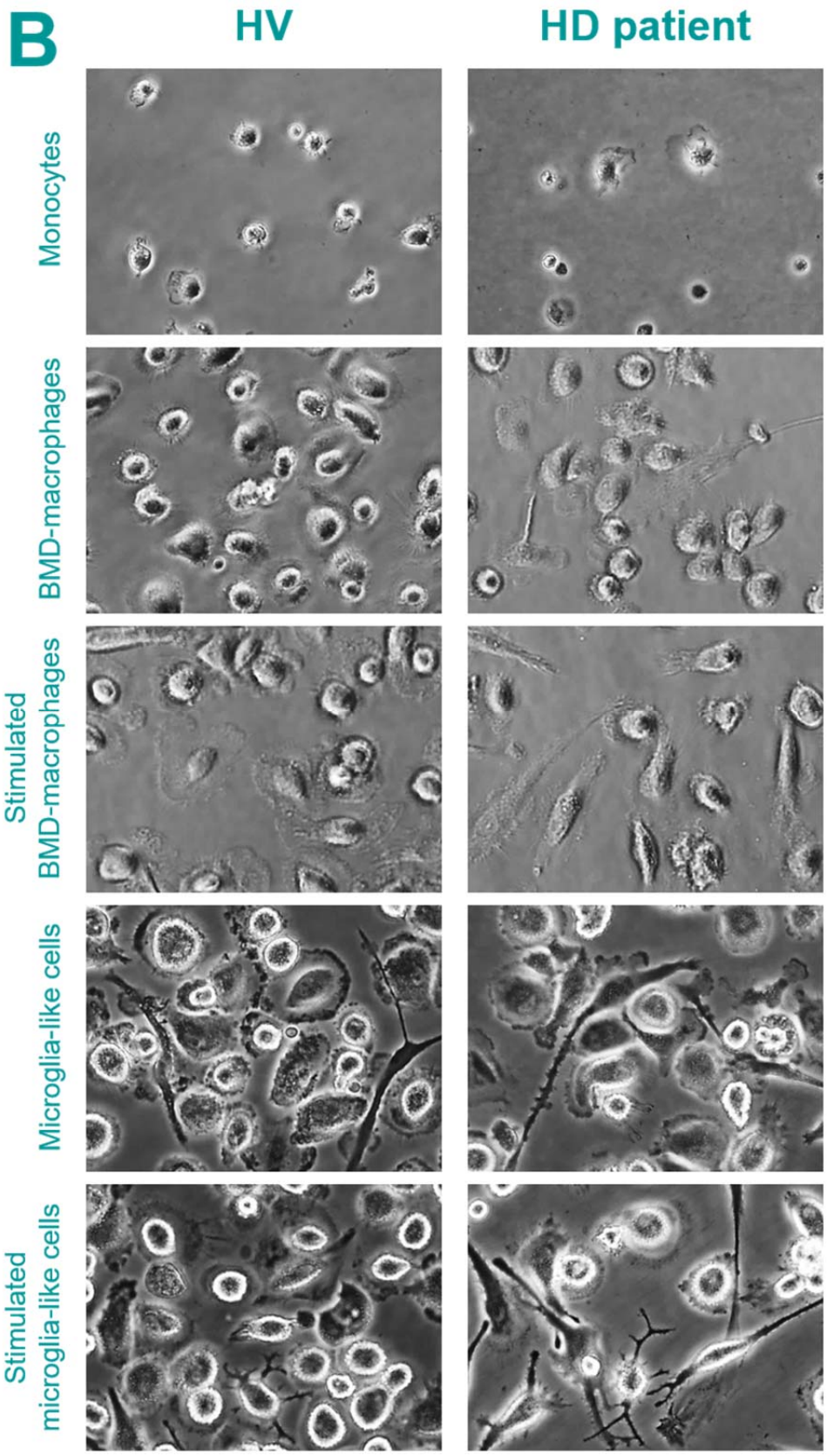

Figure 3.21: Morphological analysis of *in vitro* differentiation of primary human monocytes

Phase-contrast microscope images showing morphology of healthy volunteer (HV) and manifest HD patient myeloid cells as they are differentiated from primary monocytes to BMD-

*macrophages (induced by GM-CSF) to microglia-like cells (by media change into NM). BMD-macrophages and microglia-like cells are shown in non-stimulated and stimulated (2 µg/mL LPS and 10 ng/mL IFNγ for 24 h) conditions. Cultures were imaged using 10× objective (**A**) and 40× objective (**B**). Images are representative examples from at least five fields of view per culture, and represent similar observations made when differentiating cultures isolated from several independent healthy volunteers and HD patients.*

Monocytes were isolated from one healthy volunteer and one manifest HD patient and differentiated into BMD-macrophages. BMD-macrophages were then stimulated with 2 µg/mL LPS and 10 ng/mL IFNγ for 24 h, or were given a fresh culture medium change, and returned to the incubator for a further 4 days. Microglia-like cultures were then stimulated with 2 µg/mL LPS and 10 ng/mL IFNγ for 24 h. Cell cultures underwent morphological analysis using live-cell phase-contrast microscopy throughout the different differentiation stages and in non-stimulated and stimulated conditions as monocytes, BMD-macrophages, stimulated BMD-macrophages, microglia-like cells and stimulated microglia-like cells (Figure 3.21).

Monocytes were small round cells which grew larger and ‘fried egg’ like and proliferated during differentiation into BMD-macrophages. When stimulated, BMD-macrophages proliferated further and rounded up. Some cells became rod-like and polarised, indicative of migratory behaviour. No obvious morphological differences were observed between healthy volunteer and HD patient cells in these conditions. After four days culture in NM, BMD-macrophages grew larger and some cells had become ramified and microglia-like in their morphology, as had been observed previously in media titration experiments. This was the same in both healthy volunteer and HD patient cultures. Interestingly, when these microglia-like cells were stimulated, apparent differences were observed between healthy volunteer and HD patient cultures. In healthy volunteer cultures, approximately 10 % of the cells displayed some ramification, while the rest of the cells had rounded up and appeared activated. In HD patient cultures, around half of the cells appeared small, round and activated but the other half had become extremely ramified, sending out several long processes.

3.5.4.3 Characterisation of BMD-microglia-like cell cultures

In order to characterise stimulated HD patient microglia-like cells further, these cultures were observed in much closer detail, and comparisons were made with morphological analyses performed on primary microglia in the literature. It was found that these cell cultures shared several characteristics with primary microglia (Figure 3.22). Morphological phenotypes were similar to primary microglia isolated from human or murine brain tissue (Figure 3.22; A), and examples of various activation states were

observed, including small, round and activated forms; amoeboid forms; and ramified forms with several short processes or fewer long processes (Figure 3.22; B). This suggests that HD patient microglia-like cells are highly dynamic and can exist in a continuum of activation states, with morphologies more closely modelling microglia than peripheral macrophages. More specific morphological phenotypes were also observed, including vacuole and granular formations (Figure 3.22; C), indicative of phagocytic activities.

Microglia undergo pronounced morphological changes when they seed CNS tissue during early embryogenesis and differentiate from embryonic myeloid precursors into functionally specialised microglia. The cells change from amoeboid immature cells on CNS entry; to polarised, migrating cells; to proliferating, ramified cells with several short processes; and finally, to the typical ramified microglia with long processes which are observed throughout the adult brain parenchyma. Cells exhibiting each of these morphological transformations were present in HD patient microglia-like cell cultures (Figure 3.22; D).

When observing ramified cell populations within HD patient microglia-like cell cultures, long processes could be seen to actively survey the local micro-environment. They extended out into the extracellular space and appeared to sense neighbouring cell processes before retracting slightly and moving into free spaces. This was a dynamic process which could be observed in real time under the light microscope (Figure 3.22; E; top, left). Interestingly, in some cases processes were observed to make direct physical contact with several neighbouring cells (Figure 3.22; E; top, right), and one event was observed in real time where a microglia-like cell appeared to send out a tubule structure from its cell body, which subsequently joined with the cell body of a neighbouring cell (Figure 3.22; E; bottom, right). The tubule was of different composition than a normal process, with a narrower diameter and cytoplasmic density.

A cluster of activated microglia is commonly termed a ‘microglial nodule’, without a strict definition of the cell number. This phenomenon was observed in stimulated HD patient microglia-like cell cultures (Figure 3.22; F), but not in non-stimulated cultures, BMD-macrophage cultures, or in any cultures differentiated from healthy volunteer monocytes. Surrounding microglial nodules was an inner ring of small, round, activated cells, and an outer ring of migrating cells, polarised in the direction of the nodule. Ramified cells were found distant from the nodule. This showed that not only did these microglia-like cell cultures contain cells of varying microglial morphologies, but that these morphologies were representative of reactive phenotypes, and the cells were

responding dynamically and appropriately to their local micro-environment. Microglial nodule formation may also be a mHTT-induced phenomenon.

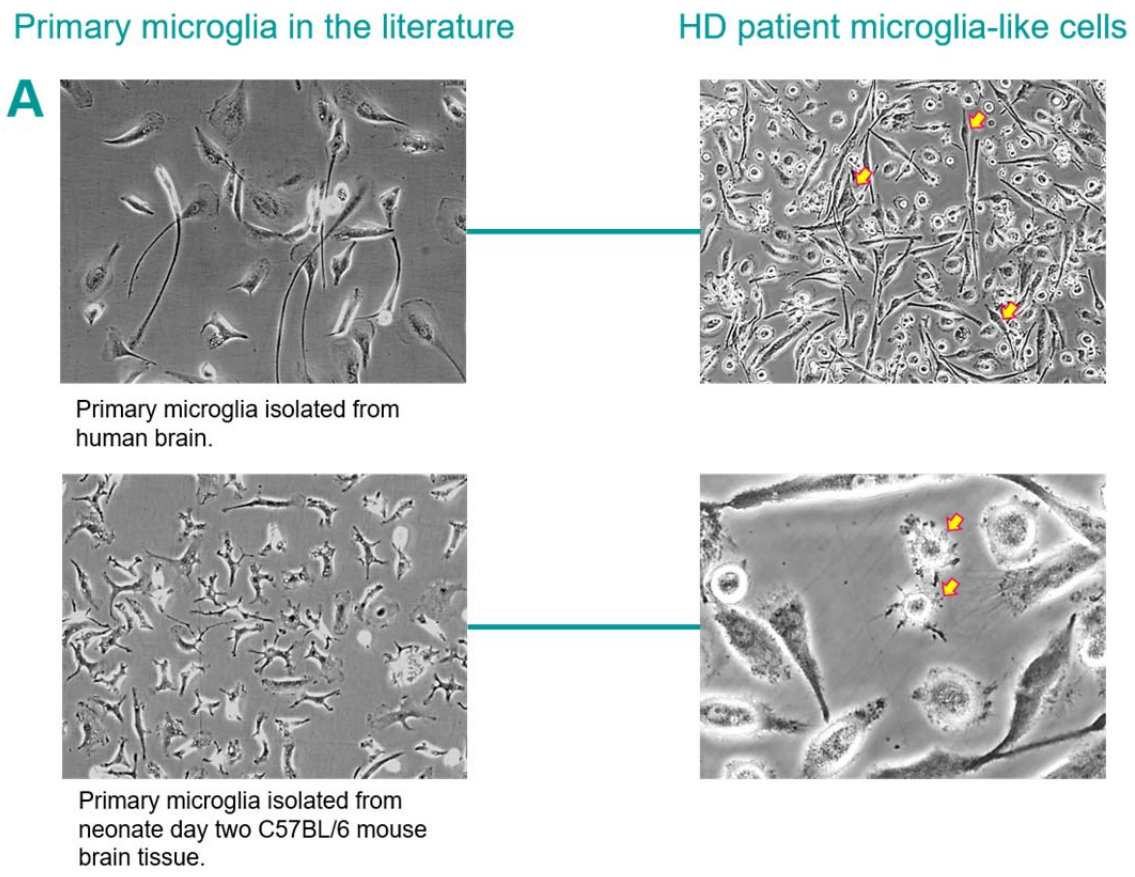

Primary microglia in the literature

HD patient microglia-like cells

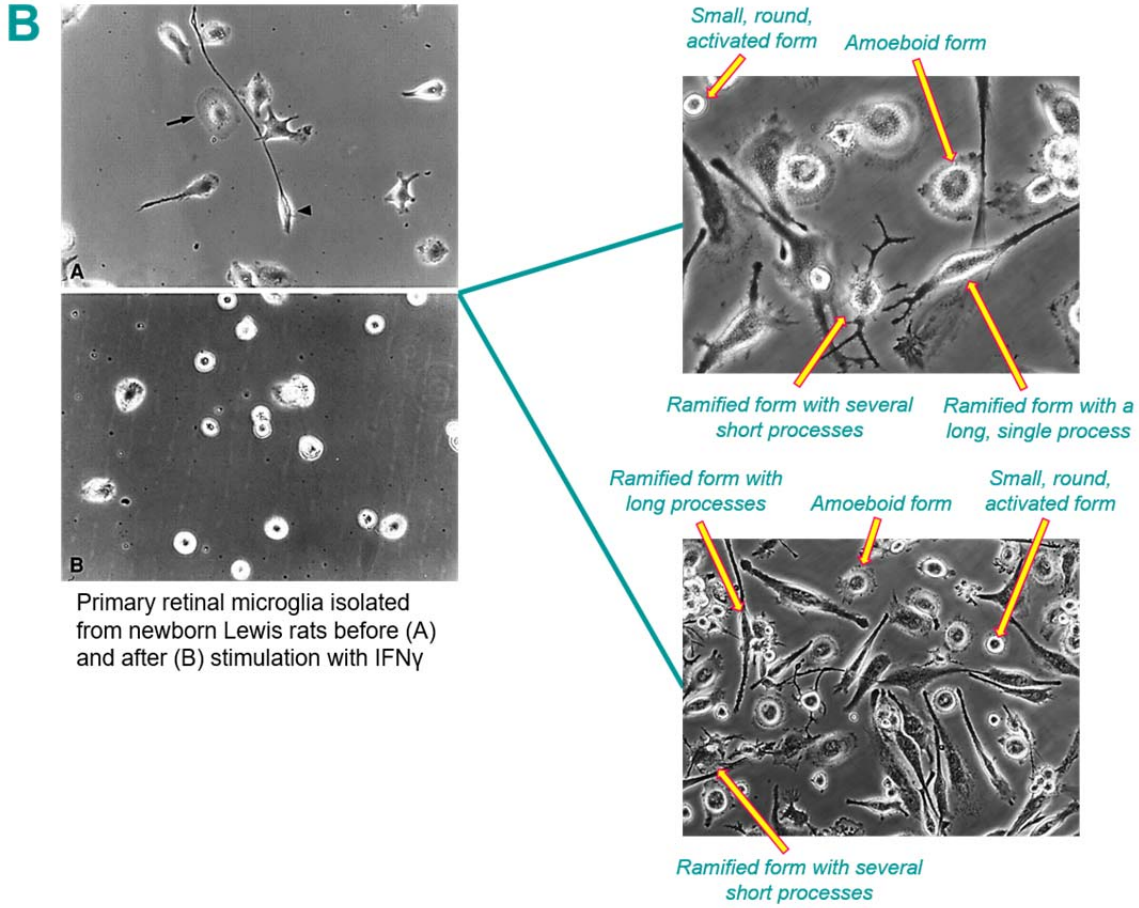

Primary retinal microglia isolated from newborn Lewis rats before (A) and after (B) stimulation with IFNγ

Primary microglia in the literature

HD patient microglia-like cells

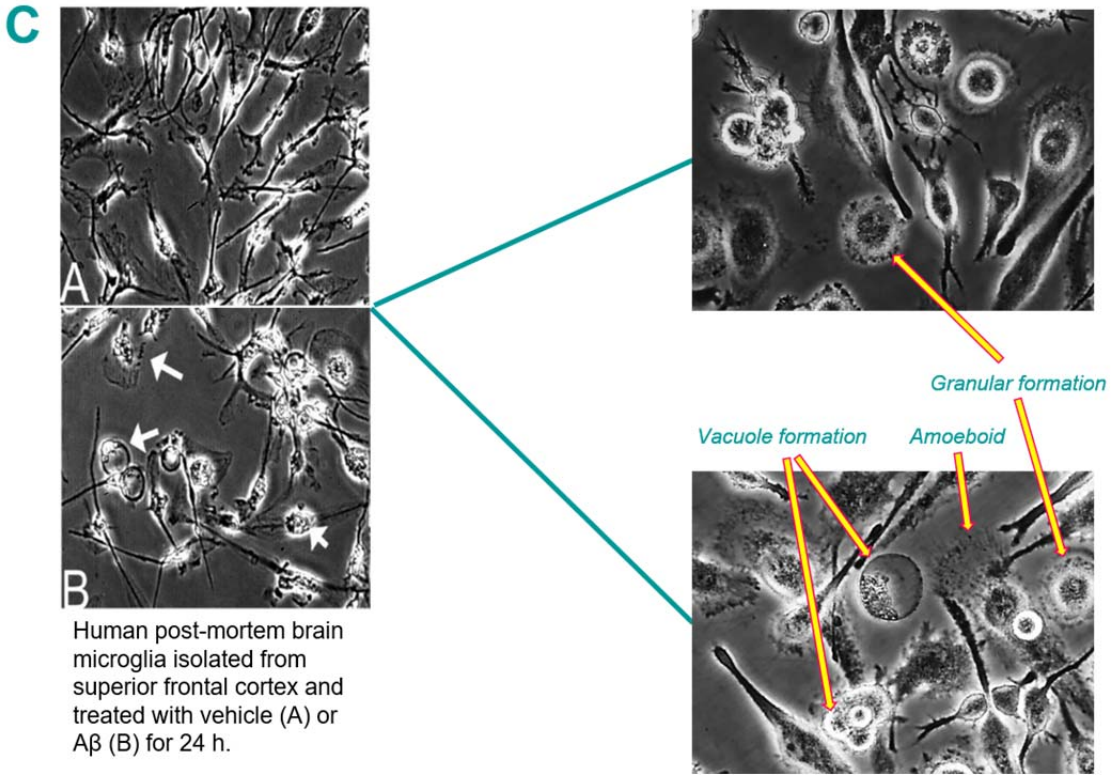

Human post-mortem brain microglia isolated from superior frontal cortex and treated with vehicle (A) or Aβ (B) for 24 h.

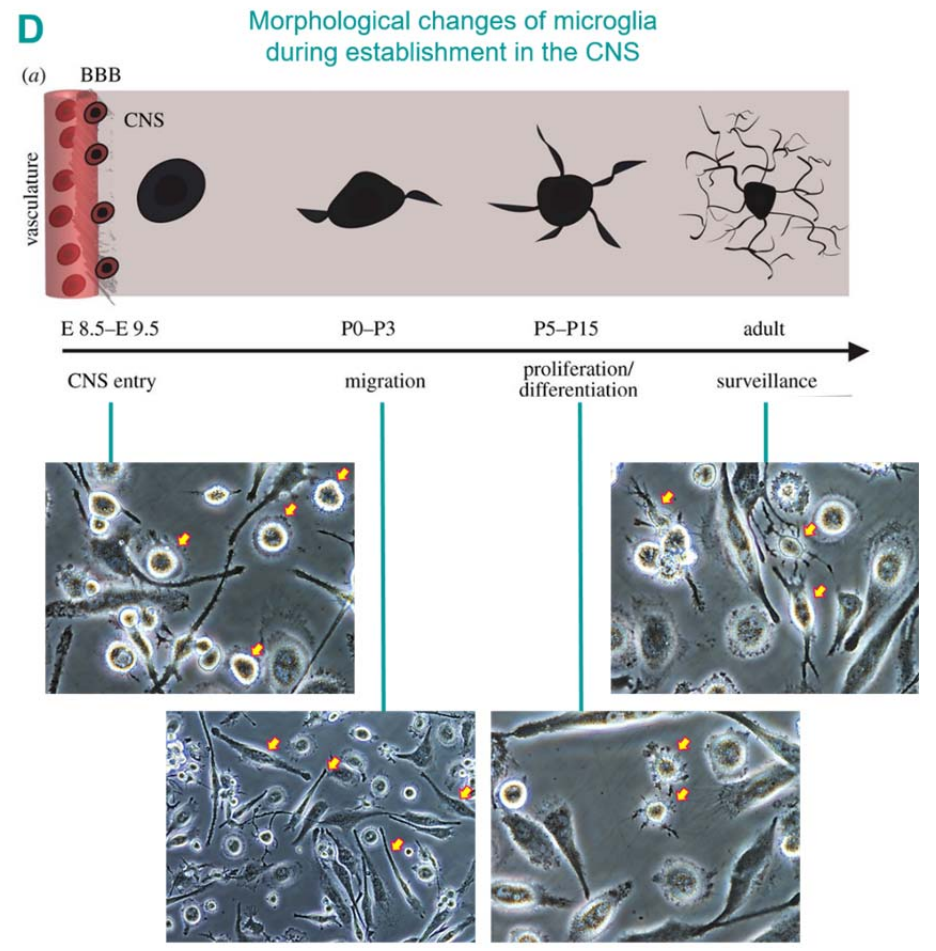

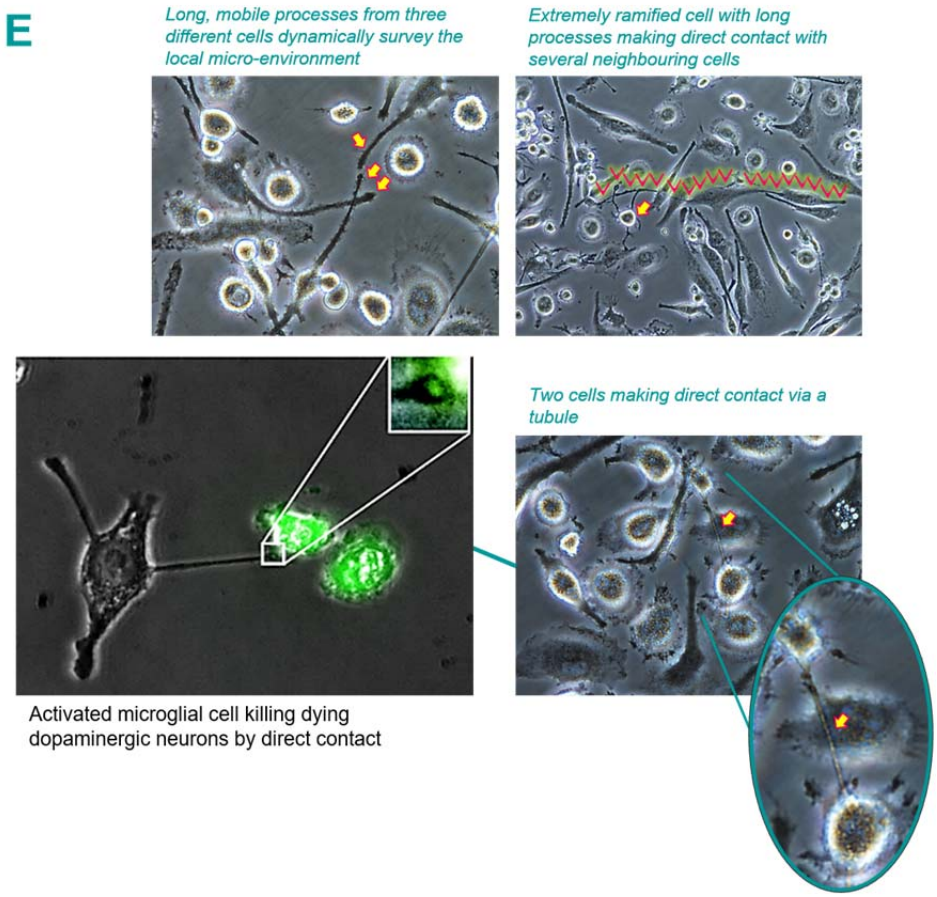

Activated microglial cell killing dying dopaminergic neurons by direct contact

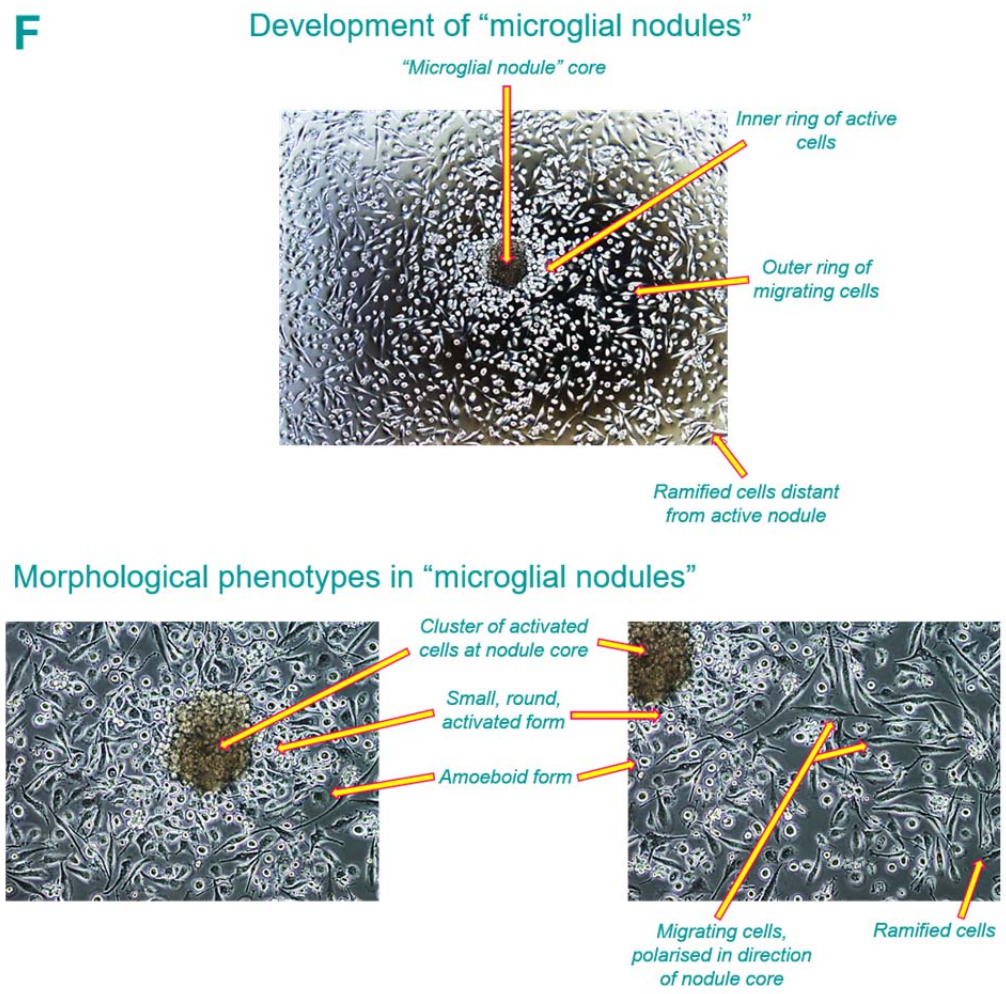

Figure 3.22: In-depth morphological analysis of HD patient microglia-like cell cultures

HD patient monocytes were differentiated into BMD-macrophages before changing culture medium into NM for 4 days. Cells were then stimulated with 2 µg/mL LPS and 10 ng/mL IFNγ for 24 h. Cultures were studied using phase-contrast microscopy and photomicrographs are presented above. Observations indicated that these cells were morphologically and phenotypically similar to primary microglia. Comparisons were made between these HD patient microglia-like cells and primary microglia cultures presented in the literature. Images presented above are representative of observations made from at least ten independent HD patient cell cultures. ***A)*** *HD patient microglia-like cells display similar morphology to primary human microglia (top) and primary mouse microglia (bottom). Yellow arrows highlight cells which specifically exemplify similar morphologies. Images taken with 10× (top, right) and 40× (bottom, right) objectives. Literature source: ScienCell Research Laboratories (http://www.sciencellonline.com/products-services/primary-cells/human-microglia.html (top, left) and http://www.sciencellonline.com/mouse-microglia-364.html (bottom, left)).* ***B)*** *A morphological comparison of rat microglia before and after stimulation with IFNγ (left). Non-stimulated microglia: both amoeboid and ramified forms could be observed, and some cells showed a long, single process or several short processes (ramified). Stimulated microglia: changed their morphology and were smaller and rounder (activated). The same morphological*

phenotypes could be observed in HD patient microglia-like cells (right), and examples are indicated with yellow arrows and labelled. Images were taken with 40× (top, right) and 20× (bottom, right) objectives. Literature source: Investigative Ophthalmology & Visual Science, Volume 40, Issue 13, Pages 3186-3193, 'Retinal microglia differentially express phenotypic markers of antigen-presenting cells in vitro' (Matsubara et al. 1999). ***C)*** *A morphological comparison of human microglia following treatment with Aβ or vehicle (left). Vehicle-treated: ramified cells. Aβ-treated: change in morphology, white arrows highlight microglia demonstrating amoeboid and vacuole formation responses. The same morphological phenotypes could be observed in HD patient microglia-like cells (right), as well as granular formations, and examples are indicated with yellow arrows and labelled. Images were taken with a 40× objective. Literature source: Journal of Leukocyte Biology, Volume 79, Issue 3, Pages 596-610, 'Gene expression changes by amyloid beta peptide-stimulated human post-mortem brain microglia identify activation of multiple inflammatory processes' (Walker et al. 2006).* ***D)*** *When microglia populate the CNS during development, they undergo pronounced morphological changes, from amoeboid immature cells to the typical ramified microglia observed throughout the brain parenchyma. These changes are depicted as illustrations (top). Similar morphological phenotypes could be observed in HD patient microglia-like cells (bottom), and examples are indicated with yellow arrows. Images were taken with 40× (top, left; top, right; bottom, right) and 20× (bottom, left) objectives. Literature source: Philosophical Transactions of the Royal Society of London. Series B, Biological Sciences, Volume 369, Issue 1654, Page 20130593, 'Fine-tuning the central nervous system: microglial modelling of cells and synapses' (Xavier et al. 2014).* ***E)*** *HD patient microglia-like cells were observed to send out long, mobile processes which appeared to actively and physically survey their local environment (top, left), and in many cases made direct physical contact with cell bodies and processes of neighbouring cells (top, right). Such cell-to-cell physical interaction has been reported in the literature between microglia and neurons, where activated microglial cells have been observed to kill dying neurons by direct contact (bottom, left). A similar example was observed between two HD patient microglia-like cells where direct contact appeared to exist via a tubule (bottom, right). Images were taken with 40× (top, left; bottom, right) and 20× (top, right) objectives. Bottom, left fluorescence microscope image of stimulated (1 µg/mL LPS) BV2 microglial cell killing a dying MN9D dopaminergic neuron in co-culture by direct contact is an unpublished image owned by, and printed with permission from, Hajji Nabil, Lecturer in cancer and epigenetics, Imperial College London Hammersmith Campus. The image relates to sources in the literature from Nature, Volume 472, Issue 7343, Pages 319-324, 'Caspase signalling controls microglia activation and neurotoxicity' (Burguillos et al. 2011a) and Neurobiology of Disease, Volume 41, Issue 1, Pages 177-188,, 'Apoptosis-inducing factor mediates dopaminergic cell death in response to LPS-induced inflammatory stimulus: evidence in Parkinson's disease patients' (Burguillos et al. 2011b).* ***F)*** *Active phenomenon similar to development of microglial nodules observed in HD patient microglia-like cell cultures. Nodule regions labelled on top micrograph, and cell morphological phenotypes within each region are indicated in bottom micrographs. Images were taken with 4× (top) and 10× (bottom) objectives.*

BMD-microglia-like cell cultures were then characterised as a model of microglia by their expression of specific markers. Monocytes were isolated from healthy volunteers and manifest HD patients and differentiated into microglia-like cells. Microglia-like cells were then stimulated with 2 µg/mL LPS and 10 ng/mL IFNγ for 24 h. ICC was performed on healthy volunteer monocytes, microglia-like cells and stimulated microglia-like cells with antibodies directed at CD11b, CD14, ionized calcium-binding adapter molecule 1 (Iba1), mannose receptor (CD206) or TREM2. N2a_R2 cells were also used as a negative control for these microglial characterisation markers. N2a_R2 had been genomically screened by Dr. Peter C. Klöhn (MRC Prion Unit, IoN, London, UK) and were found to not express the tested markers (CD11b, CD14, Iba1 and CD206), or to express them at very low levels (TREM2). Western blotting was performed on non-stimulated and stimulated healthy volunteer and manifest HD patient microglia-like cell culture lysates with antibodies directed at CD68, CSF1R, CX3CR1, Iba1, P2Y12 or PU.1.

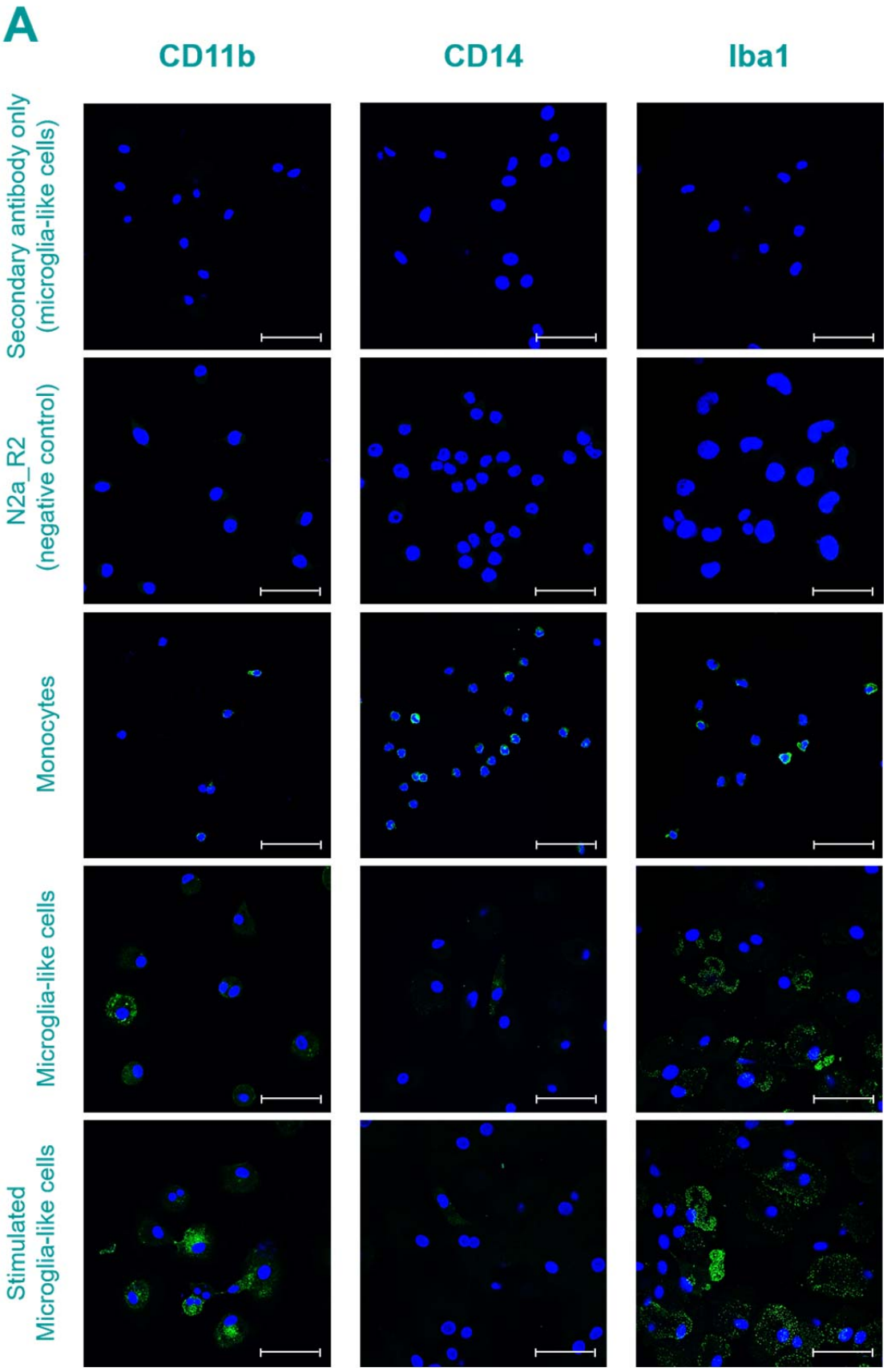
A
CD11b
CD14
Iba1
Secondary antibody only (microglia-like cells)
N2a_R2 (negative control)
Monocytes
Microglia-like cells
Stimulated Microglia-like cells

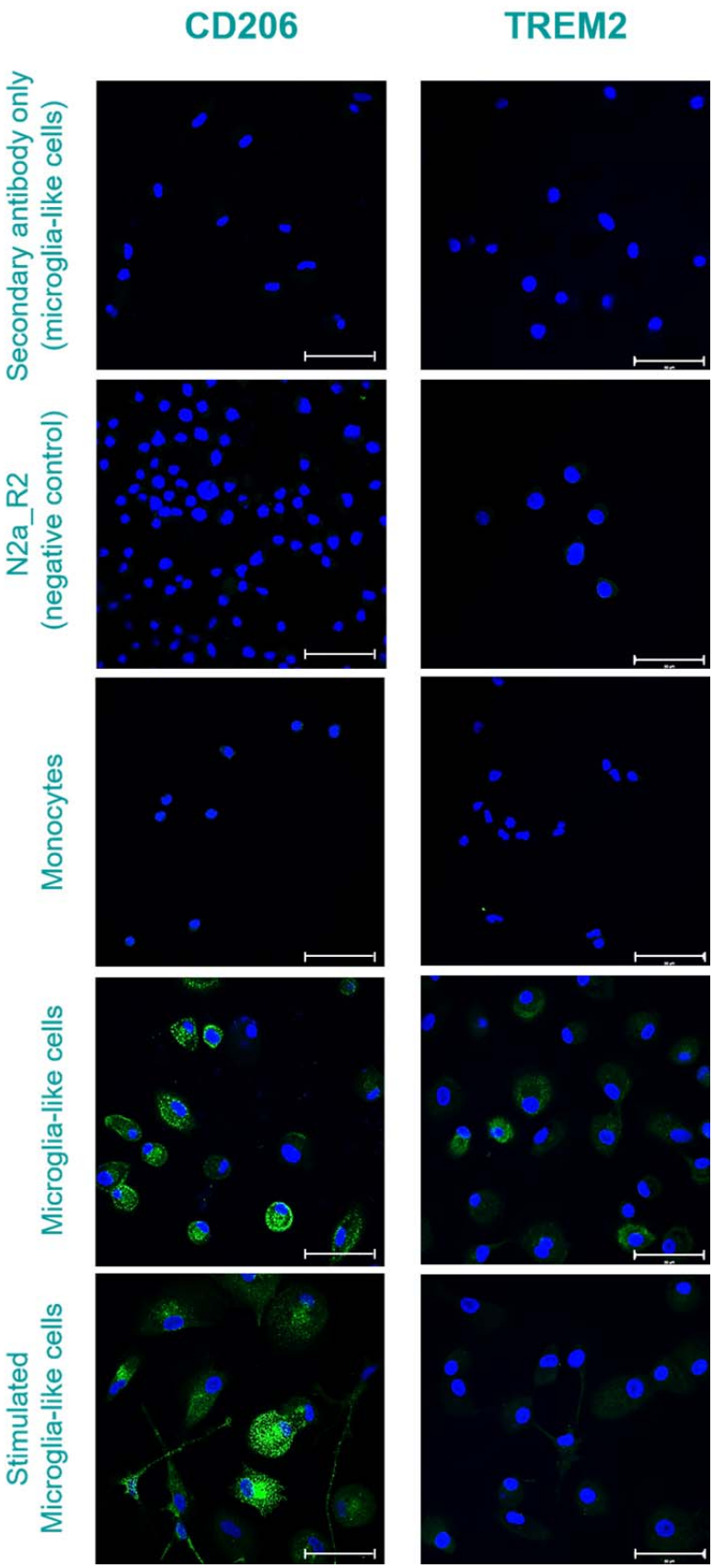
CD206
TREM2
Secondary antibody only (microglia-like cells)
N2a_R2 (negative control)
Monocytes
Microglia-like cells
Stimulated Microglia-like cells

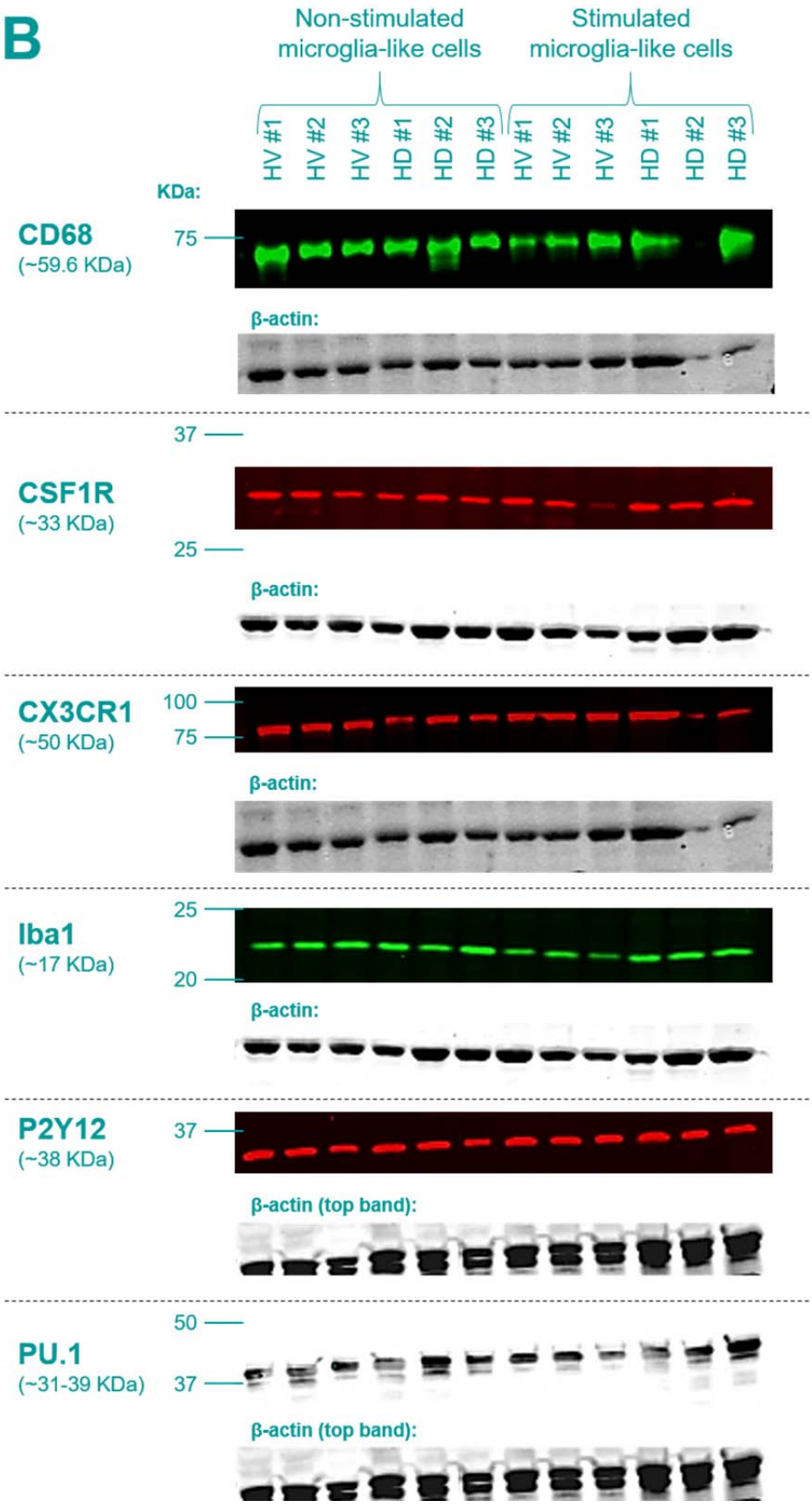

Figure 3.23: Expression of microglial markers in microglia-like cell cultures

A) *Confocal fluorescence microscope images of monocytes isolated from healthy volunteers (HV), microglia-like cells differentiated from healthy volunteer monocytes in culture, microglia-*

like cells stimulated with 2 µg/mL LPS and 10 ng/mL IFNγ for 24 h and N2a_R2 (negative control) cells. ICC was performed with antibodies directed at CD11b, CD14, Iba1, mannose receptor (CD206) or TREM2 (green). Nuclei were stained with DAPI (blue). Some microglia-like cells were probed with fluorophore-conjugated secondary antibodies only (top panels) to control for background signal. Images are representative examples from at least five fields of view from at least two independent cultures from at least two different individual donors. Images in each column are of myeloid cells from the same donor. Scale bars = 50 µm. ***B)*** *Western blot membrane scans of non-stimulated and stimulated (2 µg/mL LPS and 10 ng/mL IFNγ for 24 h) BMD-microglia-like cell lysates from three independent healthy volunteer (HV) and three independent manifest HD patient blood donors per blot. Blots were probed with antibodies directed at CD68, CSF1R, CX3CR1, Iba1, P2Y12 or PU.1, and β-actin (loading control), and secondary IRDye-conjugated secondary antibodies were detected by scanning with a LI-COR Odyssey scanner. Proteins were sized against BioRad Precision Plus All Blue protein standards.*

ICC with confocal fluorescence microscopy (Figure 3.23; A) showed that monocytes expressed the markers CD11b, CD14 and Iba1. Upon differentiation into microglia-like cells, expression of CD14 was decreased while CD11b and Iba1 expression was increased, marking differentiation into mature macrophages/microglia. CD11b and Iba1 expression was further increased in response to stimulation, which represents microglial activation. Monocytes did not express mannose receptor or TREM2, and expression of these markers was induced upon differentiation into microglia-like cells. In the microglial-like cells, mannose receptor expression was strong in both non-stimulated and stimulated conditions, confirming that these cells were both mature and polarised towards an M2 phenotype. TREM2 expression was high in non-stimulated microglia-like cells and decreased after stimulation, in accordance with its role (along with DAP12) in regulating microglial activation state. Western blots of BMD-microglia-like cell lysates (Figure 3.23; B) showed expression of microglial markers CD68, CSF1R, CX3CR1, Iba1, P2Y12 and PU.1 in both healthy volunteer and manifest HD patient cultures and in both stimulated and non-stimulated conditions.

Taking into account both the expression of key microglial markers (CD11b, CD68, CSF1R, CX3CR1, Iba1, mannose receptor, P2Y12, PU.1 and TREM2; Figure 3.23), and the microglia-specific morphological phenotypes exhibited by these cells (presence of all microglial morphological forms: small, round and activated, amoeboid, polarised, ramified with several short processes, highly ramified with very long processes; sub-cellular granule and vacuole formations indicative of phagocytic functions; process motility and cell-to-cell contact via processes and tubules; microglial nodule formations; polarised migration towards sites of activity; Figure 3.22), it was determined that the

microglia-like cultures were more similar to human microglia than to human peripheral tissue macrophages, and were henceforth referred to as BMD-microglia.

3.5.5 Development of human HD neuronal-myeloid cell co-culture models

With the aim of investigating neuronal-myeloid cell interactions in the pathogenesis of HD, co-culture models were developed. ReNcell VM+*HTT* exon 1 or ReNcell VM+full-length *HTT* neuronal cell cultures were co-cultured with BMD-macrophages or BMD-microglia differentiated from monocytes isolated from healthy volunteers, pre-manifest HD gene carriers or manifest HD patients, as outlined in Table 3.5.

Table 3.5: Neurons and myeloid cells to be used in co-culture

Neurons		Myeloid cells
ReNcell VM+*HTT* exon 1 neuronal cultures		**BMD-macrophages**
Neuronal cell line	*HTT exon 1 genotype*	
ReNcell VM +*HTT* exon 1 (29 CAG)	Normal, over-expressing	Healthy volunteers
ReNcell VM +*mHTT* exon 1 (71 CAG)	Expanded, HD, over-expressing	Pre-manifest HD gene carriers
ReNcell VM +*mHTT* exon 1 (129 CAG)	Highly expanded, HD, over-expressing	Manifest HD patients
ReNcell VM +eGFP reporter only	Normal, control	**BMD-microglia**
ReNcell VM+full-length *HTT* neuronal cultures		Healthy volunteers
Neuronal cell line	*Full-length HTT genotype*	
Wild-type ReNcell VM	Normal	Pre-manifest HD gene carriers
ReNcell VM+full-length *mHTT* (138 CAG) C8	Highly expanded, HD, over-expressing	Manifest HD patients

Details on the classification of primary human myeloid cells can be found in section 2.1.2.1.

Three different co-culture paradigms were trialled, with the aim of assessing relevant aspects of neuronal-myeloid cell communication: co-culture by conditioned medium transfer, to assess the effects of factors released from one cell-type on the phenotype of the other; co-culture by medium shared concurrently, for examination of cross-communication between both cell-types; and co-culture by direct physical contact, to determine the effects of direct cell-to-cell interactions.

3.5.5.1 Co-culture media titrations

In all three co-culture paradigms to be trialled, it was necessary for both cell-types to be cultured in the same medium, and therefore an optimised culture medium which was compatible for both cell-types was required. To achieve this, culture medium titrations were performed using standard neuronal culture medium (NM; Appendix I-v) and standard BMD-macrophage culture medium (RPMI/FBS; Appendix I-iv; without GM-CSF differentiation induction factor) in 10 DD wild-type ReNcell VM neuronal cultures (spontaneous differentiation) and healthy volunteer BMD-macrophages. Neurons and BMD-macrophages were given a medium change into a range of combination media titrations from 100 % NM to 100 % RPMI/FBS and maintained in culture for up to 7 days. To determine any confounding effects of combination culture media, cytotoxicity was assessed by ATP cell viability assay, PI viable cell exclusion and LDH cytotoxicity assay. Cultures were also monitored daily by live-cell phase-contrast microscopy.

ATP cell viability assay showed neuronal and BMD-macrophage viability to be variable across media titration conditions, but these changes were not consistent with a dose-response effect (Figure 3.24; A). Viability measurements were also higher for media combination conditions than for control standard culture medium for both cell-types, suggesting that neither neurons or BMD-macrophages were adversely affected by culture in combination media. PI viable cell exclusion and LDH cytotoxicity assay showed that neurons cultured in 100 % RPMI/FBS culture medium for 4 days did not have significantly different death levels compared with neurons cultured in 100 % NM (Figure 3.24; B and C). All cell cultures were observed to appear healthy in all conditions for up to 7 days culture in combination medium. Neuronal culture morphology was not observed to be particularly affected by any of the media titrations, however BMD-macrophage morphology was significantly altered by increasing titrations of NM (Figure 3.24; D). Surprisingly, BMD-macrophages appeared to transform into microglia-like cells. These cultures were later characterised as a model of microglia with further in-depth morphological and phenotypic analysis (section 3.5.4.2; above), and subsequently referred to as BMD-microglia. As none of the media titrations were found to reduce neuronal or BMD-macrophage viability, co-culture paradigms were developed using 100 % RPMI/FBS culture medium for neuronal-BMD-macrophage co-cultures and 100 % NM for neuronal-BMD-microglia co-cultures.

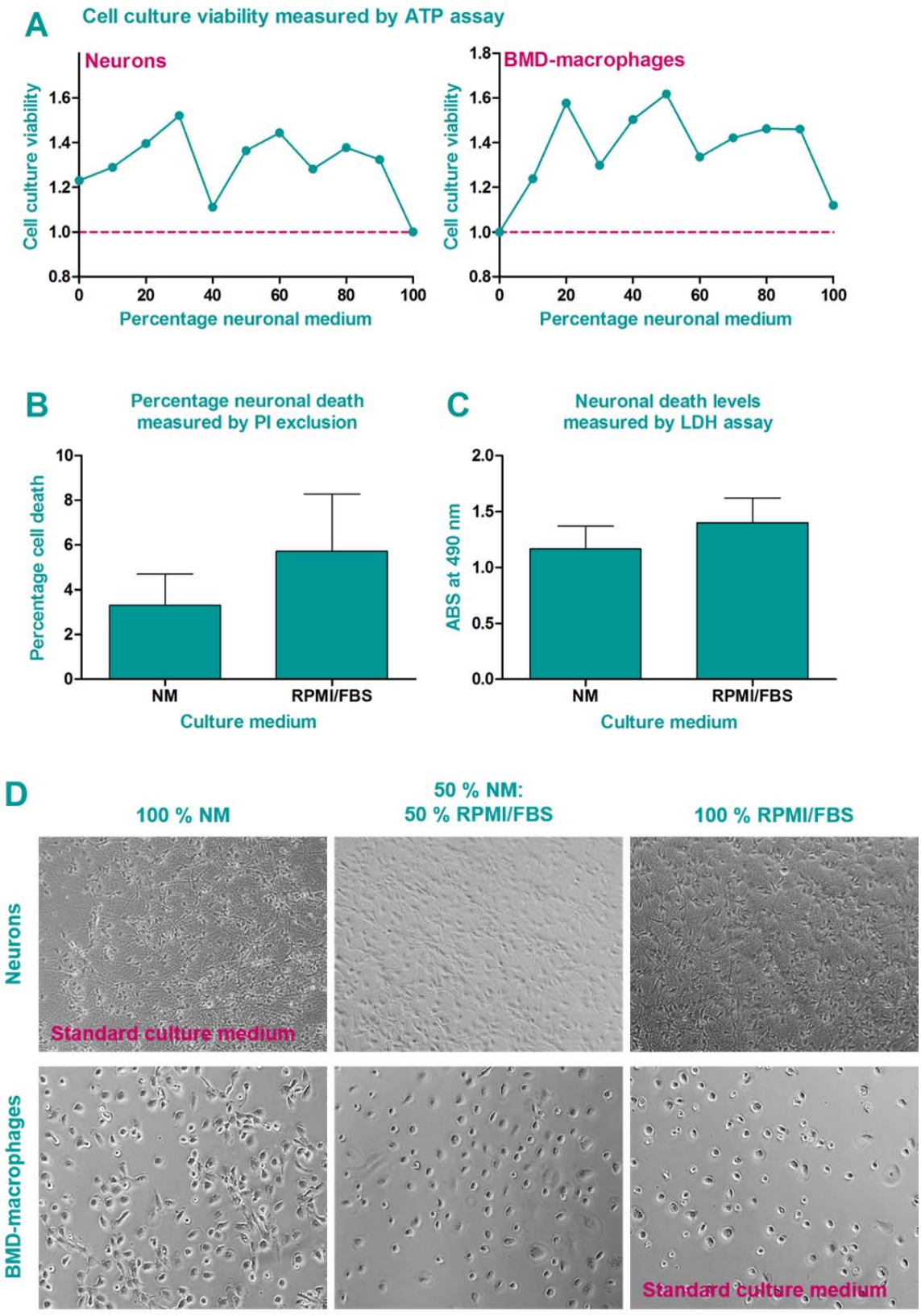

Figure 3.24: Co-culture media titrations

Co-culture NM-RPMI/FBS combination media titrations in healthy volunteer BMD-macrophages and 10 DD wild-type ReNcell VM neuronal cultures (spontaneous differentiation). ***A)*** *ATP cell viability assay at day 4 culture in combination media. Combination medium cell culture viability expressed relative to standard culture medium cell viability (100 % NM for neurons and 0 % NM*

(100 % RPMI/FBS) for BMD-macrophages; marked with dashed, purple line). ***B)*** *Percentage dead cells measured by PI viable cell exclusion in neurons following 4 days culture in 100 % NM or 100 % RPMI/FBS. Bars = mean average percentage PI-stained cells from three independent neuronal cultures per condition; error bars = ± SEM. Statistically analysed using two-tailed, unpaired t test: p=0.454 (not significant).* ***C)*** *LDH cytotoxicity assay of neurons cultured in 100 % NM or 100 % RPMI/FBS for 4 days. Neuronal death levels presented as absorbance (ABS) at 490 nm, a direct measurement of red formazan product of the LDH assay (3 internal assay replicates; media background subtracted). Bars = mean average ABS from three independent neuronal cultures per condition; error bars = ± SEM. Statistically analysed using two-tailed, unpaired t test: p=0.479 (not significant).* ***D)*** *Live-cell phase-contrast micrographs of neurons and BMD-macrophages following 3 days culture in combination media. A-D analyses were performed on different cell cultures in separate, independent media titration experiments. Each experiment included 3 replicate cell cultures per condition.*

3.5.5.2 Co-culture by conditioned medium transfer and stimulation paradigms

Procedures for co-culture by conditioned medium transfer are described in detail in sections 2.1.5.1 and 2.1.5.2.

Fourteen DD wild-type ReNcell VM neuronal cultures were treated, in duplicate, at 1:1 with Mφ-CM from non-stimulated healthy volunteer, pre-manifest HD or manifest HD BMD-macrophages and RPMI/FBS culture medium, for 4 days. BMD-macrophages were at 7 DIV and had been allowed to condition the culture medium for 4 days. Neuronal survival and morphology was observed daily by phase-contrast microscopy and at day 4 cultures were assessed by PI viable cell exclusion and LDH cytotoxicity assay to measure neurotoxicity. Final protein concentration was determined by BioRad Bradford Assay as a crude measure of overall survival and cell number.

No obvious differences were observed in neuronal cell density or morphology in any of the conditions over the 4-day treatment with conditioned medium. PI viable cell exclusion and LDH cytotoxicity assay did not reveal any significant differences in neuronal cell death following any Mφ-CM treatments compared with RPMI/FBS culture medium alone, or between healthy volunteer and HD patient Mφ-CM treatments (Figure 3.25; A). Overall, there was an observed trend for a decrease in neuronal death and an increase in total protein concentrations (Figure 3.25; B) following treatment with healthy volunteer or HD patient Mφ-CM, compared with RPMI/FBS culture medium alone. It is therefore possible that Mφ-CM from non-stimulated BMD-macrophages is neuroprotective.

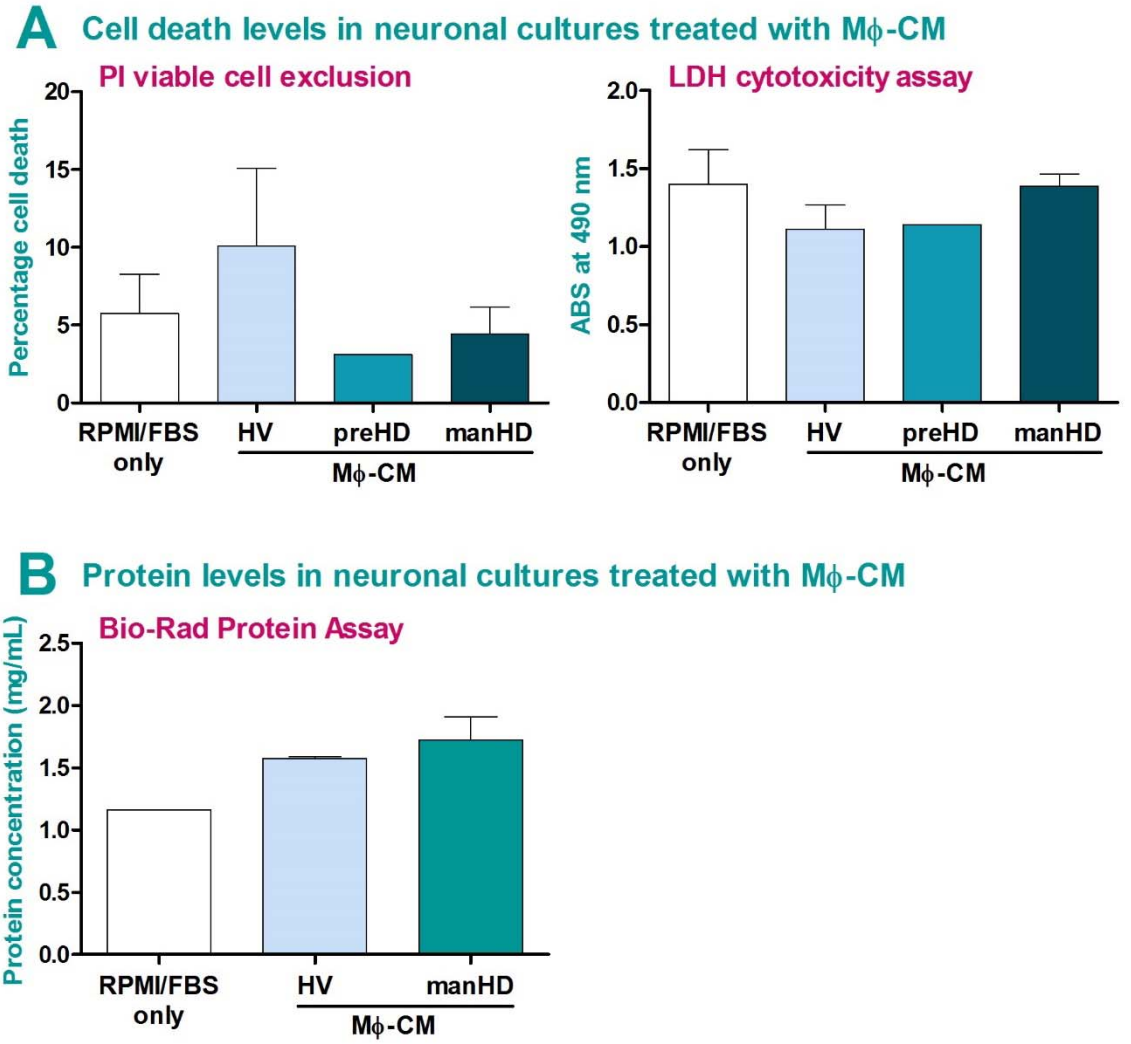

Figure 3.25: Neuronal-BMD-macrophage co-culture by conditioned medium transfer

A) *Cell death levels in 14 DD (spontaneous differentiation) wild-type ReNcell VM neuronal cultures treated for 4 days, in duplicate, with Mφ-CM from non-stimulated healthy volunteer (HV; n=3), pre-manifest HD (preHD; n=1) or manifest HD (manHD; n=4) BMD-macrophages, or RPMI/FBS culture medium only. Mφ-CM treatments were 1:1 with fresh RPMI/FBS culture medium. Cell death was measured by PI viable cell exclusion (left) and LDH cytotoxicity assay (right). Cell death levels are presented as mean average percentage PI-stained cells from six random fields of view or mean average absorbance (ABS) at 490 nm of red formazan product from LDH assay (3 internal assay replicates per condition; media background subtracted), ± SEM. Data were statistically analysed using one-way ANOVA (excluding pre-manifest HD which had an n of 1) which returned a p value of 0.451 (not significant) for PI viable cell exclusion and 0.377 (not significant) for LDH cytotoxicity assay.* ***B)*** *Protein levels in 14 DD wild-type ReNcell VM neuronal cultures treated for 4 days, in duplicate, with Mφ-CM from non-stimulated healthy volunteer (HV; n=2) or manifest HD (manHD; n=2) at 1:1 with fresh RPMI/FBS culture medium, or RPMI/FBS culture medium only. Protein levels were measured by Bio-Rad Protein Assay in neuronal cell lysates and presented as mean average protein concentration ± SEM.*

The same paradigm was then tested for neuronal-BMD-microglia co-culture. Ten DD wild-type ReNcell VM neuronal cultures were treated directly, in duplicate, with MG-CM from non-stimulated healthy volunteer or manifest HD BMD-microglia, for 4 days. BMD-microglia were at 11 DIV and had been allowed to condition the culture medium for 4 days. As Mφ-CM treatment had shown a trend for decreased neuronal death in neuronal-BMD-macrophage co-cultures, an additional conditioned medium treatment was added to control for conditioned medium in general i.e. non-myeloid cell-specific neuroprotective factors. This control treatment was neuronal conditioned medium (N-CM): NM which had been transferred from wild-type 14 DD ReNcell VM neuronal cultures after 4 days of conditioning. Following 4 days treatment with MG-CM or N-CM, neuronal death was assessed by PI viable cell exclusion and LDH cytotoxicity assay (Figure 3.26).

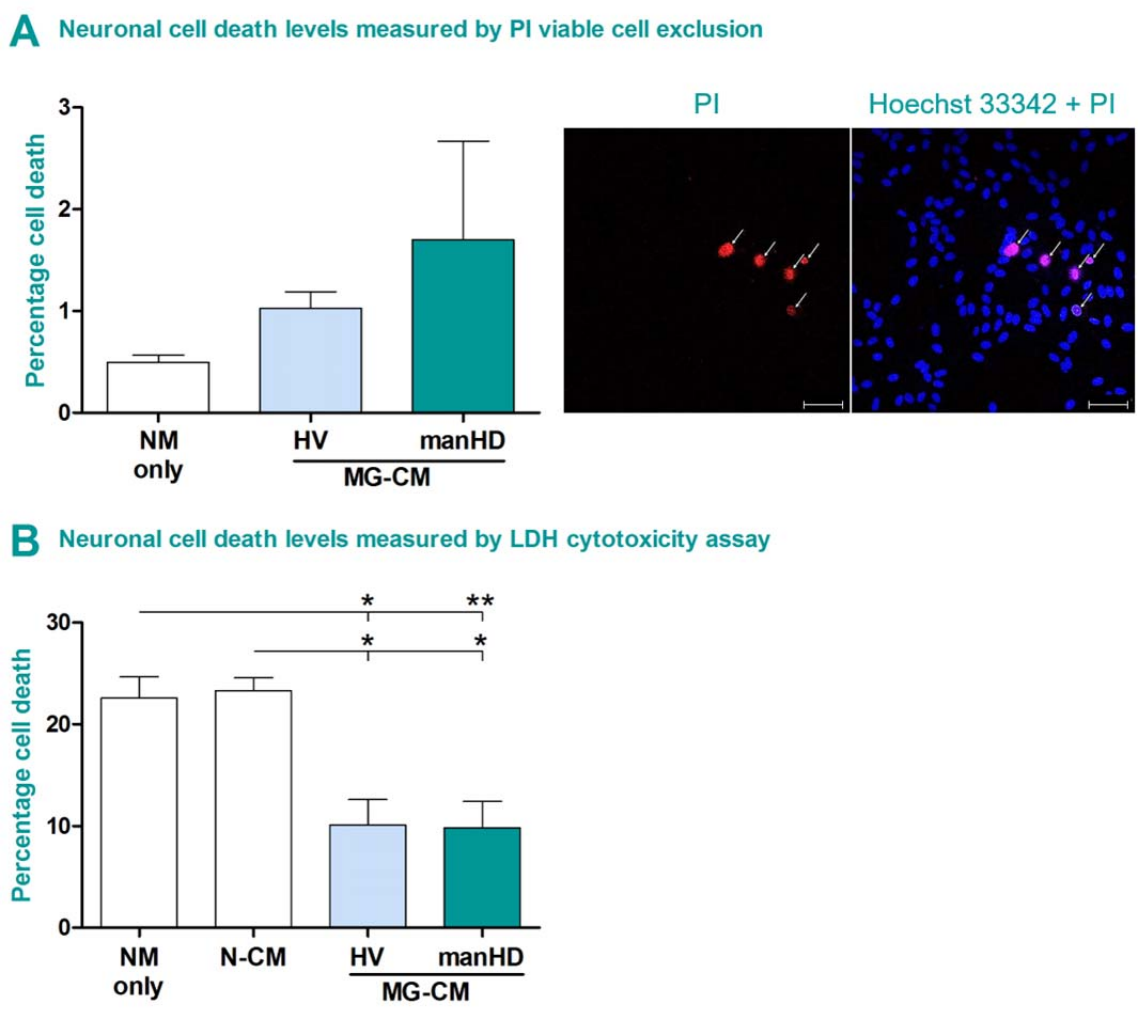

Figure 3.26: Neuronal-BMD-microglia co-culture by conditioned medium transfer

Ten DD (spontaneous differentiation) wild-type ReNcell VM neuronal cultures were treated directly for 4 days, in duplicate, with MG-CM from non-stimulated healthy volunteer (HV; n=3) or manifest HD (manHD; n=3) BMD-microglia, or in triplicate with N-CM or NM only. Neuronal

*death was assessed by PI viable cell exclusion (**A**) and LDH cytotoxicity assay (**B**). Neuronal death levels are presented as mean average percentage PI-stained cells from 10 random fields of view per culture (method representative example image shown in panel A, right (manifest HD MG-CM-treated neuronal culture); arrows highlight PI-stained nuclei; scale bars = 50 µm) or mean average percentage neuronal death (calculated as described in section 2.6.1 with total LDH calculated from 3 untreated neuronal cultures), ± SEM. Data were statistically analysed using one-way ANOVA which returned a p value of 0.385 (not significant) for PI viable cell exclusion and 0.002 (significant) for LDH cytotoxicity assay. Tukey post-hoc analysis results are presented as *p<0.05, **p<0.01.*

PI viable cell exclusion showed cell death levels to be very low in all conditions, and there were no significant differences in cell death levels detected in neuronal cultures treated with healthy volunteer or HD patient MG-CM compared with neurons cultured in NM alone (Figure 3.26; A). This method of measuring cytotoxicity does not account for cells which have already undergone complete lysis, apoptosis or necrosis, which may explain the extremely low cell death levels measured. PI viable cell exclusion may therefore be more appropriate for measuring cell death under acute conditions (minutes to hours) rather than over days as was tested in this case. LDH cytotoxicity assay revealed a significant effect of healthy volunteer ($p<0.05$) or manifest HD ($p<0.01$) MG-CM treatment on reducing neuronal death, compared with culture in NM alone (Figure 3.26; B). N-CM treatment did not affect percentage neuronal death, indicating that MG-CM-induced reduction in neuronal death was a BMD-microglia-specific effect, and not due to the medium being conditioned in general. There were no significant differences between healthy volunteer and HD patient MG-CM treatments. Overall, these results suggest that in non-stimulated conditions, both healthy volunteers and manifest HD patients BMD-microglia release factors which are neuroprotective in co-culture with wild-type neurons.

LPS/IFNγ co-stimulation paradigms were then developed to induce acute or chronic inflammatory phenotypes in healthy volunteer and HD patient BMD-macrophages or BMD-microglia. To assess the effects of HD myeloid cell hyper-reactivity on neurotoxicity, these acute and chronic co-stimulation paradigms were applied to neuronal-myeloid cell co-cultures. The procedures for acute or chronic stimulation of myeloid cells with LPS and IFNγ are described in detail in section 2.1.3.2. Briefly, the acute stimulation paradigm involved a pulse stimulation of healthy volunteer and HD patient myeloid cells with LPS and IFNγ for 1 h, followed by a fresh culture medium change. Conditioned medium was then collected at various time-points after the medium change and used to treat neurons in co-culture. Chronic stimulation was

continuous stimulation of the myeloid cells with LPS and IFNγ with collection of conditioned medium over a range of time-points from 1 to 48 h.

A range of LPS stimulation concentrations (10 -1000 ng/mL) were tested in healthy volunteer, pre-manifest HD and manifest HD BMD-macrophages. BMD-macrophages were stimulated with LPS at each of the concentrations, in duplicate, for 24 h. Conditioned medium was then collected (chronic stimulation Mφ-CM) and cells were given a fresh culture medium change (no LPS) and returned to the incubator for a further 24 h. Conditioned medium was collected again after this 24 h rest period (chronic stimulation + rest Mφ-CM). Healthy volunteer, pre-manifest HD and manifest HD Mφ-CM was then used to treat 21 DD wild-type ReNcell VM neuronal cultures, in duplicate, for 4 days, and neurotoxicity was measured by LDH cytotoxicity assay.

All Mφ-CM treatment conditions resulted in decreased neuronal death levels compared with untreated (neurons cultured in RPMI/FBS alone) (Figure 3.27), suggesting that healthy volunteer, pre-manifest HD and manifest HD Mφ-CM is neuroprotective in chronically-stimulated conditions as well as non-stimulated conditions (0 ng/mL LPS-stimulation). Following treatment with chronic stimulation Mφ-CM, LPS concentration was a significant source of variation in percentage neuronal death ($p<0.001$) (Figure 3.27; top). LPS concentration was not a significant source of variation in chronic stimulation + rest Mφ-CM conditions ($p>0.05$) (Figure 3.27; bottom), and this was most likely due to alterations in the activation state of BMD-macrophages back to a baseline, resting state during the 24 h rest period. As this was preliminary data, with a biological *n* of 1 per subject group, no conclusions could be drawn relating to subject group comparisons. It was noted, however, that the highest LPS concentration tested, 1 μg/mL, showed potential for detecting differences between healthy volunteer and HD patient Mφ-CM-effects on neuronal death.

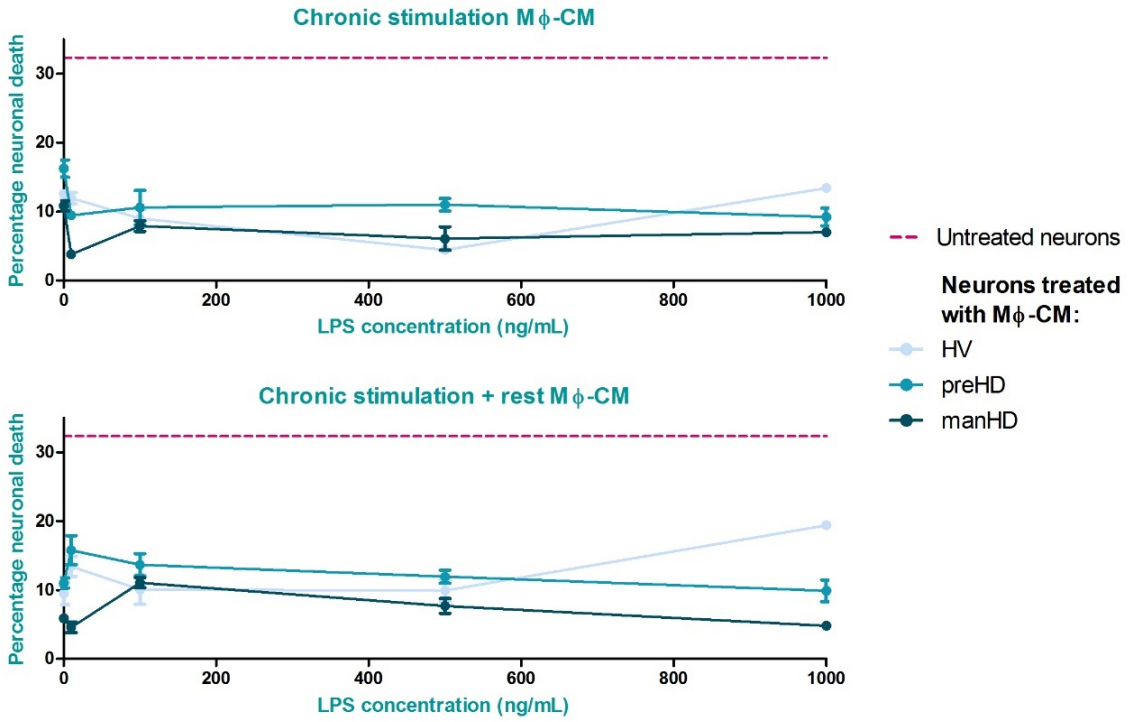

Figure 3.27: Neuronal death levels after treatment with Mφ-CM from BMD-macrophages stimulated with a range of LPS concentrations

Twenty-one DD (spontaneous differentiation) wild-type ReNcell VM neuronal cultures were treated, in duplicate, for 4 days with Mφ-CM from healthy volunteers (HV; n=1), pre-manifest HD (preHD; n=1) or manifest HD (manHD; n=1) BMD-macrophages stimulated with 0, 10, 100, 500 or 1000 ng/mL LPS, in duplicate. BMD-macrophages were stimulated for 24 h (chronic stimulation Mφ-CM; top) or were stimulated for 24 h followed by 24 h rest (chronic stimulation + rest Mφ-CM; bottom). Neurotoxicity was measured by LDH cytotoxicity assay and results are presented as mean average percentage neuronal death (calculated as described in section 2.6.1 with total LDH calculated from 3 neuronal cultures in RPMI/FBS culture medium only (untreated)) ± SEM. Percentage cell death of untreated neuronal cultures is marked with purple, dashed lines. Data were statistically analysed using two-way ANOVA which found the variation in LPS concentration to be a significant source of variation for chronic stimulation Mφ-CM ($p<0.001$) but not in chronic stimulation + rest Mφ-CM ($p=0.167$).

In chronic LPS/IFNγ stimulation paradigms (without rest), it was possible that LPS may still be present as an active stimulus in myeloid cell conditioned medium post-processing, and consequently may have direct effects on neuronal cultures. ReNcell VM neuronal cultures contain a sub-population of astrocytes which are likely to express TLR4, the LPS receptor (Trudler *et al.* 2010). Neurons have also been reported to express TLR4 (Leow-Dyke *et al.* 2012). IFNγ concentration in conditioned medium may also be higher due to presence of the original stimulus. In order to determine the direct effects of LPS and IFNγ on cell death in neuronal cultures, 10 DD wild-type ReNcell VM and ReNcell VM+full-length *mHTT* (138 CAG) neuronal cultures were treated

directly with the highest stimulus concentrations of LPS (2 µg/mL) and IFNγ (10 ng/mL), alone or in combination, for 24 h. Percentage cell death in neuronal cultures was then determined by LDH cytotoxicity assay.

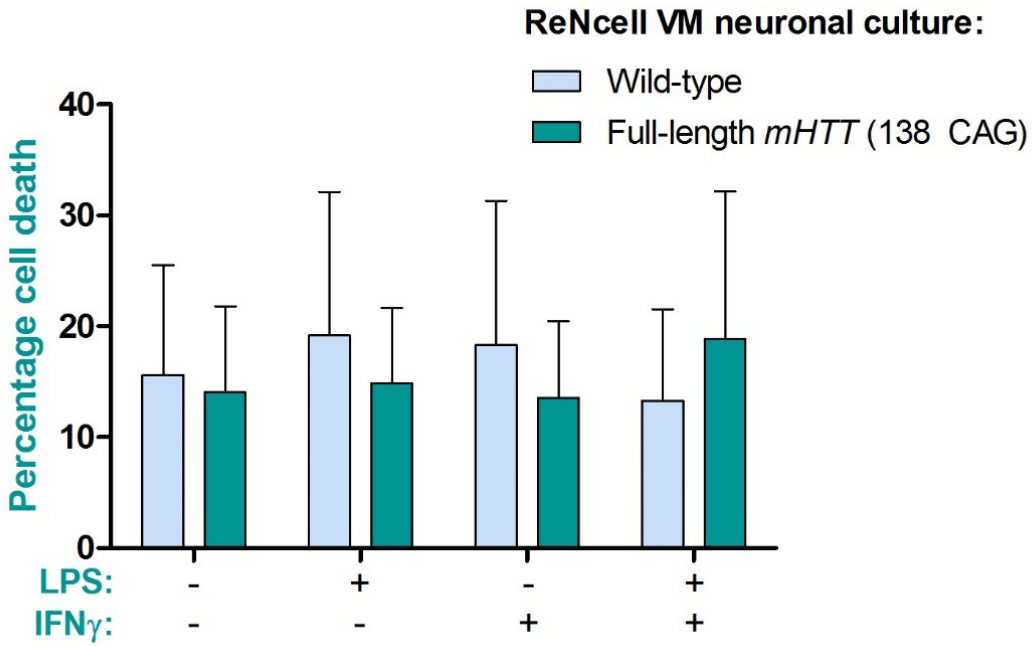

Figure 3.28: Direct treatment of wild-type and HD neurons with LPS and IFNγ

Ten DD (spontaneous differentiation) wild-type ReNcell VM or ReNcell VM+full-length mHTT (138 CAG) C8 neuronal cultures were treated directly, in duplicate, with 2 µg/mL LPS and 10 ng/mL IFNγ, alone or in combination, or received no treatment, for 24 h. Percentage cell death in neuronal cultures was determined by LDH cytotoxicity assay and is presented as mean average percentage cell death (calculated as described in section 2.6.1) of three independent biological repeats ± SEM. Data were statistically analysed using two-way ANOVA and neither treatment condition (p=0.997) or neuronal cell line (p= 0.869) were found to be significant sources of variation.

None of the stimulation treatments were found to have a significant effect on cell death compared with untreated in either wild-type or HD (full-length *mHTT* (138 CAG)) ReNcell VM neuronal cultures (Figure 3.28). There were also no significant differences in cell death between wild-type and HD neuronal cultures in untreated or treated conditions. This indicates that any differences in neuronal cell death detected following treatment with myeloid cell conditioned media are due to factors released by the myeloid cells and not due to direct effects of LPS and IFNγ. LPS and IFNγ are not directly toxic to wild-type or HD neurons in culture.

Finally, an alternative stimulation paradigm was trialled as a crude model of CNS injury. Wild-type mature neuronal cultures (21 DD by spontaneous differentiation) were

subjected to physical damage by rapid shaking (400 rpm on a shaking platform for 10 min). Supernatants, containing visible floating cell debris, were then collected from the neuronal cultures. Healthy volunteer and pre-manifest HD BMD-macrophages were stimulated, in duplicate, with these supernatants at 1:1 with fresh RPMI/FBS, for 24 h. Non-stimulated conditions were RPMI/FBS only or 1:1 NM:RPMI/FBS to control for the media composition of the stimulated condition. Mφ-CM (stimulation Mφ-CM) was then collected, processed and stored as per the usual protocol (section 2.1.5.1), including a centrifugation step to spin-out cell debris from the conditioned medium. BMD-macrophages were changed into fresh culture medium and cultured for a further 24 h before collecting Mφ-CM again (stimulation + rest Mφ-CM). Mφ-CM was then used to treat wild-type neuronal cultures for 4 days, and LDH cytotoxicity assays were performed to assess percentage cell death in neuronal cultures.

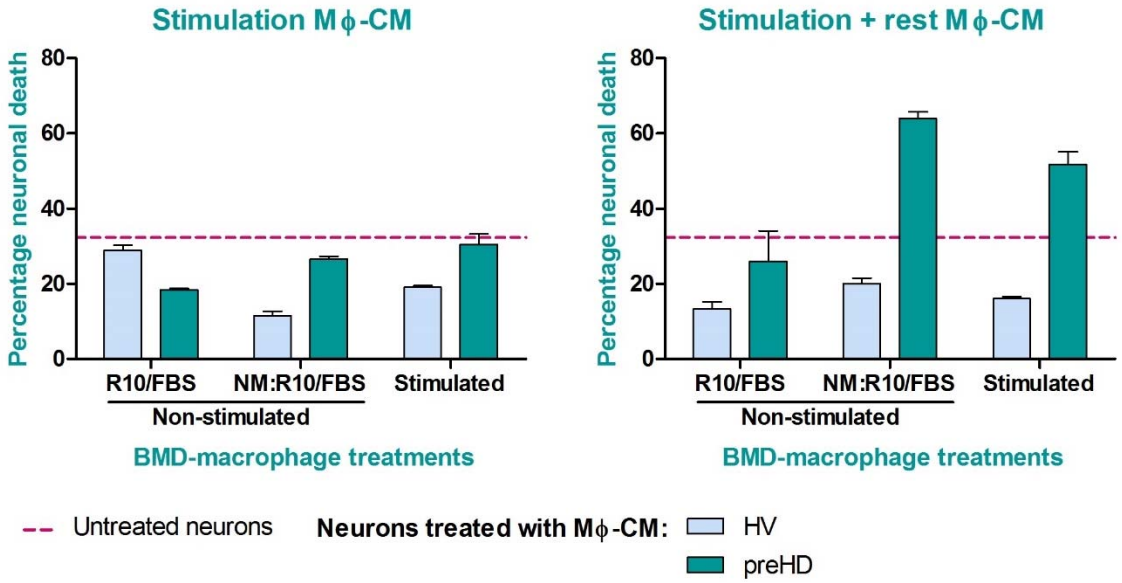

Figure 3.29: Neuronal death levels after treatment with Mφ-CM from BMD-macrophages stimulated with damaged neurons

Twenty-one DD (spontaneous differentiation) wild-type ReNcell VM neuronal cultures were treated, at least in triplicate, for 4 days with Mφ-CM from healthy volunteer (HV; n=1) or pre-manifest HD (preHD; n=1) BMD-macrophages, or were cultured in RPMI/FBS only (untreated). Mφ-CM was prepared from BMD-macrophages which had been stimulated with damaged neurons (stimulated), or cultured in R10/FBS medium or NM:RPMI/FBS culture medium (non-stimulated), for 24 h (stimulation Mφ-CM; left) or had received the same treatment followed by a 24 h rest period (stimulation + rest Mφ-CM; right). Neurotoxicity was measured by LDH cytotoxicity assay and results are presented as mean average percentage neuronal death (calculated as described in section 2.6.1 with total LDH calculated from 3 untreated neuronal cultures) ± SEM. Percentage cell death of untreated neuronal cultures is marked by purple, dashed lines.

Preliminary data showed that treatment of neuronal cultures with Mφ-CM prepared from BMD-macrophages stimulated with damaged neurons did not alter percentage cell death compared with non-stimulated Mφ-CM in the same media composition (NM:RPMI/FBS) (Figure 3.29). There were, however, differences detected between the effects of healthy volunteer and pre-manifest HD Mφ-CM on neuronal death. When BMD-macrophages had been cultured in NM:RPMI/FBS media (stimulated or non-stimulated), pre-manifest HD Mφ-CM treatment resulted in increased neuronal death compared with healthy volunteer Mφ-CM treatment in both stimulation Mφ-CM and stimulation + rest Mφ-CM conditions. Additionally, in the stimulation + rest condition, healthy volunteer Mφ-CM reduced neuronal death below baseline levels (untreated neurons) and pre-manifest HD Mφ-CM increased neuronal death above baseline levels. This suggests that in this model healthy volunteer Mφ-CM was neuroprotective and pre-manifest HD Mφ-CM was neurotoxic. With a biological *n* of 1, however, no final conclusions were drawn from these results involving subject group comparisons.

3.5.5.3 Co-culture by medium shared concurrently

Procedures for co-culture by medium shared concurrently are described in detail in section 2.1.5.3.

Wild-type ReNcell VM NSCs and healthy volunteer or manifest HD monocytes were seeded on coverslips and differentiated into 11 DD neurons (spontaneous differentiation) or BMD-macrophages, respectively. One coverslip of each cell-type (one neuronal culture and one healthy volunteer or manifest HD BMD-macrophage culture) was then transferred into one well of a 6-well plate and cultured simultaneously in RPMI/FBS culture medium for 3 days. Co-cultures were monitored daily by live-cell phase-contrast microscopy, and at day 3 coverslips were removed from co-culture and analysed independently by ATP cell viability assay.

Phase-contrast microscopy at 3 days in co-culture revealed that manifest HD BMD-macrophages appeared much healthier than healthy volunteer BMD-macrophages (Figure 3.30; A). Manifest HD BMD-macrophages had proliferated and fried-egg like morphology was maintained, while healthy volunteer BMD-macrophages had become small, round and activated and the majority of cells had subsequently died. Neuronal cultures appeared to be unaffected in co-culture with manifest HD BMD-macrophages, however in co-culture with healthy volunteer BMD-macrophages one of the neuronal cultures was adversely affected as can be seen in Figure 3.30; A, HV #2 co-culture. ATP cell viability assay of neuronal and BMD-macrophage cultures showed that neuronal viability was not affected by co-culture with healthy volunteer or manifest HD BMD-macrophages in this model (Figure 3.30; B, left). Manifest HD BMD-macrophage

viability was slightly higher than healthy volunteer BMD-macrophage viability following co-culture with neurons (Figure 3.30; B, right), however BMD-macrophage viability was highly variable overall resulting in a large SEM.

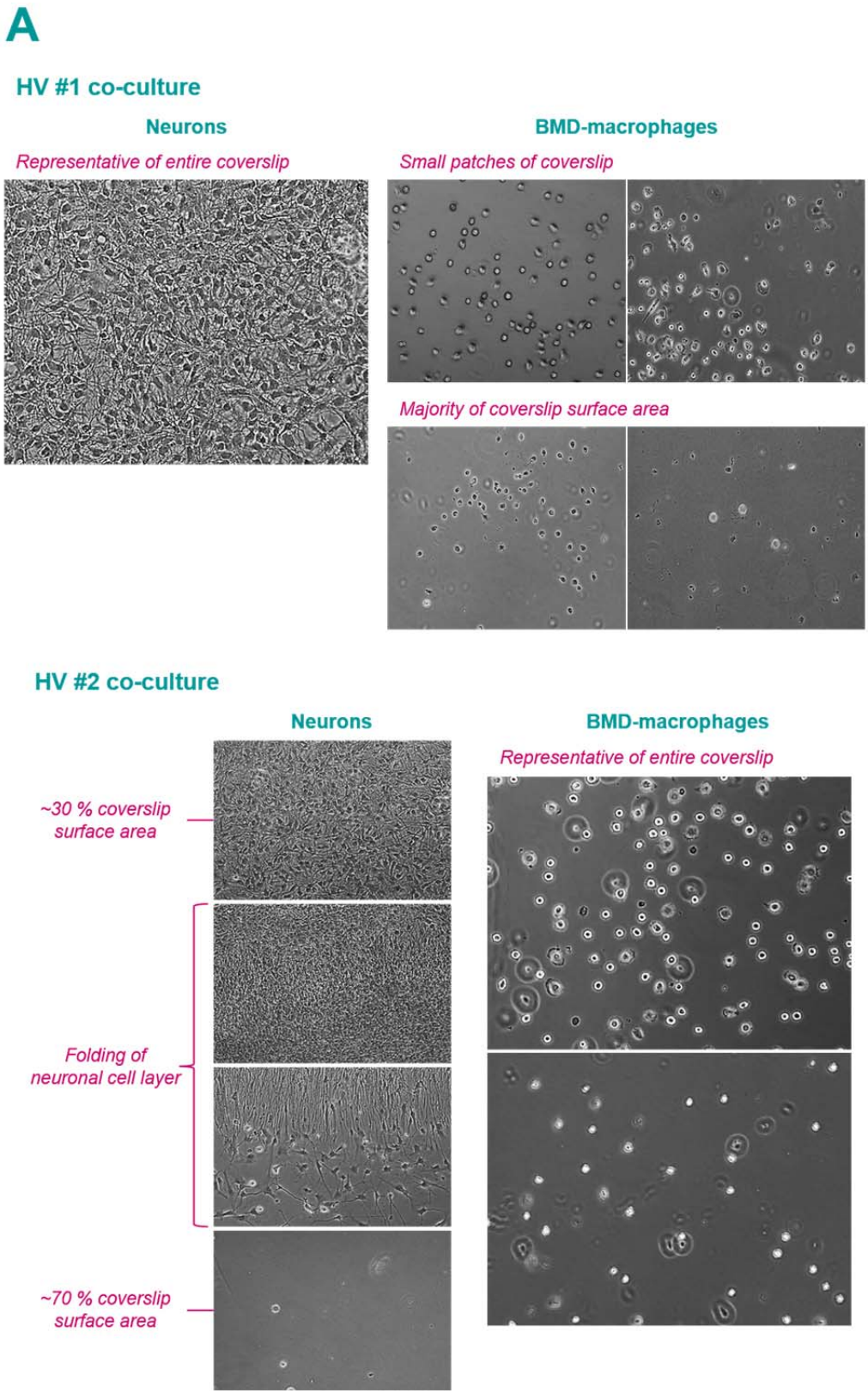

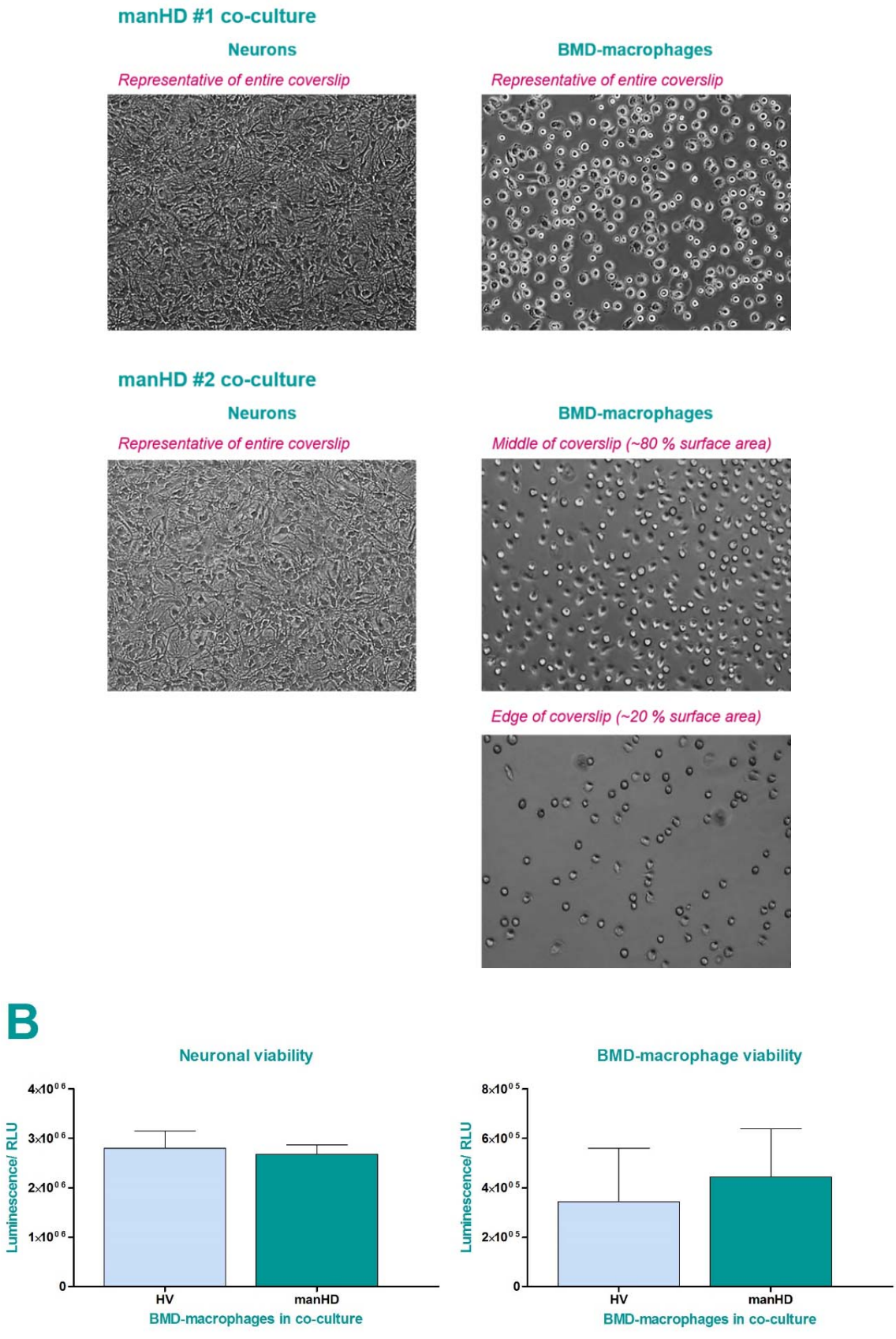

Figure 3.30: Analysis of neuronal-BMD-macrophage co-culture by medium shared concurrently

Eleven DD (spontaneous differentiation) wild-type ReNcell VM neurons and healthy volunteer (HV; n=2) or manifest HD (manHD; n=2) BMD-macrophages were cultured on coverslips and

combined in co-culture with shared culture medium (RPMI/FBS). Each co-culture combination was tested in duplicate. ***A)*** *Phase-contrast micrographs of neurons (left) and BMD-macrophages (right) after 3 days in co-culture. Representative images of each individual co-culture are presented, including 2 healthy volunteer and 2 manifest HD co-cultures with BMD-macrophages differentiated from monocytes isolated from 2 independent healthy volunteers (HV #1 and HV #2) and 2 independent manifest HD patients (manHD #1 and manHD #2) donors.* ***B)*** *Neuronal (left) and BMD-macrophage (right) viability after 3 days in co-culture as determined by ATP cell viability assay, presented as mean average luminescence in relative light units (RLU) per healthy volunteer or manifest HD co-culture ± SEM (luminescence is directly proportional to cell viability as a function of this assay).*

3.5.5.4 Co-culture by direct physical contact

Procedures for co-culture by direct physical contact are described in detail in section 2.1.5.4.

Healthy volunteer (*n*=3) or manifest HD (*n*=3) BMD-microglia were added directly on top of 18 DD (induced differentiation) wild-type ReNcell VM neuronal cultures. The co-cultures were then stimulated with 2 µg/mL LPS and 10 ng/mL IFNγ, or received no treatment (non-stimulated), and were monitored by phase-contrast microscopy. In all conditions, the following observations were made with immediate effect: all BMD-microglia transformed into small, round, activated cells and spread amongst the neurons, then large amounts of floating cell debris appeared and the neuronal cell layers lifted completely from the culture surface. It was concluded that this model of co-culture by direct physical contact was not viable for assessment of neuronal-myeloid cell interactions due to the rapid destruction of the neuronal cell layer by BMD-microglia.

3.6 Discussion

In order to investigate interactions between the CNS and innate immune system in the pathogenesis of HD, neuronal-myeloid cell co-culture models of HD were developed. Due to a lack of high-quality HD neuronal cell models which fully recapitulate relative aspects of the human condition, novel HD neuronal cell lines were generated. Additionally, a novel technique was discovered for the differentiation of primary human monocytes into microglia-like cells.

3.6.1 Human neuronal cell models of HD

3.6.1.1 ReNcell VM neuronal cultures

NSC-derived ReNcell VM neuronal cultures have been well characterised in the literature as a good model of human neurons *in vitro* (Hoffrogge *et al.* 2006; Donato *et*

al. 2007; Wood-Kaczmar *et al.* 2008; Gandhi *et al.* 2009; Morgan *et al.* 2009; Choi *et al.* 2014). In the first 7 DD using spontaneous differentiation or similar methods, ReNcell VM have been shown to display a large rearrangement of the proteome in a pattern consistent with differentiation into mature neuronal cultures (Hoffrogge *et al.* 2006). At 14-29 DD, it has been reported that some neurons express functional Na^+-channels and are electrophysiologically active, a phenomenon which occurs in a higher number of neurons if differentiation is induced rather than spontaneous (Donato *et al.* 2007).

Here, morphological and expression analyses confirmed that using the spontaneous differentiation technique, ReNcell VM NSCs can be robustly differentiated into mature neuronal cultures with a high neuronal yield and a small astroglial sub-population. The neuronal cultures were also shown to express native HTT and display similar morphology and characteristics as reported by others (Donato *et al.* 2007; Wood-Kaczmar *et al.* 2008; Gandhi *et al.* 2009; Choi *et al.* 2014). Induced differentiation increased the yield of specific neuronal sub-types within the mature cultures, including GABAergic and dopaminergic neurons, as was also reported by Wood-Kaczmar *et al.* (2008) and Gandhi *et al.* (2009). When considering the effects of inflammation on neurodegeneration, it is important to note that cell-to-cell interactions involving neurons, myeloid cells and astrocytes are necessary for the generation of neuropathogenesis in HD (Gu *et al.* 2005; Gu *et al.* 2007; Bradford *et al.* 2009; Bradford *et al.* 2010; Möller 2010; Crotti and Glass 2015). Astrocytes play important roles in the maintenance of a chronic feed-forward loop of chronic neuroinflammation as well as providing neurotrophic support to degenerating neurons (Saijo and Glass 2011; Crotti and Glass 2015; Doty *et al.* 2015). Therefore, neuronal cultures containing a small population of astrocytes were considered to be optimum for modelling neural-immune interactions in co-culture models of HD.

As ReNcell VM neuronal cultures are a well-established model of human neurons in culture, and reported morphological and phenotypic characteristics had been confirmed, this cell line was taken forward for the development of HD neuronal cell lines to study neuronal-myeloid cell interactions in HD pathogenesis. With the aim of achieving mature cultures with a pan-neuronal phenotype, the spontaneous differentiation technique was generally preferred and was used in most experiments. Spontaneous differentiation to 21-49 days was also used by Choi and colleagues, who recently published the first human neuronal culture AD model to recapitulate Aβ and tau pathology (Choi *et al.* 2014).

3.6.1.2 HD neuronal cell lines expressing HTT exon 1

Human neuronal cell models of HD were generated by lentiviral transduction of ReNcell VM NSCs with human *HTT* exon 1. Four different neuronal cell lines were developed: three expressing human *HTT* exon 1 with CAG repeats in the non-pathogenic range (ReNcell VM+*HTT* exon 1 (29 CAG)) or pathogenic range (ReNcell VM+*mHTT* exon 1 (71 CAG) and ReNcell VM+*mHTT* exon 1 (129 CAG)) in addition to an eGFP reporter, and one control line expressing the eGFP reporter only. All transgenic neuronal cell lines could be differentiated into mature neuronal cultures with a high yield of βIII-tubulin-positive neurons and some GFAP-positive astrocytes, and expression of normal or mHTT exon 1 trans-protein was confirmed in both NSC and mature neuronal cultures.

The mHTT exon 1-expressing neuronal cultures presented with characteristics similar to human HD neurons *in vivo*; including fragmentation of mHTT, inclusions composed of mHTT aggregates and neurotoxicity caused by *mHTT* expression. N-terminal fragments smaller than exon 1 were detected only in ReNcell VM+*mHTT* exon 1 (129 CAG) NSCs and neuronal cultures, which may be a result of post-translational proteolytic cleavage of the highly-expanded exon 1 fragment. N-terminal HTT fragments of this size have previously been detected in HD patient cells and not in healthy volunteer cells (Weiss *et al.* 2012). The shortest N-terminal fragments of mHTT, including an exon 1 only HTT protein, have also been demonstrated to accumulate into detergent-insoluble complexes which form cytoplasmic nuclear inclusion bodies, representing one of the neuropathological hallmarks of HD (Davies *et al.* 1997; DiFiglia *et al.* 1997; Landles *et al.* 2010). Intranuclear inclusions of mHTT were also detected in the HD neuronal cell lines (ReNcell VM+*mHTT* exon 1 (71 CAG) and ReNcell VM+*mHTT* exon 1 (129 CAG)) but not in non-HD neuronal cell lines (wild-type ReNcell VM, ReNcell VM+*HTT* exon 1 (29 CAG) and ReNcell VM+eGFP reporter only). Mutant HTT aggregates were present in both NSCs and mature neuronal cultures, and interestingly were perinuclear or cytoplasmic in NSCs and intranuclear in mature neurons. It has previously been shown that expression of mHTT exon 1 protein fragment is sufficient to cause neuronal dysfunction and death (Mangiarini *et al.* 1996; Ross and Tabrizi 2011). The same was demonstrated here, where expression of *mHTT* exon 1 (71 CAG) in ReNcell VM resulted in higher neuronal culture death levels compared with expression of *HTT* exon 1 (29 CAG), indicating mHTT-induced neurotoxicity in this neuronal cell culture model of HD.

Overall, it was demonstrated that these human NSC-derived HD neuronal cell lines over-expressing mHTT exon 1 recapitulate several features of neurons in the HD patient brain. They are an improvement on many currently available HD cell models

because they are human and neuronal, and they accurately represent the human disease like their primary human neuron counterparts whilst also being easily obtainable and useable on a large scale. Unlike iPSC-derived neurons, these neuronal cell lines can be robustly and reproducibly differentiated from NSCs into a high yield of mature HD neurons with isogenic controls. This can be conducted in a short time-frame and with minimal genetic heterogeneity and phenotypic variability between cell lines. Consequently, it is considered that ReNcell VM+*mHTT* exon 1 neuronal cell lines are a high-quality neuronal cell model of HD.

3.6.1.3 HD neuronal cell lines expressing full-length HTT

Human neuronal cell models of HD were generated by retroviral transduction of ReNcell VM NSCs with full-length human *HTT* cDNA. Two different neuronal cell lines were developed: one expressing full-length human *HTT* with 15 CAG repeats (non-pathogenic range) and one expressing full-length human *mHTT* with 138 CAG repeats (pathogenic range). Both cell lines could be differentiated from NSCs into mature neuronal cultures expressing the full-length HTT trans-proteins. This model therefore provides evidence for successful introduction of full-length human *HTT* cDNA into the genomic DNA of a NSC line by means of retroviral delivery, as well as subsequent expression of the full-length HTT protein in differentiated neuronal cultures.

Initial assessments of the HD neuronal cell line showed that expression of full-length *mHTT* (138 CAG) did not cause increased baseline cell death in neuronal cultures compared with wild-type neurons. However, due to time limitations, this cell model was not fully characterised; especially ReNcell VM+full-length *HTT* (15 CAG) which did not reach the final stages of verification after generation of clonal cell populations. In the interest of moving forward with the development of neuronal-myeloid cell co-culture models of HD, wild-type ReNcell VM were used in place of ReNcell VM+full-length *HTT* (15 CAG) as a non-HD neuronal culture alongside ReNcell VM+full-length *mHTT* (138 CAG) HD neuronal cultures.

Further work is required to complete the development and characterisation of this full-length *HTT* neuronal cell model of HD.

3.6.2 Primary human HD myeloid cells

3.6.2.1 BMD-macrophages

Differentiation of primary human monocytes into macrophages *in vitro* by GM-CSF induction promotes the development of macrophages with a proinflammatory M1-type phenotype. These BMD-macrophages have previously been shown to express several key macrophage markers including CD11b, CD11c, MHC class II human leukocyte

antigen (HLA)-DR and HLA-DQ, Fc (Fragment, crystallisable antibody region)γ receptors I and II and Scavenger Receptor type A; express important genes associated with the NFκB pathway; produce major macrophage-derived cytokines including IL-1β, IL-6, IL-8 and TNFα; and exhibit phagocytic and migratory activities (Akagawa *et al.* 2006; Kwan *et al.* 2012b; Träger *et al.* 2014a). Monocytes differentiated *in vitro* into BMD-macrophages in this way are therefore considered to be a highly representative model of tissue macrophages *in vivo*.

HD patient peripheral myeloid cells have previously been shown to express mHTT (Björkqvist *et al.* 2008; Weiss *et al.* 2012; Träger *et al.* 2014a), and likewise, HD patient BMD-macrophages were shown here to express mHTT. This has been demonstrated to lead to dysfunctional behaviours in these macrophages including aberrant NFκB signalling, increased release of proinflammatory cytokines and impaired migration (Kwan *et al.* 2012b; Träger *et al.* 2014a). HD patient BMD-macrophages have also been shown to be hyper-reactive in response to stimulation with LPS and IFNγ (Träger *et al.* 2014a). As combined stimuli, LPS and IFNγ recapitulate *in vitro* the neuroinflammatory milieu present in the degenerating HD brain, or the proinflammatory peripheral environment, and promote classical activation of BMD-macrophages. This leads to production of proinflammatory cytokines, iNOS and ROS; increased expression of MHC class II molecules and CD68; increased antigen presentation; and increased microbicidal activity (Gordon and Taylor 2005).

Whilst mHTT-induced dysfunction of HD patient BMD-macrophages has already been well described, in both non-stimulated and stimulated (LPS and IFNγ) conditions, the effects this has on neurodegeneration in the HD brain is not yet known. Therefore, HD patient BMD-macrophages were used in the development of various experimental co-culture paradigms, with the HD neuronal cell models which had been generated, in order to examine these effects.

3.6.2.2 BMD-microglia

When performing media titrations for the development of neuronal-myeloid cell co-culture models, it was discovered that the culture of BMD-macrophages in NM culture medium caused the morphological and phenotypic transformation of these macrophages into microglia-like cells (BMD-microglia).

Microglia are derived by primitive haematopoiesis in the foetal yolk sac and seed CNS tissue during early embryogenesis (Ginhoux *et al.* 2010; Saijo and Glass 2011; Goldmann *et al.* 2016). The embryonic myeloid precursors are exposed to factors in CNS tissue which drive the expression of specific genes for differentiation into functionally specialised microglia (Saijo and Glass 2011; Lavin *et al.* 2015), and

throughout this process they undergo pronounced morphological changes; from amoeboid immature cells on CNS entry; to polarised, migrating cells; to proliferating, ramified cells with several short processes; and finally to the typical ramified microglia with long processes which are observed throughout the adult brain parenchyma (Xavier *et al.* 2014). Cells exhibiting each of these morphological transformations were present in HD BMD-microglia cultures, and this could be due to differentiation of these cells from peripheral BMD-macrophages into microglia-like cells following a switch to a CNS-like environment by the change in culture medium. It is possible that the change in culture medium to NM triggered the induction of genes which drive differentiation into microglia. NM, for which the complete formulation can be found in Appendices I-v and I-vii, was developed by ReNeuron for the differentiation and maintenance of ReNcell VM prior to therapeutic surgical transplantation into the human brain, and is therefore optimised to replicate the environment of their destination.

When peripheral macrophages are recruited to the brain following injury, they adopt a functional and morphological state similar to resident microglia due to an equal response to the same environmental stimuli (O'Koren *et al.* 2016). CNS-resident microglia and CNS-infiltrating macrophages have even been deemed morphologically and phenotypically indistinguishable (Enose *et al.* 2005; Schmid *et al.* 2009; Greter *et al.* 2015). Any heterogeneity *in vivo* is therefore likely to be dependent on cellular differentiation, tissue distribution and responses to endogenous and exogenous stimuli, rather than intrinsic differences (Schmid *et al.* 2009), in which case modelling of a pro-neuronal micro-environment *in vitro* may promote a microglial phenotype in peripherally-derived myeloid cells. It is therefore possible that such microglial developmental transformation, or BMD-macrophage CNS-infiltration, has been modelled in these BMD-microglia cultures by maintaining them in NM.

Other microglial morphological phenotypes observed in HD patient BMD-microglia cultures included active and dynamic surveying of the local environment via motile processes, direct physical contact between neighbouring cells via processes and tubules, formation of microglial nodules and polarised migration. A search of the literature did not reveal any reports of direct contact occurring between two microglia cells via their processes or tubule-like structures, however similar events have been reported to occur between microglia and neurons in the context of modulating neuronal activity (Wake *et al.* 2009; Tremblay *et al.* 2010; Li *et al.* 2012) or direct killing of damaged neurons (unpublished work presented by Hajji Nabil, Lecturer in cancer and epigenetics, Imperial College London Hammersmith Campus; Figure 3.22, E). Microglial nodules can exhibit both pro- and anti-inflammatory phenotypes, and their development is a phenomenon in viral encephalitis, traumatic brain injury, brain infarct,

and MS, where microglial nodules are associated with degenerating white matter (Singh *et al.* 2013). Microglial nodules are not found in the healthy CNS (Singh *et al.* 2013). It was shown here that microglial nodules developed in BMD-microglia cultures differentiated from HD patient but not healthy volunteer monocytes, possibly occurring in response to cell-autonomous mHTT expression.

Subcellular morphological phenotypes of microglia were also observed, including vacuole and granular formations. Such phenotypes have previously been shown to occur in microglial cells in response to neurodegenerative disease or CNS injury. Exposure of human post-mortem brain-derived microglia cultures to aggregated Aβ can induce a transformation into amoeboid, reactive cells which form vacuoles (Walker *et al.* 2006). *In vivo*, microglia in the human basal ganglia have been observed to transform into compound granular corpuscles which develop into large, round, amoeboid cells heavily loaded with lipoid, in response to CNS injury leading to general paralysis (Fleming 1930). These transformations are indicative of phagocytic activities and were found in the HD BMD-microglia cultures, possibly occurring as a result of cell-autonomous mHTT expression.

BMD-microglia also expressed several key microglial markers. Upon differentiation of monocytes into BMD-microglia, expression of CD14 was decreased while CD11b and Iba1 expression was increased, marking differentiation into mature macrophages/microglia. CD14 expression has previously been shown to be much higher in blood monocytes in brain vessels than in plaque-associated microglia in AD brains (Walker and Lue 2015). CD11b and Iba1 expression further increased in response to stimulation with LPS and IFNγ. This has been shown previously to occur in microglia during neurodegenerative inflammation and nerve injury (Ito *et al.* 1998; Roy *et al.* 2006). Iba1 interacts with actin bundles and is involved with membrane ruffling and phagocytosis (Ito *et al.* 1998). Monocytes did not express mannose receptor or TREM2, and expression of these markers was induced upon differentiation into BMD-microglia. Mannose receptor is a marker of alternatively activated (M2) macrophages and is expressed by mature brain-resident microglia (Gordon and Taylor 2005; Peferoen *et al.* 2015), while monocytes have no, or very low, expression of this marker. In BMD-microglia, mannose receptor expression was strong in both non-stimulated and stimulated conditions, confirming that these cells were both mature and polarised towards an M2 phenotype. Within the CNS, TREM2 is a PRR exclusively expressed by microglia (Lucin and Wyss-Coray 2009) and, along with its core molecular complex partner DAP12, is involved in the regulation of phagocytosis and the modulation of anti-inflammatory responses through inhibition of TLR signalling (Doty *et al.* 2015; Lue *et al.* 2015). TREM2/DAP12 is also involved in the maintenance of microglia in a quiescent,

unactivated state (Saijo and Glass 2011). In BMD-microglia cultures, TREM2 expression was high in non-stimulated cells and decreased after stimulation, in accordance with its role in regulating microglial activation state. As a marker, TREM2 is also functionally similar to M2 anti-inflammatory receptors (Walker and Lue 2015), providing further support for the BMD-microglia being of M2 phenotype.

BMD-microglia were also demonstrated to express the microglial markers CD68, CSF1R, CX3CR1, P2Y12 and PU.1 in both healthy volunteer and manifest HD cultures and in both stimulated and non-stimulated conditions. CD68 is a lysosomal protein which can be used to stain microglia (Graeber *et al.* 1990; Slepko and Levi 1996), and is indicative of phagocytic activity (Zotova *et al.* 2013). High levels of CD68 expression are associated with activated microglia, whilst low levels of expression are associated with quiescent, ramified microglia (Graeber *et al.* 1990; Slepko and Levi 1996; Kingham *et al.* 1999). Microglia differentiation and proliferation is initiated by CSF1 and its receptor CSF1R, CD34 and transcription factors PU.1, C/EBPs and AP1 (Saijo and Glass 2011). Microglial-like cells were shown here to express both CSF1R and PU.1, and PU.1 expression may be higher in HD patient BMD-microglia than healthy volunteer BMD-microglia. The expression of mHTT has previously been shown to confer a cell-autonomous increase in proinflammatory gene expression associated with increased expression and transcriptional activities of PU.1 in a rat microglial cell line (Crotti et al. 2014). Microglia in the striatum and cortex of HD patient brains were also shown to express elevated levels of PU.1 (Crotti et al. 2014). Expression of CSF1R has been shown to be upregulated in microglia in the brains of patients with AD and ALS (Akiyama *et al.* 1994), and several studies have classified CSF1R signalling as similar to M2 activation (Walker and Lue 2015). The chemokine fractalkine (CX3CL1) is expressed on the surface of neurons in the CNS, and is a unique ligand for its receptor CX3CR1, which is expressed by microglia in the CNS parenchyma. When CX3CL1 activates CX3CR1 in models of inflammation, microglia are maintained in a non-neurotoxic, quiescent state and basal microglial process dynamism, motility and surveillance activities are promoted (Eyo and Wu 2013). Finally, the membrane-bound purinergic receptor P2Y12 is a microglia-specific marker in the CNS which is selectively expressed on human ramified and amoeboid microglia and elevated under neuropathologic conditions which promote alternative activation (Moore *et al.* 2015; Satoh *et al.* 2016). Expression of this marker is absent, or much reduced, in perivascular BMD-macrophages and monocytes in the human brain (Moore *et al.* 2015; Satoh *et al.* 2016). P2Y12 maintains microglia in a highly ramified state (Haynes *et al.* 2006) and mediates microglial process motility, polarisation, chemotaxis and migration (Honda *et al.* 2001; Moore *et al.* 2015; Satoh *et al.* 2016; Sipe *et al.* 2016).

Overall, characterisation of the BMD-microglia cultures by antigenic criteria revealed that the cells expressed several key microglial markers and were polarised towards an M2 alternatively activated phenotype with promotion of a ramified, surveying and quiescent phenotype. As the cells were originally differentiated from primary monocytes into macrophages by GM-CSF induction, which promotes the development of classically activated M1-type macrophages, this is evidence that the activation state of macrophages is highly dynamic and fully differentiated mature macrophages can switch from one polarisation to another. While several studies have reported certain expression markers to be microglia-specific (e.g. P2Y12), many others conclude that there is little evidence that such markers can distinguish between microglia and infiltrating peripherally-derived macrophages (Walker and Lue 2015). However, taking into account both the expression of key microglial markers (CD11b, CD68, CSF1R, CX3CR1, Iba1, mannose receptor, P2Y12, PU.1 and TREM2), and the microglia-specific morphological phenotypes exhibited by these cells (presence of all microglial morphological forms: small, round and activated, amoeboid, polarised, ramified with several short processes, highly ramified with very long processes; sub-cellular granule and vacuole formations indicative of phagocytic functions; process motility and cell-to-cell contact via processes and tubules; microglial nodule formations; and polarised migration towards sites of activity), it was determined that the BMD-microglia cultures were more similar to human microglia than to human peripheral tissue macrophages.

BMD-microglia therefore represent a novel model of human microglia in culture. They are more similar to human microglia *in vivo* or *ex vivo* by morphological and antigenic criteria than currently available immortalised human microglial cell lines (Janabi *et al.* 1995; Nagai *et al.* 2001), and unlike primary human microglia, they can be differentiated from an easily accessible and more available source. As HD patient peripheral myeloid cells express mHTT, this also represents a useful model for the study of microglial cell dysfunction and neuronal-microglial cell interactions, over the disease course, in primary HD patient cells.

3.6.3 Neuronal-myeloid cell co-culture models of HD

Three different neuronal-myeloid cell co-culture paradigms were trialled: co-culture by conditioned medium transfer, co-culture by medium shared concurrently, and co-culture by direct physical contact. This was with the aim of developing co-culture models to analyse interactions between BMD-macrophages or BMD-microglia differentiated from monocytes isolated from healthy volunteers, pre-manifest HD gene carriers or manifest HD patients with wild-type, *HTT* exon 1 or full-length *HTT* ReNcell VM neuronal cultures.

The conditioned medium transfer co-culture model was developed with the aim of determining the effects of factors secreted by myeloid cells, in various stimulated and non-stimulated conditions, on neuronal phenotypes. This will allow for comparisons to be made between the effects of healthy volunteer and HD patient myeloid cells on normal and HD neuronal cultures. Preliminary results showed that wild-type neuronal cultures treated with conditioned medium from non-stimulated healthy volunteer or HD patient BMD-microglia had decreased cell death levels compared with untreated. Cell death levels were not reduced by treatment with medium conditioned by other neurons. This suggests that both healthy volunteer and HD patient BMD-microglia, specifically, release neuroprotective factors. There were no differences between the effects of healthy volunteer and HD patient BMD-microglia on neuronal death.

To assess bi-directional communication between myeloid cells and neurons in HD, co-culture models were developed where both cell types could share the same medium. This allows neuronal-myeloid cell interactions by secreted, soluble factors such as cytokines, chemokines, ROS and RNS. In this model, morphological assessment showed HD BMD-macrophages to survive better than healthy volunteer BMD-macrophages in co-culture. Unlike the HD patient cultures, healthy volunteer BMD-macrophages transformed into small, round, activated cells and subsequently died off. However, viability analysis of both neurons and BMD-macrophages in co-culture revealed large variability between cultures and no differences were found between healthy volunteer and HD patient neuronal or BMD-macrophage viability overall.

In the CNS, microglia are dynamic cells which are free to migrate towards sites of neuronal injury. Microglia also make transient direct physical contact with neurons, functioning to support neuro-modulation during normal physiology (Eyo and Wu 2013; Heneka *et al.* 2014). Additionally, neurons suppress the activation of microglia through cell-to-cell contact (Saijo and Glass 2011). Following CNS injury or infection, ramified microglia may destroy damaged neurons by direct contact and phagocytic microglia clear neuronal debris and pathogens (Saijo and Glass 2011). Similar behaviours had also been observed here in HD patient BMD-microglia cultures. Therefore, in order to assess how these cell-to-cell interactions may be altered in HD, neuronal-BMD-microglia co-culture models were trialled where both cell-types were able to come in direct contact with each other. However, when allowed to make direct physical contact, BMD-microglia damaged the neuronal cell layer so rapidly that little analysis could be performed in this model. This could possibly have occurred due to phagocytosis and digestion of the laminin-coating used to aid neuronal adherence to the culture surface. It was concluded that this co-culture model was not viable for assessment of neuronal-

myeloid cell interactions due to the rapid destruction of the neuronal cell layer by BMD-microglia.

Co-stimulation with LPS and IFNγ is a well-established method of inducing general activation in primary human myeloid cells (Ziegler *et al.* 1988; Cramer and Klemsz 1997; Träger *et al.* 2014a; Björkqvist *et al.* 2008; Kelly and O'Neill 2015), and can also be used to model neuroinflammatory activation of microglia in neurodegenerative diseases: LPS is a PAMP, but activates TLR4 like several DAMPs associated with neurodegeneration and neurodegenerative disease (Saijo and Glass 2011; Amor *et al.* 2014; Heneka *et al.* 2014; Doty *et al.* 2015); and IFNγ is a proinflammatory cytokine which is upregulated in the brain and/or plasma of patients with ALS, HD and PD and is involved in the maintenance of chronic neuroinflammation (Nagatsu *et al.* 2000a; Björkqvist *et al.* 2008; Reale *et al.* 2009a; Wild *et al.* 2011; Ellrichmann *et al.* 2013; Doty *et al.* 2015). LPS/IFNγ co-stimulation paradigms were therefore developed to induce acute or chronic inflammatory phenotypes in healthy volunteer and HD patient BMD-macrophages or BMD-microglia. HD myeloid cells have previously been demonstrated to be hyper-reactive in response to LPS and IFNγ co-stimulation, and release elevated levels of proinflammatory cytokines compared with healthy volunteer myeloid cells (Björkqvist *et al.* 2008; Träger *et al.* 2014a). To assess the effects of HD myeloid cell hyper-reactivity on neurotoxicity, these acute and chronic co-stimulation paradigms were applied here to neuronal-myeloid cell co-cultures. BMD-macrophages stimulated with a range of LPS concentrations had differential effects on wild-type neuronal survival following conditioned medium transfer, as detected by LDH cytotoxicity assay, and the highest LPS concentration tested, 1 µg/mL, showed potential for detecting differences between the effects of healthy volunteer and HD patient Mφ-CM treatments on neuronal death.

An alternative stimulation paradigm was trialled as a crude model of CNS injury, whereby wild-type mature neuronal cultures were subjected to physical damage by shaking, and were used to directly stimulate BMD-macrophages. Mφ-CM was then used to treat wild-type neurons. As observed in other co-culture paradigms, there was a general trend for decreased neuronal death following treatment with Mφ-CM, however, unlike LPS stimulation, stimulation with damaged neurons did not lead to an effect on neuronal survival compared with non-stimulated Mφ-CM. Interestingly though, there were differences detected between the effects of healthy volunteer and pre-manifest HD Mφ-CM on neuronal survival. There was a trend for pre-manifest HD Mφ-CM treatment resulting in increased neuronal death compared with healthy volunteer Mφ-CM treatment in stimulated and non-stimulated conditions. When stimulation was followed by a rest period, healthy volunteer Mφ-CM reduced neuronal death below

baseline levels (untreated neurons) and pre-manifest HD Mφ-CM increased neuronal death above baseline levels. This suggests that in this case healthy volunteer Mφ-CM was neuroprotective and pre-manifest HD Mφ-CM was neurotoxic.

Overall, it was confirmed that co-culture by conditioned medium transfer was a suitable and viable model for assessing the effects of factors released by myeloid cells on neurotoxicity in co-culture models of HD. LDH cytotoxicity assay was the most sensitive measure of neuronal cell death and was capable of detecting differential effects of conditioned media treatments on neurotoxicity. Using this co-culture paradigm, there was some preliminary evidence that healthy volunteer and HD patient BMD-microglia are neuroprotective in co-culture with wild-type neurons, and there are potentially different effects of healthy volunteer and HD patient myeloid cell conditioned medium on neuronal survival following stimulation with the highest LPS concentration tested, 1 μg/mL. Stimulation conditions of 2 μg/mL LPS with 10 ng/mL IFNγ (peak maximal response) have previously been used to detect differences in healthy volunteer and HD myeloid cell proinflammatory cytokine release (Träger *et al.* 2014a), and these same concentrations, applied in acute or chronic paradigms, should be used in future experiments utilising this co-culture model. It was confirmed here that these stimulation conditions do not directly cause neurotoxicity.

3.7 Summary

Novel neuronal-myeloid cell co-culture models of HD were developed with the aim of studying interactions between these cell types in the pathogenesis of HD. Novel human HD and control NSC-derived neuronal cell lines expressing human *HTT* exon 1 or full-length human *HTT* were developed and characterised. Mature neuronal cultures expressing *mHTT* exon 1 exhibited several characteristics of pathologically affected neurons in the HD patient brain, including sub-fragmentation of mHTT protein, intranuclear inclusions composed of mHTT aggregates, and mHTT-induced neuronal death. A novel technique was discovered for the differentiation of primary human monocytes into microglia-like cells, and these BMD-microglia are similar to primary human microglia by morphological and antigenic criteria. BMD-macrophages and BMD-microglia were differentiated *in vitro* from primary human monocytes isolated from healthy volunteers, pre-manifest HD gene carriers and manifest HD patients and placed in various co-culture paradigms with HD or non-HD neuronal cultures. Preliminary data showed that conditioned medium transferred from healthy volunteer or HD patient BMD-microglia to neuronal cultures is neuroprotective. Co-culture by conditioned medium transfer with subsequent cell death analysis by LDH cytotoxicity

assay was determined to be a viable model for the assessment of the effects of factors released by myeloid cells, under various controlled conditions, on neurotoxicity.

4 Investigation into neuronal-myeloid cell interactions in co-culture models of HD

4.1 Background

The innate immune system is known to play a significant role in the pathogenesis of HD. Neuroinflammation, involving microglial activation, astrogliosis and elevated levels of proinflammatory factors, is an early and active component of the disease course (Singhrao *et al.* 1999; Sapp *et al.* 2001; Pavese *et al.* 2006; Tai *et al.* 2007a; Tai *et al.* 2007b; Björkqvist *et al.* 2008; Silvestroni *et al.* 2009; Politis *et al.* 2011; Tabrizi *et al.* 2013), and is accompanied by parallel inflammatory events in the periphery mediated by monocytes and macrophages (Dalrymple *et al.* 2007; Björkqvist *et al.* 2008; Wild *et al.* 2011; Ellrichmann *et al.* 2013; Heneka *et al.* 2014; Chang *et al.* 2015). These inflammatory events correlate with neurodegenerative processes and disease progression (Sapp *et al.* 2001; Pavese *et al.* 2006; Dalrymple *et al.* 2007; Tai *et al.* 2007a; Tai *et al.* 2007b; Björkqvist *et al.* 2008; Politis *et al.* 2011; Wild *et al.* 2011; Ellrichmann *et al.* 2013; Heneka *et al.* 2014). However, whether myeloid cell activation and inflammation associated with neurodegeneration in HD is protective, damaging or has no effect remains to be clearly defined.

Myeloid cells are the likely source of elevated levels of proinflammatory factors in the brain and plasma of HD patients. Microglia, monocytes and macrophages isolated from HD patients or HD mouse models are hyper-reactive when stimulated and release increased levels of cytokines, including IL-1β, IL-6, IL-8 and TNFα (Björkqvist *et al.* 2008; Träger *et al.* 2014a). This dysfunction of the innate immune system could be a reactive process to neurodegeneration and peripheral pathologies, or may be caused by cell-autonomous expression of mHTT (Crotti *et al.* 2014; Träger *et al.* 2014a). It is likely that both cell-to-cell interactions between neurons and microglia and cell-autonomous myeloid cell dysfunction are involved in generation of a feed-forward cycle of chronic inflammation in HD (Gu *et al.* 2005; Gu *et al.* 2007; Bradford *et al.* 2009; Bradford *et al.* 2010; Möller 2010; Crotti and Glass 2015). However, the effects this has on neurodegenerative processes is not clear.

Cytokines are important mediators of communication between the immune system and the CNS (Eskandari and Sternberg 2002; Wrona 2006). Microglia release cytokines which interact directly with neuronal receptors, and cytokines produced by peripheral myeloid cells regulate CNS activity directly by crossing the BBB and interacting with neuronal receptors, or indirectly by triggering the production of CNS-derived mediators via a relay involving cells at the BBB, or stimulating afferent neurons (Eskandari and Sternberg 2002; Wrona 2006). The proinflammatory cytokines IL-1β, IL-6 and TNFα, which are known to be released at elevated levels by myeloid cells in HD, have been shown to have neuromodulatory properties by impacting synaptic transmission and neuronal excitability (Vezzani and Viviani 2015). IL-2 and the Th1-type cytokines G-CSF, IFNγ, IL-1α, IL-1β, IL-6, IL-12 and TNFα regulate numerous pathways in neurons, including cytokine–receptor interactions, MAPKs, TLRs, apoptosis, PPAR signalling, cell adhesion molecules, antigen processing and Jak-STAT signalling (Benjamins 2013). These cytokines also upregulate production of certain neurotransmitters and their receptors, elements of the ubiquitin-proteasome pathway, iNOS, SOD2 and genes involved in the Wnt and Notch signalling pathways (Benjamins 2013). The Th2-type cytokines IL-4, IL-5, IL-10 and TGF-β regulate genes related to neuroactive ligand-receptors, calcium and long-term potentiation, upregulate arginase 1 expression leading to decreased NO generation and enhanced neurite outgrowth, and downregulate the gene for NCOR2 which could potentially lead to inhibition of histone demethylases and promotion of neuronal differentiation (Benjamins 2013). It is therefore likely that dysfunctional cytokine release by HD myeloid cells has an impact on neuronal function, and potentially on neurotoxicity or neuroprotection of degenerating neurons. Excessive proinflammatory cytokine release by microglia and peripheral myeloid cells has previously been demonstrated to contribute to neurotoxicity, and inhibition of IL-6 or TNFα, centrally or peripherally, has been shown to have beneficial therapeutic effects in HD (Bouchard *et al.* 2012; Hsiao *et al.* 2014). The polarisation of myeloid cells towards an M1 phenotype, which produce Th1-type cytokines, or M2 phenotype, which produce Th2-type cytokines, may also yield differential effects on neurotoxicity or neuroprotection in HD.

Neurotrophins are another major class of soluble factors involved in neuronal-myeloid cell communication, and like cytokines, levels of neurotrophins are also altered in HD. During homeostasis, microglia and peripheral myeloid cells secrete the neurotrophins NGF and BDNF which interact with their neuronal receptors to regulate neuronal survival, function, maintenance and repair (Nakajima *et al.* 2001; Saijo and Glass 2011). In response to acute striatal injury, activation of microglia and macrophages has been shown to induce expression of BDNF and stimulate dopaminergic sprouting and

repair (Batchelor *et al.* 1999). However, in HD it has been reported that there is reduced transcription and expression of BDNF and its main receptor, TrkB, in HD patient brain and HD mouse models (Zuccato *et al.* 2001; Ginés *et al.* 2006). This has been implicated as a possible contributor to striatal degeneration, and increasing BDNF levels was shown to reduce neurotoxicity and ameliorate neurological signs in animal models of HD (Puerta *et al.* 2010; Xie *et al.* 2010). Alternatively, striatal NGF expression has been shown to be increased in animal models of HD, while expression of its main receptor, TrkA, may be increased or decreased (Alberch *et al.* 2004). Microglia could be a source of these increased NGF levels, as inflammatory mediators such as cytokines, complement factors and DAMPs are potent stimulators of microglial NGF synthesis (Schindowski *et al.* 2008). It may be considered that dysregulated neuronal-myeloid cell interactions and cell-autonomous mHTT-induced toxicity in myeloid cells could result in aberrant expression and release of neurotrophins, and alterations in signalling via these essential neuroprotectants in HD could be critical for the survival or death of damaged and degenerating neurons.

Here, novel co-culture models of HD were utilised to dissect some of the complex interactions underlying neuronal-myeloid cell communication in the pathogenesis of HD. Preliminary data had shown that transfer of conditioned medium from healthy volunteer or HD patient BMD-microglia to wild-type neuronal cultures reduced neuronal cell death levels, indicating that both healthy volunteer and HD myeloid cells release neuroprotective factors. The aims of this current study were firstly to investigate further the effects of factors released by myeloid cells on neuronal death or survival in HD. Secondly, aims were to analyse the production of Th1- and Th2-type cytokines (and IL-2) and the neurotrophins NGF and BDNF in healthy volunteer and HD patient myeloid cells, to identify factors contributing to neurotoxicity or neuroprotection in HD. This will determine whether myeloid cells are neuroprotective or neurotoxic in HD, and potentially reveal altered release of specific cytokines or neurotrophins by cell-autonomous mechanisms in HD patient myeloid cells.

4.2 Aims

1) Determine the effects of healthy volunteer and HD patient Mφ-CM and MG-CM on the survival of wild-type and HD neurons in non-stimulated and stimulated conditions.
2) Analyse levels of release of Th1-type cytokines, Th2-type cytokines and IL-2 in healthy volunteer and HD patient BMD-macrophages and BMD-microglia in non-stimulated and stimulated conditions.

3) Analyse levels of release of the neurotrophins NGF and BDNF in healthy volunteer and HD patient BMD-microglia in non-stimulated and stimulated conditions.
4) Determine which factors released by healthy volunteer and HD patient BMD-macrophages and BMD-microglia contribute to neuroprotection or neurotoxicity of HD neurons in co-culture.

4.3 Methods

A summary of methods used in this Chapter is outlined below. Full details of experimental protocols can be found in Chapter 2: Materials and Methods.

BMD-macrophages and BMD-microglia were differentiated *in vitro* (as described in sections 2.1.2.4 and 2.1.2.5, respectively) from primary human monocyte cultures (isolated from whole blood samples and cultured *ex vivo* as described in sections 2.1.2.2 and 2.1.2.3). Human samples were classified as described in section 2.1.2.1. BMD-macrophages and BMD-microglia were stimulated (acute or chronic) with 2 µg/mL LPS and 10 ng/mL IFNγ, as described in section 2.1.2.6, or were non-stimulated. Neuronal cultures were differentiated by spontaneous differentiation (section 2.1.3.1) from wild-type ReNcell VM (section 2.1.1.3), ReNcell VM+*HTT* exon 1 (29/71/129 CAG or eGFP reporter only; sections 3.5.2 and 3.5.2.1) or ReNcell VM+full-length *mHTT* (138 CAG C8; sections 3.5.3 and 3.5.3.1) NSCs. Co-culture was performed by transfer of conditioned medium from myeloid cell cultures to neuronal cultures (section 2.1.4.2), and conditioned medium was collected and prepared as described in section 2.1.4.1. In some experiments, neuronal cultures were treated directly with cytokines; Recombinant Human IL-6 Protein [R&D Systems] and Recombinant Human TNF-alpha Protein [R&D Systems]. Following treatment with myeloid cell-conditioned medium or cytokines, neuronal death was analysed by LDH cytotoxicity assay (section 2.6.1). Conditioned medium content analysis was performed by MSD assay (section 2.5.6.2) for cytokines and ELISA (section 2.5.6.1) for neurotrophins. Where cytokine or neurotrophin levels are normalised to total protein, total protein levels were measured using BCA assay (section 2.4.2.2) in myeloid cell lysates which were prepared as described in section 2.1.4.1. Statistical analyses were performed as described in section 2.9.

4.4 Contributions

I, Lucianne Dobson performed all the work described in this chapter. No contributions were made by others.

4.5 Results

4.5.1 Effects of BMD-macrophage released factors on neuronal death in a co-culture model of HD

LPS-stimulation of myeloid cells *in vitro* triggers a range of intracellular processes leading to the release of soluble factors into the culture media. Some factors may be released immediately e.g. ROS and RNS, whilst proteins requiring modification or assembly may take longer e.g. cytokine pro-proteins, and expression and release of new proteins can take even longer still. Following the activation phase comes resolution of the immune response and any potential long-term phenotypic changes, or death. In order to capture released factors at each of these response phases, BMD-macrophages were subjected to acute stimulation, or were non-stimulated, and conditioned medium was collected over a time-course. Healthy volunteer, pre-manifest HD and manifest HD BMD-macrophages were stimulated with 2 µg/mL LPS and 10 ng/mL IFNγ, or were not stimulated, for 1 h then given a fresh medium change. Mφ-CM was collected at 2, 4, 8 and 24 h post-acute stimulation (or post-medium change for non-stimulated conditions) and was used to treat wild-type ReNcell VM neuronal cultures for 4 days. Neuronal culture death levels were then analysed by LDH cytotoxicity assay, and results are presented in Figure 4.1.

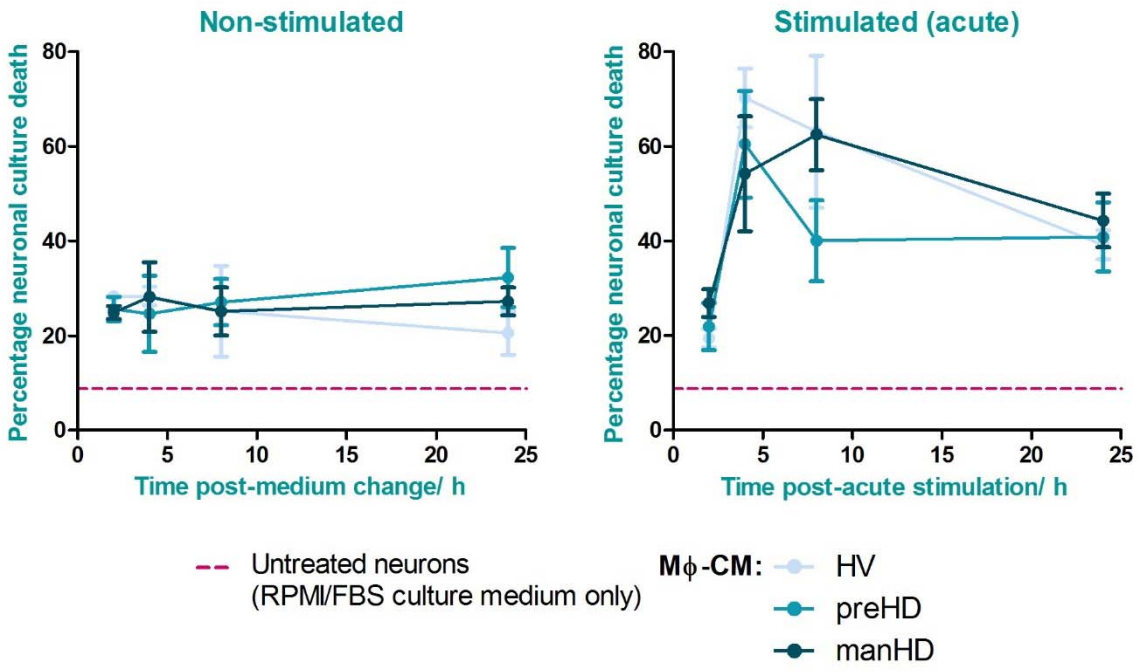

Figure 4.1: Effects of healthy volunteer and HD patient BMD-macrophage acute stimulation over time on wild-type neuronal survival

Healthy volunteer (HV; n=6), pre-manifest HD (preHD; n=5) and manifest HD (manHD; n=9) BMD-macrophage cultures were stimulated with 2 µg/mL LPS and 10 ng/mL IFNγ, or were not stimulated, for 1 h. Cultures were then given a fresh culture medium change into standard BMD-

macrophage culture medium (RPMI/FBS) and Mφ-CM was collected at 2, 4, 8 and 24 h post-acute stimulation (stimulated conditions) or post-medium change (non-stimulated conditions). Wild-type ReNcell VM neuronal cultures (6 DD) were treated with Mφ-CM, in triplicate, for 4 days, or were untreated. Neuronal culture death was then analysed by LDH cytotoxicity assay and results are presented as mean average percentage neuronal culture death (calculated as described in section 2.6.1 with total LDH calculated from 3 neuronal cultures in RPMI/FBS culture medium only (untreated)) from biological repeats, each with three internal experimental replicates, ± SEM. Percentage cell death of untreated neuronal cultures is marked with purple, dashed lines. Data were statistically analysed using two-way ANOVA: for non-stimulated conditions neither Mφ-CM subject group ($p=0.921$) or time post-medium change ($p=0.994$) were found to be significant sources of variation in percentage neuronal culture death ($p>0.05$); in stimulated conditions Mφ-CM subject group was not a significant source of variation ($p=0.544$) but time post-acute stimulation was a significant source of variation ($p<0.001$) in percentage neuronal culture death. Bonferroni post-tests did not reveal any significant differences ($p>0.05$) between any of the Mφ-CM subject groups at any of the time-points in either non-stimulated or stimulated conditions.

Results showed an increase in wild-type neuronal culture death following all non-stimulated and stimulated (acute) Mφ-CM treatment conditions compared with untreated. This indicates that Mφ-CM treatments were neurotoxic. Treatment of wild-type neurons with Mφ-CM from BMD-macrophages which had been subjected to acute stimulation resulted in significant variation in percentage neuronal culture death, and this was not found in the non-stimulated condition. Neuronal death at 2 h post-acute stimulation was similar to non-stimulated (approximately 20-25 %), but then neuronal death increased over two-fold at 4-8 h post-acute stimulation (approximately 50-70 %) before declining again at 24 h (to approximately 40-45 %). This suggests that in response to acute stimulation with LPS and IFNγ, BMD-macrophages release factors which increase in neurotoxicity over time, followed by a phase of resolution and decrease in neurotoxicity. Mφ-CM collected at 4 and 8 h post-acute stimulation was the most neurotoxic. There were no significant differences between healthy volunteer and HD Mφ-CM subject groups at any of the time-points.

To determine the effects of healthy volunteer or HD patient BMD-macrophage released factors on HD neurons, wild-type ReNcell VM and ReNcell VM+full-length *mHTT* (138 CAG) HD neuronal cultures were treated, in parallel, with Mφ-CM for 24 h. Mφ-CM had been collected from healthy volunteer, pre-manifest HD and manifest HD BMD-macrophages which had been subjected to acute stimulation, or were non-stimulated, at 2, 4, 8 and 24 h post-acute stimulation or post-medium change. Neuronal culture death levels were analysed by LDH cytotoxicity assay and results are displayed in Figure 4.2.

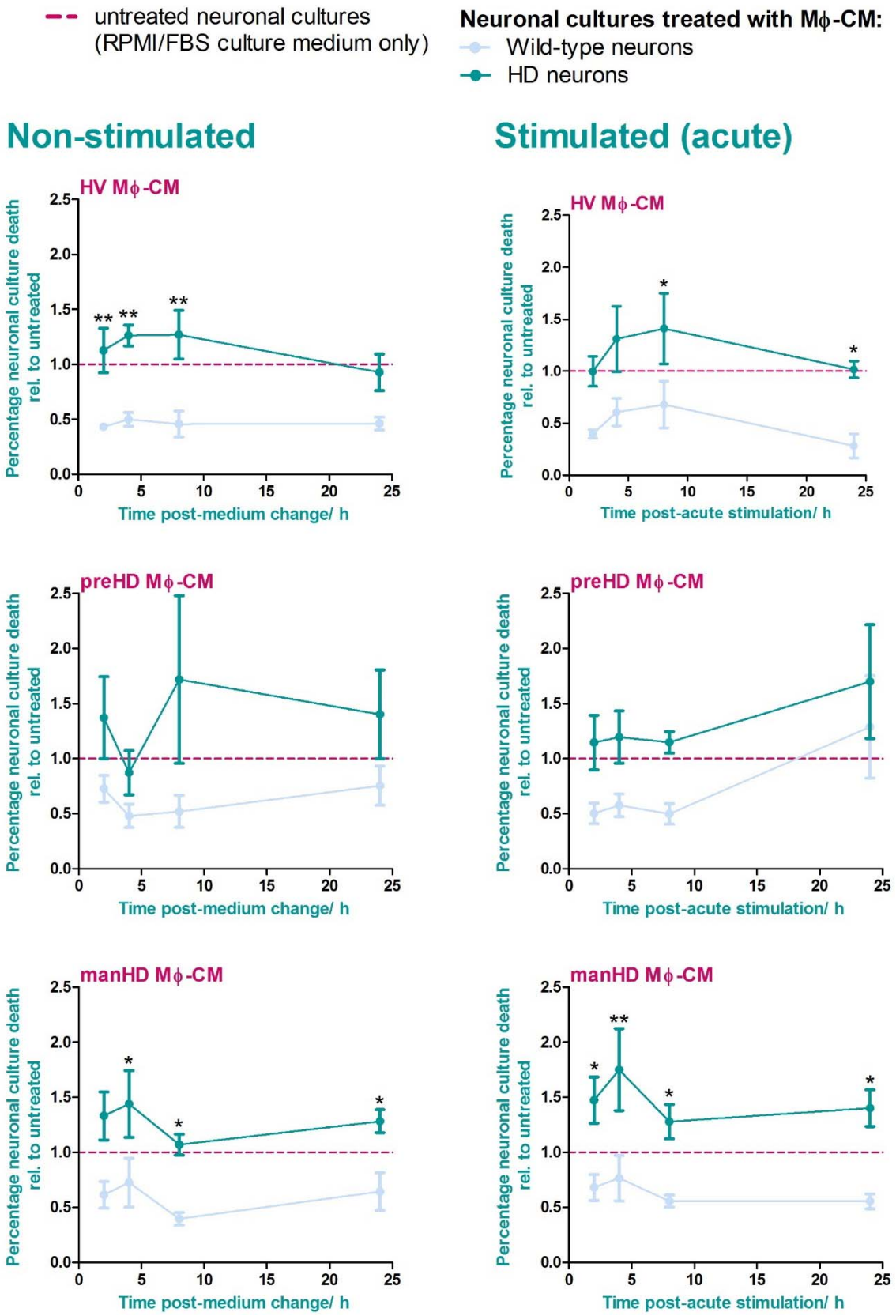

Figure 4.2: Wild-type versus HD neuronal culture death following treatment with Mφ-CM

Healthy volunteer (HV; n=5), pre-manifest HD (preHD; n=4) and manifest HD (manHD; n=8) BMD-macrophage cultures were stimulated with 2 µg/mL LPS and 10 ng/mL IFNγ, or were not stimulated, for 1 h. Cultures were then given a fresh culture medium change into standard BMD-

*macrophage culture medium (RPMI/FBS) and Mφ-CM was collected at 2, 4, 8 and 24 h post-acute stimulation (stimulated conditions) or post-medium change (non-stimulated conditions). Wild-type ReNcell VM and ReNcell VM+full-length mHTT (138 CAG) HD neuronal cultures (10 DD) were treated with Mφ-CM, in triplicate, for 24 h, or were untreated. Neuronal culture death was then analysed by LDH cytotoxicity assay and results are presented as mean average percentage wild-type or HD neuronal culture death (calculated as described in section 2.6.1) relative to untreated wild-type or HD neuronal culture death, respectively, from biological repeats, each with three internal experimental replicates, ± SEM. Data were statistically analysed using two-way ANOVA with Bonferroni post-tests; *p<0.05, **p<0.01.*

Neuronal culture type (wild-type versus HD) was found to be a significant source of variation in neuronal culture death relative to untreated, independent of time-point, following all Mφ-CM treatments over the time-course: non-stimulated healthy volunteer (p<0.0001), pre-manifest HD (p=0.022) and manifest HD (p<0.0001) Mφ-CM treatments; and stimulated (acute) healthy volunteer (p<0.0001), pre-manifest HD (p=0.0073) and manifest HD (p<0.0001) Mφ-CM treatments. HD neuronal culture death relative to untreated was significantly higher than wild-type neuronal culture death relative to untreated following 24 h treatment with Mφ-CM from healthy volunteer BMD-macrophages at 2, 4 and 8 h time-points and manifest HD BMD-macrophages at 4, 8, and 24 h time-points, in non-stimulated conditions; and healthy volunteer BMD-macrophages at 8 and 24 h time-points and manifest HD BMD-macrophages at 2, 4, 8 and 24 h time-points, in acute stimulation conditions. Pre-manifest HD Mφ-CM treatments did not significantly affect HD neuronal culture death compared with wild-type neuronal culture death at any individual time-point in non-stimulated or stimulated (acute) conditions. HD neuronal culture death levels were generally higher following Mφ-CM treatments compared with untreated, whereas wild-type neuronal culture death levels were generally lower than untreated after Mφ-CM treatments. Taken together, these results indicate that Mφ-CM treatments have a neurotoxic effect in HD neurons which leads to significantly more neuronal culture death in HD neuronal cultures compared with wild-type neuronal cultures. Overall, there were no significant differences found between healthy volunteer and pre-manifest HD or manifest HD Mφ-CM treatments on wild-type or HD neuronal culture death, in non-stimulated or stimulated (acute) conditions, over the time-course.

4.5.2 Effects of BMD-microglia released factors on neuronal death in a co-culture model of HD

4.5.2.1 Acute stimulation of BMD-microglia in co-culture

The acute stimulation time-course co-culture paradigm described above for BMD-macrophages was repeated with BMD-microglia and wild-type neurons. Healthy volunteer and manifest HD BMD-microglia were stimulated with 2 µg/mL LPS and 10 ng/mL IFNγ, or were not stimulated, for 1 h then given a fresh medium change. MG-CM was collected at 2, 4, 8, 24 and 48 h post-acute stimulation (or post-medium change for non-stimulated conditions) and was used to treat wild-type ReNcell VM neuronal cultures for 24 h. Neuronal culture death levels were then analysed by LDH cytotoxicity assay, and results are presented in Figure 4.3. Neither MG-CM subject group or time post-medium change/post-acute stimulation were significant sources of variation in non-stimulated or stimulated conditions (p>0.05). There were no significant differences between any of the MG-CM subject groups at any of the time-points in either non-stimulated or stimulated conditions (p>0.05).

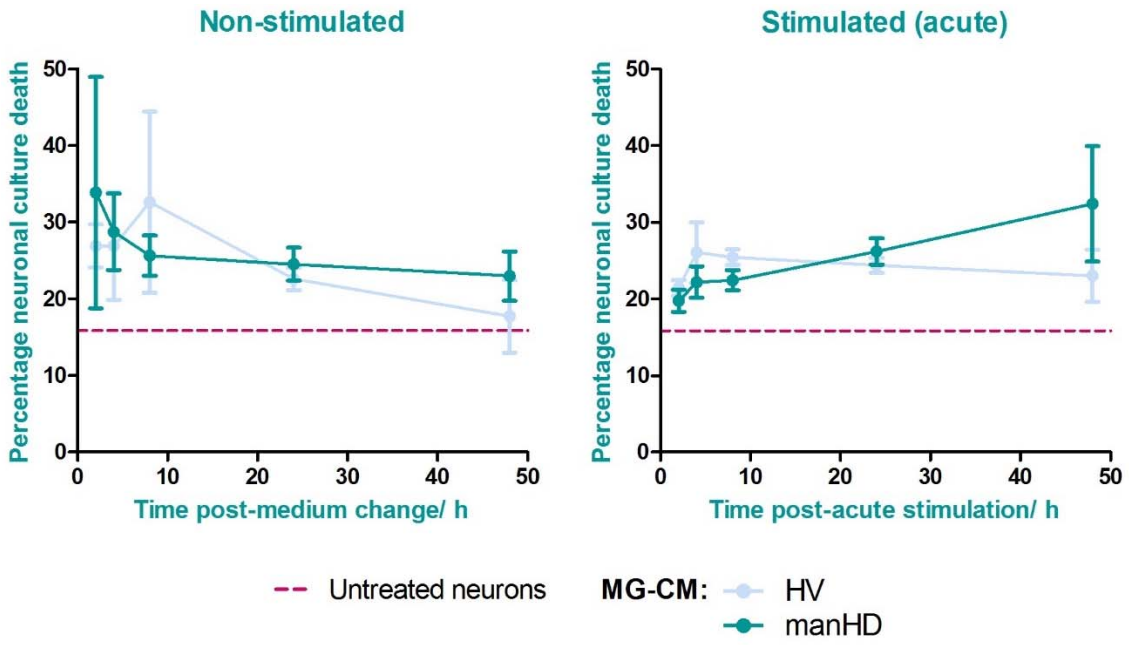

Figure 4.3: Effects of healthy volunteer and HD patient BMD-microglia acute stimulation over time on wild-type neuronal survival

Healthy volunteer (HV; n=3) and manifest HD (manHD; n=4) BMD-microglia cultures were stimulated with 2 µg/mL LPS and 10 ng/mL IFNγ, or were not stimulated, for 1 h. Cultures were then given a fresh culture medium change into standard BMD-microglia culture medium (NM) and MG-CM was collected at 2, 4, 8, 24 and 48 h post-acute stimulation (stimulated conditions) or post-medium change (non-stimulated conditions). Wild-type ReNcell VM neuronal cultures (18 DD) were treated with MG-CM, in triplicate, for 24 h, or were untreated. Neuronal culture death was then analysed by LDH cytotoxicity assay and results are presented as mean average

percentage neuronal culture death (calculated as described in section 2.6.1) from biological repeats, each with three internal experimental replicates, ± SEM. Percentage cell death of untreated neuronal cultures is marked with purple, dashed lines. Data were statistically analysed using two-way ANOVA with Bonferroni post-tests.

4.5.2.2 Chronic stimulation of BMD-microglia in co-culture

A chronic stimulation paradigm, more closely modelling the neuroinflammatory environment in the degenerating HD brain, was then assessed in BMD-microglia in co-culture with wild-type or HD neurons. Healthy volunteer, pre-manifest HD and manifest HD BMD-microglia were stimulated continuously with 2 µg/mL LPS and 10 ng/mL IFNγ, or were not stimulated. MG-CM was collected after 2, 4, 8, 24 and 48 h chronic stimulation (stimulated conditions) or post-medium change (non-stimulated conditions). MG-CM was then used to treat wild-type ReNcell VM and ReNcell VM+full-length *mHTT* (138 CAG) HD neuronal cultures, in parallel, for 24 h. Neuronal culture death after treatments was analysed by LDH cytotoxicity assay, and results are displayed in Figure 4.4.

MG-CM subject group was found to be a significant source of variation in wild-type neuronal culture death in non-stimulated conditions (p=0.040). Manifest HD MG-CM treatment resulted in significantly reduced neuronal culture death, below untreated levels, compared to healthy volunteer MG-CM at the 24 h time-point (p<0.05), and compared to pre-manifest HD MG-CM at the 48 h time-point (p<0.05). This suggests that MG-CM from non-stimulated manifest HD BMD-microglia is neuroprotective in co-culture with wild-type neurons. MG-CM subject group was not a significant source of variation (p>0.05) in wild-type neuronal culture death in stimulated (chronic) conditions, nor in HD neuronal culture death in non-stimulated or stimulated (chronic) conditions.

Duration of chronic stimulation was a significant source of variation in wild-type (p=0.007) and HD (p=0.001) neuronal culture death, and time post-medium change was not a significant source of variation in non-stimulated conditions (p>0.05). Chronic stimulation conditions showed trends for increased neuronal culture death over time, above untreated levels, indicating that chronic stimulation of BMD-microglia may lead to release of factors which increase in neurotoxicity over time.

Neuronal culture type (wild-type versus HD) was a significant source of variation in neuronal culture death following treatment with non-stimulated manifest HD MG-CM (p=0.003) or stimulated (chronic) healthy volunteer MG-CM (p=0.020). Both conditions resulted in a trend for lower death levels in wild-type neuronal cultures compared with HD neuronal cultures, indicating that these MG-CM treatments were more protective to wild-type neurons and/or more toxic to HD neurons.

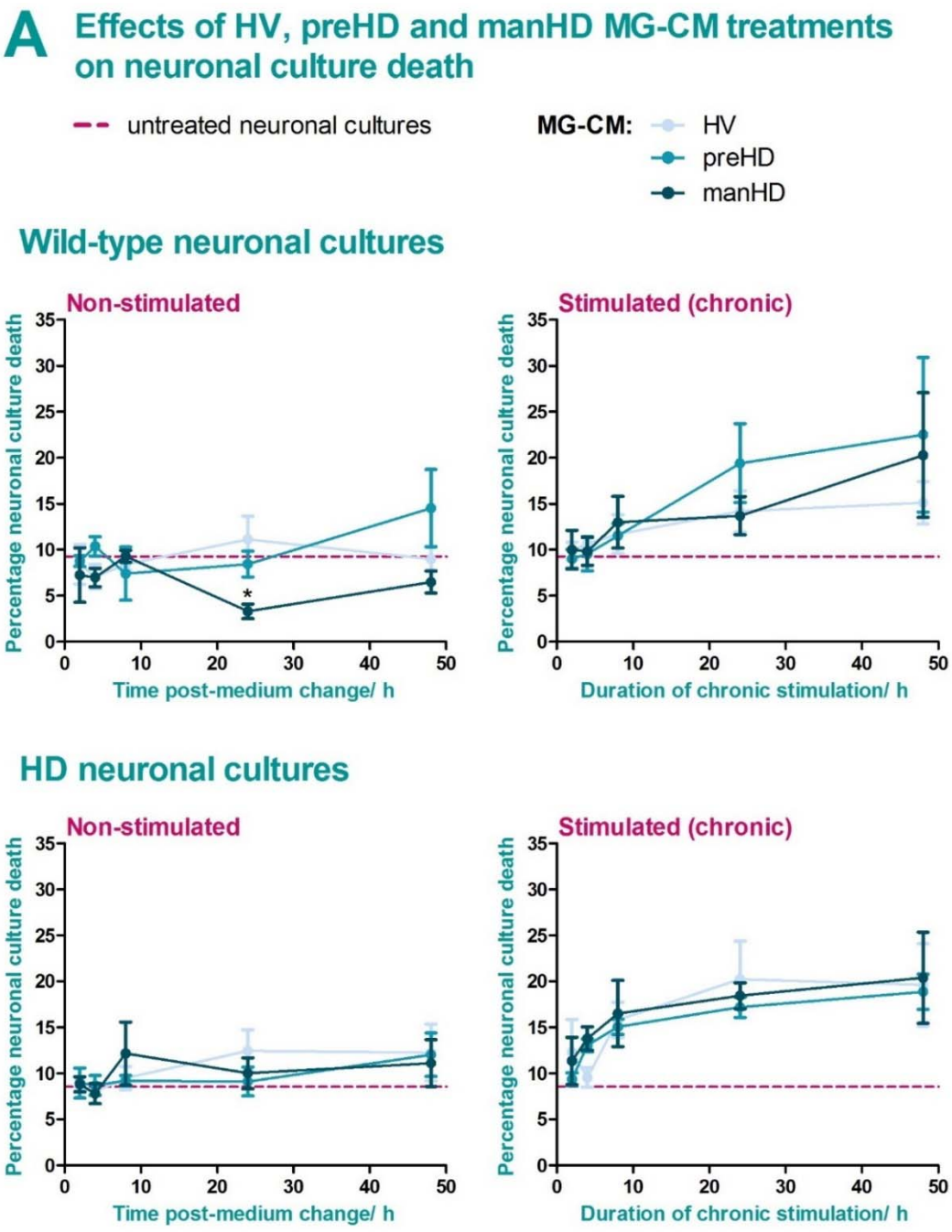
A
Effects of HV, preHD and manHD MG-CM treatments on neuronal culture death
untreated neuronal cultures
MG-CM:
HV
preHD
manHD
Wild-type neuronal cultures
Non-stimulated
Stimulated (chronic)
HD neuronal cultures
Non-stimulated
Stimulated (chronic)
Percentage neuronal culture death
Time post-medium change/ h
Duration of chronic stimulation/ h
*

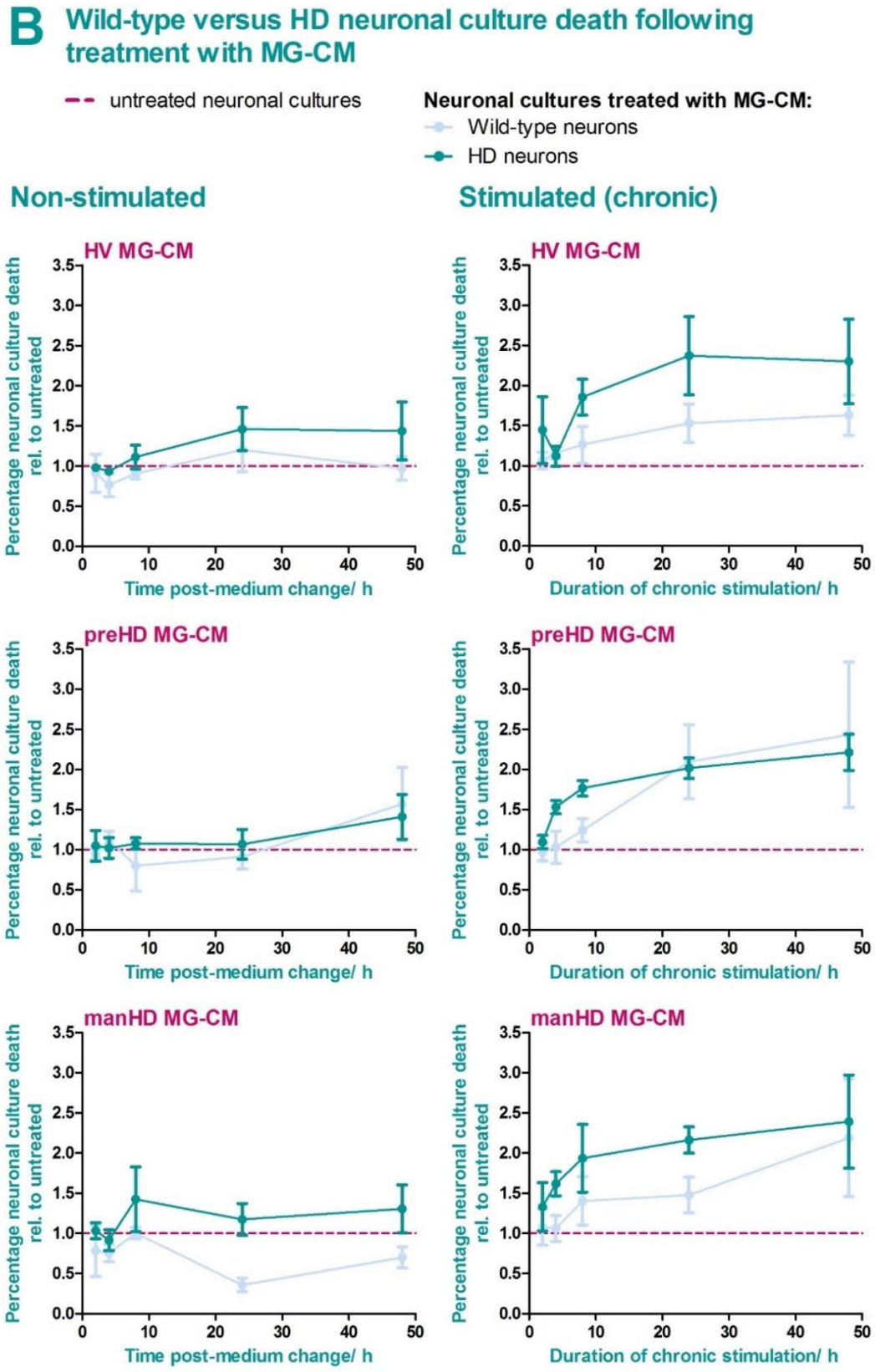

Figure 4.4: Effects of healthy volunteer, pre-manifest HD and manifest HD BMD-microglia chronic stimulation over time on wild-type and HD neuronal survival

Healthy volunteer (HV; n=3), pre-manifest HD (preHD; n=3) and manifest HD (manHD; n=3) BMD-microglia cultures were stimulated continuously with 2 µg/mL LPS and 10 ng/mL IFNγ, or

*were not stimulated, and MG-CM was collected at 2, 4, 8, 24 and 48 h chronic stimulation (stimulated conditions) or post-medium change (non-stimulated conditions). Wild-type ReNcell VM and ReNcell VM+full-length mHTT (138 CAG) HD neuronal cultures (10 DD) were treated with MG-CM, in duplicate, for 24 h, or were untreated. Neuronal culture death was then analysed by LDH cytotoxicity assay and results are presented as mean average percentage neuronal culture death (A) (calculated as described in section 2.6.1) or mean average percentage neuronal culture death relative to untreated (B) from biological repeats, each with three internal experimental replicates, ± SEM. Results are presented as comparisons of the effects of healthy volunteer, pre-manifest HD and manifest HD MG-CM treatments on neuronal culture death (**A**) and comparisons of wild-type and HD neuronal culture death in response to MG-CM treatments (**B**). Percentage cell death of untreated neuronal cultures is marked with purple, dashed lines. Data were statistically analysed using two-way ANOVA with Bonferroni post-tests.*

Differences between the effects of MG-CM treatments on wild-type neuronal culture death had begun to appear at 24 and 48 h time-points in non-stimulated and stimulated (chronic) conditions, and there was some evidence that the effects of MG-CM treatments on neuronal culture death could be different in wild-type and HD neurons at 24 and 48 h time-points in non-stimulated and stimulated (chronic) conditions (Figure 4.4). It is possible that significance was not reached in some cases due to the high level of variability in the data, and this was most likely introduced by use of human samples. To ensure that the null hypotheses (that there is no difference in the average values at 24 or 48 h time-points) were not incorrectly accepted, or rejected, power calculations were performed (as described in detail in section 2.9.4) to determine appropriate sample sizes. Test values were taken from 24 and 48 h time-point data comparing the effects of healthy volunteer, pre-manifest HD and manifest HD MG-CM on wild-type neuronal death in non-stimulated and stimulated (chronic) conditions (Figure 4.4; A) and used to calculate minimum sample sizes required to detect effect differences, or accept the null hypothesis. Results of these analyses are presented in Table 4.1.

Table 4.1: Sample size calculations for wild-type neuron-BMD-microglia co-culture experiments

Test condition	Test value	Sample condition	Sample mean	SD for sample	α-error level	β-error level	Sample size (*n*)
Wild-type neurons treated with *non-stimulated* MG-CM							
untreated	9.26	HV; 24 h	11.13	4.35	5 %	50 %	15
untreated	9.26	preHD; 24 h	8.44	2.44	5 %	50 %	24
untreated	9.26	manHD; 24 h	3.30	1.38	5 %	50 %	0
untreated	9.26	HV; 48 h	9.00	2.32	5 %	50 %	215

untreated	9.26	preHD; 48 h	14.52	7.28	5 %	50 %	5
untreated	9.26	manHD; 48 h	6.48	2.08	5 %	50 %	2
HV; 24 h	11.13	preHD; 24 h	8.44	2.44	5 %	50 %	2
HV; 24 h	11.13	manHD; 24 h	3.3	1.38	5 %	50 %	0
preHD; 24 h	8.44	HV; 24 h	11.13	4.35	5 %	50 %	7
preHD; 24 h	8.44	manHD; 24 h	3.30	1.38	5 %	50 %	0
manHD; 24 h	3.30	HV; 24 h	11.13	4.35	5 %	50 %	1
manHD; 24 h	3.30	preHD; 24 h	8.44	2.44	5 %	50 %	1
HV; 48 h	9.00	preHD; 48 h	14.52	7.28	5 %	50 %	5
HV; 48 h	9.00	manHD; 48 h	6.48	2.08	5 %	50 %	2
preHD; 48 h	14.52	HV; 48 h	9.00	2.32	5 %	50 %	0
preHD; 48 h	14.52	manHD; 48 h	6.48	2.08	5 %	50 %	0
manHD; 48 h	6.48	HV; 48 h	9.00	2.32	5 %	50 %	2
manHD; 48 h	6.48	preHD; 48 h	14.52	7.28	5 %	50 %	2
Wild-type neurons treated with *stimulated (chronic)* MG-CM							
untreated	9.26	HV; 24 h	14.17	3.87	5 %	50 %	2
untreated	9.26	preHD; 24 h	19.40	7.44	5 %	50 %	1
untreated	9.26	manHD; 24 h	13.69	3.59	5 %	50 %	2
untreated	9.26	HV; 48 h	15.10	3.99	5 %	50 %	1
untreated	9.26	preHD; 48 h	22.51	14.56	5 %	50 %	3
untreated	9.26	manHD; 48 h	20.28	11.75	5 %	50 %	3
HV; 24 h	14.17	preHD; 24 h	19.40	7.44	5 %	50 %	5
HV; 24 h	14.17	manHD; 24 h	13.69	3.59	5 %	50 %	151
preHD; 24 h	19.40	HV; 24 h	14.17	3.87	5 %	50 %	1
preHD; 24 h	19.40	manHD; 24 h	13.69	3.59	5 %	50 %	1
manHD; 24 h	13.69	HV; 24 h	14.17	3.87	5 %	50 %	176
manHD; 24 h	13.69	preHD; 24 h	19.40	7.44	5 %	50 %	5
HV; 48 h	15.10	preHD; 48 h	22.51	14.56	5 %	50 %	10
HV; 48 h	15.10	manHD; 48 h	20.28	11.75	5 %	50 %	14
preHD; 48 h	22.51	HV; 48 h	15.10	3.99	5 %	50 %	1
preHD; 48 h	22.51	manHD; 48 h	20.28	11.75	5 %	50 %	75
manHD; 48 h	20.28	HV; 48 h	15.10	3.99	5 %	50 %	2
manHD; 48 h	20.28	preHD; 48 h	22.51	14.56	5 %	50 %	115

Healthy volunteer, HV, pre-manifest HD gene carrier, preHD; manifest HD patient, manHD

The pre-manifest HD group was the most variable, having a higher SD than healthy volunteer and manifest HD groups in all conditions (non-stimulated and stimulated at 24 and 48 h). Comparisons between pre-manifest HD and healthy volunteer or manifest HD MG-CM treatments therefore require a larger sample size than other MG-CM treatment comparisons. For non-stimulated conditions, the sample size requirements had already been met (n=3) for most comparisons of MG-CM treatments.

Exceptions were healthy volunteer versus pre-manifest HD MG-CM at 24 and 48 h. In stimulated (chronic) conditions, several comparisons required a larger sample size than *n*=3 for appropriate statistical power. As a result, sample size was increased to compare healthy volunteer versus manifest HD MG-CM in stimulated (chronic) conditions at 24 and 48 h time-points (Figure 4.5; A). Non-stimulated conditions were run alongside to assess the effects of chronic stimulation of BMD-microglia on neuronal death (Figure 4.5; B).

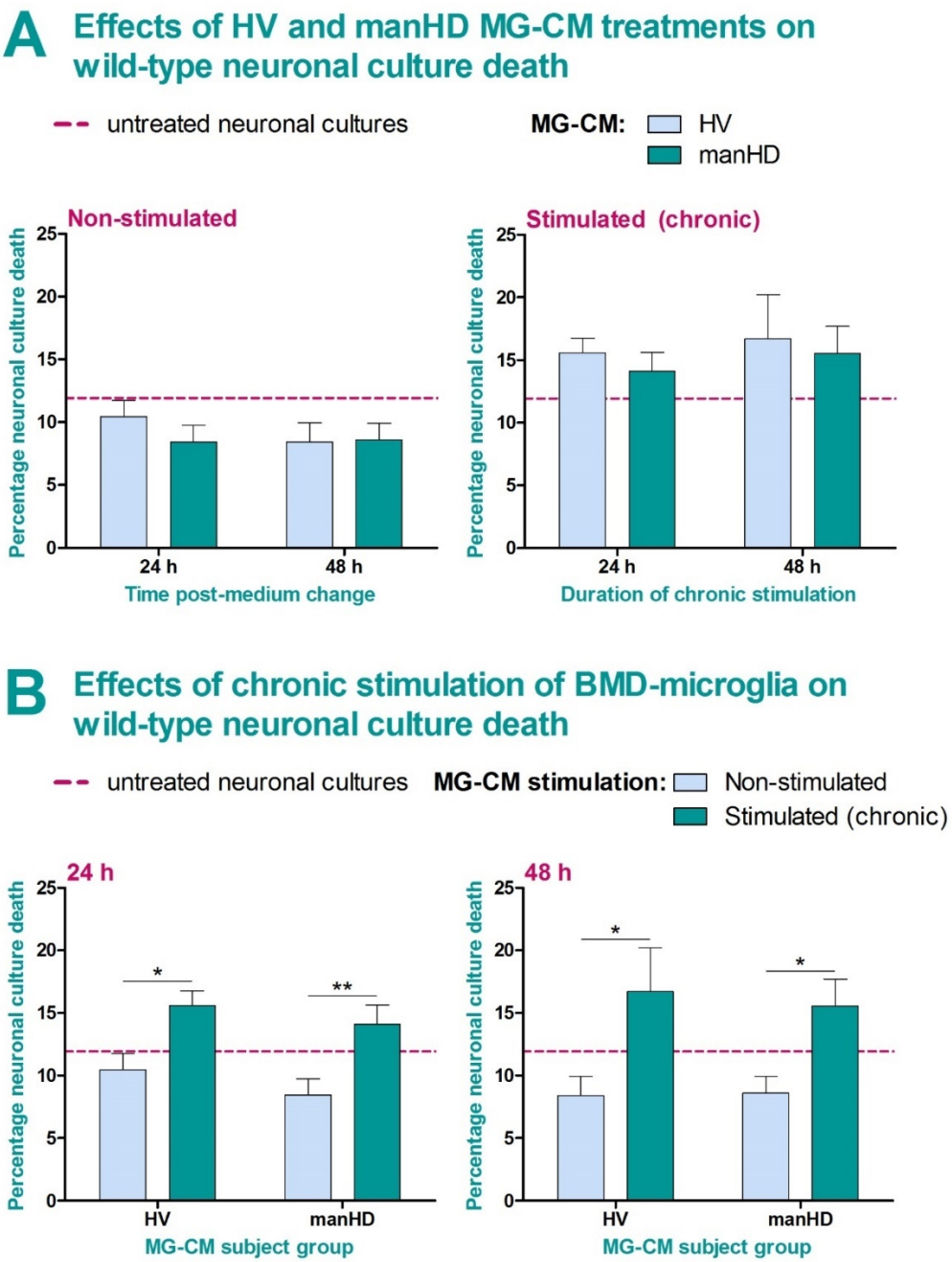

Figure 4.5: Effects of chronic stimulation of healthy volunteer versus manifest HD MG-CM on wild-type neuronal survival, at 24 and 48 h stimulation

Healthy volunteer (HV; n=12) and manifest HD (manHD; n=16) BMD-microglia cultures were stimulated continuously with 2 µg/mL LPS and 10 ng/mL IFNγ, or were not stimulated, and MG-

*CM was collected at 24 and 48 h chronic stimulation (stimulated conditions) or post-medium change (non-stimulated conditions). Wild-type ReNcell VM neuronal cultures (10 DD) were treated with MG-CM, in duplicate, for 24 h, or were untreated. Neuronal culture death was then analysed by LDH cytotoxicity assay and results are presented as mean average percentage neuronal culture death (calculated as described in section 2.6.1) from biological repeats, each with three internal experimental replicates, ± SEM. Results are presented as comparisons of the effects of healthy volunteer and manifest HD MG-CM treatments on neuronal culture death (**A**) and comparisons of the effects of non-stimulated and stimulated MG-CM treatments on neuronal culture death (**B**). Percentage cell death of untreated neuronal cultures is marked with purple, dashed lines. Data were statistically analysed using two-way ANOVA with Bonferroni post-tests: *p<0.05, **p<0.01.*

There were no significant differences (p>0.05) between the effects of healthy volunteer and manifest HD MG-CM treatments on wild-type neuronal culture death in non-stimulated or stimulated conditions at 24 or 48 h post-medium change or chronic stimulation. However, stimulation was a significant source of variation at both 24 h (p=0.0003) and 48 h (p=0.001) time-points, and treatment of wild-type neuronal cultures with stimulated MG-CM resulted in significantly higher death than treatment with non-stimulated MG-CM for both healthy volunteer (p<0.05 at 24 and 48 h) and manifest HD (p<0.01 at 24 h and p<0.05 at 48 h) subject groups. Non-stimulated healthy volunteer and manifest HD MG-CM treatments resulted in average death levels below untreated, and stimulated healthy volunteer and manifest HD MG-CM treatments resulted in average death levels above untreated. This suggests that chronic stimulation of BMD-microglia for 24 or 48 h leads to the release of neurotoxic factors, but the effects this has on wild-type neuronal culture death does not differ between healthy volunteer and manifest HD BMD-microglia.

4.5.2.3 BMD-microglia in co-culture with ReNcell VM+HTT exon 1 neurons

To further investigate the effects of microglia-released factors on HD neuronal death, co-culture was performed with BMD-microglia and ReNcell VM+*HTT* exon 1 neuronal cultures. Healthy volunteer and manifest HD BMD-microglia were stimulated continuously with 2 µg/mL LPS and 10 ng/mL IFNγ (chronic stimulation), or were not stimulated, for 24 h or 48 h. MG-CM was used to treat ReNcell VM+*HTT* exon 1 (29 CAG), ReNcell VM+*mHTT* exon 1 (71 CAG), ReNcell VM+*mHTT* exon 1 (129 CAG) and ReNcell VM+eGFP reporter only neuronal cultures, in parallel, for 24 h. Neuronal culture death was then analysed by LDH cytotoxicity assay and results are presented in Figure 4.6.

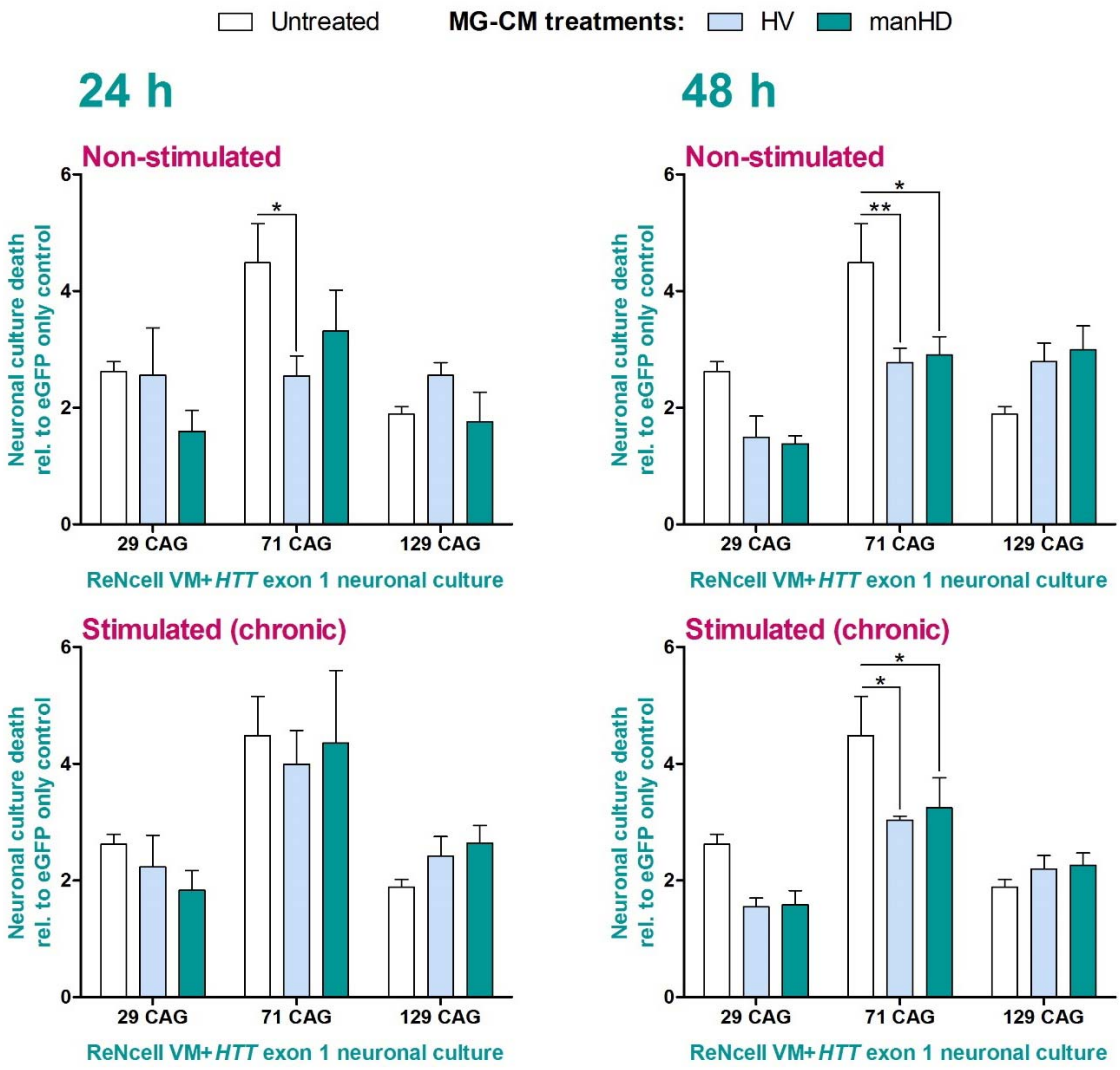

Figure 4.6: Effects of healthy volunteer and HD patient MG-CM treatments on ReNcell VM+*HTT* exon 1 non-HD and HD neuronal culture death

*Healthy volunteer (HV; n=4) and manifest HD (manHD; n=4) BMD-microglia cultures were stimulated continuously with 2 µg/mL LPS and 10 ng/mL IFNγ, or were not stimulated, and MG-CM was collected at 24 and 48 h chronic stimulation (stimulated conditions) or post-medium change (non-stimulated conditions). ReNcell VM+HTT exon 1 (29 CAG), ReNcell VM+mHTT exon 1 (71 CAG), ReNcell VM+mHTT exon 1 (129 CAG) and ReNcell VM+eGFP reporter only neuronal cultures (28 DD) were treated with MG-CM, in duplicate, for 24 h, or were untreated. Neuronal culture death was then analysed by LDH cytotoxicity assay and results are presented as mean average neuronal culture death (calculated as described in section 2.6.1) relative to untreated eGFP reporter only control neuronal culture death (baseline neuronal culture death levels), from biological repeats, each with three internal experimental replicates, ± SEM. Data were statistically analysed using two-way ANOVA with Bonferroni post-tests; *p<0.05, **p<0.01.*

Neuronal culture type (ReNcell VM+*HTT* exon 1 with 29 CAG, 71 CAG or 129 CAG) was a significant source of variation in neuronal culture death levels in non-stimulated MG-CM conditions (p=0.007 at 24 h time-point and p<0.0001 at 48 h time-point) or

stimulated MG-CM conditions (p=0.0005 at 24 h time-point and p<0.0001 at 48 h time-point). This indicates that expression of *HTT* exon 1 with 29 CAG, 71 CAG or 129 CAG in ReNcell VM neuronal cultures leads to differential effects on neuronal culture death levels, independent of MG-CM treatment conditions, and *HTT* exon 1 71 CAG had higher neuronal death than *HTT* exon 1 29 CAG or 129 CAG. MG-CM treatment (untreated, healthy volunteer MG-CM or manifest HD MG-CM) was also a significant source of variation in neuronal culture death levels in the 48 h stimulated condition (p=0.021), indicating that untreated neuronal cultures or neuronal cultures treated with 48 h stimulated MG-CM from healthy volunteers or HD patients had differential effects on neuronal culture death levels, independent of neuronal culture type. The interaction between MG-CM treatments and neuronal culture type was a significant source of variation in neuronal culture death levels in the 48 h non-stimulated condition (p=0.003), indicating that different MG-CM treatments had differential effects on different neuronal culture types in this condition.

There were no significant differences between the effects of healthy volunteer and HD patient MG-CM treatments on neuronal culture death levels in ReNcell VM+*HTT* exon 1 with 29 CAG, 71 CAG or 129 CAG, in non-stimulated or stimulated conditions. Neither healthy volunteer or HD patient MG-CM treatments altered neuronal culture death levels from untreated levels in ReNcell VM+*HTT* exon 1 (29 CAG) or ReNcell VM+*HTT* exon 1 (129 CAG) neuronal cultures. In ReNcell VM+*HTT* exon 1 (71 CAG) neuronal cultures, however, MG-CM treatments had variable effects, depending on the condition, on reducing neuronal culture death levels compared with untreated. At the 24 h time-point, in non-stimulated conditions healthy volunteer MG-CM treatment reduced ReNcell VM+*HTT* exon 1 (71 CAG) neuronal culture death levels (p<0.05) and manifest HD MG-CM treatment did not (p>0.05), suggesting that in non-stimulated conditions MG-CM from healthy volunteer BMD-microglia is neuroprotective and MG-CM from HD patient BMD-microglia is not. In stimulated conditions, neither healthy volunteer or manifest HD MG-CM treatments reduced ReNcell VM+*HTT* exon 1 (71 CAG) neuronal culture death levels (p>0.05), suggesting that MG-CM from stimulated healthy volunteer or HD patient BMD-microglia is not neuroprotective. At the 48 h time-point, both healthy volunteer and manifest HD MG-CM treatments significantly reduced ReNcell VM+*HTT* exon 1 (71 CAG) neuronal culture death levels in both non-stimulated (p<0.01 and p<0.05, respectively) and stimulated (p<0.05 for both comparisons with untreated) conditions, suggesting that MG-CM from non-stimulated or stimulated healthy volunteer or HD patient BMD-microglia is neuroprotective at this time-point.

4.5.3 Direct treatment of neurons with proinflammatory cytokines

Stimulation of myeloid cells with LPS and IFNγ triggers the production and release of cytokines, and HD patient myeloid cells release elevated levels of the proinflammatory cytokines IL-6 and TNFα in response to stimulation. To determine whether IL-6 and TNFα could contribute towards the observed neurotoxicity of BMD-macrophages and BMD-microglia following stimulation, wild-type neuronal cultures were treated directly with a range of IL-6 and TNFα concentrations, alone or in combination, for 24 h. Neuronal culture death was then analysed by LDH cytotoxicity assay and results are presented in Figure 4.7.

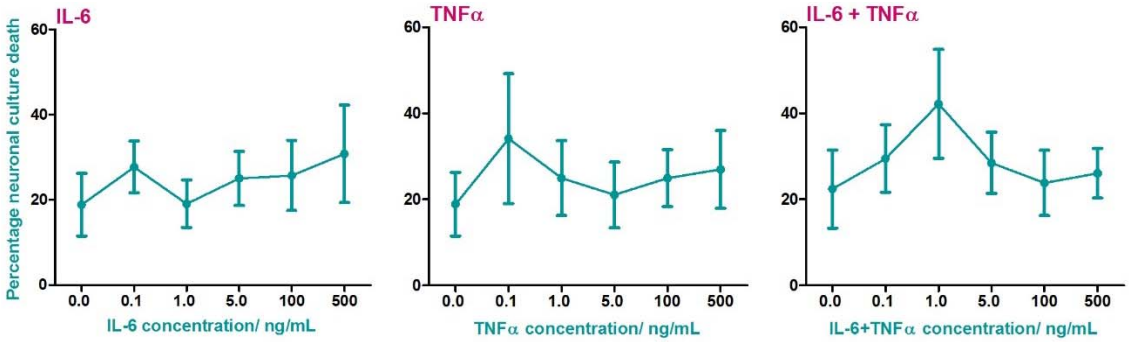

Figure 4.7: Effects of proinflammatory cytokine (IL-6 and TNFα) treatments on wild-type neuronal culture death

Wild-type ReNcell VM neuronal cultures (10 DD) were treated, in triplicate, with 0.1, 1, 5, 100 or 500 ng/mL IL-6 or TNFα or IL-6+TNFα, for 24 h, or were untreated. Neuronal culture death was then analysed by LDH cytotoxicity assay and results are presented as mean average percentage neuronal culture death (calculated as described in section 2.6.1) from 3/4 biological repeats per treatment condition, each with three internal experimental replicates, ± SEM. Data were analysed using one-way ANOVA with Dunnett's multiple comparisons tests, comparing all treatment conditions to untreated.

IL-6, TNFα or IL-6+TNFα treatments were not significant sources of variation in wild-type neuronal culture death, and no individual treatment condition resulted in significantly increased neuronal culture death compared with untreated. This suggests that the proinflammatory cytokines IL-6 and TNFα do not directly cause wild-type neuronal death, although the data was highly variable.

4.5.4 Investigation into factors released by healthy volunteer and HD patient myeloid cells

4.5.4.1 Proinflammatory cytokine release in healthy volunteer and HD patient BMD-macrophages

In section 4.5.1, treatment of neuronal cultures with Mφ-CM from non-stimulated or stimulated (acute) healthy volunteer or manifest HD BMD-macrophages was shown to result in significantly higher death levels in HD neuronal cultures compared with wild-type neuronal cultures, at several time-points post-medium change or post-acute stimulation (Figure 4.2). To assess factors which may have contributed to neurotoxicity in HD neuronal cultures in this co-culture experiment, Mφ-CM which had been collected from the same sources was analysed for proinflammatory cytokine content. Proinflammatory cytokine release in healthy volunteer, pre-manifest HD and manifest HD BMD-macrophages was compared.

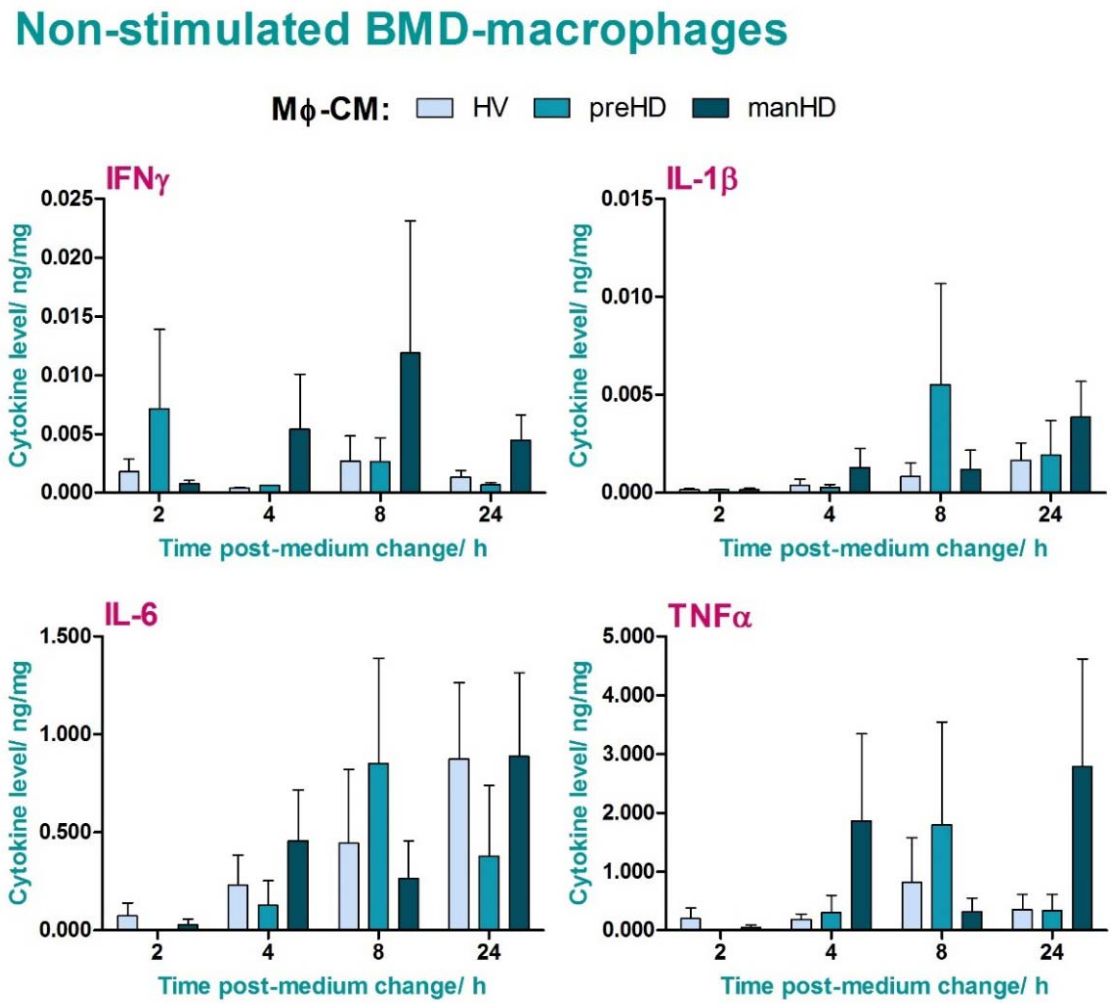

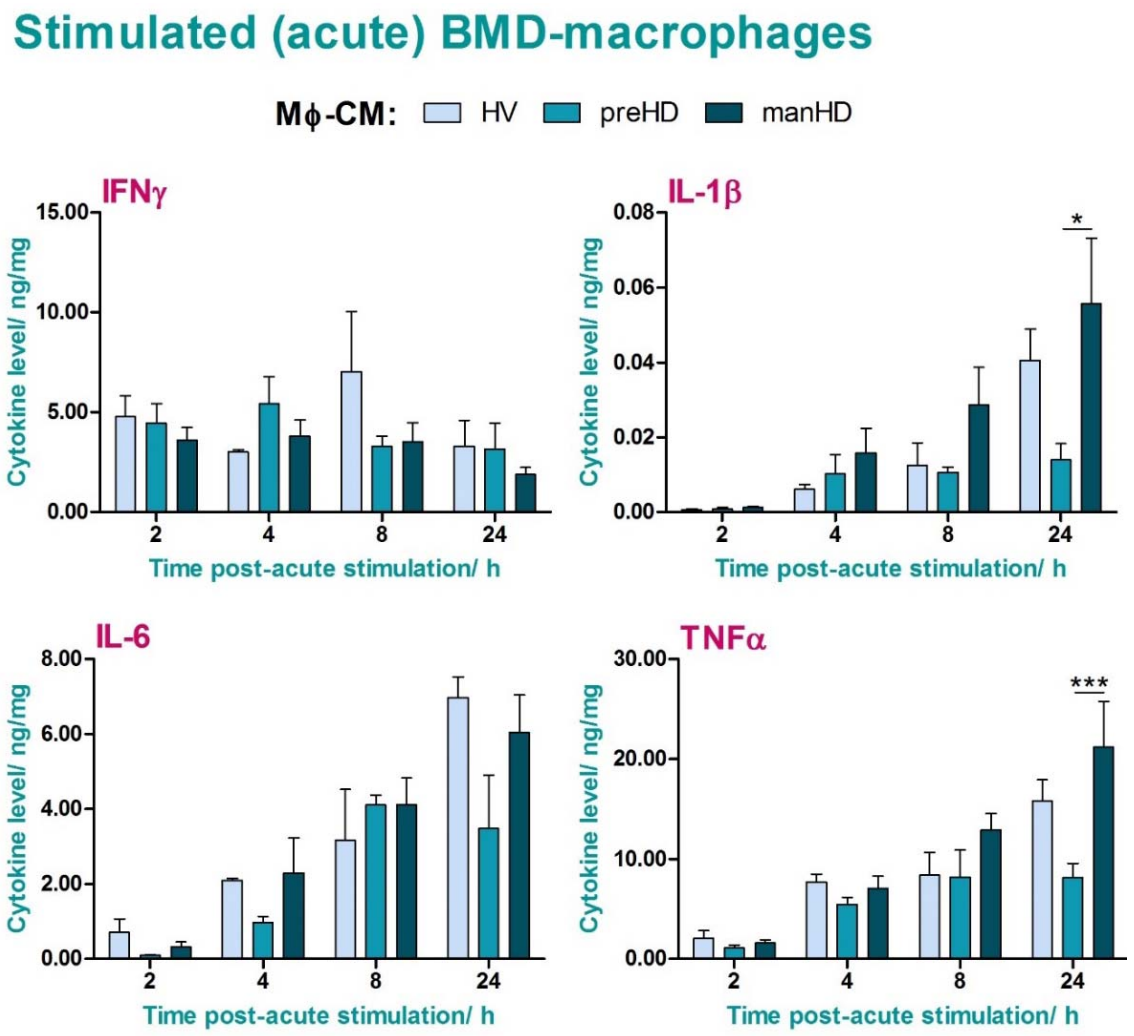

Figure 4.8: Levels of proinflammatory cytokine release in healthy volunteer, pre-manifest HD and manifest HD BMD-macrophages

*Healthy volunteer (HV; n=5), pre-manifest HD (preHD; n=4) and manifest HD (manHD; n=8) BMD-macrophage cultures were stimulated with 2 µg/mL LPS and 10 ng/mL IFNγ, or were not stimulated, for 1 h. Cultures were then given a fresh culture medium change into standard BMD-macrophage culture medium (RPMI/FBS) and Mφ-CM was collected at 2, 4, 8 and 24 h post-acute stimulation (stimulated conditions) or post-medium change (non-stimulated conditions). Cytokine levels in Mφ-CM were measured by MSD assay and normalised to total protein. Results are presented as mean average cytokine level from biological repeats, each with three internal experimental replicates, ± SEM. Data were statistically analysed using two-way ANOVA with Bonferroni post-tests; *p<0.05, ***p<0.001.*

Levels of the proinflammatory cytokines IFNγ, IL-1β, IL-6 and TNFα were measured in non-stimulated and stimulated (acute) healthy volunteer, pre-manifest HD and manifest HD Mφ-CM, over several time-points post-medium change or post-acute stimulation, using MSD assay. Results are presented in Figure 4.8. In both non-stimulated and stimulated conditions, Mφ-CM subject group was not a significant source of variation in

IFNγ, IL-1β, IL-6 or TNFα levels, indicating that healthy volunteer, pre-manifest HD and manifest HD BMD-macrophages do not release different levels of these cytokines, independent of time-point. In stimulated conditions, time post-acute stimulation was a significant source of variation in IL-1β (p=0.001), IL-6 (p<0.0001) and TNFα (p<0.0001) levels, independent of Mφ-CM subject group, and levels of these proinflammatory cytokines increased over time. At the 24 h time-point, manifest HD Mφ-CM had higher levels of IL-1β and TNFα (p<0.05 and p<0.001, respectively) compared with pre-manifest HD Mφ-CM post-acute stimulation, indicating that manifest HD BMD-macrophages release elevated levels of IL-1β and TNFα compared with pre-manifest HD BMD-macrophages, over 24 h following acute stimulation. There were no differences between healthy volunteer and pre-manifest HD or manifest HD Mφ-CM IFNγ, IL-1β, IL-6 or TNFα levels in non-stimulated or stimulated conditions.

4.5.4.2 Th1- and Th2-type (and IL-2) cytokine release in healthy volunteer and HD patient BMD-microglia

In section 4.5.2.3, non-stimulated MG-CM from healthy volunteers was shown to reduce mHTT-induced neurotoxicity in ReNcell VM+*mHTT* exon 1 (71 CAG) neuronal cultures at 24 and 48 h time-points, and non-stimulated MG-CM from manifest HD patients reduced mHTT-induced neurotoxicity in this neuronal culture at the 48 h time-point, but not at the 24 h time-point. In stimulated (chronic) conditions, both healthy volunteer and manifest HD MG-CM treatments reduced mHTT-induced neurotoxicity in ReNcell VM+*mHTT* exon 1 (71 CAG) neuronal cultures at 48 h post-stimulation, but not at 24 h post-stimulation (Figure 4.6). To assess which factors may contribute to protection from mHTT-induced neurotoxicity in this co-culture model, and whether this involved polarisation of BMD-microglia towards an M1 or M2 phenotype, levels of Th1- and Th2-type cytokines, and IL-2, were measured in MG-CM.

BMD-microglia from healthy volunteers and manifest HD patients were stimulated continuously with 2 μg/mL LPS and 10 ng/mL IFNγ (chronic stimulation), or were not stimulated, for 24 h or 48 h. MG-CM was then collected and levels of Th1-type cytokines (IFNγ, IL-1β, IL-6, IL-8, IL-12 and TNFα), Th2-type cytokines (IL-4, IL-10 and IL-13) and IL-2 were measured by MSD assay. Results are presented in Figure 4.9.

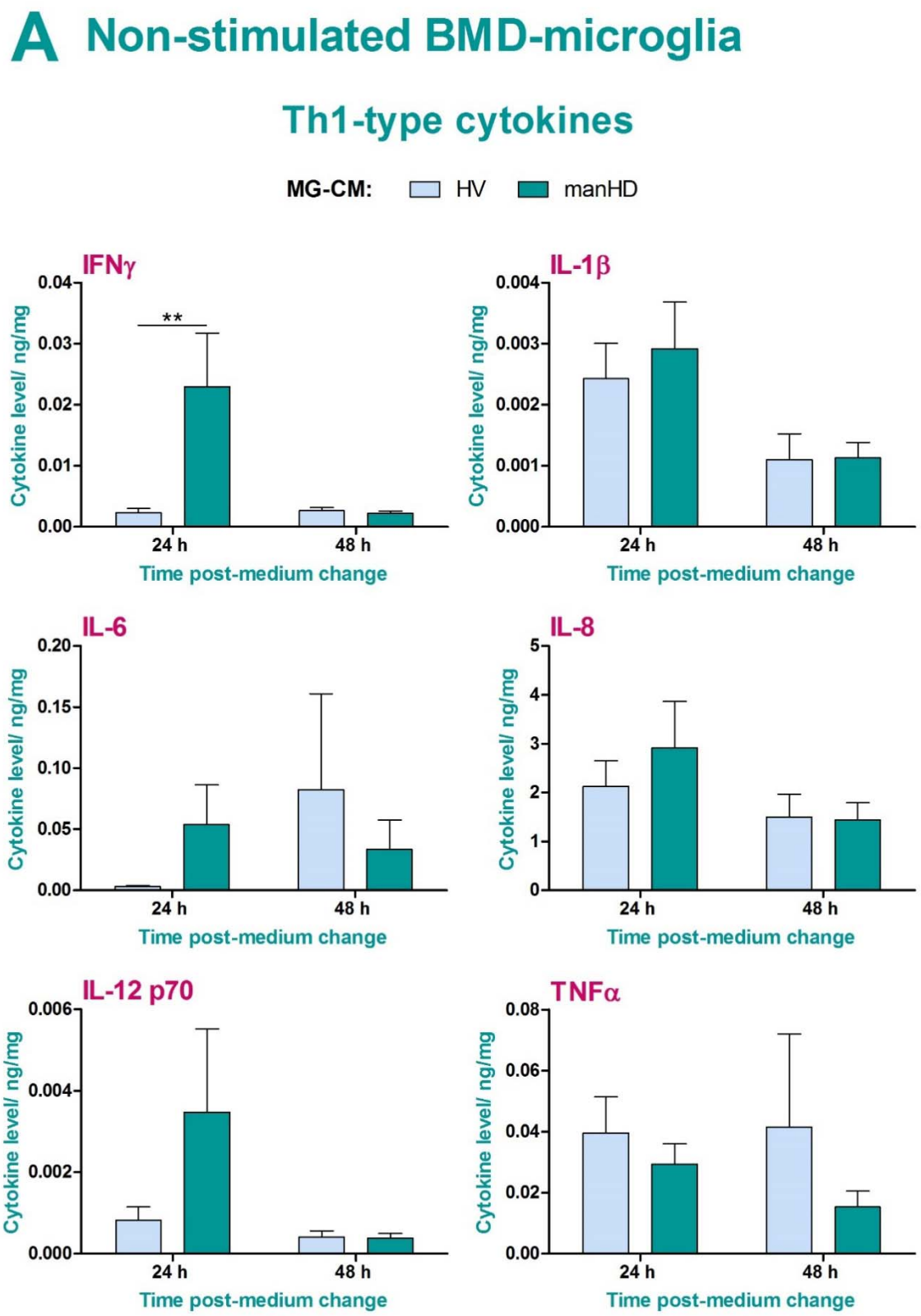
A Non-stimulated BMD-microglia
Th1-type cytokines
MG-CM: HV manHD
IFNγ
IL-1β
IL-6
IL-8
IL-12 p70
TNFα
Cytokine level/ ng/mg
Time post-medium change
24 h
48 h
**

IL-2 and Th2-type cytokines

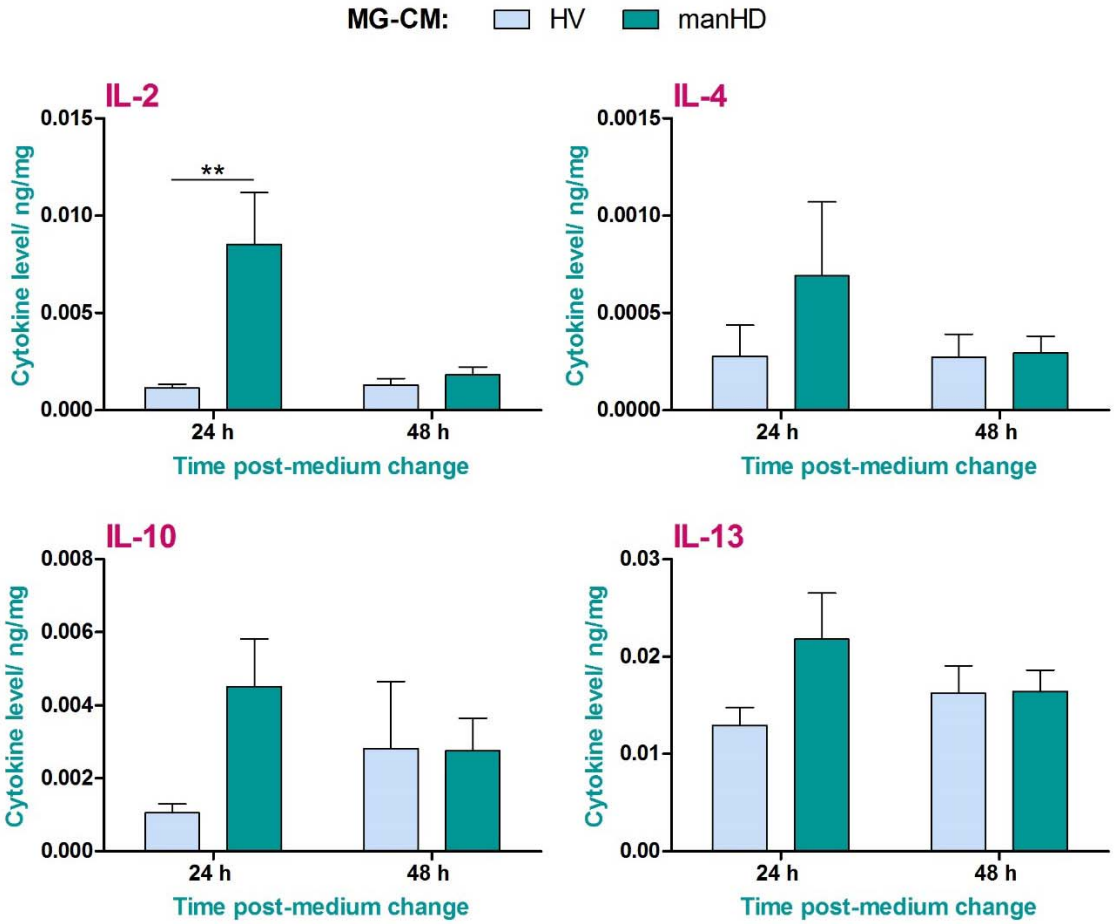

B Stimulated (chronic) BMD-microglia

Th1-type cytokines

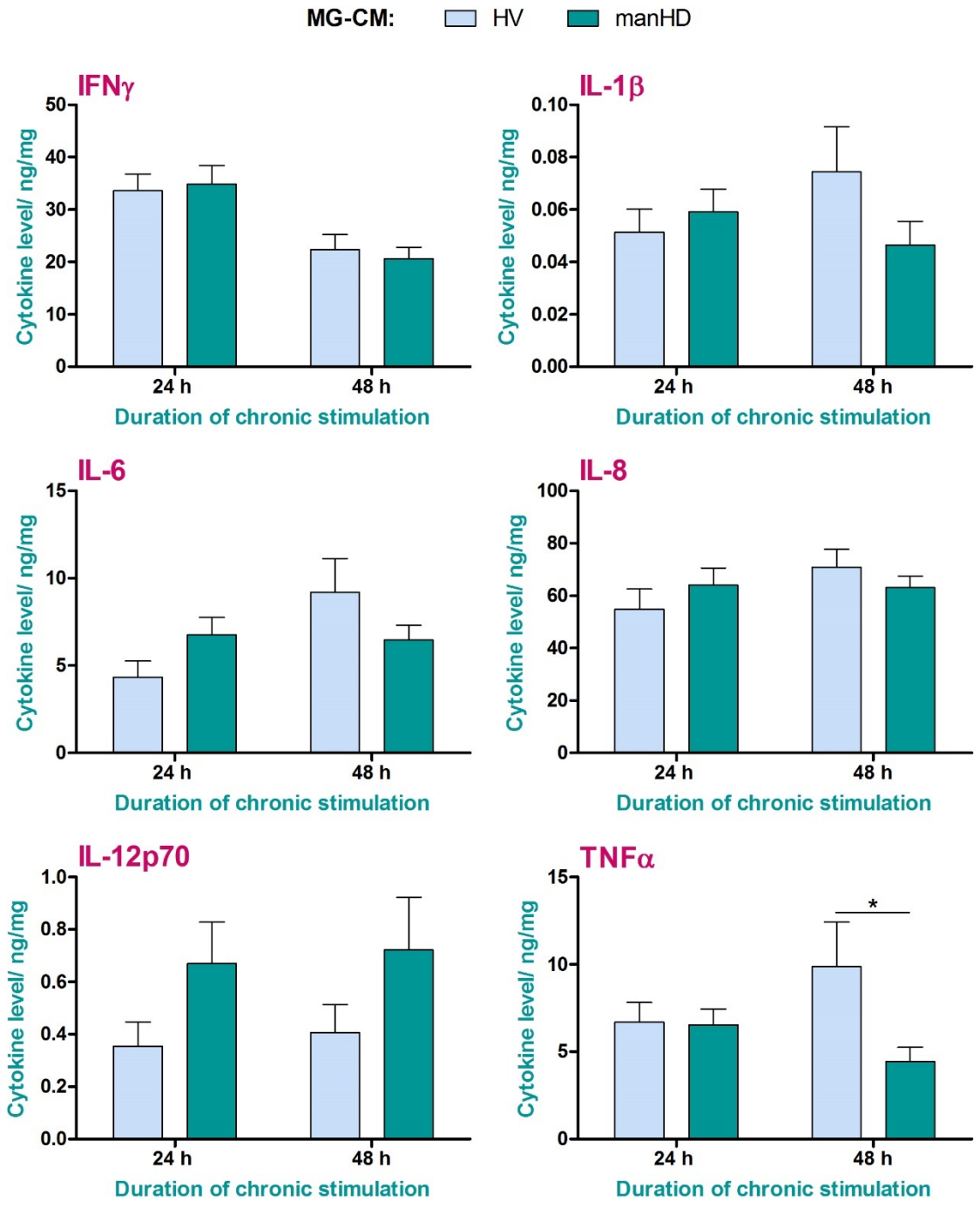

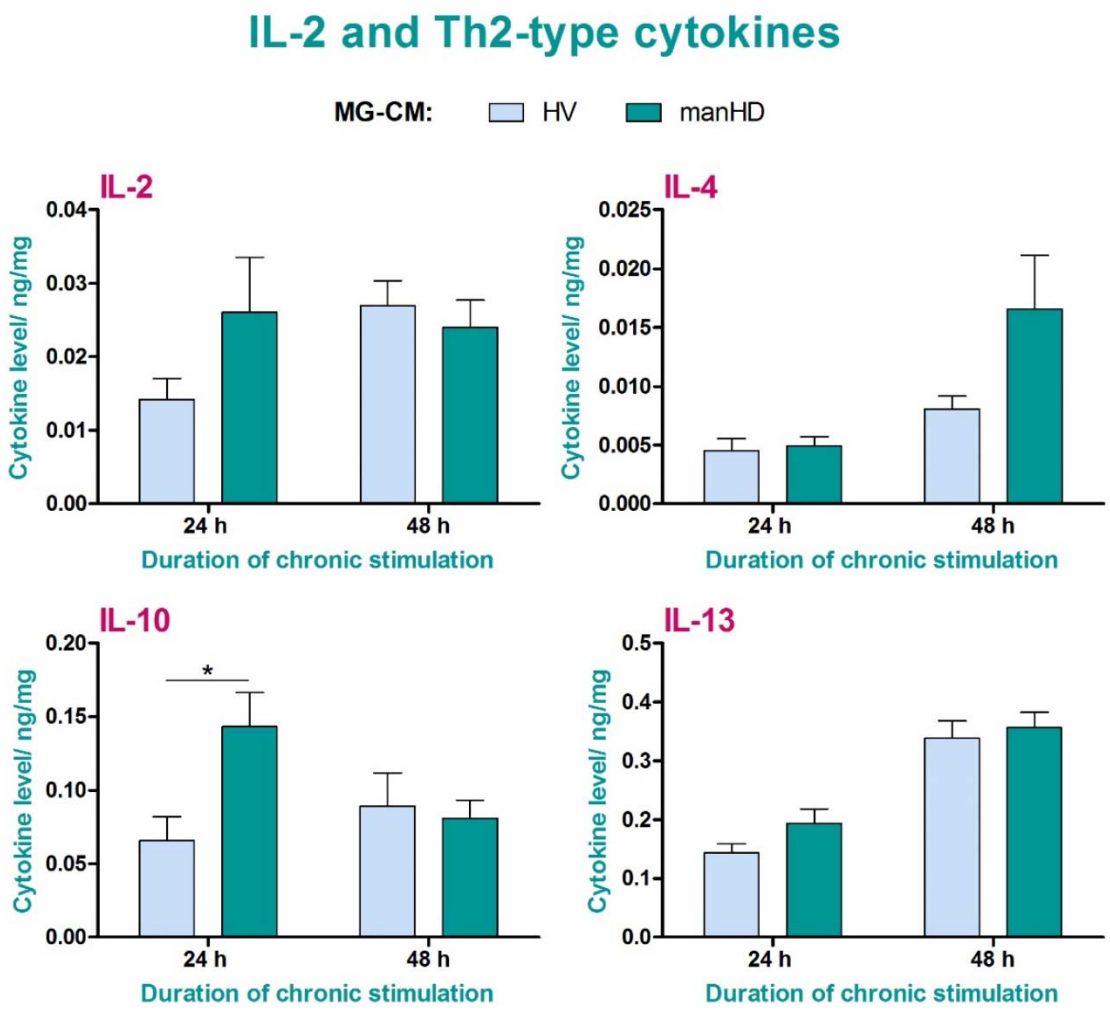

Figure 4.9: Levels of Th1- and Th2-type (and IL-2) cytokine release in healthy volunteer and manifest HD BMD-microglia

*Healthy volunteer (HV; n=17) and manifest HD (manHD; n=15) BMD-microglia cultures were stimulated continuously with 2 µg/mL LPS and 10 ng/mL IFNγ, or were not stimulated, for 24 or 48 h. Cytokine levels in MG-CM were then measured by MSD assay and normalised to total protein. Results are presented as mean average cytokine level from biological repeats, each with three internal experimental replicates, ± SEM, in MG-CM from non-stimulated BMD-microglia (**A**) and stimulated (chronic) MG-CM (**B**). Data were statistically analysed using two-way ANOVA with Bonferroni post-tests; *p<0.05, **p<0.01.*

In non-stimulated conditions, MG-CM subject group (healthy volunteer or manifest HD) was a significant source of variation in levels of IFNγ (p=0.022) and IL-2 (p=0.010), where manifest HD BMD-microglia released elevated levels of these cytokines compared with healthy volunteer BMD-microglia, independent of time-point. At the 24 h time-point, manifest HD BMD-microglia released higher levels of IFNγ (p<0.01) and IL-2 (p<0.01) than healthy volunteer BMD-microglia, but this effect was lost at 48 h. In stimulated (chronic) conditions, MG-CM subject group was a significant source of

variation in levels of IL-12 (p=0.044), where manifest HD BMD-microglia released elevated levels of this cytokine compared with healthy volunteer BMD-microglia, independent of time-point. At 24 h chronic stimulation, manifest HD BMD-microglia released elevated levels of IL-10 compared with healthy volunteer BMD-microglia (p<0.05), and at 48 h chronic stimulation manifest HD BMD-microglia released reduced levels of TNFα compared with healthy volunteer BMD-microglia (p<0.05). Duration of chronic stimulation (24 or 48 h) was a significant source of variation, independent of MG-CM subject group, in levels of IFNγ (p<0.0001), IL-4 (p=0.009) and IL-13 (p=0001), where levels of IFNγ were higher at 48 h post-stimulation than 24 h post-stimulation, and levels of IL-4 and IL-13 were lower at 48 h post-stimulation than 24 h post-stimulation. There were no significant differences detected between healthy volunteer MG-CM and manifest HD MG-CM for any of the other cytokines analysed.

4.5.4.3 Neurotrophin release in healthy volunteer and HD patient BMD-microglia

In addition to cytokine release, the release of neurotrophins by healthy volunteer and manifest HD BMD-microglia was also analysed to assess potential neuroprotective factors in MG-CM. BMD-microglia from healthy volunteers and manifest HD patients were stimulated continuously with 2 µg/mL LPS and 10 ng/mL IFNγ (chronic stimulation), or were not stimulated, for 24 h or 48 h. MG-CM was then collected and levels of the neurotrophins NGF and BDNF were measured by ELISA. Results are presented in Figure 4.10.

There was no difference between healthy volunteer and manifest HD MG-CM NGF levels in stimulated or non-stimulated conditions at 24 or 48 h time-points (p<0.05 for all comparisons). Levels of NGF release by BMD-microglia were also not affected by chronic stimulation. In non-stimulated conditions, time was a significant source of variation in BDNF levels (p=0.0006), with levels being higher at the 48 h time-point compared with the 24 h time-point, independent of MG-CM subject group (healthy volunteer or manifest HD BMD-microglia). MG-CM subject group was not a significant source of variation in BDNF levels in non-stimulated conditions. In stimulated (chronic) conditions, however, MG-CM subject group was a significant source of variation in BDNF levels (p=0.0001), and at 48 h chronic stimulation, levels of BDNF release were significantly higher in manifest HD BMD-microglia compared with healthy volunteer BMD-microglia (p<0.001). Duration of chronic stimulation was also a significant source of variation in BDNF levels in stimulated conditions (p<0.0001), with BDNF levels being higher at the 48 h time-point compared with the 24 h time-point, independent of MG-CM subject group.

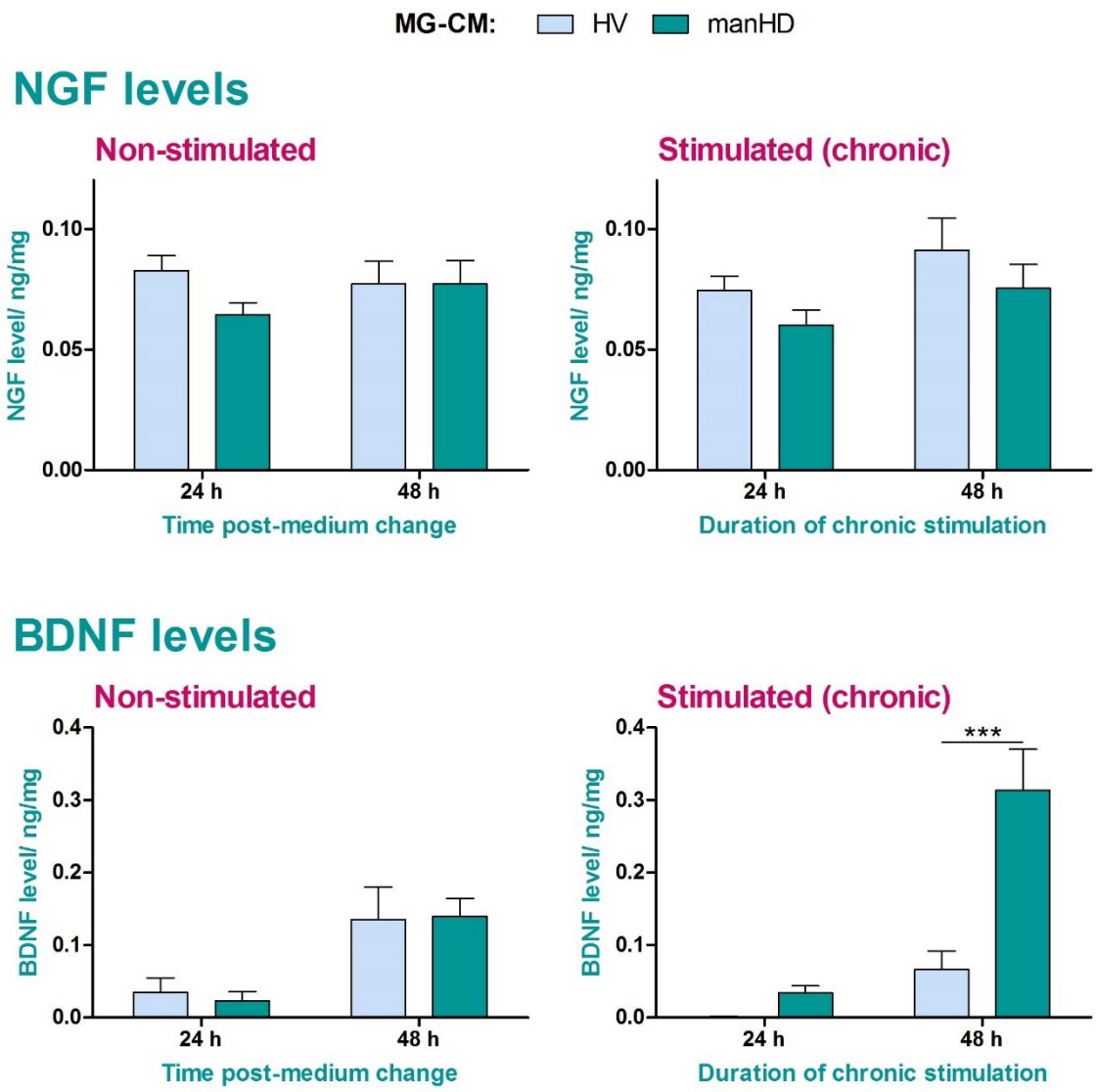

Figure 4.10: Levels of neurotrophin release in healthy volunteer and manifest HD BMD-microglia

*Healthy volunteer (HV; n=10) and manifest HD (manHD; n=10) BMD-microglia cultures were stimulated continuously with 2 µg/mL LPS and 10 ng/mL IFNγ, or were not stimulated, for 24 or 48 h. Neurotrophin levels in MG-CM were then measured by ELISA and normalised to total protein. Results are presented as mean average neurotrophin level from biological repeats, each with three internal experimental replicates, ± SEM. Data were statistically analysed using two-way ANOVA with Bonferroni post-tests; ***p<0.001.*

4.6 Discussion

4.6.1 BMD-macrophage-neuronal co-culture

4.6.1.1 Wild-type and HD (ReNcell VM+full-length mHTT (138 CAG)) neuronal culture death in co-culture with BMD-macrophages

Treatment of wild-type neuronal cultures with Mφ-CM from non-stimulated healthy volunteer, pre-manifest HD or manifest HD BMD-macrophages resulted in higher neuronal culture death levels compared with untreated, and acute stimulation of BMD-macrophages increased wild-type neuronal culture death levels over time, peaking at 4-8 h post-stimulation over a 24 h time-course. This suggests that factors released by BMD-macrophages are neurotoxic at baseline and acute stimulation increases this toxicity. The same Mφ-CM treatments also resulted in higher death levels in HD neuronal cultures compared with wild-type neuronal cultures, indicating that factors released by BMD-macrophages are less neuroprotective and/or more neurotoxic in HD neurons compared with wild-type neurons. This is in support of multiple studies which report a neurotoxic role for immune cell activation and inflammation in HD (Andre *et al.* 2016). There were no differences detected between the effects of healthy volunteer, pre-manifest HD and manifest HD BMD-macrophages on wild-type or HD neuronal culture death in co-culture.

4.6.1.2 Proinflammatory cytokine release in BMD-macrophages

To examine potential neurotoxic factors released by BMD-macrophages, levels of the proinflammatory cytokines IFNγ, IL-1β, IL-6 and TNFα were measured in the Mφ-CM used to treat wild-type and HD neurons in co-culture. In stimulated conditions, levels of IL-1β, IL-6 and TNFα were found to increase over time, over the 24 h time-course, and these increases mostly correlated with increasing neuronal culture death levels. It is possible, therefore, that BMD-macrophages are neurotoxic due to release of the proinflammatory cytokines IL-1β, IL-6 and TNFα. However, direct treatment of wild-type neuronal cultures with IL-6 and TNFα, alone or in combination, was not found to cause neurotoxicity, suggesting that these proinflammatory cytokines are not directly neurotoxic when taken in isolation.

There were no differences in proinflammatory cytokine release detected between healthy volunteer, pre-manifest HD and manifest HD BMD-macrophages in non-stimulated or stimulated (acute) conditions, other than at 24 h post-acute stimulation where manifest HD BMD macrophages released elevated levels of IL-1β and TNFα compared with pre-manifest HD BMD-macrophages. This may explain why there were no differences between the effects of healthy volunteer, pre-manifest HD and manifest HD Mφ-CM treatments on neuronal culture death levels. Träger *et al.* (2014a) also

reported that there was no difference in levels of release of IL-1β or IL-6 in pre-manifest HD or manifest HD BMD-macrophages compared with healthy volunteer BMD-macrophages, but they did report an increase in release of TNFα in pre-manifest HD and manifest HD BMD-macrophages compared with healthy volunteer BMD-macrophages after 24 h chronic stimulation.

4.6.2 BMD-microglia-neuronal co-culture

4.6.2.1 Wild-type and HD (ReNcell VM+full-length mHTT (138 CAG)) neuronal culture death in co-culture with BMD-microglia

Unlike Mφ-CM treatments, MG-CM treatments did not increase death levels in wild-type neuronal cultures compared with untreated, and acute stimulation of BMD-microglia did not increase neurotoxicity of MG-CM treatments over time, over a 48 h time-course. Chronic stimulation of BMD-microglia, however, did increase wild-type and HD neuronal culture death levels above untreated, over time, and stimulated MG-CM treatments resulted in significantly more wild-type neuronal culture death than non-stimulated MG-CM treatments at 24 and 48 h chronic stimulation. This suggests that acute stimulation of healthy volunteer, pre-manifest HD and manifest HD BMD-microglia does not affect neuronal death, but chronic stimulation is neurotoxic in wild-type and HD neuronal cultures. These findings are consistent with multiple studies which report that chronic microglial activation and inflammation is neurotoxic in HD (Cicchetti *et al.* 2009; Crotti *et al.* 2014; Heneka *et al.* 2014).

In non-stimulated conditions, treatment of wild-type neuronal cultures with MG-CM from manifest HD BMD-microglia reduced death levels below untreated levels, and these levels were lower than healthy volunteer MG-CM treatment at 24 h and pre-manifest HD MG-CM treatment at 48 h, suggesting that manifest HD BMD-microglia are more neuroprotective than healthy volunteer or pre-manifest HD BMD-microglia. Non-stimulated manifest HD MG-CM treatments also reduced wild-type neuronal culture death below HD neuronal culture death levels, overall, while non-stimulated healthy volunteer or pre-manifest HD MG-CM treatments did not; and stimulated (chronic) healthy volunteer MG-CM treatments increased HD neuronal culture death levels above wild-type neuronal culture death levels, overall, while stimulated (chronic) manifest HD MG-CM treatments did not.

4.6.2.2 ReNcell VM+HTT exon 1 (29, 71 or 129 CAG) neuronal culture death in co-culture with BMD-microglia

ReNcell VM+*HTT* exon 1 HD neurons were shown previously in this Thesis to exhibit several features similar to neurons in the HD patient brain (section 3.5.2.1). Baseline neuronal culture death levels were shown to be higher in ReNcell VM+*mHTT* exon 1

(71 CAG) neuronal cultures compared with ReNcell VM+*HTT* exon 1 (29 CAG) or ReNcell VM+*mHTT* exon 1 (129 CAG) neuronal cultures (Figure 3.11), and it was determined that this was most likely due to mHTT exon 1-induced neurotoxicity. Here, ReNcell VM+*HTT* exon 1 (29, 71 or 129 CAG) neuronal cultures were treated with MG-CM from non-stimulated and stimulated (chronic) healthy volunteer and manifest HD BMD-microglia, to assess the effects of BMD-microglia released factors on neuronal culture death.

None of the MG-CM treatments altered death levels in ReNcell VM+*HTT* exon 1 (29 CAG) or ReNcell VM+*mHTT* exon 1 (129 CAG) neuronal cultures from untreated, however, several MG-CM treatments reduced levels of death in ReNcell VM+*mHTT* exon 1 (71 CAG) neuronal cultures compared with untreated. In non-stimulated conditions, healthy volunteer MG-CM reduced neuronal death at 24 h whilst manifest HD MG-CM did not, suggesting that non-stimulated healthy volunteer BMD-microglia were neuroprotective and non-stimulated manifest HD BMD-microglia were not. By 48 h non-stimulated, however, both healthy volunteer and manifest HD MG-CM reduced neuronal death. After 24 h chronic stimulation, neither healthy volunteer nor manifest HD MG-CM reduced neuronal death, but after 48 h chronic stimulation both healthy volunteer and manifest HD MG-CM reduced neuronal death.

Overall, these results suggest that both healthy volunteer and manifest HD BMD-microglia protect HD neurons from mHTT-induced neurotoxicity leading to neuronal death. Others have also reported that microglia may be neuroprotective in HD via provision of trophic support to degenerating neurons (Andre *et al.* 2016), and Kraft *et al.* (2012) showed that wild-type microglia increased neuronal survival in mHTT-expressing neurons in co-culture. It has been considered that cell-autonomous dysfunction caused by mHTT expression in HD patient immune cells may reduce these protective functions (Heneka *et al.* 2014), however it was shown here that this is not the case under most conditions. It has also been proposed that microglial activation and neuroinflammation are neurotoxic in HD (Cicchetti *et al.* 2009; Crotti *et al.* 2014; Heneka *et al.* 2014), or are simply reactive processes; responding to neurodegeneration but not contributing to it in either a beneficial or harmful capacity (Wang *et al.* 2014a). The findings presented here, however, provide evidence for a neuroprotective role of microglia in HD.

4.6.2.3 Th1- and Th2-type (and IL-2) cytokine release in BMD-microglia

To examine potential neuroprotective factors released by BMD-microglia which may contribute to protection from mHTT-induced neurotoxicity, and to assess M1 versus M2 microglial phenotypes in co-culture, levels of Th1-type cytokines (IFNγ, IL-1β, IL-6, IL-

8, IL-12 and TNFα), Th2-type cytokines (IL-4, IL-10 and IL-13) and IL-2 were measured in non-stimulated and stimulated (chronic) MG-CM from healthy volunteer and manifest HD BMD-microglia.

In non-stimulated conditions, manifest HD BMD-microglia released elevated levels of IFNγ and IL-2 compared with healthy volunteer BMD-microglia, at the 24 h time-point. In this same condition, healthy volunteer MG-CM reduced ReNcell VM+*mHTT* exon1 (71 CAG) HD neuronal culture death and manifest HD MG-CM did not. At the 48 h time-point, these cytokine increases did not occur in manifest HD BMD-microglia, and both healthy volunteer and manifest HD MG-CM reduced ReNcell VM+*mHTT* exon1 (71 CAG) HD neuronal culture death in this condition in co-culture. This suggests that elevated release of IFNγ and IL-2 by BMD-microglia may prevent protection from mHTT-induced neurotoxicity in co-culture.

In stimulated (chronic) conditions, manifest HD BMD-microglia released elevated levels of IL-12 compared with healthy volunteer BMD-microglia, independent of time-point. Manifest HD BMD-microglia also released elevated levels of IL-10 after 24 h chronic stimulation and reduced levels of TNFα after 48 h chronic stimulation, compared with healthy volunteer BMD-microglia. Increased release of anti-inflammatory Th2-type cytokine IL-10 followed by decreased release of proinflammatory Th1-type cytokine TNFα may indicate that manifest HD BMD-microglia had become more M2-polarised than healthy volunteer BMD-microglia. Elevated release of IL-10 after 24 h chronic stimulation did not correlate with protection from mHTT-induced neurotoxicity, as both healthy volunteer and manifest HD MG-CM treatments did not decrease ReNcell VM+*mHTT* exon1 (71 CAG) HD neuronal culture death in this condition. Reduced release of TNFα may have contributed to protection from mHTT-induced neurotoxicity, as manifest HD MG-CM treatment decreased ReNcell VM+*mHTT* exon1 (71 CAG) HD neuronal culture death in this condition, however, healthy volunteer MG-CM treatment also decreased neuronal culture death.

There were no differences between healthy volunteer and manifest HD BMD-microglia in levels of cytokine release for any of the other cytokines analysed. When taken together, levels of release of Th1-type cytokine IFNγ were decreased, and levels of release of Th2-type cytokines IL-4 and IL-13 were increased in both healthy volunteer and manifest HD BMD-microglia after 48 h chronic stimulation compared with 24 h chronic stimulation. This may be indicative of polarisation of BMD-microglia towards an M2 phenotype during chronic stimulation. Altered levels of release of these cytokines also correlated with protection from mHTT-induced neurotoxicity, as both healthy volunteer and manifest HD MG-CM treatments reduced ReNcell VM+*mHTT* exon1 (71

CAG) HD neuronal culture death after 48 h chronic stimulation, but not after 24 h chronic stimulation.

4.6.2.4 Neurotrophin release in BMD-microglia

Neurotrophins are a major class of neuroprotectants in the CNS. To examine potential neuroprotective factors released by BMD-microglia which may contribute to protection from mHTT-induced neurotoxicity, levels of release of two key neurotrophins, NGF and BDNF, were analysed in non-stimulated and stimulated (chronic) healthy volunteer and manifest HD BMD-microglia. There was no difference between healthy volunteer BMD-microglia and manifest HD BMD-microglia in levels of NGF release, and levels of NGF release were not affected by chronic stimulation. Levels of BDNF release, however, were approximately 3-fold higher in manifest HD BMD-microglia compared with healthy volunteer BMD-microglia after 48 h chronic stimulation. Levels of BDNF release were also higher in both healthy volunteer and manifest HD BMD-microglia at the 48 h time-point compared with the 24 h time-point in both non-stimulated and stimulated conditions. Increased levels of BDNF release in healthy volunteer BMD-microglia correlated with reduced ReNcell VM+*mHTT* exon1 (71 CAG) HD neuronal culture death in stimulated (chronic) conditions, and increased levels of BDNF release in manifest HD BMD-microglia correlated with reduced neuronal culture death in both non-stimulated and stimulated (chronic) conditions. Taken together, these results highlight BMD-microglia BDNF release as a contributor to protection of HD neurons from mHTT-induced neurotoxicity in co-culture.

4.6.3 Protective and deleterious neuronal-myeloid cell interactions in HD

In BMD-macrophage-neuronal co-culture, increases in the release of the proinflammatory cytokines IL-1β, IL-6 and TNFα in stimulated (acute) BMD-macrophages correlated with neurotoxicity, or reduced neuroprotection, in HD neuronal cultures. Pathological roles of these proinflammatory cytokines have previously been reported in HD and they are considered to be key mediators of disease progression. Plasma levels of IL-6 and TNFα increase in correlation with disease progression and severity in HD patients (Dalrymple *et al.* 2007; Björkqvist *et al.* 2008; Heneka *et al.* 2014); and in R6/2 mice, inhibition of IL-6 diminished weight loss and reduced motor deficits (Bouchard *et al.* 2012) and inhibition of TNFα decreased neuroinflammation and neurodegeneration and improved motor function (Hsiao *et al.* 2014). IL-1β augments inflammatory signals in the CNS and is involved in neuronal death (Ona *et al.* 1999).

Peripheral inflammatory events could directly contribute to neuroinflammation and neurodegenerative processes in the CNS (Eskandari and Sternberg 2002; Wrona

2006), and multiple studies have shown peripheral immune dysfunction as a key modifier of neuroinflammation and central pathogenesis in HD (Zwilling *et al.* 2011; Bouchard *et al.* 2012; Franciosi *et al.* 2012; Kwan *et al.* 2012a). The BBB is compromised in HD (Drouin-Ouellet *et al.* 2015), and while CNS influx of peripherally-derived immune cells has not been reported (Silvestroni *et al.* 2009; Möller 2010), there may be uncontrolled passage of blood-borne factors, such as cytokines, between the periphery and the brain (Drouin-Ouellet *et al.* 2015). Peripherally-derived cytokines can also enter the CNS in non-pathological conditions by directly crossing the BBB (Eskandari and Sternberg 2002; Wrona 2006). Here, BMD-macrophages, but not BMD-microglia, released elevated levels of IL-1β, IL-6 and TNFα in response to stimulation. It is therefore possible that peripheral macrophages, and not microglia, are the source of elevated levels of IL-1β, IL-6 and TNFα which have been reported in the brain and CSF of HD patients and HD animal models (Ona *et al.* 1999; Björkqvist *et al.* 2008; Silvestroni *et al.* 2009; Bouchard *et al.* 2012; Ellrichmann *et al.* 2013; Alto *et al.* 2014).

In BMD-microglia-neuronal co-culture, manifest HD BMD-microglia released elevated levels of IFNγ and IL-2 compared with healthy volunteer BMD-microglia in non-stimulated conditions, and this correlated with a loss of neuroprotection in HD neuronal cultures. IFNγ has previously been shown to be elevated in the serum of HD patients (Kwan *et al.* 2012a) and levels of microglial IL-2 release have previously been shown to be elevated in association with brain injury (Girard *et al.* 2008). It has been reported that IFNγ can cause neurotoxicity via activation of astrocytes (Hashioka *et al.* 2015). Long-term central administration of IL-2 in rats has been shown to promote neuroinflammation, myelin damage and neuronal loss (Hanisch *et al.* 1997).

Although not released at different levels in HD BMD-microglia compared with healthy volunteer BMD-microglia, increased release of the Th2-type cytokines IL-4 and IL-13 correlated with neuroprotection of HD neurons in co-culture in stimulated (chronic) conditions. Plasma levels of IL-4 have previously been shown to increase with HD progression (Björkqvist *et al.* 2008). Th2-type cytokines are released by alternatively activated (M2) microglia, and IL-4 and IL-13 promote alternative activation (Martinez and Gordon 2014). Th1-type cytokines are released by classically activated (M1) microglia. Levels of release of anti-inflammatory Th2-type cytokine IL-10 were elevated in stimulated (chronic) manifest HD BMD-microglia compared with healthy volunteer BMD-microglia, and this was followed by a decrease in the release of Th1-type cytokine TNFα in manifest HD BMD-microglia compared with healthy volunteer BMD-microglia, which may be associated with neuroprotection of HD neurons in co-culture. This suggests that M2-polarised microglia are neuroprotective in HD whilst microglia polarised more towards M1 phenotype are not, and in conditions of chronic

inflammation, manifest HD microglia become more polarised towards an M2 phenotype than healthy volunteer microglia. M1 microglia have increased proinflammatory cytokine, iNOS and ROS production and can contribute to chronic inflammation-related neurotoxicity, while M2 microglia promote tissue repair and suppress inflammation (Berger 2000; Gordon and Taylor 2005). Analysis of striatal tissue gene expression in symptomatic R6/2 mice previously revealed Th1-type cytokines as potential regulators of disease (Crocker *et al.* 2006), and it has been reported that HD patient macrophages shift from a proinflammatory M1 phenotype to an anti-inflammatory M2 phenotype over the disease course in HD, along with an increase in IL-10-expressing macrophages in progressing symptomatic disease (Di Pardo *et al.* 2013).

Increased release of BDNF in non-stimulated and stimulated (chronic) healthy volunteer and manifest HD BMD-microglia correlated with neuroprotection of HD neurons in co-culture, and after chronic stimulation, BDNF release was highly elevated in manifest HD BMD-microglia compared with healthy volunteer BMD-microglia. Microglia constitutively secrete low levels of BDNF during homeostasis, but during CNS inflammation or following injury, BDNF production is chronically upregulated (Nakajima *et al.* 2001; Kleij and Bienenstock 2007; Venkatesan *et al.* 2010; Gomes *et al.* 2013). HTT is involved in the production and transport of BDNF (Cattaneo *et al.* 2005), so it is possible that mHTT is dysregulated in these functions, leading to elevated release in response to chronic stimulation. BDNF supports neuronal survival, function and tissue repair and maintains CNS homeostasis (Saijo and Glass 2011), and it has been shown to have neuroprotective effects in several CNS injury and neurodegenerative disease models (Linker *et al.* 2010; Lee *et al.* 2012). Pharmacological approaches for the treatment of HD have included administration of BDNF to preserve remaining neural activity (Giampà *et al.* 2013), and increasing BDNF levels was shown to reduce neurotoxicity and ameliorate neurological signs in animal models of HD (Puerta *et al.* 2010; Xie *et al*. 2010).

4.7 Summary

Healthy volunteer, pre-manifest HD and manifest HD BMD-macrophages are neurotoxic in co-culture with wild-type and HD (ReNcell VM+full-length *mHTT* (138 CAG)) neurons. Levels of neuronal death were higher in HD neurons than wild-type neurons, and neurotoxicity increased following acute stimulation with LPS and IFNγ. Increases in neuronal death were associated with elevated release of proinflammatory cytokines IL-1β, IL-6 and TNFα by BMD-macrophages.

In non-stimulated conditions, manifest HD BMD-microglia were more neuroprotective in co-culture with wild-type neurons than healthy volunteer or pre-manifest HD BMD-

microglia, and following chronic stimulation with LPS and IFNγ, HD (ReNcell VM+full-length *mHTT* (138 CAG)) neuronal culture death levels were higher than wild-type levels in co-culture with healthy volunteer BMD-microglia, but not in co-culture with manifest HD BMD-microglia. Acute stimulation of BMD-microglia with LPS and IFNγ did not affect wild-type neuronal death in co-culture.

Healthy volunteer and manifest HD BMD-microglia rescued HD neurons (ReNcell VM+*mHTT* exon 1 (71 CAG)) from mHTT-induced neurotoxicity leading to neuronal death in co-culture. Neuroprotective microglia phenotypes were associated with elevated levels of BDNF release, reduced levels of IFNγ and IL-2 release in non-stimulated conditions, and polarisation towards an M2-phenotype (decreased release of Th1-type cytokine TNFα and increased release of Th2-type cytokines IL-4, IL-10 and IL-13) during chronic stimulation with LPS and IFNγ. In conditions of chronic stimulation, manifest HD BMD-microglia were considered to be more M2-polarised than healthy volunteer BMD-microglia, and levels of BDNF release were approximately three-fold higher in manifest HD BMD-microglia than healthy volunteer BMD-microglia.

5 Investigation into the effects of laquinimod on rescuing hyper-reactive immune cell dysfunction in HD patient myeloid cells

5.1 Background

Neurodegeneration and disease progression are accompanied by central and peripheral inflammation in HD, including activation of myeloid cells and elevated levels of proinflammatory factors in the brain, CSF and plasma (Singhrao *et al.* 1999; Sapp *et al.* 2001; Pavese *et al.* 2006; Dalrymple *et al.* 2007; Tai *et al.* 2007a; Tai *et al.* 2007b; Björkqvist *et al.* 2008; Silvestroni *et al.* 2009; Politis *et al.* 2011; Wild *et al.* 2011; Tabrizi *et al.* 2013; Chang *et al.* 2015). Blood plasma levels of proinflammatory cytokines are elevated early in HD pathogenesis, before the onset of clinical symptoms, and increase in correlation with disease progression and severity (Dalrymple *et al.* 2007; Björkqvist *et al.* 2008; Heneka *et al.* 2014), indicating that peripheral inflammatory events may contribute to neurodegenerative processes and disease progression in HD. Myeloid cells are the prime candidates for the source of these elevated cytokine levels. Microglia, monocytes and macrophages isolated from HD patients or HD mouse models are hyper-reactive in response to stimulation, and release elevated levels of proinflammatory cytokines (Björkqvist *et al.* 2008; Träger *et al.* 2014a). This may be due to dysfunctional cell-autonomous mechanisms caused by mHTT expression in myeloid cells (Crotti *et al.* 2014; Träger *et al.* 2014a).

Laquinimod is a novel orally-active immunomodulatory drug which has been demonstrated to downregulate immune cell activation and inflammation in the periphery (Yang *et al.* 2004; Schulze-Topphoff *et al.* 2012) and in the CNS (Brück *et al.* 2012; Mishra *et al.* 2014). In two Phase III clinical trials, laquinimod was shown to have beneficial effects on inflammation, brain atrophy and disease progression in MS patients, and was also demonstrated to be safe and well-tolerated in humans (Comi *et al.* 2012; Filippi *et al.* 2014; Vollmer *et al.* 2014). MS and HD share some similar pathological features, including inflammation in association with myelin, axonal and neuronal loss (Ellrichmann *et al.* 2013). Therefore, laquinimod may have potential to

slow brain atrophy rate and disease progression in HD patients through central and peripheral immunomodulatory mechanisms, as it has been shown to do in MS.

HD myeloid cells have been demonstrated to release elevated levels of proinflammatory Th1-type cytokines, including IL-1β, IL-6, IL-8 and TNFα, in response to stimulation with LPS and IFNγ (Björkqvist *et al.* 2008; Träger *et al.* 2014a), and multiple studies report a neurotoxic role for immune cell activation and elevated proinflammatory Th1-type cytokines in HD (Ona *et al.* 1999; Crocker *et al.* 2006; Cicchetti *et al.* 2009; Bouchard *et al.* 2012; Crotti *et al.* 2014; Heneka *et al.* 2014; Hsiao *et al.* 2014; Andre *et al.* 2016). In Chapter 4 of this Thesis, BMD-macrophages were shown to increase wild-type and HD (ReNcell VM+full-length *mHTT* (138 CAG)) neuronal death in co-culture, and this was associated with elevated release of proinflammatory Th1-type cytokines IL-1β, IL-6 and TNFα following acute stimulation with LPS and IFNγ (section 4.6.1). BMD-microglia were demonstrated to rescue HD neurons (ReNcell VM+*mHTT* exon 1 (71 CAG)) from mHTT-induced neurotoxicity leading to neuronal death in co-culture, and this was associated with reduced levels of IL-2 and proinflammatory Th1-type cytokine IFNγ release in non-stimulated conditions, and polarisation towards an M2-phenotype (decreased release of Th1-type cytokine TNFα and increased release of Th2-type cytokines IL-4, IL-10 and IL-13) during chronic stimulation with LPS and IFNγ (sections 4.5.2.3 and 4.5.4.2). Therefore, promoting the polarisation of myeloid cells towards an M2 phenotype may be beneficial in HD.

Laquinimod has been shown to drive an immunomodulatory shift in immune cell phenotypes away from M1 and Th1-type cytokine production and towards M2 and Th2-type cytokine production *in vivo* in animal models of MS and *in vitro* in primary human microglia and PBMCs (Zou *et al.* 2002; Yang *et al.* 2004; Brück and Wegner 2011; Schulze-Topphoff *et al.* 2012; Mishra *et al.* 2014). Laquinimod may therefore have the potential to promote reparative and neuroprotective M2 and Th2-type inflammatory phenotypes whilst suppressing M1 and Th1-type proinflammatory and neurotoxic phenotypes in HD.

Hyper-reactivity of the innate immune response in HD is due partly to NFκB pathway dysregulation (Khoshnan *et al.* 2004; Hsiao *et al.* 2013; Träger *et al.* 2014a). Aberrant NFκB signalling has been demonstrated in peripheral myeloid cells isolated from HD patients, where mHTT was shown to interact with the γ subunit of IKK, leading to a more rapid degradation of IκB following LPS stimulation in HD myeloid cells compared with healthy volunteer myeloid cells (Träger *et al.* 2014a). This resulted in increased and prolonged NFκB activity and increased NFκB-dependent gene expression, leading to the elevated production and release of proinflammatory Th1-type cytokines in

response to stimulation (Khoshnan *et al.* 2004; Björkqvist *et al.* 2008; Träger *et al.* 2014a). Also, mHTT-induced transcriptional dysregulation affects key inflammatory signalling pathways in HD patient myeloid cells, including elements of the NFκB pathway (Träger *et al.* 2014a). Laquinimod mechanism of action may involve alteration of NFκB signalling. In a mouse model of MS, laquinimod administration reduced the proportion of astrocytes with nuclear NFκB (p65/RelA) immune-reactivity (Brück *et al.* 2012), and in human PBMC cultures laquinimod treatment increased IκB expression and decreased expression of downstream NFκB genes (Gurevich *et al.* 2010). Laquinimod-induced reduction of p65 translocation has also been demonstrated in primary murine astrocytes (Brück *et al.* 2012). Laquinimod may therefore have the potential to reverse NFκB pathway dysfunction in HD patient myeloid cells and dampen the elevated production of proinflammatory Th1-type cytokines in these cells.

When orally-administered, laquinimod is quickly absorbed into the blood stream from where only a small percentage (7-8 %) crosses the BBB and penetrates the CNS. It is therefore likely that laquinimod acts primarily in the periphery, although the drug has been shown to have both central and peripheral affects. Multiple studies have shown peripheral immune dysfunction as a key modifier of neuroinflammation and central pathogenesis in HD, and intervention of peripheral inflammatory events has previously been shown to modulate central neuropathology and disease progression (Zwilling *et al.* 2011; Bouchard *et al.* 2012; Franciosi *et al.* 2012; Kwan *et al.* 2012a). Changes in peripheral cytokine profile has the potential to affect neuroinflammatory processes by CNS-entry of peripherally-derived cytokines (Eskandari and Sternberg 2002; Wrona 2006; Drouin-Ouellet *et al.* 2015).

The effects of laquinimod treatment on Th1- and Th2-type cytokine release (and IL-2) in primary monocytes isolated from HD patients was investigated, to determine whether laquinimod can reduce hyper-reactive proinflammatory cytokine release in these cells, and promote a switch from M1 and Th1-type proinflammatory and neurotoxic phenotypes to M2 and Th2-type reparative and neuroprotective phenotypes. The effects of laquinimod treatment on mHTT-IKKγ protein interactions, IκB degradation kinetics and nuclear translocation of NFκB p65 was also investigated in HD patient peripheral myeloid cells, to determine if laquinimod can reverse NFκB pathway dysfunction in these cells. This was the first demonstration of the effects of laquinimod in HD patient myeloid cells.

5.2 Aims

1) Determine if laquinimod treatments are toxic in primary human monocytes.

2) Determine if laquinimod treatment alters Th1- and Th2-type (and IL-2) cytokine release away from M1 and in favour of an M2 functional signature in primary human monocytes isolated from HD patients, in non-stimulated and stimulated conditions.
3) Determine if laquinimod treatment can reverse NFκB pathway dysfunction in HD patient myeloid cells by examining mHTT-IKKγ protein interactions, IκB degradation kinetics and nuclear translocation of NFκB p65 in laquinimod-treated HD patient monocytes and BMD-macrophages.

5.3 Methods

A summary of methods used in this Chapter is outlined below. Full details of experimental protocols can be found in Chapter 2: Materials and Methods.

Human samples were classified as described in section 2.1.2.1. Primary human monocytes were isolated from healthy volunteers, pre-manifest HD gene carriers and manifest HD patients (section 2.1.2.2) and cultured *ex vivo* (section 2.1.2.3), and BMD-macrophages were differentiated *in vitro* from primary human monocyte cultures (section 2.1.2.4). In cases where myeloid cells are referred to as "stimulated", cells were stimulated as described in section 2.1.2.6. Details for laquinimod, including pharmacokinetic information on the compound, can be found in section 2.8. Laquinimod toxicity was tested in primary human monocyte cultures as described in section 2.8.1, using LDH cytotoxicity assay (section 2.6.1). Laquinimod treatment conditions were as described in section 2.8.2, and levels of cytokine release were measured in non-stimulated and stimulated conditions using MSD Human Th1/Th2 10-Plex Tissue Culture Kit or Human IL-6 Singleplex Kit (section 2.5.6.2). Investigations into laquinimod-induced NFκB pathway modulation were performed as described in section 2.8.3. Interactions between mHTT and IKKγ were assessed by PLA (section 2.5.3), IκB degradation kinetics were assessed by Western blotting techniques (sections 2.4.1.2, 2.4.3, 2.4.4 and 2.5.1.2; antibody details in section 2.5.1.3) and NFκB p65 nuclear translocation was assessed by IFC (section 2.5.5). Statistical analyses were performed as described in section 2.9.

5.4 Contributions

- Pre-clinical drug testing of laquinimod in HD patient myeloid cells was performed in collaboration with Teva Pharmaceutical Industries Ltd, who provided the compound.

- All laboratory work described in this Chapter was performed in equal parts by Dr. Ulrike Träger (Prof. Sarah J. Tabrizi's research group, UCL IoN, London, UK) and myself, Lucianne Dobson.
- Statistical analysis of levels of cytokine release in laquinimod-treated (and untreated) monocytes was performed by an independent statistician, Ruth Farmer (London School of Hygiene & Tropical Medicine, Department of Medical Statistics, London, UK).

Findings presented in this chapter were published in Journal of Neurochemistry (Appendix III-i):

Dobson L., Träger U., Farmer R., Hayardeny L., Loupe P., Hayden M. R., Tabrizi S. J. (2016) Laquinimod dampens hyperactive cytokine production in Huntington's disease patient myeloid cells. *J. Neurochem*. **137**, 782-794.

5.5 Results

5.5.1 Testing laquinimod toxicity in *ex vivo* human monocyte cultures

Before investigating the effects of laquinimod on reversing hyper-reactivity in HD patient myeloid cells, it was important to determine whether laquinimod treatments were toxic in these cells. Healthy volunteer and HD patient monocytes were treated for 24 h or 48 h with a range of laquinimod concentrations from 0.001 to 100 μM, including previously published concentrations (1 μM and 5 μM) which had been used to treat human PBMCs in culture (Brück and Wegner 2011). Cell death was then assessed by LDH cytotoxicity assay and compared with levels of death in untreated monocyte cultures. Results are presented in Figure 5.1.

Laquinimod concentration was not a significant source of variation in percentage monocyte survival after 48 h laquinimod treatment ($p>0.05$), but it was after 24 h laquinimod treatment ($p=0.016$). However, none of the individual laquinimod treatment conditions, after 24 h or 48 h treatment, showed a statistically significant difference in percentage monocyte survival compared with untreated ($p>0.05$), and confidence intervals (calculated at the 95 % confidence level) around the mean percentage survival relative to untreated cells spanned 100 % survival in all laquinimod-treated conditions, and were generally narrow. After 24 h laquinimod treatment, 1 μM and 5 μM laquinimod resulted in a mean average of 95.39 % and 101.01 % monocyte survival relative to untreated cells, respectively, and the lower limits of the confidence intervals for these results were 79.17 % for 1 μM laquinimod and 82.91 % for 5 μM laquinimod. After 48 h laquinimod treatment, 1 μM and 5 μM laquinimod resulted in a mean average of 99.84 % and 97.54 % monocyte survival relative to untreated cells,

respectively, and the lower limits of the confidence intervals for these results were 88.01 % for 1 μM laquinimod and 86.84 % for 5 μM laquinimod. These results confirmed that at concentrations of 1 μM and 5 μM, one can be confident that the true cell survival relative to untreated is above 79 % after 24 h treatment and above 86 % after 48 h treatment, which was taken to be acceptable in terms of establishing a lack of laquinimod toxicity. Therefore, previously published concentrations of 1 μM and 5 μM laquinimod (Brück and Wegner 2011) were used for subsequent experiments, which are relevant concentrations based on physiological *in vivo* data for plasma levels of laquinimod in humans (Preiningerova 2009; Sennbro *et al.* 2006) and mice (Brunmark *et al.* 2002).

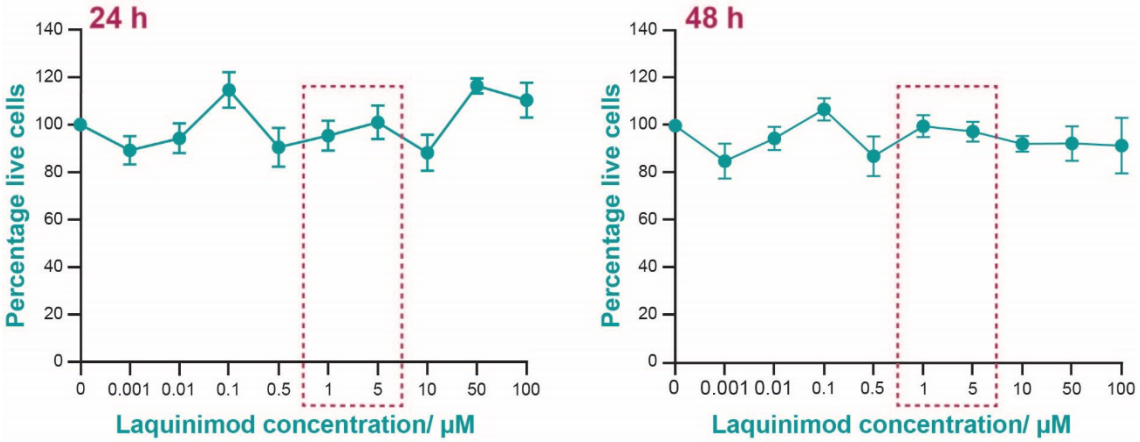

Figure 5.1: Primary human monocyte survival following laquinimod treatment

Healthy volunteer and manifest HD monocyte cultures (n=6) were treated, in duplicate, with 0, 0.001, 0.01, 0.1, 0.5, 1, 5, 10, 50 or 100 μM laquinimod for 24 or 48 h. Toxicity was then analysed by LDH cytotoxicity assay and results are presented as mean average laquinimod-treated monocyte survival from biological repeats, expressed as a percentage of untreated monocyte survival, each with three internal experimental replicates, ± SEM. Laquinimod treatment concentrations of 1 μM and 5 μM laquinimod (boxed) were used in subsequent experiments. Data were statistically analysed using one-way ANOVA with Dunnett's multiple comparison tests comparing all laquinimod treatment conditions to untreated.

5.5.2 Investigation into the effects of laquinimod on elevated cytokine release in HD patient monocytes

To determine whether laquinimod can reduce elevated proinflammatory cytokine release in HD patient myeloid cells, and promote an M1 to M2 phenotype switch in these cells, Th1- and Th2-type (and IL-2) cytokine release was measured in untreated and laquinimod-treated healthy volunteer, pre-manifest HD and manifest HD monocytes, in non-stimulated and stimulated conditions. Monocyte cultures were pre-treated with 1 μM or 5 μM laquinimod for 2 or 24 h, or were untreated. Cells were then

stimulated with 1 µg/mL LPS and 10 ng/mL IFNγ, or were non-stimulated, for 24 h (with or without continued laquinimod treatment). See Table 5.1 for details of the laquinimod treatment conditions tested. Levels of the following cytokines were then measured in monocyte culture supernatants (MC-CM), by MSD assay: Th1-type cytokines: IL-1β, IL-6, IL-8, IL-12 and TNFα; Th2-type cytokines: IL-4, IL-5, IL-10 and IL-13; and IL-2.

Table 5.1: Laquinimod treatment conditions

Laquinimod treatment duration	Laquinimod treatment concentration	Stimulation conditions
2 h pre-treatment (**2hPT**)	1 µM or 5 µM	Stimulated or non-stimulated
24 h pre-treatment (**24hPT**)	1 µM or 5 µM	Stimulated or non-stimulated
24 h pre-treatment with 24 h continued treatment (**24hPT+24hCT**)	5 µM	Stimulated or non-stimulated

5.5.2.1 Cytokine release in non-laquinimod-treated monocytes

In non-stimulated conditions, levels of all cytokines, other than IL-6, were significantly higher ($p<0.05$), or borderline ($p=0.05$-0.06), in manifest HD MC-CM compared with healthy volunteer MC-CM. Levels of IL-5, IL-8 and IL-13 ($p<0.05$) were also higher in pre-manifest HD MC-CM compared with healthy volunteer MC-CM. While the other cytokines tested were not elevated in pre-manifest HD MC-CM, both pre-manifest HD and manifest HD subject groups showed similar trends, and combining the HD subjects increased the power sufficiently to detect a statistically significant ($p<0.05$), or borderline significant ($p=0.05$-0.06), increase in all cytokines tested in HD MC-CM compared with healthy volunteer MC-CM. This suggests that in non-stimulated conditions, HD monocytes release elevated levels of both Th1-type cytokines (IL-1β, IL-6, IL-8, IL-12 and TNFα) and Th2-type cytokines (IL-4, IL-5, IL-10 and IL-13), as well as IL-2.

In stimulated conditions, there was evidence of an increase in levels of IL-1β, IL-5 and IL-13 in manifest HD MC-CM compared with healthy volunteer MC-CM, with log levels of these cytokines being approximately 0.4 higher in manifest HD MC-CM and differences being of at least borderline statistical significance ($p<0.06$). Levels of IL-4, IL-6 and IL-10 had increases of similar magnitude in manifest HD MC-CM compared with healthy volunteer MC-CM, but these differences did not reach borderline significance ($p>0.07$). IL-8 levels were lower in pre-manifest HD MC-CM compared with healthy volunteer MC-CM, with borderline statistical significance ($p=0.05$). All other

comparisons of cytokine levels in pre-manifest HD or manifest HD MC-CM compared with healthy volunteer MC-CM were not significant or borderline significant. Overall, in stimulated conditions there was little statistical evidence of differences in cytokine release between pre-manifest HD or manifest HD monocytes and healthy volunteer monocytes.

5.5.2.2 Cytokine release in laquinimod-treated non-stimulated monocytes

In non-stimulated healthy volunteer MC-CM, levels of IL-4 (p=0.009) and IL-5 (p=0.002) were increased after 2hPT with 1 μM laquinimod, compared with untreated, and there was a borderline increase in levels of IL-12 (p=0.062). After 24hPT with 1 μM laquinimod, levels of IL-4 and IL-5 were still estimated to be higher, but to a lesser degree which was not statistically significant. When treated with 5 μM laquinimod, levels of IL-5 (p=0.025) and IL-12 (p=0.036) were increased after 2hPT, compared with untreated; levels of IL-4 (p=0.014), IL-5 (p=0.002) and TNFα (p=0.022) were increased after 24hPT, compared with untreated; and levels of IL-2 (p=0.030), IL-5 (p=0.007), IL-10 (p=0.004), IL-12 (p=0.026), IL-13 (p=0.005) and TNFα (p=0.006) were increased after 24hPT+24hCT, compared with untreated, in non-stimulated healthy volunteer MC-CM. None of the laquinimod treatments had a statistically significant effect on cytokine levels compared with untreated in non-stimulated pre-manifest HD or manifest HD MC-CM (Figure 5.2). This suggests that in non-stimulated conditions, laquinimod elevates release of Th1-type cytokines, Th2-type cytokines and IL-2 in healthy volunteer monocytes, but does not affect cytokine release in pre-manifest HD or manifest HD monocytes.

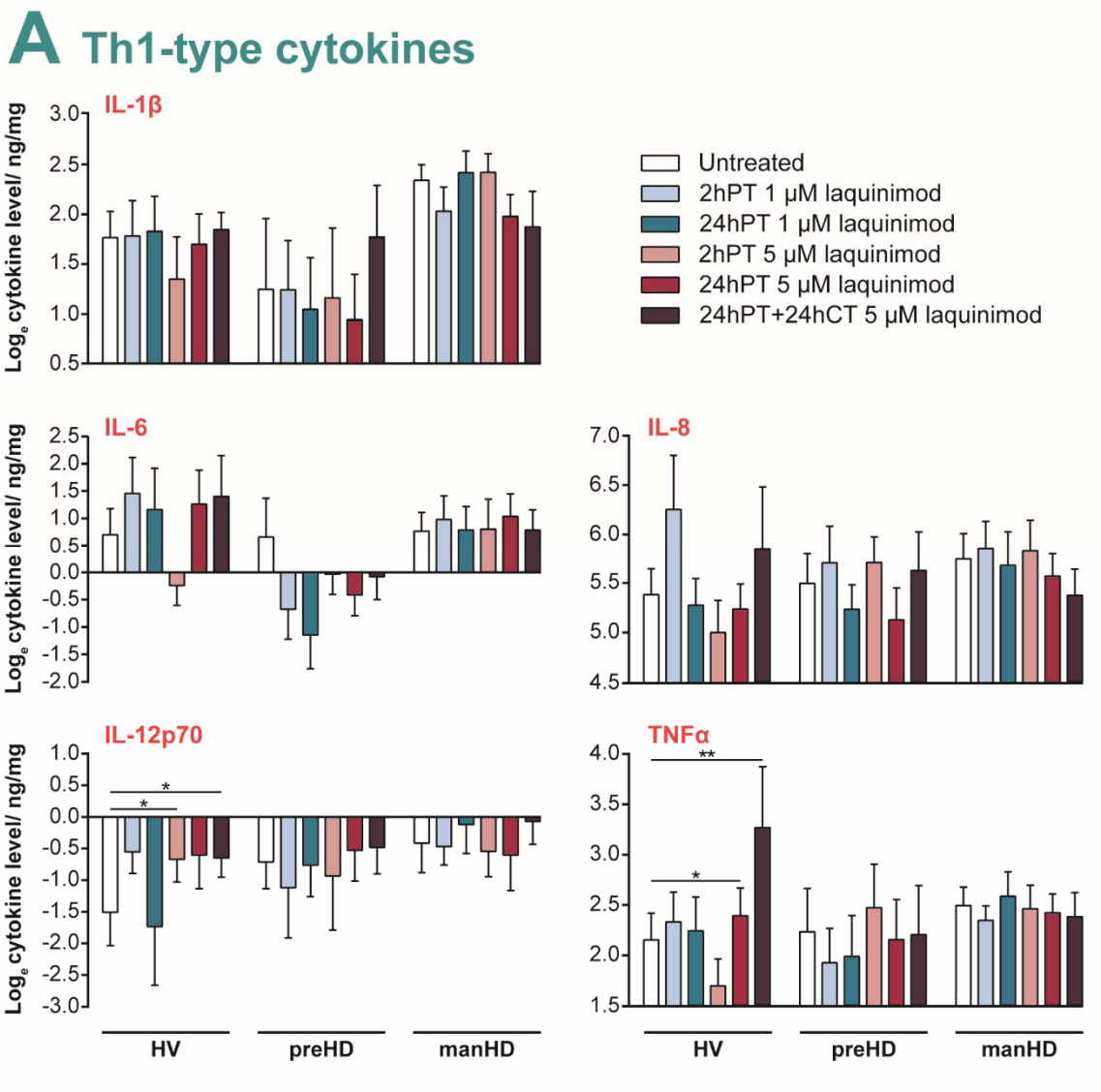
A Th1-type cytokines
IL-1β
IL-6
IL-8
IL-12p70
TNFα
Log$_e$ cytokine level/ ng/mg
Untreated
2hPT 1 µM laquinimod
24hPT 1 µM laquinimod
2hPT 5 µM laquinimod
24hPT 5 µM laquinimod
24hPT+24hCT 5 µM laquinimod
HV
preHD
manHD

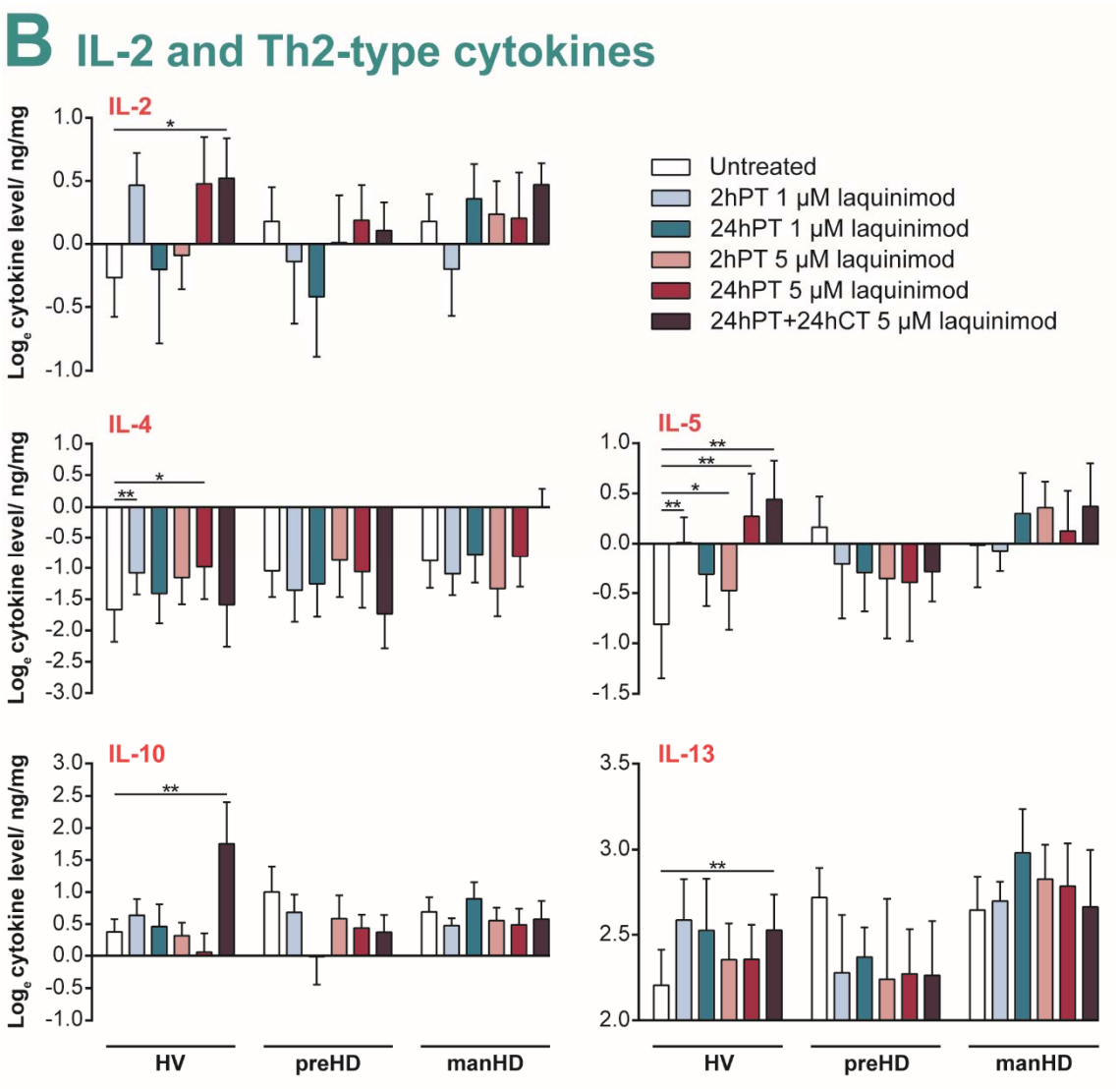

Figure 5.2: Cytokine release in non-stimulated monocytes treated with laquinimod

*Healthy volunteer (HV; n=6-15), pre-manifest HD (preHD; n=4-9) and manifest HD (manHD; n=8-18) monocyte cultures were pre-treated with 1 µM or 5 µM laquinimod, or were untreated, for 2 h or 24 h followed by 24 h rest, or were pre-treated with 5 µM laquinimod followed by 24 h continued treatment with 5 µM laquinimod. All conditions were tested in duplicate in monocyte cultures from each subject. Levels of Th1-type cytokines (**A**) and Th2-type cytokines (and IL-2) (**B**) were then measured in MC-CM by MSD assay, with two internal MSD assay experimental replicates per condition per subject culture. Results are presented as mean average log$_e$ cytokine level normalised to total protein per culture, from biological repeats, ± SD. Data were statistically analysed using a linear mixed regression model (as described in detail in section 2.9.3); *p<0.05, **p<0.01.*

5.5.2.3 Cytokine release in stimulated monocytes pre-treated with 1 μM laquinimod

In stimulated healthy volunteer monocytes, 2hPT with 1 μM laquinimod did not have a significant effect on levels of any of the cytokines measured, compared with untreated (p>0.05). After 24hPT with 1 μM laquinimod, there was a significant increase in levels of IL-5 (p=0.035) and a borderline significant increase in levels of IL-8 (p=0.064), compared with untreated.

In stimulated pre-manifest HD monocytes, 2hPT with 1 μM laquinimod resulted in a significant decrease in levels of IL-8 (p=0.004) and a borderline significant decrease in levels of IL-6 (p=0.069), compared with untreated. After 24hPT with 1 μM laquinimod, levels of IL-6 were significantly decreased compared with untreated (p=0.028).

In stimulated manifest HD monocytes, 2hPT with 1 μM laquinimod also resulted in a significant decrease in levels of IL-8 (p=0.005), compared with untreated. After 24hPT, however, there were no statistically significant effects of 1 μM laquinimod treatment, compared with untreated, on levels of any of the cytokines measured (p>0.05).

Results for cytokine release in stimulated monocytes pre-treated with 1 μM laquinimod are presented in Figure 5.3.

5.5.2.4 Cytokine release in stimulated monocytes pre-treated with 5 μM laquinimod

In stimulated healthy volunteer monocytes, 2hPT or 24hPT with 5 μM laquinimod did not have a significant effect on levels of any of the cytokines measured, compared with untreated (p>0.05). After 24hPT+24hCT with 5 μM laquinimod there was a significant decrease in levels of IL-6 (p=0.004) and a significant increase in levels of IL-5 (p=0.047) and IL-13 (p=0.041), compared with untreated.

In stimulated pre-manifest HD monocytes, although not always statistically significant, levels of cytokines following treatment with 5 μM laquinimod were generally lower than untreated. IL-2 and IL-5 were the only exceptions, which showed trends for increased levels compared with untreated. These increases, however, were small in magnitude and not statistically significant. After 2hPT with 5 μM laquinimod, there were significant decreases in levels of IL-6 (p=0.015) and IL-10 (p=0.037), compared with untreated, in stimulated pre-manifest HD MC-CM. After 24hPT, there were significant decreases in levels of IL-8 (p=0.015), IL-10 (p=0.015) and IL-13 (p=0.033) compared with untreated. After 24hPT+24hCT, there were significant decreases in levels of IL-6 (p=0.016) and IL-10 (p=0.004) compared with untreated.

In stimulated manifest HD monocytes, 2hPT with 5 μM laquinimod did not have a significant effect on levels of any of the cytokines measured, compared with untreated (p>0.05). However, after 24hPT with 5 μM laquinimod, there were at least borderline

significant decreases in levels of several cytokines compared with untreated. There were decreases in the Th1-type cytokines IL-1β (p=0.022), IL-6 (p=0.056), IL-8 (p=0.052) and TNFα (p=0.007), and the Th2-type cytokines IL-5 (p=0.053), IL-10 (p=0.044) and IL-13 (p=0.052). In addition, 24hPT with 5 μM laquinimod resulted in a statistically significant decrease in levels of the cytokines IL-1β, IL-10 and TNFα in manifest HD monocytes, which did not occur in healthy volunteer monocytes. While not statistically significant, many of the other cytokines were also decreased in manifest HD MC-CM and not in healthy volunteer MC-CM. This may suggest that 24hPT with 5 μM laquinimod has more of an effect on reducing cytokine release in manifest HD monocytes than in healthy volunteer monocytes. After 24hPT+24hCT with 5 μM laquinimod, there were significant decreases in levels of IL-12 (p=0.028) and TNFα (p=0.009), and a borderline significant decrease in levels of IL-6 (p=0.053), compared with untreated, in stimulated manifest HD monocytes. Although not statistically significant, levels of IL-2, IL-4, IL-5 and IL-13 were increased, going against the trend for a decrease in cytokine levels occurring after 2hPT and 24hPT with 5 μM laquinimod.

A secondary analysis was performed, with HD subject groups (pre-manifest HD and manifest HD) combined, to increase statistical power and assess differences in cytokine release between healthy volunteer and HD monocytes overall. In stimulated HD monocytes, 24hPT with 5 μM laquinimod resulted in at least borderline significant decreases in levels of the Th1-type cytokines IL-1β (p=0.006), IL-6 (p=0.059), IL-8 (p=0.005) and TNFα (p=0.003), and the Th2-type cytokines IL-10 (p=0.003) and IL-13 (p=0.009), compared with untreated. Additionally, the difference in change from the untreated condition between grouped HD subjects and healthy volunteers was of at least borderline significance for IL-1β (p=0.062), IL-5 (p=0.045), IL-10 (p=0.008), IL-13 (p=0.005) and TNFα (p=0.045), suggesting that 24hPT with 5 μM laquinimod has a larger effect on reducing cytokine release in HD monocytes than in healthy volunteer monocytes.

Results for cytokine release in stimulated monocytes pre-treated with 5 μM laquinimod are presented in Figure 5.3.

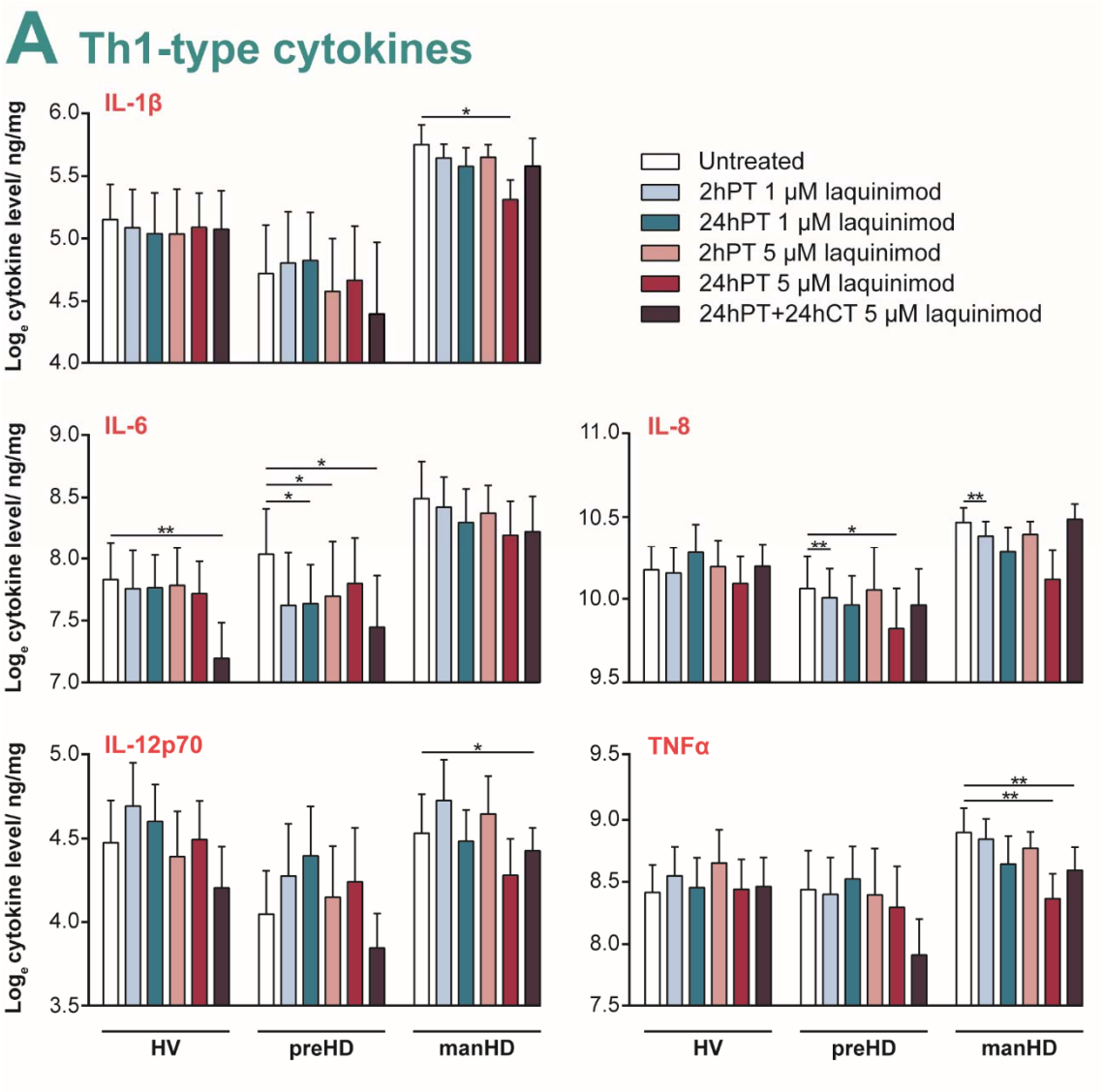
A Th1-type cytokines
IL-1β
IL-6
IL-8
IL-12p70
TNFα
Log$_e$ cytokine level/ ng/mg
Untreated
2hPT 1 μM laquinimod
24hPT 1 μM laquinimod
2hPT 5 μM laquinimod
24hPT 5 μM laquinimod
24hPT+24hCT 5 μM laquinimod
HV
preHD
manHD

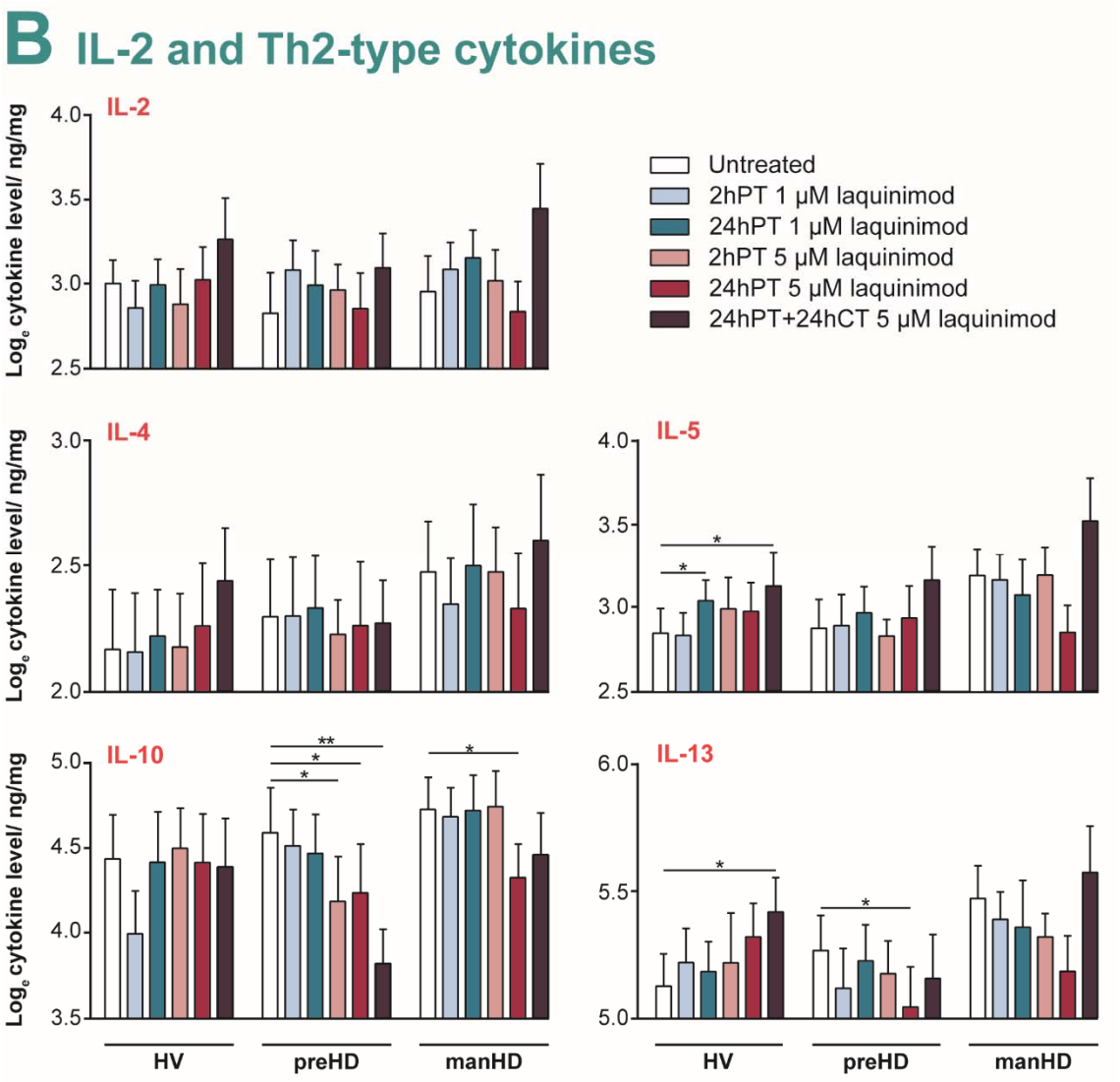

Figure 5.3: Cytokine release in stimulated monocytes pre-treated with laquinimod

*Healthy volunteer (HV; n=8-15), pre-manifest HD (preHD; n=5-9) and manifest HD (manHD; n=8-19) monocyte cultures were pre-treated with 1 µM or 5 µM laquinimod, or were untreated, for 2 h or 24 h followed by 24 h stimulation with 1 µg/mL LPS and 10 ng/mL IFNγ, or were pre-treated with 5 µM laquinimod followed by 24 h stimulation with continued treatment with 5 µM laquinimod. All conditions were tested in duplicate in monocyte cultures from each subject. Levels of Th1-type cytokines (**A**) and Th2-type cytokines (and IL-2) (**B**) were then measured in MC-CM by MSD assay, with two internal MSD assay experimental replicates per condition per subject culture. Results are presented as mean average log$_e$ cytokine level normalised to total protein per culture, from biological repeats, ± SD. Data were statistically analysed using a linear mixed regression model (as described in detail in section 2.9.3); *p<0.05, **p<0.01.*

5.5.3 Investigation into the effects of laquinimod on NFκB pathway modulation in HD patient myeloid cells

In section 5.5.2.4, 24hPT with 5 μM laquinimod was demonstrated to reduce cytokine release in response to stimulation in HD patient monocytes. To determine if laquinimod reduced cytokine release by reversing NFκB pathway dysfunction, the effects of laquinimod treatment on mHTT-IKKγ protein interactions, IκB degradation kinetics and nuclear translocation of NFκB p65 were assessed in HD patient myeloid cells.

5.5.3.1 Mutant HTT-IKKγ protein interactions in laquinimod-treated HD patient BMD-macrophages

It has previously been shown that in HD patient myeloid cells, mHTT directly interacts with the γ subunit of IKK, and it is this dysfunctional interaction which may lead to elevated IκB degradation in HD patient myeloid cells compared with healthy volunteer myeloid cells (Träger *et al.* 2014a). To determine if laquinimod can reduce, or prevent, these dysfunctional protein interactions, pre-manifest HD and manifest HD BMD-macrophages were treated with 5 μM laquinimod for 24 h, or were untreated, and PLA was performed to assess HTT-IKKγ interactions in these cells. As demonstrated by Träger *et al.* (2014a), interactions between HTT and IKKγ were detected in HD patient BMD-macrophages, however there was no significant difference between the number of HTT-IKKγ interactions (PLA spots per cell) in laquinimod-treated BMD-macrophages compared with untreated BMD-macrophages (p=0.552) (Figure 5.4). This suggests that laquinimod does not affect the interaction between mHTT and IKKγ in HD patient BMD-macrophages.

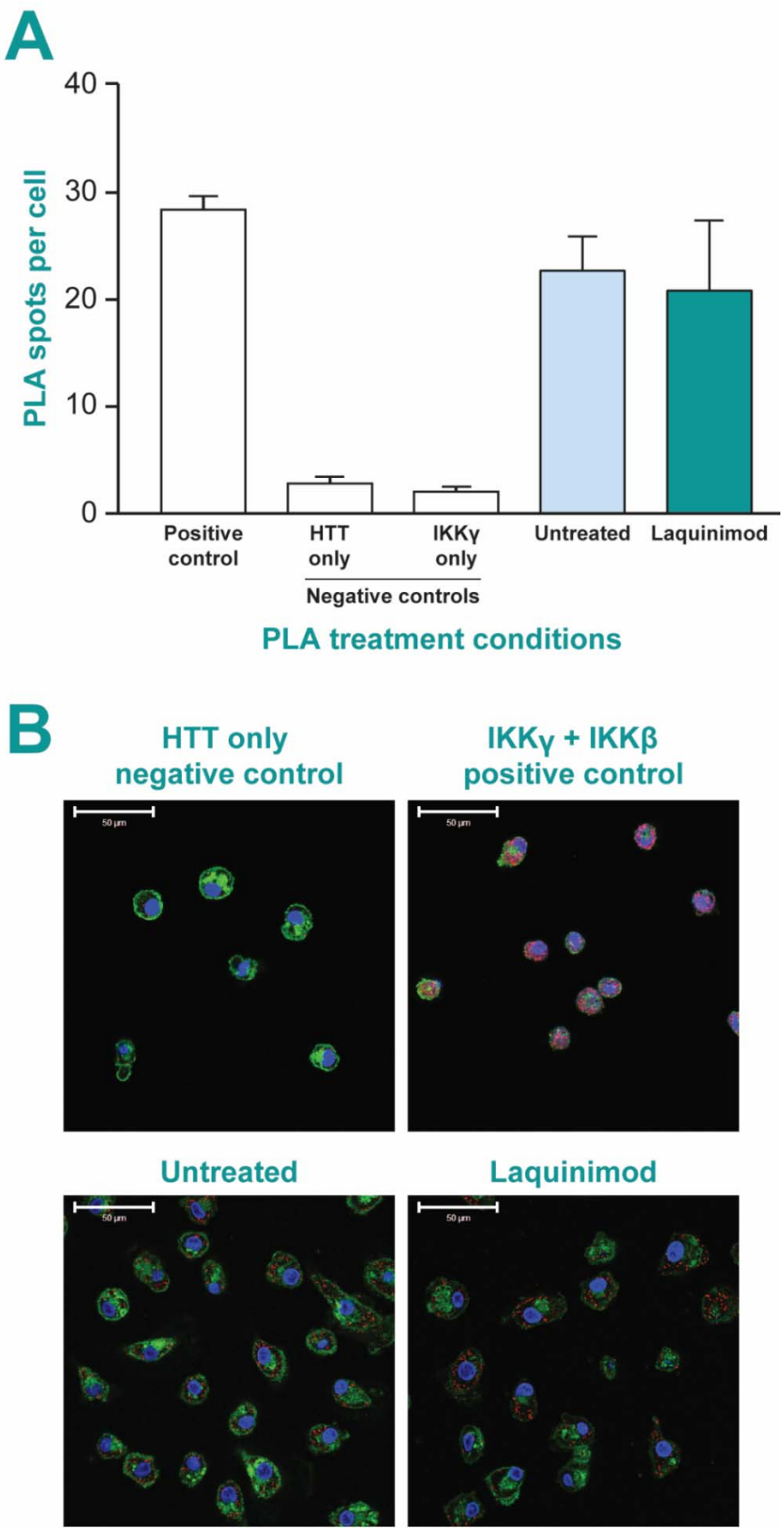

Figure 5.4: Interactions between mHTT and IKKγ in laquinimod-treated HD patient BMD-macrophages

Pre-manifest HD and manifest HD BMD-macrophage cultures (n=5-6) were treated with 5 µM laquinimod, or were untreated, for 24 h. Interactions between HTT and IKKγ were then detected

*by PLA, using primary antibodies directed at HTT (4C9) and IKKγ. Cells were imaged using confocal fluorescence microscopy, and a direct interaction between the two proteins is presented as a fluorescent red spot. Results are presented as mean average number of PLA spots per cell, from biological repeats, ± SEM (**A**). The positive control (primary antibodies directed at IKKγ and IKKβ; two proteins known to directly interact) and negative controls (primary antibodies directed at HTT only (4C9) or IKKγ only, with both secondary antibodies) indicate success of the assay. Representative example confocal fluorescence microscopy images following PLA in BMD-macrophages from the same HD patient are also presented (**B**). Nuclei were stained with DAPI (blue), membranes were stained with WGA (green), and red spots indicate direct interactions between HTT and IKKγ. Scale bars = 50 μm. Data were statistically analysed using a paired, two-tailed, Student's t-test to compare the mean differences in PLA spots per cell between laquinimod-treated and untreated HD patient BMD-macrophages (5 matched pairs).*

5.5.3.2 IκB degradation kinetics in laquinimod-treated HD patient monocytes

Träger *et al.* (2014a) had previously shown that degradation of IκB is more rapid in response to LPS stimulation in HD patient myeloid cells compared with healthy volunteer myeloid cells, leading to elevated nuclear translocation of NFκB p65. To determine if laquinimod can reduce this increased IκB degradation, IκB levels were measured by Western botting in HD patient monocyte cultures over a 60 min time-course post-LPS stimulation, in untreated cells or cells which had received 24hPT with 5 μM laquinimod. LPS stimulation resulted in the usual IκB degradation pattern for HD patient monocytes (Träger *et al.* 2014a), and laquinimod pre-treatment did not significantly alter IκB levels, compared with untreated, over time post-LPS stimulation (p=0.566) (Figure 5.5). There were also no significant differences in IκB levels between laquinimod-treated and untreated monocyte cultures at each time-point post-stimulation (p>0.05). This suggests that laquinimod does not affect IκB degradation kinetics in HD patient myeloid cells.

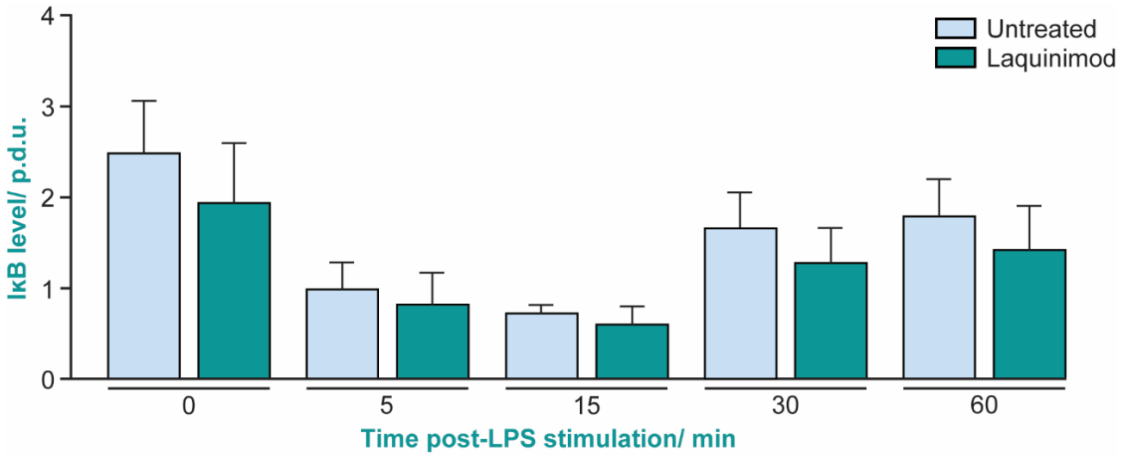

Figure 5.5: IκB degradation kinetics post-LPS stimulation in laquinimod-treated HD patient monocytes

Manifest HD patient monocyte cultures (n=4) were pre-treated with 5 µM laquinimod, or were untreated, for 24 h, then were stimulated with 1 µg/ml LPS. Cell lysates were harvested at 0, 5, 15, 30 and 60 min post-LPS stimulation and IκB levels were measured using Western blot. All IκB readings were normalised to the house-keeping protein GAPDH, and quantified by densitometry analysis giving a procedure defined unit (p.d.u.) for comparison of conditions. Results are presented as mean average IκB level from biological repeats, ± SEM. Data were statistically analysed using two-way RM ANOVA with Bonferroni post-tests.

5.5.3.3 NFκB p65 nuclear translocation in laquinimod-treated HD patient monocytes

It has previously been shown that in response to LPS stimulation, nuclear translocation of NFκB p65 is enhanced in HD patient myeloid cells compared with healthy volunteer myeloid cells (Träger *et al.* 2014a). Increased NFκB activity may be the cause for elevated proinflammatory cytokine release in these cells. Laquinimod treatment has been demonstrated to reduce p65 nuclear translocation in primary murine astrocytes (Brück *et al.* 2012). To determine if laquinimod can reduce increased nuclear translocation of p65 in HD patient myeloid cells, p65 nuclear translocation was assessed by IFC in manifest HD patient monocytes 45 min post-LPS stimulation, in untreated cells or cells which had received 24hPT with 5 µM laquinimod. There was no significant difference in the extent of p65 translocation in laquinimod-treated monocytes compared with untreated monocytes (p=0.466) (Figure 5.6). This suggests that laquinimod does not reduce increased nuclear translocation of p65 in HD patient monocytes.

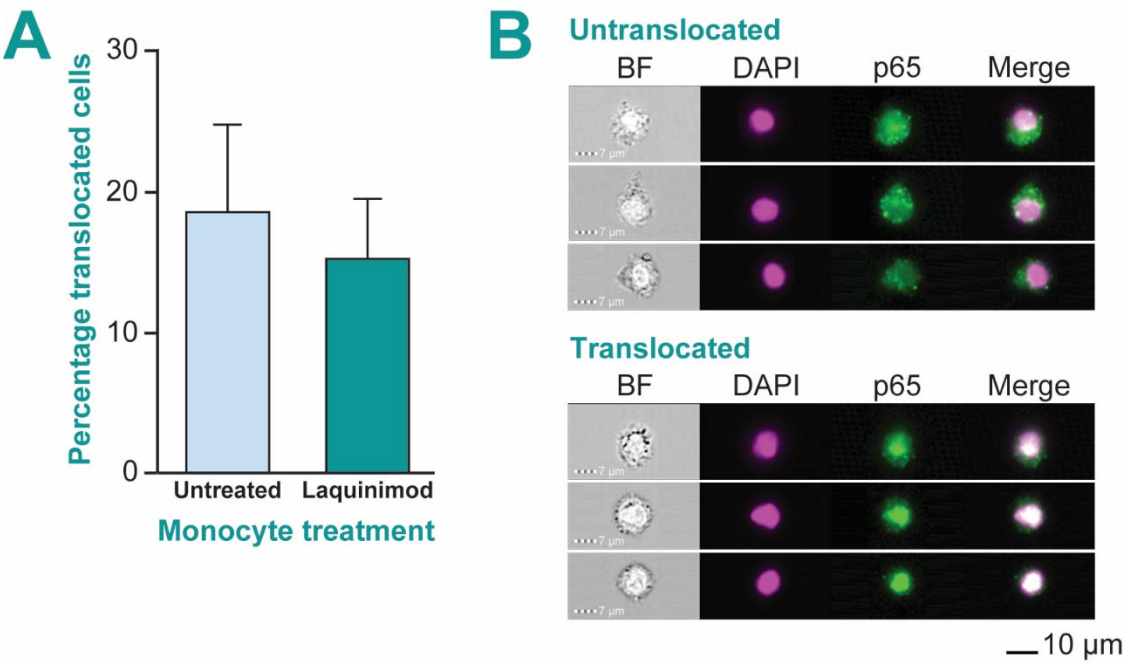

Figure 5.6: Nuclear translocation of p65 in laquinimod-treated HD patient monocytes

*Manifest HD monocyte cultures (n=7) were treated with 5 µM laquinimod, or were untreated, for 24 h, then were stimulated with 1 µg/ml LPS for 45 min. Nuclear translocation of p65 post-stimulation was assessed by IFC and results are presented as mean average percentage translocated cells, from biological repeats, ± SEM (**A**). Representative example IFC images of monocytes from the same HD patient are also presented (**B**). Monocytes were probed for p65 (green) and nuclei were stained with DAPI (pink) to determine extra- or intra-nuclear localisation of p65, and cells were considered to be "untranslocated" (top) or "translocated" (bottom), respectively. Data were statistically analysed using a paired, two-tailed, Student's t-test to compare the mean differences in percentage translocated cells between laquinimod-treated and untreated HD patient monocytes (7 matched pairs).*

5.6 Discussion

5.6.1 Cytokine release in healthy volunteer, pre-manifest HD and manifest HD monocytes

It has previously been shown that HD patient monocytes release elevated levels of the proinflammatory cytokines IL-1β, IL-6 and TNFα, compared with healthy volunteer monocytes, in response to stimulation with LPS and IFNγ (Björkqvist *et al.* 2008; Träger *et al.* 2014a). It was shown here that HD monocytes also release elevated levels of cytokines in non-stimulated conditions, including both Th1-type cytokines (IL-1β, IL-6, IL-8, IL-12 and TNFα) and Th2-type cytokines (IL-4, IL-5, IL-10 and IL-13), as well as IL-2. This suggests that HD monocytes have an inherent dysfunctional

upregulation of cytokine release, and this does not only apply to proinflammatory Th1-type cytokines, but also to Th2-type cytokines and IL-2.

In stimulated conditions, manifest HD monocytes were shown here to release increased levels of IL-1β, IL-5 and IL-13, and pre-manifest HD monocytes released reduced levels of IL-8, compared with healthy volunteer monocytes. Levels of IL-6 and TNFα release were not increased in HD monocytes, unlike findings reported by Björkqvist *et al.* (2008) and Träger *et al.* (2014a). Reasons for these differences could be the lower LPS stimulation concentration used here (1 μg/mL rather than 2 μg/mL as was used by Björkqvist *et al.* and Träger *et al.*), and also the way cytokine levels were normalised. Here, cytokine levels were normalised to total protein levels per monocyte culture to account for cell number. Björkqvist *et al.* reported an increase in IL-6 levels in pre-manifest HD monocytes, but this was not normalised, and Träger *et al.* reported increases in IL-6 and TNFα levels in pre-manifest HD and manifest HD monocytes relative to the non-stimulated condition i.e. cytokine release was increased more in HD monocytes compared with increases in healthy volunteer monocytes.

5.6.2 Effects of laquinimod treatments on cytokine release in healthy volunteer, pre-manifest HD and manifest HD monocytes

Laquinimod did not reduce the dysfunctional upregulation of proinflammatory cytokine release in non-stimulated HD patient monocytes, and did not promote a Th2-type cytokine profile in these cells. In non-stimulated healthy volunteer monocytes, laquinimod treatment resulted in increases in Th1- and Th2-type cytokine release. In stimulated conditions, however, 24hPT with 5 μM laquinimod reduced the release of several cytokines in HD patient monocytes compared with untreated, including the Th1-type cytokines IL-1β, IL-6, IL-8 and TNFα, and the Th2-type cytokines IL-5, IL-10 and IL-13, suggesting that laquinimod has an overall dampening effect on cytokine release in HD monocytes. The same laquinimod treatment also had an effect of larger magnitude in HD monocytes than in healthy volunteer monocytes for levels of IL-1β, IL-5, IL-8, IL-10, IL-13 and TNFα release, suggesting that laquinimod has more of an effect on dampening cytokine release in HD patient monocytes than in healthy volunteer monocytes. 24hPT with 5 μM laquinimod had very little effect, if any, on levels of cytokine release in stimulated healthy volunteer monocytes.

Trends in cytokine levels were generally consistent across laquinimod-treatment conditions in terms of laquinimod-induced changes being greater in magnitude at the higher drug concentration (5 μM) and with a longer pre-treatment duration (24 h). However, this did not usually extend to the 24hPT+24hCT condition, where in many cases a much smaller change from the untreated condition occurred than would have

been predicted, or there was even a change in the opposite direction. With the exception of IL-10, there were small increases in levels of release of the Th2-type cytokines after 24hPT+24hCT with 5 μM laquinimod. Interestingly, in stimulated healthy volunteer monocytes, levels of Th1-type cytokine IL-6 were decreased and levels of Th2-type cytokines IL-5 and IL-13 were increased, compared with untreated, indicating a potential laquinimod-induced M1 to M2 phenotype switch in these cells. In stimulated manifest HD patients, the same laquinimod treatment resulted in decreases in levels of Th1-type cytokines IL-12, TNFα and IL-6, and although not statistically significant, levels of IL-2 and the Th2-type cytokines IL-4, IL-5 and IL-13 were increased (levels of these cytokines were decreased in 2hPT and 24hPT conditions). It is possible that the 24hPT+24hCT treatment condition may need to be considered independently from the pre-treatment only conditions due to laquinimod being present during stimulation. An alternative mechanism of action may be occurring under these conditions, such as competitive binding or confounding cross talk between intracellular signalling pathways.

2hPT and 24hPT conditions did not show a laquinimod-induced shift from Th1- to Th2-type cytokine balance, unlike what has been reported to occur in MS (Zou *et al.* 2002; Yang *et al.* 2004; Brück and Wegner 2011; Schulze-Topphoff *et al.* 2012). However, in MS, this laquinimod-induced cytokine shift was demonstrated in different systems than used here. Zou *et al.* (2002), Yang *et al.* (2004), Schulze-Topphoff *et al.* (2012) and Brück and Wegner (2011) all showed decreases in proinflammatory Th1-type cytokines and increases in anti-inflammatory and Th2-type cytokines *in vivo* in animal models of MS, following daily laquinimod treatment. Th1- to Th2-type cytokine switches were shown in sciatic nerve sections (Zou *et al.* 2002) or spleen mononuclear cells (Yang *et al.* 2004; Schulze-Topphoff *et al.* 2012) isolated from laquinimod-treated animals. However, in lymph node mononuclear cells and PBMCs isolated from laquinimod-treated animals (Zou *et al.* 2002; Yang *et al.* 2004), or PBMCs isolated from healthy volunteers (Brück and Wegner 2011), the authors only report decreases in Th1-type cytokines. Also, in stimulated human microglia cultures, laquinimod pre-treatment was shown to reduce the release of both Th1-type cytokines TNFα, IL-1β, IL-12p70 and IL-6 and Th2-type/regulatory cytokines IL-4, IL-10 and IL-1 receptor antagonist (IL-1RA) (Mishra *et al.* 2014). Therefore, the evidence presented here for a laquinimod-induced decrease in cytokine release overall from HD patient monocytes, and lack of a Th1- to Th2-type shift in cytokine balance in pre-treatment only conditions, is supported by the current literature on laquinimod effects in MS models and primary human myeloid cells.

5.6.3 Effects of laquinimod treatments on reversing NFκB pathway dysfunction in HD patient myeloid cells

Modulation of NFκB signalling has previously been presented as a potential mechanism of action for laquinimod. Laquinimod reduced NFκB activation in a mouse model of MS and in primary human astrocyte cultures (Brück *et al.* 2012); and in laquinimod-treated PBMCs isolated from MS patients, genes downstream of NFκB signalling were downregulated (Gurevich *et al.* 2010). NFκB signalling has been shown to be pathologically enhanced in myeloid cells isolated from HD patients. This is due to a dysfunctional interaction between mHTT and IKKγ which leads to a more rapid degradation of IκB, enhanced and prolonged nuclear translocation of NFκB p65 and elevated production and release of proinflammatory cytokines in response to LPS stimulation (Träger *et al.* 2014a). While a role for NFκB modulation in laquinimod mechanism of action has been proposed, here laquinimod did not reverse NFκB pathway dysfunction in HD patient myeloid cells. Laquinimod did not affect mHTT-IKKγ protein interactions, IκB degradation kinetics or nuclear translocation of NFκB p65 in HD patient myeloid cells, compared with untreated. Similarly, whilst Brück *et al.* (2002) found NFκB activation to be markedly reduced in laquinimod-treated primary mouse astrocytes, they did not observe a reduction in NFκB activation in laquinimod-treated primary mouse microglia, in response to stimulation. This suggests that laquinimod-induced reduction in cytokine release is not via modulation of NFκB signalling in myeloid cells. It has been suggested by others that laquinimod may suppress proinflammatory signalling in myeloid cells by reducing phosphorylation and activation of the MAPKs p38 and JNK (Mishra *et al.* 2012).

5.6.4 Laquinimod as a potential therapeutic for the treatment of HD

There is evidence that systemic inflammation leads to microglial activation in the CNS and exacerbation of neurodegeneration pathology (Palin *et al.* 2008; Perry 2007; Perry *et al.* 2007; Cunningham *et al.* 2007), and peripheral immune challenges accelerate disease progression in mouse models of HD (Hsiao *et al.* 2013). This indicates that peripheral immune events directly influence neuroinflammation and neuropathology in HD. Also, modulation of the peripheral immune system has previously been shown to have therapeutic benefit in HD. Transplantation of wild-type bone marrow into YAC128 and BACHD mice reduced circulating proinflammatory cytokine levels, increased synaptic connections in the cortex, suppressed neuropathological defects and improved behavioural outcomes (Kwan *et al.* 2012a). Treatment of BACHD mice with a peripherally acting CB_2 agonist ameliorated motor deficits, synapse loss and CNS inflammation, and prolonged survival by dampening peripheral immune activation (Bouchard *et al.* 2012). There is therefore evidence that peripheral immunomodulation

is a viable therapeutic target for the treatment of HD, and as laquinimod reduced elevated cytokine release in peripheral myeloid cells isolated from HD patients, this immunomodulator is a potential candidate.

Björkqvist *et al.* (2008) reported elevated levels of Th1-type cytokines IL-6, IL-8 and TNFα as well as Th2-type cytokines IL-4 and IL-10 in plasma of HD patients compared with healthy volunteers, and a combination of IL-6, IL-8 and IL-10 cytokine increases was positively correlated with disease progression from pre-manifest HD through to manifest HD. Also, in Chapter 4 of this Thesis, elevated release of the proinflammatory Th1-type cytokines IL-1β, IL-6 and TNFα in BMD-macrophages was shown to cause neurotoxicity in co-culture. Laquinimod was shown here to reduce the release of all of these cytokines in HD patient monocytes. Laquinimod may therefore have the potential to reduce elevated plasma cytokine levels in HD patients and prevent the increasing levels associated with advancing disease, both peripherally and in the brain.

Several anti-inflammatory strategies for the treatment of HD have shown potential at pre-clinical stages of research, however few have led to meaningful benefits in patients (Soulet and Cicchetti 2011). Laquinimod, however, has already been demonstrated to have beneficial effects on inflammation, brain atrophy and disease progression in MS, as well as being safe and well-tolerated in humans, in two Phase III clinical trials (Comi *et al.* 2012; Filippi *et al.* 2014; Vollmer *et al.* 2014). In MS, laquinimod was shown to downregulate immune cell activation and inflammation in the periphery (Yang *et al.* 2004; Schulze-Topphoff *et al.* 2012) and in the CNS (Brück *et al.* 2012; Mishra *et al.* 2014), and here, for the first time, this was also demonstrated to be the case in peripheral myeloid cells isolated from HD patients. Laquinimod therefore has the potential to slow neurodegeneration and disease progression in HD by downregulating inflammatory processes, as it has been shown to do in MS. Currently, laquinimod is under investigation for its potential effects in HD and a Phase II clinical trial (LEGATO-HD) aimed at evaluating the efficacy, safety and tolerability of laquinimod as a treatment in patients with HD is in progress (Teva Pharmaceutical Industries 2016).

5.7 Summary

HD patient monocytes were shown to release elevated levels of both Th1-type cytokines (IL-1β, IL-6, IL-8, IL-12 and TNFα) and Th2-type cytokines (IL-4, IL-5, IL-10 and IL-13), as well as IL-2, compared with healthy volunteer monocytes, in non-stimulated conditions. This suggests that HD monocytes have an inherent dysfunctional upregulation of cytokine release. In stimulated conditions (LPS and IFNγ), 24hPT with 5 μM laquinimod reduced Th1- and Th2-type cytokine release in HD patient monocytes, and did not affect cytokine release in healthy volunteer monocytes.

When laquinimod treatment was continued during stimulation (24hPT+24hCT), there was evidence of a laquinimod-induced Th1- to Th2-type shift in cytokine profile in healthy volunteer monocytes. Laquinimod did not affect mHTT-IKKγ protein interactions, IκB degradation kinetics or nuclear translocation of NFκB p65 in HD patient myeloid cells, suggesting that the mechanism for laquinimod-induced modulation of cytokine release does not involve reversal of NFκB signalling dysfunction in these cells. Modulation of peripheral immune responses has been demonstrated to impact on central pathology and disease progression in HD, and therefore laquinimod may be a promising candidate for dampening the harmful effects of a dysfunctional innate immune system in HD.

6 Conclusions and future work

The innate immune system, both centrally and peripherally, is known to play a significant role in the pathogenesis of HD. However, whether the myeloid cell activation and inflammation associated with neurodegeneration and disease progression in HD is protective, damaging or has no effect remains to be clearly defined. Here, neuronal-myeloid cell interactions were examined in HD co-culture models, with the aim of investigating the contribution of myeloid cells to neurotoxicity or neuroprotection in the pathogenesis of HD. The effects of novel immunomodulatory drug laquinimod on reversing hyper-reactive immune responses in HD were also assessed.

6.1 Novel human neuronal and microglial cell models of HD

Firstly, there was a requirement for development of novel human neuronal and microglial cell models of HD which improve on the limitations of currently available cell models. Here, novel HD and non-HD human NSC-derived neuronal cell lines expressing full-length human *HTT* or human *HTT* exon 1 were developed and characterised. These cell lines can be differentiated into mature HD and non-HD neuronal cultures, and HD neuronal cultures expressing *mHTT* exon 1 exhibit several characteristics of pathologically affected neurons in the HD patient brain; including sub-fragmentation of mHTT protein, intranuclear inclusions composed of mHTT aggregates, and mHTT-induced neuronal death. Additionally, a novel technique was discovered here for the differentiation of *ex vivo* human monocyte cultures, isolated from healthy volunteers or HD patients, into microglia-like cells (BMD-microglia). BMD-microglia are similar to primary human microglia and human brain-resident microglia *in vivo* by both morphological and antigenic criteria: they exhibit microglia-specific morphological phenotypes (presence of all microglial morphological forms (small, round and activated; amoeboid; polarised; ramified with several short processes; highly ramified with very long processes); sub-cellular granule and vacuole formations indicative of phagocytic functions; process motility and cell-to-cell contact via processes and tubules; microglial nodule formations; and polarised migration towards sites of activity) and express key microglial markers (CD11b, CD68, CSF1R, CX3CR1, Iba1, mannose receptor, P2Y12, PU.1 and TREM2). BMD-microglia are polarised towards an M2 alternatively activated phenotype with promotion of a ramified, surveying and quiescent phenotype.

6.1.1 Usefulness of human HD neuronal cell models

Unlike other available cell models of HD, the novel *HTT* exon 1-expressing HD neuronal cell lines presented in this Thesis are human and stably express human *mHTT*, have an isogenic control expressing normal human *HTT*, are easily obtainable and useable on a large scale, and over a short time-frame can be robustly and reproducibly differentiated from NSCs into high yield mature neuronal cultures which display several characteristics similar to pathologically affected neurons in the HD patient brain. This neuronal cell mode of HD will be useful for studying several cellular aspects of HD in a human setting *in vitro*, including mHTT fragmentation, mHTT aggregation, mHTT exon 1 toxicity and mHTT-induced neuronal death. The full-length *HTT*-expressing neuronal cell models may also be useful for investigating the effects of the full-length mHTT protein in cellular pathology in HD, however, further development and characterisation of this model is required.

6.1.2 Usefulness of BMD-microglia as a model of human microglia *in vitro*

Microglia are known to play important roles in CNS injury and disease, and dysregulated microglial activity is involved in the pathogenesis of multiple neurodegenerative diseases, including AD, ALS, HD and PD (Amor *et al.* 2014; Heneka *et al.* 2014; Doty *et al.* 2015). Modulation of microglial responses is therefore an attractive therapeutic target. The technique presented in this Thesis for the differentiation of primary human monocytes into microglia-like cells could be highly valuable for biological, pathophysiological and therapeutic studies in patient-specific BMD-microglia. Microglia isolated from animal models of CNS injury or disease are limited in their usefulness, and primary human microglia are difficult to obtain and unavailable on a large scale. BMD-microglia, however, are similar to primary human microglia or human microglia *in vivo* by both morphological and antigenic criteria, monocytes can be easily obtained using much less invasive procedures than would be required for isolation of microglia, and the protocol for induction of microglia-like cells is simple and can be completed in ten days.

Recent coverage of the Keystone Symposium on “Microglia in the Brain” (Keystone, Colorado, USA 12-16 June 2016) (Fagan 2016) reported that three research groups independently announced that they had generated iPSC-derived microglia. Florent Ginhoux and colleagues (Agency for Science, Technology and Research, Singapore) reported their yet unpublished work demonstrating that they had recapitulated primitive haematopoiesis *in vitro* and generated primitive-like macrophages, that are genetically and phenotypically similar to *in vivo* yolk sac macrophages and microglia progenitors, from iPSCs. When placed in co-culture with neurons, these macrophages developed microglia-like processes that reached out and interacted with the neurons by direct

contact. These findings are similar to the observations made during the differentiation of BMD-macrophages into BMD-microglia described in this Thesis. Also, similarly to the technique described in this Thesis for the induction of microglia-like cells from BMD-macrophages, Julien Muffat and colleagues (Whitehead Institute for Biomedical Research, Cambridge, Massachusetts, USA) reported that they had generated microglia-like cells from iPSC-derived primitive macrophages using a fully defined culture medium which they have developed. Muffat *et al.* showed that these microglia became ramified and sprouted processes, and when placed in co-culture with neurons and astrocytes, their transcriptional signature shifted more towards that of brain microglia than BMD-macrophages (Muffat *et al.* 2016). Edsel Abud and colleagues (University of California, Irvine, California, USA) also presented their yet unpublished work demonstrating that they had generated microglia-like cells from iPSC-derived primitive hematopoietic progenitors by exposing these cells to a mixture of different factors. These microglia-like cells were shown to express typical microglia markers, including P2Y12R, TREM2, and CX3CR1, which are also expressed by the BMD-microglia presented in this Thesis, and had whole-genome transcriptional profiles which closely matched those of primary microglia. Jennifer Pocock and colleagues had previously reported their development of microglia-like cells from iPSCs at the 4th Venusberg Meeting on Neuroinflammation in May 2015 (Pocock 2015).

IPSC-derived microglia are therefore in the pipeline, and due to their differentiation via yolk sac macrophages and microglia progenitors they more closely model *in vivo* microglial developmental lineage. Also, due to their iPSC origin they are available on a much larger scale than primary human monocytes and BMD-microglia, which is necessary for high-throughput drug screening strategies. However, based on the characterisation completed to date, BMD-microglia are morphologically and phenotypically similar to primary human microglia and exhibit the same behaviours and marker expression profile as reported to be demonstrated in iPSC-derived microglia. Also, unlike iPSC-derived microglia, differentiation of BMD-microglia does not require extensive manipulation of the cells *in vitro* or complex co-culture systems, and patient-specific microglia-like cells can be generated in a much shorter time-frame.

Future directions should include further characterisation of BMD-microglia phenotypes and behaviours alongside primary human microglia cultures isolated from the same subjects for comparison; including migration, phagocytosis, cell signalling, transcriptional profiles and epigenetics. This will determine the authenticity and value of these BMD-microglia for use in translational research. An empirical approach should also be taken to analysing the factors in NM which contribute to differentiation of monocytes into microglia-like cells.

6.2 Neuroprotective and neurotoxic phenotypes of myeloid cells in HD

In co-culture, healthy volunteer and HD patient BMD-microglia rescued HD neurons (expressing *mHTT* exon 1) from mHTT-induced neurotoxicity and reduced neuronal death. In non-stimulated conditions, neuroprotective BMD-microglial phenotypes were associated with elevated levels of BDNF release and reduced levels of IFNγ and IL-2 release. Under conditions of chronic inflammation (chronic stimulation with LPS and IFNγ), BMD-microglia shifted more towards an M2 polarisation, indicated by decreased release of Th1-type cytokine TNFα and increased release of Th2-type cytokines IL-4, IL-10 and IL-13, and this was associated with neuroprotection. Manifest HD BMD-microglia became more M2-polarised than healthy volunteer BMD-microglia during chronic stimulation, and released BDNF at approximately three-fold higher levels. Also, neuronal death levels were lower in HD neurons expressing full-length *mHTT* when in co-culture with manifest HD patient BMD-microglia than when in co-culture with healthy volunteer BMD-microglia. This suggests that in HD, microglia are neuroprotective and reduce mHTT-induced neurotoxicity and neuronal death via release of BDNF and Th2-type cytokines.

In contrast, BMD-macrophages, differentiated from *ex vivo* monocyte cultures isolated from healthy volunteers, pre-manifest HD gene carriers or manifest HD patients, were neurotoxic in co-culture with HD or non-HD neurons. Elevated release of the proinflammatory Th1-type cytokines IL-1β, IL-6 and TNFα from BMD-macrophages was associated with neuronal death. This suggests that in HD, peripheral macrophages release proinflammatory cytokines which are neurotoxic. It is possible that microglia are neuroprotective in HD, whilst peripheral macrophages release neurotoxic factors which may contribute to central pathogenesis. An alternative explanation is that the neuroprotective or neurotoxic phenotypes of myeloid cells in HD, whether derived centrally or peripherally, are dependent on M1/M2 polarisation. Monocytes were differentiated into BMD-macrophages by induction with GM-CSF, which promotes the development of classically activated M1 macrophages, and they were demonstrated here to be neurotoxic. BMD-microglia, however, were shown to express markers indicative of M2-polarisation (CSF1R, mannose receptor, TREM2), and were demonstrated here to be neuroprotective. As M2-polarised BMD-microglia were differentiated from monocytes via M1-polarised BMD-macrophages, this is also evidence that M1/M2 polarisation is highly dynamic and changeable, even in mature myeloid cells.

6.2.1 Cell signalling pathway analysis in HD co-culture models

Going forward, it would be of use to interrogate intracellular signalling pathways and specific cell-to-cell interaction mechanisms in neuronal-myeloid cell co-culture models of HD. There should be a particular focus on investigations into mHTT-induced promotion of M1 to M2 polarisation and elevated BDNF release in response to stimulation in HD patient microglia-like cells; the specific effects of proinflammatory Th1-type cytokines IL-1β, IL-6 and TNFα on neurotoxicity; and the specific roles of IL-4, IL-13 and BDNF in rescuing HD neurons from mHTT-induced neurotoxicity. Understanding the cell signalling pathways involved in neuroprotective and neurotoxic myeloid cell phenotypes and the neuronal responses to factors released by myeloid cells is important. An improved knowledge may reveal specific therapeutic targets for promoting neuroprotective myeloid cell phenotypes while inhibiting neurotoxic phenotypes and/or protecting neurons from mHTT-induced neurotoxicity while reducing the impact of neurotoxic factors directly in neurons.

6.2.2 Assessment of neuronal compromise

In this Thesis, neurotoxicity of neurons in co-culture was measured by LDH cytotoxicity assay in the majority of experiments, and in some cases by PI viable dye exclusion as well. According to guidelines for the use and interpretation of assays for monitoring cell death in higher eukaryotes presented by Galluzzi *et al.* (2009), including recommendations provided by the Nomenclature Committee on Cell Death (NCCD), these methods are appropriate as a first-line approach for measuring end-stage cellular demise in the experimental settings used. However, to determine by which subroute cell death occurred, and to characterise cell death in mechanistic terms, additional techniques should be employed. It may be of interest to determine which mechanisms caused neurotoxicity of BMD-macrophages in co-culture e.g. whether neuronal death occurred by apoptotic or necrotic mechanisms; conversely, to assess whether the neuroprotective phenotypes of BMD-microglia in co-culture are due to rescue of neurons from apoptotic or necrotic cell death, and by which mechanisms this occurs. Additionally, more specific measures of neurotoxicity could be employed, including mitochondrial dysfunction, axonal degeneration and loss of synaptic integrity. These measurements can be used for assessment of subtle indications of neuronal compromise in co-culture models of HD, and also to further characterise mHTT-induced neurotoxicity in HD neuronal cell models.

6.2.3 Improvements on neuronal-myeloid cell co-culture models of HD

Recently there has been progress made in protocols for the differentiation of iPSCs into specific neuronal sub-types (Kim *et al.* 2014; Ho *et al.* 2015; Shum *et al.* 2015; Mertens *et al.* 2016). MSNs are the main neuronal sub-type affected in HD, and currently the

protocols for development of authentic MSNs are improving; time-frames required for differentiation of iPSCs into MSNs are decreasing while yields of these neurons in the finally differentiated cultures are increasing (Delli Carri *et al.* 2013; Victor *et al.* 2014; Fjodorova *et al.* 2015; Noakes *et al.* 2015; Straccia *et al.* 2015; Stanslowsky *et al.* 2016). Procedures have not yet been fully optimised, but HD iPSC-derived MSNs are in the pipeline and have the potential to improve on the neuronal cell lines presented in this Thesis for modelling HD neurons *in vitro*. Therefore, a novel improved neuronal-myeloid cell co-culture model of HD may incorporate HD iPSC-derived MSNs and BMD-microglia differentiated from monocytes isolated from the same HD patient. Alternatively, iPSC-derived MSNs could be co-cultured with iPSC-derived microglia from the same HD patient source. To maximise bi-directional interaction and communication between MSNs and microglia in co-culture, and to more closely recapitulate the *in vivo* setting, a 3-dimensional co-culture model could be utilised. Such models have previously been developed using polycaprolactone fibre scaffolds (Daud *et al.* 2012), cross-linked polystyrene scaffolds (Amsbio 2016) and collagen-filled microfluidic platforms (Kim *et al.* 2011) for neuronal-glial co-culture. A patient-specific neuronal-microglia co-culture model of HD which is highly relevant to the human disease will be valuable for the screening of potential therapeutic compounds and for pre-clinical investigations relating to the effects of microglial phenotype modulation in HD.

6.3 Inherent dysfunctional upregulation of cytokine production in HD patient monocytes

Monocytes isolated from HD patients have previously been demonstrated to be hyper-reactive in response to stimulation with LPS and IFNγ, leading to elevated release of proinflammatory Th1-type cytokines compared with monocytes isolated from healthy volunteers (Björkqvist *et al.* 2008; Träger *et al.* 2014a). Here, it was shown that HD patient monocytes also release elevated levels of cytokines in non-stimulated conditions, and this includes Th1-type cytokines (IL-1β, IL-6, IL-8, IL-12 and TNFα) and Th2-type cytokines (IL-4, IL-5, IL-10 and IL-13), as well as IL-2. This suggests that HD monocytes have an inherent dysfunctional upregulation of cytokine production overall, which does not require an external stimulus to become manifest and does not only apply to proinflammatory Th1-type cytokines. Circulating monocytes may therefore be the primary contributors to elevated cytokine levels in HD patient plasma (Dalrymple *et al.* 2007; Björkqvist *et al.* 2008; Heneka *et al.* 2014), and of particular significance, to increasing levels of IL-6, IL-8 and IL-10 which have been shown to correlate with disease progression (Björkqvist *et al.* 2008). Interestingly, levels of cytokine release are not altered in T lymphocytes in HD patients (Miller *et al.* 2015), suggesting that the

dysfunctional upregulation of cytokine release demonstrated here involves a mechanism in myeloid cells which does not occur in cells of the adaptive immune system. It may therefore be worthwhile to investigate mechanisms of cytokine production and release in monocytes which differ from those in T lymphocytes and may be uniquely affected by mHTT expression. Such investigations could yield novel therapeutic targets for specific modulation of a dysfunctional innate immune system in HD.

6.4 Laquinimod dampens hyper-reactive cytokine production in HD patient myeloid cells

Investigations into neuronal-myeloid cell interactions in the pathogenesis of HD revealed myeloid cell M1/M2 polarisation as a potential modifier of neurotoxicity. Promotion of neuroprotective M2 phenotypes over neurotoxic M1 phenotypes in HD patient myeloid cells may therefore be a therapeutic target. Laquinimod has previously been shown to drive an immunomodulatory shift in immune cell phenotypes away from M1 and Th1-type cytokine production and towards M2 and Th2-type cytokine production *in vivo* in animal models of MS and *in vitro* in primary human microglia and PBMCs (Zou *et al.* 2002; Yang *et al.* 2004; Brück and Wegner 2011; Schulze-Topphoff *et al.* 2012; Mishra *et al.* 2014). Laquinimod was also shown to have beneficial effects on inflammation, brain atrophy and disease progression in MS patients, and was demonstrated to be safe and well-tolerated, in two Phase III clinical trials for the treatment of MS (Comi *et al.* 2012; Filippi *et al.* 2014; Vollmer *et al.* 2014).

Here, 24 h pre-treatment with 5 μM laquinimod reduced the release of both Th1-type cytokines (IL-1β, IL-6, IL-8 and TNFα) and Th2-type cytokines (IL-5, IL-10 and IL-13) in HD patient myeloid cells in response to stimulation with LPS and IFNγ. The same laquinimod treatment had no effects on cytokine release in healthy volunteer monocytes. When laquinimod treatment was continued during stimulation, Th2-type cytokine release (IL-5 and IL-13) was increased along with a decrease in Th1-type cytokine release (IL-6) in healthy volunteer monocytes, indicating an M1 to M2 phenotype shift. However, this was not demonstrated in HD patient monocytes. It is possible that in response to stimulation with LPS and IFNγ, HD patient monocytes become more M1-polarised than healthy volunteer monocytes, resulting in the higher levels of release of proinflammatory cytokines which has been reported by others (Björkqvist *et al.* 2008; Träger *et al.* 2014a). As a result, when laquinimod promotes an M1 to M2 shift in these cells, healthy volunteer monocytes reach M2 polarisation whilst the phenotype of HD patient monocytes lies somewhere on the continuum between M1 and M2 activation states. Nevertheless, laquinimod did reverse hyper-reactive cytokine

production in HD patient monocytes, including IL-6, IL-8 and IL-10 for which increasing plasma levels correlate with disease progression (Björkqvist *et al.* 2008). Therefore, laquinimod is a promising candidate for dampening the harmful effects of a dysfunctional innate immune system in HD.

6.4.1 Investigating laquinimod mechanism of action

Modulation of NFκB signalling has previously been presented as a potential mechanism of action for laquinimod (Gurevich *et al.* 2010; Brück *et al.* 2012), and it had been demonstrated that hyper-reactive cytokine release in HD patient myeloid cells occurs, at least in part, as a result of dysfunctional NFκB signalling (Träger *et al.* 2014a). The work presented in this Thesis, however, does not support a role for laquinimod reversing NFκB pathway dysfunction in HD patient myeloid cells, and further work is required to establish the mechanisms by which laquinimod dampens hyper-reactive cytokine release in these cells. It has been proposed that laquinimod may also suppress another proinflammatory signalling pathway by reducing phosphorylation and activation of the MAPKs p38 and JNK (Mishra *et al.* 2012). Other mechanisms which may be worth pursuing include those that influence myeloid cell M1/M2 polarisation balance, such as PPAR, Krueppel-like factor, IRF, STAT and hypoxia-inducible factor signalling, as well as microRNAs (Wang *et al.* 2014b). It would also be of interest to assess the effects of laquinimod on promoting neuroprotective over neurotoxic myeloid cell phenotypes in the neuronal-myeloid cell co-culture models of HD presented in this Thesis.

6.5 Modulation of myeloid cell phenotypes as a therapeutic target in HD

Overall, the findings presented in this Thesis highlight myeloid cell phenotypes as an important modulator of neurotoxicity in HD. M2-type HD myeloid cells which produce Th2-type cytokines and BDNF protect neurons from mHTT-induced neurotoxicity, whilst M1-type HD myeloid cells which produce proinflammatory Th1-type cytokines increase neuronal death. Therefore, harnessing the innate immune system in order to promote neuroprotective myeloid cell phenotypes whilst inhibiting neurotoxic phenotypes is an attractive therapeutic target.

Laquinimod was demonstrated in this Thesis to be a promising candidate for dampening the harmful effects of a dysfunctional innate immune system in HD. Following on from these pre-clinical results in HD patient cells, laquinimod is currently in a Phase II clinical trial aimed at evaluating its efficacy, safety and tolerability as a treatment in patients with HD (LEGATO-HD; Teva Pharmaceutical Industries 2016).

Reference list

Aggarwal B. B. (2003) Signalling pathways of the TNF superfamily: a double-edged sword. *Nat. Rev. Immunol.* **3**, 745–756.

Aharoni R., Saada R., Eilam R., Hayardeny L., Sela M., Arnon R. (2012) Oral treatment with laquinimod augments regulatory T-cells and brain-derived neurotrophic factor expression and reduces injury in the CNS of mice with experimental autoimmune encephalomyelitis. *J. Neuroimmunol.* **251**, 14–24.

Ajami B., Bennett J. L., Krieger C., Tetzlaff W., Rossi F. M. V. (2007) Local self-renewal can sustain CNS microglia maintenance and function throughout adult life. *Nat. Neurosci.* **10**, 1538–1543.

Akagawa K. S., Komuro I., Kanazawa H., Yamazaki T., Mochida K., Kishi F. (2006) Functional heterogeneity of colony-stimulating factor-induced human monocyte-derived macrophages. *Respirol. Carlton Vic* **11 Suppl**, S32-36.

Akira S., Uematsu S., Takeuchi O. (2006) Pathogen recognition and innate immunity. *Cell* **124**, 783–801.

Akiyama H., Nishimura T., Kondo H., Ikeda K., Hayashi Y., McGeer P. L. (1994) Expression of the receptor for macrophage colony stimulating factor by brain microglia and its upregulation in brains of patients with Alzheimer's disease and amyotrophic lateral sclerosis. *Brain Res.* **639**, 171–174.

Alberch J., Pérez-Navarro E., Canals J. M. (2004) Neurotrophic factors in Huntington's disease. *Prog. Brain Res.* **146**, 195–229.

Alto L. T., Chen X., Ruhn K. A., Treviño I., Tansey M. G. (2014) AAV-dominant negative tumor necrosis factor (DN-TNF) gene transfer to the striatum does not rescue medium spiny neurons in the YAC128 mouse model of Huntington's disease. *PloS One* **9**, e96544.

Amor S., Peferoen L. A. N., Vogel D. Y. S., Breur M., Valk P. van der, Baker D., Noort J. M. van (2014) Inflammation in neurodegenerative diseases - an update. *Immunology* **142**, 151–166.

Amori L., Guidetti P., Pellicciari R., Kajii Y., Schwarcz R. (2009) On the relationship between the two branches of the kynurenine pathway in the rat brain in vivo. *J. Neurochem.* **109**, 316–325.

Amsbio (2016) *Application of Alvetex®Scaffold in the development of 3D co-culture models. Application Note 5.* http://www.amsbio.co.uk/brochures/AlvetexScaffold-in-the-Development-of-3D-Co-culture-Models.pdf (accessed online 2016).

Andre R., Carty L., Tabrizi S. J. (2016) Disruption of immune cell function by mutant huntingtin in Huntington's disease pathogenesis. *Curr. Opin. Pharmacol.* **26**, 33–38.

Andrew S. E., Goldberg Y. P., Kremer B., Telenius H., Theilmann J., Adam S., Starr E., Squitieri F., Lin B., Kalchman M. A. (1993) The relationship between trinucleotide (CAG) repeat length and clinical features of Huntington's disease. *Nat. Genet.* **4**, 398–403.

Arrasate M., Finkbeiner S. (2012) Protein aggregates in Huntington's disease. *Exp. Neurol.* **238**, 1–11.

Arrasate M., Mitra S., Schweitzer E. S., Segal M. R., Finkbeiner S. (2004) Inclusion body formation reduces levels of mutant huntingtin and the risk of neuronal death. *Nature* **431**, 805–810.

Barja G. (2004) Free radicals and aging. *Trends Neurosci.* **27**, 595–600.

Barry S. C., Harder B., Brzezinski M., Flint L. Y., Seppen J., Osborne W. R. (2001) Lentivirus vectors encoding both central polypurine tract and posttranscriptional regulatory element provide enhanced transduction and transgene expression. *Hum. Gene Ther.* **12**, 1103–1108.

Batchelor P. E., Liberatore G. T., Wong J. Y., Porritt M. J., Frerichs F., Donnan G. A., Howells D. W. (1999) Activated macrophages and microglia induce dopaminergic sprouting in the injured striatum and express brain-derived neurotrophic factor and glial cell line-derived neurotrophic factor. *J. Neurosci. Off. J. Soc. Neurosci.* **19**, 1708–1716.

Bates G. (2003) Huntingtin aggregation and toxicity in Huntington's disease. *The Lancet* **361**, 1642–1644.

Beal M. F., Matson W. R., Swartz K. J., Gamache P. H., Bird E. D. (1990) Kynurenine pathway measurements in Huntington's disease striatum: evidence for reduced formation of kynurenic acid. *J. Neurochem.* **55**, 1327–1339.

Benjamins J. A. (2013) Direct effects of secretory products of immune cells on neurons and glia. *J. Neurol. Sci.* **333**, 30–36.

Berg J., Mahmoudjanlou Y., Duscha A., Massa M. G., Thöne J., Esser C., Gold R., Haghikia A. (2016) The immunomodulatory effect of laquinimod in CNS autoimmunity is mediated by the aryl hydrocarbon receptor. *J. Neuroimmunol.* **298**, 9–15.

Berger A. (2000) Th1 and Th2 responses: what are they? *BMJ* **321**, 424.

Birnberg T., Kaye J., Weiner B., Caballero I., Barash S., Raymond E., Ben-Eliezer I., et al. (2017) Laquinimod targets the aryl hydrocarbon receptor (AhR) pathway in periphery and brains of naïve and EAE mice (P2.365). *Neurology* **88**.

Björkqvist M., Wild E. J., Thiele J., Silvestroni A., Andre R. et al (2008) A novel pathogenic pathway of immune activation detectable before clinical onset in Huntington's disease. *J. Exp. Med.* **205**, 1869–1877.

Bodner R. A., Outeiro T. F., Altmann S., Maxwell M. M., Cho S. H., Hyman B. T., McLean P. J., Young A. B., Housman D. E., Kazantsev A. G. (2006) Pharmacological promotion of inclusion formation: a therapeutic approach for Huntington's and Parkinson's diseases. *Proc. Natl. Acad. Sci. U. S. A.* **103**, 4246–4251.

Bogaard S. J. A. van den, Dumas E. M., Roos R. A. C. (2013) The role of iron imaging in Huntington's disease. *Int. Rev. Neurobiol.* **110**, 241–250.

Bouchard J., Truong J., Bouchard K., Dunkelberger D., Desrayaud S., Moussaoui S., Tabrizi S. J., Stella N., Muchowski P. J. (2012) Cannabinoid receptor 2 signaling in peripheral immune cells modulates disease onset and severity in mouse models of Huntington's disease. *J. Neurosci. Off. J. Soc. Neurosci.* **32**, 18259–18268.

Bradford J., Shin J.-Y., Roberts M., Wang C.-E., Li X.-J., Li S. (2009) Expression of mutant huntingtin in mouse brain astrocytes causes age-dependent neurological symptoms. *Proc. Natl. Acad. Sci. U. S. A.* **106**, 22480–22485.

Bradford J., Shin J.-Y., Roberts M., Wang C.-E., Sheng G., Li S., Li X.-J. (2010) Mutant huntingtin in glial cells exacerbates neurological symptoms of Huntington disease mice. *J. Biol. Chem.* **285**, 10653–10661.

Bradford M. M. (1976) A rapid and sensitive method for the quantitation of microgram quantities of protein utilizing the principle of protein-dye binding. *Anal. Biochem.* **72**, 248–254.

Brett A. C., Rosenstock T. R., Rego A. C. (2014) Current therapeutic advances in patients and experimental models of Huntington's disease. *Curr. Drug Targets* **15**, 313–334.

Brocker C., Thompson D., Matsumoto A., Nebert D. W., Vasiliou V. (2010) Evolutionary divergence and functions of the human interleukin (IL) gene family. *Hum. Genomics* **5**, 30.

Brodacki B., Staszewski J., Toczyłowska B., Kozłowska E., Drela N., Chalimoniuk M., Stepien A. (2008) Serum interleukin (IL-2, IL-10, IL-6, IL-4), TNFalpha, and INFgamma concentrations are elevated in patients with atypical and idiopathic parkinsonism. *Neurosci. Lett.* **441**, 158–162.

Brubaker S. W., Bonham K. S., Zanoni I., Kagan J. C. (2015) Innate immune pattern recognition: a cell biological perspective. *Annu. Rev. Immunol.* **33**, 257–290.

Brück W., Pförtner R., Pham T., Zhang J., Hayardeny L., Piryatinsky V., Hanisch U.-K., et al. (2012) Reduced astrocytic NF-κB activation by laquinimod protects from cuprizone-induced demyelination. *Acta Neuropathol. (Berl.)* **124**, 411–424.

Brück W., Wegner C. (2011) Insight into the mechanism of laquinimod action. *J. Neurol. Sci.* **306**, 173–179.

Brunmark C., Runström A., Ohlsson L., Sparre B., Brodin T., Aström M., Hedlund G. (2002) The new orally active immunoregulator laquinimod (ABR-215062) effectively inhibits development and relapses of experimental autoimmune encephalomyelitis. *J. Neuroimmunol.* **130**, 163–172.

Budni J., Bellettini-Santos T., Mina F., Garcez M. L., Zugno A. I. (2015) The involvement of BDNF, NGF and GDNF in aging and Alzheimer's disease. *Aging Dis.* **6**, 331–341.

Buraczynska M. J., Van Keuren M. L., Buraczynska K. M., Chang Y. S., Crombez E., Kurnit D. M. (1995) Construction of human embryonic cDNA libraries: HD, PKD1 and BRCA1 are transcribed widely during embryogenesis. *Cytogenet. Cell Genet.* **71**, 197–202.

Burg J. M. M. van der, Björkqvist M., Brundin P. (2009) Beyond the brain: widespread pathology in Huntington's disease. *Lancet Neurol.* **8**, 765–774.

Burguillos M. A., Deierborg T., Kavanagh E., Persson A., Hajji N., Garcia-Quintanilla A., Cano J., et al. (2011a) Caspase signalling controls microglia activation and neurotoxicity. *Nature* **472**, 319–324.

Burguillos M. A., Hajji N., Englund E., Persson A., Cenci A. M., Machado A., Cano J., Joseph B., Venero J. L. (2011b) Apoptosis-inducing factor mediates dopaminergic cell death in response to LPS-induced inflammatory stimulus: evidence in Parkinson's disease patients. *Neurobiol. Dis.* **41**, 177–188.

Butovsky O., Jedrychowski M. P., Moore C. S., Cialic R., Lanser A. J., Gabriely G., Koeglsperger T., et al. (2014) Identification of a unique TGF-β-dependent molecular and functional signature in microglia. *Nat. Neurosci.* **17**, 131–143.

Cagnin A., Kassiou M., Meikle S. R., Banati R. B. (2006) In vivo evidence for microglial activation in neurodegenerative dementia. *Acta Neurol. Scand.* **114**, 107–114.

Cattaneo E., Rigamonti D., Goffredo D., Zuccato C., Squitieri F., Sipione S. (2001) Loss of normal huntingtin function: new developments in Huntington's disease research. *Trends Neurosci.* **24**, 182–188.

Cattaneo E., Zuccato C., Tartari M. (2005) Normal huntingtin function: an alternative approach to Huntington's disease. *Nat. Rev. Neurosci.* **6**, 919–930.

Chakrabarty P., Li A., Ceballos-Diaz C., Eddy J. A., Funk C. C., Moore B., DiNunno N., et al. (2015) IL-10 Alters Immunoproteostasis in APP Mice, Increasing Plaque Burden and Worsening Cognitive Behavior. *Neuron* **85**, 519–533.

Chang K.-H., Wu Y.-R., Chen Y.-C., Chen C.-M. (2015) Plasma inflammatory biomarkers for Huntington's disease patients and mouse model. *Brain. Behav. Immun.* **44**, 121–127.

Chao M. V. (2003) Neurotrophins and their receptors: a convergence point for many signalling pathways. *Nat. Rev. Neurosci.* **4**, 299–309.

Chen H., O'Reilly E. J., Schwarzschild M. A., Ascherio A. (2008) Peripheral inflammatory biomarkers and risk of Parkinson's disease. *Am. J. Epidemiol.* **167**, 90–95.

Chen M., Ona V. O., Li M., Ferrante R. J., Fink K. B., Zhu S., Bian J., et al. (2000) Minocycline inhibits caspase-1 and caspase-3 expression and delays mortality in a transgenic mouse model of Huntington disease. *Nat. Med.* **6**, 797–801.

Chertoff M., Di Paolo N., Schoeneberg A., Depino A., Ferrari C., Wurst W., Pfizenmaier K., Eisel U., Pitossi F. (2011) Neuroprotective and neurodegenerative effects of the chronic expression of tumor necrosis factor α in the nigrostriatal dopaminergic circuit of adult mice. *Exp. Neurol.* **227**, 237–251.

Choi S. H., Kim Y. H., Hebisch M., Sliwinski C., Lee S., D'Avanzo C., Chen H., et al. (2014) A three-dimensional human neural cell culture model of Alzheimer's disease. *Nature* **515**, 274–278.

Cicchetti F., Saporta S., Hauser R. A., Parent M., Saint-Pierre M., Sanberg P. R., Li X. J., et al. (2009) Neural transplants in patients with Huntington's disease undergo disease-like neuronal degeneration. *Proc. Natl. Acad. Sci. U. S. A.* **106**, 12483–12488.

Comi G., Jeffery D., Kappos L., Montalban X., Boyko A., Rocca M. A., Filippi M. (2012) Placebo-controlled trial of oral laquinimod for multiple sclerosis. *N. Engl. J. Med.* **366**, 1000–1009.

Cramer L. A., Klemsz M. J. (1997) Altered kinetics of Tap-1 gene expression in macrophages following stimulation with both IFN-gamma and LPS. *Cell. Immunol.* **178**, 53–61.

Crews F. T., Vetreno R. P. (2016) Mechanisms of neuroimmune gene induction in alcoholism. *Psychopharmacology (Berl.)* **233**, 1543–1557.

Crocker S. F., Costain W. J., Robertson H. A. (2006) DNA microarray analysis of striatal gene expression in symptomatic transgenic Huntington's mice (R6/2) reveals neuroinflammation and insulin associations. *Brain Res.* **1088**, 176–186.

Crotti A., Benner C., Kerman B. E., Gosselin D., Lagier-Tourenne C., Zuccato C., Cattaneo E., Gage F. H., Cleveland D. W., Glass C. K. (2014) Mutant huntingtin promotes autonomous microglia activation via myeloid lineage-determining factors. *Nat. Neurosci.* **17**, 513–521.

Crotti A., Glass C. K. (2015) The choreography of neuroinflammation in Huntington's disease. *Trends Immunol.* **36**, 364–373.

Crouch S. P., Kozlowski R., Slater K. J., Fletcher J. (1993) The use of ATP bioluminescence as a measure of cell proliferation and cytotoxicity. *J. Immunol. Methods* **160**, 81–88.

Cunningham C., Campion S., Teeling J., Felton L., Perry V. H. (2007) The sickness behaviour and CNS inflammatory mediator profile induced by systemic challenge of mice with synthetic double-stranded RNA (poly I:C). *Brain. Behav. Immun.* **21**, 490–502.

Czirr E., Wyss-Coray T. (2012) The immunology of neurodegeneration. *J. Clin. Invest.* **122**, 1156–1163.

Dalrymple A., Wild E. J., Joubert R., Sathasivam K., Björkqvist M., Petersén A., Jackson G. S., et al. (2007) Proteomic profiling of plasma in Huntington's disease reveals neuroinflammatory activation and biomarker candidates. *J. Proteome Res.* **6**, 2833–2840.

Daud M. F. B., Pawar K. C., Claeyssens F., Ryan A. J., Haycock J. W. (2012) An aligned 3D neuronal-glial co-culture model for peripheral nerve studies. *Biomaterials* **33**, 5901–5913.

Davies S. W., Turmaine M., Cozens B. A., DiFiglia M., Sharp A. H., Ross C. A., Scherzinger E., Wanker E. E., Mangiarini L., Bates G. P. (1997) Formation of neuronal intranuclear inclusions underlies the neurological dysfunction in mice transgenic for the HD mutation. *Cell* **90**, 537–548.

Dayalu P., Albin R. L. (2015) Huntington disease: pathogenesis and treatment. *Neurol. Clin.* **33**, 101–114.

De Simone R., Ambrosini E., Carnevale D., Ajmone-Cat M. A., Minghetti L. (2007) NGF promotes microglial migration through the activation of its high affinity receptor: modulation by TGF-beta. *J. Neuroimmunol.* **190**, 53–60.

De Simoni M. G., Sironi M., De Luigi A., Manfridi A., Mantovani A., Ghezzi P. (1990) Intracerebroventricular injection of interleukin 1 induces high circulating levels of interleukin 6. *J. Exp. Med.* **171**, 1773–1778.

Delli Carri A., Onorati M., Castiglioni V., Faedo A., Camnasio S., Toselli M., Biella G., Cattaneo E. (2013) Human pluripotent stem cell differentiation into authentic striatal projection neurons. *Stem Cell Rev.* **9**, 461–474.

DeMarch Z., Giampà C., Patassini S., Bernardi G., Fusco F. R. (2008) Beneficial effects of rolipram in the R6/2 mouse model of Huntington's disease. *Neurobiol. Dis.* **30**, 375–387.

Di Pardo A., Alberti S., Maglione V., Amico E., Cortes E. P., Elifani F., Battaglia G., et al. (2013) Changes of peripheral TGF-β1 depend on monocytes-derived macrophages in Huntington disease. *Mol. Brain* **6**, 55.

DiFiglia M., Sapp E., Chase K. O., Davies S. W., Bates G. P., Vonsattel J. P., Aronin N. (1997) Aggregation of huntingtin in neuronal intranuclear inclusions and dystrophic neurites in brain. *Science* **277**, 1990–1993.

Dobson L., Träger U., Farmer R., Hayardeny L., Loupe P., Hayden M. R., Tabrizi S. J. (2016) Laquinimod dampens hyperactive cytokine production in Huntington's disease patient myeloid cells. *J. Neurochem.* **137**, 782–794.

Donato R., Miljan E. A., Hines S. J., Aouabdi S., Pollock K., Patel S., Edwards F. A., Sinden J. D. (2007) Differential development of neuronal physiological responsiveness in two human neural stem cell lines. *BMC Neurosci.* **8**, 36.

Doty K. R., Guillot-Sestier M.-V., Town T. (2015) The role of the immune system in neurodegenerative disorders: Adaptive or maladaptive? *Brain Res.* **1617**, 155–173.

Drouin-Ouellet J., Sawiak S. J., Cisbani G., Lagacé M., Kuan W.-L., Saint-Pierre M., Dury R. J., et al. (2015) Cerebrovascular and blood-brain barrier impairments in Huntington's disease: Potential implications for its pathophysiology: Vascular impairments in HD. *Ann. Neurol.* **78**, 160–177.

Duijn E. van, Kingma E. M., Mast R. C. van der (2007) Psychopathology in verified Huntington's disease gene carriers. *J. Neuropsychiatry Clin. Neurosci.* **19**, 441–448.

Durrenberger P. F., Fernando F. S., Kashefi S. N., Bonnert T. P., Seilhean D., Nait-Oumesmar B., Schmitt A., et al. (2014) Common mechanisms in neurodegeneration and neuroinflammation: a BrainNet Europe gene expression microarray study. *J. Neural Transm.* **122**, 1055–1068.

Duyao M. P., Auerbach A. B., Ryan A., Persichetti F., Barnes G. T., McNeil S. M., Ge P., Vonsattel J. P., Gusella J. F., Joyner A. L. (1995) Inactivation of the mouse Huntington's disease gene homolog Hdh. *Science* **269**, 407–410.

Ellrichmann G., Petrasch-Parwez E., Lee D.-H., Reick C., Arning L., Saft C., Gold R., Linker R. A. (2011) Efficacy of fumaric acid esters in the R6/2 and YAC128 models of Huntington's disease. *PloS One* **6**, e16172.

Ellrichmann G., Reick C., Saft C., Linker R. A. (2013) The Role of the immune system in Huntington's disease. *Clin. Dev. Immunol.* **2013**, 541259.

Enose Y., Destache C. J., Mack A. L., Anderson J. R., Ullrich F., Ciborowski P. S., Gendelman H. E. (2005) Proteomic fingerprints distinguish microglia, bone marrow, and spleen macrophage populations. *Glia* **51**, 161–172.

Eskandari F., Sternberg E. M. (2002) Neural-immune interactions in health and disease. *Ann. N. Y. Acad. Sci.* **966**, 20–27.

Evans S. J. W., Douglas I., Rawlins M. D., Wexler N. S., Tabrizi S. J., Smeeth L. (2013) Prevalence of adult Huntington's disease in the UK based on diagnoses recorded in general practice records. *J. Neurol. Neurosurg. Psychiatry* **84**, 1156–1160.

Eyo U. B., Wu L.-J. (2013) Bidirectional microglia-neuron communication in the healthy brain. *Neural Plast.* **2013**, 456857.

Fagan T. (2016) *Induced microglia make debut at Keystone Symposium*, Keystone Symposia: Common Mechanisms of Neurodegeneration/Microglia in the Brain: Part 2 of 5. Alzforum, Keystone, Colorado, USA.

Filippi M., Rocca M. A., Pagani E., De Stefano N., Jeffery D., Kappos L., Montalban X., Boyko A. N., Comi G., ALLEGRO Study Group (2014) Placebo-controlled trial of oral laquinimod in multiple sclerosis: MRI evidence of an effect on brain tissue damage. *J. Neurol. Neurosurg. Psychiatry* **85**, 851–858.

Firdaus W. J. J., Wyttenbach A., Giuliano P., Kretz-Remy C., Currie R. W., Arrigo A.-P. (2006) Huntingtin inclusion bodies are iron-dependent centers of oxidative events. *FEBS J.* **273**, 5428–5441.

Fjodorova M., Noakes Z., Li M. (2015) How to make striatal projection neurons. *Neurogenesis Austin Tex* **2**, e1100227.

Fleming G. W. T. H. (1930) Changes in the interstitial cells of the brain with morphine intoxication. *Br. J. Psychiatry* **76**, 159–160.

Forlenza O. V., Diniz B. S., Teixeira A. L., Radanovic M., Talib L. L., Rocha N. P., Gattaz W. F. (2015) Lower cerebrospinal fluid concentration of brain-derived neurotrophic factor predicts progression from mild cognitive impairment to Alzheimer's disease. *Neuromolecular Med.* **17**, 326–332.

Frakes A. E., Ferraiuolo L., Haidet-Phillips A. M., Schmelzer L., Braun L., Miranda C. J., Ladner K. J., et al. (2014) Microglia induce motor neuron death via the classical NF-κB pathway in amyotrophic lateral sclerosis. *Neuron* **81**, 1009–1023.

Franciosi S., Ryu J. K., Shim Y., Hill A., Connolly C., Hayden M. R., McLarnon J. G., Leavitt B. R. (2012) Age-dependent neurovascular abnormalities and altered microglial morphology in the YAC128 mouse model of Huntington disease. *Neurobiol. Dis.* **45**, 438–449.

Frank S. (2014) Treatment of Huntington's disease. *Neurother. J. Am. Soc. Exp. Neurother.* **11**, 153–160.

Gabrilovich D. I., Ostrand-Rosenberg S., Bronte V. (2012) Coordinated regulation of myeloid cells by tumours. *Nat. Rev. Immunol.* **12**, 253–268.

Galluzzi L., Aaronson S. A., Abrams J., Alnemri E. S., Andrews D. W., Baehrecke E. H., Bazan N. G., et al. (2009) Guidelines for the use and interpretation of assays for monitoring cell death in higher eukaryotes. *Cell Death Differ.* **16**, 1093–1107.

Gandhi S., Wood-Kaczmar A., Yao Z., Plun-Favreau H., Deas E., Klupsch K., Downward J., et al. (2009) PINK1-associated Parkinson's disease is caused by neuronal vulnerability to calcium-induced cell death. *Mol. Cell* **33**, 627–638.

Genetic Modifiers of Huntington's Disease (GeM-HD) Consortium (2015) Identification of genetic factors that modify clinical onset of Huntington's disease. *Cell* **162**, 516–526.

Giampà C., Laurenti D., Anzilotti S., Bernardi G., Menniti F. S., Fusco F. R. (2010) Inhibition of the striatal specific phosphodiesterase PDE10A ameliorates striatal and cortical pathology in R6/2 mouse model of Huntington's disease. *PloS One* **5**, e13417.

Giampà C., Montagna E., Dato C., Melone M. A. B., Bernardi G., Fusco F. R. (2013) Systemic delivery of recombinant brain derived neurotrophic factor (BDNF) in the R6/2 mouse model of Huntington's disease. *PloS One* **8**, e64037.

Ginés S., Bosch M., Marco S., Gavaldà N., Díaz-Hernández M., Lucas J. J., Canals J. M., Alberch J. (2006) Reduced expression of the TrkB receptor in Huntington's disease mouse models and in human brain. *Eur. J. Neurosci.* **23**, 649–658.

Ginhoux F., Greter M., Leboeuf M., Nandi S., See P., Gokhan S., Mehler M. F., et al. (2010) Fate mapping analysis reveals that adult microglia derive from primitive macrophages. *Science* **330**, 841–845.

Giorgini F., Guidetti P., Nguyen Q., Bennett S. C., Muchowski P. J. (2005) A genomic screen in yeast implicates kynurenine 3-monooxygenase as a therapeutic target for Huntington disease. *Nat. Genet.* **37**, 526–531.

Giorgini F., Möller T., Kwan W., Zwilling D., Wacker J. L., Hong S., Tsai L.-C. L., et al. (2008) Histone deacetylase inhibition modulates kynurenine pathway activation in yeast, microglia, and mice expressing a mutant huntingtin fragment. *J. Biol. Chem.* **283**, 7390–7400.

Girard S., Larouche A., Kadhim H., Rola-Pleszczynski M., Gobeil F., Sébire G. (2008) Lipopolysaccharide and hypoxia/ischemia induced IL-2 expression by microglia in neonatal brain. *Neuroreport* **19**, 997–1002.

Goldberg Y. P., Kalchman M. A., Metzler M., Nasir J., Zeisler J., Graham R., Koide H. B., et al. (1996) Absence of disease phenotype and intergenerational stability of the CAG repeat in transgenic mice expressing the human Huntington disease transcript. *Hum. Mol. Genet.* **5**, 177–185.

Goldmann T., Wieghofer P., Jordão M. J. C., Prutek F., Hagemeyer N., Frenzel K., Amann L., et al. (2016) Origin, fate and dynamics of macrophages at central nervous system interfaces. *Nat. Immunol.* **17**, 797–805.

Gomes C., Ferreira R., George J., Sanches R., Rodrigues D. I., Gonçalves N., Cunha R. A. (2013) Activation of microglial cells triggers a release of brain-derived neurotrophic factor (BDNF) inducing their proliferation in an adenosine A2A receptor-dependent manner: A2A receptor blockade prevents BDNF release and proliferation of microglia. *J. Neuroinflammation* **10**, 16.

Gordon S., Keshav S., Chung L. P. (1988) Mononuclear phagocytes: tissue distribution and functional heterogeneity. *Curr. Opin. Immunol.* **1**, 26–35.

Gordon S., Taylor P. R. (2005) Monocyte and macrophage heterogeneity. *Nat. Rev. Immunol.* **5**, 953–964.

Graeber M. B., Streit W. J., Kiefer R., Schoen S. W., Kreutzberg G. W. (1990) New expression of myelomonocytic antigens by microglia and perivascular cells following lethal motor neuron injury. *J. Neuroimmunol.* **27**, 121–132.

Gray M., Shirasaki D. I., Cepeda C., André V. M., Wilburn B., Lu X.-H., Tao J., et al. (2008) Full-length human mutant huntingtin with a stable polyglutamine repeat can elicit progressive and selective neuropathogenesis in BACHD mice. *J. Neurosci. Off. J. Soc. Neurosci.* **28**, 6182–6195.

Gray S. G. (2011) Targeting Huntington's disease through histone deacetylases. *Clin. Epigenetics* **2**, 257–277.

Greter M., Lelios I., Croxford A. L. (2015) Microglia versus myeloid cell nomenclature during brain inflammation. *Front. Immunol.* **6**, 249.

Gu X., André V. M., Cepeda C., Li S.-H., Li X.-J., Levine M. S., Yang X. W. (2007) Pathological cell-cell interactions are necessary for striatal pathogenesis in a conditional mouse model of Huntington's disease. *Mol. Neurodegener.* **2**, 8.

Gu X., Li C., Wei W., Lo V., Gong S., Li S.-H., Iwasato T., et al. (2005) Pathological cell-cell interactions elicited by a neuropathogenic form of mutant Huntingtin contribute to cortical pathogenesis in HD mice. *Neuron* **46**, 433–444.

Guillemin G. J., Smith D. G., Smythe G. A., Armati P. J., Brew B. J. (2003) Expression of the kynurenine pathway enzymes in human microglia and macrophages. *Adv. Exp. Med. Biol.* **527**, 105–112.

Guillot-Sestier M.-V., Doty K. R., Gate D., Rodriguez J., Leung B. P., Rezai-Zadeh K., Town T. (2015) Il10 deficiency rebalances innate immunity to mitigate Alzheimer-like pathology. *Neuron* **85**, 534–548.

Gurevich M., Gritzman T., Orbach R., Tuller T., Feldman A., Achiron A. (2010) Laquinimod suppress antigen presentation in relapsing-remitting multiple sclerosis: in-vitro high-throughput gene expression study. *J. Neuroimmunol.* **221**, 87–94.

Gusella J. F., MacDonald M. E., Lee J.-M. (2014) Genetic modifiers of Huntington's disease. *Mov. Disord. Off. J. Mov. Disord. Soc.* **29**, 1359–1365.

Ha A. D., Beck C. A., Jankovic J. (2012) Intermediate CAG Repeats in Huntington's Disease: Analysis of COHORT. *Tremor Hyperkinetic Mov. N. Y. N* **2**.

Hands S., Sajjad M. U., Newton M. J., Wyttenbach A. (2011) In vitro and in vivo aggregation of a fragment of huntingtin protein directly causes free radical production. *J. Biol. Chem.* **286**, 44512–44520.

Hanisch U. K., Neuhaus J., Rowe W., Van Rossum D., Möller T., Kettenmann H., Quirion R. (1997) Neurotoxic consequences of central long-term administration of interleukin-2 in rats. *Neuroscience* **79**, 799–818.

Hanisch U.-K. (2002) Microglia as a source and target of cytokines. *Glia* **40**, 140–155.

Harjes P., Wanker E. E. (2003) The hunt for huntingtin function: interaction partners tell many different stories. *Trends Biochem. Sci.* **28**, 425–433.

Harper P. S. (1999) Huntington's disease: a clinical, genetic and molecular model for polyglutamine repeat disorders. *Philos. Trans. R. Soc. Lond. B. Biol. Sci.* **354**, 957–961.

Hashioka S., McGeer E. G., Miyaoka T., Wake R., Horiguchi J., McGeer P. L. (2015) Interferon-γ-induced neurotoxicity of human astrocytes. *CNS Neurol. Disord. Drug Targets* **14**, 251–256.

Haynes S. E., Hollopeter G., Yang G., Kurpius D., Dailey M. E., Gan W.-B., Julius D. (2006) The P2Y12 receptor regulates microglial activation by extracellular nucleotides. *Nat. Neurosci.* **9**, 1512–1519.

Heemskerk A.-W., Roos R. A. C. (2012) Aspiration pneumonia and death in Huntington's disease. *PLoS Curr.* **4**, RRN1293.

Heneka M. T., Kummer M. P., Latz E. (2014) Innate immune activation in neurodegenerative disease. *Nat. Rev. Immunol.* **14**, 463–477.

Heng M. Y., Detloff P. J., Albin R. L. (2008) Rodent genetic models of Huntington disease. *Neurobiol. Dis.* **32**, 1–9.

Hertzog P. J., Williams B. R. G. (2013) Fine tuning type I interferon responses. *Cytokine Growth Factor Rev.* **24**, 217–225.

Heyes M. P., Saito K., Markey S. P. (1992) Human macrophages convert L-tryptophan into the neurotoxin quinolinic acid. *Biochem. J.* **283 (Pt 3)**, 633–635.

Hilditch-Maguire P., Trettel F., Passani L. A., Auerbach A., Persichetti F., MacDonald M. E. (2000) Huntingtin: an iron-regulated protein essential for normal nuclear and perinuclear organelles. *Hum. Mol. Genet.* **9**, 2789–2797.

Ho S.-M., Topol A., Brennand K. J. (2015) From "directed differentiation" to "neuronal induction": Modeling neuropsychiatric disease. *Biomark. Insights* **10**, 31–41.

Hodgson J. G., Agopyan N., Gutekunst C. A., Leavitt B. R., LePiane F., Singaraja R., Smith D. J., et al. (1999) A YAC mouse model for Huntington's disease with full-length mutant huntingtin, cytoplasmic toxicity, and selective striatal neurodegeneration. *Neuron* **23**, 181–192.

Hoebe K., Janssen E., Beutler B. (2004) The interface between innate and adaptive immunity. *Nat. Immunol.* **5**, 971–974.

Hoffrogge R., Mikkat S., Scharf C., Beyer S., Christoph H., Pahnke J., Mix E., et al. (2006) 2-DE proteome analysis of a proliferating and differentiating human neuronal stem cell line (ReNcell VM). *Proteomics* **6**, 1833–1847.

Holmes C., Cunningham C., Zotova E., Woolford J., Dean C., Kerr S., Culliford D., Perry V. H. (2009) Systemic inflammation and disease progression in Alzheimer disease. *Neurology* **73**, 768–774.

Holmes C., El-Okl M., Williams A., Cunningham C., Wilcockson D., Perry V. (2003) Systemic infection, interleukin 1beta, and cognitive decline in Alzheimer's disease. *J. Neurol. Neurosurg. Psychiatry* **74**, 788–789.

Honda S., Sasaki Y., Ohsawa K., Imai Y., Nakamura Y., Inoue K., Kohsaka S. (2001) Extracellular ATP or ADP induce chemotaxis of cultured microglia through Gi/o-coupled P2Y receptors. *J. Neurosci. Off. J. Soc. Neurosci.* **21**, 1975–1982.

Howells D. W., Porritt M. J., Wong J. Y., Batchelor P. E., Kalnins R., Hughes A. J., Donnan G. A. (2000) Reduced BDNF mRNA expression in the Parkinson's disease substantia nigra. *Exp. Neurol.* **166**, 127–135.

Hsiao H.-Y., Chen Y.-C., Chen H.-M., Tu P.-H., Chern Y. (2013) A critical role of astrocyte-mediated nuclear factor-κB-dependent inflammation in Huntington's disease. *Hum. Mol. Genet.* **22**, 1826–1842.

Hsiao H.-Y., Chiu F.-L., Chen C.-M., Wu Y.-R., Chen H.-M., Chen Y.-C., Kuo H.-C., Chern Y. (2014) Inhibition of soluble tumor necrosis factor is therapeutic in Huntington's disease. *Hum. Mol. Genet.* **23**, 4328–4344.

Hu X., Leak R. K., Shi Y., Suenaga J., Gao Y., Zheng P., Chen J. (2015) Microglial and macrophage polarization—new prospects for brain repair. *Nat. Rev. Neurol.* **11**, 56–64.

Huntington G. (1872) On Chorea. *Med. Surg. Report. Wkly. J.* **26**, 317–321.

Huntington Study Group DOMINO Investigators (2010) A futility study of minocycline in Huntington's disease. *Mov. Disord. Off. J. Mov. Disord. Soc.* **25**, 2219–2224.

Huntington Study Group HART Investigators (2013) A randomized, double-blind, placebo-controlled trial of pridopidine in Huntington's disease. *Mov. Disord. Off. J. Mov. Disord. Soc.* **28**, 1407–1415.

Ito D., Imai Y., Ohsawa K., Nakajima K., Fukuuchi Y., Kohsaka S. (1998) Microglia-specific localisation of a novel calcium binding protein, Iba1. *Brain Res. Mol. Brain Res.* **57**, 1–9.

Ivashkiv L. B., Donlin L. T. (2014) Regulation of type I interferon responses. *Nat. Rev. Immunol.* **14**, 36–49.

Iwasaki A., Medzhitov R. (2015) Control of adaptive immunity by the innate immune system. *Nat. Immunol.* **16**, 343–353.

Janabi N., Peudenier S., Héron B., Ng K. H., Tardieu M. (1995) Establishment of human microglial cell lines after transfection of primary cultures of embryonic microglial cells with the SV40 large T antigen. *Neurosci. Lett.* **195**, 105–108.

Karasuyama H., Mukai K., Tsujimura Y., Obata K. (2009) Newly discovered roles for basophils: a neglected minority gains new respect. *Nat. Rev. Immunol.* **9**, 9–13.

Kay C., Skotte N. H., Southwell A. L., Hayden M. R. (2014) Personalized gene silencing therapeutics for Huntington disease. *Clin. Genet.* **86**, 29–36.

Kaye J., Piryatinsky V., Birnberg T., Hingaly T., Raymond E., Kashi R., Amit-Romach E., et al. (2016) Laquinimod arrests experimental autoimmune encephalomyelitis by activating the aryl hydrocarbon receptor. *Proc. Natl. Acad. Sci. U. S. A.* **113**, E6145–E6152.

Kelly B., O'Neill L. A. J. (2015) Metabolic reprogramming in macrophages and dendritic cells in innate immunity. *Cell Res.* **25**, 771–784.

Kerkis I., Haddad M. S., Valverde C. W., Glosman S. (2015) Neural and mesenchymal stem cells in animal models of Huntington's disease: past experiences and future challenges. *Stem Cell Res. Ther.* **6**, 232.

Khoshnan A., Ko J., Patterson P. H. (2002) Effects of intracellular expression of anti-huntingtin antibodies of various specificities on mutant huntingtin aggregation and toxicity. *Proc. Natl. Acad. Sci. U. S. A.* **99**, 1002–1007.

Khoshnan A., Ko J., Watkin E. E., Paige L. A., Reinhart P. H., Patterson P. H. (2004) Activation of the IkappaB kinase complex and nuclear factor-kappaB contributes to mutant huntingtin neurotoxicity. *J. Neurosci. Off. J. Soc. Neurosci.* **24**, 7999–8008.

Killoran A., Biglan K. M. (2014) Current therapeutic options for Huntington's disease: good clinical practice versus evidence-based approaches? *Mov. Disord. Off. J. Mov. Disord. Soc.* **29**, 1404–1413.

Kim D.-S., Ross P. J., Zaslavsky K., Ellis J. (2014) Optimizing neuronal differentiation from induced pluripotent stem cells to model ASD. *Front. Cell. Neurosci.* **8**, 109.

Kim Y. H., Kim Y. E., Chung S., Kim B., Kim T. S., Kang J. Y. (2011) Three dimensional co-culture of neuron and astrocyte in a micro-fluidic device; 15th International Conference on Miniaturized Systems for Chemistry and Life Sciences; Conference paper published by Royal Society of Chemistry, pp. 852–854. Royal Society of Chemistry, Seattle, Washington, USA.

Kingham P., Cuzner M., Pocock J. (1999) Apoptotic pathways mobilized in microglia and neurones as a consequence of chromogranin A-induced microglial activation. *J. Neurochem.* **73**, 538–547.

Kleij H. van der, Bienenstock J. (2007) *Psychoneuroimmunology*, (Ader R., ed). Elsevier, Department of Psychiatry, Center for Psychoneuroimmunology Research, University of Rochester Medical Center, Rochester, New York, USA.

Kolaczkowska E., Kubes P. (2013) Neutrophil recruitment and function in health and inflammation. *Nat. Rev. Immunol.* **13**, 159–175.

Kraft A. D., Kaltenbach L. S., Lo D. C., Harry G. J. (2012) Activated microglia proliferate at neurites of mutant huntingtin-expressing neurons. *Neurobiol. Aging* **33**, 621.e17-33.

Kuwert T., Lange H. W., Langen K. J., Herzog H., Aulich A., Feinendegen L. E. (1989) Cerebral glucose consumption measured by PET in patients with and without psychiatric symptoms of Huntington's disease. *Psychiatry Res.* **29**, 361–362.

Kwan W., Magnusson A., Chou A., Adame A., Carson M. J., Kohsaka S., Masliah E., et al. (2012a) Bone marrow transplantation confers modest benefits in mouse models of Huntington's disease. *J. Neurosci. Off. J. Soc. Neurosci.* **32**, 133–142.

Kwan W., Träger U., Davalos D., Chou A., Bouchard J., Andre R., Miller A., et al. (2012b) Mutant huntingtin impairs immune cell migration in Huntington disease. *J. Clin. Invest.* **122**, 4737–4747.

Landles C., Sathasivam K., Weiss A., Woodman B., Moffitt H., Finkbeiner S., Sun B., et al. (2010) Proteolysis of mutant huntingtin produces an exon 1 fragment that accumulates as an aggregated protein in neuronal nuclei in Huntington disease. *J. Biol. Chem.* **285**, 8808–8823.

Lavin Y., Mortha A., Rahman A., Merad M. (2015) Regulation of macrophage development and function in peripheral tissues. *Nat. Rev. Immunol.* **15**, 731–744.

Lee D.-H., Geyer E., Flach A.-C., Jung K., Gold R., Flügel A., Linker R. A., Lühder F. (2012) Central nervous system rather than immune cell-derived BDNF mediates axonal protective effects early in autoimmune demyelination. *Acta Neuropathol. (Berl.)* **123**, 247–258.

Leow-Dyke S., Allen C., Denes A., Nilsson O., Maysami S., Bowie A. G., Rothwell N. J., Pinteaux E. (2012) Neuronal Toll-like receptor 4 signaling induces brain endothelial activation and neutrophil transmigration in vitro. *J. Neuroinflammation* **9**, 230.

Lescaudron L., Naveilhan P., Neveu I. (2012) The use of stem cells in regenerative medicine for Parkinson's and Huntington's diseases. *Curr. Med. Chem.* **19**, 6018–6035.

Li Y., Du X.-F., Liu C.-S., Wen Z.-L., Du J.-L. (2012) Reciprocal regulation between resting microglial dynamics and neuronal activity in vivo. *Dev. Cell* **23**, 1189–1202.

Linker R. A., Lee D.-H., Demir S., Wiese S., Kruse N., Siglienti I., Gerhardt E., et al. (2010) Functional role of brain-derived neurotrophic factor in neuroprotective autoimmunity: therapeutic implications in a model of multiple sclerosis. *Brain J. Neurol.* **133**, 2248–2263.

Linker R. A., Lee D.-H., Ryan S., Dam A. M. van, Conrad R., Bista P., Zeng W., et al. (2011) Fumaric acid esters exert neuroprotective effects in neuroinflammation via activation of the Nrf2 antioxidant pathway. *Brain J. Neurol.* **134**, 678–692.

Liu L., Huang J.-S., Han C., Zhang G.-X., Xu X.-Y., Shen Y., Li J., et al. (2016) Induced pluripotent stem cells in Huntington's disease: Disease modeling and the potential for cell-based therapy. *Mol. Neurobiol.* **53**, 6698–6708.

Lorigados Pedre L., Pavón Fuentes N., Alvarez González L., McRae A., Serrano Sánchez T., Blanco Lescano L., Macías González R. (2002) Nerve growth factor levels in Parkinson disease and experimental parkinsonian rats. *Brain Res.* **952**, 122–127.

Lu B., Palacino J. (2013) A novel human embryonic stem cell-derived Huntington's disease neuronal model exhibits mutant huntingtin (mHTT) aggregates and soluble mHTT-dependent neurodegeneration. *FASEB J. Off. Publ. Fed. Am. Soc. Exp. Biol.* **27**, 1820–1829.

Lu X.-H., Yang X. W. (2012) "Huntingtin Holiday": Progress toward an antisense therapy for Huntington's disease. *Neuron* **74**, 964–966.

Lucin K. M., Wyss-Coray T. (2009) Immune activation in brain aging and neurodegeneration: Too much or too little? *Neuron* **64**, 110–122.

Lue L.-F., Schmitz C. T., Serrano G., Sue L. I., Beach T. G., Walker D. G. (2015) TREM2 protein expression changes correlate with Alzheimer's disease neurodegenerative pathologies in post-mortem temporal cortices. *Brain Pathol. Zurich Switz.* **25**, 469–480.

Mahla R. S., Reddy M. C., Prasad D. V. R., Kumar H. (2013) Sweeten PAMPs: Role of sugar complexed PAMPs in innate immunity and vaccine biology. *Front. Immunol.* **4**, 248.

Mangiarini L., Sathasivam K., Seller M., Cozens B., Harper A., Hetherington C., Lawton M., et al. (1996) Exon 1 of the HD gene with an expanded CAG repeat is sufficient to cause a progressive neurological phenotype in transgenic mice. *Cell* **87**, 493–506.

Manth N., Das S. K., Das N. G. (2012) RNAi-based therapies for Huntington's disease: delivery challenges and opportunities. *Ther. Deliv.* **3**, 1061–1076.

Martinez F. O., Gordon S. (2014) The M1 and M2 paradigm of macrophage activation: time for reassessment. *F1000Prime Rep.* **6**, 13.

Mason R. P., Casu M., Butler N., Breda C., Campesan S., Clapp J., Green E. W., Dhulkhed D., Kyriacou C. P., Giorgini F. (2013) Glutathione peroxidase activity is neuroprotective in models of Huntington's disease. *Nat. Genet.* **45**, 1249–1254.

Matsubara T., Pararajasegaram G., Wu G. S., Rao N. A. (1999) Retinal microglia differentially express phenotypic markers of antigen-presenting cells in vitro. *Invest. Ophthalmol. Vis. Sci.* **40**, 3186–3193.

Maucksch C., Vazey E. M., Gordon R. J., Connor B. (2013) Stem cell-based therapy for Huntington's disease. *J. Cell. Biochem.* **114**, 754–763.

Mayberg H. S., Starkstein S. E., Peyser C. E., Brandt J., Dannals R. F., Folstein S. E. (1992) Paralimbic frontal lobe hypometabolism in depression associated with Huntington's disease. *Neurology* **42**, 1791–1797.

McKinstry S. U., Karadeniz Y. B., Worthington A. K., Hayrapetyan V. Y., Ozlu M. I., Serafin-Molina K., Risher W. C., et al. (2014) Huntingtin is required for normal excitatory synapse development in cortical and striatal circuits. *J. Neurosci. Off. J. Soc. Neurosci.* **34**, 9455–9472.

Mead E. L., Mosley A., Eaton S., Dobson L., Heales S. J., Pocock J. M. (2012) Microglial neurotransmitter receptors trigger superoxide production in microglia; consequences for microglial-neuronal interactions. *J. Neurochem.* **121**, 287–301.

Medzhitov R., Preston-Hurlburt P., Janeway C. A. (1997) A human homologue of the Drosophila Toll protein signals activation of adaptive immunity. *Nature* **388**, 394–397.

Mertens J., Marchetto M. C., Bardy C., Gage F. H. (2016) Evaluating cell reprogramming, differentiation and conversion technologies in neuroscience. *Nat. Rev. Neurosci.* **17**, 424–437.

Mestre T. A., Ferreira J. J. (2012) An evidence-based approach in the treatment of Huntington's disease. *Parkinsonism Relat. Disord.* **18**, 316–320.

Michaud J.-P., Bellavance M.-A., Préfontaine P., Rivest S. (2013) Real-time in vivo imaging reveals the ability of monocytes to clear vascular amyloid beta. *Cell Rep.* **5**, 646–653.

Michell-Robinson M. A., Touil H., Healy L. M., Owen D. R., Durafourt B. A., Bar-Or A., Antel J. P., Moore C. S. (2015) Roles of microglia in brain development, tissue maintenance and repair. *Brain J. Neurol.* **138**, 1138–1159.

Mildner A., Schmidt H., Nitsche M., Merkler D., Hanisch U.-K., Mack M., Heikenwalder M., Brück W., Priller J., Prinz M. (2007) Microglia in the adult brain arise from Ly-6ChiCCR2+ monocytes only under defined host conditions. *Nat. Neurosci.* **10**, 1544–1553.

Miller J. R. C., Träger U., Andre R., Tabrizi S. J. (2015) Mutant huntingtin does not affect the intrinsic phenotype of human Huntington's disease T lymphocytes. *PloS One* **10**, e0141793.

Miller J. R., Lo K. K., Andre R., Moss D. J. H., Träger U., Stone T. C., Jones L., Holmans P., Plagnol V., Tabrizi S. J. (2016) RNA-Seq of Huntington's disease patient myeloid cells reveals innate transcriptional dysregulation associated with proinflammatory pathway activation. *Hum. Mol. Genet.* **25**, 2893–2904.

Mishra M. K., Wang J., Keough M. B., Fan Y., Silva C., Sloka S., Hayardeny L., Brück W., Yong V. W. (2014) Laquinimod reduces neuroaxonal injury through inhibiting microglial activation. *Ann. Clin. Transl. Neurol.* **1**, 409–422.

Mishra M. K., Wang J., Silva C., Mack M., Yong V. W. (2012) Kinetics of proinflammatory monocytes in a model of multiple sclerosis and its perturbation by laquinimod. *Am. J. Pathol.* **181**, 642–651.

Mizoguchi Y., Kato T. A., Seki Y., Ohgidani M., Sagata N., Horikawa H., Yamauchi Y., et al. (2014) Brain-derived neurotrophic factor (BDNF) induces sustained intracellular Ca2+ elevation through the up-regulation of surface transient receptor potential 3 (TRPC3) channels in rodent microglia. *J. Biol. Chem.* **289**, 18549–18555.

Möller T. (2010) Neuroinflammation in Huntington's disease. *J. Neural Transm.* **117**, 1001–1008.

Möller T., Nolte C., Burger R., Verkhratsky A., Kettenmann H. (1997) Mechanisms of C5a and C3a complement fragment-induced [Ca2+]i signaling in mouse microglia. *J. Neurosci.* **17**, 615–24.

Montoya A., Price B. H., Menear M., Lepage M. (2006) Brain imaging and cognitive dysfunctions in Huntington's disease. *J. Psychiatry Neurosci. JPN* **31**, 21–29.

Moore C. S., Ase A. R., Kinsara A., Rao V. T. S., Michell-Robinson M., Leong S. Y., Butovsky O., et al. (2015) P2Y12 expression and function in alternatively activated human microglia. *Neurol. Neuroimmunol. Neuroinflammation* **2**, e80.

Morgan P. J., Ortinau S., Frahm J., Krüger N., Rolfs A., Frech M. J. (2009) Protection of neurons derived from human neural progenitor cells by veratridine. *Neuroreport* **20**, 1225–1229.

Moroni F. (1999) Tryptophan metabolism and brain function: focus on kynurenine and other indole metabolites. *Eur. J. Pharmacol.* **375**, 87–100.

Morten I. J., Gosal W. S., Radford S. E., Hewitt E. W. (2007) Investigation into the role of macrophages in the formation and degradation of beta2-microglobulin amyloid fibrils. *J. Biol. Chem.* **282**, 29691–29700.

Mrzljak L. (2013) Development of kynurenine monooxygenase (KMO) inhibitor CHDI-340246 for the treatment of Huntington's disease: A progress update. CHDI Foundation 8th Annual HD Therapeutics Conference. Venice, Italy.

Muffat J., Li Y., Yuan B., Mitalipova M., Omer A., Corcoran S., Bakiasi G., et al. (2016) Efficient derivation of microglia-like cells from human pluripotent stem cells. *Nat. Med.* **22**, 1358–1367.

Nagai A., Nakagawa E., Hatori K., Choi H. B., McLarnon J. G., Lee M. A., Kim S. U. (2001) Generation and characterization of immortalized human microglial cell lines: Expression of cytokines and chemokines. *Neurobiol. Dis.* **8**, 1057–1068.

Nagatsu T., Mogi M., Ichinose H., Togari A. (2000a) Cytokines in Parkinson's disease. *J. Neural Transm. Suppl.* 58, 143–151.

Nagatsu T., Mogi M., Ichinose H., Togari A. (2000b) Changes in cytokines and neurotrophins in Parkinson's disease. *J. Neural Transm. Suppl.* 60, 277–290.

Nakajima K., Honda S., Tohyama Y., Imai Y., Kohsaka S., Kurihara T. (2001) Neurotrophin secretion from cultured microglia. *J. Neurosci. Res.* **65**, 322–331.

Nalavade R., Griesche N., Ryan D. P., Hildebrand S., Krauss S. (2013) Mechanisms of RNA-induced toxicity in CAG repeat disorders. *Cell Death Dis.* **4**, e752.

Nance M. A., Myers R. H. (2001) Juvenile onset Huntington's disease--clinical and research perspectives. *Ment. Retard. Dev. Disabil. Res. Rev.* **7**, 153–157.

Nasir J., Floresco S. B., O'Kusky J. R., Diewert V. M., Richman J. M., Zeisler J., Borowski A., Marth J. D., Phillips A. G., Hayden M. R. (1995) Targeted disruption of the Huntington's disease gene results in embryonic lethality and behavioral and morphological changes in heterozygotes. *Cell* **81**, 811–823.

Nesargikar P. N., Spiller B., Chavez R. (2012) The complement system: history, pathways, cascade and inhibitors. *Eur. J. Microbiol. Immunol.* **2**, 103–111.

Nguyen H. P., Björkqvist M., Bode F. J., Stephan M., Hörsten S. von (2010) Serum levels of a subset of cytokines show high interindividual variability and are not altered in rats transgenic for Huntington´s disease. *PLoS Curr.* **2**, RRN1190.

Noakes Z., Fjodorova M., Li M. (2015) Deriving striatal projection neurons from human pluripotent stem cells with Activin A. *Neural Regen. Res.* **10**, 1914–1916.

Nolte C., Möller T., Walter T., Kettenmann H. (1996) Complement 5a controls motility of murine microglial cells in vitro via activation of an inhibitory G-protein and the rearrangement of the actin cytoskeleton. *Neuroscience* **73**, 1091–1107.

Norflus F., Nanje A., Gutekunst C.-A., Shi G., Cohen J., Bejarano M., Fox J., Ferrante R. J., Hersch S. M. (2004) Anti-inflammatory treatment with acetylsalicylate or rofecoxib is not neuroprotective in Huntington's disease transgenic mice. *Neurobiol. Dis.* **17**, 319–325.

Novak M. J. U., Seunarine K. K., Gibbard C. R., McColgan P., Draganski B., Friston K., Clark C. A., Tabrizi S. J. (2015) Basal ganglia-cortical structural connectivity in Huntington's disease. *Hum. Brain Mapp.* **36**, 1728–1740.

Ohgidani M., Kato T. A., Setoyama D., Sagata N., Hashimoto R., Shigenobu K., Yoshida T., et al. (2014) Direct induction of ramified microglia-like cells from human monocytes: dynamic microglial dysfunction in Nasu-Hakola disease. *Sci. Rep.* **4**, 4957.

O'Koren E. G., Mathew R., Saban D. R. (2016) Fate mapping reveals that microglia and recruited monocyte-derived macrophages are definitively distinguishable by phenotype in the retina. *Sci. Rep.* **6**, 20636.

Ona V. O., Li M., Vonsattel J. P., Andrews L. J., Khan S. Q., Chung W. M., Frey A. S., et al. (1999) Inhibition of caspase-1 slows disease progression in a mouse model of Huntington's disease. *Nature* **399**, 263–267.

Orth M., Cooper J. M., Bates G. P., Schapira A. H. V. (2003) Inclusion formation in Huntington's disease R6/2 mouse muscle cultures. *J. Neurochem.* **87**, 1–6.

Palazuelos J., Aguado T., Pazos M. R., Julien B., Carrasco C., Resel E., Sagredo O., et al. (2009) Microglial CB2 cannabinoid receptors are neuroprotective in Huntington's disease excitotoxicity. *Brain J. Neurol.* **132**, 3152–3164.

Palin K., Cunningham C., Forse P., Perry V. H., Platt N. (2008) Systemic inflammation switches the inflammatory cytokine profile in CNS Wallerian degeneration. *Neurobiol. Dis.* **30**, 19–29.

Park H.-S., Park M.-J., Kwon M.-S. (2016) Central nervous system-peripheral immune system dialogue in neurological disorders: Possible application of neuroimmunology in urology. *Int. Neurourol. J.* **20**, S8-14.

Park I.-H., Arora N., Huo H., Maherali N., Ahfeldt T., Shimamura A., Lensch M. W., Cowan C., Hochedlinger K., Daley G. Q. (2008) Disease-specific induced pluripotent stem cells. *Cell* **134**, 877–886.

Passaro A., Dalla Nora E., Morieri M. L., Soavi C., Sanz J. M., Zurlo A., Fellin R., Zuliani G. (2015) Brain-derived neurotrophic factor plasma levels: relationship with dementia and diabetes in the elderly population. *J. Gerontol. A. Biol. Sci. Med. Sci.* **70**, 294–302.

Pavese N., Gerhard A., Tai Y. F., Ho A. K., Turkheimer F., Barker R. A., Brooks D. J., Piccini P. (2006) Microglial activation correlates with severity in Huntington disease: a clinical and PET study. *Neurology* **66**, 1638–1643.

Peferoen L. A. N., Vogel D. Y. S., Ummenthum K., Breur M., Heijnen P. D. A. M., Gerritsen W. H., Peferoen-Baert R. M. B., Valk P. van der, Dijkstra C. D., Amor S. (2015) Activation status of human microglia is dependent on lesion formation stage and remyelination in multiple sclerosis. *J. Neuropathol. Exp. Neurol.* **74**, 48–63.

Perry V. H. (2007) Stress primes microglia to the presence of systemic inflammation: implications for environmental influences on the brain. *Brain. Behav. Immun.* **21**, 45–46.

Perry V. H., Cunningham C., Holmes C. (2007) Systemic infections and inflammation affect chronic neurodegeneration. *Nat. Rev. Immunol.* **7**, 161–167.

Pestka S., Krause C., Walter M. (2004) Interferons, interferon-like cytokines, and their receptors. *Immunol. Rev.* **202**, 8–32.

Pidgeon C., Rickards H. (2013) The pathophysiology and pharmacological treatment of Huntington disease. *Behav. Neurol.* **26**, 245–253.

Pocock J. M. (2015) *Microglial neurotransmitter receptors; 4th Venusberg Meeting on Neuroinflammation*. Biomedical Center (BMZ), Bonn, Germany.

Politis M., Pavese N., Tai Y. F., Kiferle L., Mason S. L., Brooks D. J., Tabrizi S. J., Barker R. A., Piccini P. (2011) Microglial activation in regions related to cognitive function predicts disease onset in Huntington's disease: a multimodal imaging study. *Hum. Brain Mapp.* **32**, 258–270.

Pollock K., Dahlenburg H., Nelson H., Fink K. D., Cary W., Hendrix K., Annett G., et al. (2016) Human mesenchymal stem cells genetically engineered to overexpress brain-derived neurotrophic factor improve outcomes in Huntington's disease mouse models. *Mol. Ther. J. Am. Soc. Gene Ther.* **24**, 965–977.

Poltorak A., He X., Smirnova I., Liu M. Y., Van Huffel C., Du X., Birdwell D., et al. (1998) Defective LPS signaling in C3H/HeJ and C57BL/10ScCr mice: mutations in Tlr4 gene. *Science* **282**, 2085–2088.

Poon D. C.-H., Ho Y.-S., Chiu K., Wong H.-L., Chang R. C.-C. (2015) Sickness: From the focus on cytokines, prostaglandins, and complement factors to the perspectives of neurons. *Neurosci. Biobehav. Rev.* **57**, 30–45.

Preiningerova J. (2009) Oral laquinimod therapy in relapsing multiple sclerosis. *Expert Opin. Investig. Drugs* **18**, 985–989.

Puerta E., Hervias I., Barros-Miñones L., Jordan J., Ricobaraza A., Cuadrado-Tejedor M., García-Osta A., Aguirre N. (2010) Sildenafil protects against 3-nitropropionic acid neurotoxicity through the modulation of calpain, CREB, and BDNF. *Neurobiol. Dis.* **38**, 237–245.

Purves D., Augustine G. J., Fitzpatrick D., Katz L. C., LaMantia A.-S., McNamara J. O., Williams M. S. (2001) Circuits within the basal ganglia system. Neuroscience 2nd edition. Sinauer Associates, Inc., Sunderland (MA).

Qin L., Wu X., Block M. L., Liu Y., Breese G. R., Hong J.-S., Knapp D. J., Crews F. T. (2007) Systemic LPS causes chronic neuroinflammation and progressive neurodegeneration. *Glia* **55**, 453–462.

Qureshi S. T., Larivière L., Leveque G., Clermont S., Moore K. J., Gros P., Malo D. (1999) Endotoxin-tolerant mice have mutations in Toll-like receptor 4 (Tlr4). *J. Exp. Med.* **189**, 615–625.

Reale M. (2015) Cytokines in chronic neurodegenerative diseases. *SRL Alzheimers Park. Dis.* **1**, 004–006.

Reale M., Greig N. H., Kamal M. A. (2009a) Peripheral chemo-cytokine profiles in Alzheimer's and Parkinson's diseases. *Mini Rev. Med. Chem.* **9**, 1229–1241.

Reale M., Iarlori C., Thomas A., Gambi D., Perfetti B., Di Nicola M., Onofrj M. (2009b) Peripheral cytokines profile in Parkinson's disease. *Brain. Behav. Immun.* **23**, 55–63.

Ren P.-H., Lauckner J. E., Kachirskaia I., Heuser J. E., Melki R., Kopito R. R. (2009) Cytoplasmic penetration and persistent infection of mammalian cells by polyglutamine aggregates. *Nat. Cell Biol.* **11**, 219–225.

Richards R. I., Samaraweera S. E., Eyk C. L. van, O'Keefe L. V., Suter C. M. (2013) RNA pathogenesis via Toll-like receptor-activated inflammation in expanded repeat neurodegenerative diseases. *Front. Mol. Neurosci.* **6**, 25.

Rock F. L., Hardiman G., Timans J. C., Kastelein R. A., Bazan J. F. (1998) A family of human receptors structurally related to Drosophila Toll. *Proc. Natl. Acad. Sci. U. S. A.* **95**, 588–593.

Romero E., Cha G.-H., Verstreken P., Ly C. V., Hughes R. E., Bellen H. J., Botas J. (2008) Suppression of neurodegeneration and increased neurotransmission caused by expanded full-length huntingtin accumulating in the cytoplasm. *Neuron* **57**, 27–40.

Romero L. I., Kakucska I., Lechan R. M., Reichlin S. (1996) Interleukin-6 (IL-6) is secreted from the brain after intracerebroventricular injection of IL-1 beta in rats. *Am. J. Physiol.* **270**, R518-524.

Rosenberg H. F., Dyer K. D., Foster P. S. (2013) Eosinophils: changing perspectives in health and disease. *Nat. Rev. Immunol.* **13**, 9–22.

Ross C. A., Tabrizi S. J. (2011) Huntington's disease: from molecular pathogenesis to clinical treatment. *Lancet Neurol.* **10**, 83–98.

Roy A., Fung Y. K., Liu X., Pahan K. (2006) Up-regulation of microglial CD11b expression by nitric oxide. *J. Biol. Chem.* **281**, 14971–14980.

Rubinsztein D. C., Carmichael J. (2003) Huntington's disease: molecular basis of neurodegeneration. *Expert Rev. Mol. Med.* **5**, 1–21.

Rubinsztein D. C., Leggo J., Coles R., Almqvist E., Biancalana V., Cassiman J. J., Chotai K., et al. (1996) Phenotypic characterization of individuals with 30-40 CAG repeats in the Huntington disease (HD) gene reveals HD cases with 36 repeats and apparently normal elderly individuals with 36-39 repeats. *Am. J. Hum. Genet.* **59**, 16–22.

Sagredo O., González S., Aroyo I., Pazos M. R., Benito C., Lastres-Becker I., Romero J. P., et al. (2009) Cannabinoid CB2 receptor agonists protect the striatum against malonate toxicity: Relevance for Huntington's disease. *Glia* **57**, 1154–1167.

Sagredo O., Pazos M. R., Valdeolivas S., Fernandez-Ruiz J. (2012) Cannabinoids: novel medicines for the treatment of Huntington's disease. *Recent Patents CNS Drug Discov.* **7**, 41–48.

Saijo K., Glass C. K. (2011) Microglial cell origin and phenotypes in health and disease. *Nat. Rev. Immunol.* **11**, 775–787.

Saleh N., Moutereau S., Durr A., Krystkowiak P., Azulay J.-P., Tranchant C., Broussolle E., Morin F., Bachoud-Lévi A.-C., Maison P. (2009) Neuroendocrine disturbances in Huntington's disease. *PloS One* **4**, e4962.

Salehi Z., Mashayekhi F. (2009) Brain-derived neurotrophic factor concentrations in the cerebrospinal fluid of patients with Parkinson's disease. *J. Clin. Neurosci. Off. J. Neurosurg. Soc. Australas.* **16**, 90–93.

Samaraweera S. E., O'Keefe L. V., Price G. R., Venter D. J., Richards R. I. (2013) Distinct roles for Toll and autophagy pathways in double-stranded RNA toxicity in a Drosophila model of expanded repeat neurodegenerative diseases. *Hum. Mol. Genet.* **22**, 2811–2819.

Sapp E., Kegel K. B., Aronin N., Hashikawa T., Uchiyama Y., Tohyama K., Bhide P. G., Vonsattel J. P., DiFiglia M. (2001) Early and progressive accumulation of reactive microglia in the Huntington disease brain. *J. Neuropathol. Exp. Neurol.* **60**, 161–172.

Sapp E., Valencia A., Li X., Aronin N., Kegel K. B., Vonsattel J.-P., Young A. B., Wexler N., DiFiglia M. (2012) Native mutant huntingtin in human brain: evidence for prevalence of full-length monomer. *J. Biol. Chem.* **287**, 13487–13499.

Sathasivam K., Hobbs C., Turmaine M., Mangiarini L., Mahal A., Bertaux F., Wanker E. E., Doherty P., Davies S. W., Bates G. P. (1999) Formation of polyglutamine inclusions in non-CNS tissue. *Hum. Mol. Genet.* **8**, 813–822.

Sathasivam K., Neueder A., Gipson T. A., Landles C., Benjamin A. C., Bondulich M. K., Smith D. L., et al. (2013) Aberrant splicing of HTT generates the pathogenic exon 1 protein in Huntington disease. *Proc. Natl. Acad. Sci. U. S. A.* **110**, 2366–2370.

Satoh J., Tosaki Y., Sakai K., Yanaizu M., Kino Y. (2016) P2Y12 expression on microglia in the human brain. *Clin. Exp. Neuroimmunol.*, DOI: 10.1111/cen3.12320.

Saxena S., Caroni P. (2011) Selective neuronal vulnerability in neurodegenerative diseases: from stressor thresholds to degeneration. *Neuron* **71**, 35–48.

Schilling S., Goelz S., Linker R., Luehder F., Gold R. (2006) Fumaric acid esters are effective in chronic experimental autoimmune encephalomyelitis and suppress macrophage infiltration. *Clin. Exp. Immunol.* **145**, 101–107.

Schindowski K., Belarbi K., Buée L. (2008) Neurotrophic factors in Alzheimer's disease: role of axonal transport. *Genes Brain Behav.* **7 Suppl 1**, 43–56.

Schmid C. D., Melchior B., Masek K., Puntambekar S. S., Danielson P. E., Lo D. D., Sutcliffe J. G., Carson M. J. (2009) Differential gene expression in LPS/IFNgamma activated microglia and macrophages: in vitro versus in vivo. *J. Neurochem.* **109 Suppl 1**, 117–125.

Schneider C. A., Rasband W. S., Eliceiri K. W. (2012) NIH Image to ImageJ: 25 years of image analysis. *Nat. Methods* **9**, 671–675.

Schoenfeld M., Myers R. H., Cupples L. A., Berkman B., Sax D. S., Clark E. (1984) Increased rate of suicide among patients with Huntington's disease. *J. Neurol. Neurosurg. Psychiatry* **47**, 1283–1287.

Schroder K., Hertzog P., Ravasi T., Hume D. (2003) Interferon-γ: an overview of signals, mechanisms and functions. *J. Leukoc. Biol.* **75**, 163–189.

Schulze-Topphoff U., Shetty A., Varrin-Doyer M., Molnarfi N., Sagan S. A., Sobel R. A., Nelson P. A., Zamvil S. S. (2012) Laquinimod, a quinoline-3-carboxamide, induces type II myeloid cells that modulate central nervous system autoimmunity. *PloS One* **7**, e33797.

Schwarcz R., Guidetti P., Sathyasaikumar K. V., Muchowski P. J. (2010) Of mice, rats and men: Revisiting the quinolinic acid hypothesis of Huntington's disease. *Prog. Neurobiol.* **90**, 230–245.

Schwarcz R., Pellicciari R. (2002) Manipulation of brain kynurenines: glial targets, neuronal effects, and clinical opportunities. *J. Pharmacol. Exp. Ther.* **303**, 1–10.

Segal R. A. (2003) Selectivity in neurotrophin signaling: theme and variations. *Annu. Rev. Neurosci.* **26**, 299–330.

Sennbro C. J., Olin M., Edman K., Hansson G., Gunnarsson P. O., Svensson L. D. (2006) Determination of the immunomodulator laquinimod in human plasma by liquid chromatography/tandem mass spectrometry; development, validation and application of two methods in clinical pharmacokinetic profiling. *Rapid Commun. Mass Spectrom. RCM* **20**, 3313–3318.

Shelbourne P. F., Killeen N., Hevner R. F., Johnston H. M., Tecott L., Lewandoski M., Ennis M., et al. (1999) A Huntington's disease CAG expansion at the murine Hdh locus is unstable and associated with behavioural abnormalities in mice. *Hum. Mol. Genet.* **8**, 763–774.

Shi C., Pamer E. G. (2011) Monocyte recruitment during infection and inflammation. *Nat. Rev. Immunol.* **11**, 762–774.

Shin J.-Y., Fang Z.-H., Yu Z.-X., Wang C.-E., Li S.-H., Li X.-J. (2005) Expression of mutant huntingtin in glial cells contributes to neuronal excitotoxicity. *J. Cell Biol.* **171**, 1001–1012.

Shirendeb U., Reddy A. P., Manczak M., Calkins M. J., Mao P., Tagle D. A., Reddy P. H. (2011) Abnormal mitochondrial dynamics, mitochondrial loss and mutant huntingtin oligomers in Huntington's disease: implications for selective neuronal damage. *Hum. Mol. Genet.* **20**, 1438–1455.

Shoham S., Youdim M. B. (2000) Iron involvement in neural damage and microgliosis in models of neurodegenerative diseases. *Cell. Mol. Biol. Noisy--Gd. Fr.* **46**, 743–760.

Shultz L. D., Brehm M. A., Garcia-Martinez J. V., Greiner D. L. (2012) Humanized mice for immune system investigation: progress, promise and challenges. *Nat. Rev. Immunol.* **12**, 786–798.

Shum C., Macedo S. C., Warre-Cornish K., Cocks G., Price J., Srivastava D. P. (2015) Utilizing induced pluripotent stem cells (iPSCs) to understand the actions of estrogens in human neurons. *Horm. Behav.* **74**, 228–242.

Silvestroni A., Faull R. L. M., Strand A. D., Möller T. (2009) Distinct neuroinflammatory profile in post-mortem human Huntington's disease. *Neuroreport* **20**, 1098–1103.

Simmons D. A., Casale M., Alcon B., Pham N., Narayan N., Lynch G. (2007) Ferritin accumulation in dystrophic microglia is an early event in the development of Huntington's disease. *Glia* **55**, 1074–1084.

Singh S., Metz I., Amor S., Valk P. van der, Stadelmann C., Brück W. (2013) Microglial nodules in early multiple sclerosis white matter are associated with degenerating axons. *Acta Neuropathol. (Berl.)* **125**, 595–608.

Singhrao S. K., Neal J. W., Morgan B. P., Gasque P. (1999) Increased complement biosynthesis by microglia and complement activation on neurons in Huntington's disease. *Exp. Neurol.* **159**, 362–376.

Sipe G. O., Lowery R. L., Tremblay M.-È., Kelly E. A., Lamantia C. E., Majewska A. K. (2016) Microglial P2Y12 is necessary for synaptic plasticity in mouse visual cortex. *Nat. Commun.* **7**, 10905.

Slepko N., Levi G. (1996) Progressive activation of adult microglial cells in vitro. *Glia* **16**, 241–246.

Slow E. J., Raamsdonk J. van, Rogers D., Coleman S. H., Graham R. K., Deng Y., Oh R., et al. (2003) Selective striatal neuronal loss in a YAC128 mouse model of Huntington disease. *Hum. Mol. Genet.* **12**, 1555–1567.

Smith A. M., Dragunow M. (2014) The human side of microglia. *Trends Neurosci.* **37**, 125–135.

Snell R. G., MacMillan J. C., Cheadle J. P., Fenton I., Lazarou L. P., Davies P., MacDonald M. E., Gusella J. F., Harper P. S., Shaw D. J. (1993) Relationship between trinucleotide repeat expansion and phenotypic variation in Huntington's disease. *Nat. Genet.* **4**, 393–397.

Song D. K., Im Y. B., Jung J. S., Cho J., Suh H. W., Kim Y. H. (2001) Central beta-amyloid peptide-induced peripheral interleukin-6 responses in mice. *J. Neurochem.* **76**, 1326–1335.

Sørensen S. A., Fenger K. (1992) Causes of death in patients with Huntington's disease and in unaffected first degree relatives. *J. Med. Genet.* **29**, 911–914.

Sorolla M. A., Reverter-Branchat G., Tamarit J., Ferrer I., Ros J., Cabiscol E. (2008) Proteomic and oxidative stress analysis in human brain samples of Huntington disease. *Free Radic. Biol. Med.* **45**, 667–678.

Soulet D., Cicchetti F. (2011) The role of immunity in Huntington's disease. *Mol. Psychiatry* **16**, 889–902.

Squitieri F., Gellera C., Cannella M., Mariotti C., Cislaghi G., Rubinsztein D. C., Almqvist E. W., et al. (2003) Homozygosity for CAG mutation in Huntington disease is associated with a more severe clinical course. *Brain J. Neurol.* **126**, 946–955.

Stanslowsky N., Reinhardt P., Glass H., Kalmbach N., Naujock M., Hensel N., Lübben V., et al. (2016) Neuronal dysfunction in iPSC-derived medium spiny neurons from Chorea-acanthocytosis patients is reversed by Src kinase inhibition and F-actin stabilization. *J. Neurosci. Off. J. Soc. Neurosci.* **36**, 12027–12043.

Steffan J. S. (2010) Does Huntingtin play a role in selective macroautophagy? *Cell Cycle Georget. Tex* **9**, 3401–3413.

Stern H. J. (2014) Preimplantation genetic diagnosis: Prenatal testing for embryos finally achieving its potential. *J. Clin. Med.* **3**, 280–309.

Straccia M., Garcia-Diaz Barriga G., Sanders P., Bombau G., Carrere J., Mairal P. B., Vinh N.-N., et al. (2015) Quantitative high-throughput gene expression profiling of human striatal development to screen stem cell-derived medium spiny neurons. *Mol. Ther. Methods Clin. Dev.* **2**, 15030.

Strand A. D., Aragaki A. K., Shaw D., Bird T., Holton J., Turner C., Tapscott S. J., et al. (2005) Gene expression in Huntington's disease skeletal muscle: a potential biomarker. *Hum. Mol. Genet.* **14**, 1863–1876.

Subramaniam S., Sixt K. M., Barrow R., Snyder S. H. (2009) Rhes, a striatal specific protein, mediates mutant-huntingtin cytotoxicity. *Science* **324**, 1327–1330.

Sun Y.-M., Zhang Y.-B., Wu Z.-Y. (2016) Huntington's disease: Relationship between phenotype and genotype. *Mol. Neurobiol.*, DOI: 10.1007/s12035-015-9662-8.

Swami M., Hendricks A. E., Gillis T., Massood T., Mysore J., Myers R. H., Wheeler V. C. (2009) Somatic expansion of the Huntington's disease CAG repeat in the brain is associated with an earlier age of disease onset. *Hum. Mol. Genet.* **18**, 3039–3047.

Tabrizi S. J., Langbehn D. R., Leavitt B. R., Roos R. A., Durr A., Craufurd D., Kennard C., et al. (2009) Biological and clinical manifestations of Huntington's disease in the longitudinal TRACK-HD study: cross-sectional analysis of baseline data. *Lancet Neurol.* **8**, 791–801.

Tabrizi S. J., Scahill R. I., Owen G., Durr A., Leavitt B. R., Roos R. A., Borowsky B., et al. (2013) Predictors of phenotypic progression and disease onset in premanifest and early-stage Huntington's disease in the TRACK-HD study: analysis of 36-month observational data. *Lancet Neurol.* **12**, 637–649.

Tai Y. F., Pavese N., Gerhard A., Tabrizi S. J., Barker R. A., Brooks D. J., Piccini P. (2007a) Imaging microglial activation in Huntington's disease. *Brain Res. Bull.* **72**, 148–151.

Tai Y., Pavese N., Gerhard A., Tabrizi S. J., Barker R., Brooks D., Piccini P. (2007b) Microglial activation in presymptomatic Huntington's disease gene carriers. *Brain* **130**, 1759–1766.

Takahashi K., Yamanaka S. (2006) Induction of pluripotent stem cells from mouse embryonic and adult fibroblast cultures by defined factors. *Cell* **126**, 663–676.

Takeda K., Akira S. (2004) TLR signaling pathways. *Semin. Immunol.* **16**, 3–9.

Takeuchi O., Akira S. (2010) Pattern recognition receptors and inflammation. *Cell* **140**, 805–820.

Tan Z. S., Beiser A. S., Vasan R. S., Roubenoff R., Dinarello C. A., Harris T. B., Benjamin E. J., et al. (2007) Inflammatory markers and the risk of Alzheimer disease: the Framingham Study. *Neurology* **68**, 1902–1908.

Tang Y., Li T., Li J., Yang J., Liu H., Zhang X. J., Le W. (2014) Jmjd3 is essential for the epigenetic modulation of microglia phenotypes in the immune pathogenesis of Parkinson's disease. *Cell Death Differ.* **21**, 369–380.

Teva Pharmaceutical Industries (2016) *A clinical study in subjects with Huntington's disease to assess the efficacy and safety of three oral doses of laquinimod. ClinicalTrials.gov Identifier: NCT02215616*.

The Huntington's Disease Collaborative Research Group (1993) A novel gene containing a trinucleotide repeat that is expanded and unstable on Huntington's disease chromosomes. *Cell* **72**, 971–983.

Thomas M., Ashizawa T., Jankovic J. (2004) Minocycline in Huntington's disease: a pilot study. *Mov. Disord. Off. J. Mov. Disord. Soc.* **19**, 692–695.

Thompson L. M., Aiken C. T., Kaltenbach L. S., Agrawal N., Illes K., Khoshnan A., Martinez-Vincente M., et al. (2009) IKK phosphorylates huntingtin and targets it for degradation by the proteasome and lysosome. *J. Cell Biol.* **187**, 1083–1099.

Träger U., Andre R., Lahiri N., Magnusson-Lind A., Weiss A., Grueninger S., McKinnon C., et al. (2014a) HTT-lowering reverses Huntington's disease immune dysfunction caused by NFκB pathway dysregulation. *Brain*.

Träger U., Andre R., Magnusson-Lind A., Miller J. R. C., Connolly C., Weiss A., Grueninger S., et al. (2014b) Characterisation of immune cell function in fragment and full-length Huntington's disease mouse models. *Neurobiol. Dis.* **73C**, 388–398.

Tremblay M.-È., Lowery R. L., Majewska A. K. (2010) Microglial interactions with synapses are modulated by visual experience. *PLoS Biol.* **8**, e1000527.

Trudler D., Farfara D., Frenkel D. (2010) Toll-like receptors expression and signaling in glia cells in neuro-amyloidogenic diseases: towards future therapeutic application. *Mediators Inflamm.* **2010**, 497987.

Untergasser A., Cutcutache I., Koressaar T., Ye J., Faircloth B. C., Remm M., Rozen S. G. (2012) Primer3--new capabilities and interfaces. *Nucleic Acids Res.* **40**, e115.

Van Raamsdonk J. M., Warby S. C., Hayden M. R. (2007) Selective degeneration in YAC mouse models of Huntington disease. *Brain Res. Bull.* **72**, 124–131.

Vega J. A., García-Suárez O., Hannestad J., Pérez-Pérez M., Germanà A. (2003) Neurotrophins and the immune system. *J. Anat.* **203**, 1–19.

Venkatesan C., Chrzaszcz M., Choi N., Wainwright M. S. (2010) Chronic upregulation of activated microglia immunoreactive for galectin-3/Mac-2 and nerve growth factor following diffuse axonal injury. *J. Neuroinflammation* **7**, 32.

Vezzani A., Viviani B. (2015) Neuromodulatory properties of inflammatory cytokines and their impact on neuronal excitability. *Neuropharmacology* **96**, 70–82.

Victor M. B., Richner M., Hermanstyne T. O., Ransdell J. L., Sobieski C., Deng P.-Y., Klyachko V. A., Nerbonne J. M., Yoo A. S. (2014) Generation of human striatal neurons by microRNA-dependent direct conversion of fibroblasts. *Neuron* **84**, 311–323.

Victorson D., Carlozzi N. E., Frank S., Beaumont J. L., Cheng W., Gorin B., Duh M. S., et al. (2014) Identifying motor, emotional-behavioral, and cognitive deficits that comprise the triad of HD symptoms from patient, caregiver, and provider perspectives. *Tremor Hyperkinetic Mov. N. Y. N* **4**, 224.

Vivier E., Tomasello E., Baratin M., Walzer T., Ugolini S. (2008) Functions of natural killer cells. *Nat. Immunol.* **9**, 503–510.

Vollmer T. L., Sorensen P. S., Selmaj K., Zipp F., Havrdova E., Cohen J. A., Sasson N., Gilgun-Sherki Y., Arnold D. L., BRAVO Study Group (2014) A randomized placebo-controlled phase III trial of oral laquinimod for multiple sclerosis. *J. Neurol.* **261**, 773–783.

Vonsattel J. P., Myers R. H., Stevens T. J., Ferrante R. J., Bird E. D., Richardson E. P. (1985) Neuropathological classification of Huntington's disease. *J. Neuropathol. Exp. Neurol.* **44**, 559–577.

Wake H., Moorhouse A. J., Jinno S., Kohsaka S., Nabekura J. (2009) Resting microglia directly monitor the functional state of synapses in vivo and determine the fate of ischemic terminals. *J. Neurosci. Off. J. Soc. Neurosci.* **29**, 3974–3980.

Walker D. G., Link J., Lue L.-F., Dalsing-Hernandez J. E., Boyes B. E. (2006) Gene expression changes by amyloid beta peptide-stimulated human postmortem brain microglia identify activation of multiple inflammatory processes. *J. Leukoc. Biol.* **79**, 596–610.

Walker D. G., Lue L.-F. (2015) Immune phenotypes of microglia in human neurodegenerative disease: challenges to detecting microglial polarization in human brains. *Alzheimers Res. Ther.* **7**, 56.

Walker F. O. (2007) Huntington's disease. *The Lancet* **369**, 218–228.

Walter S., Letiembre M., Liu Y., Heine H., Penke B., Hao W., Bode B., et al. (2007) Role of the toll-like receptor 4 in neuroinflammation in Alzheimer's disease. *Cell. Physiol. Biochem.* **20**, 947–956.

Wang N., Gray M., Lu X.-H., Cantle J. P., Holley S. M., Greiner E., Gu X., et al. (2014a) Neuronal targets for reducing mutant huntingtin expression to ameliorate disease in a mouse model of Huntington's disease. *Nat. Med.* **20**, 536–541.

Wang N., Liang H., Zen K. (2014b) Molecular mechanisms that influence the macrophage m1-m2 polarization balance. *Front. Immunol.* **5**, 614.

Wang Y., Liu H., Zhang B.-S., Soares J. C., Zhang X. Y. (2016) Low BDNF is associated with cognitive impairments in patients with Parkinson's disease. *Parkinsonism Relat. Disord.* **29**, 66–71.

Watkins L. R., Hutchinson M. R. (2014) A concern on comparing “apples” and “oranges” when differences between microglia used in human and rodent studies go far, far beyond simply species: comment on Smith and Dragunow. *Trends Neurosci.* **37**, 189–190.

Wegner C., Stadelmann C., Pförtner R., Raymond E., Feigelson S., Alon R., Timan B., Hayardeny L., Brück W. (2010) Laquinimod interferes with migratory capacity of T cells and reduces IL-17 levels, inflammatory demyelination and acute axonal damage in mice with experimental autoimmune encephalomyelitis. *J. Neuroimmunol.* **227**, 133–143.

Weinstein G., Beiser A. S., Choi S. H., Preis S. R., Chen T. C., Vorgas D., Au R., et al. (2014) Serum brain-derived neurotrophic factor and the risk for dementia: the Framingham Heart Study. *JAMA Neurol.* **71**, 55–61.

Weiss A., Grueninger S., Abramowski D., Giorgio F. P. D., Lopatin M. M., Rosas H. D., Hersch S., Paganetti P. (2011) Microtiter plate quantification of mutant and wild-type huntingtin normalized to cell count. *Anal. Biochem.* **410**, 304–306.

Weiss A., Träger U., Wild E. J., Grueninger S., Farmer R., Landles C., Scahill R. I., et al. (2012) Mutant huntingtin fragmentation in immune cells tracks Huntington’s disease progression. *J. Clin. Invest.* **122**, 3731–3736.

Wernersson S., Pejler G. (2014) Mast cell secretory granules: armed for battle. *Nat. Rev. Immunol.* **14**, 478–494.

Wexler N. S., Lorimer J., Porter J., Gomez F., Moskowitz C., Shackell E., Marder K., et al. (2004) Venezuelan kindreds reveal that genetic and environmental factors modulate Huntington’s disease age of onset. *Proc. Natl. Acad. Sci. U. S. A.* **101**, 3498–3503.

Wild E. J., Tabrizi S. J. (2007) The differential diagnosis of chorea. *Pract. Neurol.* **7**, 360–373.

Wild E., Magnusson A., Lahiri N., Krus U., Orth M., Tabrizi S. J., Björkqvist M. (2011) Abnormal peripheral chemokine profile in Huntington’s disease. *PLoS Curr.* **3**, RRN1231.

Wood-Kaczmar A., Gandhi S., Yao Z., Abramov A. Y., Abramov A. S. Y., Miljan E. A., Keen G., et al. (2008) PINK1 is necessary for long term survival and mitochondrial function in human dopaminergic neurons. *PloS One* **3**, e2455.

Wrona D. (2006) Neural-immune interactions: an integrative view of the bidirectional relationship between the brain and immune systems. *J. Neuroimmunol.* **172**, 38–58.

Wyttenbach A., Sauvageot O., Carmichael J., Diaz-Latoud C., Arrigo A.-P., Rubinsztein D. C. (2002) Heat shock protein 27 prevents cellular polyglutamine toxicity and suppresses the increase of reactive oxygen species caused by huntingtin. *Hum. Mol. Genet.* **11**, 1137–1151.

Xavier A. L., Menezes J. R. L., Goldman S. A., Nedergaard M. (2014) Fine-tuning the central nervous system: microglial modelling of cells and synapses. *Philos. Trans. R. Soc. Lond. B. Biol. Sci.* **369**, 20130593.

Xie Y., Hayden M. R., Xu B. (2010) BDNF overexpression in the forebrain rescues Huntington’s disease phenotypes in YAC128 mice. *J. Neurosci. Off. J. Soc. Neurosci.* **30**, 14708–14718.

Yang J., Zhang L., Yu C., Yang X.-F., Wang H. (2014) Monocyte and macrophage differentiation: circulation inflammatory monocyte as biomarker for inflammatory diseases. *Biomark. Res.* **2**, 1.

Yang J.-S., Xu L.-Y., Xiao B.-G., Hedlund G., Link H. (2004) Laquinimod (ABR-215062) suppresses the development of experimental autoimmune encephalomyelitis, modulates the Th1/Th2 balance and induces the Th3 cytokine TGF-beta in Lewis rats. *J. Neuroimmunol.* **156**, 3–9.

Yang W., Dunlap J. R., Andrews R. B., Wetzel R. (2002) Aggregated polyglutamine peptides delivered to nuclei are toxic to mammalian cells. *Hum. Mol. Genet.* **11**, 2905–2917.

Yang X. W., Gray M. (2011) Mouse models for validating preclinical candidates for Huntington's disease, in *Neurobiol. Huntingt. Dis. Appl. Drug Discov.*, (Lo D. C., Hughes R. E., eds). CRC Press/Taylor and Francis.

Yoshikai Y. (2001) Roles of prostaglandins and leukotrienes in acute inflammation caused by bacterial infection. *Curr. Opin. Infect. Dis.* **14**, 257–263.

Zeitlin S., Liu J. P., Chapman D. L., Papaioannou V. E., Efstratiadis A. (1995) Increased apoptosis and early embryonic lethality in mice nullizygous for the Huntington's disease gene homologue. *Nat. Genet.* **11**, 155–163.

Zhang F., Frost A. R., Blundell M. P., Bales O., Antoniou M. N., Thrasher A. J. (2010) A ubiquitous chromatin opening element (UCOE) confers resistance to DNA methylation-mediated silencing of lentiviral vectors. *Mol. Ther. J. Am. Soc. Gene Ther.* **18**, 1640–1649.

Zhang X., Zeng L., Yu T., Xu Y., Pu S., Du D., Jiang W. (2014) Positive feedback loop of autocrine BDNF from microglia causes prolonged microglia activation. *Cell. Physiol. Biochem. Int. J. Exp. Cell. Physiol. Biochem. Pharmacol.* **34**, 715–723.

Ziegler S. F., Wilson C. B., Perlmutter R. M. (1988) Augmented expression of a myeloid-specific protein tyrosine kinase gene (hck) after macrophage activation. *J. Exp. Med.* **168**, 1801–1810.

Ziegler-Heitbrock L., Ancuta P., Crowe S., Dalod M., Grau V., Hart D. N., Leenen P. J. M., et al. (2010) Nomenclature of monocytes and dendritic cells in blood. *Blood* **116**, e74-80.

Zotova E., Bharambe V., Cheaveau M., Morgan W., Holmes C., Harris S., Neal J. W., Love S., Nicoll J. A. R., Boche D. (2013) Inflammatory components in human Alzheimer's disease and after active amyloid-β42 immunization. *Brain J. Neurol.* **136**, 2677–2696.

Zou L.-P., Abbas N., Volkmann I., Nennesmo I., Levi M., Wahren B., Winblad B., Hedlund G., Zhu J. (2002) Suppression of experimental autoimmune neuritis by ABR-215062 is associated with altered Th1/Th2 balance and inhibited migration of inflammatory cells into the peripheral nerve tissue. *Neuropharmacology* **42**, 731–739.

Zuccato C., Ciammola A., Rigamonti D., Leavitt B. R., Goffredo D., Conti L., MacDonald M. E., et al. (2001) Loss of huntingtin-mediated BDNF gene transcription in Huntington's disease. *Science* **293**, 493–498.

Zwilling D., Huang S.-Y., Sathyasaikumar K. V., Notarangelo F. M., Guidetti P., Wu H.-Q., Lee J., et al. (2011) Kynurenine 3-monooxygenase inhibition in blood ameliorates neurodegeneration. *Cell* **145**, 863–874.

Appendices

Appendix I: Cell culture media

I-i DMEM/FBS culture medium

DMEM		[Life Technologies]
Foetal bovine serum (FBS)	10 %	[Life Technologies]
Penicillin;Streptomycin	5 U/mL; 5 µg/mL	[Life Technologies]

I-ii OptiMEM/FBS culture medium

OptiMEM		[Life Technologies]
FBS	10 %	
Penicillin;Streptomycin	5 U/mL; 5 µg/mL	

I-iii ReN/NSC culture medium

DMEM:F-12 *(for complete formulation see Appendix I-vii)*		[Life Technologies]
Human albumin solution	0.03%	
Transferrin (human recombinant)	5 µg/mL	
Putrescine dihydrochloride	16.2 µg/mL	
Insulin (human recombinant)	5 µg/mL	
T4	400 ng/mL	
T3	337 ng/mL	
Progesterone	60 ng/mL	
L-glutamine	2 mM	[Life Technologies]
Sodium selenite	40 ng/mL	
Heparin sodium	10 U/mL	
Corticosterone	10 ng/mL	
bFGF	10 ng/mL	[PeproTech]
EGF	20 ng/mL	[PeproTech]

I-iv RPMI/FBS culture medium

Roswell Park Memorial Institute (RPMI) medium 1640		[Life Technologies]
FBS	10 %	
L-glutamine	2 mM	
Penicillin;Streptomycin	5 U/mL; 5 µg/mL	

I-v Neuronal medium (NM)

DMEM:F-12 *(for complete formulation see Appendix I-vii)*

Human albumin solution	0.03%
Transferrin (human recombinant)	5 µg/mL
Putrescine dihydrochloride	16.2 µg/mL
Insulin (human recombinant)	5 µg/mL
L-thyroxine (T4)	400 ng/mL
Tri-iodo-thyronine (T3)	337 ng/mL
Progesterone	60 ng/mL
L-glutamine	2 mM
Sodium selenite	40 ng/mL
Heparin sodium	10 U/mL
Corticosterone	10 ng/mL

I-vi NM/cAMP/GDNF

DMEM:F-12 *(for complete formulation see Appendix I-vii)*

Human albumin solution	0.03%	
Transferrin (human recombinant)	5 µg/mL	
Putrescine dihydrochloride	16.2 µg/mL	
Insulin (human recombinant)	5 µg/mL	
T4	400 ng/mL	
T3	337 ng/mL	
Progesterone	60 ng/mL	
L-glutamine	2 mM	
Sodium selenite	40 ng/mL	
Heparin sodium	10 U/mL	
Corticosterone	10 ng/mL	
db-cAMP	0.5 mM	[Calbiochem]
GDNF	2 ng/mL	[PeproTech]

I-vii Complete formulation of DMEM:F-12

DMEM:F-12, no glutamine, no HEPES [GIBCO; ThermoFisher Scientific; #21331]

Components	Molecular weight	Concentration (mg/mL)	mM
Amino acids			
Glycine	75.0	18.750	0.250
L-Alanine	89.0	4.450	0.050
L-Arginine hydrochloride	211.0	147.500	0.700
L-Asparagine-H_2O	150.0	7.500	0.050
L-Aspartic acid	133.0	6.650	0.050
L-Cysteine hydrochloride-H_2O	176.0	17.560	0.100
L-Cystine 2HCl	313.0	31.290	0.100
L-Glutamic Acid	147.0	7.350	0.050
L-Histidine hydrochloride-H_2O	210.0	31.480	0.150
L-Isoleucine	131.0	54.470	0.416
L-Leucine	131.0	59.050	0.451
L-Lysine hydrochloride	183.0	91.250	0.499
L-Methionine	149.0	17.240	0.116
L-Phenylalanine	165.0	35.480	0.215
L-proline	115.0	17.250	0.150
L-Serine	105.0	26.250	0.250
L-Threonine	119.0	53.450	0.449
L-Tryptophan	204.0	9.020	0.044
L-Tyrosine disodium salt dehydrate	261.0	55.790	0.214
L-Valine	117.0	25.850	0.221
Vitamins			
Biotin	244.0	0.004	1.434×10^{-5}
Choline chloride	140.0	8.980	0.064
D-Calcium pantothenate	477.0	2.240	0.007
Folic acid	441.0	2.650	0.006
Niacinamide	122.0	2.020	0.017
Pyridoxine hydrochloride	206.0	2.000	0.010
Riboflavin	376.0	0.219	5.824×10^{-4}
Thiamine hydrochloride	337.0	2.170	0.006
Vitamin B12	1355.0	0.680	5.018×10^{-4}
i-Inositol	180.0	12.600	0.070

Inorganic salts			
Calcium chloride ($CaCl_2$) (anhyd.)	111.0	116.600	1.050
Cupric sulfate ($CuSO_4$-$5H_2O$)	250.0	0.001	5.2×10^{-6}
Ferric Nitrate ($Fe(NO_3)3$”$9H_2O$)	404.0	0.050	1.238×10^{-4}
Ferric sulfate ($FeSO_4$-$7H_2O$)	278.0	0.417	0.002
Magnesium chloride ($MgCl_2$) (anhyd.)	95.0	28.640	0.301
Magnesium sulfate ($MgSO_4$) (anhyd.)	120.0	48.840	0.407
Potassium chloride (KCl)	75.0	311.800	4.157
Sodium bicarbonate ($NaHCO_3$)	84.0	1200.000	14.286
Sodium chloride (NaCl)	58.0	6995.500	120.612
Sodium phosphate dibasic (Na_2HPO_4) (anhyd.)	142.0	71.020	0.500
Sodium phosphate monobasic (NaH_2PO_4-H_2O)	138.0	62.500	0.453
Zinc sulfate ($ZnSO_4$-$7H_2O$)	288.0	0.432	0.002
Other components			
D-Glucose (dextrose)	180.0	3151.000	17.506
Hypoxanthine Na	159.0	2.390	0.015
Linoleic acid	280.0	0.042	1.500×10^{-4}
Lipoic acid	206.0	0.105	5.097×10^{-4}
Phenol Red	376.4	8.100	0.022
Putrescine 2HCl	161.0	0.081	5.031×10^{-4}
Sodium pyruvate	110.0	55.000	0.500
Thymidine	242.0	0.365	0.002

Appendix II: Buffer recipes

II-i MACS buffer

Buffer used for processing PBMCs for magnetic-activated cell sorting (MACS)

DPBS		[Life Technologies]
BSA	0.5 %	
EDTA	2 mM	

II-ii Radioimmunoprecipitation assay (RIPA) buffer

Buffer used to prepare some cell lysates

Tris-HCl	25 mM; pH 7.6	[Sigma]
NaCl	150 mM	
NP-40	1.0 %	
Sodium deoxycholate	1.0 %	
Sodium dodecyl sulphate (SDS)	0.1 %	
cOmplete protease inhibitor cocktail	1 ×	[Roche]

II-iii 10× Tris/Borate/EDTA (TBE) buffer (1 L)

Buffer used to prepare agarose gels for electrophoresis of DNA fragments

Tris base	100 g	[Sigma]
Boric acid	55 g	
0.5 M EDTA	40 mL	
ddH_2O	to 1 L	

II-iv Lysis Buffer

Lysis solution used to prepare lysate samples for Western blotting or dot blotting

	Western blotting	*Dot blotting*	
PBS	1 ×	1 ×	
Triton X-100	1.0 %	0.5 %	
Tris	–	50 mM; pH 7.4	[Sigma]
Sodium deoxycholate	0.5 %	0.5 %	
NaCl	–	150 mM	
SDS	0.1 %	–	
Nonidet P-40 (NP-40)	1.0 %	–	

Benzonase	0.25 U/µL	0.25 U/µL	[Novartis]
cOmplete protease inhibitor cocktail	1 ×	1 ×	

II-v Sample buffer (5×)

Buffer added to lysates in preparation for loading gels for Western blotting

Tris-HCl	0.625 M; pH 6.8
Glycerol	50 %
SDS	10 %
Bromophenol blue	trace
β-mercaptoethanol	10%

II-vi Tris/Glycine/SDS Running buffer [National Diagnostics]

Buffer used for running SDS-PAGE

Tris	25 mM
Glycine	192 mM
SDS	0.1 %

II-vii Electroblotting buffer [National Diagnostics]

Buffer used for transferring proteins from polyacrylamide gel to membrane

Tris-HCl	25 mM; pH 8.0
Glycine	192 mM
Methanol	20 %

II-viii Tropix assay buffer [Applied Biosystems]

Buffer used for washing immunoblots before developing AP-conjugated secondary antibody signals

Tris-HCl	20 mM; pH 9.8
$MgCl_2$	1 mM

II-ix Duolink In Situ Wash Buffer A [Olink Bioscience]

Buffer used for PLA probe and oligonucleotide ligation reaction wash steps in Duolink In Situ PLA

Tris	0.01 M

NaCl	0.15 M	
Tween-20	0.05 %	
HCl	to pH 7.4	

II-x Duolink In Situ Wash Buffer B [Olink Bioscience]

Buffer used for RCA reaction wash steps in Duolink In Situ PLA

NaCl	0.1 M	
Tris	0.2 M	
HCl	to pH 7.5	

II-xi FACS buffer

Buffer used for flow cytometry cell suspension and some wash steps in IFC

PBS	1 ×	
Azide	0.02 %	
BSA	1.00 %	

II-xii MSD buffer

Buffer used for preparation of samples for quantitation of HTT using MSD assay

Tris	20 mM; pH 7.5	
NaCl	150 mM	
EDTA	1 mM	
Ethylene glycol-bis(β-aminoethyl ether)-N,N,N',N'-tetraacetic acid (EGTA)	1 mM	
Triton X-100	1 %	
Phosphatase inhibitor I and II	1 ×	[Sigma]
cOmplete protease inhibitor cocktail	1 ×	
Phenylmethylsulfonyl fluoride (PMSF)	0.5 mM	
NaF	10 mM	

Appendix III: Publications and presentations relating to this Thesis

III-i Article published in Journal of Neurochemistry

Title: Laquinimod dampens hyperactive cytokine production in Huntington's disease patient myeloid cells

Authors: Lucianne Dobson[1], Ulrike Träger[1], Ruth Farmer[2], Liat Hayardeny[3], Pippa Loupe[3], Michael R. Hayden[3], Sarah J. Tabrizi[1]

Author affiliations: [1] Department of Neurodegenerative Diseases, UCL IoN and NHNN, London, UK. [2] Department of Medical Statistics, London School of Hygiene & Tropical Medicine, London, UK. [3] Teva Pharmaceuticals, Research and Development, Netanya, Israel.

Date: June 2016 | Volume: 137 | Issue: 5 | Pages: 782-794 | doi: 10.1111/jnc.13553

Article:

III-ii Poster presented at Faculty of Brain Sciences Postgraduate Research Symposium

Date: 8 March 2016

Location: University College London, London, United Kingdom

Title: Investigation into pathogenic neuronal-myeloid cell interactions and rescue of hyper-reactive immune responses in Huntington's disease

Authors: Lucianne Dobson[1] (presenting author), Ralph André[1], Ulrike Träger[1], Rhia Ghosh[1], Liat Hayardeny[2], Sarah J. Tabrizi[1]

Author affiliations: [1] Department of Neurodegenerative Diseases, UCL IoN and NHNN, London, UK. [2] Teva Pharmaceuticals, Research and Development, Netanya, Israel.

Abstract: Huntington's disease (HD) is a genetic neurodegenerative condition hallmarked by presence of intracellular mutant huntingtin (mHTT) aggregates, neurodegeneration and loss of striatal medium spiny neurons. *mHTT* is ubiquitously expressed, so several non-neuronal pathologies also occur, including innate immune system dysfunction leading to elevated release of proinflammatory cytokines from HD myeloid cells. To investigate the direct effects of immune dysfunction on neurodegeneration in HD, a novel human neuronal-microglial cell model of HD was developed and characterised. Neurons expressing mHTT (HD neurons) had significantly more death compared to neurons expressing normal HTT (control neurons), indicating toxicity of the HD model. When in co-culture with control neurons, non-stimulated microglia were neuroprotective, while stimulated microglia were neurotoxic. However, in co-culture with HD neurons, both non-stimulated and stimulated microglia reduced neuronal death levels, indicating that microglia protect HD neurons from toxicity induced by mHTT expression. HD microglia were found to release higher levels of IFNγ, IL-2, IL-10 and IL-12 compared to HV microglia. Also, unlike HV microglia, HD microglia released high levels of brain-derived neurotrophic factor when stimulated. However, no significant differences were observed between the effects of HD or HV microglia on neuronal survival. Additionally, novel immunomodulatory drug laquinimod was found to dampen dysfunctional hyper-reactive cytokine release in HD patient myeloid cells.

Poster:

INVESTIGATION INTO PATHOGENIC NEURONAL-MYELOID CELL INTERACTIONS AND RESCUE OF HYPER-REACTIVE IMMUNE RESPONSES IN HUNTINGTON'S DISEASE

Lucianne Dobson[1], Ralph André[1], Ulrike Träger[1], Rhia Ghosh[1], Liat Hayardeny[2], Sarah J Tabrizi[1]

[1] University College London, Institute of Neurology, Department of Neurodegenerative Disease, Queen Square, London, WC1N 3BG, UK.
[2] Teva Pharmaceutical Industries Ltd., Israel.

INTRODUCTION

Huntington's disease (HD) is a genetic neurodegenerative condition. Mutant huntingtin (mHTT) is ubiquitously expressed leading to characteristic neuronal damage and loss as well as dysfunction of non-neuronal tissues, including the innate immune system (peripheral blood monocytes and macrophages and brain-resident microglia).

mHTT expression in myeloid cells and neurons: a neurodestructive cycle

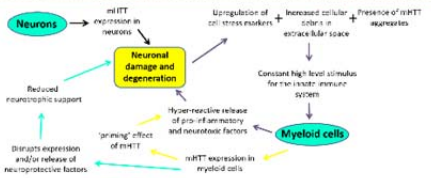

AIMS:

1. Develop and characterise a novel human neuronal-microglial co-culture model of HD
2. Define and dissect the effects of a dysfunctional immune system on neuronal survival in HD
3. Target dysfunctional myeloid cell signalling pathways pharmacologically to inhibit neurotoxic phenotypes

RESULTS

1. (A) Human neural stem cells transduced with human mHTT and differentiated into mature pan-neuronal cultures

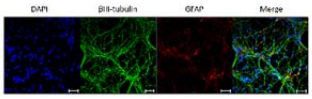

Human NSCs differentiate into mature pan-neuronal cultures (βIII-tubulin) with some astrocytes (GFAP)

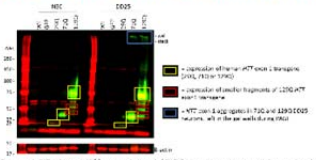

NSCs and 25 days differentiated (DD) neurons transduced with HTT exon1 express normal and/or mutant HTT protein of correct sizes. 29Q, normal HTT; 71Q and 129Q, expanded HTT (HD)

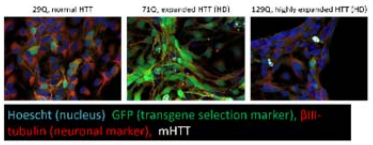

Intranuclear aggregates of mHTT appear in HD neurons

(B) Monocytes isolated from HD patient blood and differentiated into microglia *in vitro*

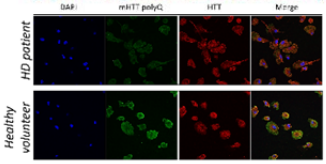

Monocytes are firstly differentiated into macrophages. HD patient macrophages express mHTT.

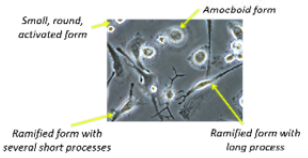

Macrophages are then differentiated into microglia, which display the same dynamic morphologies as primary human microglia in various activation states.

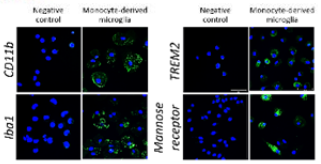

Human monocyte-derived microglia also express correct microglial markers

2. HD neurons are protected from death following treatment with media conditioned by microglia

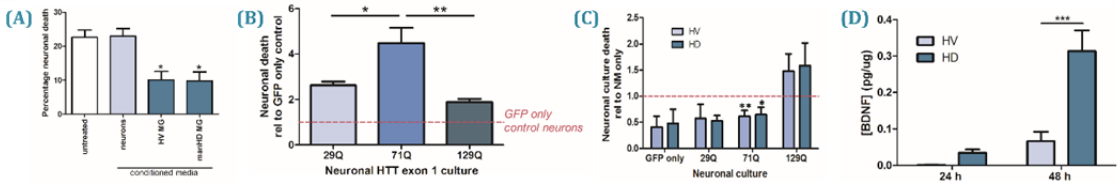

Healthy volunteer (HV) and HD microglia release factors which reduce baseline death in WT neurons (A). Neurons expressing mHTT 71Q have a neurotoxic phenotype (B), and microglia-conditioned media treatment protects HD neurons from mHTT-induced neuronal death (C). When stimulated for 48 h, HD microglia release 3-fold more of the brain-derived neurotrophic factor (BDNF) than HV microglia. Neuronal death assessed by CytoTox 96 Non-Radioactive Cytotoxicity Assay. Mean+SEM. A,B: One-way ANOVA with Tukey post-tests. C,D: Two-way ANOVA with Bonferroni post-tests. *p<0.05, **p<0.01, ***p<0.001.

3. Laquinimod dampens hyperactive cytokine production in HD patient myeloid cells
Dobson *et al.* (2016) *J Neurochem*

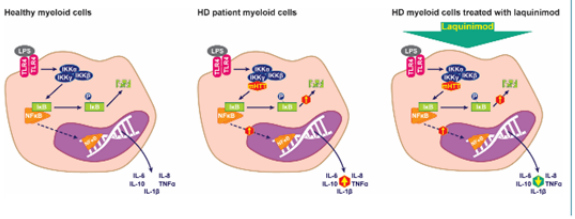

CONCLUSIONS

- Novel human HD neuronal cell lines display mHTT-induced neurotoxicity.
- Human blood monocytes differentiated into microglia using novel technique, protect HD neurons from mHTT-induced neurotoxicity in co-culture.
- No obvious differences between effects of HD and HV microglia in neuronal co-culture, although it has been observed that HD microglia release significantly higher levels of BDNF than HV microglia following stimulation.
- Immunomodulatory compound laquinimod reduces dysfunctional hyper-reactive cytokine release from stimulated HD patient myeloid cells, and shows potential for having therapeutic benefit in HD.

Lucianne Dobson is sponsored by BBSRC/GSK

III-iii Poster presented at European Huntington's Disease Network Plenary Meeting and published in Journal of Neurology Neurosurgery & Psychiatry

Dates: 19 September 2014 - 21 September 2014

Location: Hesperia Tower Hotel in Barcelona, Spain

Title: Laquinimod reduces hyper-reactive proinflammatory cytokine release from human primary Huntington's disease myeloid cells

Authors: Lucianne Dobson[1] (presenting author), Ulrike Träger[1], Liat Hayardeny[2], Sarah J. Tabrizi[1]

Author affiliations: [1] Department of Neurodegenerative Diseases, UCL IoN and NHNN, London, UK. [2] Teva Pharmaceuticals, Research and Development, Netanya, Israel.

Publication citation: Dobson L, Träger U, Hayardeny L, *et al.* M13 Laquinimod Reduces Hyper-reactive Pro-inflammatory Cytokine Release From Human Primary Huntington's Disease Myeloid Cells. *J Neurol Neurosurg Psychiatry* 2014;**85**:A98-A99.

Abstract:

Background Hyper-reactivity of the innate immune response is an early and active component of Huntington's disease (HD) and is due in part to NFκB pathway dysregulation. There is evidence that the peripheral immune system plays a disease-modifying role in HD and that targeting it may slow disease progression. Laquinimod (LAQ) is an orally active immunomodulator that has beneficial effects in multiple sclerosis and is thought to act via the NFκB pathway. We investigated whether the compound could also reverse the hyper-reactive immune responses observed in HD.

Aims Investigate the effects of LAQ on hyper-reactive HD myeloid cells.

Methods Primary human monocytes were isolated from blood collected from symptomatic HD patients, premanifest HD gene-carriers (PreHD) and healthy volunteers. Cells were pretreated with 1μM or 5μM LAQ for 2 or 24 hours (h) before being stimulated with LPS for 24h. Cytokine release was measured by ELISA. IκB degradation kinetics, nuclear translocation of NFκB, and interactions between IKK and HTT were assessed in LAQ-treated cells.

Results Twenty-four hour pretreatment with 5μM LAQ reduced cytokine release in manifest HD patient monocytes. This included IL-1β, IL-8, TNFα, IL-5, IL-13 and IL-10. Reductions in IL-6, IL-8, IL-10 and IL-13 release by preHD monocytes were also

observed using this LAQ dose. When using either 1μM LAQ or 2h pretreatment there was little evidence of a difference between active and control conditions in any of the patient subgroups. We did not observe any significant effect of LAQ on IκB degradation kinetics, NFκB translocation or interactions between IKK and HTT.

Conclusions 5μM LAQ applied to HD monocytes for 24h reduces hyper-reactive cytokine production in response to LPS stimulation. The mechanism for this does not appear to be downstream of NFκB activation. We are currently working on elucidating the mechanism of action of LAQ and will go on to determine how this impacts on neuronal survival using neuronal-myeloid cell co-culture models.

Poster:

LAQUINIMOD REDUCES HYPER-REACTIVE PRO-INFLAMMATORY CYTOKINE RELEASE FROM HUMAN PRIMARY HUNTINGTON'S DISEASE MYELOID CELLS

Lucianne Dobson[1], Ulrike Träger[1], Liat Hayardeny[2], Sarah J Tabrizi[1]

[1] University College London, Institute of Neurology, Department of Neurodegenerative Disease, Queen Square, London, WC1N 3BG, UK
[2] Teva Pharmaceutical Industries Ltd., Israel.

INTRODUCTION

Innate immune system hyper-reactivity is an early and active component of Huntington's disease (HD) and is due in part to NFκB pathway dysregulation. There is evidence that the peripheral immune system plays a disease-modifying role in HD and that targeting it may slow disease progression. Laquinimod (LAQ) is an orally active immunomodulator that has beneficial effects on disease progression and brain atrophy in multiple sclerosis and is thought to act via the NFκB pathway. We investigated whether the compound could also reverse the hyper-reactive immune responses observed in HD.

OBJECTIVE: Investigate the effects of LAQ on hyper-reactive cytokine release and increased NFκB activation in primary human HD myeloid cells.

RESULTS

1. LAQ pre-treatment reduces (A) Th1-type proinflammatory cytokine release and (B) Th2-type cytokine release from LPS-stimulated HD patient monocytes

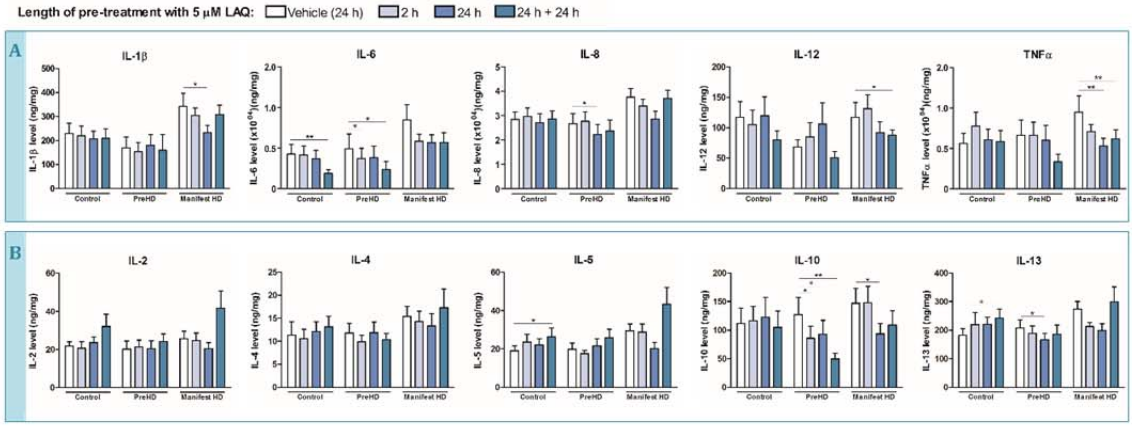

Primary human monocytes from control, premanifest HD (PreHD) and manifest HD subjects were pre-treated with 5 µM LAQ [or vehicle] for 2 or 24 h before being stimulated with 1 µg/mL LPS and 10 ng/mL IFNγ for 24 h. For the 24 + 24 h condition cells were pre-treated with 5 µM LAQ for 24 h and LAQ was added again during LPS stimulation. Levels of Th1-type (A) and Th2-type (B) cytokine release were measured in culture supernatant by multiplex ELISA (or singleplex ELISA in the case of IL-6) and normalised to total protein. Columns = mean average cytokine level of 7-14 biological repeats. Error bars = SEM. Statistical analysis performed by an external statistician's team (Ruth Farmer, London School of Hygiene and Tropical Medicine) using a linear mixed model.*p<0.05, **p<0.01.

2. LAQ does not have a significant effect on (A) IκB degradation kinetics, (B) NFκB translocation or (C) interactions between IKK and HTT in HD patient myeloid cells

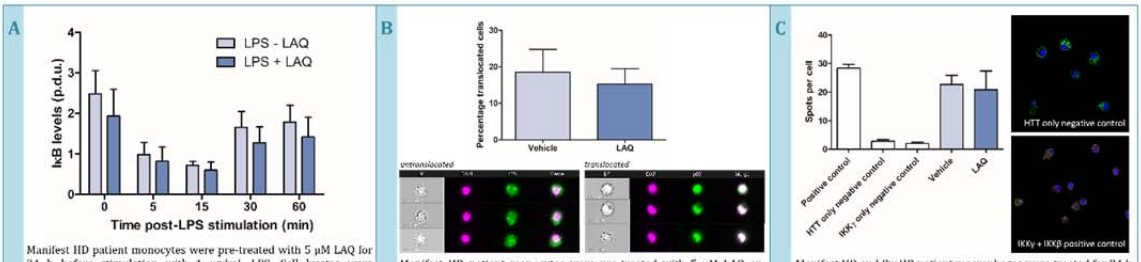

Manifest HD patient monocytes were pre-treated with 5 µM LAQ for 24 h before stimulation with 1 µg/mL LPS. Cell lysates were harvested at 0, 5, 15, 30 and 60 mins post-LPS stimulation. IκB levels were measured using Western blot and normalised to GAPDH. Readings were quantified by densitometry analysis of three exposures using ImageJ software to produce a procedure defined unit (p.d.u.) for comparison of conditions. Columns = mean average IκB level of four biological repeats. Error bars = SEM. Repeated measures (mixed model) two way ANOVA with Bonferroni post-tests found all comparisons to be not significant.

Manifest HD patient monocytes were pre-treated with 5 µM LAQ or vehicle for 24 h before stimulation with 1 µg/mL LPS for 45 mins. Monocytes were stained with anti-p65 antibody followed by FACS secondary antibody. Nuclei were stained with DAPI. Monocytes were run through ImageStream to assess intra/extra-nuclear location of p65 and images analysed using IDEAS software. Columns = mean average percentage translocated cells from seven biological repeats. Error bars = SEM. Two-tailed paired Student's *t*-test found no significant difference between vehicle and LAQ pre-treatment.

Manifest HD and PreHD patient macrophages were treated for 24 h with 5 µM LAQ or vehicle. Interaction between HTT and IKKγ was assessed using proximity ligation assay, where a direct interaction between two defined proteins is presented as a red fluorescent spot. Spots were imaged using fluorescence confocal microscopy and quantified using Volocity software. Columns = mean average spots per cell from five biological repeats. Error bars = SEM. Two-tailed paired Student's *t*-test found no significant difference between vehicle and LAQ treatments.

CONCLUSIONS AND FUTURE WORK

LAQ (5 µM) applied to HD patient myeloid cells for 24 h reduces hyper-reactive cytokine production in response to LPS stimulation. The mechanism for this does not appear to be downstream of NFκB activation in these cells. We are currently working on elucidating the mechanism of action of LAQ and will go on to determine how this impacts on neuronal survival using human neuronal-myeloid cell co-culture models of HD.

Lucianne Dobson is sponsored by BBSRC/GSK

III-iv Accepted abstract for podium presentation at Gordon Research Seminars

Seminar: CAG Triplet Repeat Disorders

Dates: 22 June 2013 - 23 June 2013

Location: Waterville Valley Resort in Waterville Valley, New Hampshire, United States

Title: Neuronal-myeloid cell co-culture models of Huntington's disease

Authors: Lucianne Dobson[1] (presenting author), Ralph Andre[1], Ulrike Traeger[1], Liat Hayardeny[3], Jennifer M. Pocock[2], Sarah J. Tabrizi[1]

Author affiliations: [1] Department of Neurodegenerative Diseases and [2] Department of Neuroinflammation, UCL IoN and NHNN, London, UK. [3] Teva Pharmaceuticals, Research and Development, Netanya, Israel.

Abstract: The innate immune system may modify the pathogenesis of several neurodegenerative diseases. In pre-manifest Huntington's disease (HD) gene carriers, inflammatory markers in the blood are elevated up to 16 years before predicted onset of clinical symptoms, and macrophages and microglia are hyper-reactive throughout the disease course. The disease-causing mutant form of the huntingtin (*HTT*) gene is expressed in HD patient myeloid cells, suggesting a cell-autonomous mechanism for immune activation. Microglial hyper-reactivity could directly contribute to neuronal damage, targeting of which could restore a protective phenotype to slow down the neurodegenerative process. Peripheral immune hyper-reactivity may parallel central pathogenic events, acting as a potential non-invasive biomarker for disease progression. It is important therefore to elucidate the mechanisms involved in the interactions between the CNS and immune system in HD. To do this, human HD neuronal-myeloid cell co-culture models have been developed. Human neural stem cells (NSCs) isolated from foetal ventral mesencephalon (ReNcell VM) or striatum (STROC05) are being studied. These NSCs can be robustly differentiated into mature, electrophysiologically active, GABAergic and dopaminergic neurons. These neurons have been co-cultured with primary human macrophages isolated from control subjects or HD patients at different disease stages, using a variety of paradigms. Human blood-derived macrophages have been characterised and data suggests they are a viable *in vitro* model of microglia, in both resting and stimulated (by LPS or neuronal cell debris) states, and in-depth analysis of cell-cell interactions is currently underway. Recent work by the Tabrizi group has shown a mechanistic link between the presence of mHTT in myeloid cells and a dysfunctional hyper-reactive phenotype, via direct interaction between the mutant protein and the NFkappaB pathway. Laquinimod (LAQ) is a novel

oral immunomodulatory drug proven to slow progression of disability and reduce relapse rate in relapsing-remitting multiple sclerosis. LAQ affects peripheral immune cells by down-regulating pro-inflammatory cytokines, tipping the Th1/Th2 cytokine balance towards anti-inflammatory cytokines. The compound is also thought to act via the NFkappaB pathway, and therefore we are currently conducting experiments looking at the effects of LAQ on HD and control myeloid cells to determine whether the hyper-reactive phenotype we have previously observed can be reversed by the drug. We are looking at the effects of LAQ on cytokine release and signalling pathway dysfunction. Once the effects of the drug are established, it will be screened in neuronal-myeloid cell co-culture models for any neuronal protection effects via actions on the co-cultured myeloid cells.

III-v Poster presented at British Neuroscience Association Event BNA2013

Event: Festival of Neuroscience

Dates: 7 April 2013 - 10 April 2013

Location: The Barbican Centre, London, United Kingdom

Title: Neuronal-myeloid cell co-culture models of Huntington's disease

Authors: Lucianne Dobson (presenting author), Jennifer Parker, Ralph André, Sarah J. Tabrizi

Author affiliation: Department of Neurodegenerative Diseases, UCL IoN and NHNN, London, UK

Abstract: The innate immune system may modify the pathogenesis of several neurodegenerative diseases. In pre-manifest Huntington's disease (HD) gene carriers, inflammatory markers in the blood are elevated up to 16 years before predicted onset of clinical symptoms, and macrophages and microglia are hyper-reactive throughout the disease course. The disease-causing mutant form of the huntingtin (HTT) gene is expressed in HD patient myeloid cells, suggesting a cell-autonomous mechanism for immune activation. Microglial hyper-reactivity could directly contribute to neuronal damage, targeting of which could restore a protective phenotype to slow down the neurodegenerative process. Peripheral immune hyper-reactivity may parallel central pathogenic events, acting as a potential non-invasive biomarker for disease progression. It is important therefore to elucidate the mechanisms involved in the interactions between the CNS and immune system in HD. To do this, human HD neuronal-myeloid cell co-culture models are being developed. Human neural stem cells

(NSCs) isolated from foetal ventral mesencephalon (ReNcell VM) or striatum (STROC05) have been immortalised with v-myc or c-myc carrying retroviruses and expanded long-term. HD and control cell lines are being created by stably transfecting NSCs with full length HTT with normal (15Q) or expanded, disease-causing (138Q) CAG repeats by retroviral transduction. HTT exon 1 cell lines will also be made by transfecting NSCs with N-terminal HTT fragments with 29 (wild-type), 71 (expanded) or 129 (highly expanded) CAG repeats. The NSCs can be robustly differentiated into mature, electrophysiologically active, GABAergic and dopaminergic neurons, with ~15% medium spiny neurons, which are the cells preferentially affected in HD patients' striata. Human microglial cell lines will also be transfected with the same full length or exon 1 HTT constructs. Various co-culture paradigms will be created with HD and control neurons together with HD central (microglia) and peripheral (monocytes, macrophages) cells of the myeloid lineage. This represents a human primary in vitro model of the in vivo HD state, allowing study of neuronal-myeloid cell-cell interactions and representing a tool for the screening of potential therapeutic compounds.

Poster:

Neuronal-myeloid cell co-culture models of Huntington's disease

Lucianne Dobson, Jennifer Parker, Ralph Andre, Sarah J Tabrizi

University College London Institute of Neurology, Department of Neurodegenerative Diseases, Queen Square, London, WC1N 3BG, UK.

Introduction

The innate immune system may modify the pathogenesis of several neurodegenerative diseases, including Huntington's disease (HD). In pre-manifest HD gene carriers, inflammatory markers in the blood are elevated up to 16 years before predicted onset of clinical symptoms, and macrophages and microglia are hyper-reactive throughout the disease course. The disease-causing form of the huntingtin (*HTT*) gene has an expanded CAG-repeat region in exon 1, which is expressed in HD patient myeloid cells, suggesting a cell-autonomous mechanism for immune activation. Microglial hyper-reactivity could directly contribute to neuronal damage, targeting of which could restore a protective phenotype to slow down the neurodegenerative process. Peripheral immune hyper-reactivity may parallel central pathogenic events, acting as a potential non-invasive biomarker for disease progression. It is important therefore to elucidate the mechanisms involved in the interactions between the CNS and immune system in HD. To do this, human HD neuronal-myeloid cell co-culture models have been developed.

Development of co-culture models

1. Human neural stem cells (NSCs) were isolated from foetal ventral mesencephalon (ReNcell VM) and expanded long-term. NSCs can be robustly differentiated into mature, electrophysiologically active, pan-neuronal cultures

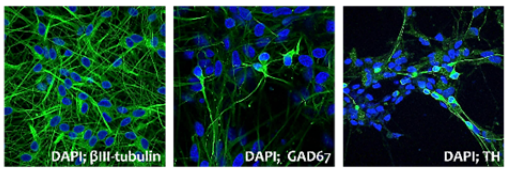

ReNcell VM NSCs were grown as neurospheres, and spontaneous differentiation was induced by removal of growth factors EGF and bFGF from the culture medium. 2 ng/ml glial cell line-derived neurotrophic factor (GDNF) was added to encourage differentiation into GABAergic and dopaminergic neuronal subtypes. Images taken after 14 days differentiation.
DAPI = *4',6-diamidino-2-phenylindole*, nuclear stain (blue); βIII-tubulin = pan-neuronal stain (green); GAD67 = *glutamic acid decarboxylase 67*, GABAergic neurons (green); TH = *tyrosine hydroxylase*, dopaminergic neurons (green).
40X magnification

2. mHTT is expressed in the peripheral myeloid cells of HD patients. Culture of human blood-derived macrophages represents an *in vitro* model of microglia, similar to the *in vivo* state.

Control subject macrophages

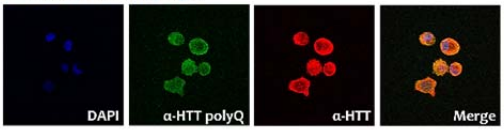

HD patient macrophages

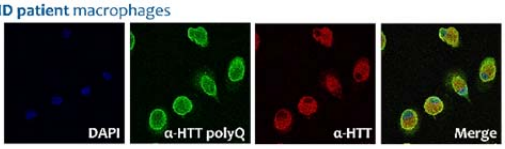

Monocytes can be isolated from human blood and differentiated into macrophages by induction with 20 ng/ml granulocyte macrophage colony-stimulating factor (GM-CSF) MW1 (*α-HTT polyQ*; green) is a HTT antibody directed at the polyQ region, with higher affinity for expanded repeats. HD patient macrophages are stained more intensely green than controls, indicating presence of the mutant protein. 2B7 (*α-HTT*; red) is a HTT antibody directed at the first 17 amino acids of the protein. Merged images show co-localisation.
63X magnification

For more information please contact lucianne.dobson@ucl.ac.uk

Thanks to:
Michael Hayden
Randolph Corteling
Jennifer M Pocock

3. Human NSC line with stable transduction of full length 138Q human HTT

Wild-type ReNcell VM NSCs

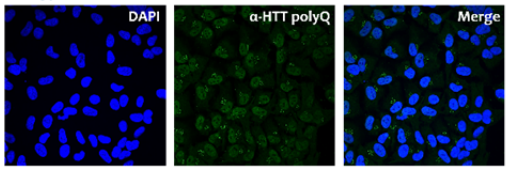

138Q (mutant) full length human HTT ReNcell VM NSCs

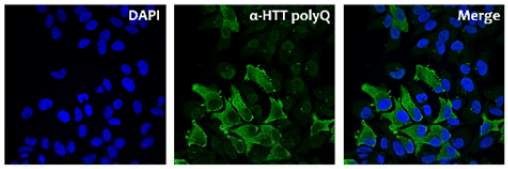

ReNcell VM NSCs have an endogenous background of 2 *HTT* alleles with 16 and 20 (wild-type length) CAG repeats. To create a stable mutant HTT cell line, NSCs were transduced with a retrovirus containing the full length human *HTT* gene (~10Kb) with 138 CAG repeats, and maintained under antibiotic selection.
Bright green α-HTT polyQ staining in the infected cells shows expression of the mutant protein, indicating successful stable transduction with the transgene.
Stable transgenic NSC lines with 15 CAG repeats are also in development.
40X magnification

Future work

- Full length human HTT 15Q and 138Q human NSCs will be made into clonal lines.
- HTT NSC lines will be differentiated into mature neurons and co-cultured with human control or HD patient macrophages.

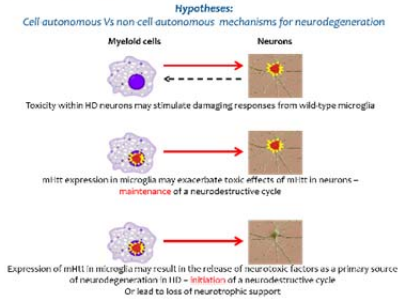

- These *in vitro* co-culture models can be used to dissect signalling pathways involved in neuronal-myeloid cell interactions in HD and to screen potential therapeutic compounds.
- These co-cultures currently represent a close *in vitro* model to the *in vivo* HD state.

III-vi Poster presented at UCL Neuroscience Symposium

Date: 22 March 2012

Location: University College London, London, United Kingdom

Title: Cellular pathobiology of Huntington's disease

Authors: Sarah J. Tabrizi and the Huntington's disease research team. Presenting authors: Lucianne Dobson and Ulrike Träger

Author affiliation: Department of Neurodegenerative Diseases, UCL IoN and NHNN, London, UK

Abstract: Huntington's disease (HD) is a fatal, inherited neurodegenerative disorder, in which the importance of the immune system is becoming increasingly recognised. We have demonstrated myeloid cell hyper-reactivity in HD patients and transgenic mouse models, contributing to elevated levels of inflammatory markers in plasma. These effects appear to be due to the cell intrinsic expression of mutant huntingtin (mHTT). Current work involves knocking-down HTT to investigate the intracellular signalling pathways that cause immune cell dysfunction. Quantification of mHTT in peripheral immune cells holds promise as a non-invasive disease biomarker for HD progression. Mutant HTT levels in peripheral immune cells differ significantly between pre-manifest and manifest HD patients, and are associated with disease burden scores and caudate atrophy rates in HD patients. Fragmentation of mHTT may explain the progressive increase in levels in these cells. To examine direct interactions between HD immune cells and neurons, co-culture paradigms with primary ex vivo cultures of HD patients' peripheral myeloid cells or human microglia cell lines are being established. This is being facilitated by the development of novel human HD neural stem cells, which could provide an invaluable tool for the broader study of cellular aspects of HD pathogenesis.

Poster:

Cellular pathobiology of Huntington's disease

Professor Sarah Tabrizi - Huntington's disease research team
UCL Institute of Neurology
Department of Neurodegenerative Disease

Introduction

We have previously described an aberrant innate immune response in Huntington's disease (HD) (Björkqvist et al., J Exp Med, 2008), in which pro-inflammatory cytokine levels are significantly increased in HD patient brain striatum, plasma and CSF, and mutant huntingtin ((m)HTT) expressing central and peripheral myeloid cells produce increased in response to LPS. These data suggest that altered myeloid cell function may be a key correlate of HD pathogenesis. The basis of these altered myeloid cell responses may lie in altered interactions between mHTT and intracellular signalling pathways such as those leading to activation of NF-κB. Myeloid cells in HD are impaired in other aspects of their function, such as their motility towards stimuli. These effects are, we believe, mediated by the cell-autonomous expression of mHTT in myeloid cells themselves. Mutant HTT is readily detected in these cells, with expression levels in monocytes increasing with disease stage and correlating with brain atrophy. This may prove to be a valuable biomarker of disease progression in HD patients. The importance of altered peripheral myeloid cell function in HD and parallel interactions of mHTT-expressing microglia with susceptible HD neurons are currently being investigated.

Results

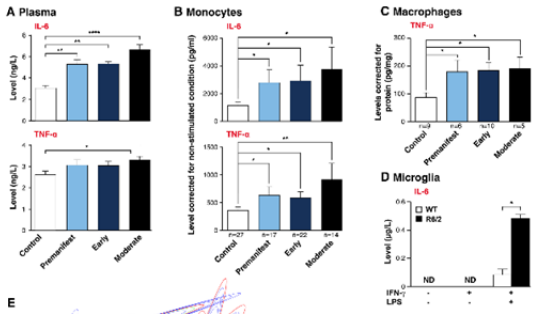

Figure 1 HD myeloid cells are hyper-reactive

(A) HD plasma has increased levels of pro-inflammatory cytokines such as IL-6 and TNFα, measured by multiplex ELISA. **(B)** HD primary monocytes, isolated from blood by magnetic cell sorting, stimulated with 10 ng/ml IFNγ and 2 ug/ml LPS for 24h have increased production of the pro-inflammatory cytokines elevated in plasma. **(C)** GM-CSF-differentiated macrophages have a similar phenotype, showing increased production of TNFα upon stimulation. **(D)** Microglia, the myeloid cells of the CNS, isolated from neonatal R6/2 mice were also hyperactive when stimulated with 10 ng/ml LPS. **(E)** Comparing mRNA expression levels in myeloid cells isolated from HD patients and controls, PCR signalling arrays and pathway analysis suggest significant changes for several key molecules within the NFκB pathway, indicating a role of NFκB in the hyper-reactive response of HD myeloid cells.

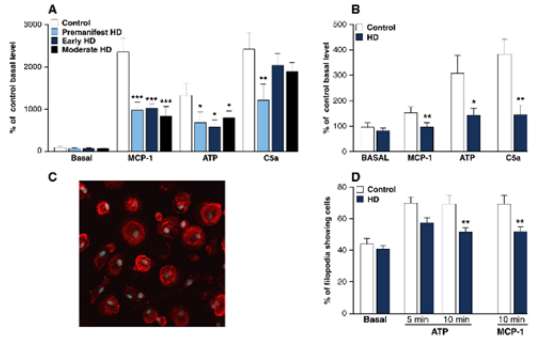

Figure 2 HD patient monocytes and macrophages have a migration defect and decreased membrane ruffling

HD **(A)** monocytes and **(B)** GM-CSF differentiated macrophages showed a significant defect in migrating towards MCP-1, ATP and C5a in a Transwell system. To access actin remodelling, macrophages were stained with phalloidin. **(C)** Example image of filopodia formation upon stimulation with ATP. **(D)** The percentage of cells with membrane ruffling was quantified after 5 or 10 min.

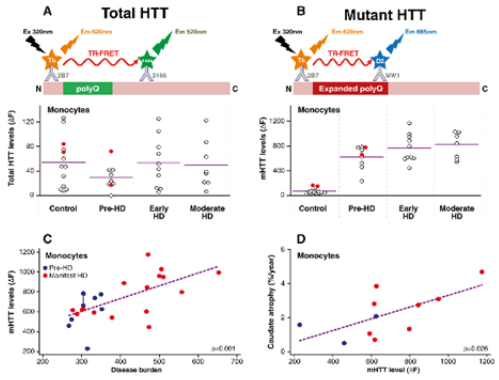

Figure 3 Mutant HTT accumulates in monocytes, correlating with disease burden and caudate atrophy rates

HTT protein levels were quantified by TR-FRET in monocytes. Total HTT quantification relies on simultaneous binding of 2B7 and 2166 anti-HTT antibodies. Mutant HTT is quantified using the 2B7 antibody and a poly-glutamine-specific antibody, MW1. **(A)** Total HTT levels in monocytes showed no significant differences between HD patients and control subjects, or between different disease stages. **(B)** Mutant HTT protein was detected in samples from HD patients and pre-manifest HD mutation carriers. Differences in mean mHTT levels in monocytes were observed between pre-manifest and manifest HD patients ($p<0.01$). **(C)** Mutant HTT protein levels in leukocytes were positively association with HD disease burden score. **(D)** Mutant HTT levels in monocytes were significantly associated with caudate atrophy rates measured by serial volumetric MRI.

Current and future work

Dissection of the NFκB pathway in HD myeloid cells, assessing kinetics of pathway activation by means of phosphorylation/degradation rate of IκB and rate of RelA translocation after TLR4 activation.

Expression of HTT exon1 in a myeloid cell line to establish whether increase in cytokine production is caused by the cell intrinsic effects of HTT expression.

Knockdown of HTT in primary myeloid cells to see whether lowering HTT protein expression can rescue the cytokine phenotype and reverse NFκB dysfunction.

Elucidation of the relative effects of the wild-type and mutant forms of HTT in myeloid and neural cells.

Dissection of neuronal-myeloid cell interactions in HD by co-culturing human HD or control macrophages with differentiated human neural stem cells (hNSCs) (see below) expressing mutant or wild-type HTT.

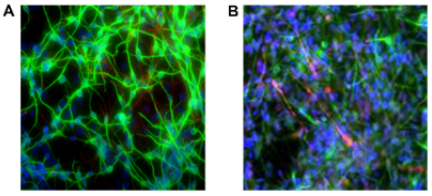

Figure 4 **(A)** Differentiated 197VM hNSCs, isolated from foetal ventral mesencephalon. **(B)** Differentiated STROC05 hNSCS isolated from foetal whole ganglionic eminence. These cells are positive for DARP32, a marker of the striatal medium spiny neurons that are particularly susceptible in HD

Contributors: Ulrike Träger, Ralph Andre, Lucianne Dobson, Ed Wild, Nayana Lahiri, Anna Maguusson

Thanks to: Andreas Weiss, Maria Bjorkqvist, Neil Aronin, Gary Ostorff , Paul Muchowksi, Thomas Möller, Chris Frost, Ruth Farmer, Stephan Grueninger, Gehan El Akabawy , TRACK-HD, Novartis, ReNeuron

Funding: European Community's Seventh Framework Programme (PADDINGTON), MRC, BBSRC, CHDI Foundation, EHDN, UCL/UCLH NIHR Biomedical Research Centre, the UK Dementia and Neurodegenerative Diseases Network, Glaxo SmithKline

Journal of Neurochemistry

JOURNAL OF NEUROCHEMISTRY | 2016 | 137 | 782–794 doi: 10.1111/jnc.13553

ORIGINAL ARTICLE

Laquinimod dampens hyperactive cytokine production in Huntington's disease patient myeloid cells

Lucianne Dobson,* Ulrike Träger,*,† Ruth Farmer,‡ Liat Hayardeny,§ Pippa Loupe,§ Michael R. Hayden§ and Sarah J. Tabrizi*

*Department of Neurodegenerative Diseases, University College London, Institute of Neurology and National Hospital for Neurology and Neurosurgery, London, UK

†Now at German Cancer Research Centre, Immune Tolerance, Tumour Immunology Program, Heidelberg, Germany

‡Department of Medical Statistics, London School of Hygiene & Tropical Medicine, London, UK

§Teva Pharmaceuticals, Research and Development, Netanya, Israel

Abstract

Huntington's disease (HD) is a neurodegenerative condition characterized by pathology in the brain and peripheral tissues. Hyperactivity of the innate immune system, due in part to NFκB pathway dysregulation, is an early and active component of HD. Evidence suggests targeting immune disruption may slow disease progression. Laquinimod is an orally active immunomodulator that down-regulates proinflammatory cytokine production in peripheral blood mononuclear cells, and in the brain down-regulates astrocytic and microglial activation by modulating NFκB signalling. Laquinimod had beneficial effects on inflammation, brain atrophy and disease progression in multiple sclerosis (MS) in two phase III clinical trials. This study investigated the effects of laquinimod on hyperactive proinflammatory cytokine release and NFκB signalling in HD patient myeloid cell cultures. Monocytes from manifest (manHD) and pre-manifest (preHD) HD gene carriers and healthy volunteers (HV) were treated with laquinimod and stimulated with lipopolysaccharide. After 24 h pre-treatment with 5 μM laquinimod, manHD monocytes released lower levels of IL-1β, IL-5, IL-8, IL-10, IL-13 and TNFα in response to stimulation. PreHD monocytes released lower levels of IL-8, IL-10 and IL-13, with no reduction observed in HV monocytes. The effects of laquinimod on dysfunctional NFκB signalling in HD was assessed by inhibitor of kappa B (IκB) degradation kinetics, nuclear translocation of NFκB and interactions between IκB kinase (IKK) and HTT, in HD myeloid cells. No differences were observed between laquinimod-treated and untreated conditions. These results provide evidence that laquinimod dampens hyper-reactive cytokine release from manHD and preHD monocytes, with a much reduced effect on HV monocytes.

Keywords: cytokines, Huntington's disease, inflammation, laquinimod, neurodegenerative disease, NFκB.

J. Neurochem. (2016) **137**, 782–794.

*Read the **Editorial Highlight** for this article on page 670.*

Received November 11, 2015; revised manuscript received January 15, 2016; accepted January 19, 2016.

Address correspondence and reprint requests to Sarah J. Tabrizi, UCL Institute of Neurology and National Hospital for Neurology and Neurosurgery, Department of Neurodegenerative Diseases, Box 104, Queen Square, London, WC1N 3BG, UK. E-mail: s.tabrizi@ucl.ac.uk

Abbreviations used: (m)HTT, (mutant) huntingtin protein; AD, Alzheimer's disease; ASO, antisense oligonucleotide; Aβ, amyloid-beta; BDNF, brain-derived neurotrophic factor; BSA, bovine serum albumin; CAG, cytosine-adenine-guanine; CB_2, cannabinoid receptor 2; CI, confidence Interval; CNS, central nervous system; CT, continued treatment; DIV, days *in vitro*; FBS, foetal bovine serum; GAPDH, glyceraldehyde 3-phosphate dehydrogenase; GM-CSF, granulocyte macrophage colony-stimulating factor; HDAC, histone deacetylase; HD, huntington's disease; *HTT*, huntingtin gene; HV, healthy volunteers; IFNγ, interferon gamma; IKK, inhibitor of kappa B kinase; IL, interleukin; iNOS, inducible nitric oxide synthase; IκB, inhibitor of kappa B; LPS, lipopolysaccharide; MACS, magnetic-activated cell sorting; manHD, manifest HD patients; MNC, mononuclear cell; MSD, MesoScale discovery; MS, multiple sclerosis; NFκB, nuclear factor kappa B; Nrf2, nuclear factor E2-related factor 2; p.d.u., procedure defined unit; PBMC, peripheral blood mononuclear cell; PE, phycoerythrin; PLA, proximity ligation assay; preHD, pre-manifest Huntington's disease gene carriers; PT, pre-treatment; RIPA, radioimmunoprecipitation assay; RPMI, roswell Park Memorial Institute; SDS, sodium dodecyl sulphate; TFC, total functional capacity; TGFβ, transforming growth factor beta; Th, T helper cell; TLR, toll-like receptor; TNFα, tumour necrosis factor alpha; UCL, University College London; WGA, wheat germ agglutinin.

Huntington's disease (HD) is a neurodegenerative condition caused by a cytosine-adenine-guanine (CAG) repeat expansion in exon 1 of the huntingtin gene (*HTT*) (The Huntington's Disease Collaborative Research Group 1993) and is characterized by progressive motor, cognitive and psychiatric symptoms including involuntary movement disturbances, dementia and depression. Symptoms display delayed onset despite presence of mHTT throughout the entire lifetime, and usually become manifest in middle age. Primary pathology involves dysfunction and loss of the GABAergic medium spiny neurons in the striatum as well as cortical neuronal degeneration, and is hallmarked by presence of intra-nuclear and cytoplasmic aggregates of mHTT. Many mechanisms have been described to contribute to tissue damage leading to neuronal degeneration in HD, including excitotoxicity, mitochondrial dysfunction, production of free radicals, impairment of protein degradation systems and transcriptional dysregulation; leading to inflammatory processes that cause microglial and astrocytic activation and neuronal loss (Ross and Tabrizi 2011; Ellrichmann *et al.* 2013).

In the central nervous system (CNS), elevated levels of inflammatory molecules are observed in postmortem HD brain tissue (Björkqvist *et al.* 2008). Substantial numbers of activated microglia are seen in affected regions of the brain such as the striatum and cortex (Sapp *et al.* 2001; Pavese *et al.* 2006), and this correlates with loss of neuronal function (Politis *et al.* 2011). Activated microglia are also present in the brains of pre-symptomatic HD gene carriers (Tai *et al.* 2007), and peripherally, inflammatory molecules are elevated in blood plasma many years before disease onset (Dalrymple *et al.* 2007; Björkqvist *et al.* 2008; Wild *et al.* 2011), suggesting a possible active role of the innate immune system during progression to symptomatic disease. Peripheral myeloid cells are the likely source of elevated systemic levels of inflammatory molecules. HD patient monocytes and macrophages produce increased levels of cytokines when stimulated *ex vivo* (Björkqvist *et al.* 2008), and are impaired in their ability to migrate towards chemo-attractant stimuli (Kwan *et al.* 2012b). These same dysfunctional phenotypes are observed in both peripheral myeloid cells and microglia isolated from HD mouse models (Björkqvist *et al.* 2008), suggesting that blood-derived myeloid cells may reflect the pathological actions of microglia in the CNS in HD. It is also possible that there is direct communication between the peripheral immune system and the CNS in HD: peripheral inhibition of kynurenine 3-monooxygenase, highly expressed in peripheral immune cells, ameliorates neurodegeneration in a HD mouse model by raising CNS levels of neuroprotective metabolite kynurenic acid and preventing hyperactive microglial activity (Zwilling *et al.* 2011).

Hyper-reactivity of the innate immune response in HD is due partly to nuclear factor (NF)κB pathway dysregulation (Khoshnan *et al.* 2004; Träger *et al.* 2014). In HD myeloid cells, dysregulation is observed upon activation of Toll-like receptors (TLRs) using lipopolysaccharide (LPS), implicating a possible mechanism of dysfunctional signalling downstream of TLR4, the principal LPS receptor (Poltorak *et al.* 1998; Qureshi *et al.* 1999). In cultured cells expressing mHTT and striatal cells from HD transgenic mice, mHTT was found to interact with inhibitor of kappa B (IκB) kinase (IKK) γ subunit, leading to elevated NFκB activity and increased NFκB-dependent gene expression (Khoshnan *et al.* 2004). This was also observed in primary human peripheral blood mononuclear cells (PBMCs), along with a more rapid degradation of IκB following LPS stimulation in HD monocytes compared to controls (Träger *et al.* 2014).

While there are treatments that manage the severity of symptoms in HD, there are no effective disease-modifying therapies and consequently, novel approaches targeting hyperactive immune cells have been investigated. Minocycline, a caspase inhibitor, reduces IL-1β and inducible nitric oxide synthase, and in the R6/2 mouse model of HD, minocycline significantly delayed disease progression (Chen *et al.* 2000). A small study in HD patients has shown minocycline to be safe and well tolerated (Thomas *et al.* 2004), however, the primary endpoint of a 25% improvement in the total functional capacity score was not met in a subsequent futility study (Huntington Study Group DOMINO Investigators 2010). More recently, dimethyl fumarate, an immunomodulator approved as a treatment for relapsing-remitting MS (Tecfidera, Biogen), has been shown to have beneficial effects on neuronal degeneration, motor functions and survival time in R6/2 and YAC128 mouse models of HD. Dimethyl fumarate is believed to exert its effects via induction of nuclear factor E2-related factor 2, a transcription factor which activates detoxification pathways and subsequently protects against oxidative damage triggered by inflammation (Ellrichmann *et al.* 2011).

Laquinimod is a novel oral immunomodulatory drug which has been shown to reduce the proportion of astrocytes with nuclear NFκB (p65/RelA) immune-reactivity in cuprizone-treated mice (Brück *et al.* 2012), and decrease cytokine release from LPS-stimulated adult human microglia (Mishra *et al.* 2014). Laquinimod effects on peripheral inflammatory phenotypes have also been described. Laquinimod-treated human PBMCs release lower levels of interleukin (IL)-17, IL-3 and granulocyte colony-stimulating factor (Brück and Wegner 2011). Mononuclear cells isolated from the spleen of a laquinimod-treated MS rat model display evidence of a shift from proinflammatory T helper (Th)1-activating to anti-inflammatory and regulatory Th2/Th3-activating cytokine expression profile, with a laquinimod-induced change in favour of the Th2 stimuli IL-4, IL-10 and transforming growth factor beta (TGFβ) and reductions in the Th1 stimuli tumour necrosis factor alpha (TNFα) and IL-12 (Yang *et al.* 2004). Laquinimod has also been shown to promote splenic

development of M2 polarized monocytes and dendritic cells in mice, leading to reduced cellular production of Th1-activating cytokines IL-6, IL-12 and TNFα with a corresponding increase in Th2-activating anti-inflammatory IL-10 production (Schulze-Topphoff *et al.* 2012).

Affymetrix GeneChip arrays on PBMCs have shown that laquinimod increases IκB expression whilst downstream NFκB genes are decreased (Gurevich *et al.* 2010), and imaging flow cytometry has shown laquinimod-induced reduction in p65 translocation in primary murine astrocytes (Brück *et al.* 2012), suggesting a potential role of NFκB signalling in laquinimod mechanism of action. It is therefore plausible that laquinimod could reverse the hyperactive proinflammatory phenotype observed in HD PBMCs, possibly by rescuing the dysfunctional NFκB signalling in these cells. Intervention of peripheral inflammatory events has previously been shown to modulate central neuropathology and disease progression in HD (Zwilling *et al.* 2011; Bouchard *et al.* 2012; Kwan *et al.* 2012a), therefore an immunomodulatory drug such as laquinimod is a potential candidate for slowing disease progression in HD patients by affecting peripheral immune cells. In addition, laquinimod has already been studied in human immunomodulation and has a very good safety profile following clinical trials for the treatment of MS (Comi *et al.* 2012; Filippi *et al.* 2014; Vollmer *et al.* 2014). Such studies have also provided evidence for laquinimod-induced immunomodulation having beneficial effects on disease progression and brain atrophy in MS (Comi *et al.* 2012). As inflammation has been implicated in myelin, axonal and neuronal loss in HD pathology (Ellrichmann *et al.* 2013), it is feasible that laquinimod may slow disease progression and reduce brain atrophy rate in HD through central and peripheral immunomodulatory mechanisms, as it has been shown to do in MS.

Therefore, the goal of this study was to determine whether laquinimod down-regulates the hyper-reactive proinflammatory phenotype of HD patient myeloid cells, and switches the functional signatures of these cells away from M1 and towards M2 polarization with a consequential shift in the balance from Th1- to Th2-activating cytokine release. This is the first demonstration of the effects of laquinimod in HD patient myeloid cells. The second aim was to elucidate a possible mechanism of action of laquinimod in the periphery, by assessing its possible effects on NFκB pathway dysregulation in HD patient myeloid cells. While a mechanism of action involving the NFκB pathway has been shown in cells of the CNS, it is not yet known whether laquinimod has the same effect in the periphery. To this end, primary human monocyte and macrophage cultures from HD patient subgroups and healthy volunteers were treated with laquinimod in stimulated and non-stimulated conditions. Cytokine release, IκB levels, NFκB translocation and IKKγ-mHTT interactions were examined.

Methods

Collection and classification of human samples

All human experiments were performed in accordance with the Declaration of Helsinki and approved by University College London (UCL)/UCL Hospitals Joint Research Ethics Committee. All blood donors provided informed written consent for research on Huntington's disease. Whole blood samples were collected from manifest HD patients with early or moderate stage disease (manHD), premanifest HD gene carriers (preHD) and healthy volunteers (HV). ManHD samples were collected from six females and 13 males with an average age of 55.32 years ranging from 27 to 70; preHD samples were collected from six females and three males with an average age of 47.45 years ranging from 33 to 62; HV samples were collected from 10 females and five males with an average age of 47.95 years ranging from 25 to 68.

Primary human monocyte isolation

Whole blood samples were decanted into 50 mL heparinized tubes (50 μL prescription grade heparin in standard 50 mL Falcon tubes). 25 mL whole blood was then carefully layered onto 20 mL Histopaque-1077 (Sigma, Dorset, UK) and separated through the gradient by centrifugation in a swinging bucket rotor at 400 *g* for 30 min at 21°C with no brake. The resulting PBMC layer was removed with a Pasteur pipette from the plasma/Histopaque-1077 interface. PBMCs were washed in magnetic-activated cell sorting (MACS) buffer [1 × Dulbecco's phosphate-buffered saline (Gibco, Life Technologies, Paisley, UK); 0.5% bovine serum albumin (Sigma); 2 mM EDTA (Sigma)] and pelleted out of wash solution by centrifugation at 350 *g* for 10 min at 4°C. Cells were re-suspended in 1 mL MACS buffer and 60 μL anti-CD14 MACS MicroBeads (Miltenyi Biotec, Surrey, UK) was added to the suspension, followed by quick vortex and 15 min incubation at 4°C. Cells were then pelleted by centrifugation at 350 *g* for 5 min at 4°C, and re-suspended in fresh MACS buffer before being applied to MACS columns (Miltenyi Biotec) mounted on a magnetic separator (Miltenyi Biotec). The flow-through was discarded and magnetically isolated CD14 + monocytes were plunged out of the columns into separate collection tubes.

Cell culture

Primary human monocytes were seeded in Primaria culture dishes (BD Falcon, BD Biosciences, Oxford, UK) at 3×10^5 cells/cm^2, and maintained in Roswell Park Memorial Institute medium 1640 (Gibco, Life Technologies); 10% foetal bovine serum (Gibco); 2 mM L-glutamine (Gibco, Life Technologies); 5 U/mL penicillin and 5 μg/mL streptomycin (Gibco PenStrep solution) in 5% CO_2 atmosphere at 37°C. Pre-testing has shown that this protocol produces monocyte cultures of at least 95% CD14$^+$ monocytes and these were used in experiments from 1 to 3 days *in vitro* (DIV). For some experiments, monocytes were differentiated into macrophages with the addition of 20 ng/mL granulocyte macrophage colony-stimulating factor (GM-CSF, R&D Systems, Oxford, UK) to the culture medium on seeding. Cells were given a complete media change with addition of fresh GM-CSF at 3 DIV and have been confirmed by factor analysis to be fully differentiated macrophages at 6 DIV and were used in experiments at this stage.

Cell treatments

Once the cells had adhered post-seeding, monocytes were treated with doses of laquinimod ranging from 0 to 100 μM for 24 or 48 h for toxicity analysis. For cytokine analysis, monocytes were treated with 1 or 5 μM laquinimod for 2 or 24 h, or were untreated. Cells were then given a media change, and relevant cultures were stimulated with 1 μg/mL LPS (Sigma, #L6529) for 24 h. 10 ng/mL interferon gamma (IFNγ, R&D Systems) was added at the same time as LPS as a priming agent. Three drug treatment durations, and two drug concentrations were used: 2 and 24 h pre-treatments of 1 and 5 μM laquinimod (before stimulation, 2hPT and 24hPT respectively) and 24 h 5 μM pre-treatment + 24 h continued 5 μM laquinimod treatment during LPS stimulation (24hPT+24hCT). After LPS stimulation, culture supernatants were collected, frozen and stored at −80°C. For western blot analysis, monocytes received 24hPT with 5 μM laquinimod, or untreated, followed by 1 μg/mL LPS stimulation over a time-course of 0–60 min. For imaging flow cytometry analysis, monocytes received 24hPT with 5 μM laquinimod, or untreated, before stimulation with 1 μg/mL LPS for 45 min. For proximity ligation assays, macrophages were treated with 5 μM laquinimod for 24 h, and then fixed.

Cytotoxicity assay

Monocytes cultures from six HD patients and HV were treated, in duplicate, with 0, 0.001, 0.01, 0.1, 0.5, 1, 5, 10, 50 or 100 μM laquinimod for 24 or 48 h. Cell survival after laquinimod treatment was assessed by CytoTox 96 Non-Radioactive Cytotoxicity Assay (Promega, Southampton, UK), as per the manufacturer's protocol, and compared to viability of untreated cells.

ELISA analysis of cytokines

Cytokine levels in monocyte culture supernatants were measured using MesoScale Discovery Human Th1/Th2 10-Plex Tissue Culture Kit analysing 10 different cytokines simultaneously (IFNγ, IL-1β, IL-2, IL-4, IL-5, IL-8, IL-10, IL-12p70, IL-13, TNFα), or Human IL-6 Singleplex Kit, according to the manufacturer's protocol. Depending on cell treatment condition, for 10-plex analysis n = 9–11 for HV, n = 9 for preHD and n = 10–14 for manHD, and for the IL-6 singleplex analysis n = 13–15 for HV, n = 6–9 for preHD and n = 15–19 for manHD. Cytokine level read-outs were normalized to protein content per culture well, which was ascertained by lysing the cultures with radioimmunoprecipitation assay buffer [consisting of 25 mM Tris-HCl pH 7.6, 150 mM NaCl, 1% Nonidet-P40, 1% sodium deoxycholate, 0.1% sodium dodecyl sulphate and protease inhibitor cocktail (Roche, West Sussex, UK)] and performing bicinchoninic acid protein assays (Pierce, Life Technologies) on the resulting lysates, according to the manufacturer's protocol. IFNγ levels were not considered because of the addition of this cytokine as a priming agent in the stimulated conditions.

Western blotting

Monocyte cultures from four manHD received 24hPT with 5 μM laquinimod, or untreated, followed by LPS stimulation. Cell lysates (made using radioimmunoprecipitation assay buffer) were harvested at 0, 5, 15, 30 and 60 min time-points after stimulation. Protein lysates were analysed by western blot using anti-IκB antibody (1:500, Santa Cruz Biotechnology, Heidelberg, Germany) to determine the rate of IκB degradation. All IκB readings were normalized to the house-keeping protein glyceraldehyde 3-phosphate dehydrogenase (anti-GAPDH antibody, 1:3000, Sigma Aldrich, Dorset, UK), and quantified by densitometry analysis of three exposures using TotalLab TL100 image analysis software (Sigma Aldrich). Western blotting and analysis were performed as previously described in detail (Träger *et al.* 2014).

Imaging flow cytometry

Monocyte cultures from seven manHD received 24hPT with 5 μM laquinimod, or untreated, followed by 45 min LPS stimulation. Monocytes were fixed and probed with NFκB p65 XP antibody (1:200, Cell Signaling Technology, New England Biolabs, Hertfordshire, UK) followed by secondary anti-rabbit IgG phycoerythrin-conjugated antibody (1 : 100, eBioscience Ltd., Hatfield, UK). Cells were stained in 1 μg/mL 4′,6-diamidino-2-phenylindole (DAPI, Sigma Aldrich) nuclear stain immediately prior to analysis. Samples were run on ImageStreamX analyser (Amnis Corporation, Seattle, WA, USA) to assess intra/extra-nuclear localization of p65 and analysed using IDEAS Software (Amnis) to calculate percentage translocated cells. Imaging flow cytometry and analysis of images were performed as previously described in detail (Träger *et al.* 2014).

Proximity ligation assay

Monocytes from six manHD and preHD were seeded on 13 mm coverslips at 5×10^3 cells/cm^2, and differentiated into macrophages. Cells were treated with 5 μM laquinimod for 24 h, or untreated, then fixed in 4% paraformaldehyde and stained with fluorescent wheat germ agglutinin (WGA, Life Technologies) to label membranes. Cells were stained with 1 μg/mL WGA for 5 min at 37°C before washing ten times with phosphate-buffered saline. Cells were then permeabilized, blocked and probed with mouse anti-HTT antibody 4C9 (1 : 300, gift from Novartis, Basel, Switzerland) and anti-IKKγ antibody (1 : 100, Santa Cruz). Instead of using fluorescently labelled secondary antibodies, a proximity ligation approach was undertaken, as per the manufacturer's instructions [Proximity Ligation Assay (PLA), Sigma]. Briefly, samples were incubated with secondary antibodies conjugated with PLUS and MINUS DNA probes, which were hybridized and ligated before amplification of the DNA template in a rolling circle amplification reaction. Detection solution was added to identify amplified DNA, and coverslips were mounted on glass slides in Duolink mounting medium (Sigma Aldrich) containing 1 μg/mL DAPI. Signals were detected using fluorescent confocal microscopy. Positive interactions appear as fluorescent spots which were quantified as average number of spots per cell using Volocity software (PerkinElmer, Waltham, MA, USA). Each of the two negative controls was made up of a single primary antibody with both PLUS and MINUS secondary antibodies. The positive control was anti-IKKβ (1 : 50; Santa Cruz) and anti-IKKγ primary antibodies with both secondary antibodies, as these proteins are known to directly interact. PLA and analysis of images were performed as previously described in detail (Träger *et al.* 2014).

Statistical analyses

All samples were labelled with an anonymized 5-digit number for blinded analysis

Cytotoxicity assay data were statistically analysed in-house. One-way ANOVA with Dunnett's multiple comparison tests comparing

all laquinimod treatment conditions to untreated were used to analyse statistically significant variations in the means.

Analysis of ELISA cytokine measurements was performed by an independent statistician (RF). The data set was split into two – stimulated and non-stimulated conditions – to perform statistical analysis. Not every subject had a measurement for every condition because of some samples failing quality control, leading to unbalanced data. Data were log transformed prior to analysis to improve normality assumptions. A linear mixed model was fitted to each of the subsets separately, assuming exchangeable correlation, with robust standard errors to allow for misspecification of the covariance structure. Comparisons of interest were calculated using linear contrasts. This approach allows for data from a subject to be used even if some of the conditions are missing, under a missing at random assumption. For the HD combined comparisons, a weighted combination of preHD and manHD was used, based on the total number of patients in those subgroups. All analyses were additionally adjusted for age. Multiple comparison adjustments were not made because of the small sample size and lack of independency in cytokine activity, and this was taken into consideration when reviewing the findings from these analyses. All results of cytokine levels and statistical analysis of this data are graphically presented and reported on the logarithmic scale. It is important to note that natural differences in cytokine release from primary human monocytes leads to highly variable data, and the sample size limits the precision for which estimates of between condition and between group differences can be made. Therefore, in cases where there is absence of statistical evidence it is not possible to determine whether this is because of no effect or that the random variation in measurements masks any effect that may be present.

NFκB mechanism of action data was analysed in-house. IκB degradation kinetics data were analysed using two-way repeated measures ANOVA comparing treatment conditions (untreated or laquinimod pre-treatment) over time post-LPS-stimulation. Two-tailed, paired Student's *t*-tests were used to compare untreated versus laquinimod treatments for imaging flow cytometry and PLA data. For PLA analysis, all conditions were tested in six subjects, however, the results for the laquinimod condition were removed for one of the subjects for quality control reasons.

Results

Laquinimod is not toxic to *ex vivo* human monocyte cultures

First, it was important to determine whether laquinimod is toxic to primary human monocytes in culture. Monocytes were treated for 24 or 48 h with previously published doses of laquinimod used to treat human PBMCs, 1 and 5 μM (Brück and Wegner 2011), as well as a range of concentrations either side. Laquinimod-treated cell survival was assessed relative to untreated cells. None of the laquinimod concentrations or treatment durations tested showed any overt toxicity to the cells (Fig. 1). Confidence intervals (CIs, calculated at the 95% confidence level) around the mean percentage survival relative to untreated cells span 100% survival in all laquinimod-treated conditions, and are generally narrow. In addition, none of the laquinimod treatment conditions showed a statistically significant difference in percentage monocyte survival ($p > 0.05$). After the longest laquinimod treatment duration of 48 h, 1 and 5 μM laquinimod resulted in an average of 99.84% and 97.54% monocyte survival, respectively, relative to untreated cells. The lower bound of the CIs for these results were 88.01% for 1 μM laquinimod and 86.84% for 5 μM laquinimod, therefore one can be confident that at these concentrations the true cell survival relative to untreated is above 86%, which was taken to be acceptable in terms of establishing a lack of laquinimod toxicity. Previously published doses of 1 and 5 μM laquinimod were therefore used for subsequent experiments, which is in accordance with physiological

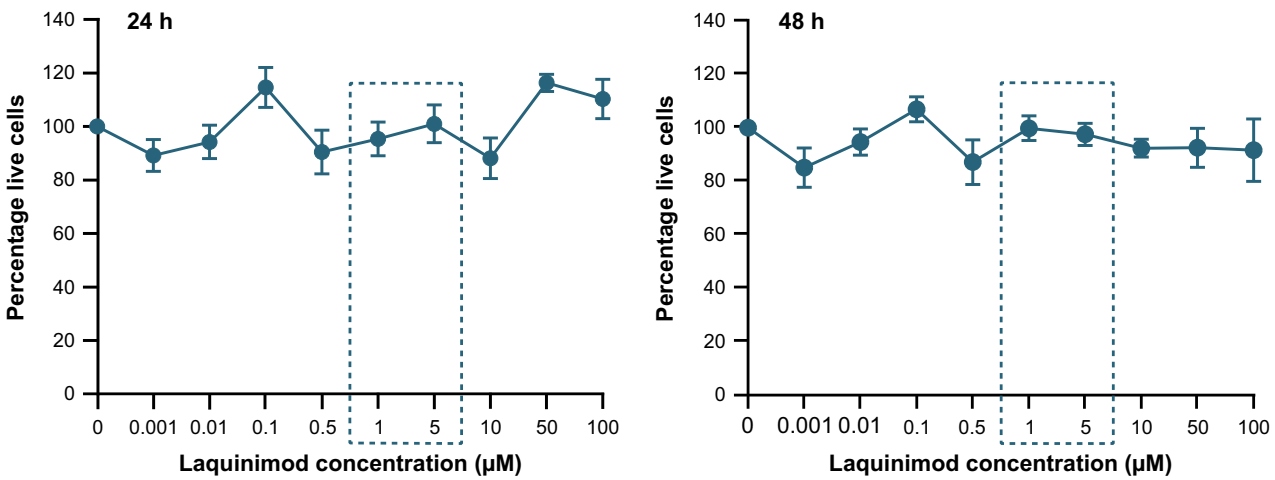

Fig. 1 Primary human monocyte survival following laquinimod treatment. Monocytes treated with a range of laquinimod concentrations for 24 or 48 h. Laquinimod-treated monocyte survival expressed as a percentage of untreated monocyte survival. Data points = mean average of six biological repeats. Error bars = SEM. Concentrations of 1 and 5 μM (boxed) were used in subsequent experiments.

in vivo data for relevant plasma levels of laquinimod in humans (Sennbro *et al.* 2006; Preiningerova 2009) and mice (Brunmark *et al.* 2002).

Laquinimod reduces hyper-reactive cytokine release from stimulated HD patient monocytes

HD monocytes and macrophages have been observed to release elevated levels of the proinflammatory Th1-activating cytokines IL-6, IL-8 and TNFα (Björkqvist *et al.* 2008), and laquinimod has been reported to drive a shift from Th1- to Th2-activating cytokine production in human PBMCs *in vitro* (Brück and Wegner 2011) and in mouse and rat models of MS *in vivo* (Zou *et al.* 2002; Yang *et al.* 2004; Brück and Wegner 2011). To determine whether laquinimod can shift the hyper-reactive proinflammatory cytokine release from HD myeloid cells by tipping the reactive cytokine balance from Th1- to Th2-activating cytokine release, *ex vivo* primary monocyte cultures from HV, preHD and manHD were treated with laquinimod, or untreated, in non-stimulated and stimulated conditions. Culture supernatants were collected and production of the following cytokines was measured: Th1-activating cytokines IL-1β, IL-6, IL-8, IL-12p70, TNFα; Th2-activating cytokines IL-4, IL-5, IL-10, IL-13, TNFα; and IL-2.

Baseline cytokine release in untreated monocytes

Levels of all cytokines, other than IL-6, were significantly higher ($p < 0.05$), or borderline, in manHD compared to HV in monocyte cultures which had received no laquinimod treatment or stimulation. IL-5, IL-8 and IL-13 were also elevated in preHD compared to HV under these conditions. While not all cytokines tested were higher in preHD compared to HV, both preHD and manHD subgroups showed similar trends, and combining the HD subjects increased the power sufficiently to see a statistically significant ($p < 0.05$), or borderline increase in all cytokines tested in HD compared to HV cultures (data not shown) suggesting that HD monocytes inherently release higher levels of cytokines.

Cytokine release in laquinimod-treated non-stimulated monocytes

Monocytes from HV showed at least borderline significant evidence for an increase in Th1-activating cytokine IL-12 ($p = 0.062$) (Figure S1) and the Th2-activating cytokines IL-4 ($p = 0.009$) and IL-5 ($p = 0.002$) (Figure S2), after 2hPT with 1 μM laquinimod. After 24hPT with 1 μM laquinimod, IL-4 and IL-5 levels were still estimated to be higher, but to a lesser degree which was not statistically significant. When HV monocytes were treated with 5 μM laquinimod, there was evidence of an increase in levels of the Th1-activating cytokines IL-12 and TNFα (Figure S1) compared to untreated: IL-12 was increased after 2hPT and 24hPT+24hCT ($p = 0.036$ and $p = 0.026$ respectively), and TNFα was increased after 24hPT and 24hPT+24hCT ($p = 0.022$ and $p = 0.006$ respectively). IL-2 and the Th2-activating cytokines IL-4, IL-5, IL-10 and IL-13 were also increased (Figure S2): IL-2 was increased after 24hPT+24hCT ($p = 0.030$), IL-4 was increased after 24hPT ($p = 0.014$), IL-5 was increased after 2hPT, 24hPT and 24hPT+24hCT ($p = 0.025$, $p = 0.002$ and $p = 0.007$ respectively), IL-10 was increased after 24hPT+24hCT ($p = 0.004$) and IL-13 was increased after 24hPT+24hCT ($p = 0.005$). There was no evidence of a statistically significant effect of laquinimod treatment at any of the concentrations or treatment durations on non-stimulated preHD or manHD monocytes.

Cytokine release in non-laquinimod-treated stimulated monocytes

In LPS(+IFNγ)-stimulated conditions, there was some evidence of an increase in IL-1β, IL-5 and IL-13 release in manHD compared to HV monocytes. The log levels of these cytokines in manHD were all estimated to be around 0.4 higher than in HV, with these differences being of at least borderline statistical significance. IL-4, IL-6 and IL-10 had differences in similar magnitude but did not reach borderline significance. IL-8 levels were lower in preHD compared to HV, with borderline statistical significance. Overall there was little statistical evidence of differences between HD subgroups and HV monocyte cytokine release in stimulated conditions (data not shown).

Cytokine release in 1 μM laquinimod-treated stimulated monocytes

There was no evidence of an effect of 2hPT with 1 μM laquinimod in LPS(+IFNγ)-stimulated HV monocytes. Following 24hPT at the same concentration, HV monocytes showed a borderline significant increase in Th1-activating cytokine IL-8 ($p = 0.064$; Fig. 2) and a significant increase in Th2-activating cytokine IL-5 ($p = 0.035$; Figure 3) compared to untreated cells. PreHD subjects showed decreases in Th1-activating cytokines IL-6 and IL-8 ($p = 0.069$ and $p = 0.004$ respectively; Figure 2) compared to untreated, following 2hPT with 1 μM laquinimod. After a longer pre-treatment duration, 24hPT, at the same concentration, IL-6 levels were significantly decreased compared to untreated ($p = 0.028$; Figure 2). Like the preHD group, manHD monocytes also showed a significant decrease in IL-8 levels following 2hPT with 1 μM laquinimod in stimulated cells ($p = 0.005$; Figure 2). There was no statistical evidence of an effect of 1 μM laquinimod on stimulated manHD monocyte cytokine release following 24hPT (Figures 2 and 3).

Cytokine release in 5 μM laquinimod-treated stimulated monocytes

In HV monocytes, 2hPT or 24hPT with the higher laquinimod concentration of 5 μM resulted in no significant effects

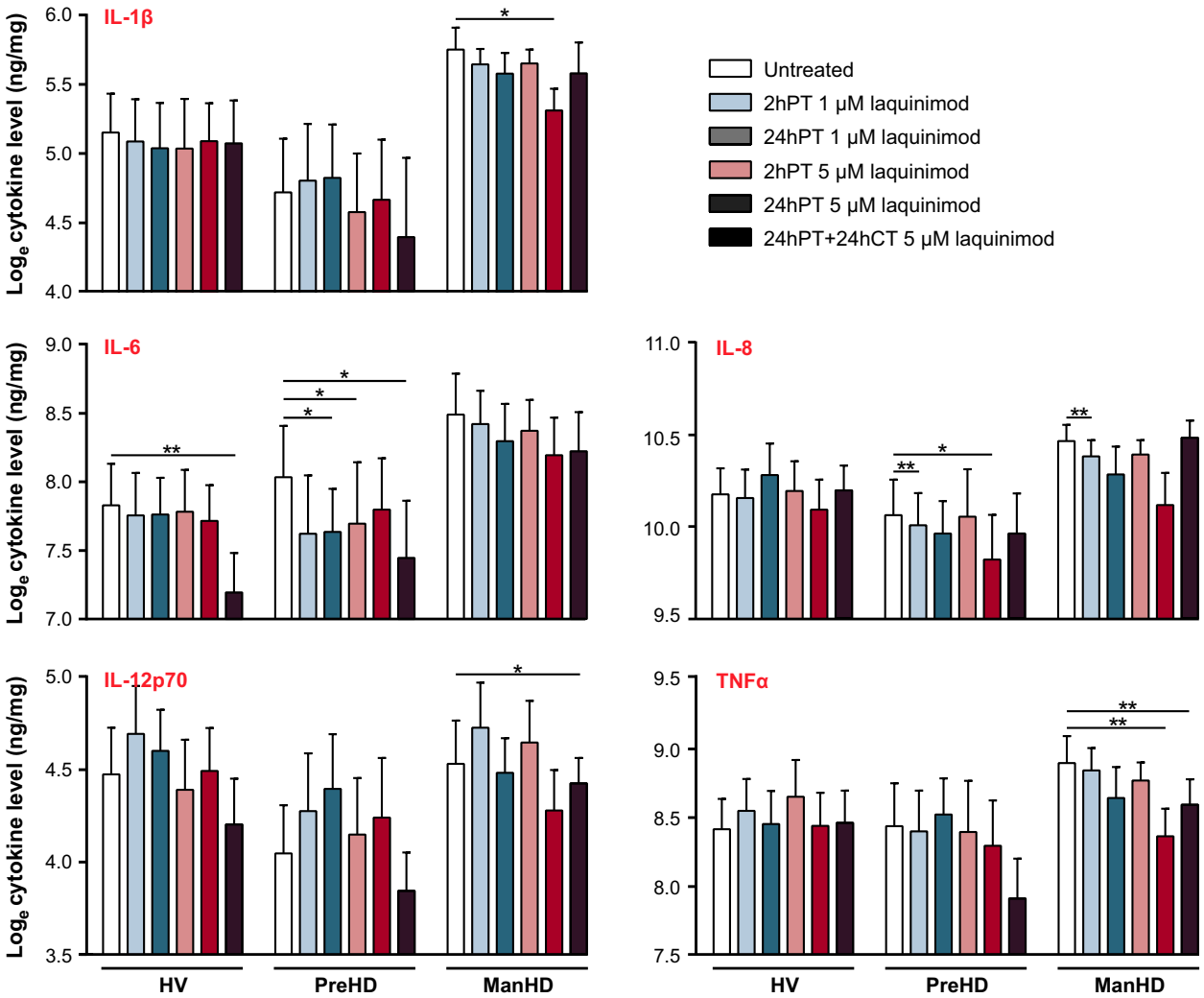

Fig. 2 Th1-activating cytokine release in stimulated monocytes pre-treated with laquinimod. *Primary* stimulated human monocyte cultures from HV, preHD and manHD received 2hPT or 24hPT with 1 or 5 μM laquinimod, or 24hPT+24hCT with 5 μM laquinimod. Levels of cytokine release were measured in monocyte culture supernatants and normalized to cell culture protein. Figure 2 displays results for the Th1-activating cytokines and Fig. 3 displays results for IL-2 and the Th2-activating cytokines measured. Columns = mean average log cytokine level of biological repeats; error bars = SEM; $^*p < 0.05$, $^{**}p < 0.01$.

on levels of cytokine release ($p > 0.05$ for all comparisons; Figures 2 and 3). Levels of Th1-activating cytokine IL-6 were significantly lower in HV monocytes which received 24hPT+24hCT with 5 μM laquinimod compared to untreated ($p = 0.004$; Figure 2), and levels of Th2-activating cytokines IL-5 and IL-13 were significantly higher in the same condition ($p = 0.047$ and $p = 0.041$ respectively; Fig. 3).

In the preHD group, although not always statistically significant, the estimates comparing treatments for 2hPT, 24hPT and 24hPT+24CT with the untreated condition generally showed decreases in levels of cytokines. The exceptions were IL-2 and IL-5, where the general trend shows increases in cytokine levels following laquinimod treatments, but these differences were small in magnitude. Th1-activating cytokines IL-6 and IL-8 were reduced (Fig. 2): IL-6 was reduced after 2hPT and 24hPT+24hCT ($p = 0.015$ and $p = 0.016$ respectively), and IL-8 was reduced after 24hPT ($p = 0.015$). Th2-activating cytokines IL-10 and IL-13 were also reduced (Fig. 3): IL-10 was reduced after 2hPT, 24hPT and 24hPT+24hCT ($p = 0.037$, $p = 0.015$ and $p = 0.004$ respectively), and IL-13 was reduced after 24hPT ($p = 0.033$).

In manHD monocytes, 2hPT with 5 μM laquinimod did not show a statistically significant change in cytokine levels compared to untreated, however, the 24hPT effect was of at least borderline statistical significance for several cytokines, with evidence of a reduction in the proinflammatory, Th1-activating cytokines IL-1β ($p = 0.022$), IL-6 ($p = 0.056$), IL-8 ($p = 0.052$) and TNFα ($p = 0.007$) (Fig. 2), and the Th2-activating cytokines IL-5 ($p = 0.053$), IL-10 ($p = 0.044$) and

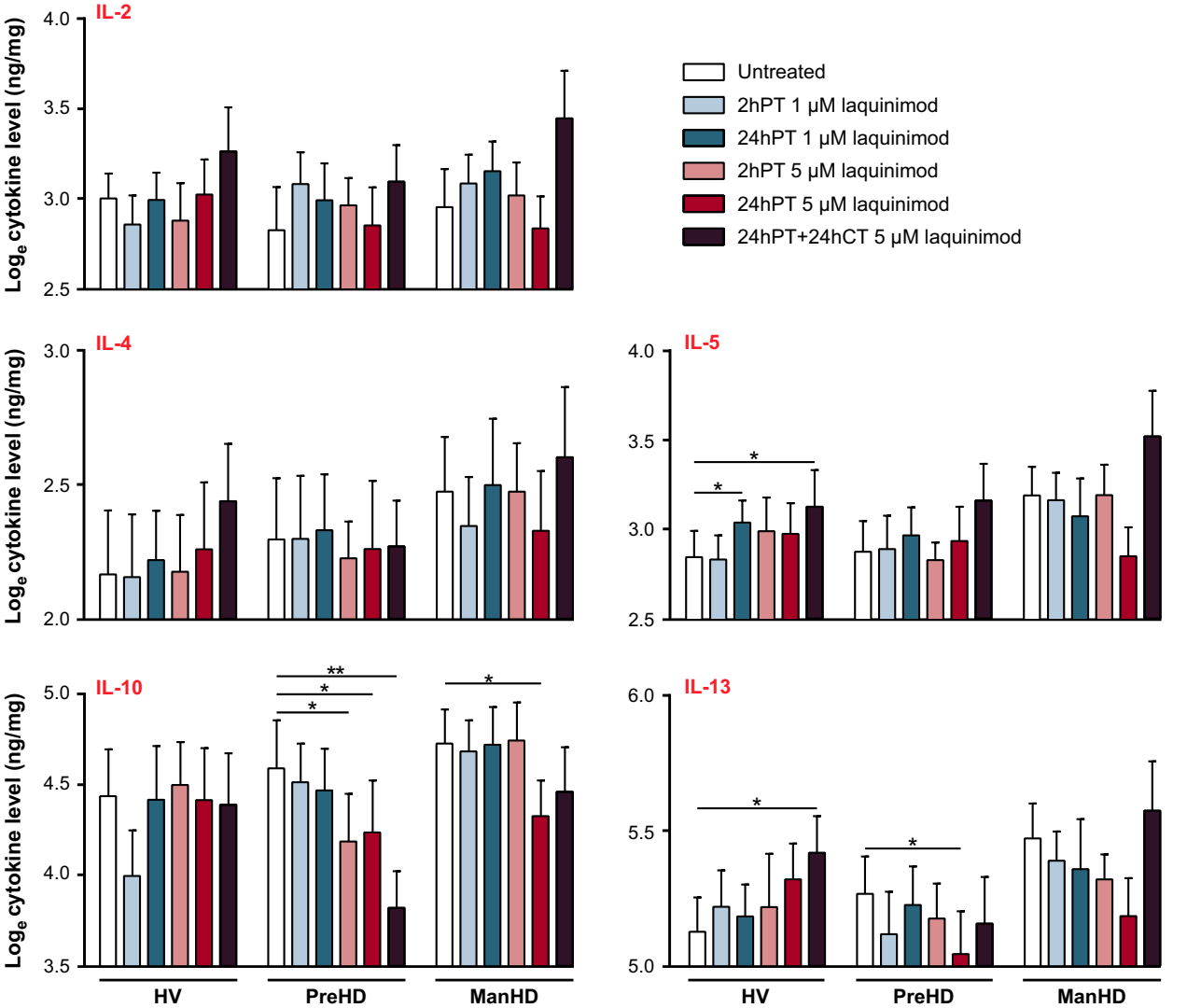

Fig. 3 IL-2 and Th2-activating cytokine release in stimulated monocytes pre-treated with laquinimod. Primary stimulated human monocyte cultures from HV, preHD and manHD received 2hPT or 24hPT with 1 or 5 μM laquinimod, or 24hPT+24hCT with 5 μM laquinimod. Levels of cytokine release were measured in monocyte culture supernatants and normalized to cell culture protein. Figure 2 displays results for the Th1-activating cytokines and Figure 3 displays results for IL-2 and the Th2-activating cytokines measured. Columns = mean average log cytokine level of biological repeats; error bars = SEM; $^*p < 0.05$, $^{**}p < 0.01$.

IL-13 ($p = 0.052$) (Fig. 3). In addition, for the cytokines IL-1β, IL-10 and TNFα, 24hPT with 5 μM laquinimod resulted in a statistically significant reduction in cytokine release from manHD monocytes that was not seen in HV. While not statistically significant, many of the other cytokines also showed this trend. This could suggest that 24hPT with 5 μM laquinimod has more of an effect on reducing cytokine production in manHD monocytes than in HV monocytes. After 24hPT+24hCT, there were decreases in the Th1-activating cytokines IL-6 ($p = 0.053$), IL-12 ($p = 0.028$) and TNFα ($p = 0.009$) compared to untreated in manHD monocytes (Fig. 2). Although not statistically significant, levels of IL-2 and Th2-activating cytokines IL-4, IL-5 and IL-13 were increased following 24hPT+24hCT (Fig. 3), going against the trend seen with 2hPT and 24hPT.

A secondary analysis was performed to increase power and look at the differences between HV and HD overall. When manHD and preHD subgroup data were combined, 24hPT with 5 μM laquinimod resulted in at least a borderline significant decrease in the Th1-activating cytokines IL-1β ($p = 0.006$), IL-6 ($p = 0.059$), IL-8 ($p = 0.005$) and TNFα ($p = 0.003$), and the Th2-activating cytokines IL-10 ($p = 0.003$) and IL-13 ($p = 0.009$) compared to the untreated condition. In addition, the difference in change from the untreated condition between grouped HD subjects and HV was of at least borderline significance for IL-1β ($p = 0.062$),

IL-5 ($p = 0.045$), IL-10 ($p = 0.008$), IL-13 ($p = 0.005$) and TNFα ($p = 0.045$), suggesting that 24hPT with 5 μM laquinimod has a larger effect on reducing cytokine release from HD cells than HV cells.

Laquinimod does not affect NFκB signalling in HD monocytes

Laquinimod-induced down-regulation of proinflammatory factors in monocytes has previously been shown to be because of a switch from MI to M2 phenotype (Zou *et al.* 2002; Yang *et al.* 2004; Brück and Wegner 2011; Schulze-Topphoff *et al.* 2012). The exact mechanism for this remains unclear, although in astrocytes the down-regulation has been shown to be a result of reduced NFκB activation (Brück *et al.* 2012). In HD myeloid cells, the enhanced release of proinflammatory factors is at least in part because of elevated NFκB activation (Träger *et al.* 2014), so investigations were made into a role of the NFκB pathway in the observed overall dampening of cytokine release from stimulated HD monocytes pre-treated with laquinimod.

To determine whether laquinimod has the potential to improve NFκB dysfunction in HD, the effect of the compound on IκB degradation kinetics was assessed in HD monocytes. IκB binds NFκB transcription factor p65 in the cytoplasm, preventing its nuclear translocation. Degradation of IκB, however, liberates p65, which then translocates into the nucleus to modulate transcription (Hayden and Ghosh 2012). Consequently, monitoring IκB kinetics is an indirect measure for monitoring p65 nuclear translocation; decreased IκB levels indicates increased nuclear translocation of p65. ManHD monocytes were stimulated with LPS, with or without 24hPT with 5 μM laquinimod, and IκB levels were measured by western blotting at 0, 5, 15, 30 and 60 min post-stimulation. LPS stimulation resulted in the usual degradation pattern of IκB for HD monocytes (Träger *et al.* 2014), and laquinimod pre-treatment did not significantly alter ($p = 0.566$) IκB levels from the untreated condition over time post-LPS stimulation (Fig. 4a). As IκB degradation kinetics were not affected by laquinimod treatment, this suggests that laquinimod may not alter nuclear translocation of the NFκB transcription factor p65 in monocytes. However, because of the indirect method of measuring p65 translocation used, it was necessary to directly monitor nuclear translocation using an alternative method before ruling out an effect of laquinimod in this mechanism.

Imaging flow cytometry was implemented to directly assess p65 nuclear translocation. ManHD monocytes received 24hPT with 5 μM laquinimod, or untreated, for 24 h before 45 min LPS stimulation. Monocytes were labelled with anti-p65 antibody and DAPI nuclear stain, and run through ImageStream to detect intra/extra-nuclear localization of p65. NFκB translocation has previously been shown to be pathologically enhanced in HD patient myeloid cells, leading to a hyper-reactive response to LPS stimulation and increased release of proinflammatory cytokines (Träger *et al.* 2014). 24hPT with 5 μM laquinimod did not significantly alter ($p = 0.466$) the extent of p65 translocation compared to untreated in HD monocytes (Fig. 4b).

It has previously been shown in HD myeloid cells that mHTT directly interacts with the γ subunit of IKK, and it is this dysfunctional interaction which may lead to the observed increase in IκB degradation (Träger *et al.* 2014). PLA was conducted to assess the interaction between mHTT and IKKγ in HD macrophages after 24hPT with 5 μM laquinimod, or untreated. Laquinimod did not significantly alter ($p = 0.552$) the number of observed positive HTT-IKKγ interactions (spots per cell) compared to untreated, suggesting that laquinimod does not affect the interaction between mHTT and IKKγ in HD macrophages (Fig. 4c).

Discussion

Systemic levels of proinflammatory cytokines in HD gene carriers are elevated many years before disease manifestation, and monocytes and macrophages are the likely source (Björkqvist *et al.* 2008). HD patient monocytes produce higher levels of cytokines than HV monocytes when stimulated *ex vivo* (Björkqvist *et al.* 2008) and are impaired in their ability to migrate towards chemoattractant stimuli (Kwan *et al.* 2012b). There is evidence that systemic inflammatory processes activate CNS microglia leading to exacerbation of neurodegeneration pathology (Cunningham *et al.* 2007; Perry 2007; Perry *et al.* 2007; Palin *et al.* 2008), and peripheral immune challenges have been shown to exacerbate disease progression in mouse models of HD (Hsiao *et al.* 2013). Therefore, peripheral immune events may directly influence neuroinflammation and neuropathology in HD.

Laquinimod appears to alter hyperactivity of the peripheral immune system in HD as shown by its reduction in cytokine release from HD patient blood-derived monocytes. In non-stimulated conditions, laquinimod showed significant effects on HV cytokines but not preHD or manHD cytokine levels. In stimulated monocytes, laquinimod had an overall dampening effect on cytokine release; however, these changes were variable depending on the cytokine, subject group, and laquinimod pre-treatment conditions. Laquinimod pre-treatment reduced the release of nearly all cytokines from stimulated preHD and/or manHD monocytes compared to the untreated condition. This effect was most consistent following 24hPT, and interestingly had an effect of larger magnitude on HD monocytes than on HV monocytes, where the changes (if any) in the HV group were relatively minor. In particular, our data provides evidence for this for the Th1-activating proinflammatory cytokines IL-1β, IL-8 and TNFα and the Th2-activating cytokines IL-5, IL-13 and anti-inflammatory IL-10. It is important to note that the natural differences in cytokine release from primary human mono-

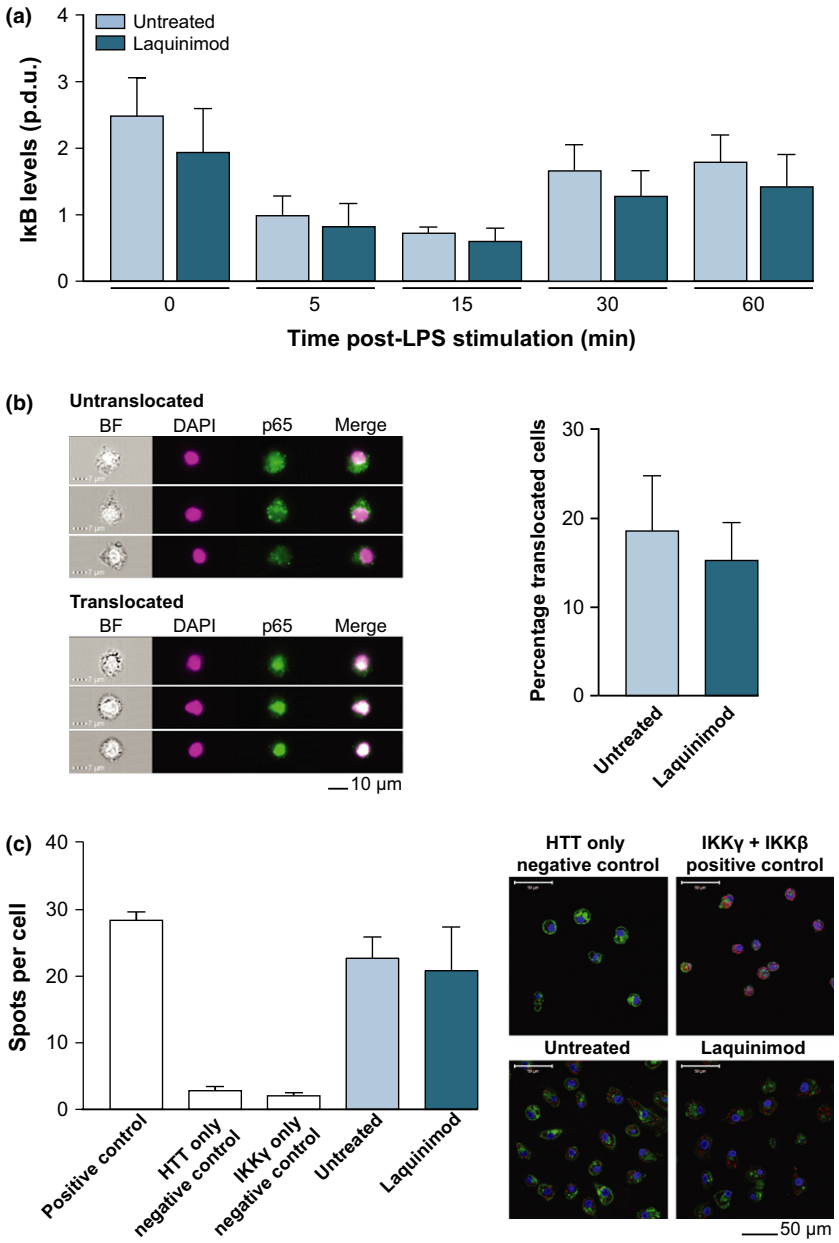

Fig. 4 Laquinimod does not affect (a) IκB degradation kinetics, (b) p65 translocation or (c) IKKγ-mHTT interaction in HD patient myeloid cells. (a) IκB degradation kinetics in lipopolysaccharide (LPS)-stimulated HD monocytes, with and without 24hPT with 5 μM laquinimod. IκB levels measured using western blotting of cell lysates harvested at 0, 5, 15, 30 and 60 min post-LPS stimulation. Blots quantified using densitometry giving a procedure defined unit (p.d.u.) for comparison of conditions. Columns = mean average p.d.u. of four biological repeats; error bars = SEM. (b) Nuclear translocation of NFκB transcription factor p65 in manHD monocytes 45 min post-LPS stimulation, as assessed by imaging flow cytometry. Monocytes received 24hPT with 5 μM laquinimod or untreated. Monocytes were probed for p65 (green) and nuclei were stained with DAPI (pink), as can be seen in example images all taken from the same untreated sample, and percentage translocated cells assessed. Columns = mean average percentage translocated cells from seven biological repeats; error bars = SEM. (c) Interaction between HTT and IKKγ in HD macrophages with or without 24 h 5 μM laquinimod treatment, as assessed by proximity ligation assay (PLA). Cells imaged using fluorescence confocal microscopy. A direct interaction between the two proteins is presented as a fluorescent red spot, nuclei stained with DAPI (blue) and membranes withwheat germ agglutinin (WGA) (green), as can be seen in example images all taken from the same patient cells. Positive and negative controls indicate success of the assay. Columns = mean average spots per cell (untreated condition from 6 biological repeats, laquinimod condition from five biological repeats; five matched pairs); error bars = SEM.

cytes (HV and HD) leads to large variations in cytokine level measurements, which introduces some limitations to this system. Consequently, it is not always possible to determine whether lack of a statistically significant effect is because of there being no effect or because of random variation in measurements masking an effect that may be present. Overall, the sample size limits the precision for which between condition and between subject group differences can be assessed. However, there is evidence that laquinimod does have an effect on cytokine release from HD monocytes, and that this effect may be different than the effect of laquinimod on HV monocytes.

Cytokine level trends across laquinimod treatment conditions are generally consistent in terms of laquinimod-induced changes being greater in magnitude at the 5 μM drug concentration and a longer pre-treatment duration. However, this did not usually extend to the 24hPT+24hCT condition, where in many cases a much smaller change from the untreated condition occurred than would have been predicted, or there was even a change in the opposite direction. Indeed, with the exception of IL-10, there were small increases in the Th2-activating cytokines in the 24hPT+24hCT condition. Thus, it is important to note that the 24hPT+24hCT condition may need to be considered independently from the pre-treatment only conditions, as laquinimod was present during stimulation. It is possible that an alternative mechanism of action is at play under these conditions, such as competitive binding or confounding cross talk between intracellular signalling pathways.

We did not observe an overall shift in cytokine balance from Th1- to Th2-activating cytokine release in HD monocytes, which has been reported previously in MS (Zou *et al.* 2002; Yang *et al.* 2004; Brück and Wegner 2011; Schulze-Topphoff *et al.* 2012). The shift in cytokine balance previously reported was identified in systems quite different than those used here. Zou *et al.* (2002) and Yang *et al.* (2004) both describe a decrease in proinflammatory cytokines along with an increase in Th2-activating and anti-inflammatory cytokines *in vivo* in rat models of MS following 15 days of daily laquinimod administration. Zou *et al.* found a decrease in the number of IFNγ- and TNFα-expressing cells, with an increase in the number of IL-4-expressing cells in sciatic nerve sections, but in mononuclear cells (MNCs) isolated from lymph node they only looked at release of the proinflammatory cytokines, which decreased. Yang *et al.* describe an increase in the number of spleen MNCs expressing mRNA for the Th2-activating cytokines IL-4, TGFβ1 and IL-10 and a decrease in the number of cells expressing mRNA for proinflammatory IL-12 and TNFα, however, in PBMCs they report a decrease in the number of cells expressing TNFα mRNA with no change in the other cytokines. Schulze-Topphoff *et al.* (2012) also report their findings in an *in vivo* animal model of MS, describing a laquinimod-induced cytokine shift in cells isolated from spleen. Brück and Wegner (2011) report a Th1- to Th2-activating shift following daily laquinimod administration in a MS mouse model, but in PBMCs isolated from HVs they only describe decreases in proinflammatory cytokines. In our model, we push isolated PBMCs towards an M1 phenotype by stimulating them with LPS and IFNγ. In this setting an increase in Th2-activating cytokines was unlikely to be observed, however, laquinimod pre-treatment did reduce overall cytokine production, including those which promote Th1 activation, suggesting that the functional signatures of laquinimod-treated HD monocytes are somewhere between the M1 and M2 polarization extremes following stimulation (Martinez and Gordon 2014). Overall, our evidence for a laquinimod-induced decrease in cytokine release from human HD monocytes is supported by the current literature on laquinimod effects in MS models. Our findings for lack of a Th1- to Th2-activating shift in cytokine balance is also consistent with the effects seen following laquinimod pre-treatment of LPS-activated human microglial cultures, where laquinimod significantly reduced the secretion of the proinflammatory cytokines TNFα, IL-1β, IL-12p70 and IL-6, and the anti-inflammatory/regulatory cytokines IL-4, IL-10 and IL-1ra (Mishra *et al.* 2014).

In the Björkqvist *et al.* (2008) study comparing peripheral cytokine levels in the plasma of HV and HD patient subgroups, there were increased levels of both Th1- and Th2-activating cytokines in HD compared to HV, and these increases correlated with disease progression. The Th1-activating cytokines IL-6, IL-8 and TNFα, and the Th2-activating cytokines IL-4 and anti-inflammatory IL-10 were elevated in HD patient plasma compared to HV plasma. A combination of IL-6, IL-8 and IL-10 cytokine increases was positively correlated with disease progression from preHD through to manHD, and could also be used to discriminate HV from HD gene carriers (both pre-manifest and manifest). In this study, laquinimod shows dampening of the hyper-reactive release of cytokines by HD monocytes, and this may be a way of reducing the elevated plasma cytokine levels observed in HD patients and the increasing levels in advancing disease, both peripherally and in the brain.

It may seem counterintuitive to reduce potent proinflammatory factors such as IL-1β and TNFα whilst additionally decreasing the key anti-inflammatory cytokine IL-10. However, IL-10 levels, which are shown to be high in HD patients, are also abnormally elevated in Alzheimer's disease (AD) patient brains (Guillot-Sestier *et al.* 2015), and IL-10 has recently been highlighted as harmful in mouse models of AD; increasing brain amyloid-β (Aβ) accumulation, exacerbating memory impairment and suppressing microglial Aβ phagocytosis (Chakrabarty *et al.* 2015). As HD and AD share similar pathologies of protein aggregation and neurodegeneration, and are both diseases exacerbated by dysregulated inflammation, it may be that the laquinimod-induced reduction in IL-10 from HD peripheral myeloid cells

is beneficial, and may contribute to resolution of the innate immune system cytokine balance.

Previous studies on laquinimod mechanism of action present evidence for a role of the NFκB pathway in astrocytes. Laquinimod reduced astrocytic NFκB activation in cuprizone-treated mice and primary human astrocyte cultures (Brück *et al.* 2012), and gene expression microarrays on laquinimod-treated PBMCs isolated from MS patients revealed down-regulation of key genes downstream of NFκB signalling (Gurevich *et al.* 2010). The results of this study, however, do not support a role for laquinimod mechanism of action downstream of NFκB activation in primary human HD monocytes. Laquinimod did not affect IκB degradation kinetics, nuclear translocation of p65 nor IKKγ-mHTT protein–protein interactions, from the untreated condition. This is in accordance with work by Brück *et al.* who found that NFκB activation was markedly reduced by laquinimod in astrocytes, but not in microglia, the resident myeloid cells of the CNS, in stimulated primary mouse cultures (Brück *et al.* 2012).

In summary, 5 μM laquinimod applied to HD patient peripheral myeloid cells for 24 h appears to reduce hyperreactive cytokine production in response to LPS stimulation. This is true for Th1-activating proinflammatory cytokines and Th2-activating cytokines including IL-10. Altering peripheral immune responses modulates central pathology and disease progression in HD, hence laquinimod is a promising candidate for dampening the harmful effects of a dysfunctional innate immune system in HD. The mechanism for this does not appear to be downstream of NFκB activation in these cells. Laquinimod mechanism of action is currently under investigation.

Acknowledgements and conflict of interest disclosure

This work was undertaken at UCLH/UCL who acknowledges support from the Department of Health's NIHR Biomedical Research Centre.

Conflicts of interest

Laquinimod is produced by Teva Pharmaceutical Industries Ltd, Israel. LH, MRH and PL are employees of Teva. LD has received travel expenses for attending meetings and SJT has received financial grant support for research from Teva Pharmaceutical Industries Ltd, Israel.

Supporting information

Additional supporting information may be found in the online version of this article at the publisher's web-site:

Figures S1 and S2. Primary non-stimulated human monocyte cultures from HV, preHD and manHD received 2hPT or 24hPT with 1 or 5 μM laquinimod, or 24hPT+24hCT with 5 μM laquinimod. Levels of cytokine release were measured in culture supernatants and normalized to cell culture protein. Supplementary figure 1 displays results for the Th1-activating cytokines and Figure S2 displays results for IL-2 and the Th2-activating cytokines measured. Columns = mean average log cytokine level of biological repeats; error bars = SEM; *$p<0.05$, **$p<0.01$.

References

Björkqvist M., Wild E. J., Thiele J. *et al.* (2008) A novel pathogenic pathway of immune activation detectable before clinical onset in Huntington's disease. *J. Exp. Med.* **205**, 1869–1877.

Bouchard J., Truong J., Bouchard K., Dunkelberger D., Desrayaud S., Moussaoui S., Tabrizi S. J., Stella N. and Muchowski P. J. (2012) Cannabinoid receptor 2 signaling in peripheral immune cells modulates disease onset and severity in mouse models of Huntington's disease. *J. Neurosci. Off. J. Soc. Neurosci.* **32**, 18259–18268.

Brück W. and Wegner C. (2011) Insight into the mechanism of laquinimod action. *J. Neurol. Sci.* **306**, 173–179.

Brück W., Pförtner R., Pham T. *et al.* (2012) Reduced astrocytic NF-κB activation by laquinimod protects from cuprizone-induced demyelination. *Acta Neuropathol. (Berl.)* **124**, 411–424.

Brunmark C., Runström A., Ohlsson L., Sparre B., Brodin T., Aström M. and Hedlund G. (2002) The new orally active immunoregulator laquinimod (ABR-215062) effectively inhibits development and relapses of experimental autoimmune encephalomyelitis. *J. Neuroimmunol.* **130**, 163–172.

Chakrabarty P., Li A., Ceballos-Diaz C. *et al.* (2015) IL-10 alters immunoproteostasis in APP mice, increasing plaque burden and worsening cognitive behavior. *Neuron* **85**, 519–533.

Chen M., Ona V. O., Li M. *et al.* (2000) Minocycline inhibits caspase-1 and caspase-3 expression and delays mortality in a transgenic mouse model of Huntington disease. *Nat. Med.* **6**, 797–801.

Comi G., Jeffery D., Kappos L., Montalban X., Boyko A., Rocca M. A. and Filippi M. (2012) Placebo-controlled trial of oral laquinimod for multiple sclerosis. *N. Engl. J. Med.* **366**, 1000–1009.

Cunningham C., Campion S., Teeling J., Felton L. and Perry V. H. (2007) The sickness behaviour and CNS inflammatory mediator profile induced by systemic challenge of mice with synthetic double-stranded RNA (poly I:C). *Brain Behav. Immun.* **21**, 490–502.

Dalrymple A., Wild E. J., Joubert R. *et al.* (2007) Proteomic profiling of plasma in Huntington's disease reveals neuroinflammatory activation and biomarker candidates. *J. Proteome Res.* **6**, 2833–2840.

Ellrichmann G., Petrasch-Parwez E., Lee D.-H., Reick C., Arning L., Saft C., Gold R. and Linker R. A. (2011) Efficacy of fumaric acid esters in the R6/2 and YAC128 models of Huntington's disease. *PLoS ONE* **6**, e16172.

Ellrichmann G., Reick C., Saft C. and Linker R. A. (2013) The role of the immune system in Huntington's disease. *Clin. Dev. Immunol.* **2013**, 541259.

Filippi M., Rocca M. A., Pagani E., De Stefano N., Jeffery D., Kappos L., Montalban X., Boyko A. N. and Comi G., ALLEGRO Study Group (2014) Placebo-controlled trial of oral laquinimod in multiple sclerosis: MRI evidence of an effect on brain tissue damage. *J. Neurol. Neurosurg. Psychiatry* **85**, 851–858.

Guillot-Sestier M.-V., Doty K. R., Gate D., Rodriguez J., Leung B. P., Rezai-Zadeh K. and Town T. (2015) Il10 deficiency rebalances

innate immunity to mitigate Alzheimer-like pathology. *Neuron* **85**, 534–548.

Gurevich M., Gritzman T., Orbach R., Tuller T., Feldman A. and Achiron A. (2010) Laquinimod suppress antigen presentation in relapsing-remitting multiple sclerosis: in-vitro high-throughput gene expression study. *J. Neuroimmunol.* **221**, 87–94.

Hayden M. S. and Ghosh S. (2012) NF-κB, the first quarter-century: remarkable progress and outstanding questions. *Genes Dev.* **26**, 203–234.

Hsiao H.-Y., Chen Y.-C., Chen H.-M., Tu P.-H. and Chern Y. (2013) A critical role of astrocyte-mediated nuclear factor-κB-dependent inflammation in Huntington's disease. *Hum. Mol. Genet.*, **22**, 1826–1842.

Huntington Study Group DOMINO Investigators (2010) A futility study of minocycline in Huntington's disease. *Mov. Disord. Off. J. Mov. Disord. Soc.* **25**, 2219–2224.

Khoshnan A., Ko J., Watkin E. E., Paige L. A., Reinhart P. H. and Patterson P. H. (2004) Activation of the IkappaB kinase complex and nuclear factor-kappaB contributes to mutant huntingtin neurotoxicity. *J. Neurosci. Off. J. Soc. Neurosci.* **24**, 7999–8008.

Kwan W., Magnusson A., Chou A. *et al.* (2012a) Bone marrow transplantation confers modest benefits in mouse models of Huntington's disease. *J. Neurosci. Off. J. Soc. Neurosci.* **32**, 133–142.

Kwan W., Träger U., Davalos D. *et al.* (2012b) Mutant huntingtin impairs immune cell migration in Huntington disease. *J. Clin. Invest.* **122**, 4737–4747.

Martinez F. O. and Gordon S. (2014) The M1 and M2 paradigm of macrophage activation: time for reassessment. *F1000prime Rep.* **6**, 13.

Mishra M. K., Wang J., Keough M. B., Fan Y., Silva C., Sloka S., Hayardeny L., Brück W. and Yong V. W. (2014) Laquinimod reduces neuroaxonal injury through inhibiting microglial activation. *Ann. Clin. Transl. Neurol.* **1**, 409–422.

Palin K., Cunningham C., Forse P., Perry V. H. and Platt N. (2008) Systemic inflammation switches the inflammatory cytokine profile in CNS Wallerian degeneration. *Neurobiol. Dis.* **30**, 19–29.

Pavese N., Gerhard A., Tai Y. F., Ho A. K., Turkheimer F., Barker R. A., Brooks D. J. and Piccini P. (2006) Microglial activation correlates with severity in Huntington disease: a clinical and PET study. *Neurology* **66**, 1638–1643.

Perry V. H. (2007) Stress primes microglia to the presence of systemic inflammation: implications for environmental influences on the brain. *Brain Behav. Immun.* **21**, 45–46.

Perry V. H., Cunningham C. and Holmes C. (2007) Systemic infections and inflammation affect chronic neurodegeneration. *Nat. Rev. Immunol.* **7**, 161–167.

Politis M., Pavese N., Tai Y. F., Kiferle L., Mason S. L., Brooks D. J., Tabrizi S. J., Barker R. A. and Piccini P. (2011) Microglial activation in regions related to cognitive function predicts disease onset in Huntington's disease: a multimodal imaging study. *Hum. Brain Mapp.* **32**, 258–270.

Poltorak A., He X., Smirnova I. *et al.* (1998) Defective LPS signaling in C3H/HeJ and C57BL/10ScCr mice: mutations in Tlr4 gene. *Science* **282**, 2085–2088.

Preiningerova J. (2009) Oral laquinimod therapy in relapsing multiple sclerosis. *Expert Opin. Investig. Drugs* **18**, 985–989.

Qureshi S. T., Larivière L., Leveque G., Clermont S., Moore K. J., Gros P. and Malo D. (1999) Endotoxin-tolerant mice have mutations in Toll-like receptor 4 (Tlr4). *J. Exp. Med.* **189**, 615–625.

Ross C. A. and Tabrizi S. J. (2011) Huntington's disease: from molecular pathogenesis to clinical treatment. *Lancet Neurol.* **10**, 83–98.

Sapp E., Kegel K. B., Aronin N., Hashikawa T., Uchiyama Y., Tohyama K., Bhide P. G., Vonsattel J. P. and DiFiglia M. (2001) Early and progressive accumulation of reactive microglia in the Huntington disease brain. *J. Neuropathol. Exp. Neurol.* **60**, 161–172.

Schulze-Topphoff U., Shetty A., Varrin-Doyer M., Molnarfi N., Sagan S. A., Sobel R. A., Nelson P. A. and Zamvil S. S. (2012) Laquinimod, a quinoline-3-carboxamide, induces type II myeloid cells that modulate central nervous system autoimmunity. *PLoS ONE* **7**, e33797.

Sennbro C. J., Olin M., Edman K., Hansson G., Gunnarsson P. O. and Svensson L. D. (2006) Determination of the immunomodulator laquinimod in human plasma by liquid chromatography/tandem mass spectrometry; development, validation and application of two methods in clinical pharmacokinetic profiling. *Rapid Commun. Mass Spectrom. RCM* **20**, 3313–3318.

Tai Y., Pavese N., Gerhard A., Tabrizi S. J., Barker R., Brooks D. and Piccini P. (2007) Microglial activation in presymptomatic Huntington's disease gene carriers. *Brain* **130**, 1759–1766.

The Huntington's Disease Collaborative Research Group (1993) A novel gene containing a trinucleotide repeat that is expanded and unstable on Huntington's disease chromosomes. *Cell* **72**, 971–983.

Thomas M., Ashizawa T. and Jankovic J. (2004) Minocycline in Huntington's disease: a pilot study. *Mov. Disord. Off. J. Mov. Disord. Soc.* **19**, 692–695.

Träger U., Andre R., Lahiri N. *et al.* (2014) HTT-lowering reverses Huntington's disease immune dysfunction caused by NFκB pathway dysregulation. *Brain*, **137**, 819–833.

Vollmer T. L., Sorensen P. S., Selmaj K., Zipp F., Havrdova E., Cohen J. A., Sasson N., Gilgun-Sherki Y. and Arnold D. L., BRAVO Study Group (2014) A randomized placebo-controlled phase III trial of oral laquinimod for multiple sclerosis. *J. Neurol.* **261**, 773–783.

Wild E., Magnusson A., Lahiri N., Krus U., Orth M., Tabrizi S. J. and Björkqvist M. (2011) Abnormal peripheral chemokine profile in Huntington's disease. *PLoS Curr.* **3**, RRN1231.

Yang J.-S., Xu L.-Y., Xiao B.-G., Hedlund G. and Link H. (2004) Laquinimod (ABR-215062) suppresses the development of experimental autoimmune encephalomyelitis, modulates the Th1/Th2 balance and induces the Th3 cytokine TGF-beta in Lewis rats. *J. Neuroimmunol.* **156**, 3–9.

Zou L.-P., Abbas N., Volkmann I., Nennesmo I., Levi M., Wahren B., Winblad B., Hedlund G. and Zhu J. (2002) Suppression of experimental autoimmune neuritis by ABR-215062 is associated with altered Th1/Th2 balance and inhibited migration of inflammatory cells into the peripheral nerve tissue. *Neuropharmacology* **42**, 731–739.

Zwilling D., Huang S.-Y., Sathyasaikumar K. V. *et al.* (2011) Kynurenine 3-monooxygenase inhibition in blood ameliorates neurodegeneration. *Cell* **145**, 863–874.

Supplementary

Title: Laquinimod dampens hyperactive cytokine production in Huntington's disease patient myeloid cells

Authors: Lucianne Dobson[1], Ulrike Träger[1,5], Ruth Farmer[2], Liat Hayardeny[3], Pippa Loupe[3], Blair R Leavitt[4], Michael R Hayden[3], and Sarah J Tabrizi[1].

Author affiliations:

1. University College London, Institute of Neurology and National Hospital for Neurology and Neurosurgery, Department of Neurodegenerative Diseases, London, UK
2. London School of Hygiene & Tropical Medicine, Department of Medical Statistics, London, UK
3. Teva Pharmaceuticals, Research and Development, Netanya, Israel.
4. The University of British Colombia, Centre for Molecular Medicine and Therapeutics, Vancouver, Canada
5. Now at German Cancer Research Centre, Immune Tolerance, Tumour Immunology Program, Heidelberg, Germany

Supplementary figures 1 and 2 legend: *Primary non-stimulated human monocyte cultures from HV, preHD and manHD received 2hPT or 24hPT with 1 or 5 µM laquinimod, or 24hPT+24hCT with 5 µM laquinimod. Levels of cytokine release were measured in culture supernatants and normalised to cell culture protein. Supplementary figure 1 displays results for the Th1-activating cytokines and supplementary figure 2 displays results for IL-2 and the Th2-activating cytokines measured. Columns = mean average log cytokine level of biological repeats; error bars = SEM; *p<0.05, **p<0.01.*

SUPPLEMENTARY FIGURE 1: Th1-activating cytokine levels in non-stimulated monocytes pre-treated with laquinimod

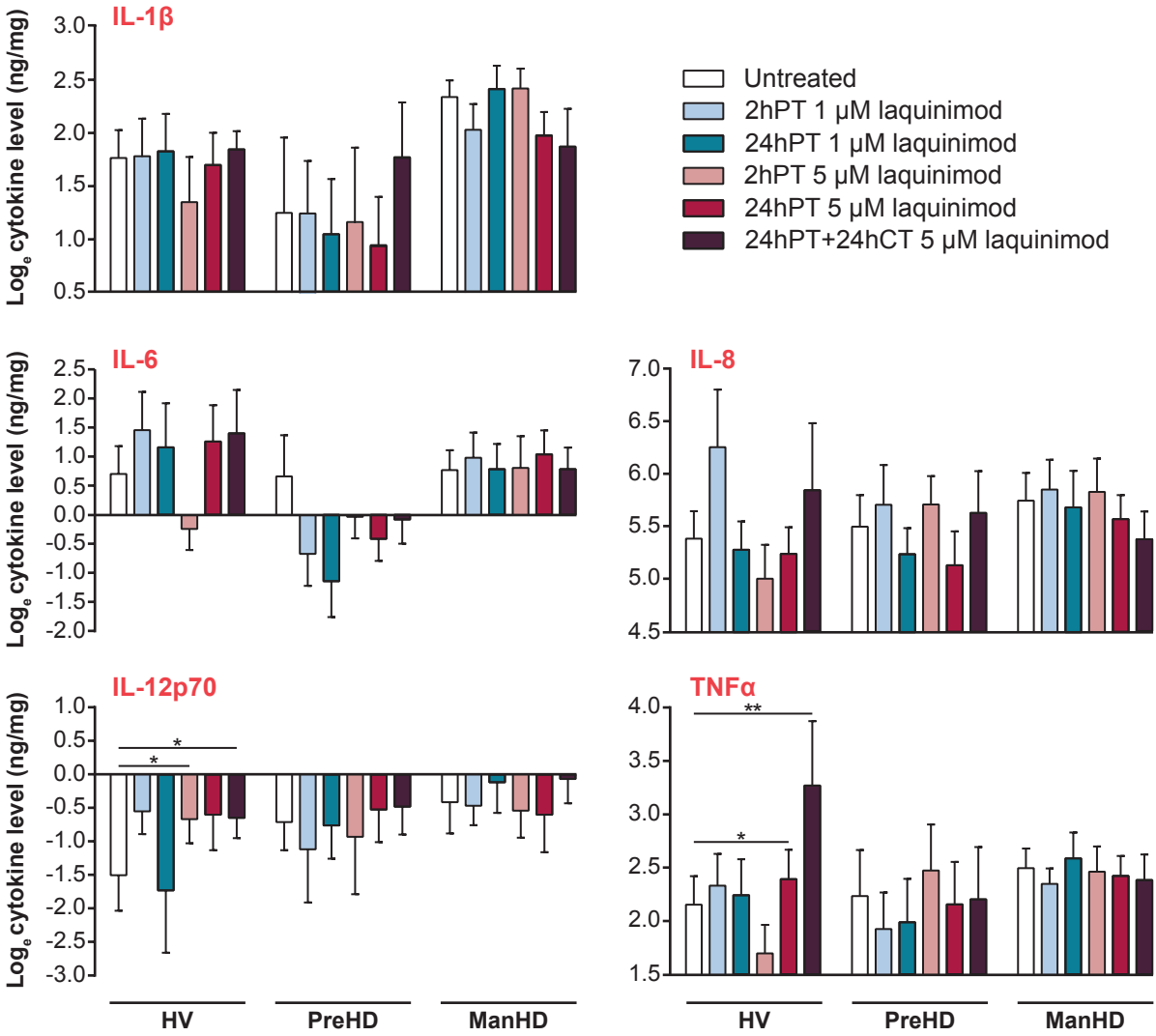

SUPPLEMENTARY FIGURE 2 IL-2 and Th2-activating cytokine levels in non-stimulated monocytes pre-treated with laquinimod